THE UNIVERSITY OF ADELAIDE

DEPARTMENT OF MECHANICAL ENGINEERING

UNSTEADY GAS TO WALL HEAT TRANSFER

LOCAL INSTANTANEOUS MEASUREMENTS in an I.C. ENGINE COMBUSTION CHAMBER

by

GARTH A. MORGAN B.E.

May 1968

A thesis submitted to the Faculty of Engineering of the University of Adelaide to fulfil the requirements for the degree of Doctor of Philosophy.

TABLE OF CONTENTS

ABSTRACT

The present thesis deals with an experimental and theoretical study of local heat transfer in the combustion chamber of a spark ignition engine.

A critical survey of the previous heat transfer work in reciprocating engine combustion chambers is carried out. The main conclusion that may be drawn from this survey is that the most profitable field of further investigation is the direct measurement of local instantaneous heat transfer conditions.

In order to undertake this work it was necessary to develop suitable methods of measurement and analysis of certain variables which had to be recorded simultaneously.

One of the important aspects was to obtain by direct measurement a representative local instantaneous gas temperature.

Various methods of gas temperature measurement were considered and the most suitable technique for this study was found to be a single fine wire thermocouple electrically corrected by a passive compensating network.

A modulated voltage data acquisition system was designed and built and this enabled the direct simultaneous recording of all time varying data during a test run with a flat frequency response from D.C. to 15 kc/s.

Steady-state and cyclic heat transfer experiments were carried out on a Ricardo E6/S research engine. The combustion chamber was instrumented so that measurements could be made at three regions; Inlet, Exhaust and Knock-Zone respectively.

Tests were carried out under motoring and firing conditions for a range of operating parameters and both steady-state and instantaneous measurements made. The cyclic data recorded on magnetic tape were capable of being digitised at rates of up to 12000 samples per second and these were analysed on a CDC 6400 digital computer.

The results of these experimental and theoretical considerations led to the following conclusions:

(1) The concept of a quasi-steady gas-wall heat transfer coefficient breaks down due to phase differences between the heat flux and the gas-wall temperature difference and more advanced theoretical methods are thus required.

(2) The phase relationships experimentally observed between the variables more accurately conform to the predictions of the Heat Transfer Coefficient concept than to those of the Temperature Profile Method.

(3) The cycle of quasi-steady heat transfer coefficient was found to resemble closely the cycle of mass velocity measured by Horvatin.

(4) A "thermal layer" thickness was defined by measurement and was found to vary considerably over the cycle, as well as with engine operating parameters.

(5) Although the induction and compression strokes showed negative and infinite heat transfer coefficients due to the breakdown in the concept, the expansion and exhaust strokes showed a continuous variation of heat transfer coefficient with a maximum occuring near e.v.o.

(6) Over this latter phase, existing empirical formulae were found to be deficient compared to experimental observations. Although modifications to these formulae are suggested, no satisfactory relationship presently exists.

(7) It appears that measurements of local instantaneous gas velocities in a combustion chamber are of prime importante for further advances in this field.

STATEMENT

This thesis contains no material which has been accepted for the award of any other degree or diploma in any University. To the best of the author's knowledge and belief, this thesis contains no material previously published or written by any other person except where due reference is made in the text.

Garth A. Morgan

May, 1968

ACKNOWLEDGEMENTS

The author wishes to express his sincere appreciation to the following persons and organisations for their valuable assistance during this project:

Professor H.H.Davis, Dr.J.Mannam and the staff of the Mechanical Engineering Department, University of Adelaide and Professor R.G.Barden, Chairman, Department of Mechanical Engineering, Monash University (formerly of Adelaide); for their continued guidance, suggestions and encouragement throughout this investigation.

Messrs. M.Hale, R.Schumann and R.Garnham who helped with the design and construction of the data acquisition system.

Messrs. A.Symes, H.Bode and R.Trueman for the construction, development and maintenance of the experimental apparatus.

Messrs. J.Dunne, L.Lock and staff of the Computer Electronics Division of the Weapons Research Establishment (W.R.E.), Salisbury, South Australia; for their enthusiastic cooperation during development of the voltage-to-frequency converters.

Messrs. J.H.Fowler of the Mechanical Engineering Department, D.Knight and B.McDowall of the Computing Research Section, Commonwealth Scientific and Industrial Research Organisation (C.S.I.R.O.); for their assistance whilst developing the computer programmes.

Miss P.Yates and staff of the Mathematical Services Division of W.R.E. for help in the logical design of the data acquisition system and for the processing of the recorded information on their Analogue-to-Digital Converter.

The use of the computing facilities of the Department of Computing Science, University of Adelaide, and of the Computing Research Section, C.S.I.R.O. is

greatly appreciated.

To the Department of Supply of the Commonwealth Government of Australia, the author is indebted for the research scholarship and financial assistance which enabled this research to be carried out.

INTRODUCTION

Engine designers are continually striving to increase specific power output of reciprocating IC Engines commensurate with reliability.

Unfortunately, this "uprating" procedure has lately emphasised the undersirable effects due to thermal loading of the components. The most disastrous effects of high local thermal loading have been recently observed in highly rated turbocharged diesel engines in the form of failure of piston crowns, valve seat bridges and thermal straining and cracking of other local "hot spots".

Unfortunately, if overall metal temperatures are reduced by removing more heat to the coolant, then thermal efficiency suffers. For best performance, only the minimum coolant flow rate required to keep the walls at a safe operating temperature is necessary. Alternatively, localised heat extraction should be provided at those areas subject to high thermal loading. Thus it would seem desirable to study local heat transfer to various regions of the combustion chamber in order to improve the empirical heat transfer formulae currently used in engine design.

However, since an engine undergoes a cyclic working process it would be required to predict the local heat transfer rate over the cycle as a function of crank angle or time.

Thus a knowledge of local instantaneous heat transfer would be useful because:

(1) The large variation in temperature of the working fluid over the cycle causes cyclic fluctuations in wall surface temperature which can induce thermal stresses of considerable magnitude in the material of the containing walls as mentioned above.

(2) An interrelationship exists between valve timing and the "direction" of heat transfer which can adversely affect volumetric efficiency. If valve timing is such that there is a significant flow of heat from the chamber walls back into the gas during the induction stroke, then the specific volume of the charge will increase with a consequent decrease of charge mass and hence volumetric efficiency will drop.

(3) The simulation of engine operation by digital computer program is becoming a powerful tool for preliminary engine design; and in the interests of more realistic simulation, more suitable expressions than those empirical expressions currently used for instantaneous heat transfer are required.

Based on the classical approach to steady-state heat transfer; it could be expected that instantaneous heat transfer from the working fluid to the combustion chamber walls of an engine would possibly be simply expressed by an instantaneous heat transfer coefficient.

However, recent experimental evidence has tended to refute even the concept of an instantaneous heat transfer coefficient under unsteady conditions due to negative and even infinite coefficients being observed at some times in the cycle. (1), (2) *

While this breakdown in the validity of the heat transfer coefficient concept can be predicted on the basis of simple theories there exists also an uncertainty in much of the literature due to the scanty experimental evidence available.

* Numbers in brackets refer to references.

In most investigations to date, some of the required variables have been obtained by calculation, on the basis of certain simplifying assumptions; rather than by direct measurement.

Furthermore, due to the limitations of previous recording procedures and methods of analysis; the various unsteady data required have invariably not been measured over the same engine cycle nor even for the same operating conditions.

All recent authors agree that further direct experimental measurement is a prerequisite to advances in this field.

AIMS

The aims of the study presented in this thesis were therefore:

(1) To develop suitable methods of measurement of each of the following quantities at a given region at each instant in the cycle:-

(a) Wall surface Temperature

(b) Surface Heat Flux

(c) Bulk Gas Temperature

(d) Gas Pressure

For correlation purposes a knowledge of the properties of the working fluid, (fuel/air/residuals mixture) as a function of gas temperature is also required, i.e. viscosity, thermal conductivity, specific heat.

(2) To build a recording system capable of collecting all the required local heat transfer data simultaneously over any particular unique engine cycle or cycles.

(3) To develop suitable methods of recovery and analysis of this data.

(4) To use this system to obtain new experimental evidence on local instantaneous heat transfer coefficients; and if possible to obtain correlation with existing unsteady heat transfer predictions.

(5) To investigate the local heat transfer at different locations in the chamber under a range of engine operating conditions.

The experimental investigation was carried out on a single cylinder 4-stroke spark ignition petrol engine in order to eliminate consideration of the radiative mode of heat transfer which is possibly more significant in the case of a Diesel Engine.

DEFINITIONS

The following concepts are defined here for the purposes of this study:

Steady-State or Mean Component

is that part of the total value of a measured variable which is independent of time in the cycle, but which changes with variation of engine operating parameters.

Unsteady-State or Cyclic Component

is that portion of a measured variable which changes continuously with crank angle or time in the cycle.

The Total Instantaneous Value

of a variable is the sum of the steady-state (mean) component and the unsteady-state (cyclic) component.

A Transient

is a special case of the unsteady-state whereby the change in the variable takes place between two definite limits over a given interval of time.

A Quasi-Steady Process

is one in which laws and definitions accepted for steady-state conditions are deemed also to hold good over a short interval of time in the unsteady-state.

Continuous Recording

is the process of measuring a variable continuously in time over any one cycle or over a consecutive number of cycles.

Point-by-Point Recording

also known as the Null method whereby the transducer signal is measured and recorded at only one particular point of time (or crank angle) in any one

cycle. A 'psuedo-cycle' is then synthesised by making a number of such measurements over a large number of cycles, not necessarily consecutive.

The Bulk-gas* Free Stream or Peak Fluid Temperature

is the gas temperature in the central region of the combustion chamber where the effect of temperature gradients at the walls can be neglected i.e. the temperature in the 'turbulent gas nucleus'.

The Space-mean Temperature

is the total instantaneous temperature integrated over a finite path length through the gas in the combustion chamber.

Optical methods give a 'line of sight' space mean temperature, including the unknown effect of the thermal gradients at the walls.

A resistance thermometer gives a space mean temperature in the region covered by the finite length of the sensing element.

The Mass-Average Temperature

is that temperature which would exist if all the gas in the cylinder volume were adiabatically mixed. An application of perfect gas laws to the cylinder gas at any time would yield this temperature.

The Local Instantaneous Gas Temperature

is that temperature measured at a point in the gas volume at any instant of time in the cycle. A point in the gas volume is defined for this study by a given spatial distance from the wall at a given peripheral location of the probe within the clearance volume.

The Thermal Layer Thickness (steady-state)

is that distance from the wall into the gas at any given location under a given set of operating conditions, at which the measured local mean gas temperature becomes identical with the mean Bulk gas temperature.

* Preferred term.

The Thermal Gradient (instantaneous)

is the distance rate of change of local instantaneous gas temperature through the thermal layer at any time in the cycle.

Note the difficulty of measuring a truly instantaneous thermal gradient due to the impossibility of taking a number of simultaneous point temperature measurements without mutual interference.

For this reason, thermal gradients in this study were estimated by comparing the temperature cycles recorded at different depths of insertion into the gas at any location. These recordings were made within the space of a few minutes under constant engine conditions.

The Quench Layer

is the distance from the wall at which internal or chemical energy heat sources become evident.

There is some evidence (63) that engine exhaust contaminants important in 'smog' formation are produced in this region near the combustion chamber wall where the flame is 'quenched' by the relatively cool wall.

Heat Flux

Applying to either the steady-state or the cyclic component the heat flux is the density of heat transfer per unit area of the wall per unit time. The sign convention used is that positive heat flux passes from the gas into the wall, while negative heat flux indicates a flow from the wall back into the gas.

Thermal Loading

denotes the strains imposed upon an engine structure by thermal impingement or more specifically by the potential cooling heat flux density. (Thermal impingement = cause, thermal straining = effect)

The Potential Cooling Heat Flux Density

has been physically interpreted by Steiger and Aue, (11), as the heat flux which would occur if the gas-side wall temperature was at the absolute zero point.

i.e. $q_{pc} = T_g \times h_{mean}$ BTU/ft^{2}sec.

ABBREVIATIONS

C.T.D.C.	Compression Top Dead Centre
B.C.T.D.C.	Before Compression Top Dead Centre
A.C.T.D.C.	After Compression Top Dead Centre
i.v.o.	Inlet valve opens
i.v.c.	Inlet valve closes
e.v.o.	Exhaust valve opens
e.v.c.	Exhaust valve closes
W.O.T.	Wide Open Throttle
M.B.T.	Minimum spark advance for Best Torque
C.R.	Compression Ratio
r.p.m.	Revolutions per minute
b.m.e.p.	Brake Mean Effective Pressure
b.s.f.c.	Brake Specific Fuel Consumption

1. LITERATURE SURVEY

The present section surveys briefly the theoretical and experimental investigations reported in the technical literature to date.

Nusselt-type formula

In 1923 Nusselt (3) put forward a formula for the combined convective and radiative modes of heat transfer based on measurements from a cylindrical combustion bomb after combustion of a quiescent air-fuel mixture. He also carried out experiments on forced convection heat transfer from flat plates at very low (Re); and tested his formula with time average data of Clerk (4) from a gas engine.

The convective part of Nusselt's formula is:-

$$h = 5.24 \times 10^5 \ (1 + 0.38V_{Pm}) \ (P^2T)^{1/3} \qquad CHU/ft^2 sec^oC$$

or $$h = 0.99 \ \sqrt[3]{P^2T} \ (1 + 1.24V_{Pm}) \qquad kcal/m^2hr^oc \qquad (1)$$

Annand (5) shows that this reduces, with certain simplifications, to the form

$$(Nu) = (\alpha^1 + B^1 (Re)) \ (P_r) \qquad (2)$$

where the 'constants' have dimensions thus limiting application of the formula.

The Nusselt expression forms the background to several modifications summarised recently by Stambuleanu (6) and used mainly in the USSR.

Jaklisch (quoted (6)) has rewritten Nusselt's formula in the more general form:

$$h = 0.0224(228.3)^{m} P^{m} T^{1-m} . \ (1+1.24\ V_{Pm}) \qquad \text{kcal/m}^2\text{hr}^{\circ}\text{C} \qquad (3)$$

Instead of using the index 2/3 of Nusselt, Jaklisch proposed that m varies with temperature in the range 0.44 to 0.90.

Briling (quoted also in (6)) found that the convective part of Nusselt's formula gave heat transfer coefficients 2 to 3 times higher than his own results from large stationary diesel engines and proposed:

$$h = 0.99 \sqrt[3]{P^2 T} \ (1+d+b.V_{Pm}) \qquad \text{kcal/m}^2\text{hr}^{\circ}\text{C} \qquad (4)$$

Where the coefficient of mean piston speed b = 0.185 (instead of 1.24 in the Nusselt and Jaklisch formulae) & d = 0 for a carburetted engine, 1.45 for a supercharged diesel engine.

Some considerations limiting the application of the above formulae are as follows:

(1) The multiplying factor $(1 + b.V_{Pm})$ in all the above expressions is a mean factor valid only for the overall cycle. Thus it is impossible to use these expressions to predict instantaneous heat transfer rate, or even that over the different phases of the engine cycle.

Nusselt himself pointed out (3) that his expression was an approximation and could not be applied indiscriminantly to the exhaust and inlet strokes.

(2) Although the effect of mean piston speed on the gas motion and hence the time-mean convection term has been accounted for, other important factors

such as cylinder head configuration, compression ratio, valve timing, and spark advance have been neglected. Nusselt recommended that his formula should not be applied if the mean piston speed was greater than 5 metre/sec.

(3) The fact that these expressions are not dimensionally homogeneous as shown by Annand (5), precludes their use under conditions very far removed from those for which they were determined.

However, Stambuleanu (6), 1967 determined time mean heat transfer with good result from Nusselt-type formula applied to a petrol engine heat balance.

Although Stambuleanu retained the Nusselt-type formula for its simplicity, he modified it by determining the form of the multiplying factor separately for different phases of the cycle as follows:

(1) Compression and Combustion Phase

From experimental data of Untaru (quoted (6)) using measurements of turbulence intensity of Semenov and Sokolik (8), 1958; Stambuleanu proposed that during compression the absolute intensity of turbulence is proportional to mean piston speed up to 20^{o} crank angle ATDC. i.e.

$$h = 0.08 \sqrt[3]{P^2T}\ (1 + 1.24\ V_{Pm}) \qquad \text{kcal/m}^2\text{hr}^{o}\text{C} \qquad (5)$$

but that toward end of compression and during combustion a greater turbulence level ensues giving:

$$h = 0.08 \sqrt[3]{P^2T}\ (1 + 1.24\ V_{Pm}^{1.2}) \qquad \text{kcal/m}^2\text{hr}^{o}\text{C} \qquad (6)$$

(2) Expansion Phase

From Semonov's measurements, this high degree of turbulence continues

over a fairly large portion of the expansion stroke.

(i.e. approximately for the first 35-40%):

$$h = 0.08 \sqrt[3]{P^2T} \quad (1 + 1.24\ V_{Pm}^{1.5}) \qquad \text{kcal/m}^2\text{hr}^\circ\text{C} \qquad (7)$$

But for the latter part of the expansion stroke the turbulent oscillations decrease to about 1/3 - 1/2 of this level i.e. for the latter 50 - 65% of expansion:

$$h = 0.08 \sqrt[3]{P^2T} \quad \frac{(1+ 1.24\ V_{Pm})}{2.5} \qquad \text{kcal/m}^2\text{hr}^\circ\text{C} \qquad (8)$$

(3) Exhaust Phase

As this phase progresses the gas flow becomes more directed toward the exhaust port, so for the initial blowdown portion of this exhaust phase, the same conditions exist as during the latter part of expansion i.e. for both cylinder wall and piston crown:

$$\text{(a)} \quad h = 0.08 \sqrt[3]{P^2T} \quad \frac{(1 + 1.24\ V_{Pm})}{2.5} \qquad \text{Kcal/m}^2\text{hr}^\circ\text{C} \qquad (9)$$

Whereas for the combustion chamber roof (similar to flow over a flat plate)Stambuleanu writes:

$$\text{(b)} \quad h = 34.5\, l^{-0.25} (\rho c_p)^{0.75} \lambda_t^{0.25} \omega^{0.75} \qquad \text{kcal/m}^2\text{hr}^\circ\text{C} \qquad (10)$$

Where $l = \frac{d-D}{2}$

ω = radial mean gas velocity along roof.

λ_t = thermal conductivity of gas at mean of gas and wall temps.

and for the combustion chamber walls - he proposes a pipe flow approximation.

$$(c) \quad h = 22.6\, l^{-0.05}\, d^{-0.16} (\rho C_p)^{0.79}\, \lambda_t^{0.21} (\rho w)^{0.79} \qquad (11)$$

Where l varies with crank angle i.e. $l = S/(\varepsilon - 1)$, $\varepsilon = C.R.$

p = gas pressure

& w = mean velocity of gases along cylinder wall; S = distance of piston from TDC

and for the Exhaust Stroke proper Stambuleanu writes:

(a) For Combustion chamber roof:

$$h = 34.5\, l^{-0.25} (\rho C_p)^{0.75}\, \lambda_t^{0.25}\, w^{0.75} \qquad (12)$$

(b) For cylinder walls:

$$h = 22.6\, l^{-0.05} d^{-0.16} (\rho C_p)^{0.79}\, \lambda_t^{0.21} (\rho w)^{0.79} \qquad (13)$$

(c) For the Piston crown:

$h = 14.5 w^{0.45}$ from Jakob (9) where w = piston speed relative to gas in cylinder. (14)

(4) Inlet Phase

From experiments on a model cylinder in 1935, Stambuleanu (10) proposed an expression to predict the heat transfer coefficient for the inlet phase - i.e. heat transferred back from cylinder wall to gas:-

$$h = 3600 \cdot A_m C_{Pc} \eta_c^{1/4} (T/T_c)^2 (V_{Pm} \rho)^{0.75} \text{ kcal/m}^2\text{hr}^\circ\text{C} \qquad (15)$$

where:- C_{p_c} = specific heat, η_c = dynamic viscosity of gas mix. at T_c

$(V_{p_m} \rho)$ = mass flow rate, T_c = mean wall temperature

and A_m = a coefficient taking into account the location of the inlet valve and the ratios:

$$\frac{h}{d} = \frac{\text{Instantaneous Exhaust Valve Lift}}{\text{Cylinder bore } \emptyset}$$

$$\frac{D}{d} = \frac{\text{Valve Port Diameter}}{\text{Cylinder bore } \emptyset}$$

$$\frac{l}{d} = \frac{\text{Instantaneous Piston Displacement}}{\text{Cylinder bore } \emptyset}$$

Stambuleanu applied the above equations for heat transfer coefficient to the experimental results of Untaru (6) by integrating the relevant coefficient over the phase period for which it applies. Using the exposed area of the cylinder head and barrel, together with approximations of wall temperature based on empirical laws of the form $T_w = a(V_{pm})^n$; he calculated the separate rates of heat transfer to the cooling water for head and barrel.

The percentage heat lost to coolant over the different phases were also compared with similar data approximated by Taylor & Taylor (7) of the form $q \propto V_{pm}^{0.8}$.

Fair agreement in both comparisons led Stambuleanu to the conclusion that his expressions could be applied successfully to the different phases of the operating cycle of a 4-stroke petrol engine.

Note however that this expression is also dimensionally incorrect.

A further development of Briling's version of the Nusselt formula by Chirkov and Stefanovski was reviewed by Annand and shown to be incorrect; being of the form $(N_u) = \text{constant} \times D^{5/12} (R_e)^{1/4}$.

The Eichelberg Formula

The expression put forward by Eichelberg (21) in 1939 is still the most

widely used; recent examples being in the papers of Walker (12), Henein (13), Brown (14), Huber & Brown (15), Whitehouse etal (16), Smyth and Wallace (17), Borman etal (18).

Eichelberg apparently modified the Nusselt formula equation (1) on the basis of his own experiments (19) and those of Hug (20) on a large low speed 2-stroke diesel engine:-

$$h = 0.0564\ (V_{Pm})^{1/3}\ (PT)_g^{1/2} \quad BTU/hrft^2F^o \qquad (16)$$

His modification of the Nusselt PT group by increasing the power of T and decreasing that of P appears to be an arbitrary method of allowing for radiation which would be more predominant in a diesel engine than in Nusselt's bomb.

Eichelberg's analysis for obtaining experimental measurements of instantaneous wall surface heat flux appears to be well proven, however.

His method, used by all subsequent investigators involves differentiation of the harmonic series representing the wall surface temperature cycle.

Because Eichelberg used sub-surface thermocouples, he had to apply an exponential correction to each term of the recorded temperature in order to obtain the true surface temperature. However, this correction technique is no longer necessary with modern miniature thermocouples.

There is actually a strong case for Eichelberg's approach of using a "mean effective" or "mass average" gas temperature calculated from the pressure record. This facilitates comparison of heat transfer between different engines in an analogous manner to performance comparisons by b.m.e.p.

However, for local investigations of heat transfer in the same engine even Eichelberg (21) recognised that the gas temperature during combustion is not uniform throughout the whole cylinder as he assumed it to be when calculating a mean value of the instantaneous gas temperature for the total mass of gas. The real gas temperature, for example near the piston is probably much higher than the mean for the total mass and much more heat (than predicted by Eichelberg) will be transferred to the piston because the real temperature difference is greater.

Pflaum (22) in 1961 proposed a modified Eichelberg expression, based on the results of tests on a large supercharged marine diesel engine. His modification was arranged to make the heat transfer finite at zero piston speed and asymptotic to some higher value at infinite piston speed:-

$$h = k_1 k_2 \, f(V_p) \, (PT)^{1/2} \qquad \text{CHU/ft}^2\text{sec}^{\circ}\text{C} \qquad (17)$$

where $$f(V_p) = 3 \pm 2.57 \, [1 - e^{\pm (1.5 - 0.127 V_p)}] \qquad (18)$$

and k_1 = 1 for liner, 3 for cylinder head and piston.

k_2 = effect of induction manifold pressure

The signs are taken + if $V_p > 11.8$ ft/sec

- if $V_p < 11.8$ ft/sec

However, Annand (5) pointed out that there is likely to be a discontinuous change of flow regime as speed tends to zero giving rise also to a discontinuous change in the mode of variation of the heat transfer.

The use of wholly empirical factors and the limited range of tests upon which these were based also renders this method doubtful for wide application.

Henien (13), simply applied Eichelberg's formula to develop expressions for combustion-chamber wall temperature and thermal loading in terms of manifold pressure, temperature, mean piston speed and i.m.e.p. for a small turbocharged diesel engine.

A comparison of the Nusselt and Eichelberg expressions was made by Van Tiejen (23). He integrated the $\sqrt[3]{P^2T}$ of the Nusselt expression and also the $\sqrt{PT}$ of the Eichelberg equation for several different cycles and found that the ratio of the two integrals was constant to within $\pm$ 5%.

Walker (24) compared the heat transfer rate for compression and expansion calculated by the Nusselt, Eichelberg and Briling formulae for a hypothetical cycle as a function of r.p.m. He found close agreement of the former two methods up to 2000 r.p.m. but thereafter the results diverged the prediction of Nusselt, equation (1), exceeding that of Eichelberg, equation (16), by almost a factor of 2.

Briling's formula, equation (4), gave heat transfer rates much lower (1/2 to 1/3) than the other two formulae over the entire speed range. This confirms Stambuleanu's criticism of Briling's formula.

Overbye's Expression

Overbye (1) 1961 reported a most extensive experimental investigation of local unsteady heat transfer in a C.F.R. spark ignition engine with port injection. Advances of his work over previous investigations included:

(1) The use of a fast-response plated (Ni-Fe) thermocouple for measurement of wall surface temperature variation.

(2) More advanced methods of recording and analysing wall temperature records

i.e. recording of temperature traces from an oscilloscope by drum camera and subsequent measurement of a large number of ordinates from the film record by optical comparator.

(3) The use of a digital computer for a much more extensive Fourier analysis of the records than previously obtained.

(4) Attempts to correlate over a range of engine variables under motoring and firing conditions.

Since Overbye's engine was not instrumented for gas temperature measurements he used only the computed "mass-average" gas temperature irrespective of position of his wall thermocouple. (This method is discussed in Appendix A1).

In order to 'experimentally' determine heat transfer coefficients, Overbye attempted to use the flame temperature data of Millar (25), also from a C.F.R. engine, together with the wall temperature and heat flux measurements from his own engine.

However, he found that this was unworkable because for the same spark advance, his engine gave wall temperatures which peaked earlier than the gas temperatures from Millar's engine.

A possible explanation of this anomaly is that the burning behaviour of two similar engines can be quite different even under the same operating conditions.

Thus, Overbye's principal recommendation for further work was that a gas temperature measurement was required simultaneously with the wall temperature measurement.

Overbye refrained from using a correlation involving an instantaneous heat transfer coefficient due to the observation of discontinuous experimental

coefficients and the theoretical evidence, as described later in Section 1.2, that these difficulties may not be entirely due to experimental error.

He thus presented an empirical expression based on experiments with an engine motored with air under maximum turbulence conditions:

$$N_o^*/3600 = P_e' \times 10^{-4}(0.26P^* - 0.035) + 0.1P^* - 0.02 \qquad (19)$$

where N_o^* = $q_o L_o / K_g T_o$ (a modified Nusselt No.)

and q_o = instantaneous surface heat flux (BTU/hr.ft^2)

L_o = stroke of engine (ft)

k_g = gas thermal conductivity (BTU.ft/hr.ft^2.F^o)

T_o = absolute temperature of intake manifold air (^oR)

P_e' = Peclet No. = $R_e \times (P_r)_i$ where $(P_r)_i$ = Prandtl No. at inlet manifold conditions.

and P^* = P/rP_i = cylinder pressure/(compression ratio x manifold pressure)

and (R_e) = $VPL\rho_i/\mu_i$ i.e. based on mean piston speed and stroke.

However, it can be seen that although dimensionless, equation (19) does not include wall temperature and thus cannot be expressed in terms of h.

He further suggested an empirical method to correct equation (19) to firing conditions by multiplying No^* by the ratio of gas-wall temperature difference on the compression stroke to the corresponding temperature difference at the same crank angle on the expansion stroke. This appears to be unwieldly and without justification as a practical method.

Overbye summed up his most exhaustive investigation ( ) in the following manner: ..."although Eichelberg's equation does not agree with the experimental data of this study, it is a simple expression and is an attempt to account for 3 factors important to heat transfer in an engine i.e. turbulence, gas density and gas temperature-wall temperature difference. The correlations attempted (by Overbye) do not present a more satisfactory expression for heat transfer in a fired engine, and our present state of knowledge in this area must be regarded as unsatisfactory,....".

Annand's Correlation

In addition to most of the above formulae, Annand (5) reviewed two other basic formulae which he has shown to be incorrect. These are the expressions of Elser (26) and of Oguri (27). They are given herein for completeness, but will not be used further in this study.

From Eichelberg-type experiments on low speed two and four stroke diesel engines using sub-surface thermopiles Elser applied dimensional analysis to form the expression:

$$(N_u) = 6.5\ (1 + 0.5\ \Delta S/C_p).\ [(R_e)(P_r)]^{1/2} \qquad (20)$$

where ΔS = increase of entropy per unit mass from the start of compression.

Elser intended the $\Delta S/C_p$ term to allow for radiant heat transfer, but Annand showed that this term resulted from a mistake; and is in fact finite after combustion.

Oguri(40),(28),1960, conducted an experimental study using a plated surface thermocouple on the piston crown of a small single cylinder spark ignition Engine, but once again computed the gas temperature from an indicator diagram. He accepted Elser's expression and developed from this the more complex version (27) :

$$(N_u) = 1.75(1 + \Delta S/C_p)\ [R_e).\ (P_r)]^{1/2}\ [2 + \quad (\theta - 20^o)] \qquad (21)$$

where θ = crank angle from TDC.

In re-examining the date of Elser, Oguri, and Overbye (of which only Elser's data appeared to be suitable), and in the light of a complete dimensional analysis, Annand decided that for any given location in a particular engine, the Reynold's Number based on piston diameter and mean piston speed was the most important parameter for local convective heat transfer. Thus he proposed the power law relationship:

$$(N_u) = a(R_e)^b \qquad (22)$$

By extensive statistical analysis of Elser's data at 300 r.p.m. for the compression and expansion phases, Annand determined the exponent 'b' and the multiplying constant 'a' for both Elser's two and four-stroke engines. His predicted heat fluxes fitted Elser's data generally better than did Elser's own formula. There appeared to be close agreement between predicted and experimental values in the region of zero gas-wall temperature difference (infinite heat transfer coefficient) due to the low level of heat flux at that time.

It is also interesting to note that Annand's results gave the least scatter when the required gas thermal properties were calculated directly from the gas temperature rather than from the mean of this and the wall temperature as used by Elser. The information presented in Appendix A2 on the thermal transport properties of a number of fuel/air/residual mixtures would thus seem to be useful in this regard, over the range of applicability considered i.e. for the compression phase and up to the dissociation temperature limit.

Moreover, Annand's use of mean piston speed neglects the effect of local gas motion and results in an overall Reynolds No. Thus his expression could be restrictive when applied to localised unsteady investigations.

Annand also appears to have justified the use of a (Nu) - (Re) exponent of 0.7 for the motored and fired data of Overbye and for a considerable amount of other time-mean heat transfer data.

However, from considerations of the energy equation, Overbye (1) showed that the rate of change of pressure term probably plays an important part in heat transfer to the wall. Therefore the omission of a pressure work term in Annand's equation may reduce the generality of his prediction.

Some recent attempts have been made to approximate instantaneous gas velocities especially by Knight (29) and Henien (30). Early experiments to determine instantaneous mass flow rates by hot wire anemometer techniques have been reported by Semenov (31) and Horvatin (32) and these are discussed in detail later.

Overbye (33) also investigated calculations of 'swirl' velocity component reporting that angular swirl velocities could be of the order of 10 times engine r.p.m.

Henien (30) recently modified Eichelberg's equation with apparently good result by using an approximate gas velocity instead of mean piston speed. The gas velocity used was the resultant of crude calculations of the squish and swirl components; the peak velocity amounting to about 9 times the mean piston speed.

Knight (29) has stated that quite crude gas velocity assessments could substantially improve engine heat transfer correlations and also widen their field of usefuleness by making it possible to allow for different heat fluxes to the various internal surfaces.

Annand did realise the limitations of his correlation, however, as he stated that with the experimental evidence available it was impossible to formulate any more than the simplest of empirical equations.

The evidence referred to included at his time of writing both true local instantaneous heat transfer measurements and gas velocity data.

The Work of Knight

Knight (29) 1964, carried out experiments on motoring and firing engines using a surface thermocouple to measure wall surface temperature fluctuations.

He also obtained mass-average temperatures from cyclic pressure measurements. For the motoring case he confirmed these calculated temperatures by hot wire resistance thermometer measurements.

He then applied the temperature profile theory (given later) to check his measured wall temperature swing. For this purpose he used the turbulent boundary layer thickness developed in a pipe having the same flow velocity as the peak gas velocity. He approximated this gas velocity by energy conservations including the "squish" effect of the trapped mass of gas using simplified valve timing.

While this step towards a measure of true instantaneous gas velocity seems to be plausible, the direct application of steady-state pipe flow boundary layer thicknesses would need verification.

2. UNSTEADY HEAT TRANSFER PREDICTIONS

2.1 The Quasi-Steady Heat Transfer Coefficient

Under steady state conditions, the rate of transfer of heat from a fluid to a wall by convection is given by Newton's Law of cooling:

$$q/A = h(T_g - T_w) \tag{23}$$

where: q/A = heat flux ($BTU/hr.ft^2$)

Tg = Bulk gas temperature (^oF)

Tw = Wall surface temperature (^oF)

h = film coefficient of heat transfer ($BTU/hr.ft^2F^o$)

An unsteady heat transfer process can be thought of as being comprised of a number of quasi-steady processes taking place over short intervals of time.

Therefore for each interval of time an unsteady heat transfer coefficient can be obtained according to equation (23).

Elser (2) and Overbye (1) both noted from experiment that gas-wall temperature difference and heat flux were out of phase. Thus, at certain points in the cycle, negative or infinite coefficients result.

This discontinuity caused them to doubt the usefulness of a quasi-steady heat transfer coefficient.

Annand (5) commented however that in the practical case, the use of a formula yielding continuous finite values of h will only be slightly in error due to the fact that the quantity of heat transferred at the discontinuities is only a small fraction of the total heat transferred during the cycle.

Again, the results of previous investigations with regard to phase relations between the variables cannot be relied upon due to the restrictive nature of the experimental data.

It will now be shown that the two main opposing theories of instantaneous heat transfer, i.e. the Heat Transfer Coefficient Concept and the Temperature Profile Method, predict quite different phase relations between the variables.

2.2 The Heat Transfer Coefficient Concept

The general energy equation for a control volume located either in the gas or in the cylinder wall is given in (34) as follows:

$$\frac{\partial}{\partial t}(\rho C_p T) = -(\nabla \cdot \rho C_p T \vec{V}) - (\nabla \cdot \vec{q}) - (\tau : \vec{\nabla} V) + \frac{1}{J}\left(\frac{\partial \log_e (1/\rho)}{\partial \log_e T}\right) \cdot \frac{Dp}{Dt} + \rho T \left(\frac{DC_p}{Dt}\right) + q_i \qquad (24)$$

where t = time (hr)

ρ = density (lb/ft^3)

C_p = specific heat at constant pressure (BTU/lb^oF)

T = absolute temperature (^oR)

V = velocity (a vector) (ft/hr)

q = heat flux (a vector) ($BTU/hr.ft^2$)

τ = shear stress (a tensor)

p = absolute pressure (lb/ft^2)

q_i = rate of energy conversion (BTU/ft^{3}hr)

D = a substantial derivative

J = Joule's mechanical equivalent of heat (ft/lb$_f$/BTU)

or in words: The time rate of change of thermal energy within the control volume consists of:-

(1) Energy variations due to mass flow in and out of the control volume (convection).

(2) Heat conduction into and out of the volume.

(3) Viscous dissipation of fluid energy into thermal energy as it flows into the control volume (Frictional effects).

(4) Pressure work done on the gas in the control volume due to cyclic pressure variation.

(5) Energy changes due to variation in specific heat of the gas.

(6) Internal energy generation within the control volume due to combustion.

Now if we assume for the solid wall only that:-

(1) Convective heat transfer is zero.

(2) Frictional effects are absent.

(3) Pressure work is zero.

(4) Density is independent of temperature and pressure.

(5) Internal energy sources are absent.

(6) Thermal properties of the solid wall are independent of temperature.

Then the heat transfer in one-dimensional form will be given by:

$$\frac{\partial T}{\partial t} = \alpha \frac{\partial^2 T}{\partial x^2} \qquad (25)$$

i.e. the one-dimensional Fourier heat conduction equation

where $\alpha = (k/\rho C_p)_w$ = diffusivity of the wall material.

k_w = thermal conductivity of the wall material

Cp_w = specific heat of wall material

x = distance from gas-wall interface.

Hobson (35) and Kelvin (36) modified equation (23) so that it could be applied to the Unsteady-state; and this was summarised by Overbye (1) from Jakob (19) as follows:

It is assumed that the temperature in the bulk gas region varies sinusoidally with time:

$$\theta_g = \theta_{og} \cdot \cos(n\omega t - \gamma) \qquad (26)$$

where θ_{og} is the maximum of the nth harmonic of gas temperature about the steady-state mean (Tgm) i.e. $\theta_{og} = T_{g\infty} - T_{gm}$

γ is the phase angle of this harmonic

ω is the fundamental cyclic frequency

t is time in the cycle.

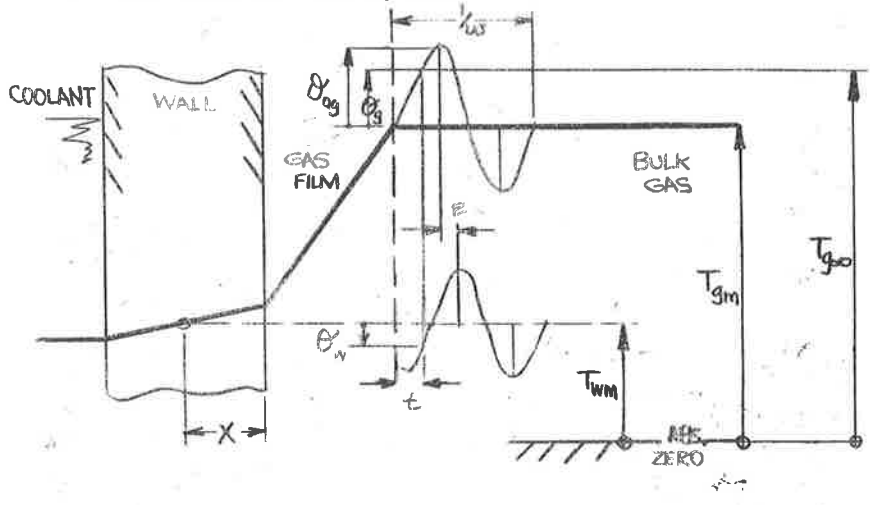

It is then assumed that the temperature variation with time induced at any depth in the wall by this harmonic of gas temperature can be expressed as

$$\theta_w = \theta_{og}\,\eta\, e^{-mx}\cdot\cos(n\omega t - mx - \varepsilon) \qquad (27)$$

where w is the wall temperature above its mean value

X is distance into the wall from the gas-wall interface,

η, m & ε are constants to be determined by boundary conditions.

If Fourier's heat conduction equation (25) is satisfied the boundary conditions required for a solution of this equation are:

(a) at x = o, $\left(\frac{dT}{dx}\right)_w = \left(\frac{dT}{dx}\right)_g$ hence $q_w = q_g$

(b) at x = o, $\theta_g = \theta_w$

These two conditions are satisfied by:

$$-k_w \frac{\partial \theta_w}{\partial X} = h_o\left(\theta_g - \theta_w\right)\Big|_{X=0} \qquad (28)$$

where h_o is a time mean heat transfer coefficient.

It can be shown from these boundary conditions Ref. (1) that:

$$\varepsilon = \tan^{-1}(1/(1 + b/m)) \qquad (29)$$

$$\eta = 1/\sqrt{1 + 2m/b + 2(m/b)^2} \qquad (30)$$

where $b = h_o / k_w$

and $m = \sqrt{n\omega/2\alpha}$

Using typical values for an S.I. engine for the fundamental component of gas temperature at 1000 RPM:

$n = 1$, $w = 60{,}000\pi$ rad/hr, $= 0.52$ ft^2/hr $\therefore m = \sqrt{nw/2\alpha} = \underline{425}$

and if $h_o = 100$ BTU/hr/ft^{2}F^o

and $k_w = 29.0$ BTU/hr.ft.F^o $\therefore$ $b = h_o/k_w = 100/29.0 = \underline{3.45}$

$\therefore$ $b/m = \underline{0.00814}$

From the tabulated variation of η & ε with b/m given in Ref. (9) at b/m = 0.008, ε lies between 44^o 50' & 45^o 00' and furthermore will approach more closely to 45^o 00' as n increases.

Differentiating equation (27) with respect to X, evaluating at X = 0 and multiplying by $(-k_w)$ gives:

$$q_o = \sqrt{2}\, k_w r \theta_{og} \eta \cos(n\omega t - \varepsilon + \pi/4) \qquad (31)$$

and, if as shown ε is exactly equal to $\pi/4$ for each harmonic, then the

surface heat transfer will be exactly in phase with the fluctuations of the bulk gas temperature. Thus the important implications of this theory are:

(1) The gas temperature fluctuations are attenuated in the gas film adjacent to the wall surface. (the factor η in equation (30))

(2) A particular harmonic of the variation in gas temperature at a great distance from the wall leads the corresponding wall surface temperature harmonic by 1/8 of its period i.e. 90^{o} crank angle for the fundamental component.

(3) The wall surface heat transfer variation is in phase with the cycle of gas temperature at a great distance from the wall.

In discussing this theory in relation to his own investigation Overbye (1) observed that his wall temperature cycle did not lag his gas temperature cycle by 90^{o} and that the phase shifts between the gas temperature, wall temperature, and heat transfer were not large.

2.3 The Temperature Profile Method

The previous heat transfer coefficient concept makes no allowance for energy variations in the gas film next to the wall. It assumed constant thermal resistance giving a linear temperature gradient in the gas film. Thus the layer only entered into the heat transfer process as a purely conducting medium in that theory.

In order to solve the general energy equation (24) for a control volume situated in the gas film, Pfriem (37) and Elser (2) gave separate developments. The former represented the pressure work term (Dp/Dt) as a harmonic function, whereas the latter expressed the internal energy generation term (q_i) as a harmonic function.

Both assumed that these energy contributions were uniformly distributed throughout the gas volume.

The energy equation for the gas volume can now be written:

$$\rho C_p \frac{\partial T}{\partial t} + C_p T \frac{\partial \rho}{\partial t} = k_g \frac{\partial^2 T}{\partial x^2} + \frac{1}{J} \frac{\partial P}{\partial t} + q_i \qquad (32)$$

Both Pfriem and Elser made the assumption that gas density was constant, implying that pressure or internal heat generation fluctuations are small compared to their absolute values and that gas properties can thus be regarded as independent of pressure and temperature. Also, the gas velocity component perpendicular to the wall was assumed to be negligible near the wall surface. Hence convective energy transport is zero in the stagnant gas film and a further simplification of (32) is:

$$\frac{\partial \theta_g}{\partial t} = \alpha_g \frac{\partial^2 \theta_g}{\partial x^2} + \frac{1}{J(\rho C_p)_g} \cdot \frac{\partial P}{\partial t} + \frac{q_i}{(\rho C_p)_g} \qquad (33)$$

Elser's analysis assumed zero pressure term and hence:

$$\frac{\partial \theta_g}{\partial t} = \alpha_g \frac{\partial^2 \theta_g}{\partial x^2} + \frac{q_i}{(\rho C_p)_g} \qquad (34)$$

where $\theta_g = (T_g - T_m)$

$$\alpha_g = (k/\rho C_p)_g$$

At a great distance from the wall in the turbulent bulk gas region where conduction is zero, the gas temperature variation is of the form:

$$\theta_{g\infty} = \theta_{og} \sin \omega t \tag{35}$$

θ_{og} = Amplitude of Bulk gas temperature.

and the heat generation term is:

$$q_i = \omega (\rho C_p)_g \cdot \theta_{og} \cos \omega t \tag{36}$$

Using the boundary conditions

(a) $\theta_w = \theta_g$ at x = o (37)

and (b) $k_w \frac{\partial \theta_w}{\partial x} = k_g \frac{\partial \theta_g}{\partial x}$ at x = o (38)

Equation (34) may be solved to give:

$$\theta_g = \theta_{og} \sin \omega t - A e^{rx} \sin(\omega t + rx + \gamma) \tag{39}$$

where $r = \sqrt{\omega / 2\alpha_g}$ & $\alpha_g = (k/\rho C_p)_g$

A = amplitude) of a given harmonic of the
) gas temperature at any
γ = phase) location in the gas volume.

The exponential term e^{rx} represents attenuation as the wall is approached.

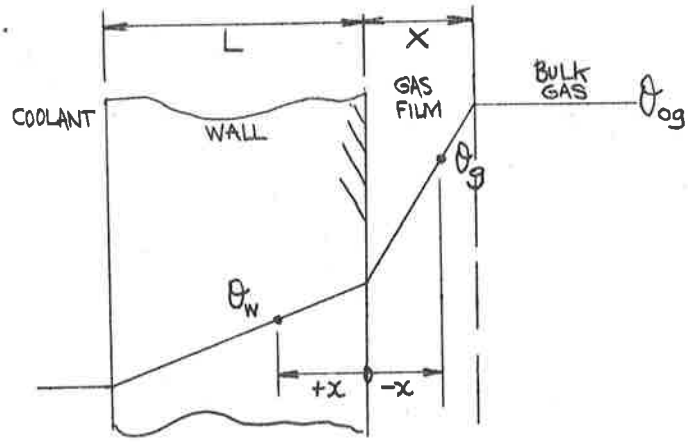

It can be shown, Ref. (1), that if a gas temperature variation of the above form (39) induces a sinusoidal surface temperature on an infinitely thick slab, then the temperature variation in the wall is given by:

$$\vartheta_w = \vartheta_{ow} e^{-mx} \sin(\omega t - mx + \beta) \tag{40}$$

where ϑ_{ow} = amplitude of surface temperature variation.

β = phase angle between wall surface temperature and the gas temperature at $x = \infty$

$m = \sqrt{\omega / 2\alpha_w}$ for the wall material

if equations (39) and (40) are used with the boundary conditions (37) and (38); it can be seen that:

$$\vartheta_{og} \sin \omega t - A \sin(\omega t + \gamma) = \vartheta_{ow} \sin(\omega t + \beta) \tag{41}$$

and

$$A\sqrt{(k\rho c_p)_g} \begin{bmatrix} \sin(\omega t + \gamma) \\ + \\ \cos(\omega t + \gamma) \end{bmatrix} = \vartheta_{ow}\sqrt{(k\rho c_p)_w} \begin{bmatrix} \sin(\omega t + \beta) \\ + \\ \cos(\omega t + \beta) \end{bmatrix} \tag{42}$$

Thus, from equation (42) it can be seen that:

$$\gamma = \beta \quad \& \quad \frac{\theta_{ow}}{A} = \sqrt{(k\rho C_p)_g} \Big/ \sqrt{(k\rho C_p)_w} \tag{43}$$

and using equation (41) $\gamma = \beta = 0$, $\&$ $$\frac{\theta_{ow}}{\theta_{og}} = \frac{b_g}{(b_g + b_w)} \tag{44}$$

where b = thermal penetration No. $= \sqrt{k/\rho C_p}$

Equation (39) can now be rewritten:

$$\theta_g = \theta_{og}\left[\sin\omega t - (b_w/(b_w+b_g).e^{-rx}.\sin(\omega t + rx)\right] \tag{45}$$

from which it can be seen that the net result of energy generation and conduction into and out of the gas layer near the wall is:

(1) The wall surface temperature is in phase with the gas temperature at a great distance from the wall ($x \longrightarrow \infty$) and is a miniature replica of it, reduced by the ratio of thermal penetration numbers of gas and wall. Note that "a great distance from the wall", or the gas film thickness to the adiabatic or bulk gas region becomes smaller at higher frequencies.

(2) The heat transfer through the wall surface leads the wall surface temperature by a phase angle of 1/8 of the period for any harmonic.

It can thus be seen that the predictions of this theory are opposed to those of the heat transfer coefficient concept. However, both theories are oversimplified, the first assuming a constant heat transfer coefficient and the second assuming a constant gas density in order to obtain a solution.

If, however, a variable 'h' is used with the results of the temperature profile method, then using equations (40) and (44), the surface heat flux can be expressed from equation (23) as:

$$q_0 = [b_w b_g \theta_0 \sqrt{\omega}/(b_w + b_g)] \sin(wt + 45^o) \qquad (46)$$

and since $\theta_{g\infty}$ & $\theta_w \big| x = o$ are in phase and related by the thermal penetration numbers (bg, bw), the H.T. coefficient is

$$h = b_g \sqrt{\omega} \sin (wt + 45^o)/\sin wt \qquad (47)$$

from which it can be seen that h can be zero, negative and even infinite which is contrary to the concept of a heat transfer coefficient as used in steady-state heat transfer.

Pfriem (37) has taken this concept a step further by writing equation (23) in the polar form

$$q_0 = h_m . h_\phi (\theta_{g\infty} - \theta_w)\big|_{x=0} \qquad (48)$$

where h_m is the modulus of the HT Coefficient and hØ is the phase angle between gas-wall temperature difference and the surface heat transfer.

From equation (47) above hØ = 45^o

and $h_m = b_g \sqrt{\omega}$ and thus a continuous heat flux will result from (48) above.

A different approach to deriving a coefficient of heat transfer than the two methods just discussed will now be shown.

2.4 A Heat Transfer Coefficient From Kadrinov's Kinetic Theory, Ref. (38)

The basic assumptions from the Kinetic theory of Matter are:-

(1) Atoms of the solid wall perform oscillatory movements near their equilibrium states in the direction of the thermal flux i.e. normal to the wall in the one-dimensional case.

(2) The gas molecules are in a continuous random motion constantly colliding between each other and the oscillating atoms of the wall.

(3) Collisions between the gas molecules and also between gas molecules and atoms of the solid wall are considered to be elastic.
There will be an energy exchange between the gas molecules and the wall atoms if they have different kinetic energies.

(4) The temperature of the gas characterizes the average kinetic energy of the motion of the molecules. Similarly, the wall temperature expresses the average kinetic energy of its oscillating atoms.
Considering a vessel containing a gas with a temperature higher than that of the walls.

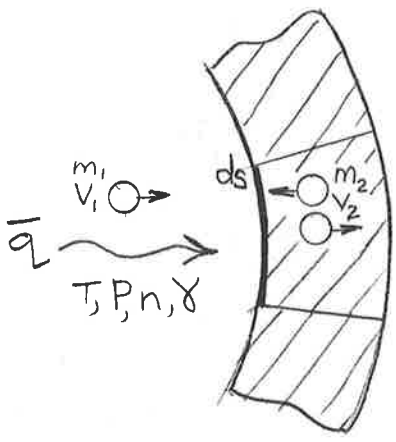

The above assumptions can be summarised as follows:-
There is a continuous process of heat transfer by which thermal energy is transmitted from the higher to the lower energy level until equilibrium is reached.

Nomenclature for Kadrinov's Theory

ds = elemental wall area receiving heat flux

x = distance along X-axis (normal to wall element ds) radially outwards.

V_1 = average velocity of forward motion of gas molecules at start of a collision with atoms of the wall.

u_1 = velocity of these molecules at the end of a collision.

m_1 = the mass of the gas molecule.

V_2 = the average velocity of the oscillatory motion of the atoms on the wall surface that are in collision with the gas molecules.

m_2 = the mass of these atoms.

ν = the no. of gas molecules/unit volume (gas concentration).

T = the representative gas temperature (either Tg or Tp)

T_g = the bulk gas temperature.

T_w = the wall surface temperature.

T_p = temperature in the gas-wall boundary layer.

u'_1 = velocity of gas molecules at the end of a collision with atoms of a wall element ds moving in the direction of the inside normal.

u''_1 = velocity of gas molecules after collision moving in the direction of the outside normal.

P = gas pressure per unit area ds.

$\bar{q}$ = the amount of energy lost by the gas molecules per unit time to a unit area of the wall. (Heat Flux).

μ = weight of a single mole of gas (μ = gNm)

N = number of molecules in 1 kg-mole.

n = number of degrees of freedom = $2/\gamma - 1 = \frac{2}{Cp}(Cp - R/J)$

γ = adiabatic index = Cp/c_v

Cp = specific heat at constant pressure.

C_v = specific heat at constant volume.

R = $\bar{R}/M$

$\bar{R}$ = Universal gas constant = 1544.

J = Mechanical equivalent of heat.

g = gravitational constant.

Consider the elemental surface area ds of the wall and let the number of molecules striking the element during a time interval $dt = \nu V_1 ds.dt/6$.

If half these molecules collide with atoms of the wall element that are moving towards the gas-wall interface and the other half collide with atoms that are moving away from the gas-wall interface then, by the theorem of momemtum as applied to gas molecules colliding with atoms of the solid wall, we can write:

$$P ds.dt = \frac{\nu \nu_1 ds/dt}{12} (2m_1 \nu_1 + m_1 u_1' + m_1 u_1'') \qquad (49)$$

and the velocities u_1' and u_1'' can be determined from the following known formulae of theoretical mechanics

$$\left.\begin{aligned} u_1' &= \frac{2m_2}{m_1+m_2} \cdot (\nu_1 + \nu_2) - \nu_1 \\ u_1'' &= \frac{2m_2}{m_1+m_2} \cdot (\nu_1 - \nu_2) - \nu_1 \end{aligned}\right\} \qquad (50)$$

Substituting (50) in (49):-

$$\text{pds.dt} = \frac{\rho v_1 ds.dt}{12}\left(2m_1v_1 + m_1u_1' + m_1u_1''\right)$$

$$= \frac{\rho v_1 ds.dt}{12}\left(2m_1v_1 + \frac{2m_1m_2}{m_1+m_2}(v_1+v_2) - m_1v_1 + \frac{2m_1m_2}{m_1+m_2}(v_1-v_2) - m_1v_1\right)$$

$$\therefore \text{pds.dt} = \frac{\rho v_1 ds\,dt}{12} \cdot \frac{4m_1m_2v_2}{(m_1+m_2)}$$

$$\therefore p = \frac{\rho}{3}\frac{m_1m_2v_1^2}{(m_1+m_2)}$$

$$\therefore p = \frac{\rho}{3}\cdot\frac{m_2}{(m_1+m_2)} \cdot \frac{m_1v_1^2}{2} \qquad (51)$$

The amount of energy lost per unit time by the gas molecules to the atoms of the wall per unit elemental area is given by:-

(number of gas molecule-wall atom collisions) x (change in kinetic energy due to one collision)

$$\therefore \bar{q} = \frac{\rho v_1}{6}\cdot\left(\frac{m_1v_1^2}{2} - \frac{1}{2}\left(\frac{m_1u_1'^2}{2} + \frac{m_1u_1''^2}{2}\right)\right)$$

$$= \frac{\rho v_1}{12}\left(m_1v_1^2 - \frac{m_1u_1'^2}{2} - \frac{m_1u_1''^2}{2}\right)$$

& (50)→

$$\therefore \bar{q} = \frac{\rho v_1}{12}\left(m_1v_1^2 - \frac{m_1}{2}\left(\frac{2m_2}{m_1+m_2}(v_1+v_2) - v_1\right)^2 - \frac{m_1}{2}\left(\frac{2m_2}{m_1+m_2}(v_1+v_2) - v_1^2\right)\right)$$

$$\therefore \bar{q} = \frac{2}{3}\rho m_1v_1 \cdot \frac{m_2}{(m_1+m_2)^2}\cdot\left(\frac{m_1v_1^2}{2} - \frac{m_2v_2^2}{2}\right) \text{ kcal/sec for an elemental area.} \qquad (52)$$

and substituting (51) in (52)

$$P = \frac{2}{3}\nu \cdot \frac{m_2}{(m_1+m_2)} \cdot \frac{m_1 v_1^2}{2}$$

$$\therefore \frac{2P}{v_1} = \frac{2}{3}\nu\, v_1 m_1 \cdot \frac{m_2}{(m_1+m_2)}$$

$$\therefore \bar{q} = \frac{2P}{v_1}\left(\frac{m_1 v_1^2}{2} - \frac{m_2 v_2^2}{2}\right)\Big/(m_1+m_2) \qquad (53)$$

Also from the kinetic theory:

$$\frac{m_1 v_1^2}{2} = \frac{3}{2}\cdot\frac{848}{N}\cdot T \qquad \& \quad \frac{m_2 v_2^2}{2} = \frac{3}{2}\cdot\frac{848}{N}\cdot T_w \qquad (54)$$

Where N = number of molecules/kg-mole

and substituting these in (53)

$$\bar{q} = \frac{2P}{v_1}\cdot\frac{1}{(m_1+m_2)}\cdot\frac{3}{2}\cdot\frac{848}{N}(T-T_w)$$

$$\therefore \bar{q} = \frac{P}{(m_1+m_2)}\cdot\frac{2544}{N}\cdot\frac{(T-T_w)}{v_1}$$

& from (54)

$$v_1 = \sqrt{\frac{2544\,T_g}{m_1 N}}$$

$$\therefore \bar{q} = \frac{P}{m_1+m_2}\cdot\frac{2544}{N}\cdot\sqrt{\frac{m_1 N}{2544\,T_g}}\cdot(T-T_w)$$

$$\therefore \bar{q} = \frac{P}{m_1+m_2}\cdot\sqrt{\frac{2544\,m_1}{N T_g}}\cdot(T-T_w) \qquad \frac{\text{kg-mole}}{\text{m}^2\,\text{sec}} \qquad (55)$$

The above equation holds for a MONATOMIC gas having 3 degrees of freedom.

For a POLYATOMIC gas of n degrees of freedom the RHS of equation (55) is multiplied by n/3 (from Maxwell-Boltzmann), where $n = (2/\gamma - 1)$, $\gamma = C_p/C_v$.

Noting that gNm = μ kg/mole and that 1 kg.metre = 427 Kcal. then $\bar{q}$ in thermal units is given by:-

$$\bar{q} = \frac{P.n/3}{427\left(\frac{\mu_1}{gN} + \frac{\mu_2}{gN}\right)} \cdot \sqrt{\frac{2544\,\mu_1}{gN.NT}} \cdot (T - T_w) \quad \text{Kcal/m}^2\text{sec} \qquad (56)$$

$$= \frac{P.gNn}{1281(\mu_1 + \mu_2)} \cdot \sqrt{\frac{2544\,\mu_1}{gN^2T}} \cdot (T - T_w)$$

$$= \frac{\sqrt{2544}}{1281} \cdot \frac{nP}{(\mu_1 + \mu_2)} \cdot \sqrt{\frac{\mu_1 g^2 N^2}{gN^2T}} (T - T_w)$$

Thus:

$$\bar{q} = 0.0394 \frac{nP}{\mu_1 + \mu_2} \sqrt{\frac{\mu_1 g}{T}} (T - T_w) \quad \text{Kcal/m}^2\text{sec} \qquad (57)$$

Where T = the characteristic gas temperature.

For turbulent heat transfer only, the total gas volume is at bulk gas temperature, i.e. $T = T_g$, and combining equations (23) and (57) yields:

$$h = 0.0394 \frac{nP}{\mu_1 + \mu_2} \sqrt{\frac{\mu_1 g}{T}} \quad \text{Kcal/m}^2\text{sec} \qquad (58)$$

However, considering a boundary layer to be present at the wall, the characteristic temperature may by written $T = (T_g + T_w)/2$ and equation (57) becomes:

$$\bar{q} = 0.0394 \frac{nP}{\mu_1 + \mu_2} \sqrt{\frac{2\mu_1 g}{T + T_w}} \cdot \left(\frac{T_g + T_w}{2} - T_w\right)$$

$$\therefore \bar{q} = 0.0394 \frac{nP}{\mu_1 + \mu_2} \sqrt{\frac{2\mu_1 g}{T + T_w}} \cdot \left(\frac{T_g - T_w}{2}\right) \quad \text{Kcal/m}^2\text{sec} \qquad (59)$$

and substituting in (23):

$$h = 0.0394 \frac{nP}{\mu_1 + \mu_2} \sqrt{\frac{2\mu_1 g}{T_g + T_w}} \cdot \frac{1}{2}$$

$$\therefore h = 0.0394 \frac{nP}{\mu_1 + \mu_2} \sqrt{\frac{\mu_1 g}{2(T_g - T_w)}} \quad \text{Kcal/m}^2\text{sec}^{\circ}\text{C} \qquad (60)$$

The constant term has dimensions $[MT^{-1}L^{-1/2}\theta^{-1/2}]$ and thus in Absolute British units:

$$C = 0.0394 \times 2.205 \times \frac{1}{3.781} \times \frac{1}{1.8} = \underline{0.0357}$$

Where P is in lbal/ft^2, T in $^{\circ}\text{R}$

Thus (60) becomes:

$$h = \frac{0.0357 \times 3600 \times 144}{32.2} \cdot \frac{nP}{\mu_1 + \mu_2} \sqrt{\frac{\mu_1 g}{2(T_g + T_w)}}$$

$$h = 575 \frac{nP}{\mu_1 + \mu_2} \sqrt{\frac{\mu_1 g}{2(T_g + T_w)}} \quad \text{BTU/hr.ft}^2\text{F}^{\circ} \text{ with P in psia} \qquad (61)$$

For a stoichiometric octane-air mixture:

$\mu_1 = 30.094$ (Table 7 Appendix A2)

and for an iron wall $\mu_2 = 55.85$

and substituting these values in (61):

$$h = 147\, hP / \sqrt{T_g + T_w} \quad \text{BTU/hr.ft}^2\text{F}^\circ \qquad (62)$$

Values for n were calculated from

$$n = 2/(\gamma - 1) \quad \text{where} \quad \gamma = \frac{C_p}{C_v}$$

$$\therefore\ n = \frac{2}{C_p}\left(C_p - \frac{R}{J}\right) = \frac{2}{C_p}\left(C_p - \frac{\bar{R}}{W.J}\right)$$

and since C_p and W are given for the Fuel/Air/Residuals mixture in Appendix A2, the number of degrees of freedom n, can be found to be approximately $n = \frac{2}{C_{pmix}}\,(C_{pmix} - 0.066)$

Hence the heat transfer coefficient can be found from Kadrinov's formula up to the dissociation limit of the C_{pmix} data in Appendix A2.

It can be seen from the above analysis that:

(1) The coefficient of heat transfer from a gas to a wall in all cases is directly proportional to the absolute pressure of the gas.

(2) In the presence of a strongly turbulent gas flow having an identical temperature throughout its volume, the heat transfer coefficient is inversely proportional to the square root of the average temperature T of this gas and can be found from equation (58).

(3) In cases of a non-uniform temperature distribution, the heat transfer coefficient depends on both gas temperature and wall temperature and can be found from equation (59). For this it is first necessary to determine the temperature T_p of the gas boundary layer which is always lower than its average temperature.

(4) The heat transfer coefficient depends on the physical properties of the gas and also on the molecular weight of the wall material adjacent to it.

3. THE EXPERIMENTAL APPROACH

3.1 Measurements Required

In order to determine experimentally the variation of local quasi-steady heat transfer coefficient over the cycle, it has been seen that it is necessary to measure simultaneously the instantaneous values of:

(1) Wall surface temperature

(2) Wall surface heat flux

(3) Bulk gas temperature, and

(4) Pressure (for correlation purposes)

The method used for wall surface temperature measurement in this investigation was to locate a miniature Chromel-Alumel sheathed thermocouple (0.001"Ø wires) with its junction at the wall surface. It was found that this gave comparable measurements to those of Overbye (1), Bennethum (39) and Oguri (40).

To determine surface heat flux an harmonic analysis of the recorded wall temperature cycle was carried out as detailed in Section (5.2) again following the methods used by the above authors but with the advantage of more advanced sampling and analysis.

The extremely difficult measurement of local instantaneous Bulk gas temperature has been avoided by previous authors, as mentioned earlier, by the use of the "mass average" temperature calculated from the measured pressure-time diagram.

It is realised that the method finally chosen, i.e. electrical compensation of a single fine-wire thermocouple, is still only approximate and has definite limitations. But it is relatively simple

and appears to give at least an indication of the instantaneous temperature variation at any location in the combustion space.

A point measurement is necessary because the gas temperature required in the definition of the quasi-steady heat transfer coefficient is the Bulk-gas temperature or that measured outside the gas-wall "thermal boundary layer".

Unfortunately there is scanty knowledge of the extent of this thermal layer thickness in a fired or even in a motored engine. Due to the complex flow patterns existing in the combustion chamber at any time it is rather difficult to calculate a theoretical boundary layer thickness although approximations from pipe flow theory have been made by Knight (29).

Thus, as a prerequisite to the measurement of local instantaneous bulk gas temperature, it is necessary to determine the instantaneous boundary layer thickness.

This in turn must be estimated from the instantaneous temperature gradient in the gas layer near the wall.

The gas pressure cycle was also required to be measured simultaneously with the other measurements for use in the Eichelberg, Kadrinov and other formulae.

3.2 The Test Engine

The test engine used in this investigation was the Ricardo E6/S variable CR research engine shown in Figs. (1) and (2). The main specifications are given in Fig. (3).

The engine was run in carburetted petrol engine form for all tests so that:

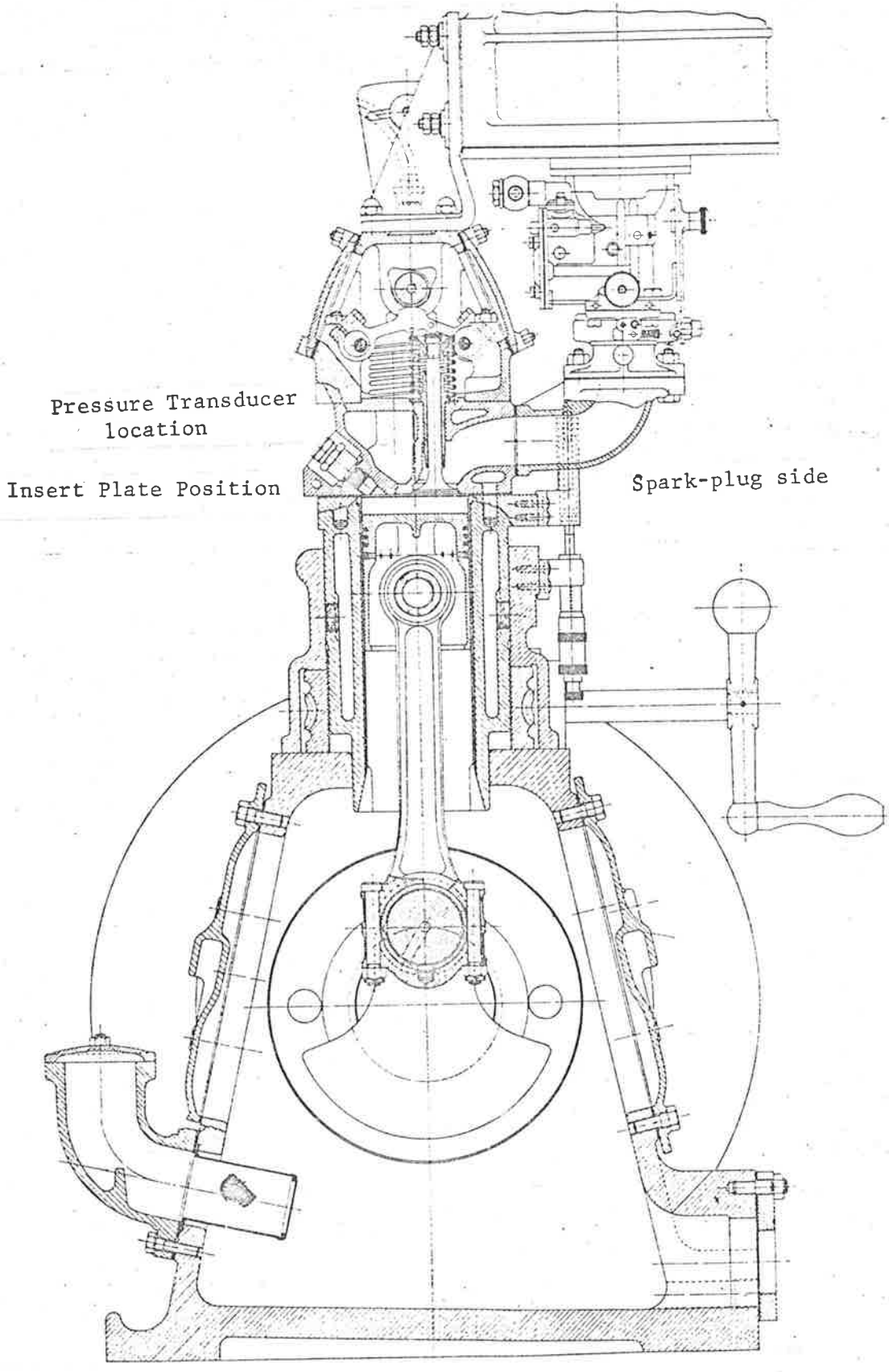

Fig.(1) Cross-section of research engine

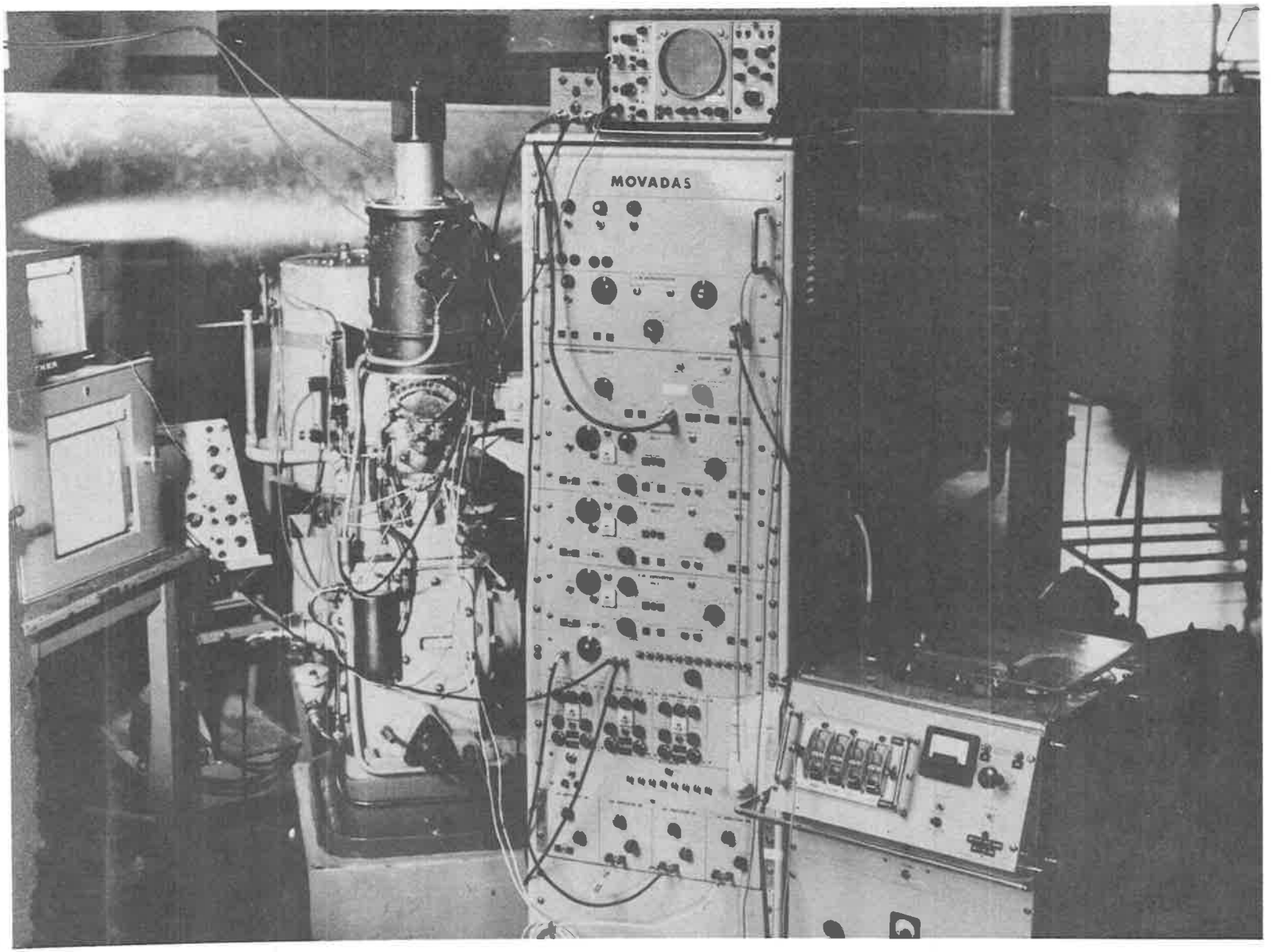

Fig. 2 General view of the Instrumented Engine

Fig.(3) Specifications of Test Engine

Make :	RICARDO E6/S, Serial No.25/48
Type :	Single Cylinder, Overhead valve, Flat chamber
Bore x Stroke:	3" x 4 $\frac{3}{8}$"
Speed Range:	500 to 3000 r.p.m.
C.R. Range (Std.)	4.5:1 to 20:1
C.R. Range (Mod.)	to 7:1
Spark Advance Range:	20^{o} to 50^{o}
Valve Timing:	Inlet Stroke:
	i.v.o. 8^{o}BTDC
	i.v.c. 34^{o}ABDC
	Exhaust Stroke:
	e.v.o. 44^{o}BBDC
	e.v.c. 6^{o}ATDC

Ancillary Equipment:

Swinging field electric dynamometer

Auxiliary motor-driven coolant pump

" " " oil pump

Oil and cooling water heat exchangers

Air preheater - not used in tests

Exhaust calorimeter - not used

Other: No inlet air swirl was induced, no supercharge

Fuels: 85 and 95 Octane pump petrols

(1) The radiant mode of heat transfer evident in Diesel combustion would be largely eliminated. (In line with other investigations (1), (5), (30) a working assumption of negligible radiant heat transfer is made in this study).

(2) Most experimental work in the past has been carried out on large diesel engines. Thus it was considered to be more profitable to investigate a small spark ignition engine and to determine the suitability of the various current empirical formulae to this type.

The only modification to the test engine to enable the heat transfer measurements to be made was the addition of an Insert Plate 0.55" thick, Figs.(4)(5), between the cylinder head and the block.

This required installation of longer cylinder head studs and had the effect of:

(1) Increasing the clearance volume to a measured 84.53 cc ($5.157 in^3$) and hence

(2) Reducing the maximum attainable C.R. from a standard 20:1 to 7:1.

The insert plate had identical water jacket spaces to those in the engine block, and three radial positions Fig. (6), were available for the installation of the probes.

When a probe was not in use at any particular location, it was removed and the probe hole blanked off by a solid steel plug. This allowed engine warmup and adjustments to both the engine and the recording apparatus to be made prior to a run without exposing the probe unduly.

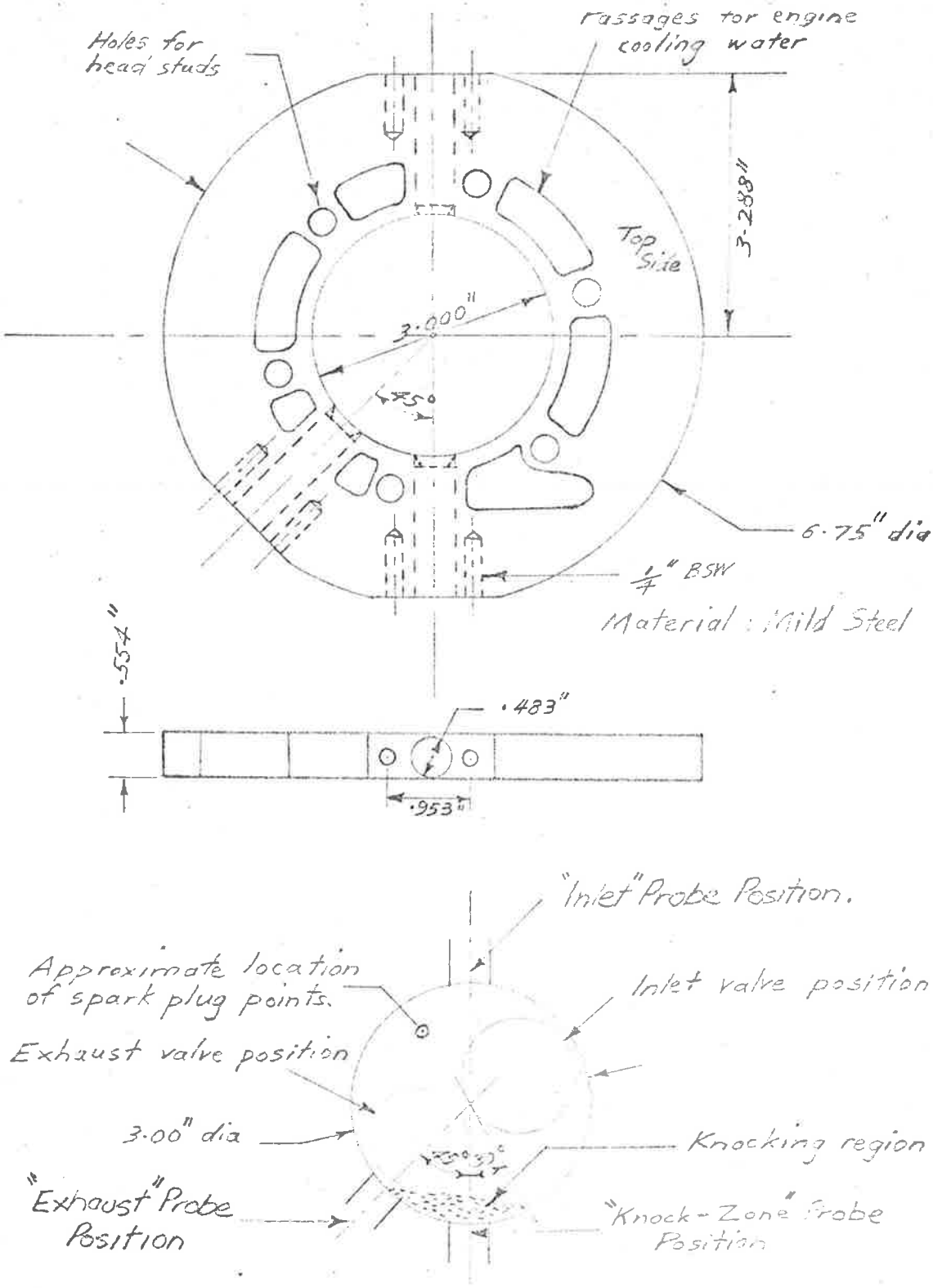

Fig. 4 Insert Plate & Probe Locations.

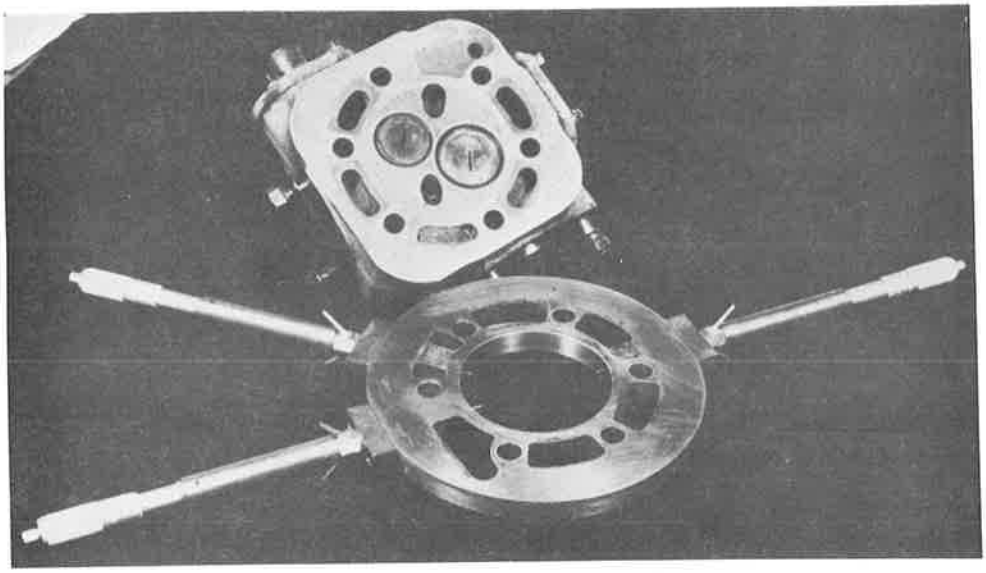

Fig. 5 Cylinder head & Insert Plate

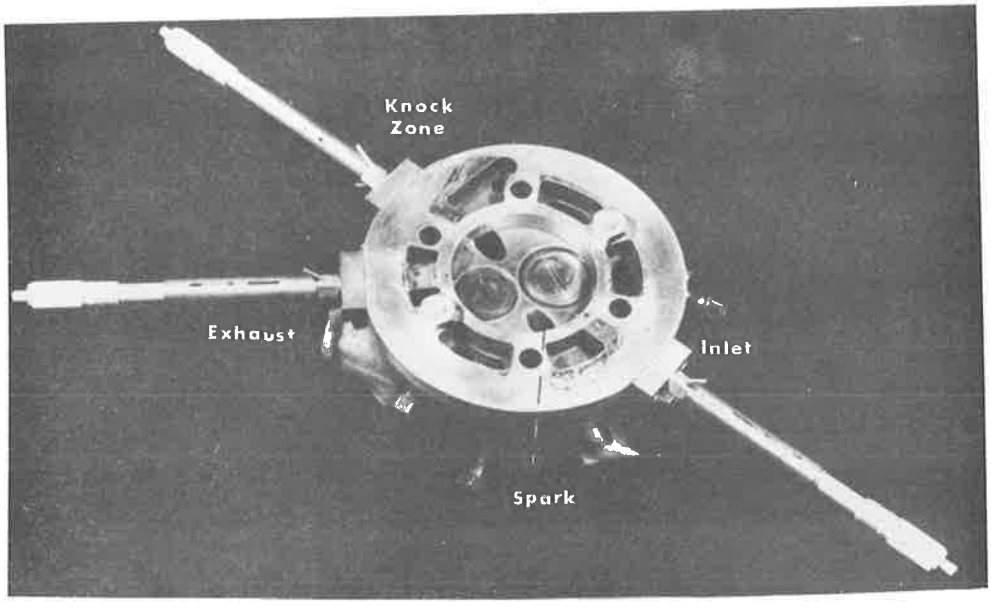

Fig. 6 Probe locations in clearance space

3.3 Probe Design

The basic tool for the engine heat transfer studies, both steady-state and instantaneous, was a multi-purpose probe as shown in Figs. (7), (8), (9), designed to incorporate the following functions:-

(1) A steady Flow Calorimeter to provide a measure of the mean of steady-state heat transfer rate from the gas to a small area of the combustion chamber wall at any of the probe positions.

(2) An embedded surface thermocouple on the gas-wall interface of the probe to give the instantaneous wall temperaturecycle. The cyclic component of the instantaneous heat flux through the probe surface could be derived.

(3) A traversable gas thermocouple which could be moved a known distance into the gas, between 0.000 and 0.500" from the wall, in a radial direction at the probe location.

This could be used to measure, either the steady-state temperature gradient in the gas near the wall; or the instantaneous gas temperature over the cycle at any point in the gas but particularly outside the "thermal boundary layer".

Design details to accomplish each of these functions are as follows:-

(1) The Calorimeter:

Each probe is fitted into a radial hole in the steel insert plate Fig. (4), which, since the cylinder head is a plane flat surface Fig. (5) serves merely to increase the clearance space above the piston TDC position. Thus the probe face is always exposed to the gas throughout the cycle and it is not necessary to consider piston ring friction or heat transfer by conduction to the piston.

The arrangement available between the water jacket spaces for probe installation quite fortuitously gave the following regions Fig. (6):-

(a) The INLET region - between the inlet valve and the spark plug.

(b) The KNOCK ZONE - diametrically opposite region (a) and in the area known to sustain knocking under certain conditions (see Ref. (41), Barden, 1956).

(c) The EXHAUST region - alongside (b) and in close proximity to the exhaust valve.

The calorimeter probe body, Fig. (7), consists of a flanged hollow steel plug the exposed end of which butts around its circumference onto a tapered annular seat in the insert plate leaving a circular area of 5/16" Ø exposed to the gas.
The tapered seat forms a pressure seal and also presents a minimum path area to transverse heat conduction into the probe body.

This latter effect was largely eliminated in the final probe design by moulding a high temperature silicone rubber of low thermal conductivity around the probe body.

Earlier probe designs, Fig. (10) had experienced difficulty through excess transverse heat "leakage" due to deterioration of the probe insulating material but the silicone rubber greatly reduced this effect.

Bennethum (39) recommended that surface temperature probes should be completely insulated from the surrounding walls because he had difficulty in obtaining uniform thermal contact

with loose fitting metal-metal probes. An insulated probe also has the effect of approximating one-dimensional heat flow through the probe surface.

Cooling water was introduced into the probe by means of a long stainless-steel tube positioned so that it would discharge at the inner face. The cooling water outlet was at the outer end of the probe toward the top, ensuring a full flow of coolant.

Coolant temperature change was measured by a differential thermopile while flow rate was measured by means of a rising-ball flowmeter. Flow rate could be adjusted by means of a needle valve.

(2) The Probe wall thermocouple

A Chromel-Alumel thermocouple of 0.001" wire diameter was embedded in the wall at the surface as shown in Fig. (11). The junction was produced by arc-welding in an inert atmosphere as described in Appendix A1 and was then carefully silver-soldered into a groove in the probe face.

The response time of the wall thermocouple was estimated to be 10μ sec - see Ref. (42).

(3) The Traversing gas thermocouple

This thermocouple, shown in Fig. (12) was designed to minimise flow disturbance and alteration of the gas temperature field near the wall. The thermocouple wires, 0.001" Ø were stripped of their 0.010" Ø stainless-steel sheathing and the junction was formed, again by arc-welding in an inert gas, approximately 1/32" from the end of the sheathing. This was then resealed with a high temperature

ceramic cement to prevent shorting of the elements.

Approximately 1/4" of the sheathing was left protruding from a stainless-steel hyperdermic tube of 15 gauge B & S (0.057" Ø which was also sealed with the ceramic cement.

Although some investigators (43), (44) & (45) have used finer thermoelements (about 0.0005" Ø) spot-welded to larger gauge wire than that presently used, it is believed that the present method of construction is more robust and also being more compact does not present so great a disturbance near the measuring point. (See Fig. (11)).

Although the 0.001" Ø wire was found to have a time constant of approximately 10 msec, this was electrically corrected to give an equivalent thermocouple wire diameter of 0.0002" with a response time of 1.0 msec.

The methods used for determination of the response time and for correction of the thermocouple output are detailed in Appendix A1.

(4) The Traversing Mechanism

The arrangement for traversing the thermocouple is shown in Figs. (8) and (14).

The spindle of a 0-1" x 0.001" micrometer rotates inside a collar carrying the hyperdermic tube which is constrained to move in the axial direction only. The hyperdermic tubing containing the thermocoax slides inside another stainless-steel tube silver-soldered to the probe face. Neoprene glands also provide a pressure seal.

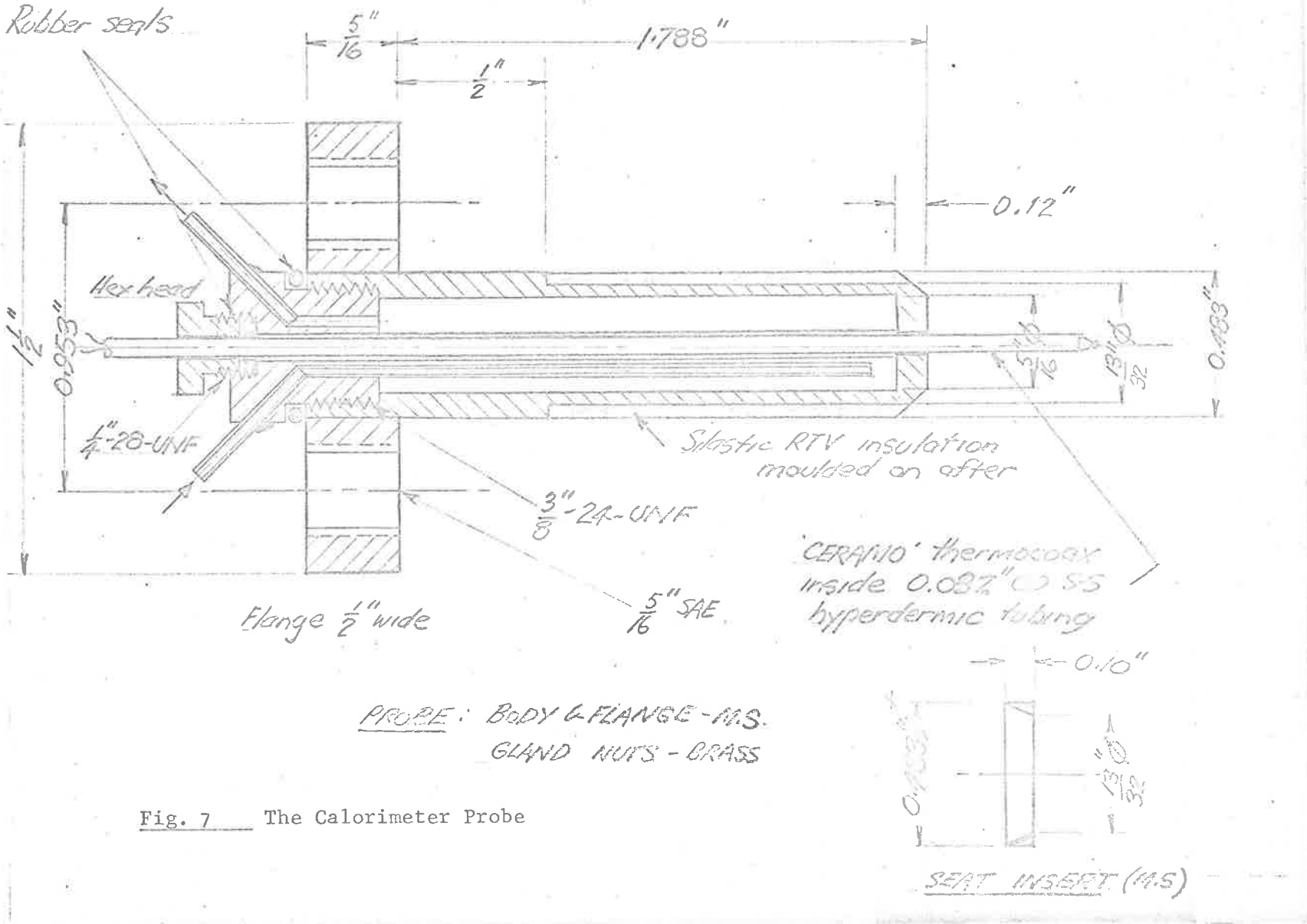

Fig. 7 The Calorimeter Probe

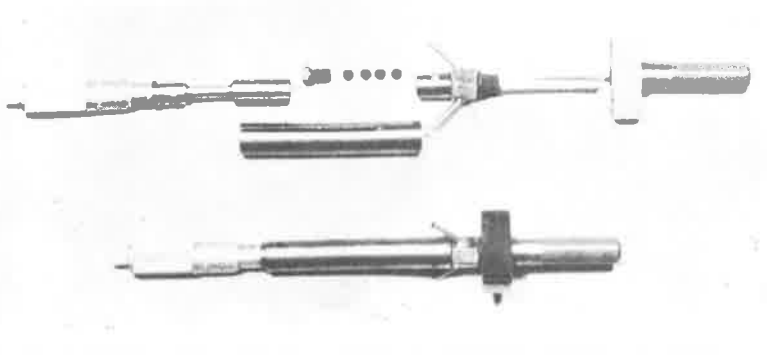

Fig.8 Assembly of the Probe

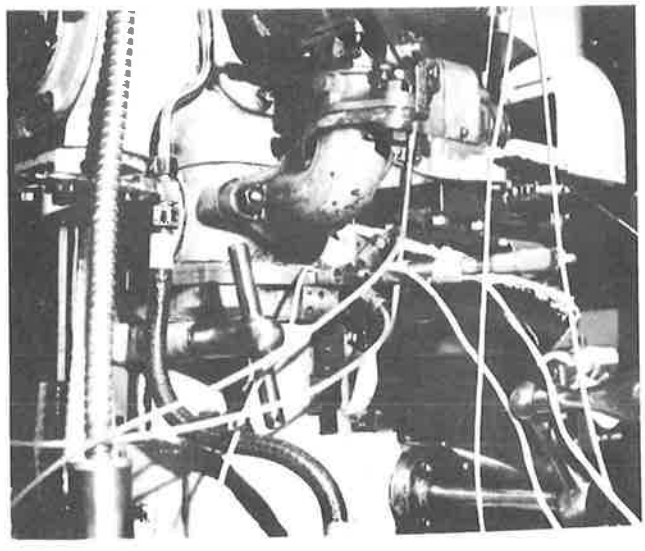

Fig.9 Installation of Probe on
Inlet side of the Test Engine

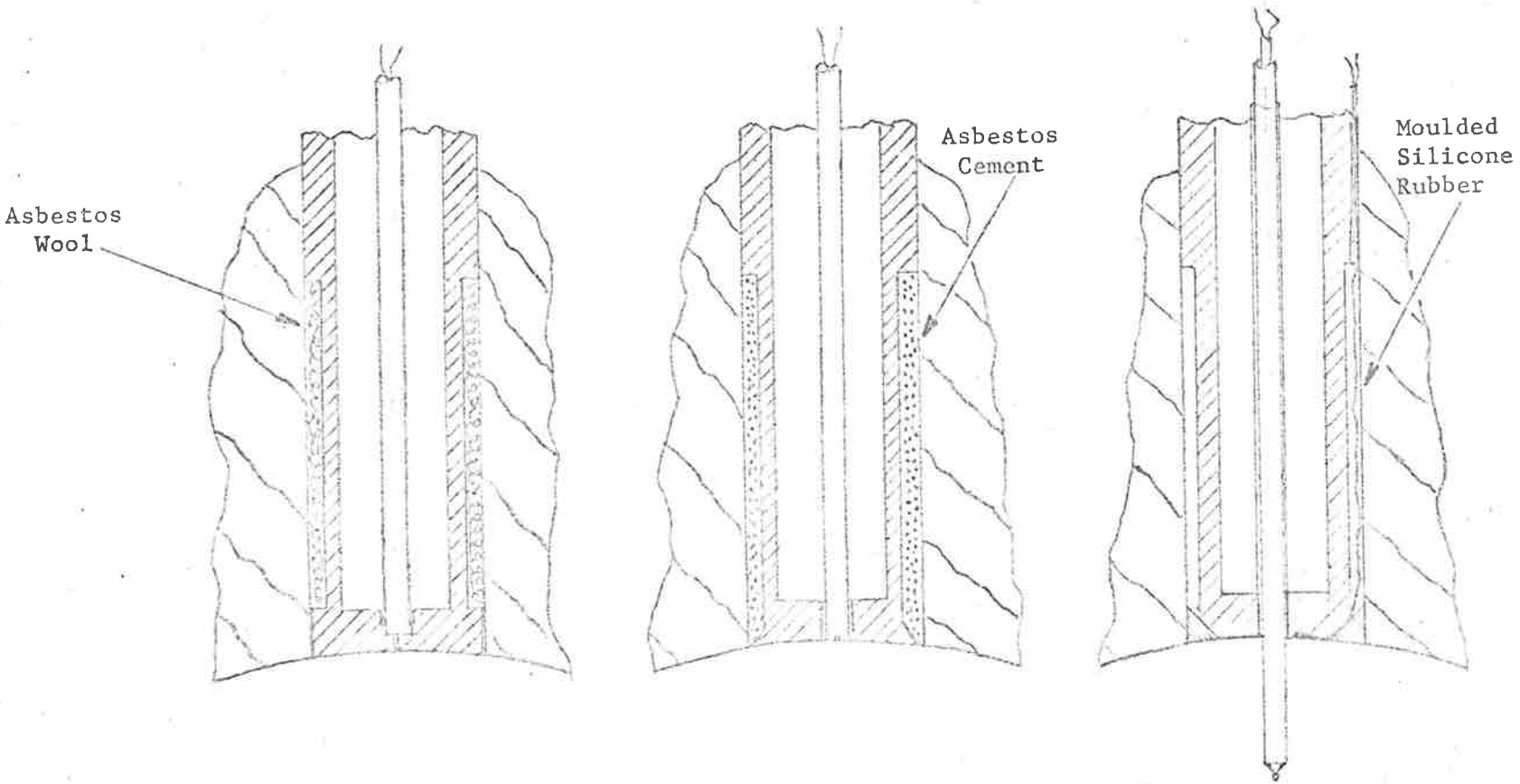

(a) Gas leakage
Poor insulation

(b)

(c)
Final Design
No leakage - Good insulation

Fig.10 Stages of Development of the Probe Tip.

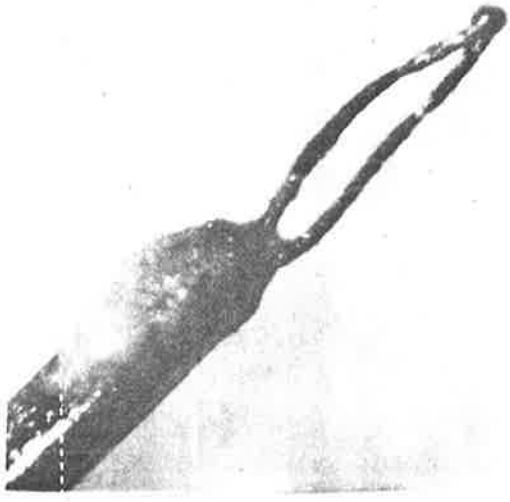

Thermocoax Junction
Wire 0.001" Ø
(18X)

Fig. 12

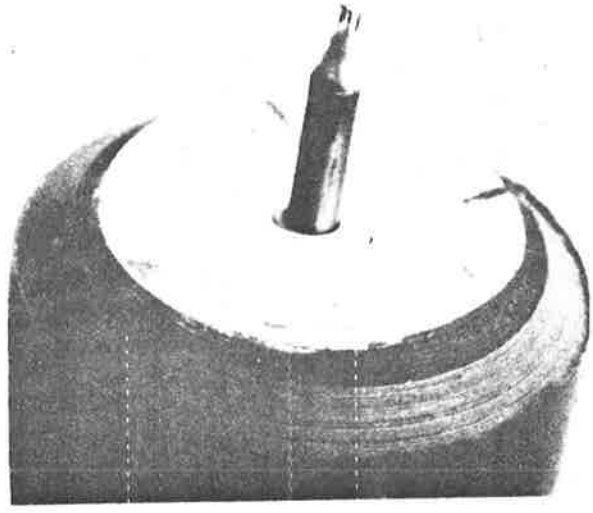

3-Wire probe
Wires 1.0, 1.5, 1.97X0.001"Ø
(8X)

Fig. 13

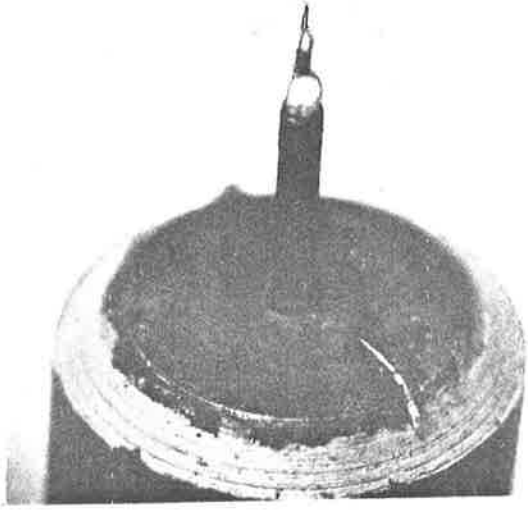

Single Wire probe
Wire 0.001" Ø (7X)

Fig. 11

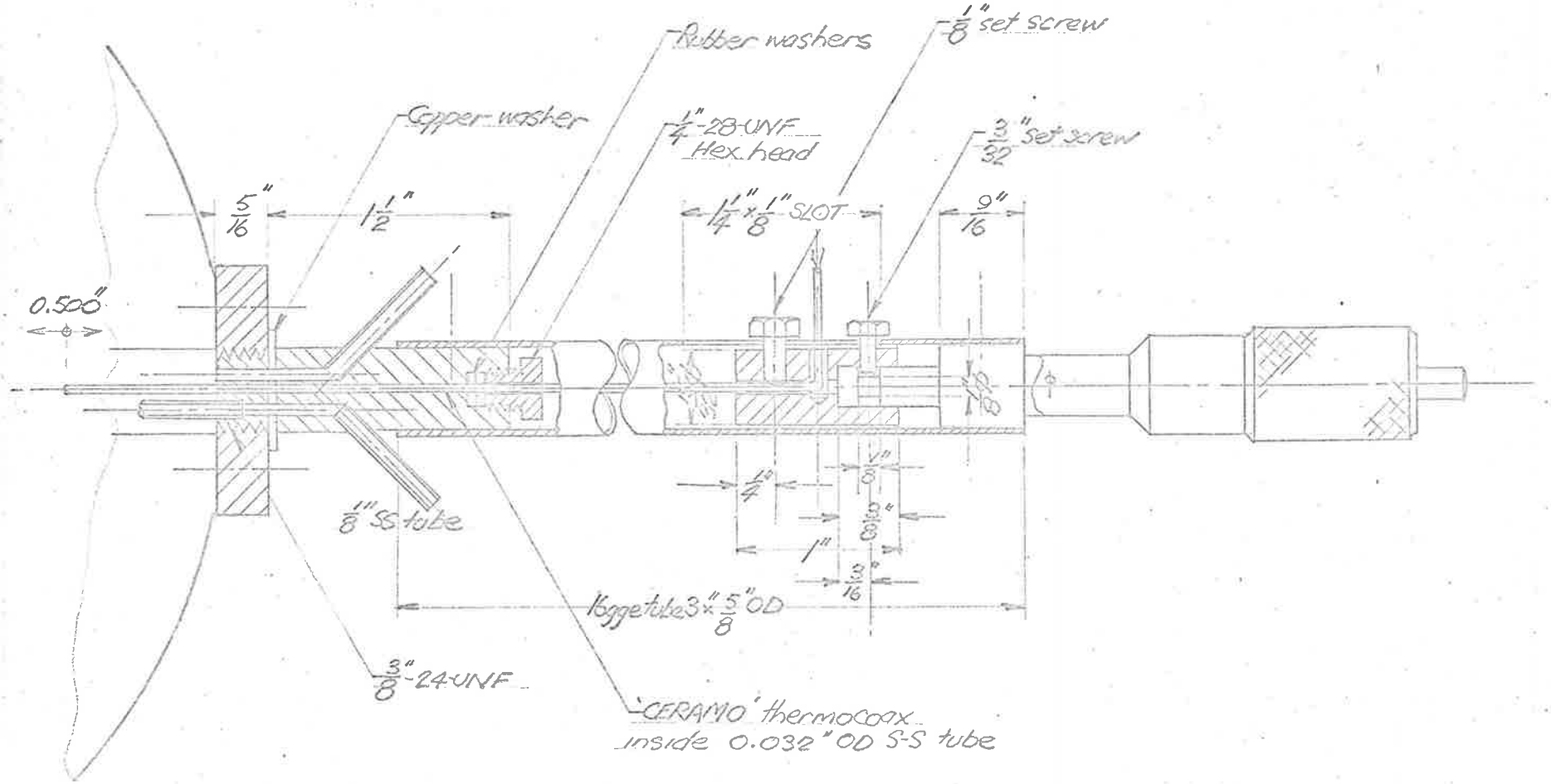

Fig.14 Thermocouple Traversing Mechanism.

This method of traversing was found to be most satisfactory, giving consistent positioning of the junction and also facilitating easy repair of the thermocouple.

3.4 Scope of the experiments

The engine tests carried out were as follows:-

(1) Engine Performance Calibration

As a basis of reference for the steady state and cyclic heat transfer experiments it was required to determine the optimum engine settings for any given engine speed, C.R., and grade of fuel i.e. the Minimum Spark advance for best torque (MBT) and the Air/Fuel (A/F) ratio for Maximum Power were required. Test results were reduced for this purpose by a computer programme given in Appendix A4.

(2) Motoring Tests

(a) Steady-State Traverse

The gas thermocouple was traversed out from the wall and mean reading instruments used to determine the mean temperature-distance profile in the gas near the wall under motoring conditions. The effect of r.p.m. and C.R. on layer thickness was observed.

(b) Cyclic Traverse

Successive gas temperature cycles were recorded at different depths in the gas in order to examine the change in temperature profile over the cycle. It should be noted that a truly instantaneous temperature profile could not be obtained as a large number of thermocouples in proximity would interfere with

each other by disturbing the temperature field in the region.

In this investigation, traverse cycles at all depths were recorded within the space of a few minutes under any given steady engine setting.

(3) Firing Runs

(a) Variation of Steady-State data with Engine Parameters

The mean gas and wall temperatures and the steady-state calorimeter heat flux were investigated over the speed range 500 - 2500 r.p.m. for various spark advance and with two fuels of different octane rating.

(b) Steady-state Traverse

Under firing conditions the mean gas temperature was measured as a function of distance from the wall as for (2a) above.

At each speed and compression ratio investigated, the spark advance and mixture strength were set for maximum power as determined in (1) above.

From these temperature measurements the extent of the thermal layer at the inlet and knock zone regions was estimated.

Gas temperature traverses were not made at the exhaust probe position due to persistent failure of the thermocouple in this location.

(c) Cyclic Traverse

At the two regions just mentioned gas temperature cycles were recorded as for the motored traverse at various fired engine settings.

(d) Cyclic Heat Transfer Measurements

Under low speed firing conditions, all data were collected simultaneously with the bulk gas temperature measured at a point outside the estimated boundary layer, so that instantaneous heat transfer data could be correlated and compared with predictions.

3.5 Data Recording Improvements

Since all data being studied execute periodic variations at engine cyclic frequency (1/2 engine r.p.m.) it was decided to express each variable by a Fourier Series.

In order to obtain a true comparison in time between the variables they were all referenced to a common datum point in each cycle. The reference point chosen for 0^{o} crank angle was the compression-stroke Top Dead Centre point (CTDC).

Cyclic temperature and pressure records are sometimes obtained by sampling at distinct points in the cycle over a large number of cycles. These "point-by-point" methods are more fully described in Appendix A1.

In this investigation such a technique would mask the cycle-to-cycle fluctuations in gas pressure, gas temperature and wall temperature caused by combustion irregularities. Therefore an erroneous correlation could result between these data, especially with regard to their relative phase angles.

For this reason it was necessary to record all the required data simultaneously by direct and continuous recording.

Thus, the design and construction of a high speed multitrack F.M. magnetic tape recording facility was undertaken which is discussed in

Section (4.3) and in detail in Appendix A3.

Since extensive facilities were available for analogue-to-digital conversion of the recorded data tapes and for the processing by computer of the resulting digital information; Fourier coefficients for any given cycle and for each of the recorded data could be determined analytically with reference to the CTDC point.

The analytical Fourier analysis technique used is detailed in Section (5.2). It was convenient to manipulate the data in terms of Fourier coefficients also for the following reasons:-

(1) The method of determining the cyclic component of instantaneous heat flux required the differentiation of the Fourier series representating the wall surface temperature cycle (Section 5.3).

(2) For presentation of the cyclic information, it was relatively simple to sum the Fourier series for the variable concerned and to plot the required (resynthesised) cycle against crank angle beginning from the CTDC point. This obviated the need for taking detailed manual measurements from analogue data e.g. oscilloscope Photographs, and allowed a uniform manner of presentation of the data.

(3) An insight into possible numerical methods of correction of the gas thermocouple signals could result from a consideration of the Fourier coefficients of the data (See Appendix A1).

If necessary, the FM analogue tapes could also be demodulated for playback and monitored on an oscilloscope for purposes of checking the records prior to digitising. The units comprising the data recording system are shown in the Block Diagram of Fig. (15).

The accuracy of the recording system and analogue to digital conversion(A-D) was very good. The linearity of the voltage to frequency converters(V-F) was to within 0.5% over the range. For the standard input voltage range to the driver amplifiers of the V-F converters (± 1.4 volt), the range of the digital information after A-D conversion was approximately 700 units. At the conversion rate of 4000 samples per second used for all tests, there were at least 32 digital samples per cycle of the 15th harmonic of the engine thermal cycle at 1000r.p.m. Thus, the computational errors due to aliasing were small even for the higher harmonics.

Further advantages of using such an advanced data recording and analysis system are discussed in Section 5 in comparison to previous methods used in this field. Details of each unit of the system and its calibration are given in the following Section 4.3 and in Appendix A3.

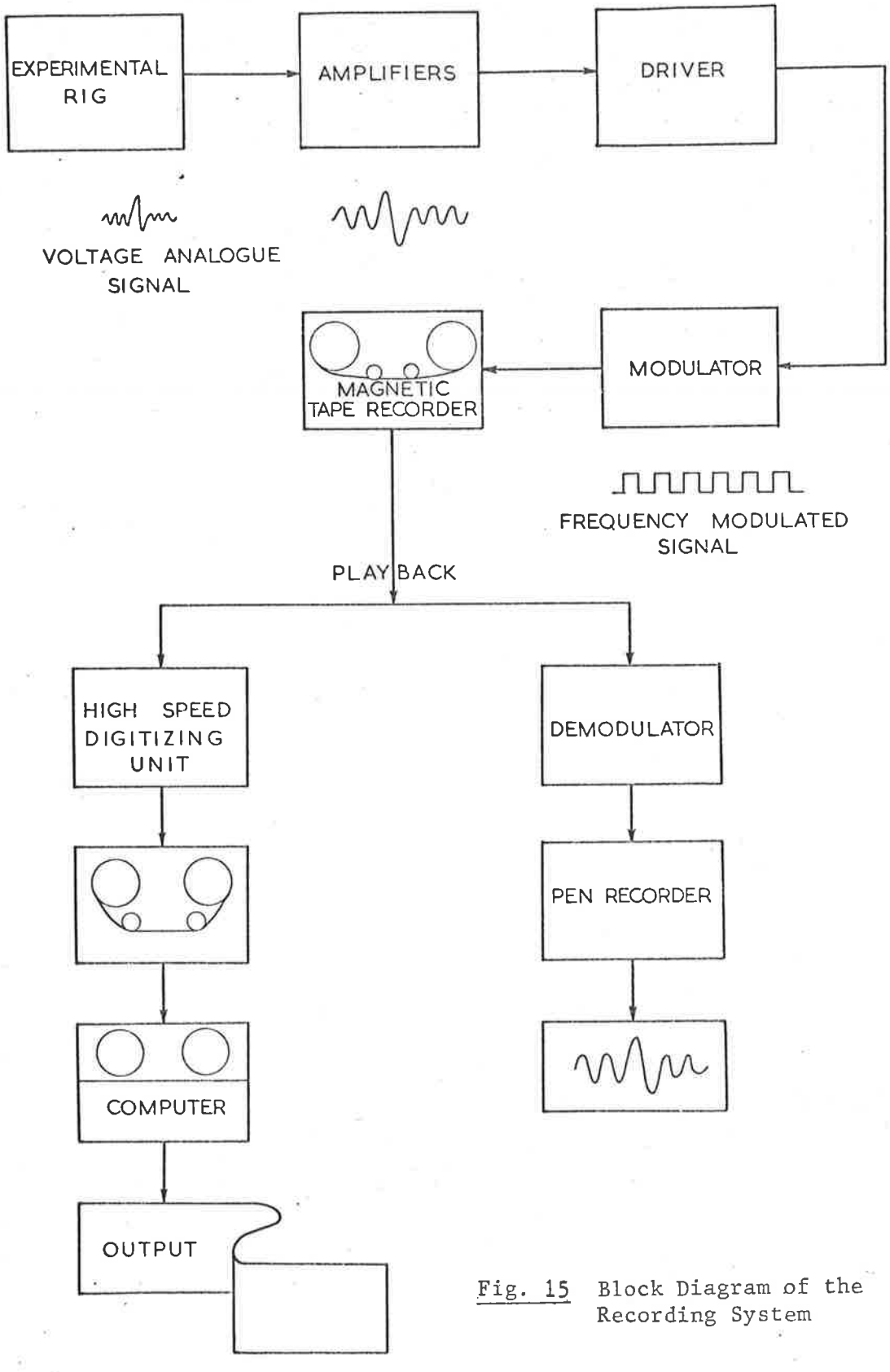

Fig. 15 Block Diagram of the Recording System

4. INSTRUMENTATION AND APPLIED MEASUREMENT

The recording system can be divided into the following basic groups:

(1) Transducers and Sensors

(2) Mean Reading Instruments

(3) Signal Amplifiers and Conditioning Units

(4) Recording System - High Speed Tape-Recorder.

4.1 Transducers and Sensors

4.1.1 Gas Thermocouple

All gas thermocouples used were of the thermocoax type * using Chromel-Alumel elements to the ISA 'K' specification.

In this type of thermocouple the two fine wire elements are contained in a stainless steel sheathing and are isolated from this and from each other by a Magnesium oxide insulation. The various types of thermocoax used had wire diameters of 1.0, 1.5 and 1.97 thousandths of an inch diameter.

It was found by experiment that for gas temperature measurement wire gauges greater than 0.002" Ø had an inadequate response (time constant $>$ 20 msec) while thermocouples with wires of less than 0.001" Ø would not withstand the rigors of combustion.

The thermocoax finally used for all cyclic gas temperature measurements was the finest commercially available and had elements of 0.001" Ø and an uncorrected response time of approximately 10 msec.

* Wires tradenamed "Ceramo" U.S.A. and "Sodern Thermocoax" France.

As it was obvious that the signals from even this size thermocouple were attenuated from the true gas temperature, extensive investigations were carried out to find a suitable method of correcting the thermocouple signals.

Accordingly a 3-wire probe was built, Fig. (13) using all three gauges of thermocoax previously mentioned. An attempt was made using the methods of Benson and Brundrett (46) to determine true gas temperature by numerical calculation from the 3 simultaneous temperature records. As described in Appendix A1 this method was unsuccessful by the numerical methods tried and was abandoned in favour of an approximate but simple electrical method using the single fine wire. This involved correction of the thermocouple signal before FM recording by means of a passive compensating network and required an experimental method of determining the thermocouple response time under representative flow conditions. A shock-tube technique was used for this purpose (Appendix A1).

The final corrected thermocouple had a measured response time of about 1.5 msec; this being equivalent to a wire diameter of approximately 0.0002".

The use of Chromel-Alumel thermocouples also had the advantage that the output was practically linear over the working temperature range. (22.4 μv/^{o}F)

4.1.2 Gas Side Wall Thermocouple

Again Chromel-Alumel 'K' calibration thermocoax of the finest wire diameter (0.001") was used although early wall temperature measurements used 0.008" Ø wire with a similar result. As shown in

Fig. (11) the wall thermocouple was positioned in a radial groove on the probe face with its junction at about the 1/2 radius point. This was a difficult operation performed under the microscope as care was needed to ensure that the junction was exactly at the surface and did not affect the wall smoothness.

The amplitude and form of the variation in wall surface temperature proved to be quite comparable with the results of other studies (1), (39), (40).

4.1.3 Water-side Wall thermocouple

In the course of the investigation, it became necessary to measure the temperature of the probe wall on the water side to check that the cyclic component of this temperature was negligible. The 0.001" Ø thermocoax was used again for this purpose and silver-soldered to the wall.

4.1.4 Gas Pressure Transducer

This was a CAV-Ricardo transducer using the Photoelectric principle to measure the deflection of a diaphragm under the gas pressure fluctuations.

This transducer had an estimated flat response to 5 kc/s and since rapid pressure rise effects (knocking and detonation) were not studied, this was considered adequate. The transducer was statically calibrated before and after a run by applying a known pressure from a Nitrogen gas cylinder to the diaphragm. The nominal output was 1.2 mv/psi.

The location of the pressure transducer for all tests was in the Knock-Zone region or practically diametrically opposite the spark plug

position and the transducer was cooled by laboratory air.

4.1.5 Event Marker Transducer

This transducer used a photoelectric cell to give a voltage spike once per engine cycle at the reference CTDC datum.

After amplification this voltage signal triggered a monostable multivibrator to generate a square pulse which after voltage-to frequency conversion was recorded in FM form on the tape recorder. See Fig. (16) and Appendix A1 for details of the units comprising the Event Marker.

In the subsequent mathematical analysis (Section 5 and Appendix A4) the phase of the Fourier coefficients of all cyclic data were determined with respect to the onset of the Event Marker signal.

4.2 Mean Reading Instruments

As the data acquisition system recorded only the AC or fluctuating components, suitable mean recording instruments were required to measure the DC or steady state components. These were as follows:-

Mean Gas and Wall Temperatures were either:-

(a) recorded continuously on a Philips 12 channel automatic compensating chart recorder which incorporated a constant temperature cold junction or

(b) 'Spot' voltage measurements were taken with a Pye potentiometer and the readings reduced to temperature using the Chromel-Alumel calibration tables and applying a correction for ambient temperature.

Mean Heat Flux Measurement

This was obtained from the steady-state calorimeter probe which acted as an 'element of wall' with its own water jacket. It will be shown later that the varying gas-side temperature fluctuations are damped out before reaching the water-side wall.

The mass flow rate and temperature rise of the probe cooling water was measured assuming that the heat picked up came mainly through the probe surface, i.e. 1-Dimensional heat transfer, since the probe body was insulated from the insert plate.

The coolant flow rate was measured by a Fischer & Porter rising ball flowmeter No. 10A3135N calibrated from 1-10 gal/hr against direct measurement using beaker and stop-watch.

The rise of coolant temperature was obtained by a Sierra Model 189B Differential thermopile, the nominal sensitivity of which was 1.7 mv/^{o}c. This supplied an Ether model chart recorder and was calibrated against direct measurement from 0-100^{o}C Mercury thermometers in special lagged thermometer pockets.

The general layout of the instrumentation can be seen in Fig. (2).

4.3 Signal Amplifiers and Conditioning Units

The signal amplifiers and conditioning units form a data acquisition system designated by the acronym "MOVADAS" (Modulated Voltage Analogue Data Acquisition System) which was capable of recording time varying data with a flat frequency response from DC to 15Kc/s. MOVADAS incorporated the following units, see Fig. (17) described in Appendix A3 :-

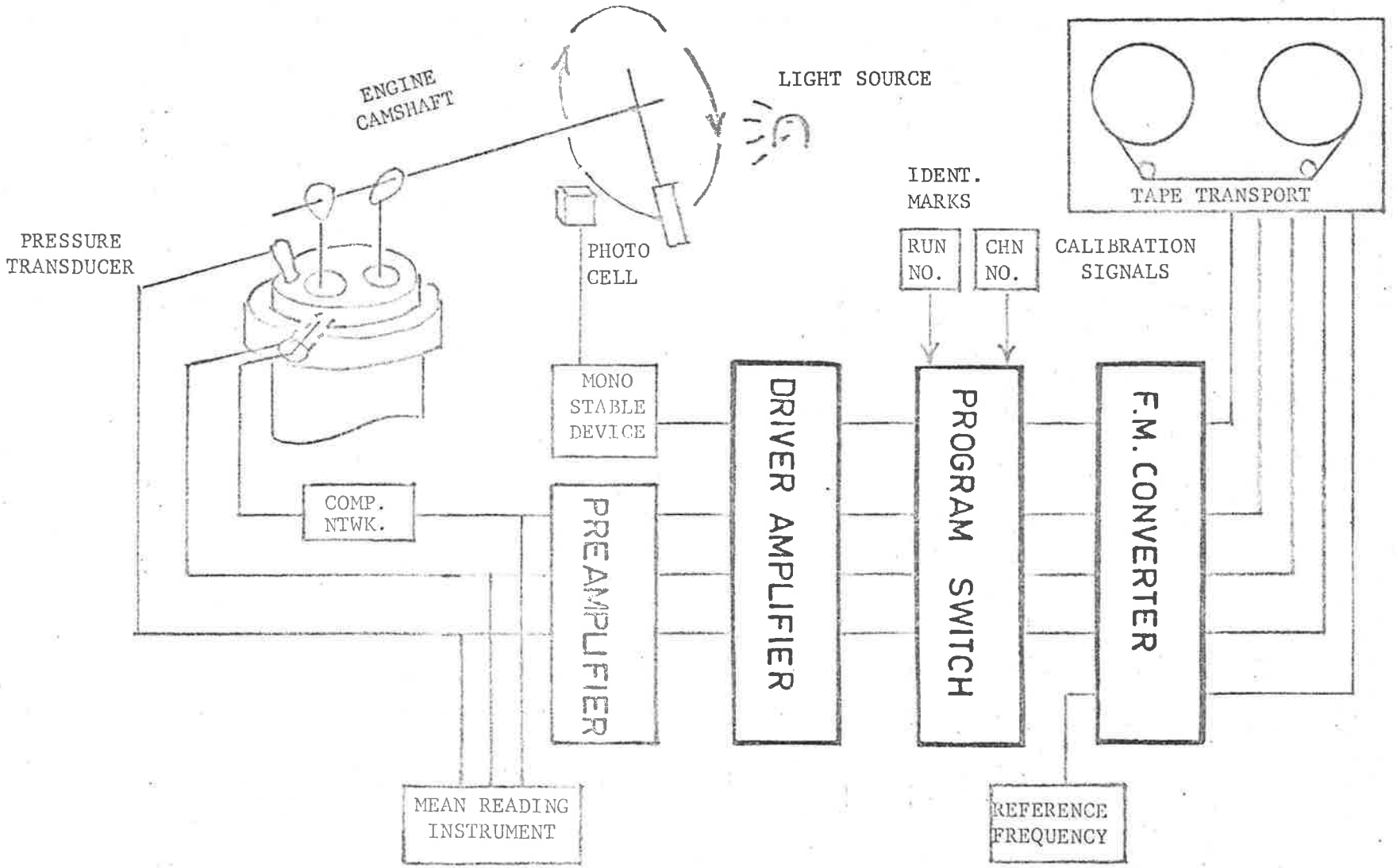

Fig.16 - Block Diagram of Instrumentation.

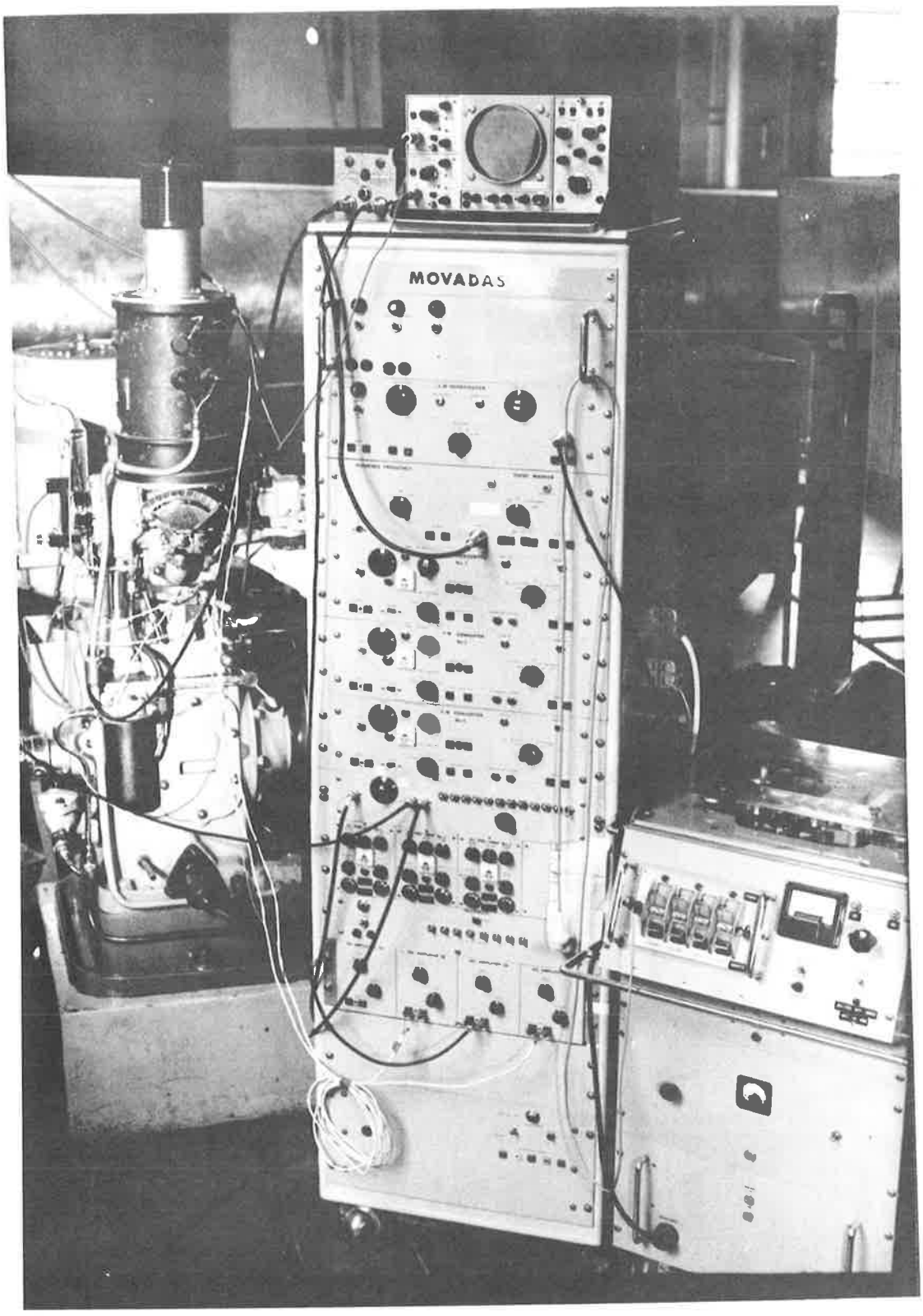

Fig.17 The Data Acquisition System

(1) DC Voltage Pre-amplifiers

(2) Driver Amplifiers

(3) Voltage-to-frequency Converters

(4) Reference 'Clock'

(5) Programming Switch.

The latter two devices are herein briefly described since they control the whole recording/analysis procedure.

The programming switch utilises a multibank rotary switch (uniselector) to:-

(a) Bring the tape transport up to the steady recording speed on initiation of the recording process.

(b) When this is achieved to automatically switch on current to the tape recording heads.

(c) To impress on each data channel immediately prior to the modulated data signal a sequence of binary-coded pulses representing the Run number, Channel number (or Track No.) and a series of calibration voltage levels for an instantaneous calibration of each voltage to frequency converter.

(d) To switch off the recording head current and to stop the tape transport after a given recording time in readiness for the next run.

The identification and calibration signals were applied to all active data channels simultaneously so that the resultant digital information could be cross-correlated between channels.

The data signals recorded at 60 ips were frequency modulated in

the range 54kc/s ± 40% to conform to the IRIG* International specification.

The analogue-to-digital conversion process required a separate reference frequency or 'Clock' channel and thus a 50.00 kc/s signal was generated from a crystal oscillator and subsequently modulated and recorded on a separate track. Run and Channel numbers were not recorded on this track.

The A-D conversion process could be carried out at 1500, 4000 or 8000 samples/sec of actual recording time, and it was found that the intermediate rate was adequate for all runs recorded in this study.

Tape Transport

An Epsylon Model 580 data tape recorder was modified as described described in Appendix A3 to conform to IRIG specifications and for automatic operation.

The designation of tracks on the analog tape were as follows:-

Track	1)		Wall surface temperature
	)		
	2)	Data Channels	Gas temperature
	)		
	3)		Gas pressure
	4	Voice only - not used	
	5	Reference Clock Frequency 50.00 kc/s	
	6)		Cyclic Event Marker
	)	Data Channels	
	7)		Spare - unused.

The operation of the MOVADAS complex was intrinsic in the computing procedures described in Appendix A4 used to carry out the mathematical analyses given in the next section.

* Inter-Range Instrumentation Group.

5. MATHEMATICAL ANALYSIS AND CORRELATION

5.1 General

After analogue to digital (A-D) conversion, the recorded information was identified and converted into words compatible with the word structure of the CDC 6400 digital computer used in subsequent analyses (see Appendix A4 for details of Programme 'CONVERT').

The list of digits constituting a single experimental recording of any one variable was termed a file, and each file contained a number of engine cycles of the variable depending on the recording time.

It was possible to select from any given file the list of binary numbers corresponding to any one or more cycles of the recorded data, because the identification pulses from the programming switch were recorded simultaneously on all active channels - including the Event Marker Channel.

5.2 Fourier Analysis

A Fourier analysis of the recorded signals was performed by considering the samples from any one cycle as constituting a series of psuedo square waves, the Fourier coefficients of which could be expressed mathematically. The rigorous derivation of this method of Fourier analysis was given by Clarke Ref. (49). Briefly it is as follows:-

The Fourier Series expansion of a continuous function f(t) in the range $0 \leq t \leq 2c$ is

$$f(t) = a_0 + \sum_{n=1}^{\infty} \left(a_n \cos \frac{n\pi t}{c} + b_n \sin \frac{n\pi t}{c} \right) \qquad (63)$$

where $a_o = \frac{1}{2C} \int_0^{2C} f(t).dt$

$$a_n = \frac{1}{C} \int_0^{2C} f(t).\cos\frac{n\pi t}{C} . dt$$

and $$b_n = \frac{1}{C} \int_0^{2C} f(t).\sin\frac{n\pi t}{C} . dt$$

An estimate A'_n of A_n for a series of N equally spaced points f(h,K) where h is the sampling interval and K = 0,1, ...N-1 is:-

$$a'_n = \frac{2}{N-1} \sum_{k=0}^{N-1} W_k . f(h,k) \cos k\theta \qquad (64)$$

where W_k = weighting coefficients

and $\theta = \frac{2n\pi}{N-1}$

Consider now a series defined by:-

$$a''_n = \frac{2}{N-1} \sum_{k=0}^{N-1} W_k \cdot f(h,k) . \frac{\cos k\theta}{|\cos k\theta|} \qquad (65)$$

and since $\frac{\cos k\theta}{|\cos k\theta|}$ is mathematically represented by

$$\frac{4}{\pi} \sum_{j=1}^{\infty} \frac{(-1)^{j-1}}{(2j-1)} .\cos(2j-1) . k\theta \qquad (66)$$

then equation (65) can be expressed as:-

$$a''_n = \frac{4}{\pi} \sum_{j=1}^{\infty} \frac{(-1)^{j-1}}{(2j-1)} . a'(2j-1).n \qquad (67)$$

A similar solution is given in Ref. (49) for b_n'' and b_n'. The ratio $\cos k\theta / |\cos k\theta|$ for a fixed θ and varying k is obtained by sampling the squarewave of frequency θ at time intervals of k.

After summation of the series in equation (65) the linear system equation (67) is solved by back substitution.

This method of solving for the Fourier coefficients is faster than normal methods. The programme listing (Sub-routine FASQW) is given together with a definition of symbols used, in Appendix A4.

5.3 Heat Flux Calculation

The 1-Dimensional Fourier heat conduction equation (25) was derived to be:-

$$\frac{\partial T}{\partial t} = \alpha \frac{\partial^2 T}{\partial x^2}$$

where the symbols are as previously defined.

If it can be demonstrated that the temperature of the wall on the water side does not fluctuate (See Section (5.5)) then the boundary conditions for the solution of equation (25) are :-

$$\left.\begin{aligned} &\text{(i)} \quad T_w = A_{ow} + \sum_{n=1}^{\infty} \left[A_n \cos n\omega t + B_n \sin n\omega t\right] \quad \text{at } x=0 \\ &\text{and} \quad \text{(ii)} \quad T_w = A_{0j} = \text{constant at } x = L \end{aligned}\right\} \quad (68)$$

where A_0 = the time averaged component of temperature defined mathematically as:-

$$A_o = \frac{1}{2\pi}\int_0^{2\pi} T(\omega t).\, d(\omega t) \qquad (69)$$

and A_{ow} = time averaged wall temperature at gas/wall interface

A_{oj} = time averaged wall temperature at wall/water interface

and where L = wall thickness

A_n, B_n = Fourier Coefficients

ω = angular frequency

n = harmonic No.

w = subscript denoting wall.

Thus, the steady-state temperature distribution through the wall is

$$T(x,t) = A_{ow} - (A_{ow} - A_{oj}).\, x/L \qquad (70)$$

and it can be seen that this satisfies the Fourier heat conduction equation (25).

As was assumed in section 2.3, equation (40), the temperature profile within the slab with the boundary conditions of equation (68) can be written:-

$$T(x,t) = B_n e^{-px} \sin(n\omega t - qx) \qquad (71)$$

where as shown $p = q = \sqrt{n\omega/2\alpha}$

Thus, by superposition for the nth sine and cosine terms of equation (71) and using the boundary conditions (68), the total temperature at any depth x and any time t is:

$$T(x,t) = A_{ow} - (A_{ow} - A_{oj})\,x/L + \sum_{n=1}^{\infty} e^{-px} \left\{ \begin{matrix} A_n \cos(n\omega t - px) \\ + \\ B_n \sin(n\omega t - px) \end{matrix} \right\} \quad (72)$$

In order to obtain the surface heat flux, it is necessary to differentiate equation (72) with respect to x according to the expression:

$$q/A = -k_w \frac{\partial T}{\partial x} \quad (73)$$

by taking the limit as $x \rightarrow o$.

However, term by term differentiation of a Fourier series can only be permitted if the series does not diverge. It is fortunate that a convergent series always results from a solution satisfying equation (25) since the damping exponential term in equation (72) acts as a convergence factor.

Hence we can write:

$$q_{(o,t)} = k_w (A_{ow} - A_{oj})/L + k_w \sqrt{\frac{n\omega}{2\alpha_w}} \sum_{n=1}^{\infty} \left\{ \begin{matrix} (B_n - A_n) \sin(n\omega t) \\ + \\ (B_n + A_n) \cos(n\omega t) \end{matrix} \right\} \quad (74)$$

where the 1st term on the RHS represents the steady-state or time-mean component of surface heat flux (measured by the calorimeter) and the 2nd term gives the cyclic or unsteady component i.e.

$$q_{(o,t)} = q_{ss} + k_w \sqrt{\frac{n\omega}{2\alpha_w}} \sum_{n=1}^{\infty} \left\{ \begin{matrix} (B_n - A_n) \sin(n\omega t) \\ + \\ (B_n + A_n) \cos(n\omega t) \end{matrix} \right\} \quad (75)$$

This method of obtaining instantaneous heat flux was programmed as given in Appendix A4 (Sub-routine HFLUX).

5.4 Criteria for Sampling and Re-synthesis

The problem of determing a suitable number of samples per cycle and the number of harmonics required to adequately synthesise a cycle will now be discussed.

Overbye (1) defined wall temperature variations by a finite Expansion of the form:

$$T(0,t) = A_{0w} + \sum_{n=1}^{N/2} A_n \cos(n\omega t) + \sum_{n=1}^{N/2} B_n \sin(n\omega t) \qquad (76)$$

where N = the number of equally spaced temperature ordinates used in the cycle analysis.

A_n = the amplitude of the nth cosine harmonic component

B_n = the amplitude of the nth sine harmonic component

Overbye arbitrarily used N = 144 ordinates to yield 72 harmonics. This was 6 times the number of samples used by previous investigators who were limited by manual computation and desk calculators.

However, in an analysis of an elementary ramp function temperature cycle Overbye found that this number was inadequate. His derived heat flux cycle exhibited severe oscillations when the initial surface temperature rise occurred in a time interval of 1/144 of the cycle time.

He concluded that although a given number of ordinates may adequately represent a surface temperature-time function, they may not be satisfactory for heat transfer purposes.

In deciding on the number of ordinates, Overbye seems to have been guided by Shannon's Rule, Ref. (47), which states that the

sampling frequency required to completely define the trace is twice the highest frequency present in the trace.

In this investigation, however, instead of using a finite expansion the recorded data fluctuations were expressed as an infinite Fourier series. i.e.

$$T_{(o,t)} = A_{ow} + \sum_{n=1}^{\infty} A_n \cos(n\omega t) + B_n \sin(n\omega t) \qquad (77)$$

Experience in numerical analysis has shown that it is in fact better to exceed the Shannon's Rule requirement and use at least six times the highest harmonic as the criterion for the minimum number of samples required in the series of equation (76).

An application of the concept of numerical transfer functions to this criterion as suggested by Hamming Ref. (48), will show that it is then possible to determine the highest harmonic component to within 10% relative accuracy.

Since the data reduction procedure in the present work used a fixed sampling rate of 4000 samples per second, the number of samples per cycle was related to the engine RPM as follows:-

RPM	Cycles/min	Cycles/sec	Period msec/cycle	Samples/cycle at 4 kc
500	250	4.16	240	960
1000	500	8.33	120	480
1500	750	12.50	80	320
2000	1000	16.66	60	240

In all cases the number of samples per cycle exceeded that used by Overbye.

With regard to the number of Fourier coefficients required in equation (77), it was observed that for gas and wall temperature cycles recorded in this study Fig. (18) the moduli ceased to decrease in a monotone manner after a given number of terms and merely oscillated about a mean. This indicated that the level of signal noise had been reached. Further increase in the number of terms would thus only add further error to the synthesis. In practically all cycles analysed, the number of harmonic terms required to reach the noise level was approximately 15.

This agreed with the findings of Chistyakov (50) who recommended that engine temperature data be sampled at not less than 72 points per cycle, and that the number of terms in the series should be between 7 and 15. This also confirms the sampling criterion proposed above.

Using the infinite Fourier series method the steepest ramp function tested by Overbye was analysed. The resulting heat flux cycle Fig. (19) did not exhibit the violent oscillations noticed by him.

5.5 Expected Fluctuation in Water-Side Wall Temperature

It was shown in Section 2 (equations (27) and (40), that the temperature variation in a wall is given by:

$$\theta_x = \theta_0 e^{-x\sqrt{n\omega/2\alpha}}$$

where θ_x = amplitude of attenuated temperature wave at distance X from the surface

θ_0 = amplitude of temperature wave at the surface (X = 0)

X = distance into the wall from the surface

ω = frequency of temperature fluctuations

α = thermal diffusivity of wall material

n = harmonic number.

If we assume values for the probe of Fig. (7) as follows:-

ϑ_o = 40F° (≡ unity), x = 0.12", ω = 8.3 cps at 1000 RPM,

α = 0.52 and considering the fundamental component only,

then $\vartheta_x = 1 . e^{-\frac{0.120}{12}\sqrt{\frac{60000\pi}{2\times 0.52}}}$

$= e^{-4.25}$

$\therefore \quad \vartheta_x = 14.3 \times 10^{-3}$

= 1.43% of the gas side fluctuation.

i.e. the water side wall temperature is constant. This fact was also experimentally verified.

Higher harmonics are damped even more than this.

1000RPM WOT*0.25,FIRING 24DEG SPK, KZ COMPENSATED, X=0.200
ANALOG TAPE 6 TRANSMITTAL TAPE 1558

SERIAL	RUN	CHANNEL	TYPE	NO PERIODS	COEFF
7	12	123	1	1	30

FOURIER COEFFICIENTS AT CYCLE FREQUENCY

CYCLE HARMONIC	TEMPERATURE (DEG.F)	PHASE ANGLE CRANK ANG.DEG)
1	22.175	123.77
2	7.626	154.38
3	3.727	195.39
4	1.576	220.31
5	.758	228.47
6	.826	225.53
7	.666	263.11
8	.276	284.49
9	.261	247.42
10	.366	256.05
11	.372	292.01
12	.136	325.22
13	.080	211.92
14	.249	273.58
15	.208	323.61
16	.195	15.36
17	.087	274.36
18	.225	331.02
19	.268	41.78
20	.186	99.71
21	.074	199.95
22	.148	4.04
23	.252	67.00
24	.227	128.66

Fig.18

Moduli & Phase Angles for harmonics of a typical wall temperature cycle.

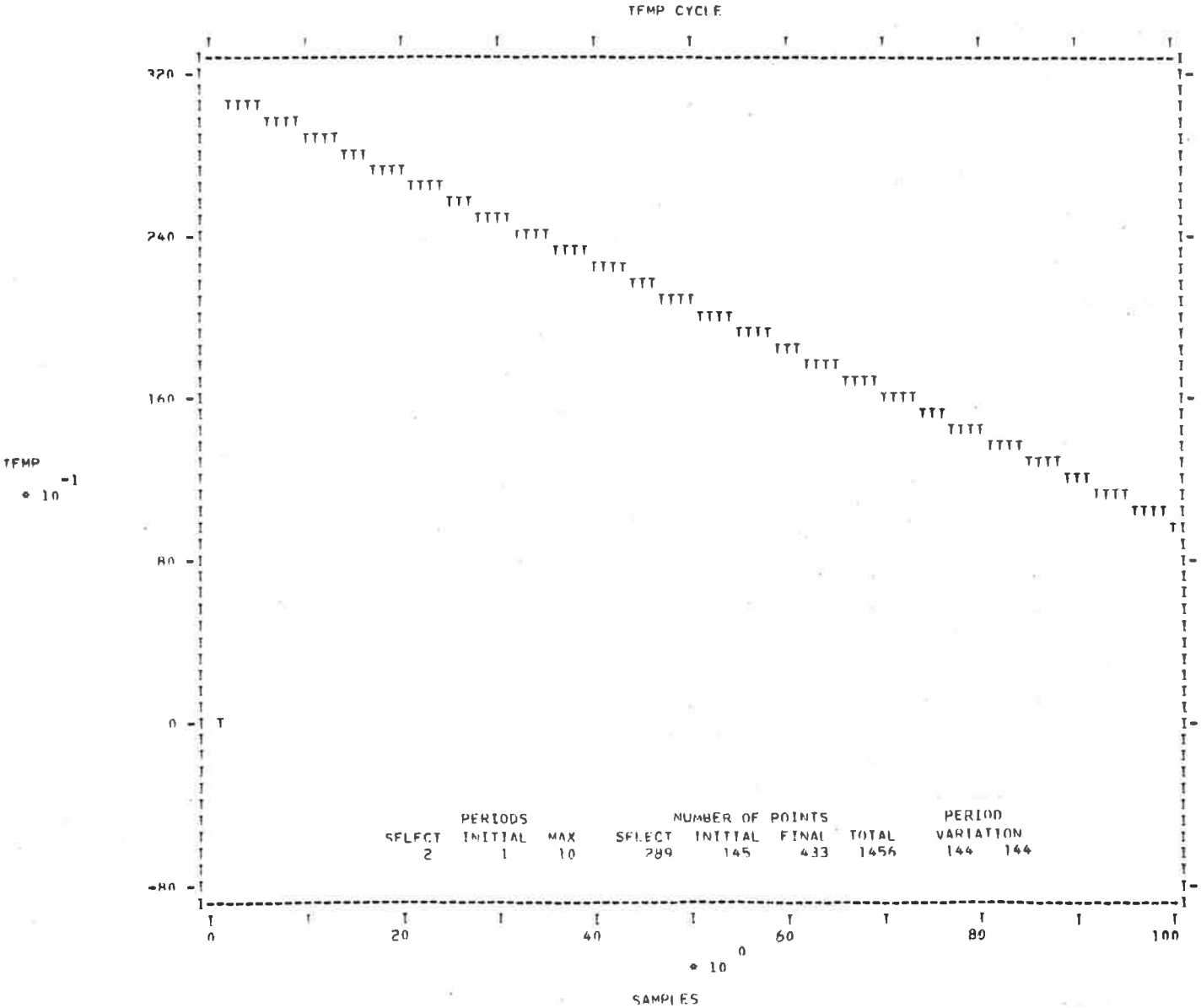

Fig. 19 (a) Test Ramp function of wall temperature

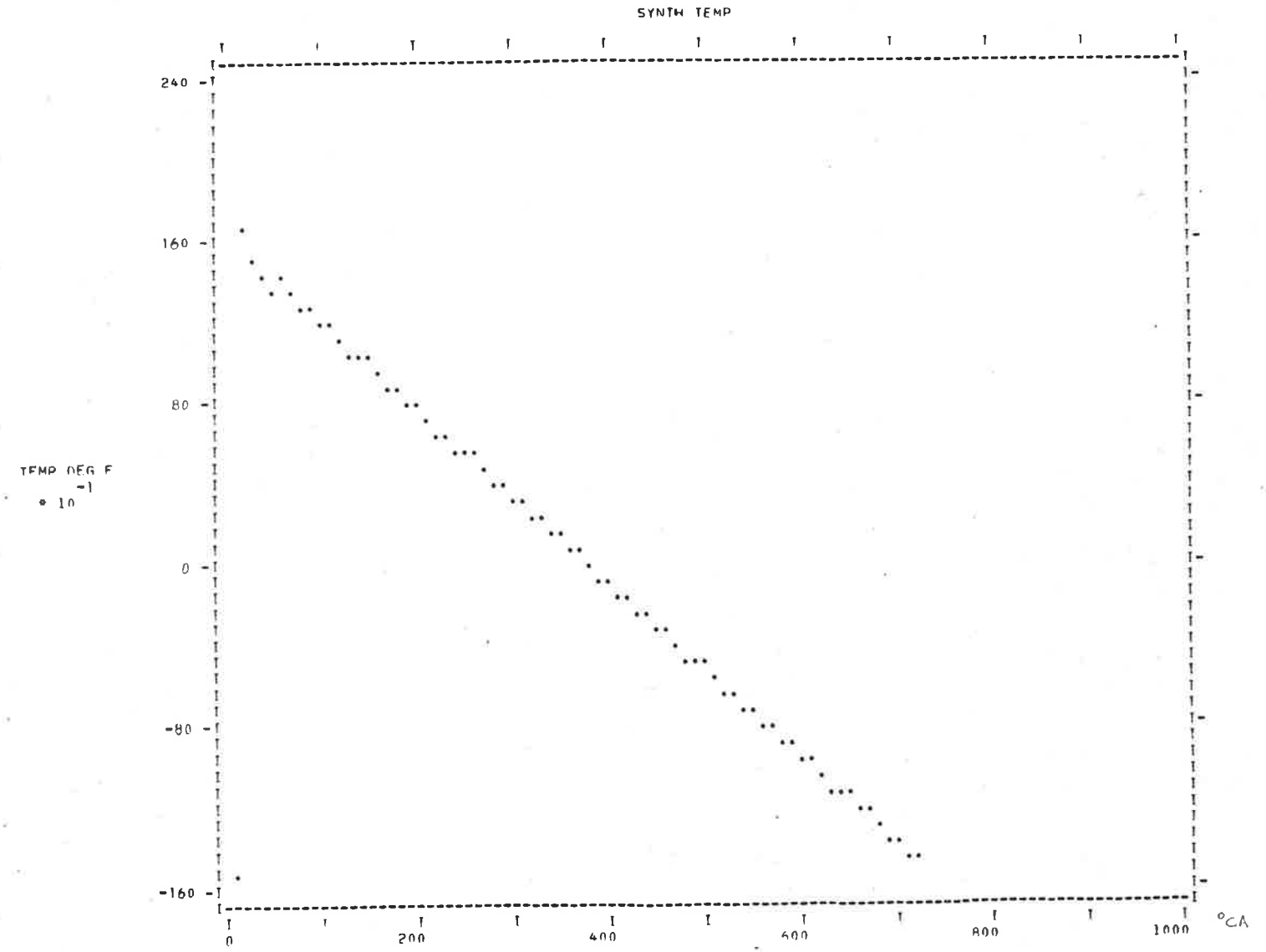

Fig. 19 (b) Synthesised Ramp function wall temperature

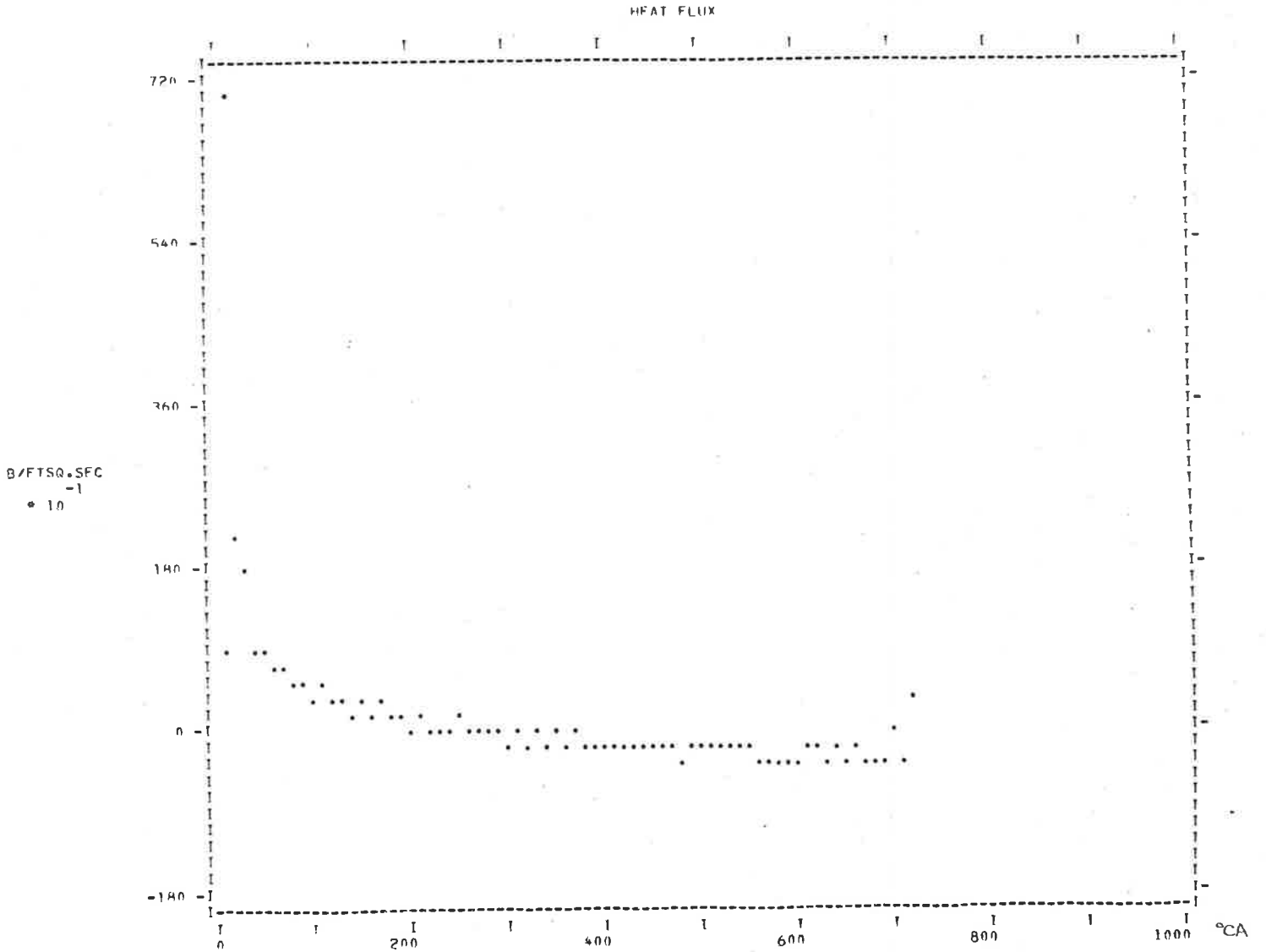

Fig. 19 (c) Synthesised heat flux cycle derived from 19 (b)

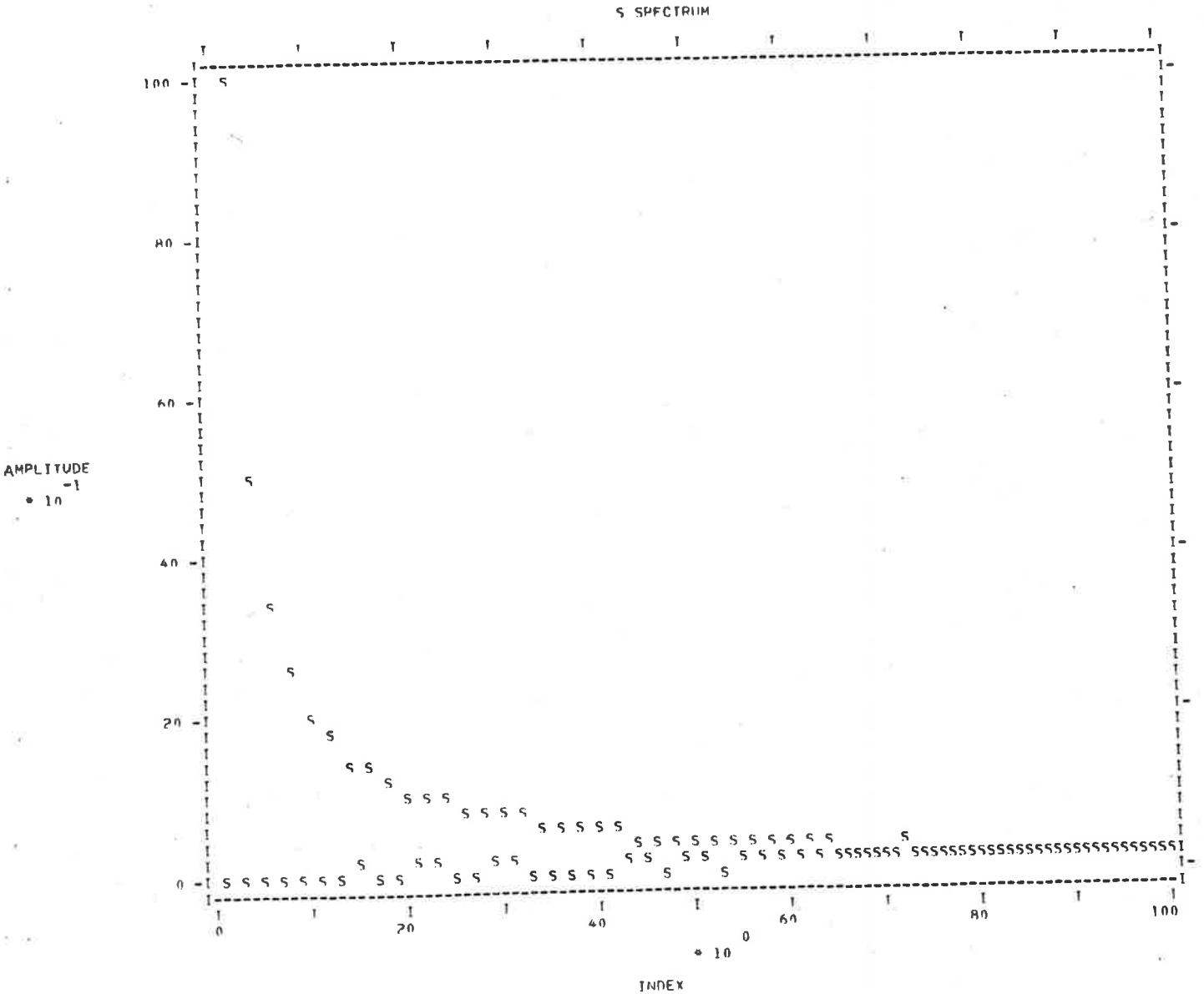

Fig. 19 (d) Sine Spectrum of Ramp function wall temperature

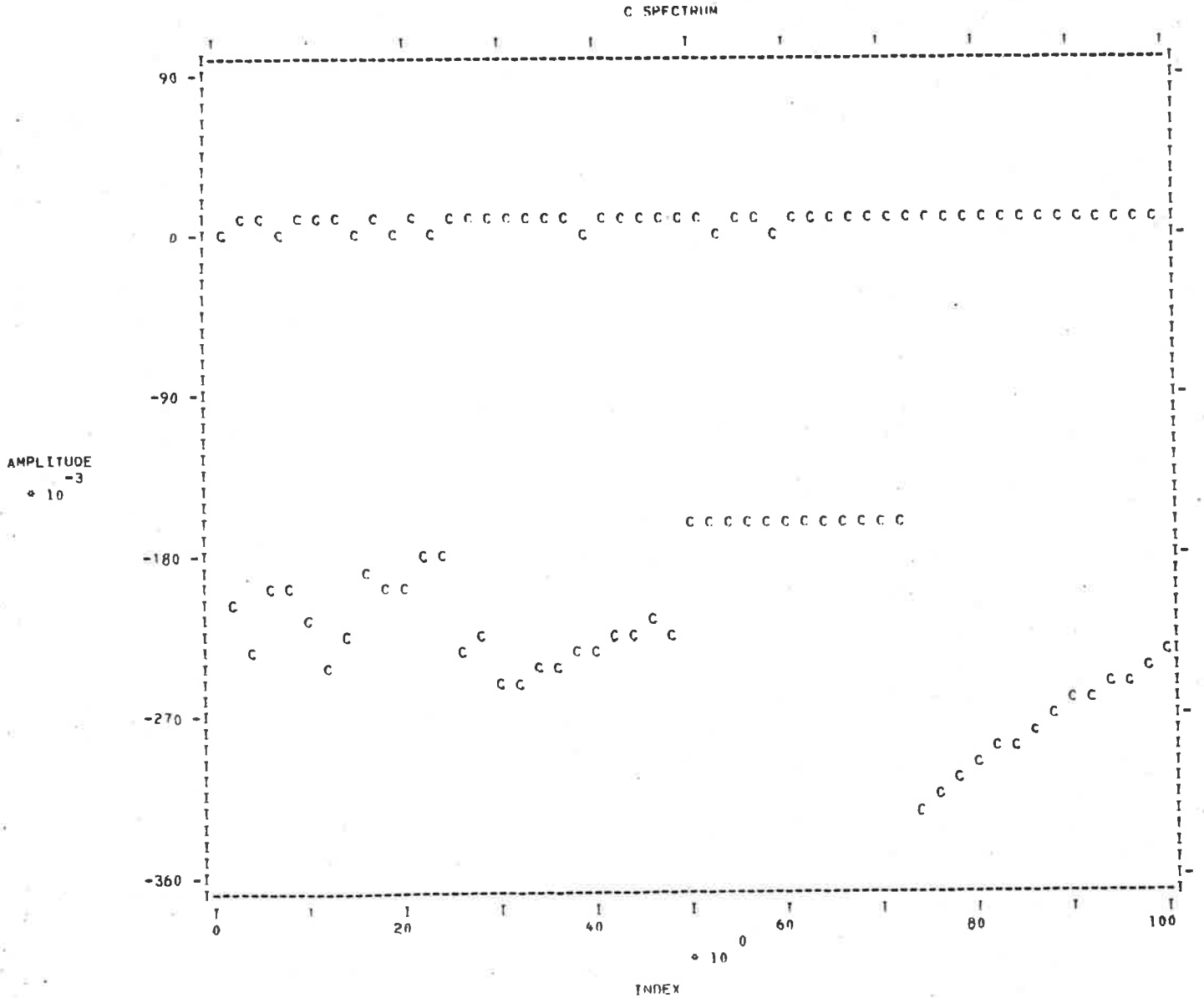

Fig. 19 (e) Cosine Spectrum of Ramp function wall temperature

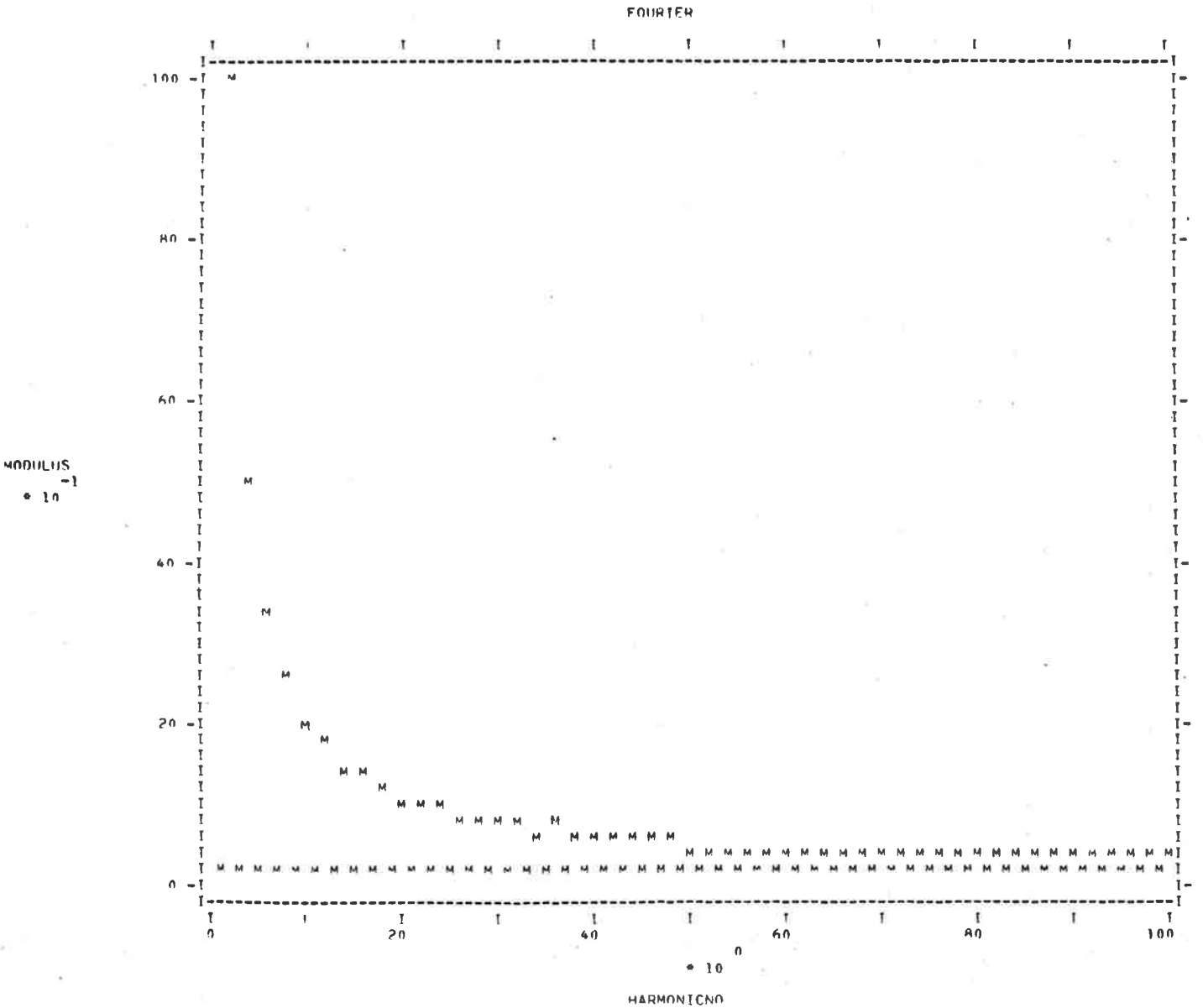

Fig. 19 (f) Moduli of Ramp function wall temperature harmonics

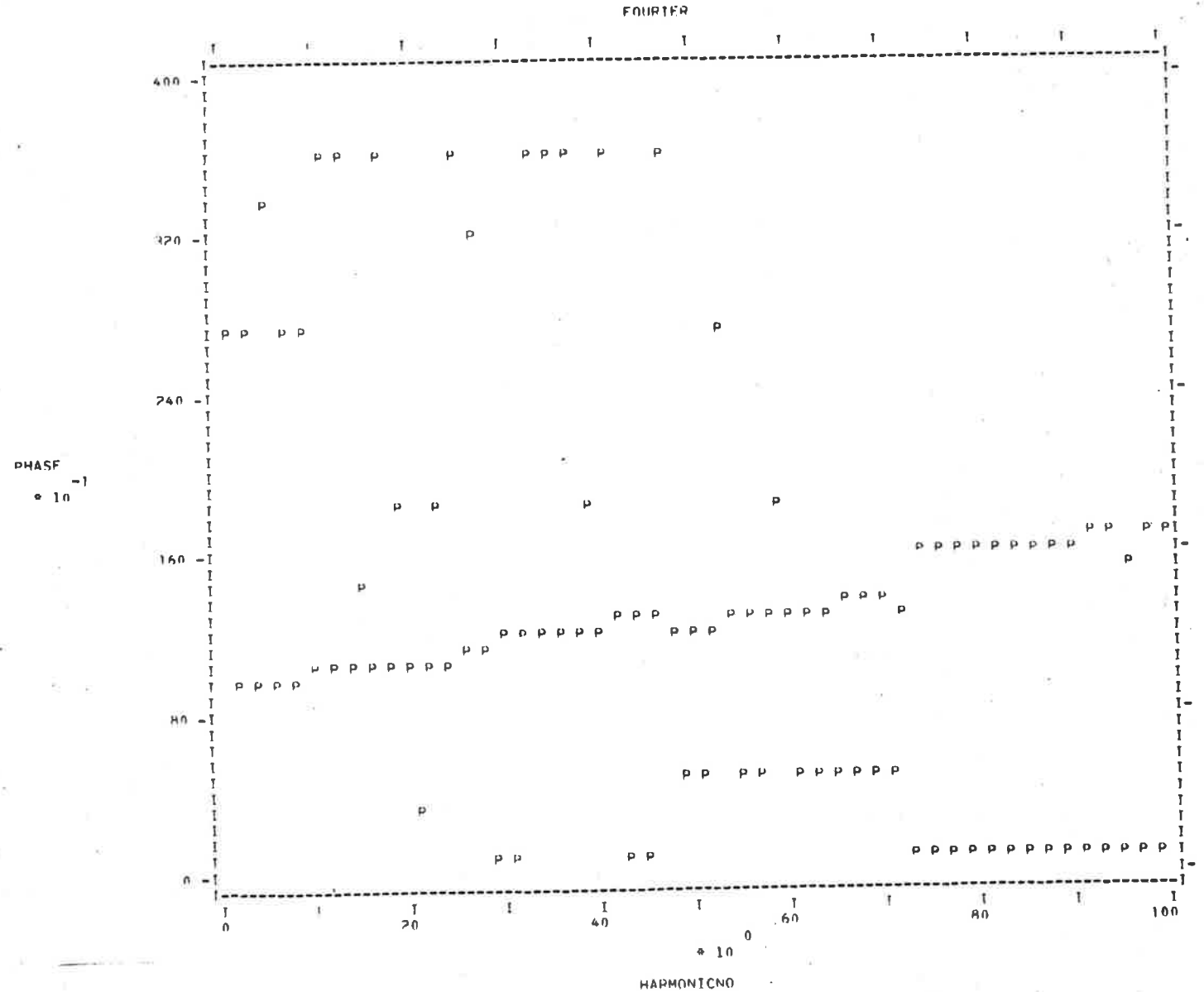

Fig. 19 (g) Phase angles of Ramp function wall temperature harmonics

6. EXPERIMENTAL RESULTS

6.1 Experimental Procedure

Prior to a traverse recording run the test engine with dummy probes installed in the insert plate, was warmed up until the water jacket temperatures had stabilised. This condition was maintained throughout the run by adjusting the secondary coolant flow rate to the heat exchanger. At the same time the mixture strength and spark advance were adjusted to the predetermined optimum values for the r.p.m., compression ratio and fuel type used. (See Performance Calibration next Section).

Adjustments to the data acquisition system were also made at this time. All units had been switched on for some hours prior to the test and had thus stabilised.

It was necessary to carry out the following adjustments to the system:

(1) The coarse and fine driver amplifier potentiometers were balanced.

(2) The centre frequencies of the voltage-to-frequency converters were adjusted to 54Kc/s and the square wave mark-to-space ratio checked. It was verified that the output frequency for open circuit input was the same as that for short circuit input.

(3) The frequency swing for calibration voltage levels of $\pm$ 1 Volt was checked for each channel (38.57, 69.43 Kc/s respectively).

(4) The 5 calibration voltage levels were measured.

(5) The interconnecting coaxial wiring between units was arranged to give the desired Amplifier/Converter/Channel Number combinations.

(6) The Event marker photocell was tested to ensure that it triggered without failure over the engine speed range.

(7) It was verified that the internal reference (clock) frequency was 50.00 Kc/s.

When all the checks were completed satisfactorily, the engine was shut down for a short time (no more than 5 mins.) while the dummy plugs were removed, the thermocouple probes were installed, and the thermocouple compensating leads connected to the pre-amplifiers. At this stage all thermocouples were tested for continuity and special earthing precautions were taken to ensure that there were no significant earth-loop currents which would impose electrical noise on the signals.

Also at this time the preamplifiers and DC recorders were switched on to stabilise. The following preparations were then made for recording:

(1) The tape transport was switched on and tape speed selectors on each channel set to 60 ips.

(2) The relevant Run Number was encoded on the binary switches.

(3) The AC coupling, Attenuation and desired Driver Amplifier gain settings were selected for each channel.

(4) The recording time was selected on the test panel (0.5 sec usually).

(5) The Programming switch was activated with the Tape Transport switched on and the panel switch set to Remote control.

The engine was restarted and set to the required speed, with the traversing thermocouple retracted into the probe.

The input signals to each converter channel were monitored in turn on an oscilloscope via the channel selector switch. The relevant preamplifier and driver amplifier gains were adjusted to ensure that no signal exceeded the permissable maximum input to the voltage-to-frequency converters of 2.8 volt peak-to-peak.

After 2-3 minutes when water jacket temperatures had once again stabilised, the gas thermocouple was traversed to the required depth and the recording process initiated by the remote hand held trigger.

The thermocouple was traversed to a new position immediately the tape had stopped, the next run number was encoded, and the recording process again initiated. This sequence was repeated until the analogue tape was full (approximately 15 runs or 5 minutes). The gas and wall thermocouples were then connected to the DC recorders and the traverse repeated. This repitition was unfortunately necessary because it was found that cyclic and mean measurements could not be made simultaneously since the Philips multichannel DC recorder radiated a 'noise spike' to the thermocouple preamplifiers whenever it printed a character. However the whole procedure could be accomplished within 10 minutes. During this time interval the drift in the mean temperature at any location under constant engine conditions was negligible.

Before changing to a different engine setting the probe coolant flow rate and differential temperature were recorded.

6.2 Engine Performance Calibration

The dynamometer load, fuel and air flow rates, engine coolant flow rate and temperature differential were recorded for different mixture strengths at each speed over the range 500 - 2500 r.p.m. Spark advance was adjusted to M.B.T. for each setting.

The data were programmed to give the performance figures at each setting. Details of the computing procedure are given in Fig. (4) Appendix A4.

An example of the output of this programme is given in Fig. (20) for the 2500 r.p.m. case. From this output the mixture strength and the M.B.T. spark advance for the maximum b.m.e.p. condition was selected.

It will also be noticed from Fig. (20) that the total heat transfer rate to the engine coolant (HTRE) peaks approximately at the maximum power mixture strength and drops off markedly for richer or leaner mixtures. This fact agrees with the experimental findings of Kerley and Thurston (51), 1962, for a single cylinder engine of similar quiescent combustion chamber design to that of the engine used in this investigation.

Fuel-loop curves of b.m.e.p. against b.s.f.c. were also plotted from the programme output for each test condition. Examples of these are presented in Fig. (21).

6.3 Motoring Investigations

6.3.1 Steady-state gas temperature traverse

Mean temperature-distance profiles in the gas near to the wall are presented in Fig. (22) for the Inlet region and in Fig. (23) for the knock-zone region for the following motoring conditions:

Wide Open Throttle (W.O.T.)

Compression ratios 5:1 & 7:1

Engine speeds 500 r.p.m. and 2000 r.p.m.

Some observations from these figures are:-

(1) The thermal layer is thickest at the lower speed and lower C.R.

(2) At 7:1 C.R. the Inlet thermal layer thickness decreases from approximately 0.350" to 0.300" with speed increase from 500 to 2000 r.p.m.

(3) Also at 7:1 C.R. the Knock-Zone layer is thinner than at Inlet and varies from approximately 0.300" to 0.275" with speed change from 500 to 2000 r.p.m.

(4) At 5:1 C.R. however, the Inlet region shows a much greater change in thickness from 0.400" to 0.275" with the same speed change as above.

(5) Also at 5:1 C.R. in the Knock-Zone the thickness changes only from 0.350" to 0.250" with the speed change.

(6) The Knock-Zone bulk gas temperature is about $16^{\circ}F$ and $30^{\circ}F$ higher than the Inlet bulk gas temperature at 500 and 2000 r.p.m., respectively.

It should be borne in mind that these gas temperatures were measured with a finite size thermocouple (0.003" Ø wires). Thus the mean measurements are subject to a static error under this unsteady heat transfer situation; refer to Gordov and Kovshev (52), 1961.

This error is due to the increased heating of the thermocouple in the first half of the cycle and the decreased cooling over the

second half of the cycle. Data given in (52) indicates that for this size wire, the static error could be as much as 15%, but this error is independent of frequency.

Due therefore to this latter fact, Figs. (22) and (23) probably give a valid comparison between the two regions at the different speeds and C.R. even although the absolute levels are not correct. It was thus considered sufficient to plot the potentiometer readings above atmospheric temperature.

(7) The Knock-Zone wall temperature is 25°F and 60°F higher than the Inlet wall temperature at 500 and 2000 r.p.m. respectively. Ratios of Wall temperature to bulk gas temperature ($T_w \backslash T_\infty$) from these traverses also agree with motoring data in (29).

From the above it can be seen that in general the rate of change of layer thickness with speed is more marked at the lower C.R. and in the cooler region.

Referring to Figs. (22) and (23) it is of interest to compare the form of the two temperatures profiles. It will be observed that in the Inlet region a steep gradient extends to a small plateau in the close vicinity of the wall. In the Knock-Zone region however the temperature profile is a smooth curve extending to the bulk-gas region.

The "sub-layer" thickness in the Inlet region (from A to X in Fig. (22)) for both 500 and 2000 r.p.m. approximate to those selected

by Knight (29) for use in the Temperature Profile Theory (Section 2.3), equation (45)).

His selected values for the turbulent boundary layer thickness from Goldstein (53) were 0.047" and 0.034" for motoring at 500 r.p.m. and 2000 r.p.m. respectively.

It was apparent that the quenching effect of the wall on the gas extended much further into the gas than the above theoretically predicted boundary layer, and for heat transfer measurements the bulk gas temperature was measured outside the previously discussed thermal layer.

It should also be pointed out that these mean temperature profiles could be quite consistently repeated over a period of time at constant running conditions by traversing the thermocouple away from and towards the wall a number of times, Fig. (24).

For the Knock-Zone, steady-state gas temperature profiles were plotted for speeds ranging from 300 - 2500 r.p.m., Fig. (25), and the extent of the thermal layer was estimated at each speed (curve A-A).

The estimated thermal layer thickness for each speed was then plotted against mean piston speed on a log-log basis, Fig. (26). This curve approximated to a straight line resulting in an expression of the form

$$x = a\ (V_{pm})^{-1/4} \qquad (78)$$

Equation (78) infers also that the time-mean heat transfer coefficient at this location is directly proportional to the 4th root of r.p.m. since the thermal resistance is directly proportional

PERFORMANCE RUN 3/7/64 DURATION 2HR 10MIN

NTEST= 36 NRUN= 1

CR= 7.0 NOCT= 85 THROT= 1.000

NRPM =	2500				*					
MIX =	1	2	3	4	5	6	7	8	9	
MBT =	60	35	32	32	32	32	32	32	32	DEGBTDC
F =	12.73	9.06	8.50	7.78	7.54	6.99	6.43	5.55	4.27	LB/HR
A =	93.30	93.13	93.13	93.13	92.95	92.95	92.78	92.78	92.78	LB/HR
AF =	7.325	10.272	10.947	11.956	12.312	13.296	14.423	16.703	21.688	
FA =	.136	.097	.091	.083	.081	.075	.069	.059	.046	
FA/FC=	2.05	1.46	1.37	1.25	1.22	1.13	1.04	.90	.69	
BHP =	8.70	9.94	10.52	10.82	10.82	11.18	10.74	3.21	3.21	
BSFC =	1.498	.933	.827	.736	.714	.639	.612	1.767	1.361	LB/BHP.HR
BMEP =	89.0	101.7	107.7	110.7	110.7	114.4	110.0	32.9	32.9	PSI
EVOL =	55.47	55.36	55.36	55.36	55.26	55.26	55.15	55.15	55.15	
ECFLO=	438.2	441.4	441.4	441.4	441.4	441.4	443.3	443.3	443.3	GAL/HR
HTRE =	16.56	18.27	19.07	20.66	20.66	22.25	22.34	21.54	15.96	KBTU/HR

Fig.20 Example of output- Engine Performance Calibration - * indicates Optimum

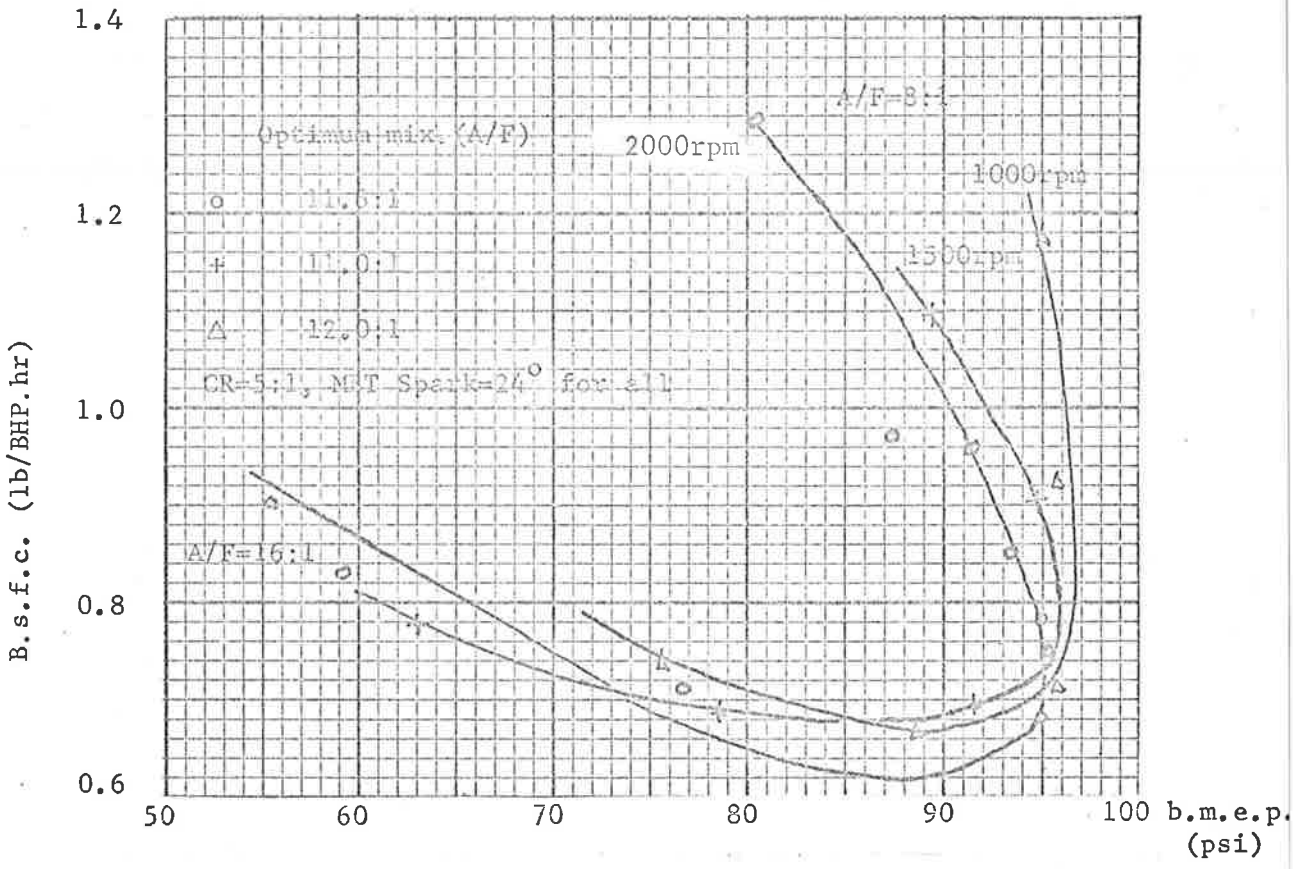

Fig.21 Mixture range loops from performance data

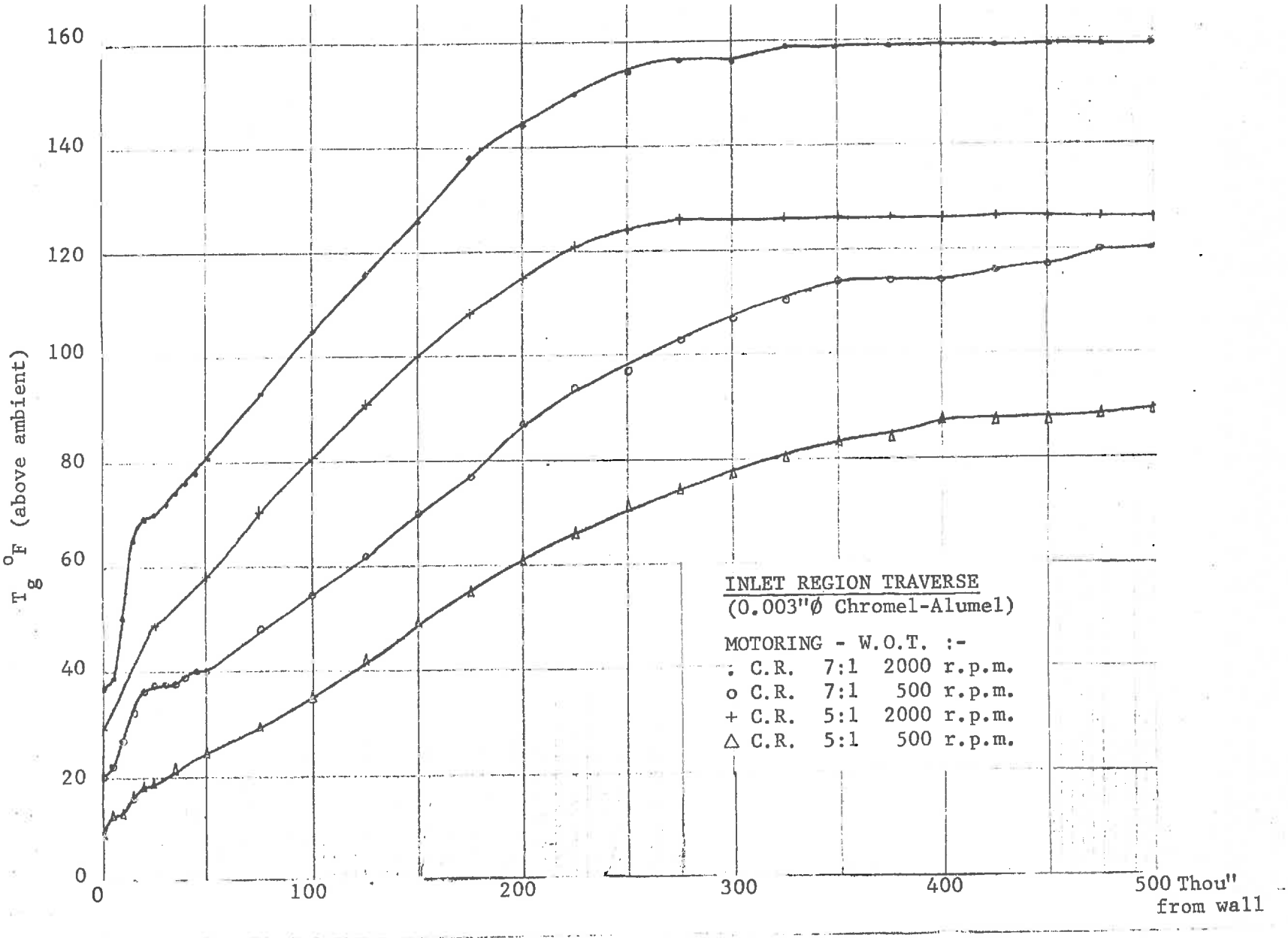

Fig. 22 Steady-state Motoring traverse- INLET

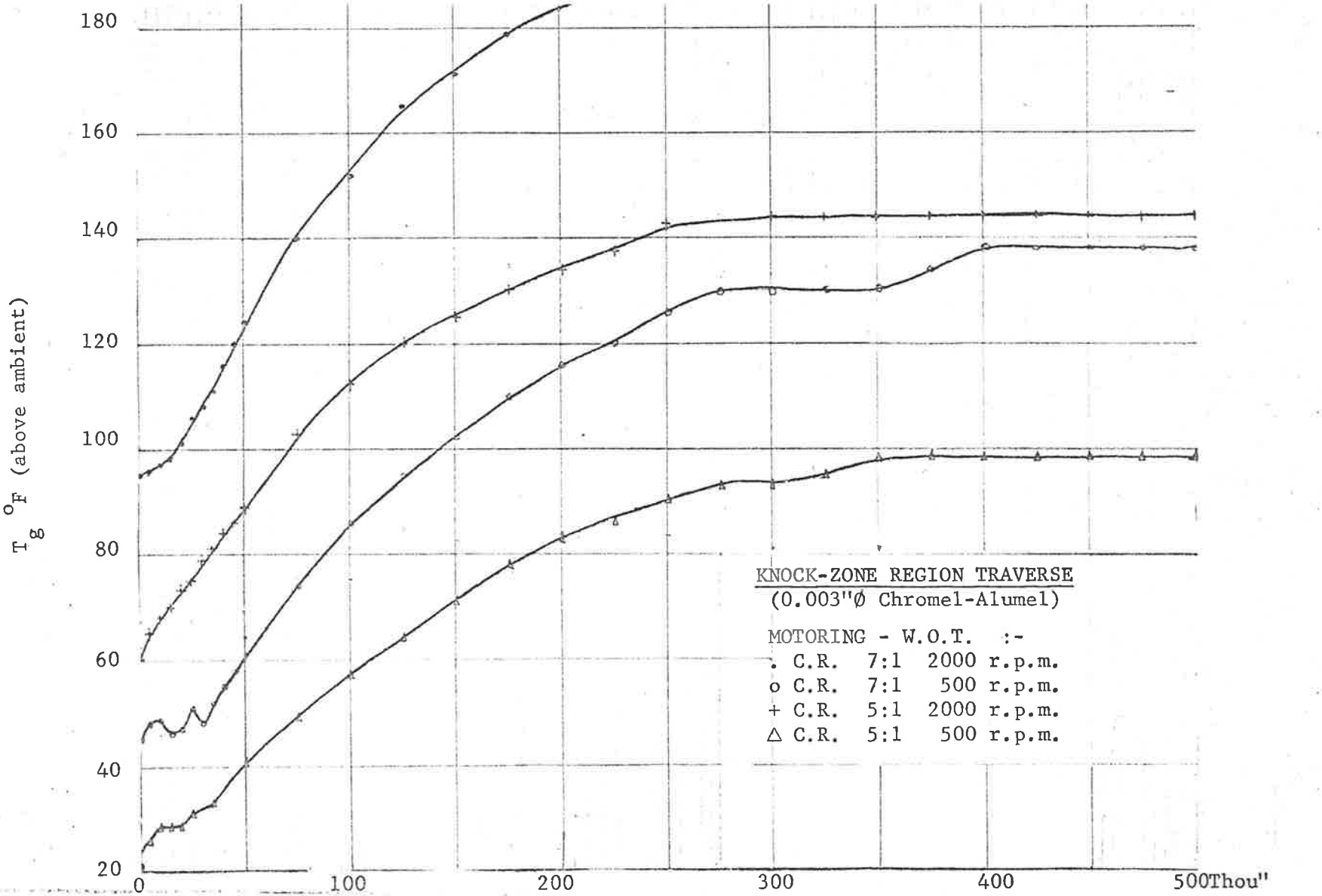

Fig. 23 Steady-state Motoring Traverse- KNOCK-ZONE

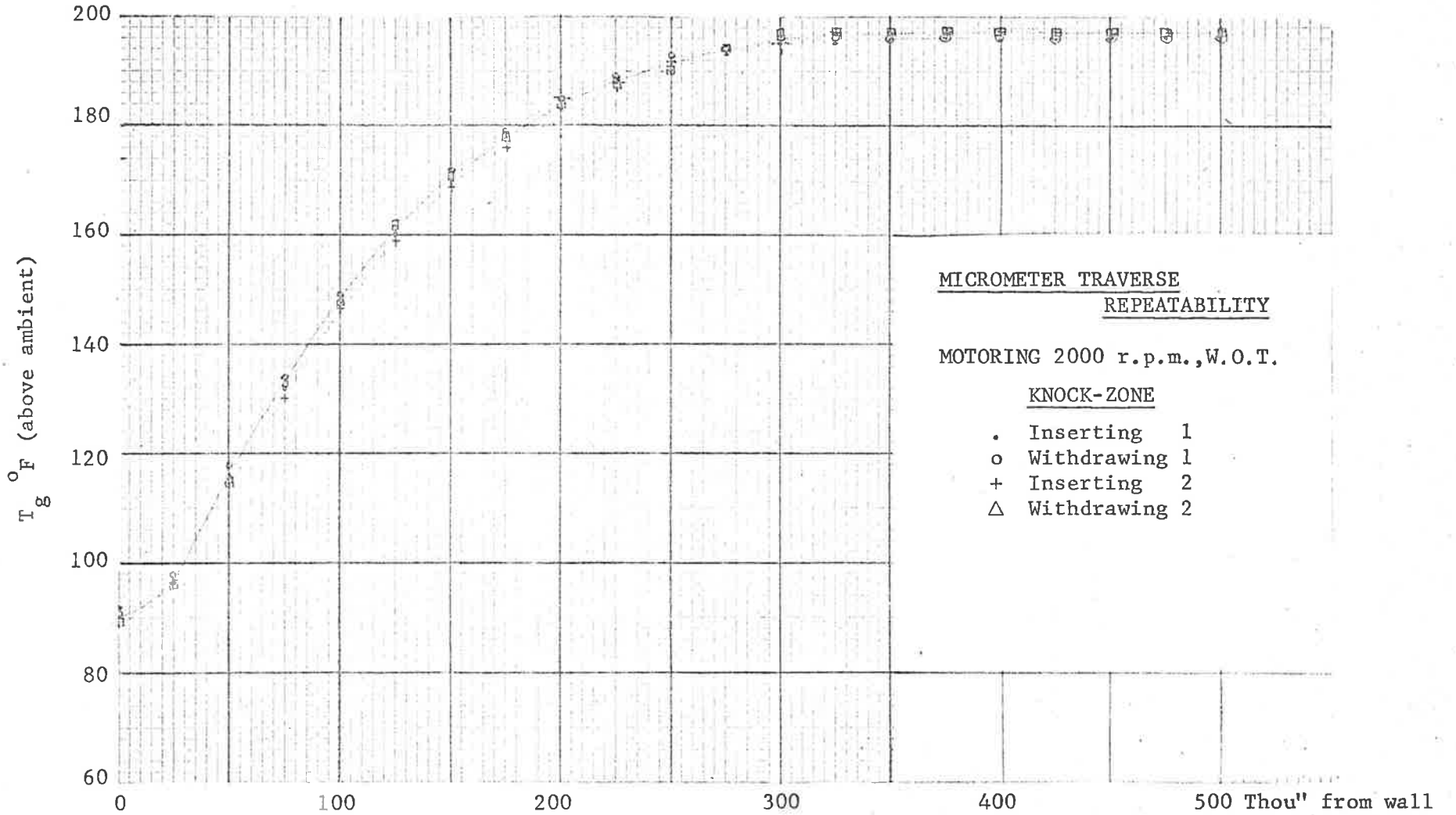

Fig. 24 Repeatability of Temperature Profile

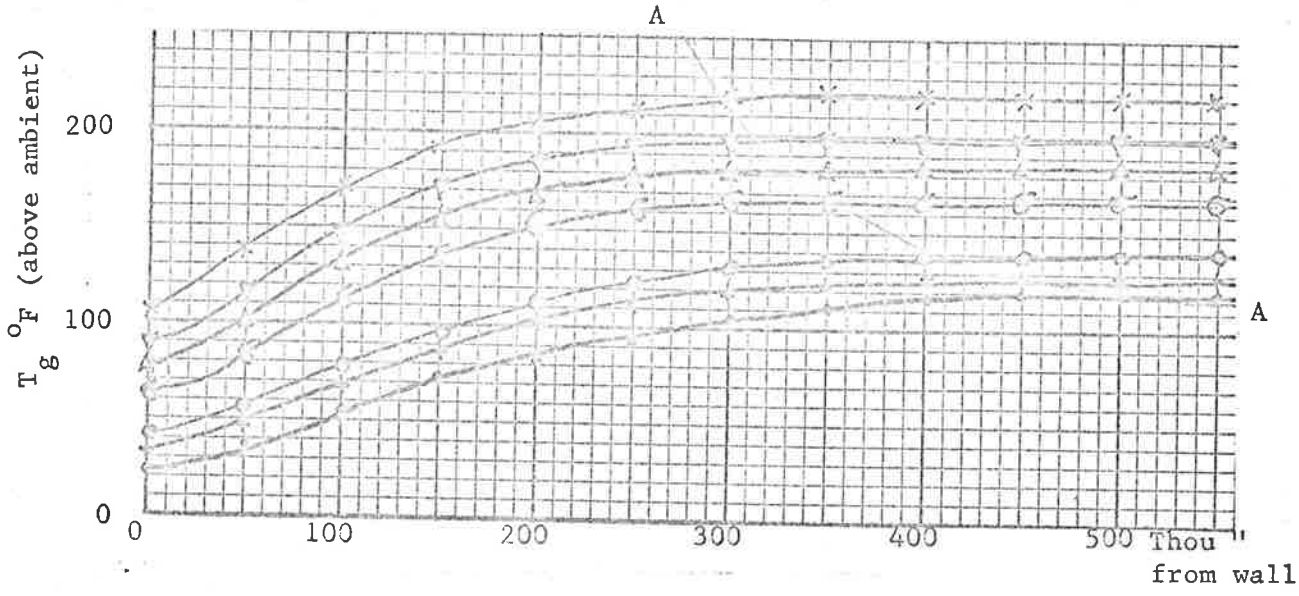

X	2500	r.p.m.
▽	2000	"
△	1300	"
Ó	1200	"
o	500	"
+	400	"
•	300	"

C.R 7:1 , W.O.T.

Fig.25 Knock-Zone Motoring traverse showing extent of the " Thermal Layer " at various speeds (curve A-A)

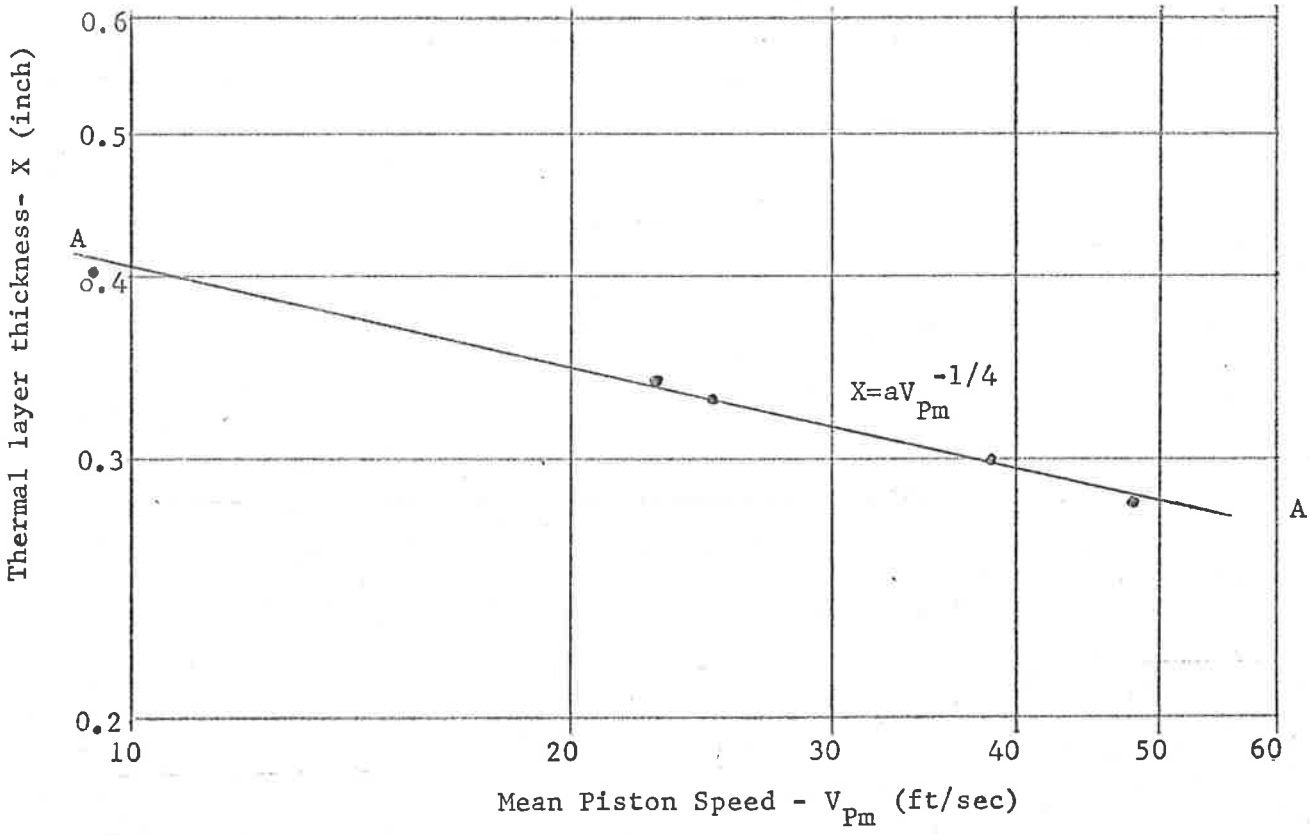

Fig.26 Thermal layer thickness v. mean piston speed for Motored engine, W.O.T., Knock-Zone (Fig.25)

to the layer thickness.

Annand (5) commented that experimental evidence generally (54), (55), (56) gave variation of overall time mean heat transfer with powers of r.p.m. between 0.5 and 0.8 and never as low as the 0.33 proposed by Eichelberg (21).

However, the foregoing observation tends to support the exponent used by Eichelberg if his formula is applied to a localised region since the investigations cited by Annand were only for overall heat transfer to the cylinder head and barrel.

6.3.2 Motored Engine Cyclic Traverse

The gas temperature traverse given in Fig.(27) shows the marked change of thermal gradient experienced over the cycle within the gas layer at the Knock-Zone under conditions of motoring at 700 r.p.m., w.o.t., 5:1 C.R. Presented in this figure are gas temperature cycles recorded for different depths of insertion of the thermocouple ranging from 0.000" to 0.200". If we plot the instantaneous temperature profile at various time intervals over the cycle, we will note considerable variations in the boundary layer thickness (Fig.27 - (a),(b),(c)). The results of this Figure are only qualitative because they were obtained with an uncorrected 0.001"Ø thermocouple (Appendix A1).

Still, it does clearly show that the thermal layer is thinnest toward the end of compression, and that it grows over the expansion and exhaust strokes, becoming thickest during the inlet phase.

A corrected thermocouple was used for the traverse in Fig.(29); this shows the Inlet region at 750 r.p.m., w.o.t., 5:1 C.R. It can be seen that all cycles reach their maxima before 20^{o} ACTDC.

Fig. (30) gives a traverse under these same conditions for the next consecutive series of cycles to each of those in Fig. (29). This illustrates that despite cycle-to-cycle temperature variations, the temperature profiles in the gas are repeatable, being quite similar to those of the first cycle.

These traverses were used to determine the rate of growth of the layer as a function of crank angle (time) in the cycle. This was carried out in the following manner.

(1) From the list of temperatures at each depth at any given crank angle, Fig. (28), the temperature - distance profiles were plotted at 100^{o} crank angle intervals over the cycle in Fig. (31).

(2) From this figure, the layer thickness was estimated from the slopes of each profile and plotted as a function of crank angle (time) over the cycle.

It can be seen from the ensuing curve, Fig. (32), that over the expansion stroke and for about 50% of the exhaust stroke, the thermal layer grows at the rate of about 0.001"/msec. For the latter half of the exhaust stroke and over the inlet stroke, the layer thickness increases at the rate of 0.0001"/msec only. For the first 70 - 80% of the compression stroke, the layer thickness begins to decrease at the rate of 0.0008"/msec.

Since the thickness of this layer is a measure of the thermal resistance of the gas near the wall, it could be expected that the heat transfer coefficient would follow an inverse trend to the variations shown in Fig. (32).

CONVERT TAPE NO 4
750 RPM 60T MOTORING P+TO K7,UNCOMPENSATED
ANALOG TAPE 9 TRANSMITTAL TAPE 503

SERIAL	RUN	CHANNEL	TYPE	NO PER1009	COEFF
6	11	123	1	1	15

	A	B	C	D	E
1	5.49995E+02	5.72743E+02	5.85800E+02	5.98809E+02	6.00833E+02
2	5.53618E+02	5.80512E+02	5.96937E+02	5.95809E+02	6.00443E+02
3	5.57173E+02	5.88484E+02	6.08702E+02	6.03578E+02	6.16670E+02
4	5.61303E+02	5.96359E+02	6.20992E+02	6.11408E+02	6.25178E+02
5	5.65734E+02	6.04019E+02	6.33010E+02	6.18988E+02	6.33756E+02
6	5.70289E+02	6.11143E+02	6.44272E+02	6.26710E+02	6.42265E+02
7	5.74669E+02	6.17401E+02	6.54232E+02	6.33051E+02	6.50109E+02
8	5.78564E+02	6.23054E+02	6.62544E+02	6.39517E+02	6.57637E+02
9	5.81702E+02	6.27734E+02	6.68036E+02	6.45584E+02	6.63720E+02
10	5.83912E+02	6.31044E+02	6.72737E+02	6.51107E+02	6.68841E+02
11	5.85157E+02	6.32304E+02	6.74994E+02	6.54109E+02	6.72401E+02
12	5.85530E+02	6.31004E+02	6.75750E+02	6.54223E+02	6.72747E+02
13	5.85212E+02	6.32404E+02	6.75533E+02	6.53343E+02	6.72684E+02
14	5.84421E+02	6.32034E+02	6.74847E+02	6.55174E+02	6.70781E+02
15	5.83352E+02	6.30713E+02	6.74311E+02	6.56435E+02	6.79144E+02
16	5.82143E+02	6.29111E+02	6.74074E+02	6.66464E+02	6.79031E+02
17	5.80886E+02	6.27354E+02	6.74274E+02	6.65756E+02	6.79445E+02
18	5.79534E+02	6.25922E+02	6.74791E+02	6.66864E+02	6.77547E+02
19	5.78144E+02	6.27411E+02	6.75352E+02	6.63708E+02	6.76284E+02
20	5.76893E+02	6.21610E+02	6.75625E+02	6.61844E+02	6.74715E+02
21	5.75200E+02	6.10507E+02	6.75309E+02	6.60335E+02	6.72664E+02
22	5.73713E+02	6.17704E+02	6.74216E+02	6.58745E+02	6.70795E+02
23	5.72240E+02	6.15037E+02	6.72206E+02	6.57016E+02	6.65542E+02
24	5.70940E+02	6.12740E+02	6.69656E+02	6.55004E+02	6.66300E+02
25	5.69807E+02	6.10531E+02	6.66881E+02	6.52969E+02	6.64044E+02
26	5.68781E+02	6.08801E+02	6.63015E+02	6.50479E+02	6.61845E+02
27	5.67800E+02	6.06494E+02	6.59455E+02	6.48701E+02	6.59715E+02
28	5.66899E+02	6.04595E+02	6.55923E+02	6.45924E+02	6.57842E+02
29	5.66003E+02	6.02844E+02	6.52491E+02	6.43627E+02	6.55081E+02
30	5.65110E+02	6.01256E+02	6.49156E+02	6.41425E+02	6.53544E+02
31	5.64220E+02	5.99714E+02	6.45909E+02	6.39135E+02	6.51592E+02
32	5.63337E+02	5.98430E+02	6.42694E+02	6.37298E+02	6.49490E+02
33	5.62508E+02	5.97134E+02	6.39573E+02	6.35204E+02	6.47405E+02
34	5.61870E+02	5.95963E+02	6.36561E+02	6.33240E+02	6.45527E+02
35	5.61215E+02	5.94760E+02	6.33700E+02	6.31208E+02	6.43618E+02
36	5.60541E+02	5.93666E+02	6.30941E+02	6.29179E+02	6.41720E+02
37	5.59972E+02	5.92804E+02	6.28100E+02	6.27198E+02	6.39818E+02
38	5.59203E+02	5.92017E+02	6.25704E+02	6.25251E+02	6.37749E+02
39	5.58139E+02	5.88136E+02	6.23009E+02	6.23152E+02	6.35582E+02
40	5.57519E+02	5.90812E+02	6.20154E+02	6.21454E+02	6.33144E+02
41	5.56554E+02	5.89780E+02	6.17693E+02	6.19522E+02	6.30510E+02
42	5.55566E+02	5.88861E+02	6.15369E+02	6.17509E+02	6.27701E+02
43	5.54720E+02	5.87856E+02	6.13985E+02	6.15610E+02	6.25004E+02
44	5.53882E+02	5.86240E+02	6.08311E+02	6.13768E+02	6.22324E+02
45	5.53015E+02	5.77052E+02	6.03035E+02	6.11120E+02	6.19850E+02
46	5.52221E+02	5.71146E+02	6.00194E+02	6.09041E+02	6.17609E+02
47	5.51486E+02	5.69890E+02	5.97887E+02	6.07216E+02	6.15844E+02
48	5.50731E+02	5.68513E+02	5.96027E+02	6.05568E+02	6.14204E+02
49	5.50038E+02	5.67562E+02	5.94569E+02	6.04117E+02	6.12978E+02
50	5.49377E+02	5.66843E+02	5.93251E+02	6.02875E+02	6.11743E+02
51	5.48746E+02	5.65719E+02	5.91947E+02	6.01713E+02	6.10819E+02
52	5.48254E+02	5.64731E+02	5.90501E+02	6.00571E+02	6.09408E+02
53	5.47774E+02	5.63628E+02	5.88856E+02	5.99302E+02	6.08108E+02
54	5.47322E+02	5.62403E+02	5.87032E+02	5.98147E+02	6.06715E+02
55	5.46886E+02	5.61376E+02	5.85124E+02	5.96884E+02	6.05253E+02
56	5.46471E+02	5.60316E+02	5.83241E+02	5.95502E+02	6.03765E+02
57	5.45835E+02	5.59054E+02	5.81474E+02	5.94146E+02	6.02294E+02
58	5.45260E+02	5.58145E+02	5.79882E+02	5.92853E+02	6.00888E+02
59	5.44701E+02	5.57112E+02	5.78444E+02	5.91584E+02	5.99534E+02
60	5.44160E+02	5.56076E+02	5.77125E+02	5.90131E+02	5.98262E+02
61	5.43634E+02	5.55088E+02	5.75886E+02	5.89147E+02	5.97084E+02
62	5.43292E+02	5.54041E+02	5.74551E+02	5.87941E+02	5.95872E+02
63	5.42940E+02	5.54005E+02	5.73220E+02	5.86799E+02	5.94717E+02
64	5.42608E+02	5.53054E+02	5.71886E+02	5.85659E+02	5.93537E+02

65	5.42256E+02	5.52134E+02	5.70519E+02	5.84553E+02	5.92443E+02
66	5.41857E+02	5.51234E+02	5.69234E+02	5.83407E+02	5.91337E+02
67	5.41410E+02	5.50406E+02	5.68004E+02	5.82441E+02	5.90237E+02
68	5.40932E+02	5.49546E+02	5.66946E+02	5.81413E+02	5.89226E+02
69	5.40458E+02	5.48448E+02	5.65976E+02	5.80340E+02	5.88130E+02
70	5.40028E+02	5.47562E+02	5.65033E+02	5.79333E+02	5.87144E+02
71	5.39655E+02	5.46570E+02	5.64116E+02	5.78278E+02	5.86068E+02
72	5.39354E+02	5.45866E+02	5.63184E+02	5.77243E+02	5.84991E+02
73	5.39101E+02	5.45207E+02	5.62237E+02	5.76247E+02	5.83918E+02
74	5.38845E+02	5.47140E+02	5.61291E+02	5.75166E+02	5.82866E+02
75	5.38617E+02	5.46756E+02	5.60372E+02	5.74060E+02	5.81742E+02
76	5.38341E+02	5.46305E+02	5.59587E+02	5.73021E+02	5.80633E+02
77	5.38046E+02	5.45842E+02	5.58784E+02	5.71951E+02	5.79535E+02
78	5.37732E+02	5.45336E+02	5.57963E+02	5.70896E+02	5.78424E+02
79	5.37441E+02	5.44794E+02	5.57265E+02	5.69848E+02	5.77344E+02
80	5.37182E+02	5.44190E+02	5.56566E+02	5.68818E+02	5.76267E+02
81	5.36958E+02	5.43529E+02	5.55796E+02	5.67733E+02	5.75073E+02
82	5.36728E+02	5.42902E+02	5.54496E+02	5.66718E+02	5.73994E+02
83	5.36455E+02	5.42110E+02	5.54136E+02	5.65661E+02	5.72930E+02
84	5.36116E+02	5.41373E+02	5.53140E+02	5.64607E+02	5.71897E+02
85	5.35887E+02	5.40652E+02	5.52019E+02	5.63447E+02	5.70792E+02
86	5.35177E+02	5.39934E+02	5.50946E+02	5.62384E+02	5.69669E+02
87	5.34819E+02	5.39203E+02	5.49715E+02	5.61293E+02	5.68617E+02
88	5.34059E+02	5.38478E+02	5.48340E+02	5.60092E+02	5.67574E+02
89	5.33534E+02	5.37602E+02	5.46946E+02	5.58951E+02	5.66420E+02
90	5.33007E+02	5.36890E+02	5.45622E+02	5.57853E+02	5.65319E+02
91	5.32666E+02	5.36040E+02	5.43961E+02	5.56725E+02	5.64165E+02
92	5.32281E+02	5.35475E+02	5.42242E+02	5.55625E+02	5.63040E+02
93	5.31882E+02	5.33564E+02	5.40872E+02	5.54469E+02	5.61851E+02
94	5.31443E+02	5.32450E+02	5.39177E+02	5.53269E+02	5.60525E+02
95	5.30943E+02	5.31405E+02	5.37785E+02	5.52068E+02	5.59295E+02
96	5.30407E+02	5.30410E+02	5.36507E+02	5.50943E+02	5.58146E+02
97	5.29886E+02	5.29534E+02	5.35133E+02	5.49798E+02	5.56967E+02
98	5.29421E+02	5.28703E+02	5.34241E+02	5.48678E+02	5.55810E+02
99	5.29041E+02	5.28100E+02	5.33201E+02	5.47605E+02	5.54709E+02
100	5.28767E+02	5.27648E+02	5.32192E+02	5.46518E+02	5.53593E+02
101	5.28580E+02	5.27187E+02	5.31205E+02	5.45463E+02	5.52507E+02
102	5.28287E+02	5.26745E+02	5.30243E+02	5.44387E+02	5.51395E+02
103	5.27999E+02	5.26320E+02	5.29123E+02	5.43345E+02	5.50216E+02
104	5.27650E+02	5.25131E+02	5.28443E+02	5.42281E+02	5.49107E+02
105	5.27237E+02	5.24556E+02	5.27695E+02	5.41236E+02	5.48034E+02
106	5.26794E+02	5.24022E+02	5.27020E+02	5.40187E+02	5.46911E+02
107	5.26344E+02	5.23547E+02	5.25447E+02	5.39117E+02	5.45822E+02
108	5.26077E+02	5.23118E+02	5.25971E+02	5.38086E+02	5.44720E+02
109	5.25875E+02	5.22831E+02	5.25582E+02	5.37017E+02	5.43618E+02
110	5.25779E+02	5.22593E+02	5.25268E+02	5.35979E+02	5.42587E+02
111	5.25742E+02	5.22413E+02	5.25006E+02	5.34935E+02	5.41595E+02
112	5.25704E+02	5.22214E+02	5.24787E+02	5.33913E+02	5.40620E+02
113	5.25613E+02	5.22164E+02	5.24593E+02	5.32882E+02	5.39607E+02
114	5.25444E+02	5.22005E+02	5.24412E+02	5.31881E+02	5.38646E+02
115	5.25215E+02	5.21843E+02	5.24234E+02	5.30845E+02	5.37649E+02
116	5.24971E+02	5.21666E+02	5.24061E+02	5.29787E+02	5.36513E+02
117	5.24770E+02	5.21494E+02	5.23900E+02	5.28784E+02	5.35436E+02
118	5.24655E+02	5.21338E+02	5.23738E+02	5.27815E+02	5.34284E+02
119	5.24632E+02	5.21237E+02	5.23606E+02	5.26854E+02	5.33208E+02
120	5.24672E+02	5.21170E+02	5.23484E+02	5.25934E+02	5.32154E+02
121	5.24714E+02	5.21109E+02	5.23363E+02	5.25025E+02	5.31136E+02
122	5.24707E+02	5.21027E+02	5.23230E+02	5.24137E+02	5.30150E+02
123	5.24651E+02	5.20915E+02	5.23047E+02	5.23268E+02	5.29160E+02
124	5.24454E+02	5.20708E+02	5.22877E+02	5.22405E+02	5.28178E+02
125	5.24208E+02	5.20486E+02	5.22722E+02	5.21552E+02	5.27191E+02
126	5.24194E+02	5.22154E+02	5.25203E+02	5.24956E+02	5.28072E+02
127	5.24247E+02	5.22563E+02	5.25627E+02	5.25237E+02	5.28243E+02

128	5.24480E+02	5.22104E+02	5.26124E+02	5.25044E+02	5.24631E+02
129	5.24868E+02	5.23465E+02	5.26732E+02	5.25047E+02	5.24134E+02
130	5.25334E+02	5.24146E+02	5.27403E+02	5.25081E+02	5.23813E+02
131	5.25780E+02	5.25137E+02	5.28041E+02	5.25119E+02	5.23582E+02
132	5.26130E+02	5.25981E+02	5.29595E+02	5.27055E+02	5.24061E+02
133	5.26368E+02	5.26925E+02	5.30959E+02	5.28109E+02	5.24360E+02
134	5.26561E+02	5.27846E+02	5.32524E+02	5.29414E+02	5.24736E+02
135	5.26865E+02	5.28146E+02	5.34298E+02	5.30947E+02	5.24987E+02
136	5.27423E+02	5.28644E+02	5.36300E+02	5.32742E+02	5.25604E+02
137	5.28433E+02	5.29512E+02	5.38602E+02	5.34863E+02	5.26744E+02
138	5.29998E+02	5.30970E+02	5.41317E+02	5.37024E+02	5.28222E+02
139	5.32109E+02	5.32880E+02	5.44593E+02	5.39542E+02	5.29145E+02
140	5.34680E+02	5.34980E+02	5.48631E+02	5.42552E+02	5.30321E+02
141	5.37561E+02	5.44688E+02	5.53624E+02	5.46330E+02	5.31794E+02
142	5.40599E+02	5.45199E+02	5.59755E+02	5.50088E+02	5.32605E+02
143	5.41477E+02	5.54684E+02	5.67194E+02	5.57502E+02	5.34772E+02
144	5.40788E+02	5.65336E+02	5.75878E+02	5.61095E+02	5.33804E+02

Data List for Fig.27

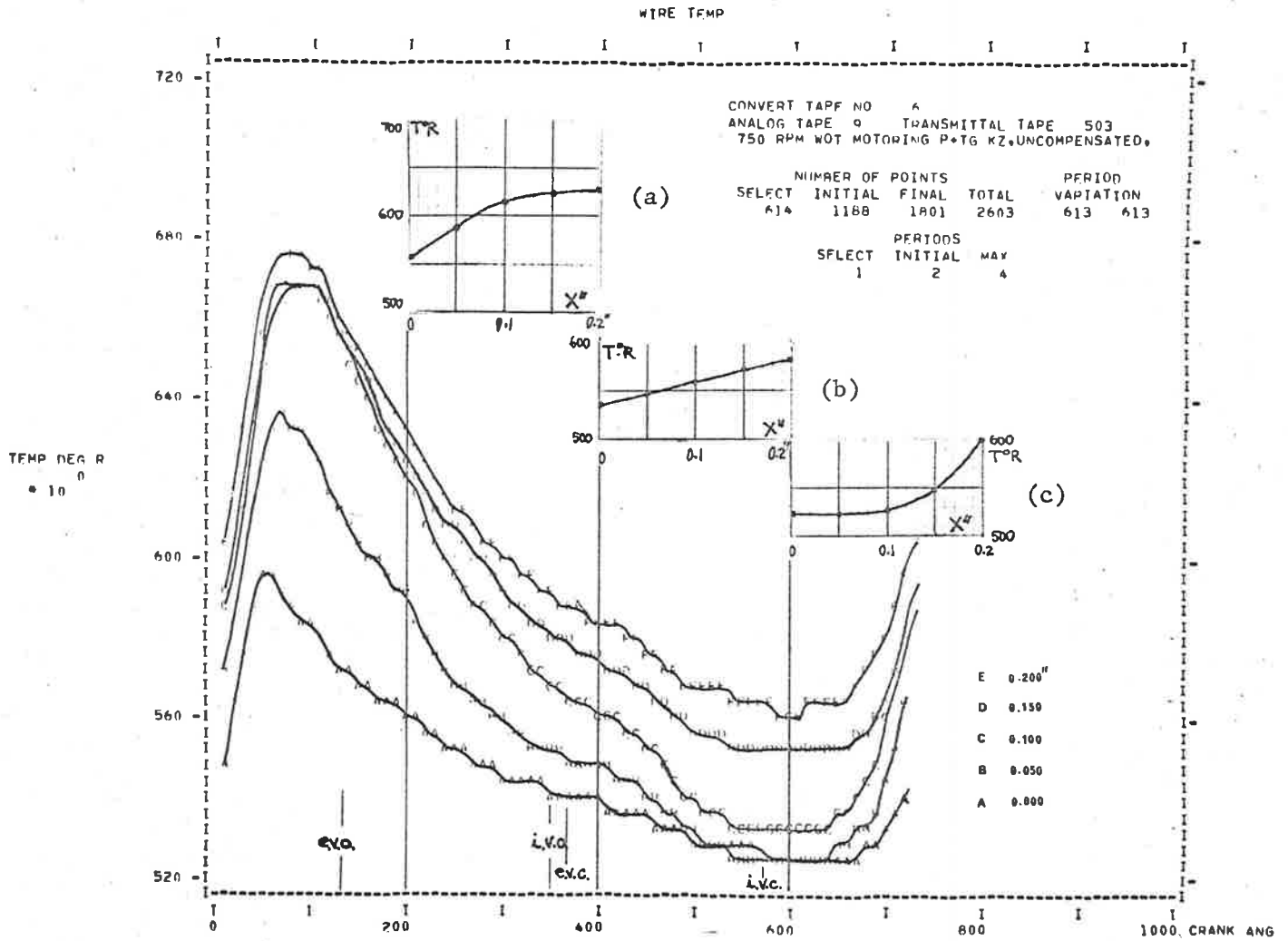

Fig.27 Knock-Zone Cyclic Traverse(uncorrected)
Motored engine, W.O.T.,5:1C.R.

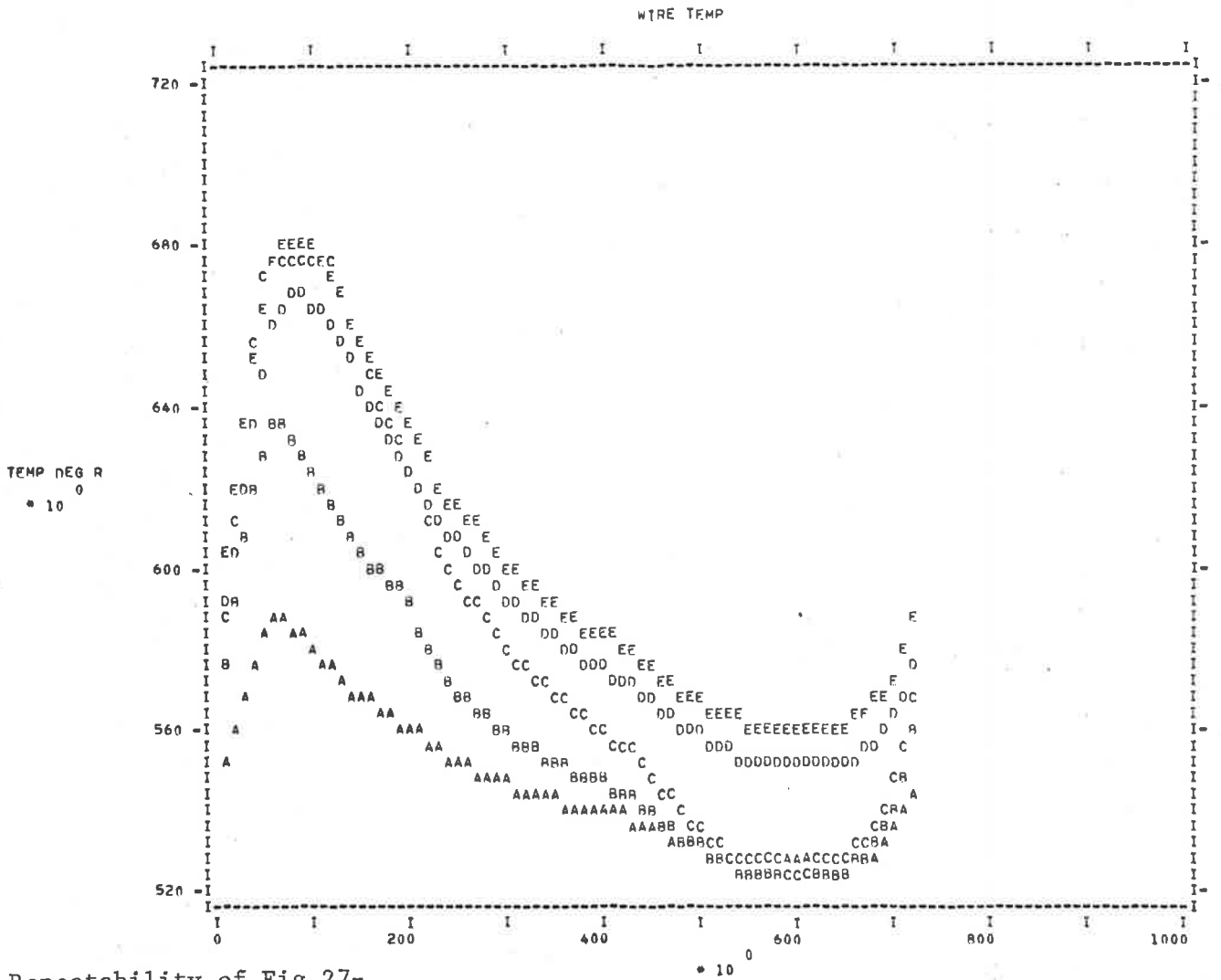

Repeatability of Fig.27-
Next consecutive cycle

[illegible]
700 RPM.CR 5/1. [illegible] INLET CORRECTED.
[illegible] 1545

T_g (°R)

	A	B	C	D
1	[illegible]	[illegible]	7.51705E+02	[illegible]
2	[illegible]	7.11253E+02	[illegible]	[illegible]
3	[illegible]	7.33931E+02	7.50017E+02	[illegible]
4	6.57370E+02	7.36741E+02	[illegible]	[illegible]
5	6.54865E+02	7.33711E+02	[illegible]	[illegible]
6	6.49614E+02	7.30943E+02	[illegible]	7.79152E+02
7	6.42605E+02	7.26414E+02	[illegible]	7.75175E+02
8	6.35742E+02	7.21465E+02	7.40511E+02	7.70320E+02
9	6.29965E+02	7.16632E+02	7.37828E+02	7.66847E+02
10	6.26347E+02	7.11270E+02	7.34077E+02	7.59054E+02
11	6.23903E+02	7.06590E+02	7.29600E+02	7.53257E+02
12	6.21161E+02	7.02602E+02	7.26212E+02	[illegible]
13	6.21302E+02	6.99214E+02	7.19036E+02	[illegible]
14	6.21700E+02	6.96173E+02	7.14315E+02	7.39204E+02
15	6.21400E+02	6.97132E+02	7.10206E+02	7.36514E+02
16	6.20216E+02	6.89836E+02	7.06929E+02	7.31294E+02
17	6.14311E+02	6.86143E+02	7.06067E+02	7.28516E+02
18	6.16196E+02	6.82100E+02	7.01344E+02	7.26052E+02
19	6.14410E+02	6.78170E+02	6.98661E+02	7.23707E+02
20	6.13806E+02	6.74740E+02	6.95853E+02	7.21682E+02
21	6.13252E+02	6.71003E+02	6.93000E+02	7.19676E+02
22	6.13709E+02	6.69200E+02	6.90242E+02	7.17773E+02
23	6.14531E+02	6.65937E+02	6.87810E+02	7.15963E+02
24	6.15067E+02	6.64055E+02	6.85757E+02	7.14222E+02
25	6.15092E+02	6.62405E+02	6.86114E+02	7.12638E+02
26	6.14563E+02	6.60405E+02	6.82818E+02	7.10715E+02
27	6.13676E+02	6.50601E+02	6.81735E+02	7.18774E+02
28	6.12768E+02	6.54267E+02	6.80736E+02	7.06537E+02
29	6.12071E+02	6.57729E+02	6.79710E+02	7.04095E+02
30	6.11765E+02	6.58733E+02	6.78555E+02	7.01208E+02
31	6.11736E+02	6.55734E+02	6.77154E+02	6.97965E+02
32	6.11717E+02	6.54360E+02	6.75759E+02	6.94616E+02
33	6.11406E+02	6.52528E+02	6.72909E+02	6.90478E+02
34	6.10594E+02	6.49781E+02	6.69926E+02	6.86925E+02
35	6.09291E+02	6.44091E+02	6.66903E+02	6.83359E+02
36	6.07681E+02	6.41601E+02	6.61677E+02	6.80188E+02
37	6.06144E+02	6.37070E+02	6.56809E+02	6.77577E+02
38	6.05071E+02	6.32813E+02	6.52763E+02	6.75617E+02
39	6.06521E+02	6.29612E+02	6.48545E+02	6.74794E+02
40	6.06627E+02	6.27670E+02	6.45931E+02	6.73487E+02
41	6.05104E+02	6.26451E+02	6.44601E+02	6.72993E+02
42	6.05591E+02	6.27107E+02	6.44641E+02	6.72573E+02
43	6.05765E+02	6.27540E+02	6.45348E+02	6.72013E+02
44	6.05376E+02	6.27765E+02	6.44155E+02	6.71175E+02
45	6.04507E+02	6.27320E+02	6.46470E+02	6.70031E+02
46	6.03372E+02	6.26141E+02	6.45749E+02	6.68663E+02
47	6.02300E+02	6.24615E+02	6.44096E+02	6.67223E+02
48	6.01586E+02	6.23006E+02	6.41521E+02	6.65892E+02
49	6.01373E+02	6.22046E+02	6.38741E+02	6.64769E+02
50	6.01504E+02	6.21844E+02	6.36744E+02	6.63930E+02
51	6.02030E+02	6.22300E+02	6.34442E+02	6.63120E+02
52	6.02366E+02	6.23307E+02	6.33459E+02	6.62931E+02
53	6.02361E+02	6.24093E+02	6.33109E+02	6.62338E+02
54	6.01926E+02	6.24730E+02	6.32943E+02	6.61754E+02
55	6.01160E+02	6.23660E+02	6.32625E+02	6.61067E+02
56	6.00300E+02	6.21806E+02	6.31719E+02	6.60741E+02
57	5.99618E+02	6.19806E+02	6.30207E+02	6.59688E+02
58	5.99306E+02	6.18030E+02	6.28327E+02	6.59216E+02
59	5.99390E+02	6.17069E+02	6.26405E+02	6.58977E+02
60	5.99720E+02	6.17076E+02	6.25179E+02	6.58930E+02
61	6.00066E+02	6.19071E+02	6.24577E+02	6.58948E+02
62	6.00143E+02	6.19545E+02	6.24831E+02	6.58853E+02
63	5.99806E+02	6.20969E+02	6.25655E+02	6.58491E+02
64	5.99066E+02	6.21472E+02	6.26623E+02	6.57740E+02
65	5.98101E+02	6.20766E+02	6.27298E+02	6.56652E+02
66	5.97170E+02	6.18807E+02	6.27337E+02	6.55369E+02
67	5.96555E+02	6.15985E+02	6.26602E+02	6.54028E+02
68	5.96367E+02	6.12967E+02	6.25509E+02	6.52883E+02
69	5.96590E+02	6.10466E+02	6.24008E+02	6.52036E+02
70	5.97040E+02	6.09005E+02	6.22727E+02	6.51475E+02
71	5.97659E+02	6.08749E+02	6.21507E+02	6.51071E+02
72	5.97602E+02	6.09640E+02	6.20669E+02	6.50595E+02
73	5.97376E+02	6.10575E+02	6.19732E+02	6.49706E+02
74	[illegible]	6.11406E+02	6.18511E+02	6.48675E+02
75	[illegible]	[illegible]	[illegible]	[illegible]
76	5.96776E+02	6.10613E+02	6.14514E+02	6.44054E+02
77	5.94937E+02	6.08563E+02	6.11868E+02	6.41155E+02
78	5.93314E+02	6.05771E+02	6.09105E+02	6.38064E+02
79	5.92906E+02	6.02711E+02	6.06851E+02	6.34902E+02
80	5.92598E+02	5.99859E+02	6.05141E+02	6.32004E+02
81	5.92265E+02	5.97560E+02	6.04208E+02	6.29449E+02
82	5.91810E+02	5.95948E+02	6.03857E+02	6.27048E+02
83	5.91219E+02	5.95060E+02	6.03709E+02	6.24927E+02
84	5.90585E+02	5.94701E+02	6.03674E+02	6.23009E+02
85	5.89969E+02	5.94720E+02	6.03201E+02	6.21327E+02
86	5.89553E+02	5.95012E+02	6.02278E+02	6.19931E+02
87	5.89389E+02	5.95667E+02	6.01006E+02	6.18895E+02
88	5.89677E+02	5.96037E+02	5.99628E+02	6.18214E+02
89	5.89756E+02	5.96652E+02	5.98630E+02	6.17972E+02
90	5.90120E+02	5.97203E+02	5.97621E+02	6.18025E+02
91	5.90510E+02	5.97566E+02	5.97249E+02	6.18267E+02
92	5.90881E+02	5.97530E+02	5.97292E+02	6.18567E+02
93	5.91202E+02	5.97111E+02	5.97477E+02	6.18734E+02
94	5.91480E+02	5.96208E+02	5.97641E+02	6.18754E+02
95	5.91690E+02	5.95255E+02	5.97715E+02	6.18604E+02
96	5.91771E+02	5.94215E+02	5.97637E+02	6.18361E+02
97	5.91632E+02	5.93417E+02	5.97516E+02	6.18054E+02
98	5.91195E+02	5.93017E+02	5.97472E+02	6.17822E+02
99	5.90438E+02	5.93031E+02	5.97580E+02	6.17685E+02
100	5.89434E+02	5.93335E+02	5.97818E+02	6.17629E+02
101	5.88364E+02	5.93707E+02	5.98066E+02	6.17601E+02
102	5.87441E+02	5.93926E+02	5.98159E+02	6.17534E+02
103	[illegible]	[illegible]	[illegible]	6.17377E+02
104	[illegible]	[illegible]	[illegible]	6.17117E+02
105	[illegible]	[illegible]	[illegible]	6.16784E+02
106	[illegible]	[illegible]	[illegible]	6.16436E+02
107	[illegible]	[illegible]	[illegible]	6.16129E+02
108	[illegible]	[illegible]	[illegible]	6.15912E+02
109	[illegible]	[illegible]	[illegible]	6.15749E+02
110	[illegible]	[illegible]	[illegible]	6.15746E+02
111	[illegible]	[illegible]	[illegible]	6.15861E+02
112	[illegible]	[illegible]	[illegible]	6.16040E+02
113	[illegible]	[illegible]	[illegible]	6.16341E+02
114	[illegible]	[illegible]	[illegible]	6.16883E+02
115	[illegible]	[illegible]	[illegible]	6.17659E+02
116	[illegible]	[illegible]	[illegible]	6.18708E+02
117	[illegible]	[illegible]	[illegible]	6.19948E+02
118	[illegible]	[illegible]	[illegible]	6.21306E+02
119	[illegible]	[illegible]	[illegible]	6.22794E+02
120	[illegible]	[illegible]	[illegible]	6.24027E+02
121	[illegible]	[illegible]	[illegible]	6.25030E+02
122	[illegible]	[illegible]	[illegible]	6.25820E+02
123	[illegible]	[illegible]	[illegible]	6.26505E+02
124	[illegible]	[illegible]	[illegible]	6.27245E+02
125	[illegible]	[illegible]	[illegible]	6.28295E+02
126	[illegible]	[illegible]	[illegible]	6.29740E+02
127	[illegible]	[illegible]	[illegible]	6.31656E+02
128	[illegible]	[illegible]	[illegible]	6.34006E+02
129	[illegible]	[illegible]	[illegible]	6.36701E+02
130	[illegible]	[illegible]	[illegible]	6.39670E+02
131	[illegible]	[illegible]	[illegible]	6.42942E+02
132	[illegible]	[illegible]	[illegible]	6.46696E+02
133	[illegible]	[illegible]	[illegible]	6.51254E+02
134	[illegible]	[illegible]	[illegible]	6.57069E+02
135	[illegible]	[illegible]	[illegible]	6.64524E+02
136	[illegible]	[illegible]	[illegible]	6.73937E+02
137	[illegible]	[illegible]	[illegible]	6.85210E+02
138	[illegible]	[illegible]	[illegible]	6.98178E+02
139	[illegible]	[illegible]	[illegible]	7.12224E+02
140	[illegible]	[illegible]	[illegible]	7.26590E+02
141	[illegible]	[illegible]	[illegible]	7.40418E+02
142	[illegible]	[illegible]	[illegible]	7.52938E+02
143	[illegible]	[illegible]	[illegible]	7.63567E+02
144	[illegible]	[illegible]	[illegible]	7.71991E+02

Fig.28 Data list for corrected wire traverse of Fig.29

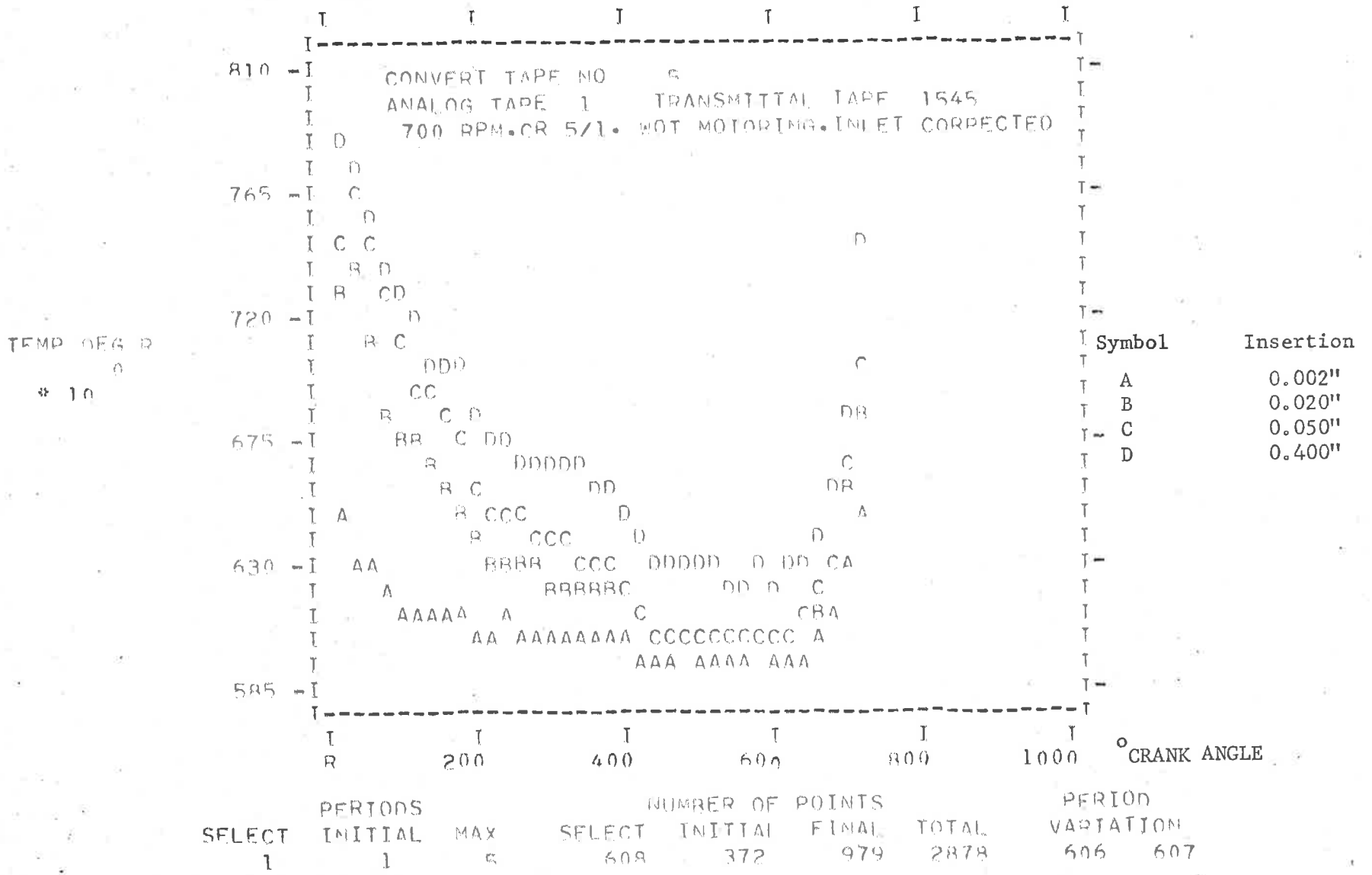

Fig.29 Inlet region Cyclic Traverse(corrected)
Motored engine,W.O.T. - 1st.cycle

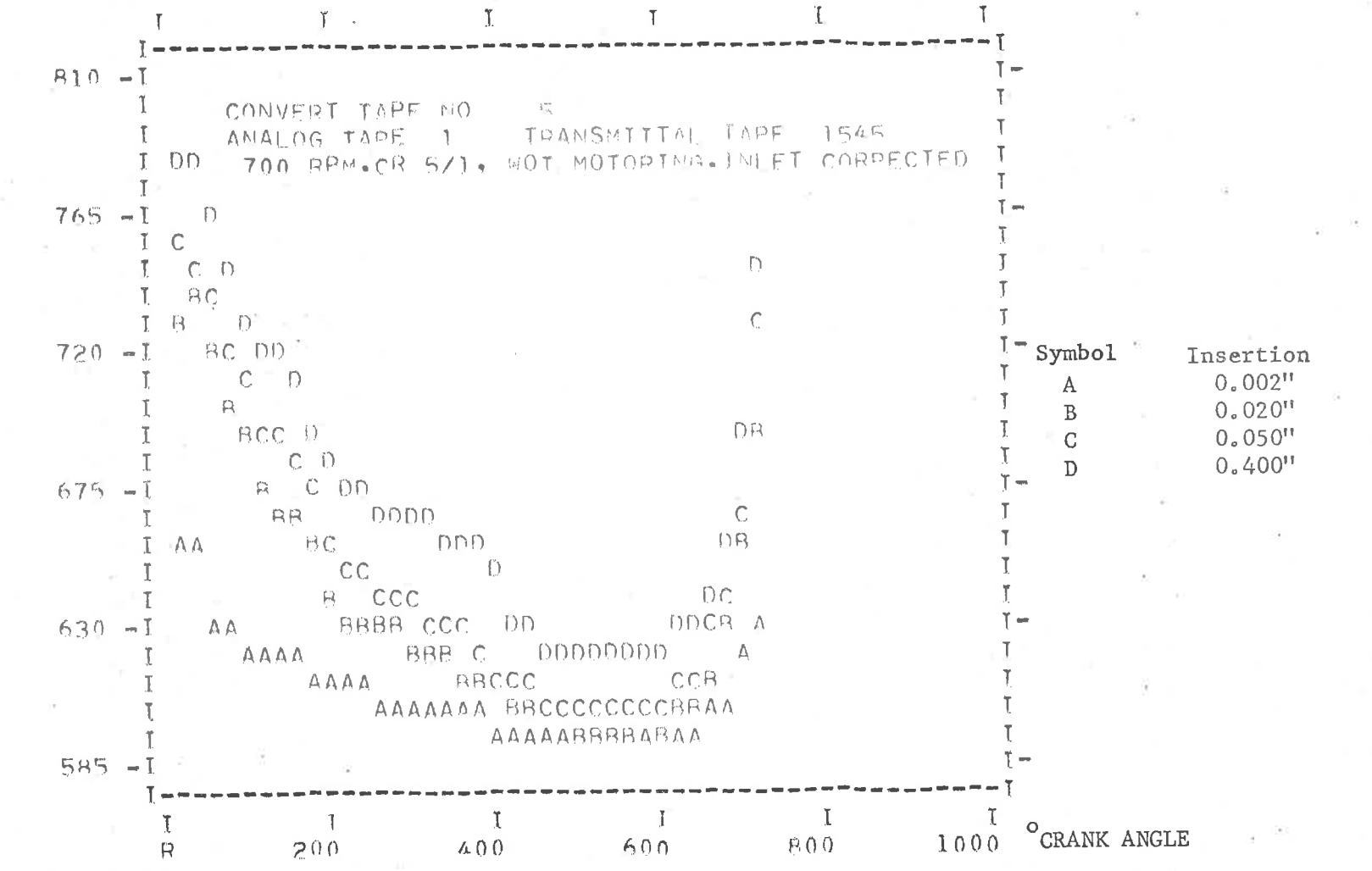

Fig.30 Inlet region Cyclic Traverse(corrected)
Motored engine,W.O.T. - 2nd.cycle

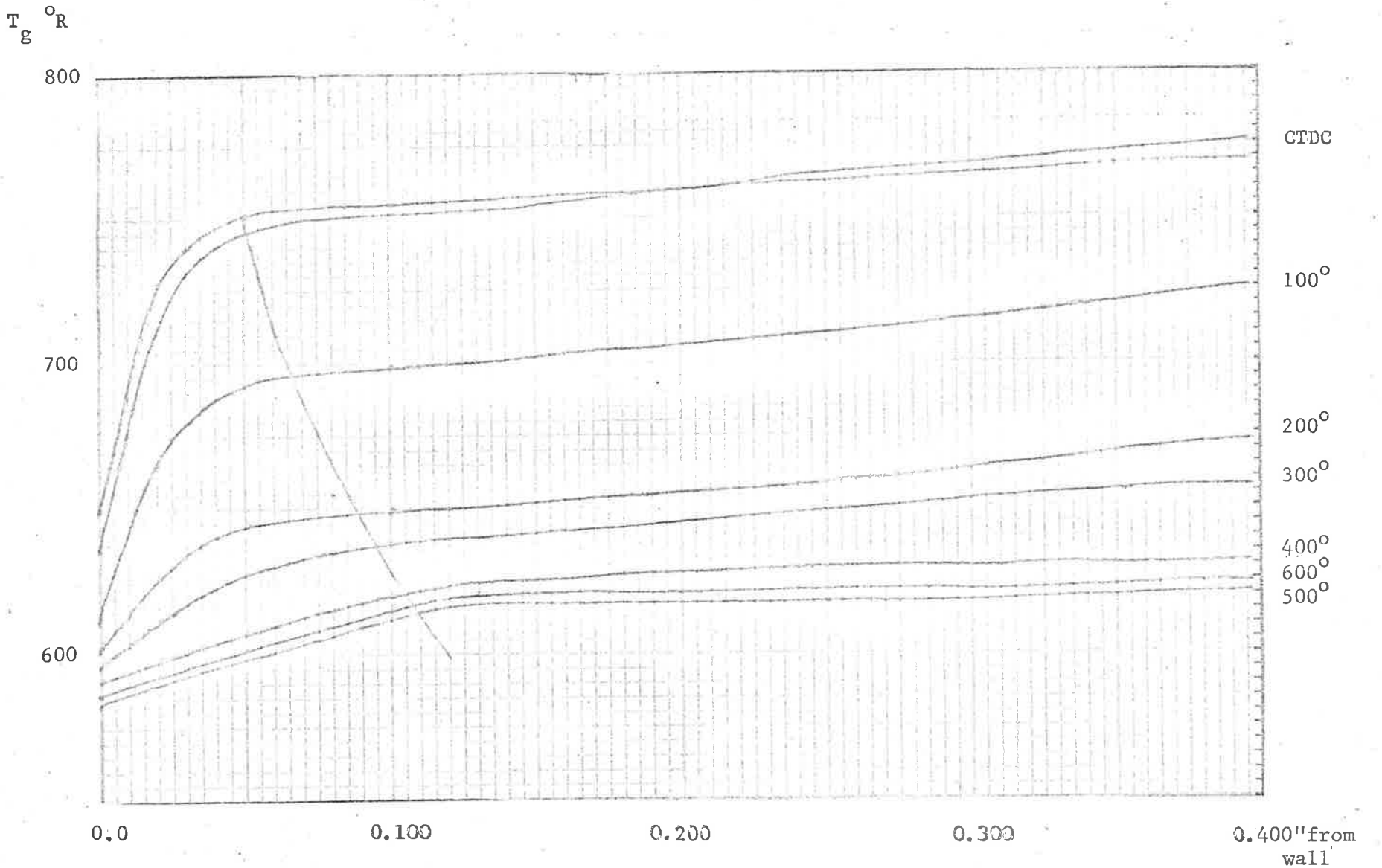

Fig.31 Temperature profiles at 100° crank angle intervals over the cycle of Fig.29 (Inlet, motoring, W.O.T.)

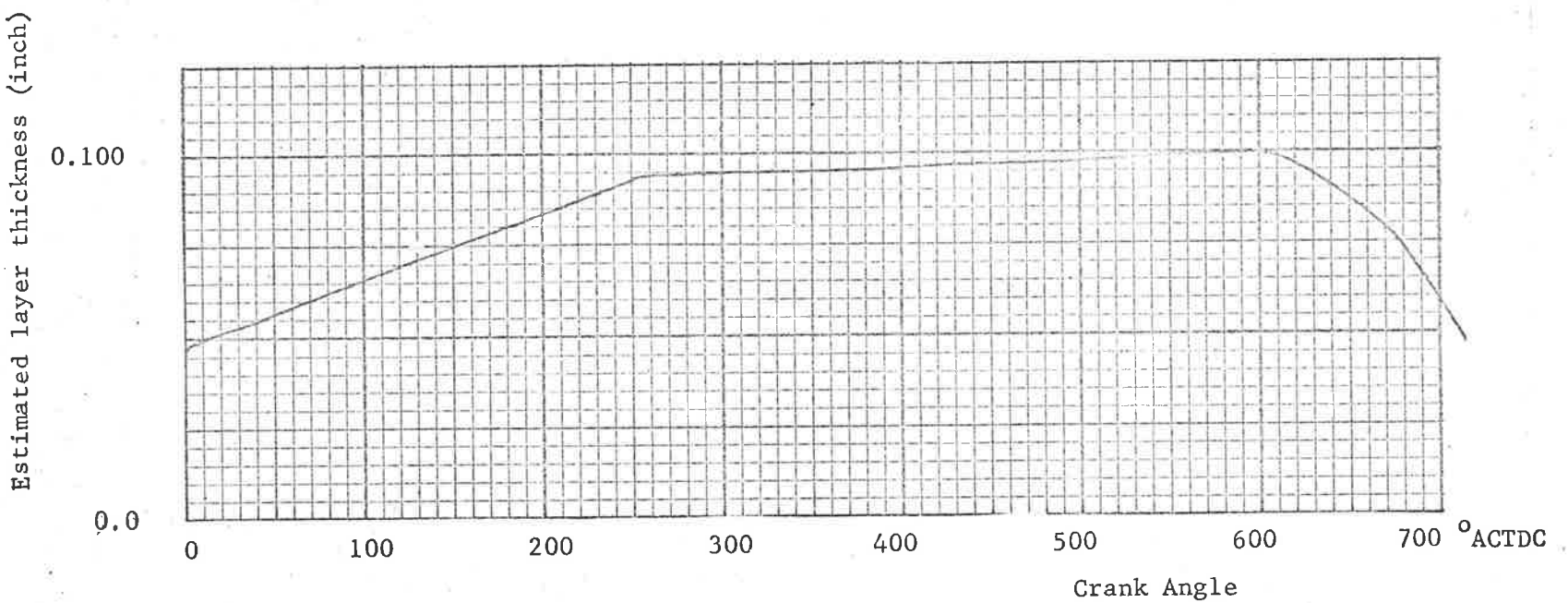

Fig.32 Approximate thermal layer thickness variation over the cycle (from Fig.31 for Inlet region, motoring, W.O.T., 700rpm, 5:1C.R.)

6.4 Fired Engine Results

6.4.1 Steady-state Heat Transfer Data Reduction

A computer programme was written to give mean local and overall heat transfer data from calorimeter probe experiments - using probes of type (a) in Fig. (10).

The heat transfer data reduction programme is given in Fig. (5) Appendix A4. A sample of these results is presented in Fig. (33). The computed local mean heat transfer coefficients presented here are incorrect because they were measured with large diameter uncorrected thermocouples (0.008" Ø wire), within the boundary layer (x = 0.100").

Still the trends of steady-state heat transfer with variation of engine parameters are of interest.

(1) In Fig. (34), the mean heat transfer rates at the Inlet and Exhaust regions together with the overall rate of heat transferred to the water jackets is plotted as a function of r.p.m. The overall data are also compared to the findings of Stambuleanu (6), Walker (12) and Annand (5).

This in general confirms Annand's prediction that for the overall heat transfer to the engine coolant

$$\bar{q}_{\text{ss overall}} \propto (N)^{0.5 \text{ to } 0.8}$$

(an exponent of 0.6 is evident in Fig. (34)).

However, for local heat transfer to the calorimeter probe, Eichelberg's prediction held approximately true i.e.

$$\bar{q}_{\text{ss local}} \propto (N)^{0.33}$$

(an exponent of 0.2 is evident in Fig. (34)).

This tends to confirm the results discussed in Section 6.3.1.

(2) The local and overall data from the aforementioned programme were also compared on the basis of fuel flow rate, Fig. (35),

with predictions of Annand (5) and Alcock (57) with fair agreement as follows:

(a) $\bar{q}_{\text{ss overall}} \propto (F)^{1.1}$ where F = fuel flow rate

Alcock determined exponents between 0.75 to 1.25.

(b) $\bar{q}_{\text{local}} \propto (F)^{0.53}$ for the exhaust region

& $\bar{q}_{\text{local}} \propto (F)^{0.41}$ for the inlet region

Annand gives exponents of 0.48 to 0.50 and 0.65 to 0.76, respectively.

(3) Data for variation of steady-state heat transfer rate with spark advance are given in Fig. (36).

The overall heat transfer rate to the engine coolant can be seen to follow a similar trend as that shown by Taylor (58), although the level is somewhat lower.

The summation of the heat transfer rates to probes located at the Inlet, Exhaust and Knock-Zone regions is compared in Fig. (37) with the data of Ku (55) for a calorimeter probe located inside the combustion chamber gases.

The trends coincide almost exactly up to 35^{o} spark advance but diverged for earlier spark.

However, this is not surprising since audible knocking was often detected at advanced spark settings during this series of tests.

The variation of gas temperature with spark advance as measured by the large thermocouple within the boundary layer is shown in Fig. (38) for conditions of w.o.t. at 7:1 C.R. using 95 octane fuel.

For all r.p.m. there is coincidental agreement with the statement by Hottel, (59) that the unburned gas temperature near the end of combustion is approximately 100°F higher for each 20° increase in spark advance.

This could not be confirmed for the bulk gas region by traversing tests, since, as mentioned earlier, the fine wire thermocouple repeatedly failed during traverses in the exhaust region.

(4) During the engine performance calibration (Section 5.1), spark plug tip temperatures were also taken using a specially made spark plug. These temperatures are shown as a function of mixture strength in Fig. (39) for various r.p.m. These are of incidental interest and were not used directly but a marked decrease of tip temperature on either side of maximum power mixture strength is evident. A similar trend was reported by Brewster & Kerley, (60).

(5) The steady-state knock-zone surface temperature at a given C.R. showed an dependence on fuel Octane No. (Fig. (40)).

For 95 octane fuel at 7:1 C.R. and w.o.t. the knock-zone surface temperature as a function of r.p.m. was considerably lower (75°F) for all spark advance than for 85 octane fuel. Furthermore, the latter rating showed a wider temperature variation with spark advance than the former.

Also for the lower Octane No. a pronounced increase in wall temperature was evident at the lowest speed for all spark.

Comparing this to the dependence of mean heat transfer on spark advance observed in Fig. (37) in (3) above, a possible

connection could be explained as follows:

At a low r.p.m. the fuel of lower octane rating is most susceptible to knocking especially in this end-gas region, see Barden (41).

Therefore, with progressively earlier spark normal combustion gives a decrease in wall temperature and a corresponding increase in heat transfer rate until the onset of knocking is reached. Thereafter, increasing spark advance gives both an increase in wall temperature and also a greatly increased rate of heat transfer to the wall.

6.4.2 Steady-state Gas Temperature Profiles

Mean gas temperature profiles for the Inlet region at 1000 r.p.m., w.o.t. are shown in Fig. (41) for both 5:1 and 7:1 C.R. Mixture strength and spark advance were set for maximum power as determined in Section 5.1.

The gas temperature profile in the knock-zone at 5:1 C.R., 1000 r.p.m. w.o.t. is shown in Fig. (42), while an indication of the variation in the profile with r.p.m. in this region is shown in Fig. (43).

Due to frequent failure of the fine wire (0.001" Ø) thermocouples used in these traverses, the scope of the results is not as extensive as those for the motored engine.

In general, however, the same trends were evident in layer thickness as were discussed for the motored case in Section 5.2.1.

Again, a sub-layer effect was evident in the Inlet region.

The surprising feature of the firing engine temperature profiles is that the total layer thickness is not greatly different to that

```
 CR= 7.0 THROT= 1.000 NOCT= 95
 NSPK= 40 DEG.BTDC
 NRPM=          700       1000       1500       2000       2500
 BHP=          2.54       3.80       6.12       8.40      10.35
 F=             .039       .057       .071       .083       .097  LB/MIN
 A=             .355       .497       .710       .841      1.202  LB/MIN
 F/A=           .109       .115       .100       .098       .081
 A/F=          9.105      8.691      9.933     10.112     12.327
 ECFLO=         38.5       38.5       38.5       42.3       45.6  LB/MIN
 HTRE=       10813.6    11645.4    14556.7    18308.1    21671.4   BTU/HR
PLUG COOLANT RATE=HIGH
INLET SIDE P2WALL(TEST 20),P3GAS(TEST 26)
 CFLO=           .86        .83        .82        .82        .82 LB/MIN
 HTR=          416.8      401.0      434.5      457.6      467.9  BTU/HR
 HFLUX=     277604.5   265163.8   291493.0   309706.5   317740.2  BTU/HFTSQ
 HTC=          425.7      400.5      363.9      374.0      360.2  BTU/HFTSQF
ENGINE HEAT TRANSFER 16/1/63 TO 12/2/63
 CR= 7.0 THROT= 1.000 NOCT= 95
 NSPK= 20 DEG.BTDC
 NRPM=          700       1000       1500       2000       2500
 BHP=          2.84       4.28       6.77       8.57      10.00
 F=             .039       .057       .078       .091       .097  LB/MIN
 A=             .322       .526       .747       .933      1.250  LB/MIN
 F/A=           .120       .108       .104       .097       .077
 A/F=          8.268      9.198      9.574     10.258     12.824
 ECFLO=         58.5       58.5       58.5       58.5       58.5  LB/MIN
 HTRE=        7582.2     9477.8    12637.0    16428.2    18955.6   BTU/HR
PLUG COOLANT RATE=LOW(TESTS 12TO16 AND 31TO35)
INLET SIDE  P2WALL(TEST 12),P3GAS (TEST 31)
 CFLO=           .55        .56        .55        .55        .56 LB/MIN
 HTR=          563.8      580.3      597.3      635.4      602.7  BTU/HR
 HFLUX=     393116.7   406104.6   419474.0   449430.9   423717.3  BTU/HFTSQ
 HTC=          832.8      835.6      751.7      768.2      672.5  BTU/HFTSQF

 CR= 7.0 THROT= 1.000 NOCT= 95
 NSPK= 25 DEG.BTDC
 NRPM=          700       1000       1500       2000       2500
 BHP=          2.82       4.20       6.64       8.80      10.35
 F=             .039       .057       .071       .084       .097  LB/MIN
 A=             .340       .483       .725       .873      1.208  LB/MIN
 F/A=           .114       .118       .098       .096       .080
 A/F=          8.730      8.448     10.138     10.333     12.391
 ECFLO=         58.5       58.5       58.5       58.5       58.5  LB/MIN
 HTRE=        9477.8     9477.8    15164.4    16428.2    22114.8   BTU/HR
PLUG COOLANT RATE=LOW
INLET SIDE  P2WALL(TEST13),P3GAS(TEST32)
 CFLO=           .58        .55        .56        .54        .55 LB/MIN
 HTR=          577.2      334.4      602.7      588.1      616.4  BTU/HR
 HFLUX=     403639.7   212858.4   423717.3   412214.3   434477.8  BTU/HFTSQ
 HTC=          773.2      400.8      797.9      645.0      635.2  BTU/HFTSQF
```

Fig.33 Example of output- Steady State Heat Transfer

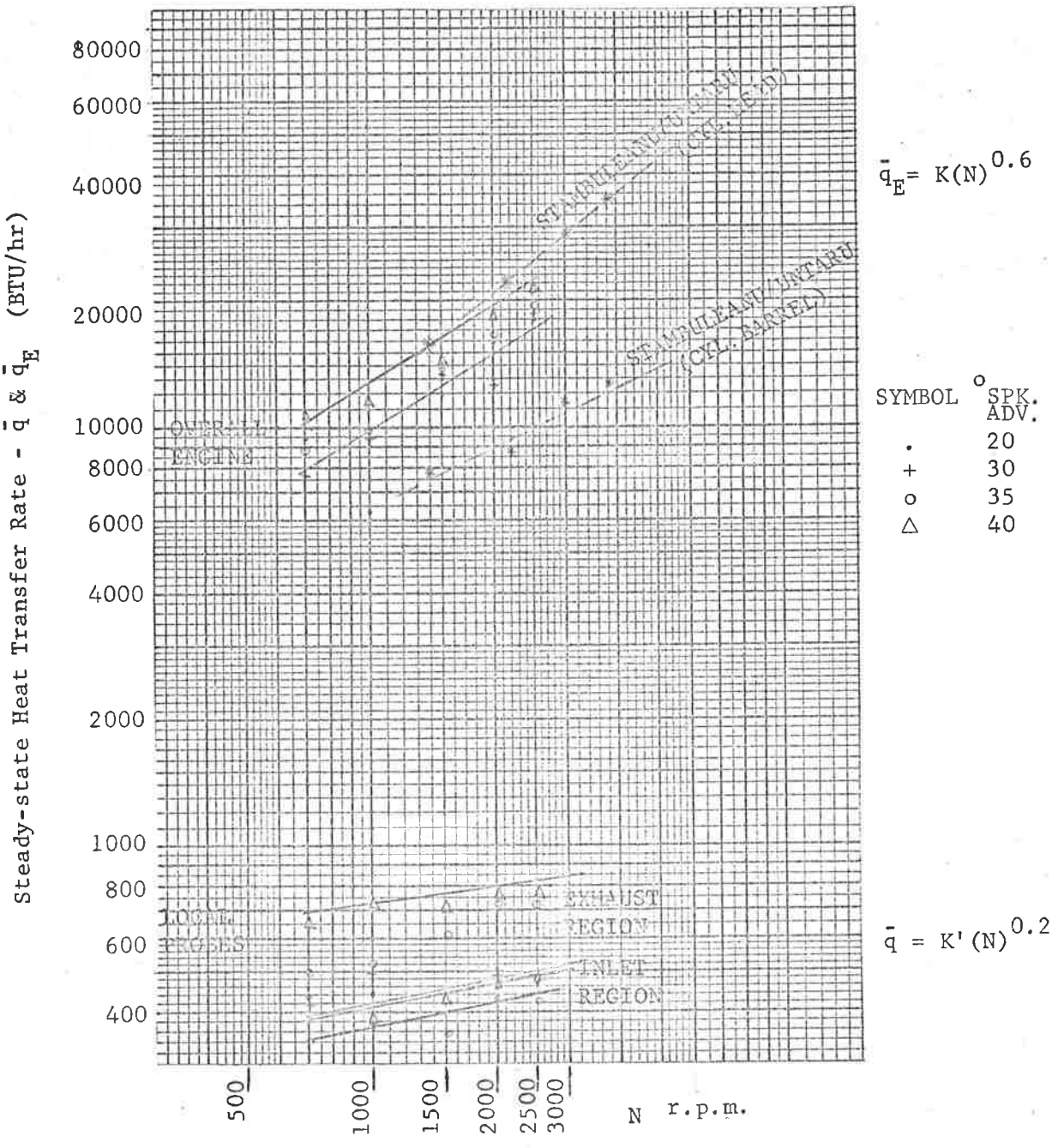

Fig.34 Mean Local & Overall Heat Transfer Rates v. r.p.m.

Fig.35 Mean Local & Overall Heat Transfer Rates v. Fuel Flow Rate from steady-state heat transfer data (F/A ≠ constant)

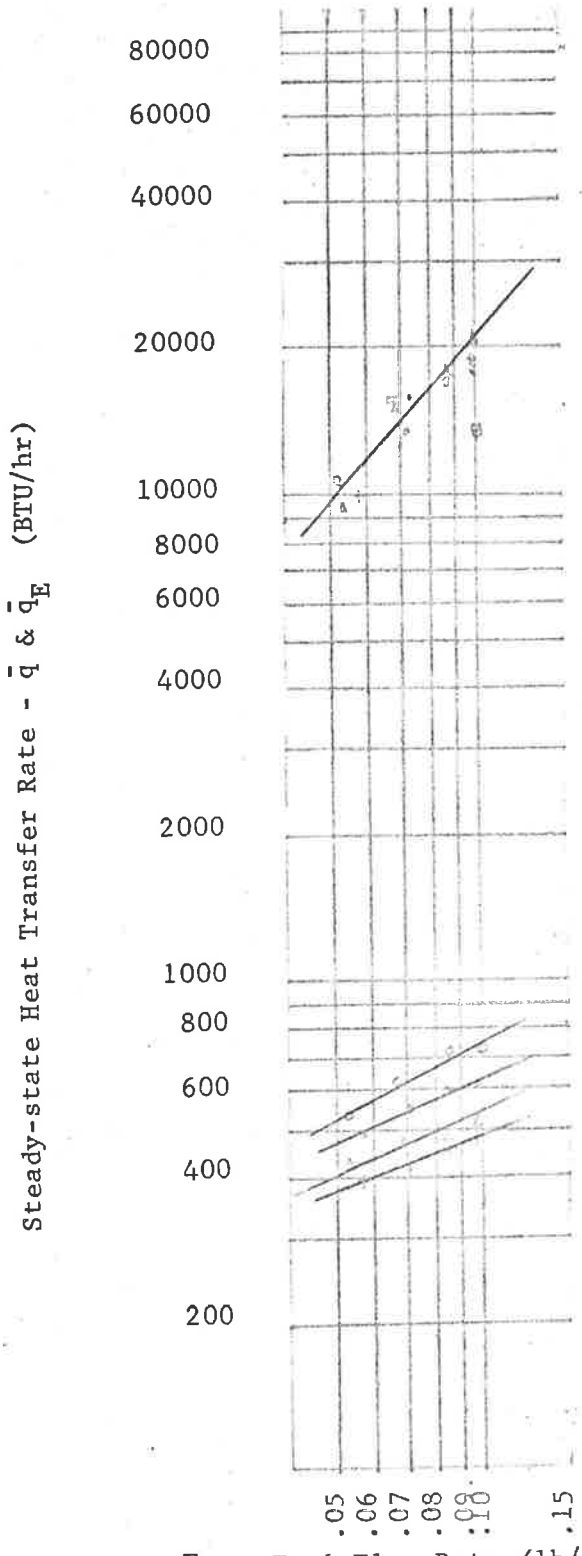

Overall Engine

$\bar{q}_E = K''(F)^{1.1}$

Local Probes

Exhaust (m = 5gal/hr)
Inlet (m = 3gal/hr)
Exhaust (m = 3gal/hr)
Inlet (m = 5gal/hr)

m = probe coolant flow rate.

$\bar{q}_{Ex} = K'(F)^{0.53}$

$\bar{q}_{In} = K(F)^{0.41}$

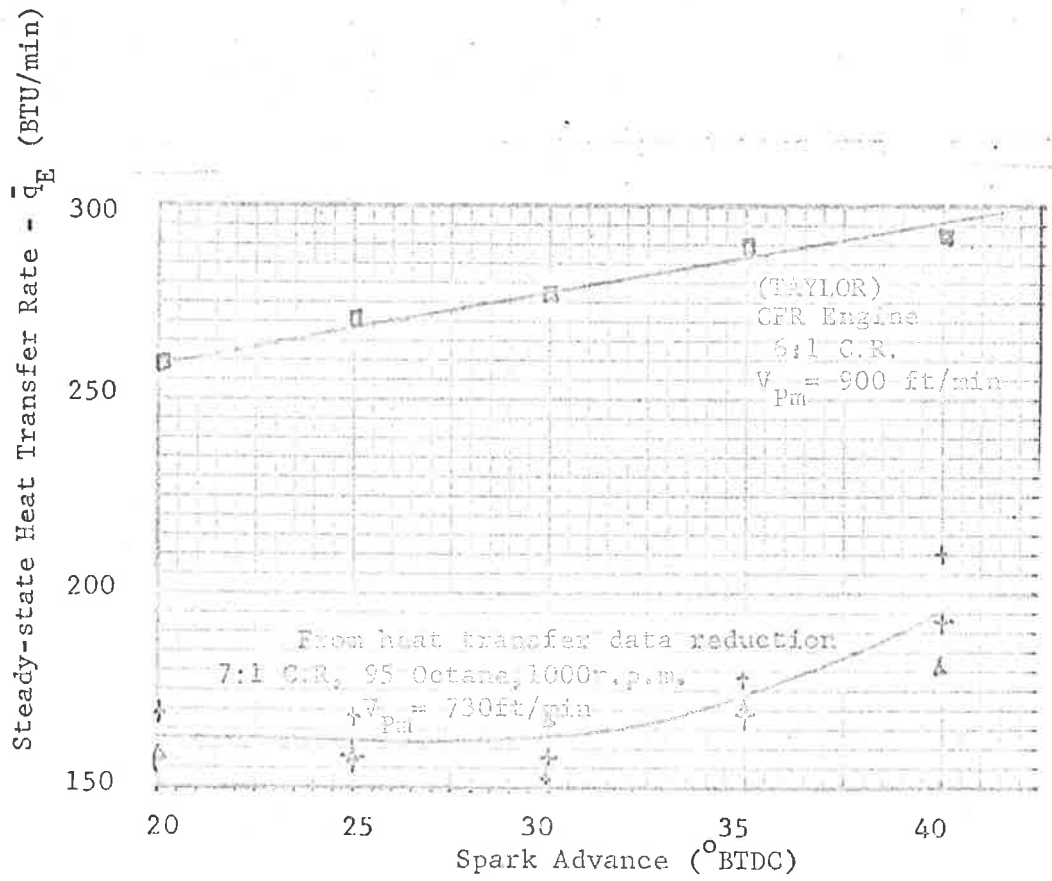

Fig.36 Overall Heat Transfer Rate to engine coolant v. spark advance

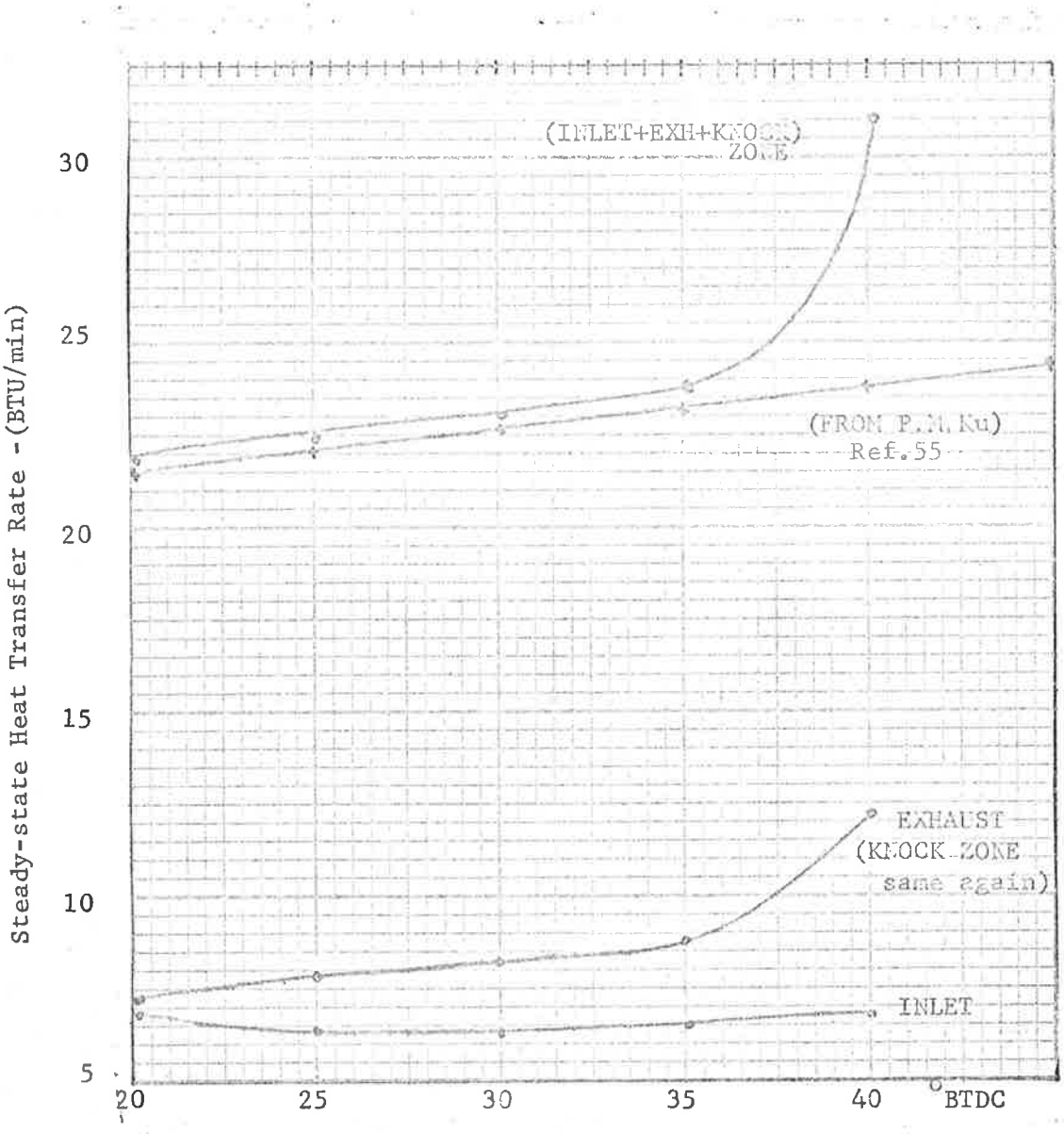

Fig.37 Summation of Steady-state heat transfer to Probes as a function of Spark Advance compared with the data of P.M.Ku (Ref.55)

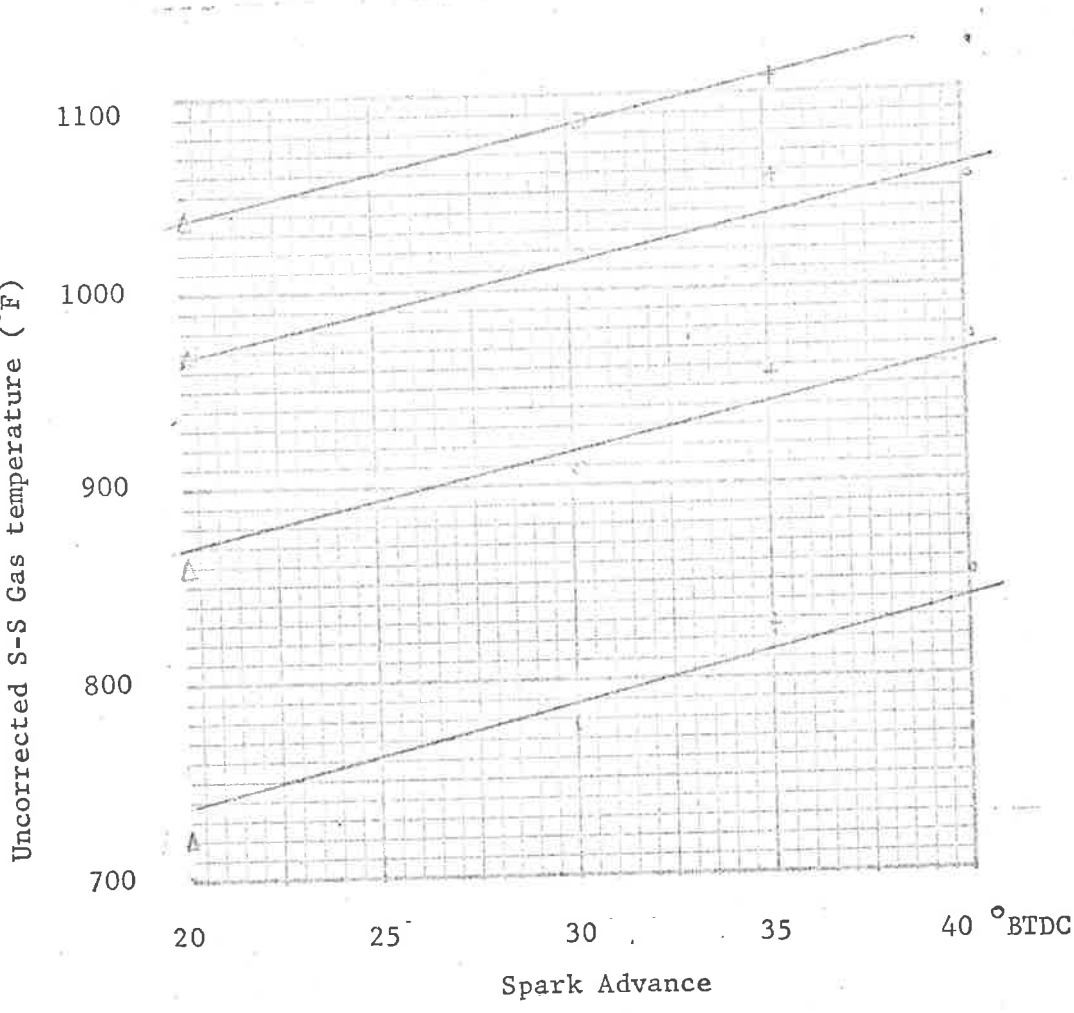

Fig.38 Gas temperature within boundary layer at Exhaust region as a function of Spark Adv. for various r.p.m. - W.O.T.,7:1 C.R.,95 Octane.

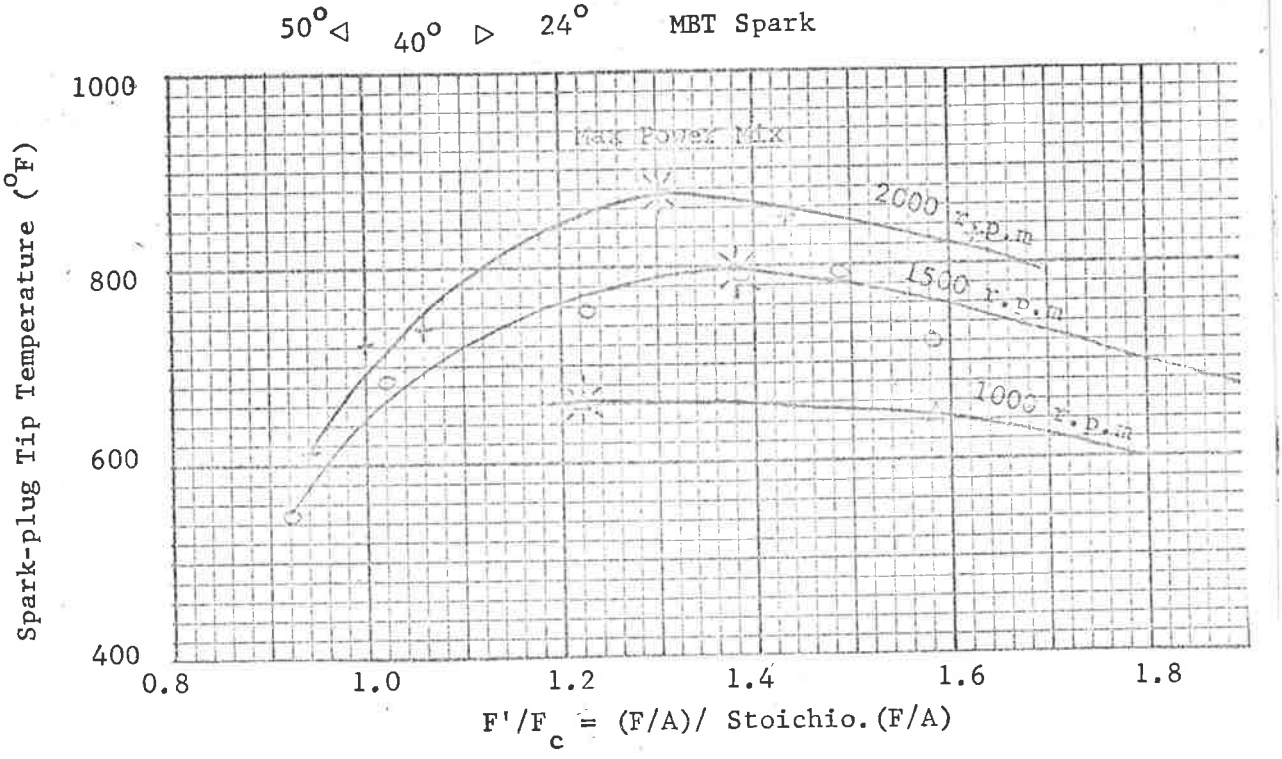

Fig.39 Spark-plug Tip Temperature v. mixture strength for various r.p.m. (Champion L7/TC) From Performance calibration for 5:1 C.R., W.O.T.

SYMBOL	°Spark Adv.
•	20
+	25
o	30
ó	35
△	40

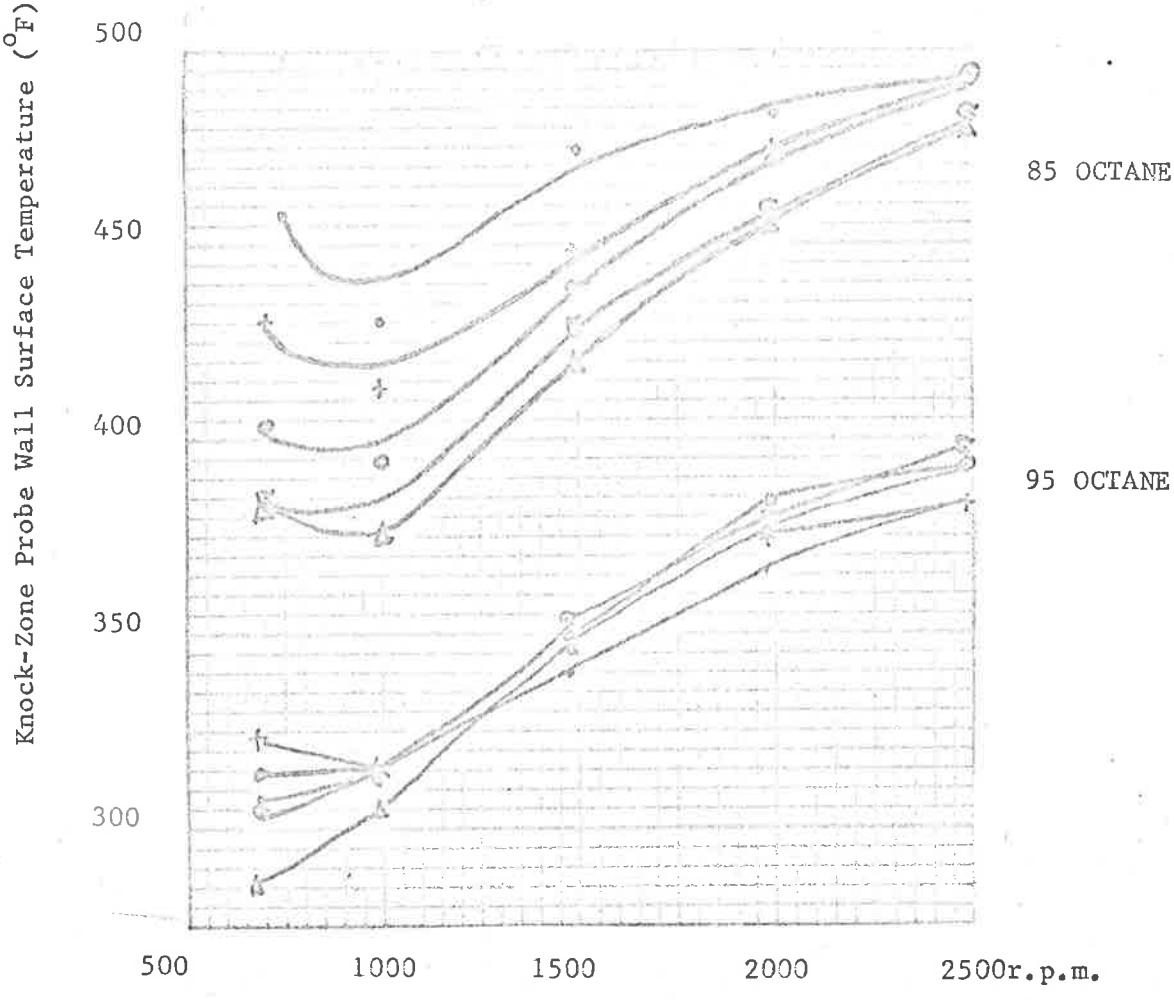

Fig.40 Knock Zone Surface Temperature v. r.p.m. for various spark & two fuel ratings 7:1 C.R., W.O.T.

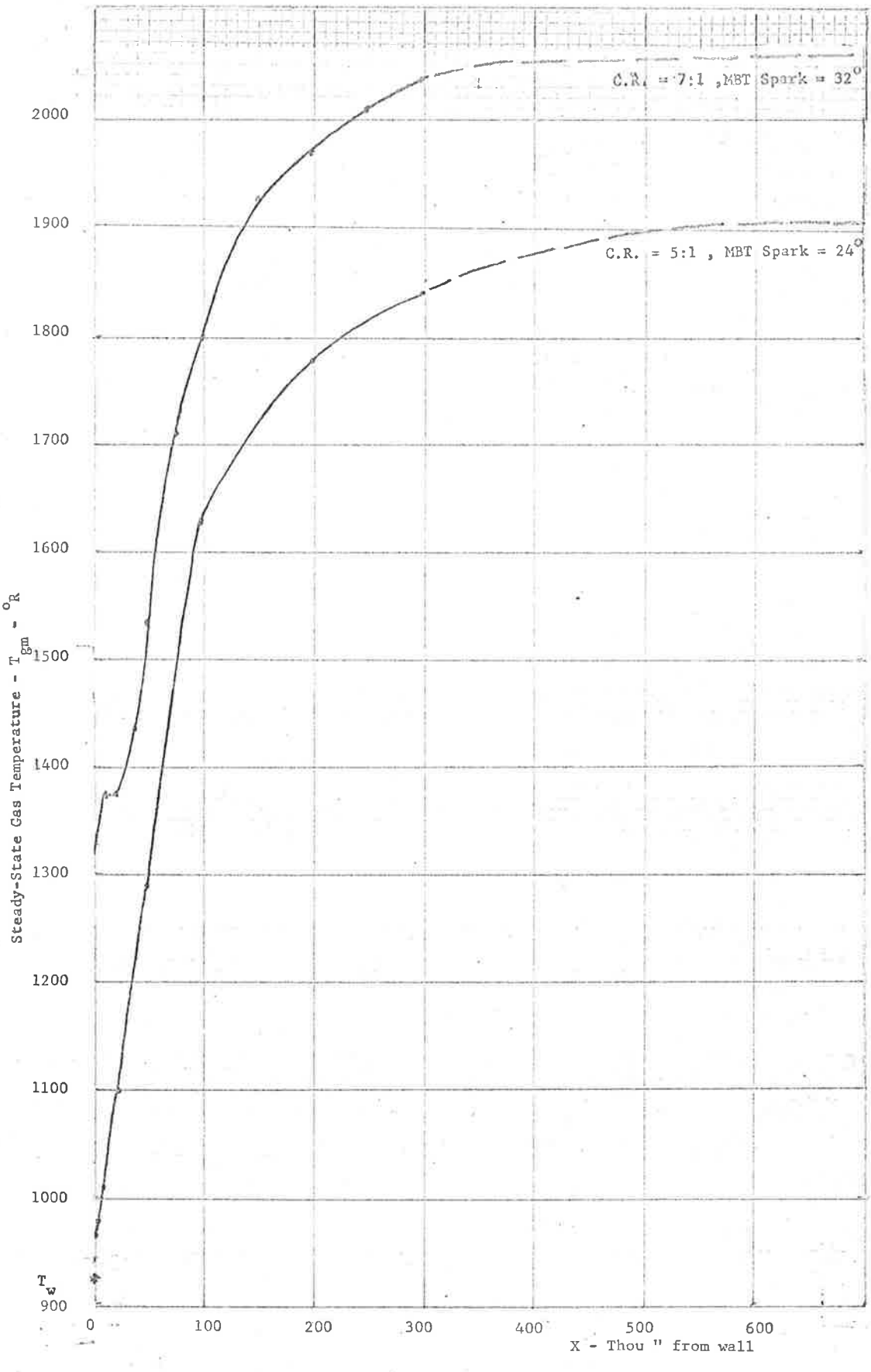

Fig.41 Steady-State Gas Temperature Traverse - INLET region for two C.R. at 1000 r.p.m., W.O.T., $(F/A)_{max.power}$

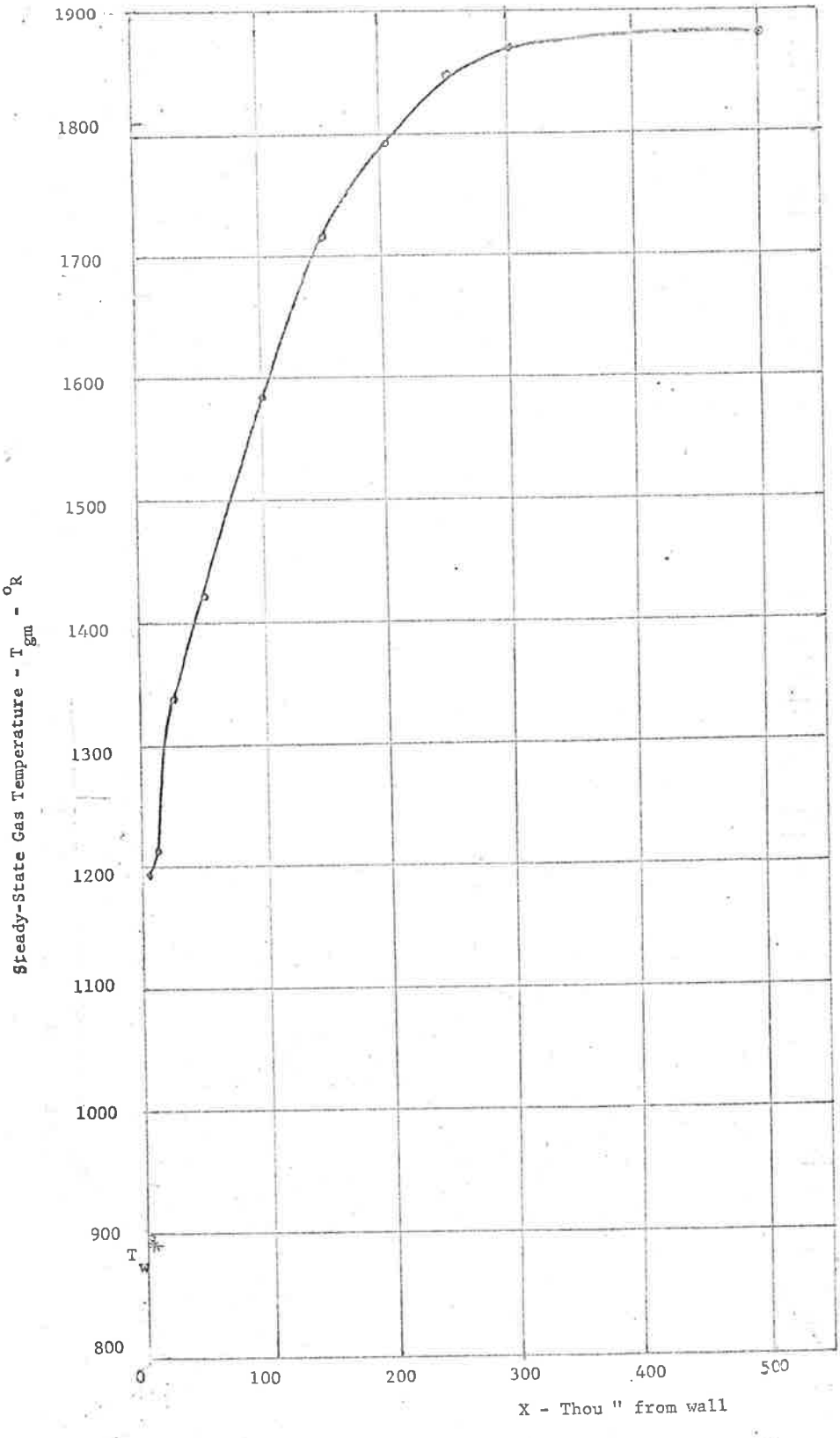

Fig 42 Steady-State Gas Temperature Traverse - KNOCK ZONE
1000 r.p.m., W.O.T., 32° spark, 5:1 C.R., $(F/A)_{max.power}$

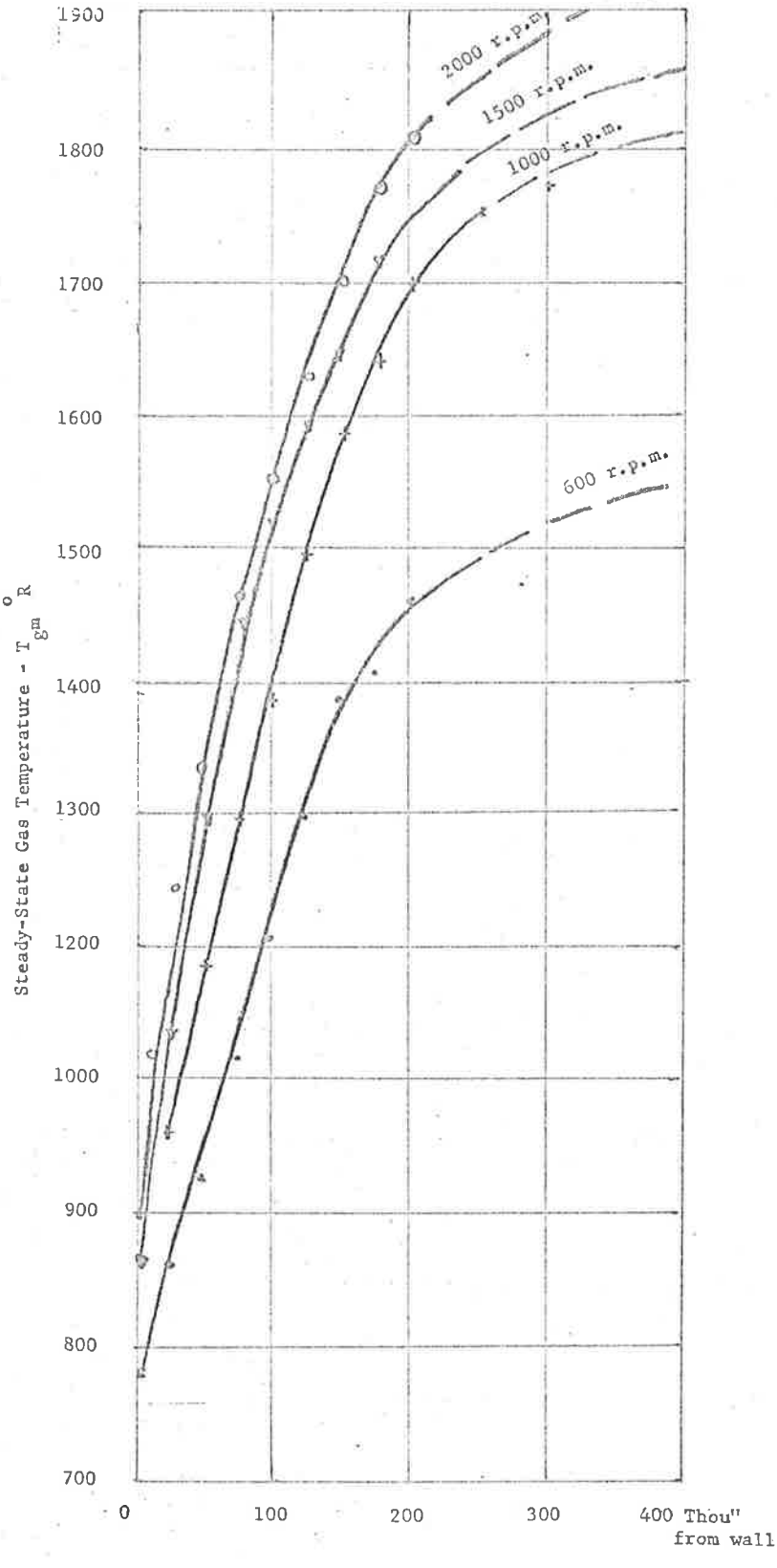

Fig.43 Variation of Knock-Zone Temperature Profile with r.p.m. C.R. 5:1, W.O.T., MBT, $(F/A)_{max.power}$

for the motored case.

6.4.3 Fired Engine Cyclic Heat Transfer Results

General

The main results presented in Figs. (44) to (97) are for the knock-zone location. It was thought that this would be a relatively quiescent region (under non-knocking conditions) remote from the influence of gas velocity fluctuations induced by valve motion.

Most of the data are for part throttle engine operation since some early difficulty was experienced at w.o.t. with short life of the gas thermocouple. Later in the test period it was found that deterioration of the ceramic cement used to seal the thermocoax in the hyperdermic tubing, Fig. (11), resulted in a high velocity gas leakage to atmosphere along the tubing. This rapidly eroded the thermocouple wires causing failure only a few firing cycles after ignition.

Thus, initial data was taken at 1/4 throttle with maximum power mixture strength and MBT ignition. This problem was eventually solved by using a different type of cement. Thereafter, a w.o.t. firing run could continue for over an hour without damage to the thermocouple.

All data are herein presented in the form of a single cycle computer plot for each variable using the plotting routine given in Appendix A4. This gave an approximate indication only since the plotting interval (abscissa) was usually 20^{o} crank angle (sometimes 10^{o}).

More detailed information for each variable over a given single

cycle is presented in the respective output lists at 5^{o} crank angle intervals.

It should be noted that the plots for heat transfer coefficient were deliberately limited to +1500 and -500 BTU/hr.ft^{2}F^{o} at the discontinuities in order to obtain a reasonable scale over the continuous portion of the cycle.

Although a number of consecutive cycles were recorded at any one setting, it was not the purpose of this study to obtain data truly representative of a particular setting over a range of conditions. For such 'average' cycles a smoothing technique or alternatively a statistical selection method such as that used by Overbye (33) would be required.

It appeared to be more desirable to observe accurately the phase relations between the recorded variables in each unique cycle in order to compare these with the predictions of the opposing theories given in Section (2). Also, comparisons were sought between the experimental heat transfer coefficients for a given cycle, and those calculated for that identical cycle by the various empirical methods described earlier.

Discussion of data presented

Typical instantaneous heat transfer data for the fired engine at 1/4 throttle, 5:1 C.R., 85 octane fuel are shown in Figs. (44) to (60) for the knock-zone.

These data compare sets of simultaneous wall temperature, heat flux, gas temperature, pressure and experimental heat transfer coefficient. Each set is repeated for each of four insertions of the gas thermocouple i.e. x = 0.200, 0.250, 0.400 and 0.450" respectively.

The latter two are probably outside the thermal layer as estimated in the previous section, Thus the heat transfer coefficients at these insertions represent more correctly the true quasi-steady heat transfer coefficient under these conditions.

The former two sets, Figs. (44) to (61) are included to show details of the discontinuous heat transfer coefficient arising when the gas temperature is measured within the thermal layer. These will be discussed later.

It is evident from phase comparisons of all gas and wall temperature cycles that the gas temperature invariably peaks at about 90 - 100° crank angle before the wall temperature. In most cases also the heat flux cycle bears a remarkable similarity in form to the gas temperature cycle e.g. see Figs. (56) and (58).

The repeatability of this evidence tends to directly confirm the theoretical predictions of the Heat Transfer Coefficient Concept in Section (2) as opposed to those of the Temperature Profile Method.

There appears to be at least one discontinuity in the heat transfer coefficient cycle, e.g. Fig. (52), when the gas-wall temperature difference becomes very small while the heat flux is still finite.

Of the continuous part of the heat transfer coefficient cycle, the peak occurs at approximately 100° ACTDC in all cases i.e. just before e.v.o. This would seem to bear some relationship to the observation by Stambuleanu (6) mentioned earlier that a more directed gas flow occurs as the exhaust phase progresses.

Also the expansion-exhaust (working) phase is approximated by a modified Eichelberg expression in which the mean piston speed is replaced by the instantaneous piston velocity and the whole expression is arbitrarily multiplied by a factor of 3. This supports the technique of Pflaum (22), equation (17) to some extent. However, instantaneous piston velocity does not appear to be a suitable parameter over the induction compression phase due to the fact that it becomes zero and changes direction every 180^{o} crank angle.

Again, in agreement with Henien (30), the original formula of Eichelberg appears to predict heat transfer coefficients much lower than the experimental values of Fig. (52). Nusselt's expression as modified by Stambuleanu (equations 5, 6, 7, 8) for the various phases was also tried but this appeared to be even less successful than Eichelberg's formula.

Fig. (81) gives a typical spectrum of the heat transfer coefficient calculated from the moduli of heat flux and that of gas-wall temperature difference, showing those harmonics of engine frequency which predominate.

A modification of Pfriem's method of expressing the instantaneous heat transfer coefficient in polar form (equation (48)) was investigated. A synthesised heat transfer coefficient was computed as follows:

$$h(\theta) = h_{ss} + \sum_{K=1}^{KK} h(K) \cdot \cos(K\theta - \phi_K) \qquad (78)$$

where hss = the mean heat transfer coefficient

i.e.; $h_{ss} = (q/A)_{ss} / (T_{gm} - T_{wm})$

θ = crank angle , ϕ_k = phase angle

$$h(k) = \frac{(q/A)_k}{\sqrt{(T_g(k) - T_w(k))^2 \cos^2 k\theta + (T_g(k) - T_w(k))^2 \sin^2 k\theta}}$$

k = the harmonic No. 1, 2 ------ kk

Since ϕ_k was unknown for each harmonic, the corresponding phase angle of heat flux for each harmonic was used.

An example of the resulting synthesised coefficient is shown in Fig. (82) for the data of x = 0.400".

While the magnitudes do not correspond to the previous quasi-steady values, Fig. (70), it is interesting to observe that a large peak is observed approximately at CTDC and a secondary peak appears at the e.v.o. position as was evident in the previous direct plot of heat transfer coefficient.

This observation could indicate that apart from the discontinuity near CTDC when the concept of a quasi-steady heat transfer coefficient breaks down (due to the phase lag between driving temperature difference and heat flux); the most rigorous part of the cycle from the heat transfer point of view occurs near e.v.o. The heat transfer at this time may thus bear a direct relationship to piston velocity as suggested by Stambuleanu and this will be investigated further in the next section.

It can be seen that negative heat transfer coefficients result from the experimental data over certain parts of the cycle. A viable physical explanation for these negative values and for the variations over the induction-compression phase is difficult to provide.

In most data analysed the instantaneous heat flux passes through zero and becomes negative at approximately 400^{o}ACTDC or soon after the i.v.o. point. This in itself is not unexpected since the cooler incoming charge would be expected to absorb heat from the wall; i.e. to reverse the direction of heat flow.

The apparently perplexing feature of all the data is, that there is not an immediate reversal of gas-wall temperature difference consequent on this negative heat flux. This gives rise to the meaningless negative coefficients observed.

Due to the aforementioned theoretical phase lag considerations it seems obvious that an immediate and simultaneous change in the direction of heat flux and driving temperature difference cannot take place. As the driving temperature difference becomes smaller, so oscillations are introduced into the experimental heat transfer coefficient curve. These become noticeable discontinuities when the gas temperature drops below wall temperature (e.g. see Fig. (52)).

Some doubt was therefore cast on the mean measurements, especially that of heat flux.

Considering the data for Fig. (47), if negative heat fluxes were to be avoided, a mean value of 67.0 BTU/ft^2sec would be required instead of the value of 30.0 used.

Fig. (83) shows a cycle of heat transfer coefficient when this artificially high value of mean heat flux is used.

Henein (30) does show a heat transfer coefficient cycle of almost exactly this form with peaks of practically identical magnitude. However, his computations were carried out by desk calculator from ordinates read from polaroid photographs of the variables at only 68 points per cycle. Furthermore he appears to have ignored the phase differences when computing the cycle of heat transfer coefficient from his data.

Since the gas and wall temperatures used by Henein were much the same as those used in this investigation, his mean heat flux would need to assume the high value above in order to obtain positive coefficients over the cycle. This value seems to be impossibly high compared to the measured steady-state heat flux when conservatively corrected for heat leakage into the probe through the fastening end. Also, the values of mean heat flux reported herein are of the order reported by Overbye (33) and Bennethum (39).

It is also logical that part throttle operation would give rise to lower mean values and probably wider swings than for w.o.t.

A large negative heat flux would thus seem probable, but this is incompatible with the observation that bulk gas temperature is always greater than wall temperature.

When the mean wall temperature is artificially adjusted so that wall temperature does become greater than the gas temperature during the negative heat flux period the resulting heat transfer coefficient is shown in Fig. (84). This can be seen to again

contain discontinuities over the induction-compression phase. The periodicity of the discontinuities seems to be quite well defined at between 120 and 130° crank angle.

It would appear to be more than a coincidence that compensated hot wire anemometer measurements of instantaneous mass flow rate carried out by Horvatin (32), 1965, for a motored engine show an exactly similar pattern.

A cycle of mass flow rate as measured by Horvatin is reproduced in Fig. (85). It can be seen that the similarity to Fig. (84) is pronounced. The first half of the cycle shows a continuous variation while the second half exhibits violent oscillations of approximately 120° period.

This coincidence emphasises the need for instantaneous gas velocity measurements over the fired engine cycle simultaneously with the information recorded in this study.

A rather conjectural physical explanation for the variations of heat transfer near the wall observed in Fig. (84) is as follows:

(1) Soon after i.v.o. the new charge is inducted and begins to rapidly cool the gas in the main core. The new charge also acts as a vast absorber of heat from the walls and net heat flux becomes "negative".

(2) Compression begins to reduce the flow of heat from the walls to the gas soon after i.v.c.

The discontinuities in this part of the cycle may very well be a result of velocity fluctuations penetrating the boundary layer. Alternatively the rapid rate of decrease in layer thickness itself at this time (see Fig. (32)) may be a contributing factor.

(3) It seems an anomaly that the heat transferred to the wall should rapidly decrease again during the compression stroke (2) - (3) but as the piston crown approaches CTDC it comes in close proximity to the measuring point and an alternative path becomes available for heat transfer from the region,

(4) Ignition arrests heat transfer from the walls and combustion reverses the flow of heat until soon after CTDC.

(5) As the piston begins on the expansion stroke the burning gases are exposed to a progressively greater wall area and so the specific amount of heat transferred at the measuring point at first drops rapidly.

(6) However, this trend is again quickly reversed as combustion progresses (or perhaps due to afterburning) and the heat transfer to the walls reaches a peak finite value at approximately the e.v.o. position when a steady continuous drop in gas-wall heat transfer occurs due to mass efflux and the cycle returns to (1) above.

It should be stressed that this explanation is purely arbitrary and a more rigorous study should be made of the inter-relationship between the variables over the various phases.

Several miscellaneous heat transfer coefficient cycles are shown in Figs. (86) to (97) for w.o.t. knock-zone conditions at 7:1 C.R. Figs. (96) and (97) illustrate the pronounced delay and reduction in heat transfer caused by retarding the ignition from the MBT point.

It can also be seen that the w.o.t. data both for the experimental heat transfer coefficient cycle and for that synthesised by

Pfriem's method, (Figs. (94) and (95)) do not display the pronounced peak at e.v.o. as did the 1/4 w.o.t. data.

6.4.4 Fired Engine Cyclic Traverse

Further light was thrown onto the occurence of negative heat flux over the induction-compression phase when a cyclic gas temperature traverse was performed near the knock-zone wall in the firing engine. The results of this traverse are presented in Fig. (98) From this figure it will be noticed that at 400^{o} ACTDC or very soon after i.v.o., the gas temperature near the wall becomes greater than that further away and remains so over the whole inlet phase. Thus, during this phase for the layer from 0.000" to 0.075" it appears that heat is transferred away from the wall in the gas layer.

The observation that the gas temperature at the wall is greater than the wall temperature appears to be due to experimental error since a stagnant gas pocket may be formed when the thermocouple is withdrawn to the wall.

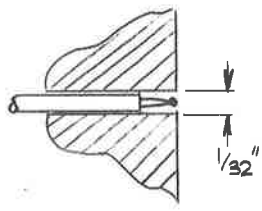

Also, the wall-thermocouple radiation error is likely to increase in this position.

However, the notion of "hot gas pockets" has been proposed by previous workers to justify the peculiarities of their heat flux measurements e.g. (29), (33), (39).

Knight (29) who also observed negative heat fluxes from his experiments on a diesel engine, suggested that these may be caused

by a mass of gas being compressed and expanded against the wall surface thermocouple with a loss of heat greater than that experienced by the main body of the gas.

Overbye (33) and Bennethum (39) observed similar effects which they attributed to either two-dimensional heat transfer to the probe or to the existance of a stagnant hot gas layer at the probe position.

Since a cyclic gas temperature traverse for the Inlet region, Fig. (99), exhibited no such reversal of gradient near i.v.o., the phenomenon observed is probably characteristic of the knock-zone or stagnant 'end-gas' region.

Another possible physical explanation which could be put forward concerns the possible catalytic action of deposits on the adjacent gas layer.

Bennethum (39) reported that the ignition temperature of deposits not containing phosphorus could be as low as 750^{o}F. The deposits observed on the knock-zone probe were certainly quite different to those at the Inlet position opposite. The latter were usually black, soft and thick, while the former were greyish-white, hard and much thinner.

Thus there is the possibility of a hot gas layer due to deposit glowing. However, since an effort was made to keep the probes deposit-free in order not to affect the steady-state heat transfer to the calorimeter, this possibility was not investigated in detail.

6.5 Correlations

Due to the discontinuities observed in the experimental heat transfer coefficient over the induction and compression strokes, correlations were only attempted for the continuous portion of the

working phase.

These were as follows:

(1) A correlation between experimental data and that predicted by Annand's equation, equation (22). The Nusselt No. was defined for this purpose as:

$$(Nu) = (h_i D_p / 3600 K_g)$$

where D_p = piston diameter (ft.)

h_i = instantaneous experimental heat transfer coefficient (BTU/hr.ft^{2}F^o)

and $(Re) = V_{Pm} \cdot D_p \cdot \rho_g / \mu_g$

where V_{Pm} = mean piston speed (ft/sec)

ρ_g = gas density = $0.00169\ (P/14.7)^{0.7}$ (lb/ft^3)

μ_g = gas mixture dynamic viscosity (Appendix A2), (lb/ft.sec).

Note: the above mixture properties are not strictly applicable to this part of the cycle but are used in the absence of suitable data including the products of combustion and probable dissociation effects.

This correlation is plotted in log-log form in Fig. (100). For the data of Fig. (79) an exponent of 0.5 resulted for this phase compared to Annand's value of 0.7.

(2) When the instantaneous piston velocity was used instead of the mean piston speed in Reynold's No., the resulting exponent Fig. (100), was 0.33 which agreed with that given by Eichelberg.

(3) Kadrinov's theory (equation (62)) was used at 10^{o} intervals over the expansion stroke. The number of degrees of freedom, n, was calculated from the specific heat data (Appendix A2) at the corresponding temperature and pressure for each point.

It was thought that since Kadrinov's formula represented conductive heat transfer only, a better correlation for convection might result if this value for h were subtracted from the experimental value.

i.e. $h_{conv.} = (h_{expt.} - h_{Kadrinov})$

However, the effect of velocity was still of the form $(Nu) = a\ (Re)^{0.33}$.

Thus convection is probably the dominant mode over this part of the cycle.

(4) In order to examine further the effect of h on conduction through the gas, the following model was considered.

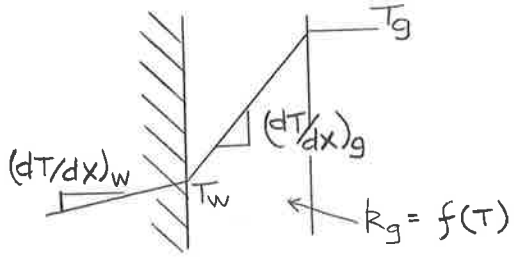

$$(q/A) = kg\ (dT/dx)_g$$

and from experimental measurement

$$h_i = \left(\frac{q/A}{Tg-Tw}\right)_i$$

thus, we can write:

$$h_i = \frac{Kg(dT/dx)}{(Tg-Tw)}g$$

If we plot h_i versus $\left(\frac{dT/dx}{Tg-Tw}\right)_i$

then the slope of the curve over the various phases should equal the value of the relevant gas thermal conductivity.

This does in fact agree fairly well during the compression phase with the mixture conductivity data applicable to this phase (Appendix A2).

Thus for this phase the measured instantaneous temperature gradients in the gas are verified.

1000RPM WOT=0.25*FIRING 2ND/FD SPK, KZ COMPENSATED, X=0.200
ANALOG TAPE A TRANSMITTAL TAPE 1550

PERIODS SELECT 1 INITIAL 1 MAX 3

NUMBER OF POINTS SELECT 439 INITIAL 149 FINAL 588 TOTAL 2902

PERIOD VARIATION 437 438

CYCLE COUNT	CRANK ANG	PRESSURE	GAS TEMP.	WALL TEMP.	HEAT FLUX	PISTON VELOC.	HEAT TRANSFER COEFF. EXPT.	FICH VP.	FICH. VPM
1	0	9.334E+01	7.418E+02	7.790E+02	-6.598E+01	0.	1.088E+04	0.	1.43E+01
2	4	1.127E+02	8.454E+02	7.787E+02	-4.398E+01	2.046E+00	-1.928E+03	6.420E+01	1.994E+01
3	10	1.384E+02	1.011E+03	7.783E+02	-3.170E+01	4.447E+00	-5.913E+02	1.001E+02	4.813E+01
4	15	1.497E+02	1.199E+03	7.793E+02	-1.445E+01	6.068E+00	-1.254E+03	1.379E+02	5.803E+01
5	20	2.014E+02	1.407E+03	7.807E+02	1.194E+01	7.042E+00	6.930E+01	1.790E+02	6.838E+01
6	25	2.206E+02	1.627E+03	7.827E+02	4.324E+01	7.761E+00	1.889E+02	2.178E+02	7.781E+01
7	30	2.443E+02	1.849E+03	7.853E+02	7.432E+01	1.146E+01	2.711E+02	2.550E+02	8.628E+01
8	35	2.521E+02	1.065E+03	7.883E+02	1.044E+02	1.301E+01	3.254E+02	2.745E+02	9.009E+01
9	40	2.458E+02	2.048E+03	7.914E+02	1.284E+02	1.447E+01	3.837E+02	2.929E+02	9.210E+01
10	45	2.293E+02	2.209E+03	7.945E+02	1.441E+02	1.587E+01	3.711E+02	2.991E+02	9.15?E+01
11	50	2.067E+02	2.319E+03	7.974E+02	1.529E+02	1.679E+01	3.748E+02	2.975E+02	8.906E+01
12	55	1.825E+02	2.408E+03	8.000E+02	1.582E+02	1.770E+01	3.732E+02	2.900E+02	8.82?E+01
13	60	1.605E+02	2.449E+03	8.025E+02	1.737E+02	1.846E+01	3.752E+02	2.791E+02	8.697E+01
14	65	1.432E+02	2.449E+03	8.048E+02	1.807E+02	1.898E+01	3.847E+02	2.647E+02	8.480E+01
15	70	1.312E+02	2.448E+03	8.072E+02	1.984E+02	1.935E+01	4.107E+02	2.550E+02	7.307E+01
16	75	1.234E+02	2.381E+03	8.095E+02	1.985E+02	1.954E+01	4.198E+02	2.459E+02	8.972E+01
17	80	1.180E+02	2.241E+03	8.119E+02	2.028E+02	1.965E+01	5.019E+02	2.339E+02	8.444E+01
18	85	1.129E+02	2.120E+03	8.141E+02	2.071E+02	1.968E+01	5.714E+02	2.268E+02	8.294E+01
19	90	1.060E+02	1.993E+03	8.161E+02	2.089E+02	1.970E+01	6.446E+02	2.248E+02	8.922E+01
20	95	9.964E+01	1.873E+03	8.179E+02	2.077E+02	1.966E+01	7.098E+02	1.922E+02	6.655E+01
21	100	9.190E+01	1.757E+03	8.195E+02	2.048E+02	1.949E+01	7.595E+02	1.781E+02	5.232E+01
22	105	8.469E+01	1.723E+03	8.209E+02	2.013E+02	1.916E+01	7.681E+02	1.688E+02	4.984E+01
23	110	7.877E+01	1.747E+03	8.221E+02	1.981E+02	1.865E+01	7.390E+02	1.588E+02	4.827E+01
24	115	7.451E+01	1.817E+03	8.233E+02	1.957E+02	1.804E+01	7.092E+02	1.550E+02	4.751E+01
25	120	7.142E+01	1.884E+03	8.244E+02	1.935E+02	1.744E+01	6.819E+02	1.511E+02	4.736E+01
26	125	7.027E+01	1.941E+03	8.254E+02	1.905E+02	1.687E+01	6.727E+02	1.473E+02	4.733E+01
27	130	7.211E+01	1.955E+03	8.263E+02	1.955E+02	1.624E+01	6.504E+02	1.421E+02	4.705E+01
28	135	7.861E+01	1.913E+03	8.270E+02	1.790E+02	1.570E+01	6.489E+02	1.355E+02	4.629E+01
29	140	8.794E+01	1.804E+03	8.275E+02	1.704E+02	1.511E+01	6.270E+02	1.271E+02	4.505E+01
30	145	9.921E+01	1.747E+03	8.277E+02	1.415E+02	8.898E+00	6.002E+02	1.139E+02	4.357E+01
31	150	1.019E+02	1.736E+03	8.277E+02	1.439E+02	7.481E+00	5.792E+02	1.058E+02	4.216E+01
32	155	9.859E+01	1.802E+03	8.276E+02	1.493E+02	6.796E+00	5.519E+02	9.945E+01	4.108E+01
33	160	9.184E+01	1.833E+03	8.273E+02	1.492E+02	5.118E+00	5.310E+02	9.091E+01	4.042E+01
34	165	8.205E+01	1.844E+03	8.268E+02	1.490E+02	3.842E+00	5.201E+02	8.197E+01	4.009E+01
35	170	6.864E+01	1.859E+03	8.263E+02	1.424E+02	2.543E+00	5.181E+02	7.111E+01	3.990E+01
36	175	4.906E+01	1.840E+03	8.259E+02	1.533E+02	1.282E+00	5.206E+02	5.556E+01	3.981E+01
37	180	2.464E+01	1.888E+03	8.256E+02	1.499E+02	-6.819E-07	5.206E+02	4.377E-01	3.979E+01
38	185	4.266E+01	1.915E+03	8.256E+02	1.410E+02	-1.282E+00	5.160E+02	5.990E+01	3.988E+01
39	190	3.774E+01	1.770E+03	8.256E+02	1.268E+02	-2.563E+00	4.880E+02	5.940E+01	3.975E+01
40	195	3.270E+01	1.713E+03	8.257E+02	1.499E+02	-3.842E+00	4.443E+02	5.191E+01	3.929E+01
41	200	2.717E+01	1.641E+03	8.259E+02	1.503E+02	-5.114E+00	3.907E+02	4.149E+01	3.843E+01
42	205	2.364E+01	1.617E+03	8.275E+02	1.498E+02	-6.394E+00	3.731E+02	4.048E+01	3.805E+01
43	210	2.098E+01	1.581E+03	8.262E+02	1.732E+02	-7.661E+00	2.972E+02	4.020E+01	3.762E+01
44	215	1.987E+01	1.568E+03	8.251E+02	1.431E+02	-8.898E+00	2.808E+02	4.097E+01	3.758E+01
45	220	1.971E+01	1.581E+03	8.243E+02	1.434E+02	-1.011E+01	2.790E+02	4.204E+01	3.722E+01
46	225	1.980E+01	1.678E+03	8.237E+02	1.430E+02	-1.130E+01	2.164E+02	4.457E+01	3.720E+01
47	230	1.983E+01	1.666E+03	8.234E+02	1.470E+02	-1.246E+01	1.516E+02	4.587E+01	3.179E+01
48	235	1.993E+01	1.620E+03	8.232E+02	1.353E+02	-1.357E+01	1.772E+02	4.532E+01	3.131E+01
49	240	1.984E+01	1.610E+03	8.229E+02	1.190E+02	-1.463E+01	1.794E+02	4.419E+01	3.074E+01
50	245	1.956E+01	1.620E+03	8.227E+02	1.487E+02	-1.563E+01	1.563E+02	4.414E+01	3.028E+01
51	250	1.891E+01	1.648E+03	8.222E+02	1.416E+02	-1.657E+01	1.117E+02	4.299E+01	3.013E+01
52	255	1.801E+01	1.647E+03	8.216E+02	1.286E+02	-1.734E+01	2.476E+02	4.089E+01	3.040E+01
53	260	1.760E+01	1.627E+03	8.211E+02	1.594E+02	-1.805E+01	2.383E+02	3.910E+01	3.103E+01
54	265	1.841E+01	1.554E+03	8.206E+02	1.431E+02	-1.844E+01	2.144E+02	3.635E+01	3.178E+01
55	270	1.924E+01	1.570E+03	8.202E+02	1.442E+02	-1.900E+01	2.124E+02	3.800E+01	3.237E+01
56	275	1.940E+01	1.543E+03	8.199E+02	1.429E+02	-1.940E+01	2.181E+02	3.909E+01	3.256E+01
57	280	1.956E+01	1.513E+03	8.197E+02	1.425E+02	-1.965E+01	2.247E+02	3.942E+01	3.231E+01
58	285	1.898E+01	1.504E+03	8.194E+02	1.417E+02	-1.986E+01	2.314E+02	3.843E+01	3.175E+01
59	290	1.824E+01	1.475E+03	8.190E+02	1.124E+02	-1.995E+01	2.264E+02	3.749E+01	3.112E+01
60	295	1.783E+01	1.454E+03	8.184E+02	3.494E+01	-1.999E+01	2.095E+02	3.707E+01	3.071E+01
61	300	1.784E+01	1.444E+03	8.181E+02	3.206E+01	-1.844E+01	1.842E+02	3.728E+01	3.068E+01
62	305	1.851E+01	1.444E+03	8.175E+02	2.755E+01	-1.778E+01	1.577E+02	3.154E+01	2.105E+01
63	310	1.904E+01	1.455E+03	8.169E+02	2.431E+01	-1.639E+01	1.376E+02	3.232E+01	2.165E+01
64	315	2.044E+01	1.459E+03	8.163E+02	2.213E+01	-1.457E+01	1.239E+02	3.295E+01	2.222E+01
65	320	2.101E+01	1.469E+03	8.158E+02	2.115E+01	-1.443E+01	1.183E+02	3.151E+01	2.251E+01
66	325	2.102E+01	1.467E+03	8.153E+02	2.057E+01	-1.701E+01	1.142E+02	3.000E+01	2.268E+01
67	330	2.051E+01	1.441E+03	8.149E+02	1.984E+01	-1.145E+01	1.131E+02	3.505E+01	2.212E+01
68	335	1.974E+01	1.431E+03	8.145E+02	1.902E+01	-9.761E+00	1.051E+02	3.427E+01	2.162E+01
69	340	1.900E+01	1.418E+03	8.140E+02	1.837E+01	-7.943E+00	9.534E+01	3.352E+01	2.121E+01
70	345	1.893E+01	1.424E+03	8.134E+02	1.276E+01	-6.040E+00	7.434E+01	3.014E+01	2.110E+01
71	350	1.908E+01	1.439E+03	8.129E+02	1.000E+01	-4.047E+00	5.752E+01	3.441E+01	2.131E+01
72	355	1.970E+01	1.447E+03	8.123E+02	7.970E+00	-2.045E+00	4.493E+01	3.507E+01	2.176E+01
73	360	2.037E+01	1.448E+03	8.119E+02	5.899E+00	-2.130E+00	3.910E+01	3.777E+01	2.221E+01
74	365	2.072E+01	1.447E+03	8.114E+02	5.175E+00	-2.045E+00	3.411E+01	3.717E+01	2.241E+01
75	370	2.065E+01	1.454E+03	8.110E+02	4.552E+00	-4.047E+00	3.443E+01	4.467E+01	2.225E+01
76	375	1.974E+01	1.439E+03	8.106E+02	4.251E+00	-6.040E+00	3.582E+01	5.154E+01	2.189E+01
77	380	1.847E+01	1.410E+03	8.102E+02	5.213E+00	-7.943E+00	3.127E+01	5.435E+01	2.088E+01
78	385	1.762E+01	1.377E+03	8.098E+02	5.242E+00	-9.741E+00	2.470E+01	5.584E+01	2.006E+01
79	390	1.695E+01	1.343E+03	8.092E+02	5.522E+00	-1.145E+01	1.724E+00	5.708E+01	1.961E+01
80	395	1.685E+01	1.310E+03	8.087E+02	-2.435E+00	1.701E+01	-1.820E+01	5.868E+01	1.912E+01
81	400	1.729E+01	1.279E+03	8.081E+02	-5.567E+00	1.443E+01	-4.257E+01	5.975E+01	1.912E+01
82	405	1.795E+01	1.243E+03	8.075E+02	-8.215E+00	1.170E+01	-6.743E+01	6.288E+01	1.925E+01
83	410	1.852E+01	1.214E+03	8.069E+02	-1.047E+01	1.170E+01	-9.257E+01	6.444E+01	1.939E+01
84	415	1.843E+01	1.179E+03	8.063E+02	-1.240E+01	1.177E+01	-1.198E+02	6.492E+01	1.909E+01
85	420	1.817E+01	1.143E+03	8.057E+02	-1.429E+01	1.866E+01	-1.524E+02	6.472E+01	1.864E+01
86	425	1.740E+01	1.110E+03	8.051E+02	-1.635E+01	1.894E+01	-1.931E+02	6.273E+01	1.802E+01
87	430	1.694E+01	1.084E+03	8.045E+02	-1.844E+01	1.935E+01	-2.404E+02	6.109E+01	1.744E+01
88	435	1.653E+01	1.057E+03	8.039E+02	-2.111E+01	1.955E+01	-2.889E+02	6.000E+01	1.708E+01
89	440	1.641E+01	1.040E+03	8.032E+02	-2.351E+01	1.955E+01	-3.296E+02	5.800E+01	1.707E+01
90	445	1.719E+01	1.041E+03	8.025E+02	-2.554E+01	1.940E+01	-3.574E+02	5.990E+01	1.737E+01
91	450	1.806E+01	1.065E+03	8.019E+02	-2.751E+01	1.909E+01	-3.783E+02	6.217E+01	1.783E+01
92	455	1.880E+01	1.087E+03	8.013E+02	-2.917E+01	1.864E+01	-3.948E+02	6.303E+01	1.822E+01
93	460	1.914E+01	1.086E+03	8.008E+02	-3.047E+01	1.805E+01	-4.224E+02	6.284E+01	1.836E+01
94	465	1.905E+01	1.053E+03	8.000E+02	-3.198E+01	1.736E+01	-4.680E+02	6.174E+01	1.817E+01
95	470	1.829E+01	1.018E+03	7.993E+02	-3.521E+01	1.651E+01	-5.158E+02	5.886E+01	1.771E+01
96	475	1.765E+01	1.017E+03	7.988E+02	-3.785E+01	1.563E+01	-6.243E+02	5.589E+01	1.714E+01
97	480	1.693E+01	9.994E+02	7.979E+02	-4.040E+01	1.443E+01	-7.212E+02	5.323E+01	1.668E+01
98	485	1.644E+01	9.873E+02	7.970E+02	-4.247E+01	1.303E+01	-8.048E+02	5.134E+01	1.640E+01
99	490	1.701E+01	9.809E+02	7.965E+02	-4.377E+01	1.134E+01	-8.584E+02	5.025E+01	1.661E+01
100	495	1.767E+01	9.747E+02	7.959E+02	-4.420E+01	1.137E+01	-8.702E+02	4.954E+01	1.692E+01
101	500	1.828E+01	9.771E+02	7.953E+02	-4.400E+01	1.011E+01	-8.712E+02	4.951E+01	1.719E+01
102	505	1.844E+01	9.717E+02	7.947E+02	-4.342E+01	8.886E+00	-8.473E+02	4.959E+01	1.724E+01
103	510	1.808E+01	9.609E+02	7.942E+02	-4.351E+01	7.641E+00	-8.151E+02	4.954E+01	1.694E+01
104	515	1.715E+01	9.574E+02	7.937E+02	-4.409E+01	5.986E+00	-1.103E+03	3.985E+01	1.631E+01
105	520	1.606E+01	9.595E+02	7.932E+02	-4.511E+01	5.114E+00	-1.414E+03	3.493E+01	1.553E+01
106	525	1.520E+01	9.754E+02	7.928E+02	-4.691E+01	3.843E+00	-2.039E+03	3.034E+01	1.484E+01
107	530	1.500E+01	9.913E+02	7.923E+02	-4.818E+01	2.543E+00	-3.194E+03	2.589E+01	1.447E+01
108	535	1.557E+01	9.178E+02	7.918E+02	-4.924E+01	1.282E+00	-6.733E+03	2.059E+01	1.452E+01
109	540	1.673E+01	8.840E+02	7.909E+02	-4.939E+01	-2.564E-06	-1.352E+04	2.484E-01	1.492E+01
110	545	1.806E+01	8.457E+02	7.904E+02	-4.844E+01	-1.282E+00	-1.142E+04	2.200E+01	1.551E+01
111	550	1.900E+01	8.264E+02	7.900E+02	-4.775E+01	-2.563E+00	-6.895E+03	2.477E+01	1.610E+01
112	555	1.925E+01	8.098E+02	7.895E+02	-4.727E+01	-3.842E+00	-4.425E+03	3.384E+01	1.655E+01
113	560	1.876E+01	8.076E+02	7.891E+02	-4.777E+01	-5.116E+00	-1.453E+03	3.774E+01	1.678E+01
114	565	1.779E+01	8.407E+02	7.886E+02	-4.903E+01	-6.394E+00	-1.032E+03	4.072E+01	1.682E+01
115	570	1.688E+01	1.011E+03	7.881E+02	-5.179E+01	-7.661E+00	-8.378E+02	4.119E+01	1.680E+01
116	575	1.653E+01	1.047E+03	7.875E+02	-5.481E+01	-8.898E+00	-7.659E+02	4.574E+01	1.692E+01
117	580	1.700E+01	1.041E+03	7.870E+02	-5.672E+01	-1.011E+01	-7.442E+02	4.875E+01	1.728E+01
118	585	1.819E+01	1.048E+03	7.865E+02	-5.782E+01	-1.130E+01	-7.984E+02	5.200E+01	1.776E+01
119	590	1.948E+01	1.078E+03	7.857E+02	-5.758E+01	-1.258E+01	-9.607E+02	5.471E+01	1.809E+01
120	595	2.075E+01	1.115E+03	7.852E+02	-5.628E+01	-1.385E+01	-1.280E+03	5.602E+01	1.800E+01
121	600	2.107E+01	1.123E+03	7.848E+02	-5.378E+01	-1.484E+01	-2.288E+03	5.861E+01	1.780E+01
122	605	2.015E+01	1.088E+03	7.844E+02	-5.043E+01	-1.543E+01	-6.208E+03	5.966E+01	1.744E+01
123	610	1.845E+01	1.042E+03	7.838E+02	-5.234E+01	-1.563E+01	-1.103E+04	6.066E+01	1.693E+01
124	615	1.694E+01	1.015E+03	7.838E+02	-5.254E+01	-1.574E+01	5.784E+03	6.009E+01	1.653E+01
125	620	1.612E+01	1.007E+03	7.834E+02	-5.329E+01	-1.580E+01	1.604E+04	6.007E+01	1.616E+01
126	625	1.640E+01	1.140E+03	7.830E+02	-5.389E+01	-1.584E+01	-4.254E+03	5.173E+01	1.695E+01
127	630	1.856E+01	1.474E+03	7.825E+02	-5.407E+01	-1.590E+01	-2.298E+03	5.491E+01	1.672E+01
128	635	2.164E+01	1.734E+03	7.822E+02	-5.324E+01	-1.604E+01	-1.455E+03	5.737E+01	1.808E+01
129	640	2.407E+01	1.892E+03	7.819E+02	-5.149E+01	-1.625E+01	-1.175E+03	6.028E+01	1.971E+01
130	645	2.487E+01	1.870E+03	7.814E+02	-4.994E+01	-1.654E+01	-1.134E+03	7.117E+01	2.082E+01
131	650	2.487E+01	1.769E+03	7.814E+02	-4.874E+01	-1.695E+01	-1.298E+03	7.457E+01	2.129E+01
132	655	3.113E+01	1.823E+03	7.812E+02	-4.845E+01	-1.808E+01	-1.725E+03	7.420E+01	2.132E+01
133	660	3.243E+01	1.819E+03	7.809E+02	-4.898E+01	-1.868E+01	-2.482E+03	7.349E+01	2.119E+01
134	665	3.488E+01	1.942E+03	7.805E+02	-4.944E+01	-1.877E+01	-3.047E+03	7.480E+01	2.200E+01
135	670	3.933E+01	1.988E+03	7.802E+02	-4.967E+01	-1.879E+01	-2.634E+03	7.809E+01	2.353E+01
136	675	4.614E+01	2.033E+03	7.800E+02	-4.977E+01	-1.879E+01	-1.680E+03	8.491E+01	2.596E+01
137	680	5.479E+01	2.215E+03	7.799E+02	-4.981E+01	-1.881E+01	-1.114E+03	9.181E+01	2.890E+01
138	685	6.381E+01	2.459E+03	7.799E+02	-4.976E+01	-1.891E+01	-8.073E+02	9.726E+01	3.169E+01
139	690	7.149E+01	2.556E+03	7.800E+02	-3.287E+01	-1.914E+01	-6.721E+02	9.886E+01	3.381E+01
140	695	7.664E+01	2.544E+03	7.802E+02	-2.956E+01	-1.943E+01	-7.021E+02	9.864E+01	3.474E+01
141	700	7.913E+01	2.472E+03	7.804E+02	-2.752E+01	-1.990E+01	-1.103E+03	9.767E+01	3.390E+01
142	705	7.913E+01	2.423E+03	7.803E+02	-3.021E+01	-2.068E+01	-2.047E+03	9.685E+01	3.225E+01
143	710	7.873E+01	2.467E+03	7.800E+02	-3.593E+01	-2.188E+01	3.873E+03	9.699E+01	3.119E+01
144	715	8.378E+01	2.779E+03	7.795E+02	-4.711E+01	-2.348E+01	2.038E+03	9.230E+01	3.158E+01

1000RPM WOT=0.25*FIRING 2ND/FD SPK, KZ COMPENSATED, X=0.200

Fig.44

Data set X = 0.2

CONVERT TAPE NO 4
1000RPM WOT*0.25,FIRING 24DEG SPK, KZ COMPENSATED, X=0.200
ANALOG TAPE 6 TRANSMITTAL TAPE 1558

SERIAL	RUN	CHANNEL	TYPE	NO PERIODS	COEFF
7	12	123	1	1	15

NO POINTS	INITIAL	MAX PERIODS
439	1	7

FOURIER COEFFICIENTS AT CYCLE FREQUENCY

CYCLE HARMONIC	TEMPERATURE (DEG.F)	PHASE ANGLE CRANK ANG.DEG)
1	22.192	123.79
2	7.627	154.41
3	3.719	195.48
4	1.535	219.28
5	.790	226.70
6	.895	226.14
7	.672	265.16
8	.239	299.21
9	.223	236.95
10	.409	251.72
11	.372	292.01
12	.136	325.22
13	.080	211.92
14	.249	273.58
15	.208	323.61
	8.3E+02	7.8E+02

Fig.45 Fourier Coefficients of Wall Temperature cycle following

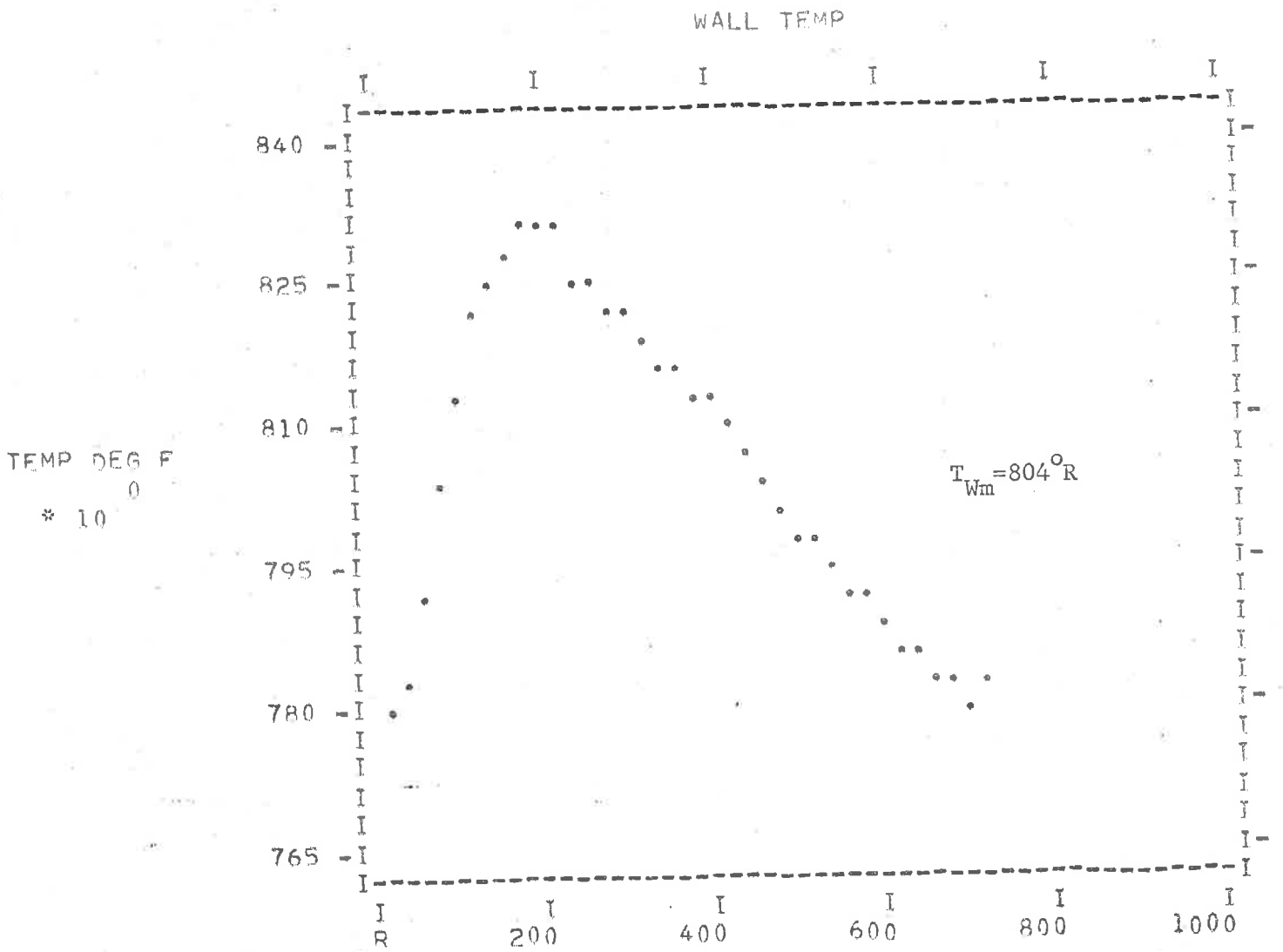

Fig.46 Wall Temperature cycle

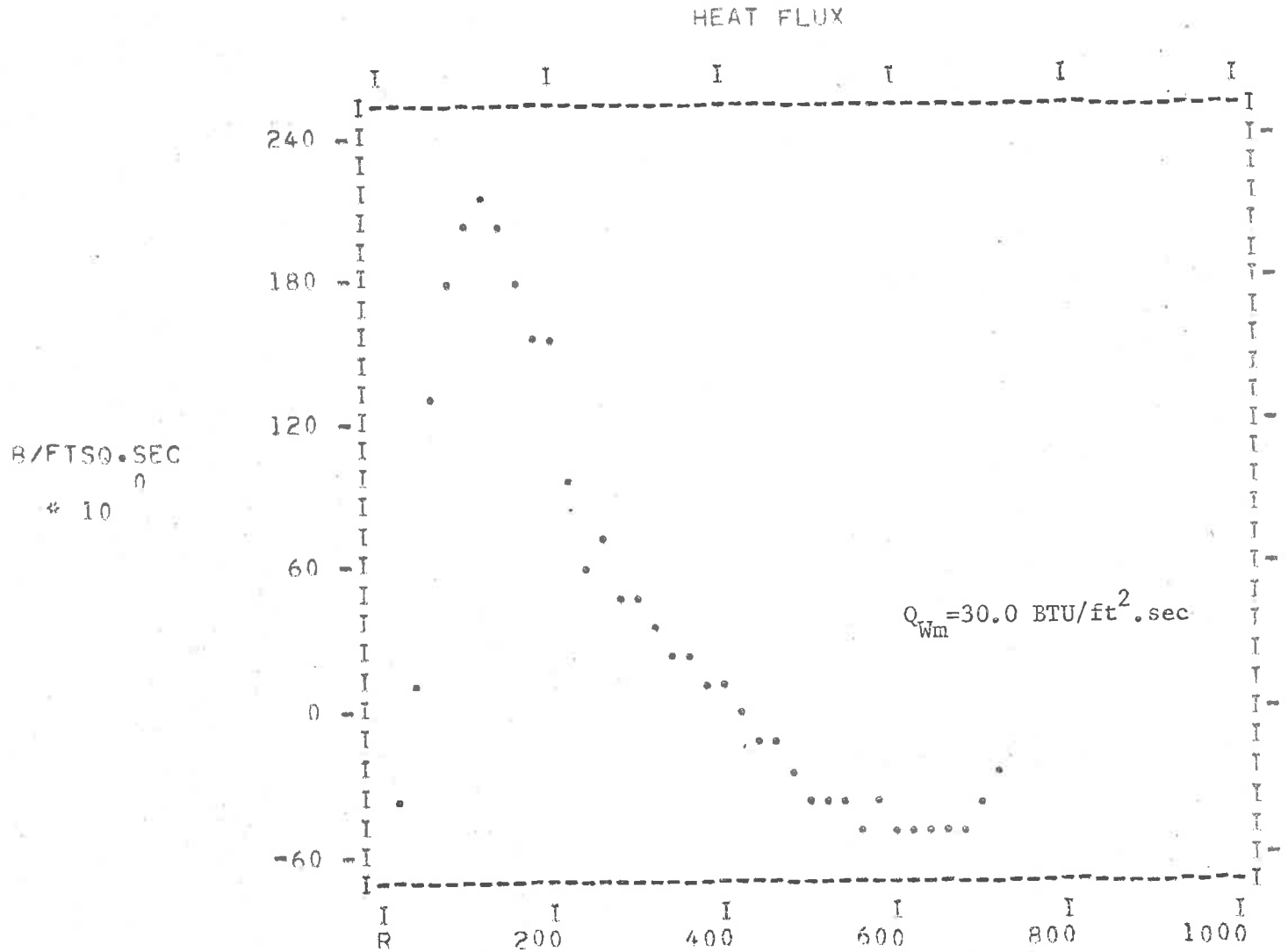

Fig.47 Heat Flux cycle derived from preceding T_w cycle

FOURIER COEFFICIENTS AT CYCLE FREQUENCY

CYCLE HARMONIC	TEMPERATURE (DEG.F)	PHASE ANGLE CRANK ANG.DEG)
1	496.866	87.46
2	223.396	87.66
3	180.113	129.41
4	111.342	120.31
5	120.263	139.56
6	104.522	167.44
7	120.898	209.40
8	48.595	194.89
9	28.418	190.57
10	25.509	283.13
11	32.050	299.01
12	18.623	203.83
13	25.905	150.85
14	33.243	136.01
15	25.826	184.06
	2.5E+03 7.3E+02	

Fig.48 Fourier Coefficients of Gas Temperature cycle following (X=0.200")

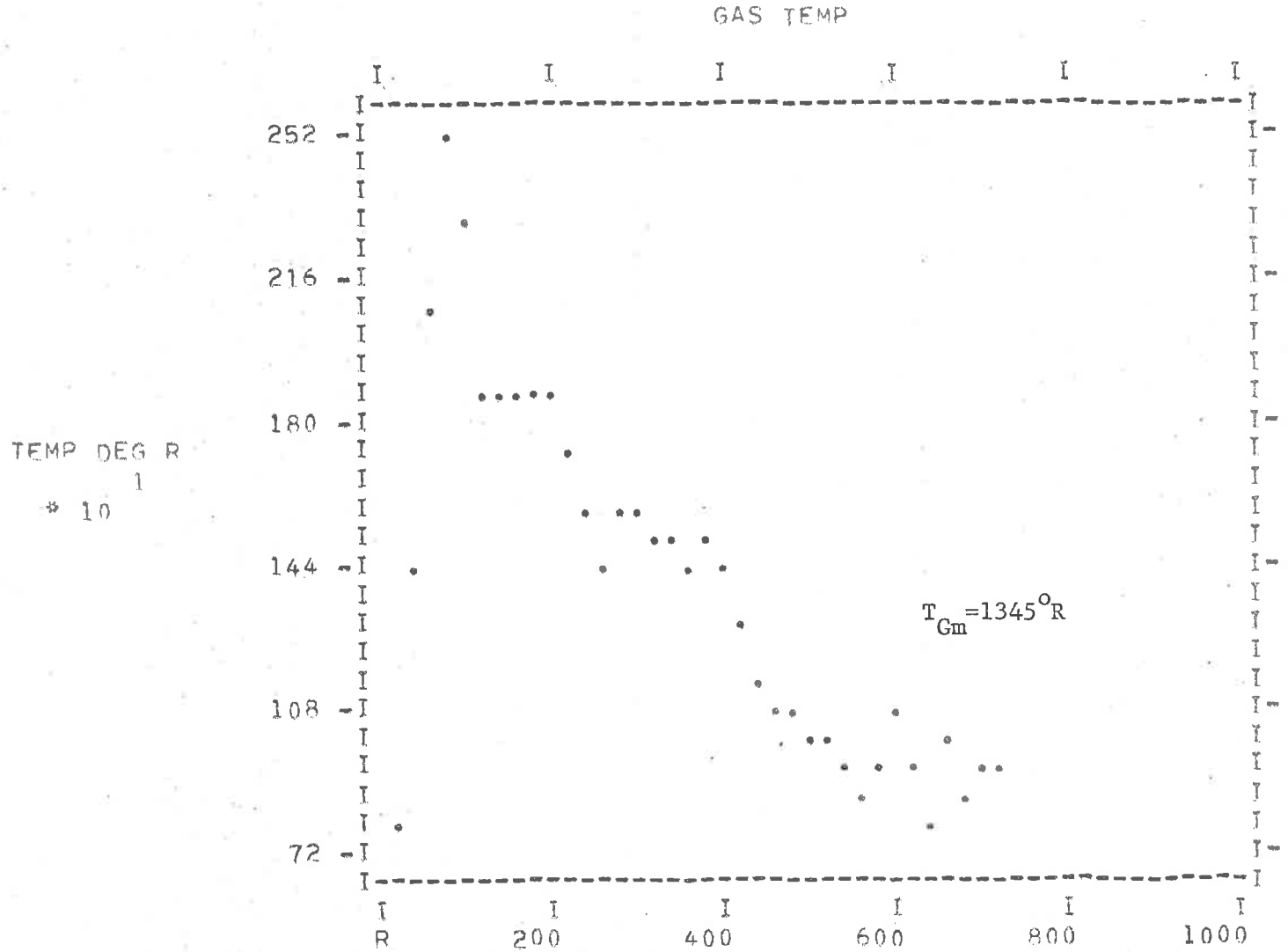

Fig.49 Gas Temperature cycle (X = 0.200")

FOURIER COEFFICIENTS AT CYCLE FREQUENCY

CYCLE HARMONIC	TEMPERATURE (DEG.F)	PHASE ANGLE CRANK ANG.DEG)
1	54.289	26.87
2	38.708	48.57
3	23.557	64.25
4	16.150	68.69
5	14.013	85.28
6	11.153	111.47
7	9.097	137.17
8	7.363	148.61
9	6.776	157.19
10	6.236	172.07
11	5.287	187.19
12	4.288	197.11
13	3.924	207.42
14	3.548	219.84
15	2.836	233.63
	2.5E+02 1.5E+01	

Fig.50 Fourier Coefficients of Gas Pressure cycle following

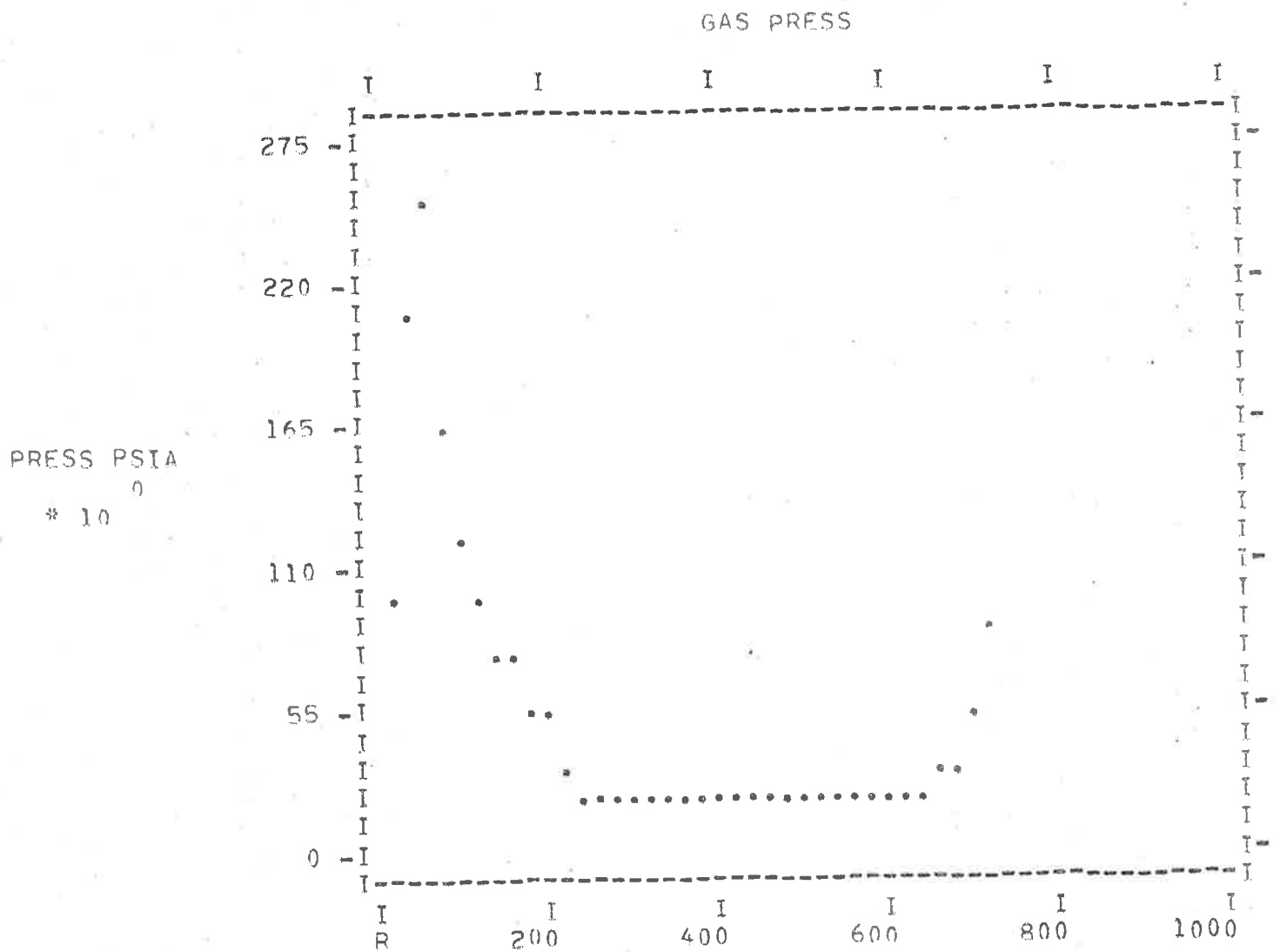

Fig.51 Gas Pressure cycle

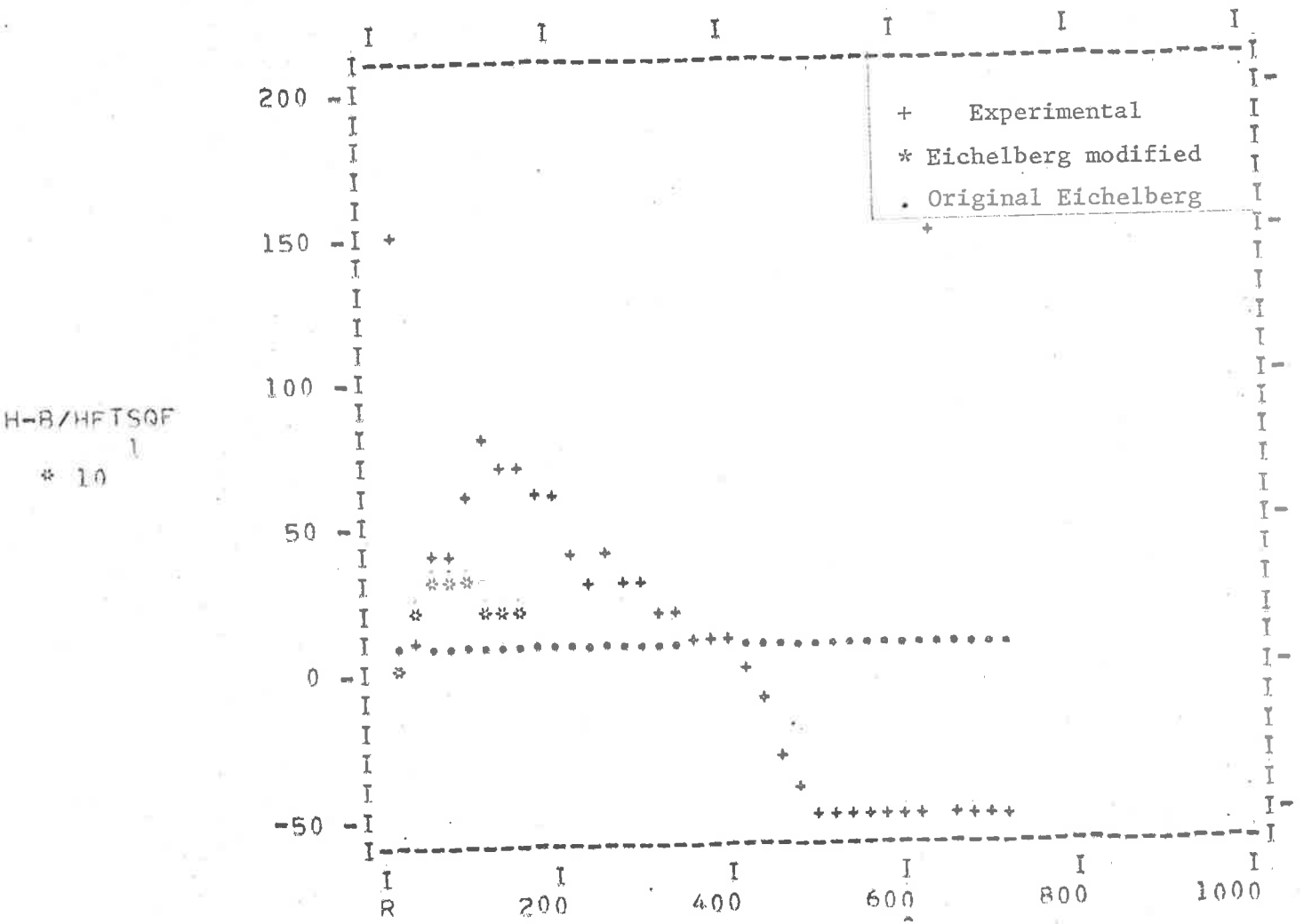

Fig.52 Cycle of Heat Transfer Coefficient
from preceding simultaneous data (X = 0.200")

CONVERT TAPE NO.
1000RPM +07F0,25.4TIMING 2ND63 50K± KZ COMPENSATED. ISD.290
ANALOG TAPE 4 TRANSMITTAL TAPE 1990

	REGIONS SELECT	INITIAL	FINAL	NUMBER OF POINTS SELECT	INITIAL	FINAL	TOTAL	REGION VARIATION
	1	1	1	438	46	481	2198	438 438

CYCLE COUNT	CRANK ANG	PRESSURE	GAS TEMP.	WALL TEMP.	HEAT FLUX	PISTON VELOC.	HEAT TRANSFER COEFF. EXPT.	EICH VP.	EICH. VPM
1	0	0.550E+01	0.633E+03	7.047E+02	1.113E+01	0.	0.427E+03	0.	1.671E+01
2	5	0.731E+01	0.963E+03	7.092E+02	1.417E+01	2.065E+00	0.508E+03	0.780E+01	1.688E+01
3	10	1.041E+02	0.913E+03	7.100E+02	1.452E+01	4.447E+00	0.577E+04	0.715E+01	1.703E+01
4	15	1.271E+02	0.902E+03	7.099E+02	1.413E+01	6.040E+00	0.781E+03	0.000E+00	1.707E+01
5	20	1.440E+02	0.853E+03	7.096E+02	2.037E+01	7.063E+00	0.003E+03	0.110E+02	0.031E+01
6	25	1.707E+02	0.720E+03	7.089E+02	2.922E+01	9.561E+00	1.029E+03	0.170E+02	0.101E+01
7	30	1.984E+02	0.454E+03	7.091E+02	4.555E+01	1.114E+01	1.688E+03	0.142E+02	0.196E+01
8	35	2.104E+02	0.417E+03	7.093E+02	5.745E+01	1.191E+01	1.698E+03	0.854E+02	0.171E+01
9	40	2.189E+02	0.333E+03	7.094E+02	6.866E+01	1.443E+01	1.813E+03	0.720E+02	0.192E+01
10	45	2.179E+02	0.347E+03	7.093E+02	6.403E+01	1.537E+01	1.094E+03	0.114E+02	0.429E+01
11	50	2.042E+02	0.709E+03	7.089E+02	3.137E+03	1.470E+01	2.232E+03	0.722E+02	0.444E+01
12	55	1.792E+02	0.722E+03	0.011E+02	1.575E+03	1.377E+01	2.689E+03	0.143E+02	0.707E+01
13	60	1.729E+02	0.455E+03	0.013E+02	1.433E+02	1.244E+01	2.785E+03	0.704E+02	0.717E+01
14	65	1.579E+02	0.514E+03	0.052E+02	1.494E+02	1.090E+01	3.104E+03	0.789E+02	0.860E+01
15	70	1.375E+02	0.417E+03	0.470E+02	1.420E+02	1.937E+01	3.414E+03	0.594E+02	0.807E+01
16	75	1.295E+02	0.511E+03	0.505E+03	1.529E+03	1.765E+01	3.677E+03	0.435E+02	0.902E+01
17	80	1.164E+02	0.334E+03	0.509E+02	1.523E+02	1.000E+01	3.841E+03	0.301E+02	0.653E+01
18	85	1.107E+02	0.195E+03	0.511E+02	1.521E+02	1.000E+01	3.957E+03	0.219E+02	0.337E+01
19	90	1.055E+02	0.212E+03	0.124E+03	1.519E+02	1.000E+01	3.990E+03	0.153E+02	0.176E+01
20	95	1.007E+02	0.217E+03	0.135E+02	1.519E+02	1.000E+01	3.992E+03	0.098E+02	0.071E+01
21	100	0.922E+01	0.159E+03	0.144E+03	1.518E+02	1.000E+01	3.989E+03	0.049E+02	0.031E+01
22	105	0.915E+01	0.133E+03	0.152E+02	1.484E+02	1.234E+01	3.974E+03	0.000E+00	0.597E+01
23	110	0.913E+01	0.128E+03	0.158E+03	1.342E+02	1.483E+01	3.940E+03	0.377E+02	0.341E+01
24	115	0.926E+01	0.129E+03	0.162E+02	1.309E+02	1.563E+01	3.904E+03	0.444E+02	0.109E+01
25	120	0.939E+01	0.988E+03	0.165E+02	1.217E+02	1.443E+01	3.854E+03	0.478E+02	0.033E+01
26	125	0.148E+01	0.964E+03	0.167E+02	1.181E+02	1.267E+01	3.791E+03	0.483E+02	0.829E+01
27	130	0.040E+01	0.920E+03	0.169E+02	1.165E+02	1.266E+01	3.688E+03	0.444E+02	0.791E+01
28	135	0.047E+01	0.888E+03	0.172E+02	1.143E+02	1.130E+01	3.615E+03	0.407E+02	0.787E+01
29	140	0.071E+01	0.810E+03	0.175E+02	1.154E+02	1.011E+01	3.490E+03	0.348E+02	0.780E+01
30	145	0.090E+01	0.907E+03	0.180E+02	1.176E+02	8.884E+00	3.502E+03	0.298E+02	0.740E+01
31	150	0.437E+01	0.732E+03	0.185E+02	1.187E+02	7.661E+00	3.527E+03	0.196E+02	0.692E+01
32	155	0.163E+01	0.704E+03	0.190E+02	1.179E+02	6.706E+00	3.516E+03	0.179E+02	0.626E+01
33	160	0.731E+01	0.714E+03	0.193E+02	1.145E+02	5.114E+00	3.449E+03	0.855E+01	0.373E+01
34	165	0.375E+01	0.704E+03	0.195E+02	1.098E+02	3.843E+00	3.370E+03	0.411E+01	0.222E+01
35	170	0.060E+01	0.701E+03	0.195E+02	1.015E+02	2.543E+00	3.095E+03	0.299E+01	0.085E+01
36	175	0.722E+01	0.706E+03	0.193E+02	9.409E+01	1.282E+00	2.853E+03	0.417E+01	0.959E+01
37	180	0.197E+01	0.714E+03	0.191E+02	8.728E+01	-0.819E-07	2.629E+03	0.421E+01	0.829E+01
38	185	0.931E+01	0.715E+03	0.188E+02	8.182E+01	-1.282E+00	2.457E+03	0.270E+01	0.869E+01
39	190	0.632E+01	0.999E+03	0.185E+02	7.712E+01	-2.564E+00	2.353E+03	0.192E+01	0.868E+01
40	195	0.187E+01	0.950E+03	0.182E+02	7.324E+01	-3.842E+00	2.311E+03	0.573E+01	0.915E+01
41	200	0.740E+01	0.898E+03	0.179E+02	6.973E+01	-5.115E+00	2.311E+03	0.599E+01	0.914E+01
42	205	0.187E+01	0.922E+03	0.176E+02	6.692E+01	-6.389E+00	2.328E+03	0.632E+01	0.657E+01
43	210	0.731E+01	0.786E+03	0.172E+02	6.502E+01	-7.661E+00	2.328E+03	0.623E+01	0.621E+01
44	215	0.837E+01	0.674E+03	0.163E+02	6.461E+01	-8.933E+00	2.297E+03	0.607E+01	0.525E+01
45	220	0.784E+01	0.627E+03	0.142E+02	6.236E+01	-1.021E+01	2.191E+03	0.137E+01	0.149E+01
46	225	0.717E+01	0.602E+03	0.157E+02	6.512E+01	-1.131E+01	2.075E+03	0.209E+01	0.146E+01
47	230	0.747E+01	0.590E+03	0.153E+02	6.294E+01	-1.268E+01	1.971E+03	0.619E+01	0.155E+01
48	235	0.786E+01	0.607E+03	0.149E+02	6.138E+01	-1.396E+01	1.909E+03	0.745E+01	0.187E+01
49	240	0.761E+01	0.620E+03	0.146E+02	6.234E+01	-1.525E+01	1.893E+03	0.809E+01	0.191E+01
50	245	0.683E+01	0.632E+03	0.144E+02	6.331E+01	-1.653E+01	1.908E+03	0.852E+01	0.132E+01
51	250	0.612E+01	0.638E+03	0.142E+02	6.410E+01	-1.653E+01	1.931E+03	0.847E+01	0.091E+01
52	255	0.563E+01	0.641E+03	0.141E+02	6.452E+01	-1.783E+01	1.939E+03	0.847E+01	0.057E+01
53	260	0.544E+01	0.642E+03	0.139E+02	6.417E+01	-1.886E+01	1.928E+03	0.771E+01	0.050E+01
54	265	0.550E+01	0.644E+03	0.138E+02	6.334E+01	-1.884E+01	1.875E+03	0.177E+01	0.075E+01
55	270	0.650E+01	0.645E+03	0.136E+02	6.250E+01	-1.908E+01	1.822E+03	0.640E+01	0.125E+01
56	275	0.737E+01	0.641E+03	0.134E+02	6.190E+01	-1.960E+01	1.782E+03	0.619E+01	0.179E+01
57	280	0.786E+01	0.644E+03	0.133E+02	6.147E+01	-1.985E+01	1.771E+03	0.729E+01	0.218E+01
58	285	0.804E+01	0.646E+03	0.132E+02	6.233E+01	-1.056E+01	1.792E+03	0.811E+01	0.229E+01
59	290	0.786E+01	0.652E+03	0.131E+02	6.267E+01	-1.915E+01	1.832E+03	0.734E+01	0.208E+01
60	295	0.743E+01	0.671E+03	0.130E+02	6.352E+01	-1.899E+01	1.870E+03	0.544E+01	0.187E+01
61	300	0.690E+01	0.688E+03	0.129E+02	6.451E+01	-1.844E+01	1.886E+03	0.329E+01	0.129E+01
62	305	0.680E+01	0.697E+03	0.129E+02	7.050E+01	-1.737E+01	1.842E+03	0.182E+01	0.101E+01
63	310	0.690E+01	0.671E+03	0.126E+02	7.704E+01	-1.639E+01	1.753E+03	0.029E+01	0.103E+01
64	315	0.780E+01	0.578E+03	0.125E+02	8.419E+01	-1.478E+01	1.639E+03	0.962E+01	0.131E+01
65	320	0.813E+01	0.578E+03	0.120E+02	9.221E+01	-1.344E+01	1.522E+03	0.903E+01	0.173E+01
66	325	0.850E+01	0.570E+03	0.117E+02	1.009E+02	-1.191E+01	1.458E+03	0.788E+01	0.211E+01
67	330	0.903E+01	0.548E+03	0.115E+02	1.074E+02	-1.018E+01	1.433E+03	0.555E+01	0.232E+01
68	335	0.905E+01	0.579E+03	0.113E+02	1.113E+02	-9.761E+00	1.427E+03	0.229E+01	0.231E+01
69	340	0.880E+01	0.655E+03	0.111E+02	1.229E+02	-8.048E+00	1.428E+03	0.769E+01	0.212E+01
70	345	0.871E+01	0.654E+03	0.111E+02	1.208E+02	-6.868E+00	1.412E+03	0.199E+01	0.187E+01
71	350	0.868E+01	0.628E+03	0.110E+02	1.281E+02	-5.642E+00	1.452E+03	0.421E+01	0.170E+01
72	355	0.877E+01	0.635E+03	0.109E+02	1.194E+02	-4.395E+00	1.434E+03	0.594E+01	0.159E+01
73	360	0.901E+01	0.638E+03	0.107E+02	1.134E+02	-3.198E+00	1.557E+03	0.711E+01	0.182E+01
74	365	0.922E+01	0.633E+03	0.105E+02	1.048E+02	-2.005E+00	1.439E+03	0.749E+01	0.201E+01
75	370	0.921E+01	0.597E+03	0.103E+02	1.047E+02	-1.726E+00	1.426E+03	0.695E+01	0.210E+01
76	375	0.887E+01	0.567E+03	0.100E+02	2.551E+01	6.040E+00	1.296E+03	0.225E+01	0.194E+01
77	380	0.825E+01	0.554E+03	0.098E+02	2.447E+01	7.063E+00	1.215E+03	0.525E+01	0.166E+01
78	385	0.768E+01	0.526E+03	0.098E+02	2.450E+01	9.751E+00	1.231E+03	0.840E+01	0.170E+01
79	390	0.685E+01	0.499E+03	0.098E+02	2.415E+01	1.116E+01	1.278E+03	0.991E+01	0.203E+01
80	395	0.656E+01	0.466E+03	0.097E+02	2.431E+01	1.191E+01	1.331E+03	0.992E+01	0.209E+01
81	400	0.686E+01	0.398E+03	0.096E+02	2.467E+01	1.443E+01	1.356E+03	0.204E+01	0.194E+01
82	405	0.711E+01	0.339E+03	0.095E+02	2.512E+01	1.537E+01	1.709E+03	0.152E+01	0.194E+01
83	410	0.770E+01	0.294E+03	0.094E+02	2.579E+01	1.470E+01	1.188E+03	0.509E+01	0.198E+01
84	415	0.813E+01	0.271E+03	0.093E+02	1.704E+01	1.377E+01	9.365E+01	0.641E+01	0.953E+01
85	420	0.819E+01	0.259E+03	0.075E+02	8.284E+00	1.244E+01	6.413E+01	0.709E+01	0.947E+01
86	425	0.794E+01	0.254E+03	0.070E+02	4.886E+00	1.088E+01	3.932E+01	0.493E+01	0.923E+01
87	430	0.712E+01	0.253E+03	0.068E+02	2.015E+00	0.935E+00	1.844E+01	0.490E+01	0.884E+01
88	435	0.637E+01	0.250E+03	0.060E+02	-1.614E-01	1.096E+01	-1.149E+00	0.645E+01	0.840E+01
89	440	0.586E+01	0.243E+03	0.055E+02	-1.686E+00	1.095E+01	-1.536E+01	0.164E+01	0.805E+01
90	445	0.574E+01	0.250E+03	0.050E+02	-3.331E+00	1.040E+01	-2.794E+01	0.285E+01	0.793E+01
91	450	0.601E+01	0.223E+03	0.268E+02	-4.773E+00	1.009E+01	-4.107E+01	0.299E+01	0.806E+01
92	455	0.668E+01	0.212E+03	0.274E+02	-6.174E+00	1.026E+01	-5.413E+01	0.325E+01	0.829E+01
93	460	0.726E+01	0.200E+03	0.277E+02	-8.219E+00	1.005E+01	-7.481E+01	0.332E+01	0.850E+01
94	465	0.756E+01	0.196E+03	0.272E+02	-1.133E+01	1.776E+01	-9.722E+01	0.258E+01	0.853E+01
95	470	0.730E+01	0.187E+03	0.227E+02	-1.254E+01	1.443E+01	-1.242E+02	0.075E+01	0.828E+01
96	475	0.668E+01	0.184E+03	0.221E+02	-1.445E+01	1.443E+01	-1.564E+02	0.784E+01	0.777E+01
97	480	0.580E+01	0.118E+03	0.216E+02	-1.647E+01	1.443E+01	-1.041E+02	0.467E+01	0.713E+01
98	485	0.524E+01	0.088E+03	0.211E+02	-1.878E+01	1.367E+01	-2.356E+02	0.154E+01	0.656E+01
99	490	0.500E+01	0.066E+03	0.208E+02	-2.018E+01	1.268E+01	-2.758E+02	0.915E+01	0.625E+01
100	495	0.527E+01	0.047E+03	0.201E+02	-2.186E+01	1.130E+01	-3.068E+02	0.784E+01	0.627E+01
101	500	0.594E+01	0.041E+03	0.198E+02	-2.151E+01	1.211E+01	-3.211E+02	0.675E+01	0.657E+01
102	505	0.671E+01	0.043E+03	7.992E+02	-2.177E+01	8.806E+00	-3.214E+02	0.491E+01	0.698E+01
103	510	0.724E+01	0.048E+03	7.988E+02	-2.202E+01	7.441E+00	-3.174E+02	0.448E+01	0.731E+01
104	515	0.735E+01	0.053E+03	7.981E+02	-2.259E+01	6.784E+00	-3.218E+02	0.206E+01	0.737E+01
105	520	0.698E+01	0.044E+03	7.979E+02	-2.374E+01	5.116E+00	-3.648E+02	0.852E+01	0.712E+01
106	525	0.620E+01	0.031E+03	7.975E+02	-2.654E+01	3.842E+00	-3.944E+02	0.340E+01	0.665E+01
107	530	0.565E+01	0.049E+03	7.970E+02	-2.791E+01	2.543E+00	-4.187E+02	0.883E+01	0.614E+01
108	535	0.539E+01	0.040E+03	7.966E+02	-3.467E+01	1.282E+00	-4.888E+02	0.244E+01	0.592E+01
109	540	0.531E+01	0.046E+03	7.959E+02	-3.923E+01	-2.046E-06	-7.048E+02	0.439E+01	0.584E+01
110	545	0.560E+01	0.057E+03	7.953E+02	-3.523E+01	-1.282E+00	-7.176E+02	0.302E+01	0.623E+01
111	550	0.727E+01	0.053E+03	7.947E+02	-3.437E+01	-2.563E+00	-7.479E+02	0.307E+01	0.683E+01
112	555	0.871E+01	0.821E+03	7.942E+02	-3.459E+01	-3.842E+00	-7.613E+02	0.545E+01	0.744E+01
113	560	0.914E+01	0.802E+03	7.938E+02	-3.409E+01	-5.116E+00	-8.234E+02	0.810E+01	0.781E+01
114	565	0.893E+01	0.817E+03	7.934E+02	-3.527E+01	-6.394E+00	-8.868E+02	0.922E+01	0.785E+01
115	570	0.811E+01	0.821E+03	7.930E+02	-3.568E+01	-7.661E+00	-8.449E+02	0.449E+01	0.750E+01
116	575	0.780E+01	0.812E+03	7.927E+02	-3.435E+01	-8.884E+00	-8.432E+02	0.571E+01	0.691E+01
117	580	0.823E+01	0.827E+03	7.923E+02	-3.468E+01	-1.011E+01	-8.229E+02	0.407E+01	0.633E+01
118	585	0.903E+01	0.838E+03	7.919E+02	-3.541E+01	-1.130E+01	-7.163E+02	0.482E+01	0.599E+01
119	590	0.925E+01	0.815E+03	7.915E+02	-3.517E+01	-1.268E+01	-8.139E+02	0.439E+01	0.600E+01
120	595	0.781E+01	0.833E+03	7.911E+02	-3.467E+01	-1.367E+01	-8.850E+02	0.072E+01	0.630E+01
121	600	0.781E+01	0.865E+03	7.908E+02	-3.435E+01	-1.443E+01	-8.783E+02	0.131E+01	0.671E+01
122	605	0.826E+01	0.838E+03	7.905E+02	-3.543E+01	-1.562E+01	-7.541E+02	0.550E+01	0.702E+01
123	610	0.813E+01	0.733E+03	7.902E+02	-3.425E+01	-1.663E+01	-8.772E+02	0.435E+01	0.708E+01
124	615	0.744E+01	0.744E+03	7.899E+02	-3.307E+01	-1.734E+01	-8.112E+02	0.695E+01	0.686E+01
125	620	0.671E+01	0.807E+03	7.897E+02	-3.234E+01	-1.805E+01	-8.850E+02	0.459E+01	0.643E+01
126	625	0.663E+01	0.843E+03	7.895E+02	-3.224E+01	-1.844E+01	-8.984E+02	0.669E+01	0.639E+01
127	630	0.714E+01	0.813E+03	7.892E+02	-3.274E+01	-1.899E+01	-8.139E+02	0.817E+01	0.668E+01
128	635	0.790E+01	0.791E+03	7.889E+02	-3.340E+01	-1.948E+01	-8.323E+02	0.140E+01	0.757E+01
129	640	0.820E+01	0.831E+03	7.886E+02	-3.373E+01	-1.985E+01	-8.242E+02	0.482E+01	0.893E+01
130	645	0.853E+01	0.827E+03	7.883E+02	-3.331E+01	-1.965E+01	-8.467E+02	0.109E+01	0.908E+01
131	650	0.900E+01	0.803E+03	7.881E+02	-3.202E+01	-1.935E+01	-8.572E+02	0.476E+01	0.892E+01
132	655	0.918E+01	0.804E+03	7.879E+02	-3.014E+01	-1.898E+01	-8.098E+02	0.807E+01	0.901E+01
133	660	0.903E+01	0.946E+03	7.878E+02	-2.822E+01	-1.844E+01	-8.911E+02	0.167E+01	0.967E+01
134	665	0.840E+01	0.893E+03	7.877E+02	-2.490E+01	-1.770E+01	-8.761E+02	0.167E+01	0.802E+01
135	670	0.849E+01	0.913E+03	7.876E+02	-2.454E+01	-1.679E+01	-8.459E+02	0.379E+01	0.439E+01
136	675	0.922E+01	0.964E+03	7.874E+02	-2.731E+01	-1.579E+01	-8.163E+02	0.189E+01	0.600E+01
137	680	0.774E+01	0.726E+03	7.872E+02	-2.824E+01	-1.444E+01	-1.222E+03	0.331E+01	0.422E+01
138	685	0.684E+01	0.450E+03	7.869E+02	-2.967E+01	-1.331E+01	-1.254E+03	0.413E+01	0.809E+01
139	690	0.679E+01	0.218E+03	7.868E+02	-2.741E+01	-1.165E+01	-0.197E+03	0.949E+01	0.763E+01
140	695	0.723E+01	0.337E+03	7.867E+02	-2.190E+01	-9.976E+00	-0.984E+03	0.167E+01	0.298E+01
141	700	0.803E+01	0.437E+03	7.866E+02	-1.771E+01	-7.963E+00	-1.522E+03	0.989E+01	0.691E+01
142	705	0.872E+01	0.995E+03	7.871E+02	-0.852E+00	-5.940E+00	-1.791E+03	0.598E+01	0.805E+01
143	710	0.144E+01	0.650E+03	7.875E+02	-1.615E+00	-3.940E+00	-3.404E+01	0.739E+01	0.816E+01
144	715	0.266E+01	0.190E+03	7.881E+02	5.487E+00	-2.448E+00	1.618E+03	0.834E+01	0.945E+01

1000RPM +07F0,25.4TIMING 2ND63 50K± KZ COMPENSATED. ISD.290

Fig.53
Data set X = 0.25"

CONVERT TAPE NO 4
1000RPM WOT*0.25,FIRING 240EG SPK, KZ COMPENSATED, X=0.250
ANALOG TAPE 6 TRANSMITTAL TAPE 1558

SERIAL	RUN	CHANNEL	TYPE	NO PERIODS	COEFF
7	13	123	1	1	15

NO POINTS	INITTAL	MAX PERIODS
438	1	7

FOURIER COEFFICIENTS AT CYCLE FREQUENCY

CYCLE HARMONIC	TEMPERATURE (DEG.F)	PHASE ANGLE CRANK ANG.DEG)
1	14.244	128.24
2	5.007	139.61
3	2.401	191.19
4	.926	212.26
5	.525	223.48
6	.454	228.96
7	.437	296.71
8	.275	339.29
9	.166	8.03
10	.128	36.02
11	.100	33.12
12	.105	353.57
13	.097	40.74
14	.170	44.36
15	.100	91.62
	8.2E+02	7.9E+02

Fig.54 Fourier Coefficients of Wall Temperature cycle following

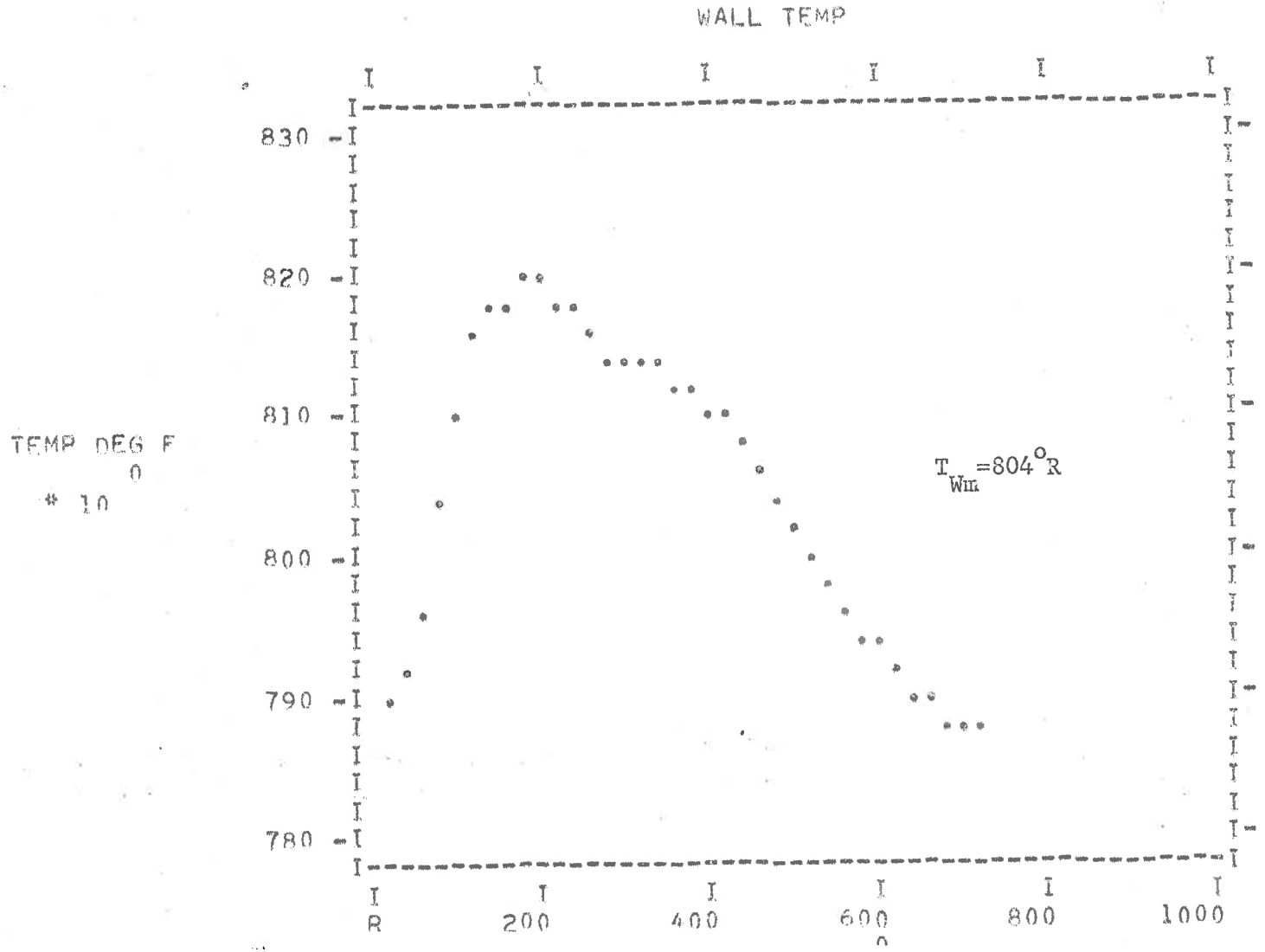

Fig.55 Wall Temperature cycle

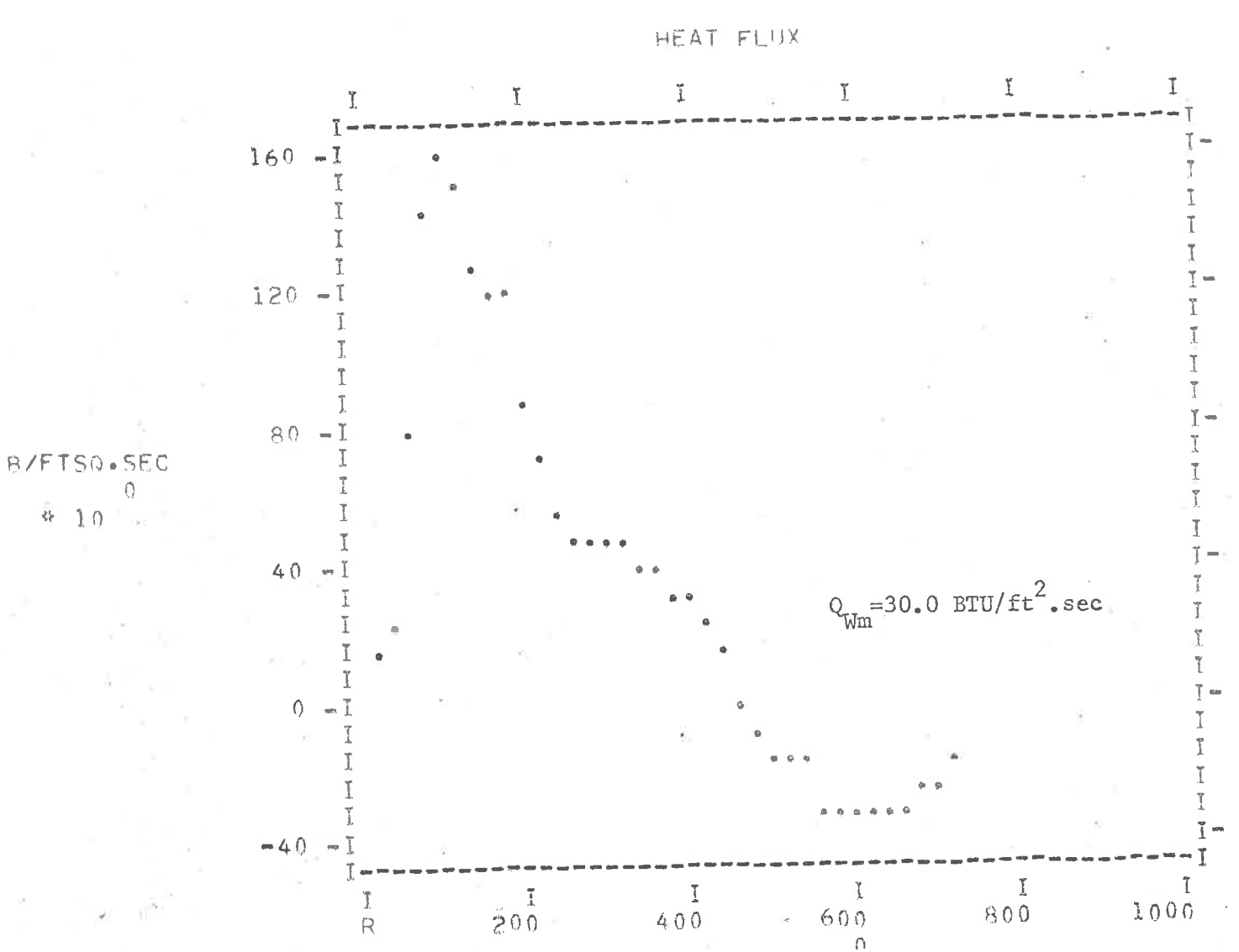

Fig.56 Heat Flux cycle derived from preceding T_w cycle

FOURIER COEFFICIENTS AT CYCLE FREQUENCY

CYCLE HARMONIC	TEMPERATURE (DEG.F)	PHASE ANGLE CRANK ANG.DEG)
1	534.670	91.07
2	240.922	97.66
3	184.866	136.85
4	119.980	137.11
5	130.766	147.88
6	122.991	171.60
7	108.424	207.33
8	47.697	219.25
9	62.379	229.55
10	58.440	247.36
11	63.720	280.23
12	40.579	271.39
13	36.779	299.07
14	34.373	311.15
15	34.740	336.92
	2.7E+03 7.9E+02	

Fig.57 Fourier Coefficients of Gas Temperature cycle following (X=0.250")

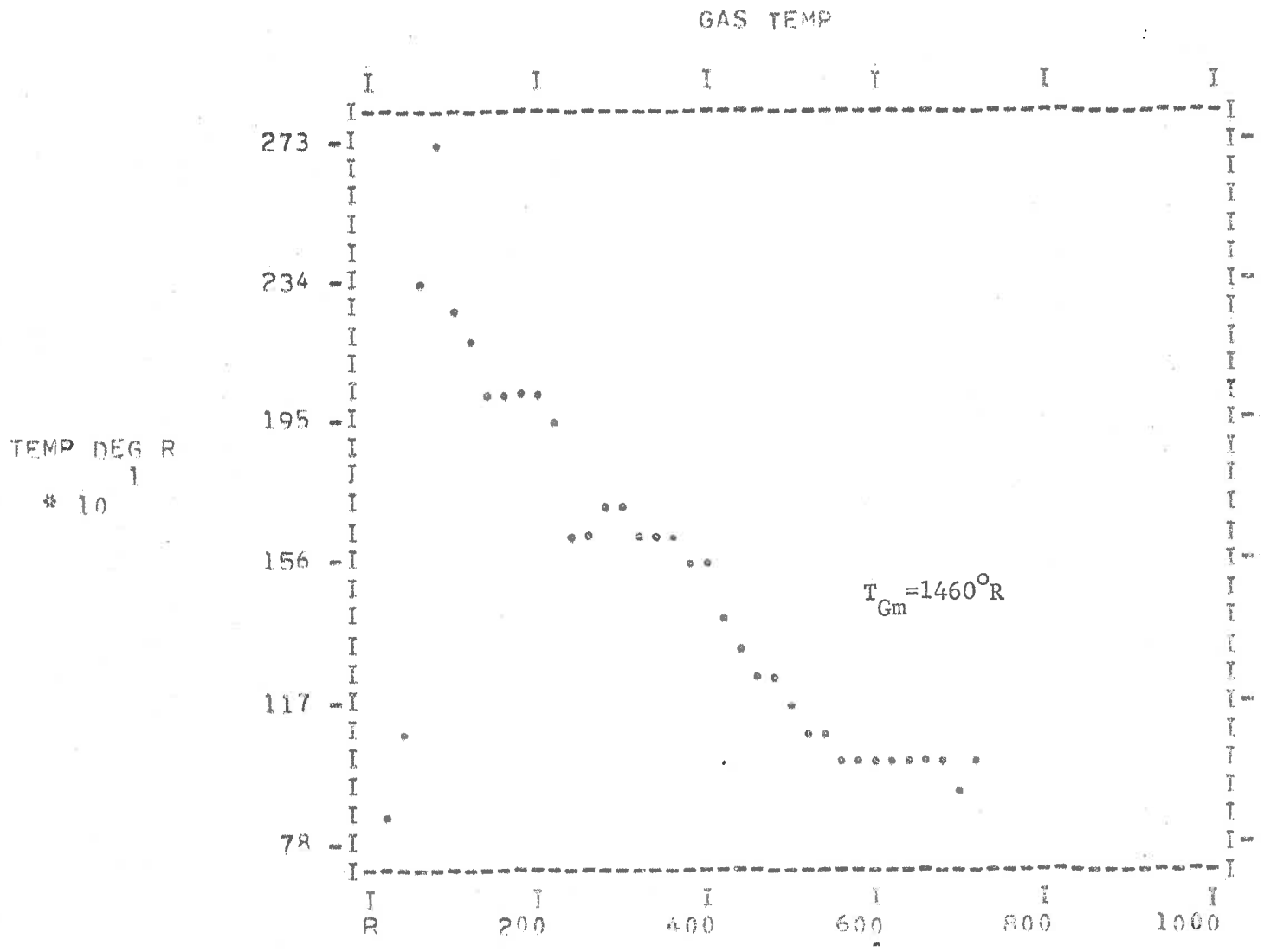

Fig.58 Gas Temperature cycle (X = 0.250")

FOURIER COEFFICIENTS AT CYCLE FREQUENCY

CYCLE HARMONIC	TEMPERATURE (DEG.F)	PHASE ANGLE CRANK ANG.DEG)
1	50.609	28.72
2	35.444	53.62
3	20.094	73.54
4	12.596	78.02
5	10.538	97.42
6	9.213	130.77
7	7.913	160.87
8	5.848	180.13
9	4.916	190.50
10	4.498	207.67
11	4.146	224.33
12	3.476	244.51
13	2.790	256.12
14	2.527	274.23
15	1.991	283.84
	2.2E+02 1.5E+01	

Fig.59 Fourier Coefficients of Gas Pressure cycle following

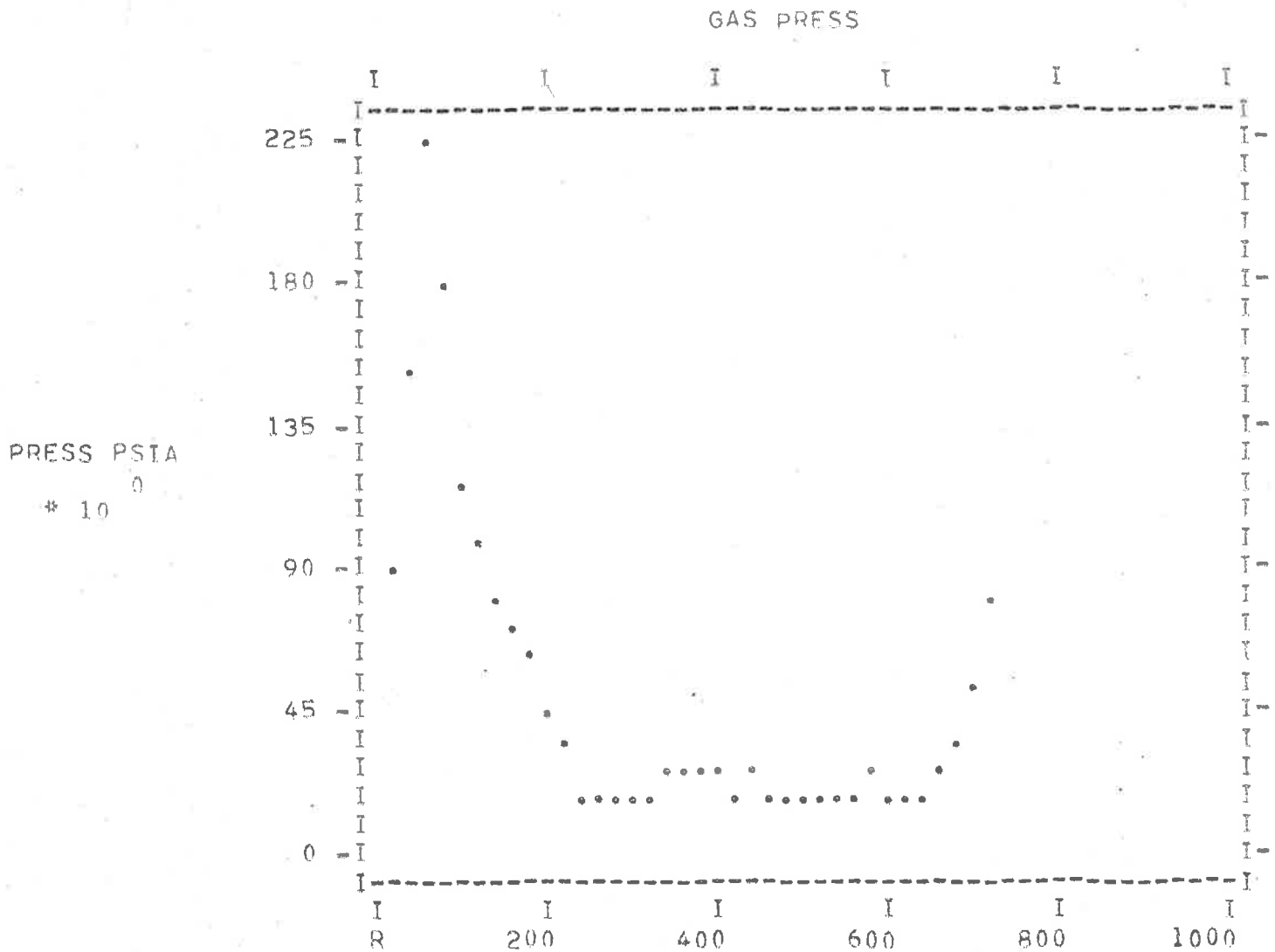

Fig.60 Gas Pressure cycle

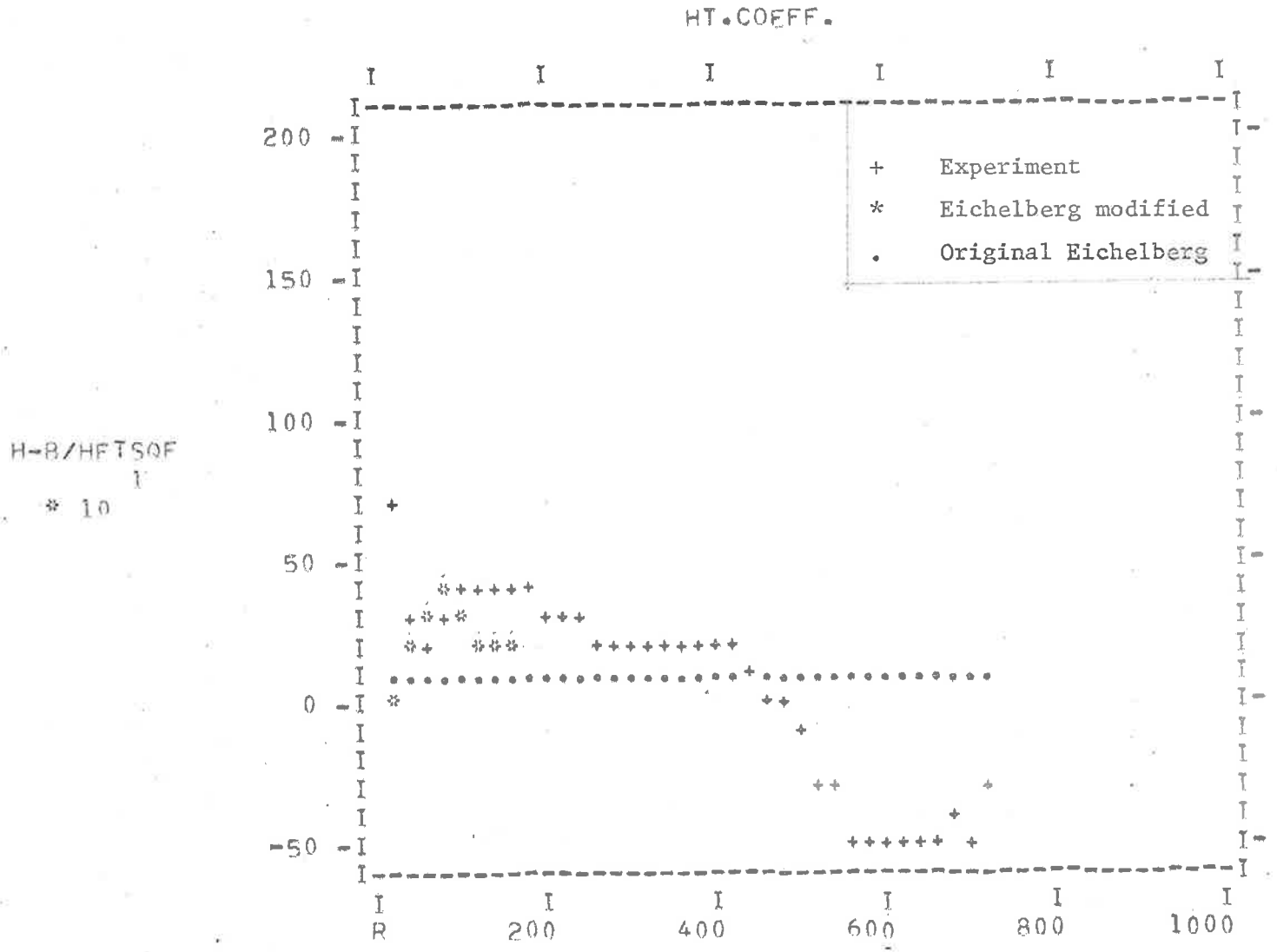

Fig.61 Cycle of Heat Transfer Coefficient
from preceding simultaneous data (X=0.250")

SYMMETRIC TAPE FOR
100000PSI WATER,3%FIBING 24DEG SPR, KZ COMPENSATED, RUN,400
ANALOG TAPE A TRANSMITTAL TAPE 1850

PERIODS SELECT	PERIODS INITIAL	PERIODS WAY	NUMBER OF POINTS SELECT	NUMBER OF POINTS INITIAL	NUMBER OF POINTS FINAL	NUMBER OF POINTS TOTAL	PERIOD VARIATION
1	1	7	491	1AR	498	2989	429 430

CYCLE POINT	FRAME NO	PRESSURE	GAS TEMP.	WALL TEMP.	HEAT FLUX	PISTON VELOC.	HEAT TRANSFER COEFF. PERT.	HEAT TRANSFER COEFF. PITCH VP.	HEAT TRANSFER COEFF. PITCH VPH
1	A	9.842E+01	8.468E+02	7.944E+02	-2.119E+01	0.	-1.358E+03	0.	1.700E+01
2	8	1.171E+02	1.027E+03	7.944E+02	-1.175E+01	2.084E+00	-7.801E+03	7.390E+01	4.498E+01
3	10	1.412E+02	1.147E+03	7.947E+02	-8.256E+00	4.247E+00	-5.184E+01	1.177E+02	5.451E+01
4	18	1.682E+02	1.273E+03	7.955E+02	7.875E+00	6.048E+00	2.732E+01	1.493E+02	7.123E+01
5	20	1.983E+02	1.395E+03	7.947E+02	3.054E+01	7.042E+00	7.150E+01	2.251E+02	8.868E+01
6	28	2.153E+02	2.787E+03	7.888E+02	5.194E+01	9.951E+00	1.044E+02	2.774E+02	9.984E+01
7	30	2.202E+02	1.220E+03	7.910E+02	8.716E+01	1.114E+01	1.342E+02	3.197E+02	1.087E+02
8	35	2.311E+02	1.288E+03	7.937E+02	1.149E+02	1.391E+01	1.451E+02	3.441E+02	1.174E+02
9	40	2.269E+02	1.247E+03	1.944E+02	1.344E+02	1.443E+01	2.003E+02	3.513E+02	1.104E+02
10	45	2.104E+02	1.131E+03	7.994E+02	1.444E+02	1.557E+01	2.428E+02	3.410E+02	1.044E+02
11	50	1.925E+02	1.031E+03	8.022E+02	1.449E+02	1.670E+01	2.054E+02	3.190E+02	9.648E+01
12	55	1.770E+02	9.437E+02	8.047E+02	1.434E+02	1.774E+01	1.891E+02	2.932E+02	8.583E+01
13	60	1.651E+02	9.134E+02	8.070E+02	1.424E+02	1.844E+01	1.798E+02	2.644E+02	7.742E+01
14	65	1.603E+02	9.091E+02	8.091E+02	1.421E+02	1.898E+01	1.953E+02	2.470E+02	7.097E+01
15	70	1.598E+02	9.047E+02	8.112E+02	1.427E+02	1.935E+01	5.417E+02	2.339E+02	6.674E+01
16	75	1.598E+02	9.071E+02	8.132E+02	1.437E+02	1.960E+01	5.481E+02	2.257E+02	6.424E+01
17	80	1.615E+02	9.098E+02	8.151E+02	2.812E+02	1.965E+01	5.498E+02	2.209E+02	6.298E+01
18	85	1.670E+02	9.131E+02	8.170E+02	2.812E+02	1.964E+01	5.498E+02	2.173E+02	6.099E+01
19	90	1.806E+02	9.201E+02	8.188E+02	2.814E+02	1.960E+01	5.709E+02	2.055E+02	5.894E+01
20	95	9.359E+01	9.054E+02	8.199E+02	1.941E+02	1.854E+01	5.722E+02	1.951E+02	5.840E+01
21	100	8.607E+01	9.000E+02	8.209E+02	1.947E+02	1.805E+01	5.719E+02	1.913E+02	5.165E+01
22	105	8.118E+01	1.014E+03	8.218E+02	1.764E+02	1.714E+01	5.624E+02	1.729E+02	4.911E+01
23	110	7.868E+01	1.013E+03	8.220E+02	1.659E+02	1.493E+01	5.464E+02	1.560E+02	4.934E+01
24	115	7.351E+01	1.011E+03	8.223E+02	1.547E+02	1.542E+01	5.145E+02	1.478E+02	4.831E+01
25	120	7.183E+01	1.004E+03	8.226E+02	1.498E+02	1.443E+01	4.810E+02	1.530E+02	4.794E+01
26	125	7.098E+01	1.002E+03	8.228E+02	1.451E+02	1.357E+01	4.511E+02	1.490E+02	4.788E+01
27	130	6.982E+01	2.017E+03	8.231E+02	1.420E+02	1.246E+01	4.278E+02	1.444E+02	4.774E+01
28	135	6.821E+01	2.035E+03	8.234E+02	1.387E+02	1.138E+01	4.122E+02	1.381E+02	4.722E+01
29	140	6.363E+01	2.033E+03	8.236E+02	1.342E+02	1.011E+01	3.994E+02	1.305E+02	4.427E+01
30	145	6.072E+01	2.016E+03	8.237E+02	1.279E+02	8.894E+00	3.841E+02	1.214E+02	4.501E+01
31	150	5.778E+01	2.000E+03	8.236E+02	1.201E+02	7.441E+00	3.681E+02	1.121E+02	4.171E+01
32	155	5.450E+01	1.991E+03	8.234E+02	1.117E+02	6.194E+00	3.485E+02	1.031E+02	4.259E+01
33	160	5.284E+01	2.003E+03	8.231E+02	1.044E+02	5.116E+00	3.175E+02	9.392E+01	4.174E+01
34	165	5.030E+01	2.010E+03	8.228E+02	9.783E+01	3.842E+00	2.918E+02	8.603E+01	4.110E+01
35	170	4.771E+01	2.044E+03	8.225E+02	9.371E+01	2.543E+00	2.718E+02	7.218E+01	4.037E+01
36	175	4.464E+01	2.091E+03	8.223E+02	9.127E+01	1.282E+00	2.584E+02	5.470E+01	3.926E+01
37	180	4.284E+01	2.098E+03	8.221E+02	8.944E+01	-4.210E-07	2.524E+02	4.141E+01	3.717E+01
38	185	3.425E+01	2.088E+03	8.220E+02	8.724E+01	-1.282E+00	2.484E+02	3.011E+01	3.532E+01
39	190	3.163E+01	2.040E+03	8.218E+02	8.473E+01	-2.543E+00	2.477E+02	2.993E+01	3.267E+01
40	195	2.733E+01	1.994E+03	8.215E+02	7.893E+01	-3.842E+00	2.429E+02	2.127E+01	2.993E+01
41	200	2.348E+01	1.974E+03	8.211E+02	7.211E+01	-5.114E+00	2.329E+02	2.211E+01	2.762E+01
42	205	2.139E+01	1.994E+03	8.208E+02	6.600E+01	-6.394E+00	2.180E+02	4.347E+01	2.588E+01
43	210	1.989E+01	1.849E+03	8.208E+02	5.869E+01	-7.681E+00	2.007E+02	6.185E+01	2.484E+01
44	215	1.923E+01	1.957E+03	8.194E+02	5.128E+01	-8.844E+00	1.849E+02	6.575E+01	2.433E+01
45	220	1.883E+01	1.947E+03	8.189E+02	4.494E+01	-1.011E+01	1.760E+02	6.795E+01	2.405E+01
46	225	1.859E+01	1.941E+03	8.184E+02	4.134E+01	-1.139E+01	1.698E+02	6.948E+01	2.373E+01
47	230	1.884E+01	1.903E+03	8.180E+02	4.025E+01	-1.266E+01	1.691E+02	7.022E+01	2.321E+01
48	235	1.741E+01	1.743E+03	8.176E+02	4.518E+01	-1.367E+01	1.723E+02	7.013E+01	2.253E+01
49	240	1.693E+01	1.716E+03	8.172E+02	4.189E+01	-1.443E+01	1.747E+02	6.977E+01	2.187E+01
50	245	1.656E+01	1.674E+03	8.169E+02	4.227E+01	-1.493E+01	1.767E+02	6.991E+01	2.144E+01
51	250	1.640E+01	1.658E+03	8.165E+02	4.659E+01	-1.465E+01	1.737E+02	7.111E+01	2.140E+01
52	255	1.722E+01	1.650E+03	8.162E+02	5.422E+01	-1.734E+01	1.674E+02	7.144E+01	2.175E+01
53	260	1.702E+01	1.641E+03	8.159E+02	5.869E+01	-1.805E+01	1.601E+02	7.061E+01	2.231E+01
54	265	1.687E+01	1.714E+03	8.156E+02	5.837E+01	-1.844E+01	1.539E+02	7.017E+01	2.289E+01
55	270	1.841E+01	1.765E+03	8.154E+02	5.862E+01	-1.909E+01	1.494E+02	8.088E+01	2.318E+01
56	275	1.824E+01	1.743E+03	8.151E+02	5.896E+01	-1.940E+01	1.469E+02	8.088E+01	2.308E+01
57	280	1.752E+01	1.741E+03	8.149E+02	5.791E+01	-1.955E+01	1.444E+02	7.961E+01	2.259E+01
58	285	1.686E+01	1.742E+03	8.147E+02	5.822E+01	-1.954E+01	1.440E+02	7.706E+01	2.193E+01
59	290	1.680E+01	1.716E+03	8.144E+02	5.365E+01	-1.915E+01	1.446E+02	7.483E+01	2.134E+01
60	295	1.598E+01	1.699E+03	8.140E+02	5.475E+01	-1.898E+01	1.268E+02	7.357E+01	2.114E+01
61	300	1.668E+01	1.674E+03	8.137E+02	2.919E+01	-1.844E+01	1.179E+02	7.358E+01	2.139E+01
62	305	1.731E+01	1.675E+03	8.133E+02	2.856E+01	-1.778E+01	1.110E+02	7.449E+01	2.191E+01
63	310	1.792E+01	1.699E+03	8.130E+02	2.809E+01	-1.647E+01	1.077E+02	7.547E+01	2.259E+01
64	315	1.807E+01	1.708E+03	8.127E+02	2.852E+01	-1.577E+01	1.067E+02	7.543E+01	2.315E+01
65	320	1.820E+01	1.722E+03	8.125E+02	2.717E+01	-1.443E+01	1.075E+02	7.411E+01	2.339E+01
66	325	1.803E+01	1.725E+03	8.123E+02	2.724E+01	-1.301E+01	1.076E+02	7.136E+01	2.324E+01
67	330	1.933E+01	1.713E+03	8.121E+02	2.807E+01	-1.134E+01	1.062E+02	6.703E+01	2.279E+01
68	335	1.770E+01	1.699E+03	8.119E+02	2.346E+01	-9.751E+00	9.624E+01	6.302E+01	2.224E+01
69	340	1.732E+01	1.662E+03	8.118E+02	1.987E+01	-7.042E+00	8.356E+01	5.681E+01	2.182E+01
70	345	1.735E+01	1.638E+03	8.109E+02	1.588E+01	-6.046E+00	8.020E+01	5.195E+01	2.164E+01
71	350	1.774E+01	1.625E+03	8.104E+02	1.218E+01	-4.467E+00	5.370E+01	4.551E+01	2.186E+01
72	355	1.829E+01	1.624E+03	8.099E+02	9.895E+00	-2.046E+00	4.178E+01	3.674E+01	2.217E+01
73	360	1.842E+01	1.631E+03	8.095E+02	9.185E+00	-2.180E-04	4.008E+01	3.482E+01	2.246E+01
74	365	1.874E+01	1.640E+03	8.091E+02	9.613E+00	2.046E+00	4.126E+01	3.738E+01	2.255E+01
75	370	1.834E+01	1.665E+03	8.088E+02	1.059E+01	4.087E+00	4.557E+01	4.455E+01	2.234E+01
76	375	1.743E+01	1.693E+03	8.084E+02	1.119E+01	6.046E+00	4.853E+01	5.194E+01	2.186E+01
77	380	1.684E+01	1.721E+03	8.083E+02	1.174E+01	7.042E+00	4.726E+01	5.395E+01	2.126E+01
78	385	1.692E+01	1.718E+03	8.080E+02	1.124E+01	8.751E+00	4.181E+01	5.277E+01	2.072E+01
79	390	1.615E+01	1.640E+03	8.077E+02	1.145E+01	1.100E+01	3.700E+01	4.806E+01	2.062E+01
80	395	1.645E+01	1.635E+03	8.072E+02	1.177E+01	1.301E+01	1.743E+01	4.254E+01	2.038E+01
81	400	1.702E+01	1.693E+03	8.068E+02	1.198E+01	1.443E+01	4.307E+00	6.613E+01	2.050E+01
82	405	1.759E+01	1.662E+03	8.063E+02	-9.899E-01	1.557E+01	-5.491E+00	6.739E+01	2.061E+01
83	410	1.780E+01	1.615E+03	8.059E+02	-1.007E+00	1.670E+01	-1.091E+01	6.886E+01	2.066E+01
84	415	1.774E+01	1.612E+03	8.055E+02	-2.341E+00	1.770E+01	-1.742E+01	6.922E+01	2.034E+01
85	420	1.721E+01	1.593E+03	8.051E+02	-2.493E+00	1.844E+01	-1.851E+01	6.866E+01	1.992E+01
86	425	1.651E+01	1.578E+03	8.048E+02	-3.831E+00	1.898E+01	-2.607E+01	6.759E+01	1.940E+01
87	430	1.509E+01	1.569E+03	8.043E+02	-4.731E+00	1.935E+01	-3.042E+01	6.649E+01	1.898E+01
88	435	1.543E+01	1.566E+03	8.039E+02	-5.221E+00	1.954E+01	-3.300E+01	6.606E+01	1.880E+01
89	440	1.557E+01	1.556E+03	8.033E+02	-1.293E+01	1.965E+01	-3.376E+01	6.578E+01	1.898E+01
90	445	1.624E+01	1.562E+03	8.027E+02	-1.448E+01	1.966E+01	-3.068E+01	6.713E+01	1.915E+01
91	450	1.688E+01	1.569E+03	8.021E+02	-1.524E+01	1.950E+01	-1.267E+01	6.741E+01	1.939E+01
92	455	1.725E+01	1.572E+03	8.015E+02	-2.447E+01	1.954E+01	-1.456E+01	6.719E+01	1.943E+01
93	460	1.732E+01	1.590E+03	8.010E+02	-2.417E+01	1.805E+01	-1.636E+01	6.683E+01	1.915E+01
94	465	1.706E+01	1.726E+03	8.005E+02	-2.206E+01	1.734E+01	-1.868E+01	6.778E+01	1.859E+01
95	470	1.683E+01	1.178E+03	8.001E+02	-2.257E+01	1.643E+01	-2.199E+01	9.351E+01	1.791E+01
96	475	1.616E+01	1.122E+03	7.996E+02	-2.378E+01	1.642E+01	-2.452E+01	5.448E+01	1.732E+01
97	480	1.607E+01	1.091E+03	7.991E+02	-2.443E+01	1.467E+01	-3.182E+01	5.430E+01	1.702E+01
98	485	1.629E+01	1.076E+03	7.985E+02	-2.449E+01	1.317E+01	-3.407E+01	5.317E+01	1.704E+01
99	490	1.681E+01	1.024E+03	7.979E+02	-1.119E+01	1.206E+01	-3.795E+01	5.279E+01	1.745E+01
100	495	1.761E+01	1.115E+03	7.974E+02	-1.324E+01	1.139E+01	-3.765E+01	5.249E+01	1.793E+01
101	500	1.778E+01	1.115E+03	7.968E+02	-1.418E+01	1.411E+01	-3.636E+01	5.154E+01	1.827E+01
102	505	1.767E+01	1.144E+03	7.963E+02	-1.393E+01	9.884E+00	-3.613E+01	4.962E+01	1.829E+01
103	510	1.751E+01	1.176E+03	7.959E+02	-1.282E+01	1.461E+01	-3.487E+01	4.613E+01	1.789E+01
104	515	1.631E+01	1.111E+03	7.955E+02	-3.158E+01	6.394E+00	-1.597E+01	4.195E+01	1.731E+01
105	520	1.561E+01	1.098E+03	7.952E+02	-3.466E+01	5.116E+00	-1.888E+01	3.758E+01	1.670E+01
106	525	1.529E+01	1.053E+03	7.948E+02	-3.844E+01	3.842E+00	-2.703E+01	3.334E+01	1.632E+01
107	530	1.552E+01	1.040E+03	7.944E+02	-3.216E+01	2.567E+00	-4.718E+01	2.922E+01	1.636E+01
108	535	1.628E+01	1.045E+03	7.940E+02	-3.134E+01	1.292E+00	-4.933E+01	2.380E+01	1.678E+01
109	540	1.726E+01	1.045E+03	7.935E+02	-3.497E+01	-2.064E-04	-4.908E+01	2.904E+01	1.744E+01
110	545	1.807E+01	1.041E+03	7.929E+02	-3.027E+01	-1.293E+00	-4.734E+01	2.542E+01	1.806E+01
111	550	1.834E+01	1.112E+03	7.924E+02	-4.477E+01	-2.562E+00	-4.588E+01	1.784E+01	1.839E+01
112	555	1.794E+01	1.120E+03	7.919E+02	-4.132E+01	-3.842E+00	-4.530E+01	1.774E+01	1.825E+01
113	560	1.720E+01	1.113E+03	7.915E+02	-4.114E+01	-5.114E+00	-4.606E+01	1.992E+01	1.775E+01
114	565	1.602E+01	1.047E+03	7.911E+02	-4.054E+01	-6.394E+00	-4.768E+01	1.729E+01	1.705E+01
115	570	1.521E+01	1.081E+03	7.907E+02	-3.894E+01	-7.661E+00	-4.945E+01	1.240E+01	1.650E+01
116	575	1.500E+01	1.077E+03	7.903E+02	-3.984E+01	-8.884E+00	-4.981E+01	1.419E+01	1.636E+01
117	580	1.550E+01	1.090E+03	7.900E+02	-3.978E+01	-1.011E+01	-4.790E+01	1.715E+01	1.672E+01
118	585	1.563E+01	1.116E+03	7.896E+02	-4.189E+01	-1.113E+01	-4.613E+01	1.118E+01	1.768E+01
119	590	1.765E+01	1.163E+03	7.893E+02	-4.041E+01	-1.236E+01	-4.845E+01	1.855E+01	1.835E+01
120	595	1.848E+01	1.141E+03	7.888E+02	-4.142E+01	-1.367E+01	-5.803E+01	1.915E+01	1.801E+01
121	600	1.875E+01	1.192E+03	7.885E+02	-4.193E+01	-1.443E+01	-5.742E+01	1.955E+01	1.823E+01
122	605	1.849E+01	1.179E+03	7.881E+02	-4.231E+01	-1.562E+01	-5.992E+01	1.995E+01	1.899E+01
123	610	1.782E+01	1.149E+03	7.877E+02	-4.254E+01	-1.643E+01	-6.254E+01	1.143E+01	1.850E+01
124	615	1.785E+01	1.178E+03	7.873E+02	-4.269E+01	-1.714E+01	-6.784E+01	1.137E+01	1.809E+01
125	620	1.841E+01	1.176E+03	7.870E+02	-4.228E+01	-1.805E+01	-6.710E+01	1.191E+01	1.807E+01
126	625	1.984E+01	1.158E+03	7.867E+02	-4.141E+01	-1.844E+01	-6.488E+01	1.481E+01	1.865E+01
127	630	2.202E+01	1.043E+03	7.864E+02	-3.982E+01	-1.909E+01	-6.179E+01	1.864E+01	1.984E+01
128	635	2.461E+01	1.082E+03	7.863E+02	-3.767E+01	-1.940E+01	-5.672E+01	1.729E+01	2.091E+01
129	640	2.649E+01	1.191E+03	7.861E+02	-3.494E+01	-1.955E+01	-3.998E+01	1.719E+01	2.194E+01
130	645	2.787E+01	1.105E+03	7.860E+02	-3.253E+01	-1.954E+01	-3.478E+01	1.931E+01	2.267E+01
131	650	2.864E+01	1.058E+03	7.860E+02	-3.092E+01	-1.915E+01	-3.120E+01	1.987E+01	2.296E+01
132	655	2.906E+01	1.048E+03	7.859E+02	-3.058E+01	-1.898E+01	-4.252E+01	1.951E+01	2.295E+01
133	660	2.911E+01	8.990E+02	7.857E+02	-3.159E+01	-1.844E+01	-5.357E+01	1.813E+01	2.267E+01
134	665	2.855E+01	9.557E+02	7.854E+02	-3.352E+01	-1.778E+01	-6.494E+01	1.990E+01	2.150E+01
135	670	2.693E+01	9.647E+02	7.851E+02	-3.954E+01	-1.647E+01	-7.048E+01	2.478E+01	2.038E+01
136	675	2.402E+01	1.008E+03	7.848E+02	-3.441E+01	-1.577E+01	-5.899E+01	2.748E+01	2.031E+01
137	680	2.284E+01	1.093E+03	7.845E+02	-3.401E+01	-1.443E+01	-4.374E+01	1.913E+01	2.190E+01
138	685	2.339E+01	1.169E+03	7.844E+02	-3.167E+01	-1.301E+01	-3.214E+01	1.987E+01	2.382E+01
139	690	2.211E+01	1.209E+03	7.843E+02	-2.947E+01	-1.134E+01	-2.498E+01	1.117E+01	2.398E+01
140	695	2.027E+01	1.243E+03	7.844E+02	-2.512E+01	-9.751E+00	-2.159E+01	1.884E+01	2.389E+01
141	700	1.787E+01	1.213E+03	7.845E+02	-2.144E+01	-7.042E+00	-1.939E+01	9.939E+01	2.314E+01
142	705	1.655E+01	1.208E+03	7.845E+02	-1.990E+01	-5.049E+00	-3.208E+01	8.403E+01	2.420E+01
143	710	1.654E+01	8.793E+02	7.846E+02	-2.008E+01	-4.247E+00	-7.434E+01	7.136E+01	2.428E+01
144	715	1.691E+01	8.439E+02	7.845E+02	-2.114E+01	-2.046E+00	-3.927E+01	9.423E+01	2.393E+01

100000PSI WATER,3%FIBING 24DEG SPR, KZ COMPENSATED, RUN,400

Fig.62
Data set X = 0.4"

CONVERT TAPE NO 4
1000RPM WOT*0.25.FIRING 24DEG SPK, KZ COMPENSATED, X=0.400
ANALOG TAPE 6 TRANSMITTAL TAPE 1558

SERIAL	RUN	CHANNEL	TYPE	NO PERIODS	COEFF
7	16	123	1	1	15

NO POINTS	INITTAL	MAX PERIODS
431	1	7

FOURIER COEFFICIENTS AT CYCLE FREQUENCY

CYCLE HARMONIC	TEMPERATURE (DEG.F)	PHASE ANGLE CRANK ANG.DEG)
1	17.181	119.79
2	6.479	140.68
3	3.439	179.17
4	1.792	203.22
5	1.042	221.89
6	.815	233.81
7	.417	260.57
8	.239	270.91
9	.156	263.46
10	.151	278.43
11	.112	318.94
12	.146	279.31
13	.190	289.22
14	.120	294.18
15	.162	353.25
	8.2E+02	7.8E+02

Fig.63 Fourier Coefficients of Wall Temperature cycle following

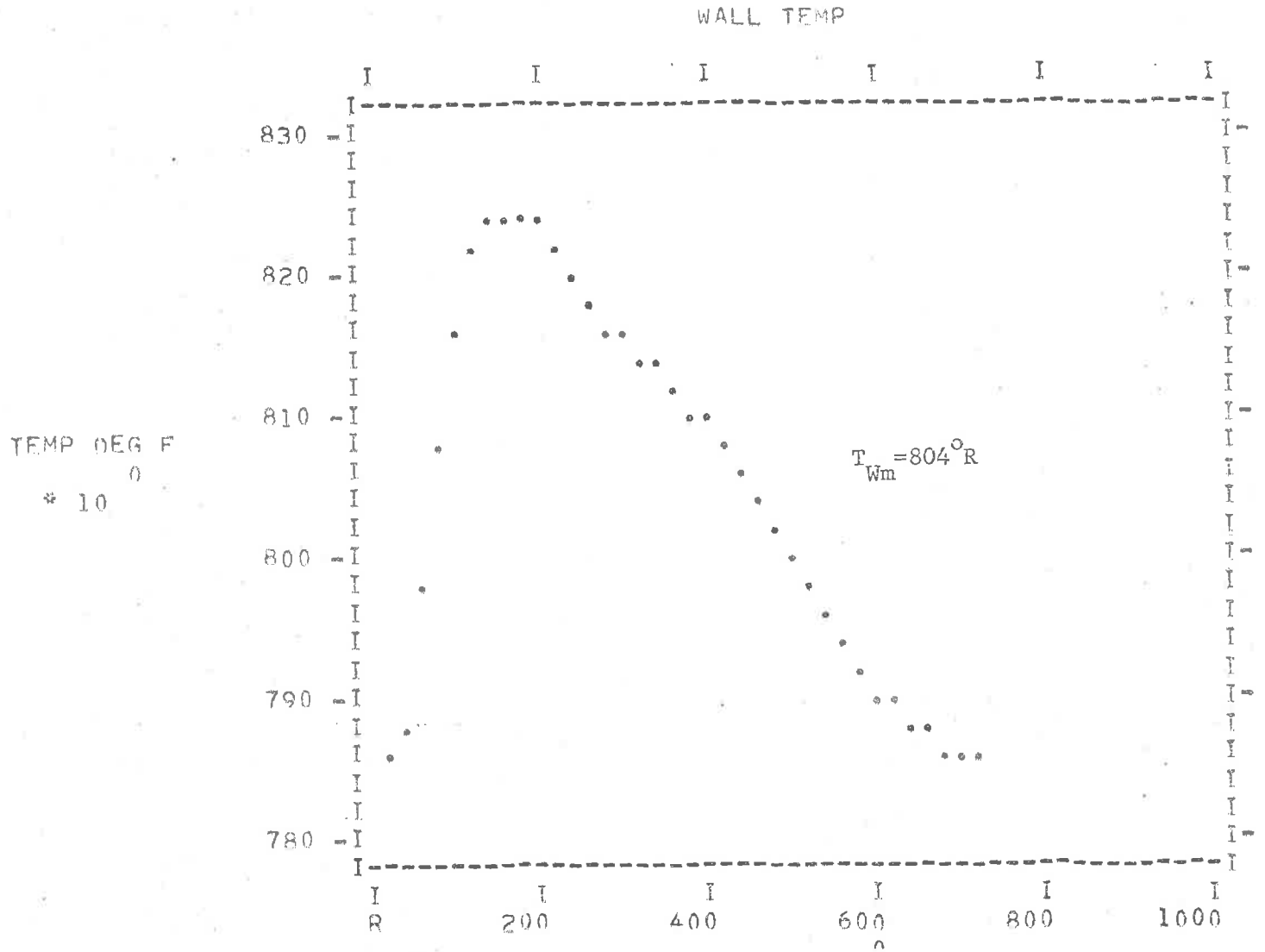

Fig.64 Wall Temperature Cycle

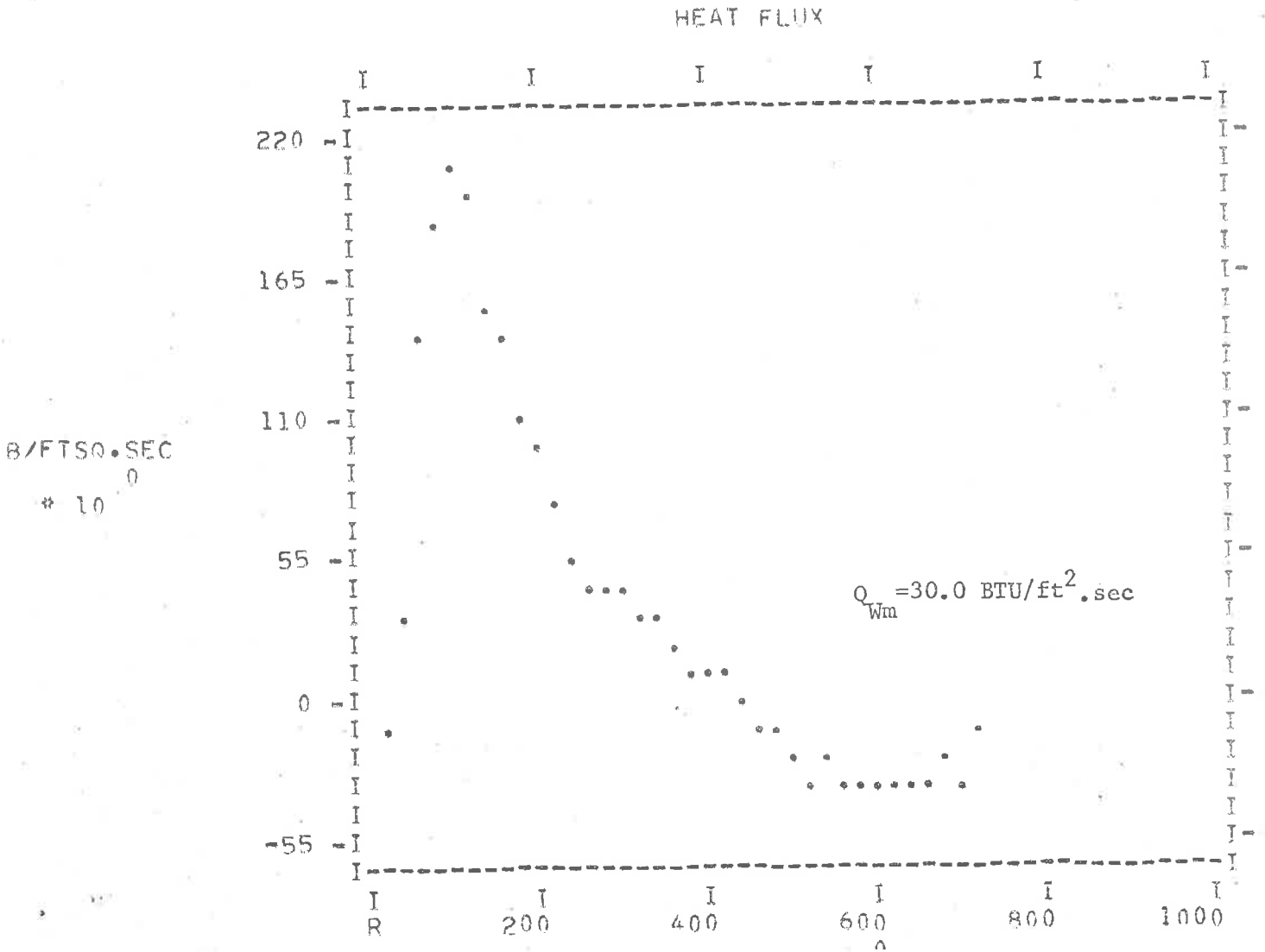

Fig.65 Heat Flux cycle derived from preceding T_w cycle

FOURIER COEFFICIENTS AT CYCLE FREQUENCY

CYCLE HARMONIC	TEMPERATURE (DEG.F)	PHASE ANGLE CRANK ANG.DEG)
1	517.652	83.58
2	230.658	71.91
3	162.162	103.73
4	181.437	88.39
5	178.718	104.91
6	145.524	131.06
7	116.417	146.41
8	105.869	153.42
9	118.582	171.32
10	97.069	176.46
11	84.033	197.19
12	86.174	198.13
13	54.864	217.41
14	67.210	219.33
15	52.047	233.79
	3.3E+03 8.0E+02	

Fig.66 Fourier Coefficients of Gas Temperature cycle following (X=0.400")

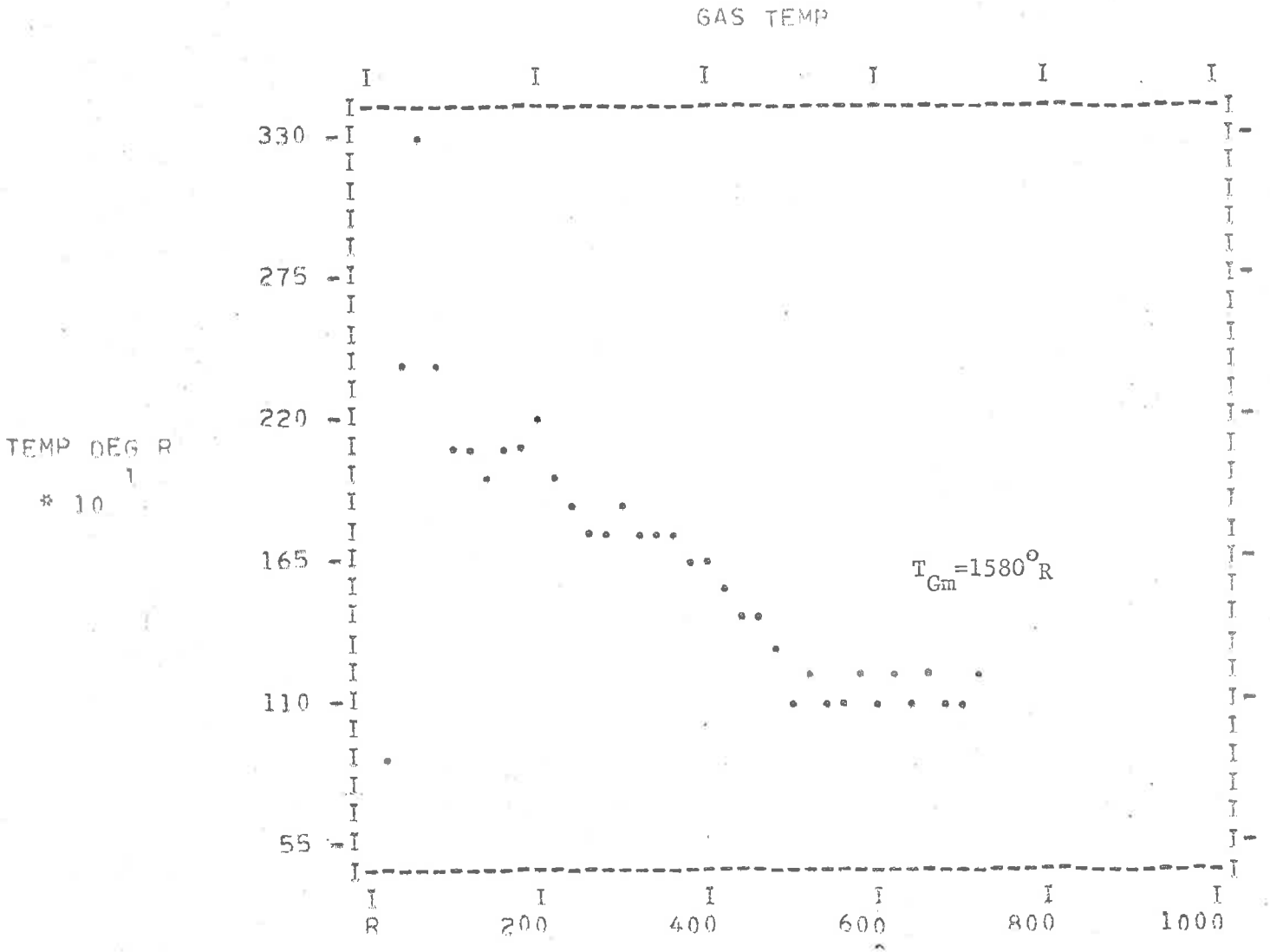

Fig.67 Gas Temperature cycle (X = 0.400")

FOURIER COEFFICIENTS AT CYCLE FREQUENCY

CYCLE HARMONIC	TEMPERATURE (DEG.F)	PHASE ANGLE CRANK ANG.DEG)
1	52.519	25.66
2	37.071	47.20
3	22.221	62.41
4	14.646	67.18
5	12.320	82.90
6	10.249	107.84
7	7.955	133.51
8	5.889	149.60
9	5.208	156.81
10	5.146	171.44
11	4.487	182.01
12	3.585	190.00
13	2.948	199.83
14	2.360	203.44
15	2.037	209.65
	2.3E+02 1.5E+01	

Fig,68 Fourier Coefficients of Gas Pressure cycle following

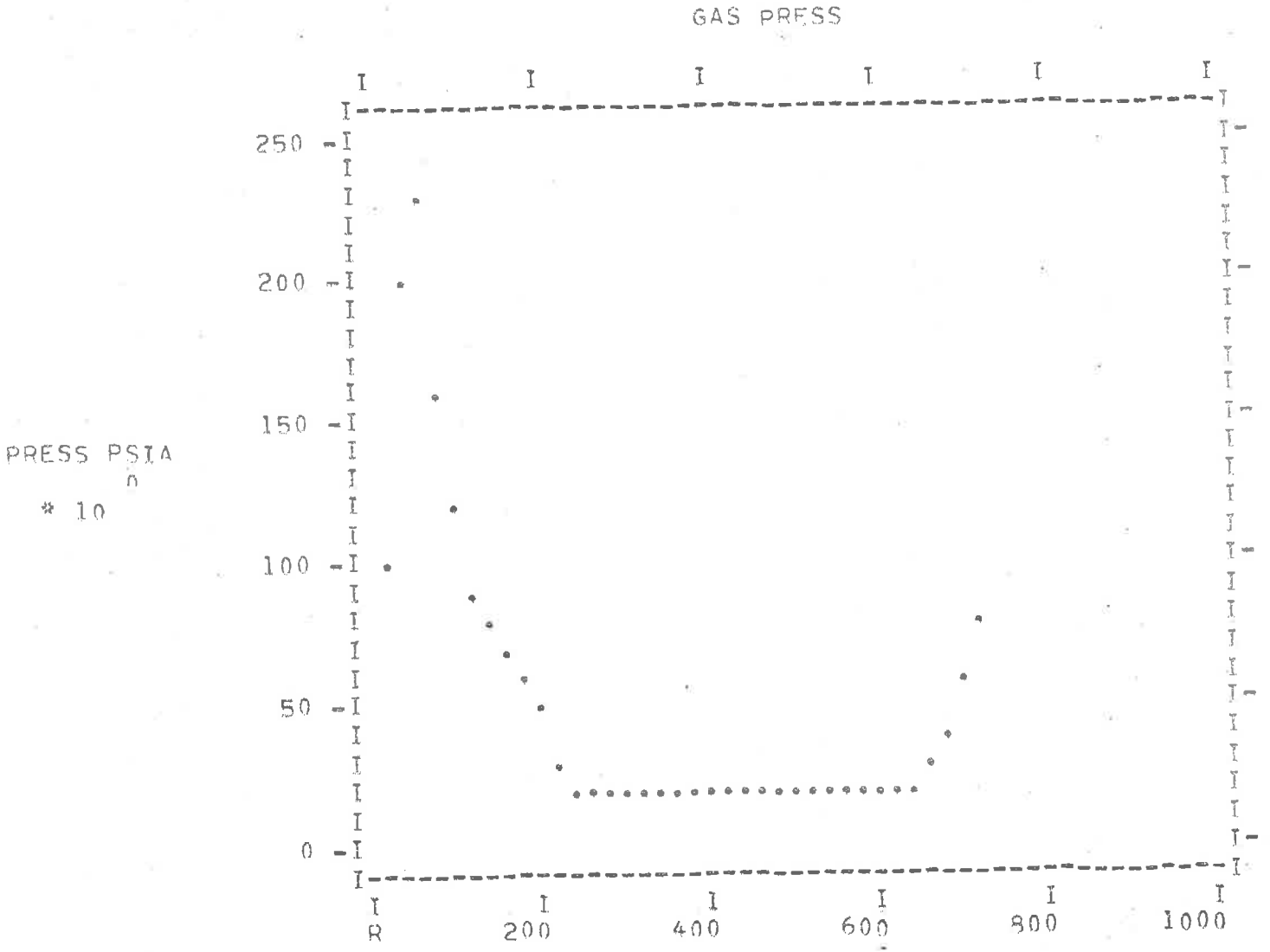

Fig.69 Gas Pressure cycle

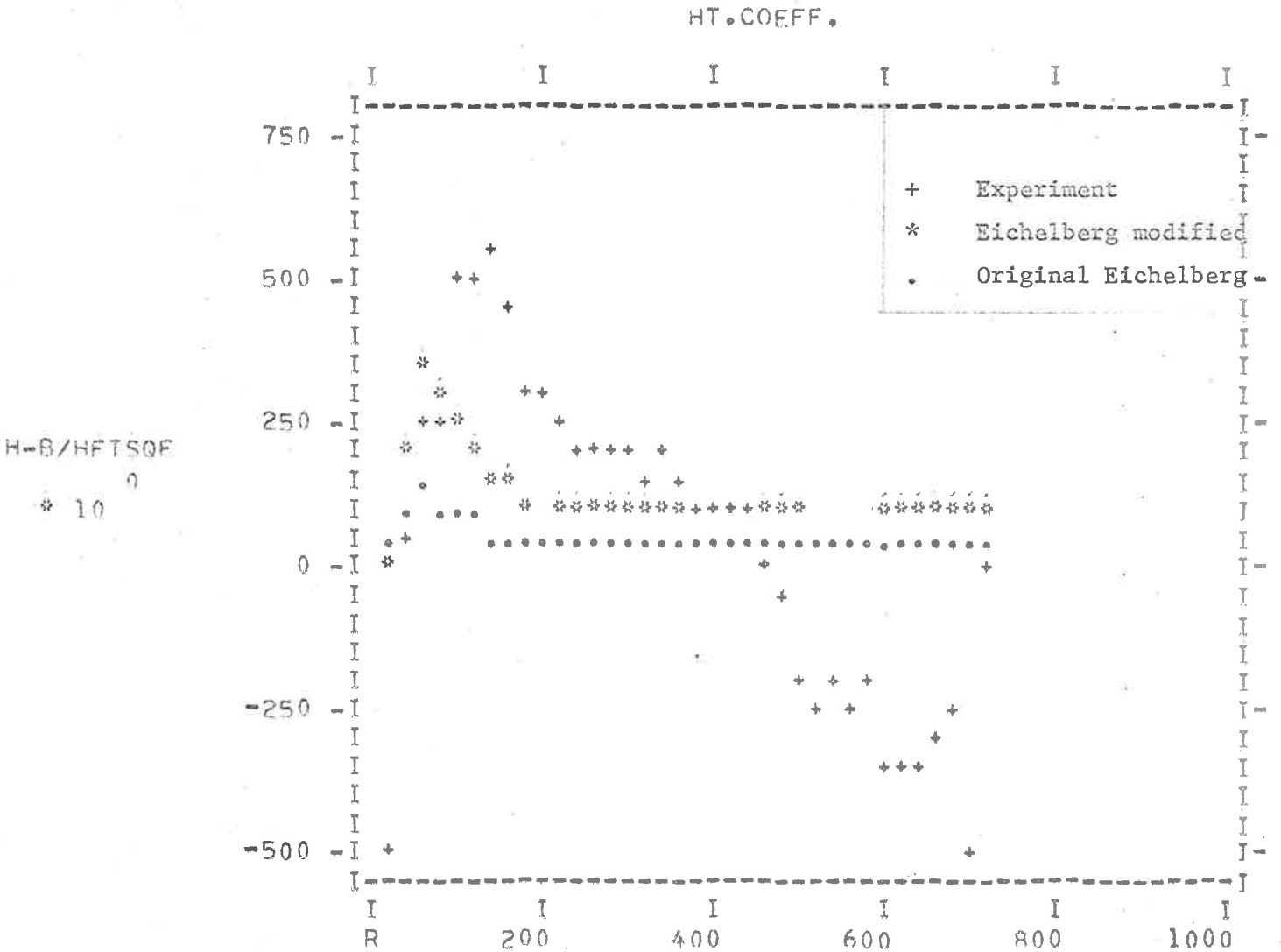

Fig.70 Cycle of Heat Transfer Coefficient
from preceding simultaneous data (X=0.400")

CONVERT TAPE =0 4
10000RPM =0TR0,25=FIRING 24PER 90K= KZ COMPENSATED, R=0.450
ANALOG TAPE A TRANSMITTAL TAPE 1990

PERIODS SELECT	INITIAL	FINAL	NUMBER OF POINTS SELECT	INITIAL	FINAL	TOTAL	PERIOD VARIATION
1	1	9	416	325	738	2885	412 417

CYCLE COUNT	CRANK ANG	PRESSURE	GAS TEMP.	WALL TEMP.	HEAT FLUX	PISTON VELOCITY	HEAT TRANSFER COEFF. FDOT,	FICM VP,	FICM, VDM
1	0	1.020E+03	1.000E+03	7.958E+02	-4.481E+01	0.	-7.931E+02	0.	4.138E+01
2	5	1.211E+03	9.425E+02	7.967E+02	-5.261E+01	2.065E+00	-1.362E+03	7.137E+01	4.130E+01
3	10	1.484E+03	9.142E+02	7.982E+02	-4.522E+01	4.067E+00	-1.224E+03	9.758E+01	4.481E+01
4	15	1.783E+03	1.023E+03	7.966E+02	-2.421E+01	6.060E+00	-1.078E+03	1.279E+02	5.191E+01
5	20	1.985E+03	1.227E+03	7.958E+02	-2.530E+00	7.993E+00	1.858E+01	1.471E+02	6.426E+01
6	25	2.118E+03	1.454E+03	7.972E+02	1.443E+01	9.781E+00	1.927E+03	2.141E+02	7.441E+01
7	30	2.291E+03	1.693E+03	7.997E+02	3.444E+01	1.145E+01	1.944E+03	2.422E+02	8.917E+01
8	35	2.330E+03	1.856E+03	7.974E+02	4.974E+01	1.301E+01	2.051E+03	2.639E+02	9.902E+01
9	40	2.274E+03	1.941E+03	7.945E+02	5.398E+01	1.443E+01	2.056E+03	2.725E+02	1.047E+02
10	45	2.164E+03	1.913E+03	7.927E+02	5.338E+01	1.570E+01	2.015E+03	2.648E+02	1.055E+02
11	50	1.994E+03	1.798E+03	8.008E+02	5.398E+01	1.678E+01	2.088E+03	2.488E+02	1.020E+02
12	55	1.770E+03	1.641E+03	8.018E+02	5.604E+01	1.770E+01	2.208E+03	2.235E+02	9.514E+01
13	60	1.540E+03	1.472E+03	8.015E+03	5.414E+01	1.844E+01	2.442E+03	2.048E+02	8.473E+01
14	65	1.342E+03	1.340E+03	8.053E+02	5.441E+01	1.898E+01	2.487E+03	2.735E+02	7.930E+01
15	70	1.208E+03	1.260E+03	8.045E+02	5.492E+01	1.934E+01	2.489E+03	2.489E+02	7.189E+01
16	75	1.204E+03	1.249E+03	8.083E+02	5.656E+01	1.954E+01	2.305E+03	2.305E+02	6.959E+01
17	80	1.130E+03	1.206E+03	8.100E+02	5.421E+01	1.955E+01	2.492E+03	2.179E+02	6.199E+01
18	85	1.044E+03	1.205E+03	8.115E+02	5.462E+01	1.940E+01	2.030E+03	2.098E+02	5.974E+01
19	90	1.009E+03	1.204E+03	8.131E+02	5.471E+01	1.909E+01	2.488E+03	2.032E+02	5.826E+01
20	95	9.681E+02	1.172E+03	8.145E+02	5.427E+01	1.862E+01	2.713E+03	1.966E+02	5.677E+01
21	100	8.777E+02	1.078E+03	8.154E+02	5.488E+01	1.800E+01	4.672E+03	1.888E+02	5.494E+01
22	105	8.211E+02	1.047E+03	8.163E+02	5.455E+03	1.738E+01	4.568E+03	1.781E+02	5.274E+01
23	110	7.747E+02	1.027E+03	8.170E+02	5.416E+02	1.663E+01	4.674E+03	1.674E+02	5.062E+01
24	115	7.495E+02	1.004E+03	8.177E+02	5.488E+02	1.582E+01	4.032E+03	1.575E+02	4.930E+01
25	120	7.170E+02	1.015E+03	8.184E+02	5.448E+02	1.488E+01	5.206E+03	1.489E+02	4.644E+01
26	125	7.000E+02	1.029E+03	8.190E+02	5.447E+02	1.387E+01	5.337E+03	1.419E+02	4.560E+01
27	130	6.868E+02	1.033E+03	8.194E+02	5.408E+02	1.266E+01	5.190E+03	1.343E+02	4.507E+01
28	135	6.656E+02	1.043E+03	8.199E+02	5.339E+02	1.130E+01	4.792E+03	1.311E+02	4.489E+01
29	140	6.629E+02	1.079E+03	8.201E+02	5.248E+02	1.011E+01	4.594E+03	1.241E+02	4.417E+01
30	145	6.155E+02	1.016E+03	8.200E+02	5.145E+02	9.084E+00	3.699E+03	1.200E+02	4.439E+01
31	150	5.884E+02	1.028E+03	8.197E+02	5.068E+02	7.881E+00	3.259E+03	1.134E+02	4.382E+01
32	155	5.584E+02	1.003E+03	8.194E+02	9.752E+01	6.395E+00	2.967E+03	1.083E+02	4.703E+01
33	160	5.322E+02	1.011E+03	8.192E+02	9.344E+01	5.115E+00	2.829E+03	1.044E+02	4.209E+01
34	165	5.069E+02	1.009E+03	8.191E+02	9.191E+01	3.882E+00	2.817E+03	1.019E+02	4.105E+01
35	170	4.780E+02	1.007E+03	8.192E+02	9.134E+01	2.663E+00	2.859E+03	1.011E+02	3.992E+01
36	175	4.487E+02	1.008E+03	8.193E+02	9.664E+01	1.282E+00	2.895E+03	1.023E+02	3.842E+01
37	180	4.114E+02	1.038E+03	8.195E+02	9.513E+01	-5.819E-07	2.542E+03	1.080E+02	3.776E+01
38	185	3.681E+02	1.022E+03	8.195E+02	9.151E+01	-1.282E+00	2.740E+03	1.088E+02	3.515E+01
39	190	3.243E+02	1.031E+03	8.194E+02	8.481E+01	-2.563E+00	2.542E+03	5.881E+01	3.291E+01
40	195	2.912E+02	1.007E+03	8.190E+02	7.510E+01	-3.843E+00	2.107E+03	6.347E+01	3.054E+01
41	200	2.844E+02	1.079E+03	8.185E+02	6.718E+01	-5.114E+00	2.081E+03	6.144E+01	2.829E+01
42	205	2.170E+02	1.042E+03	8.179E+02	5.956E+01	-6.384E+00	1.907E+03	6.194E+01	2.641E+01
43	210	1.995E+02	1.003E+03	8.174E+02	5.642E+01	-7.641E+00	1.812E+03	6.443E+01	2.504E+01
44	215	1.908E+02	1.047E+03	8.169E+02	5.264E+01	-8.884E+00	1.709E+03	6.556E+01	2.425E+01
45	220	1.842E+02	1.040E+03	8.166E+02	5.234E+01	-1.011E+01	1.961E+03	6.717E+01	2.381E+01
46	225	1.815E+02	1.021E+03	8.163E+02	5.298E+01	-1.130E+01	1.898E+03	6.886E+01	2.352E+01
47	230	1.801E+02	1.008E+03	8.161E+02	5.320E+01	-1.244E+01	1.935E+03	7.019E+01	2.320E+01
48	235	1.783E+02	1.000E+03	8.160E+02	5.223E+01	-1.357E+01	1.931E+03	7.091E+01	2.278E+01
49	240	1.781E+02	1.760E+03	8.157E+02	5.211E+01	-1.463E+01	1.892E+03	7.121E+01	2.231E+01
50	245	1.844E+02	1.745E+03	8.154E+02	4.748E+01	-1.562E+01	1.886E+03	7.149E+01	2.192E+01
51	250	1.845E+02	1.731E+03	8.151E+02	4.512E+01	-1.653E+01	1.801E+03	7.225E+01	2.174E+01
52	255	1.840E+02	1.705E+03	8.149E+02	4.435E+01	-1.734E+01	1.793E+03	7.174E+01	2.184E+01
53	260	1.784E+02	1.703E+03	8.147E+02	4.478E+01	-1.805E+01	1.815E+03	7.509E+01	2.217E+01
54	265	1.780E+02	1.715E+03	8.146E+02	4.519E+01	-1.866E+01	1.986E+03	7.927E+01	2.261E+01
55	270	1.841E+02	1.710E+03	8.145E+02	4.769E+01	-1.918E+01	1.857E+03	8.030E+01	2.301E+01
56	275	1.848E+02	1.768E+03	8.145E+02	4.835E+01	-1.960E+01	1.929E+03	8.144E+01	2.324E+01
57	280	1.819E+02	1.788E+03	8.144E+02	4.758E+01	-1.993E+01	1.763E+03	8.148E+01	2.318E+01
58	285	1.774E+02	1.791E+03	8.143E+02	4.534E+01	-1.996E+01	1.672E+03	8.048E+01	2.291E+01
59	290	1.725E+02	1.777E+03	8.140E+02	4.231E+01	-1.975E+01	1.578E+03	7.904E+01	2.254E+01
60	295	1.701E+02	1.758E+03	8.133E+02	3.933E+01	-1.908E+01	1.505E+03	7.780E+01	2.224E+01
61	300	1.714E+02	1.754E+03	8.125E+02	3.729E+01	-1.866E+01	1.476E+03	7.690E+01	2.214E+01
62	305	1.757E+02	1.788E+03	8.132E+02	3.657E+01	-1.777E+01	1.477E+03	7.549E+01	2.224E+01
63	310	1.803E+02	1.802E+03	8.131E+02	3.700E+01	-1.672E+01	1.507E+03	7.537E+01	2.254E+01
64	315	1.851E+02	1.795E+03	8.129E+02	3.785E+01	-1.570E+01	1.528E+03	7.665E+01	2.288E+01
65	320	1.844E+02	1.773E+03	8.128E+02	3.920E+01	-1.463E+01	1.510E+03	7.729E+01	2.306E+01
66	325	1.844E+02	1.743E+03	8.127E+02	3.736E+01	-1.351E+01	1.443E+03	7.594E+01	2.309E+01
67	330	1.808E+02	1.756E+03	8.125E+02	3.492E+01	-1.234E+01	1.434E+03	6.737E+01	2.291E+01
68	335	1.764E+02	1.740E+03	8.122E+02	3.194E+01	-9.761E+00	1.208E+03	6.101E+01	2.260E+01
69	340	1.737E+01	1.729E+03	8.119E+02	2.787E+01	-7.042E+00	1.088E+03	5.885E+01	2.229E+01
70	345	1.737E+01	1.700E+03	8.115E+02	2.455E+01	-5.015E+00	9.947E+01	5.856E+01	2.211E+01
71	350	1.782E+01	1.672E+03	8.111E+02	2.374E+01	-3.947E+00	9.595E+01	5.831E+01	2.208E+01
72	355	1.797E+01	1.655E+03	8.108E+02	2.234E+01	-2.626E+00	9.570E+01	5.837E+01	2.219E+01
73	360	1.822E+01	1.655E+03	8.105E+02	2.208E+01	2.180E-04	9.764E+01	5.799E+01	2.236E+01
74	365	1.813E+01	1.649E+03	8.103E+02	2.341E+01	2.564E+00	9.900E+01	5.714E+01	2.241E+01
75	370	1.782E+01	1.648E+03	8.101E+02	2.350E+01	4.847E+00	9.479E+01	5.449E+01	2.231E+01
76	375	1.731E+01	1.701E+03	8.099E+02	2.219E+01	5.040E+00	9.069E+01	5.232E+01	2.201E+01
77	380	1.655E+01	1.615E+03	8.098E+02	2.000E+01	7.042E+00	8.129E+01	5.412E+01	2.155E+01
78	385	1.609E+01	1.668E+03	8.093E+02	1.696E+01	9.451E+00	7.124E+01	5.871E+01	2.106E+01
79	390	1.594E+01	1.683E+03	8.089E+02	1.403E+01	1.168E+01	6.281E+01	6.070E+01	2.064E+01
80	395	1.617E+01	1.668E+03	8.085E+02	1.196E+01	1.301E+01	5.827E+01	6.244E+01	2.034E+01
81	400	1.655E+01	1.674E+03	8.081E+02	1.087E+01	1.443E+01	5.694E+01	6.448E+01	2.015E+01
82	405	1.700E+01	1.692E+03	8.078E+02	1.090E+01	1.570E+01	6.192E+01	6.513E+01	2.000E+01
83	410	1.715E+01	1.696E+03	8.075E+02	1.109E+01	1.679E+01	6.004E+01	6.424E+01	1.993E+01
84	415	1.696E+01	1.670E+03	8.073E+02	1.073E+01	1.770E+01	6.457E+01	6.446E+01	1.990E+01
85	421	1.660E+01	1.672E+03	8.070E+02	9.227E+00	1.844E+01	5.977E+01	6.451E+01	1.990E+01
86	425	1.673E+01	1.707E+03	8.068E+02	8.461E+00	1.898E+01	6.028E+01	6.502E+01	1.987E+01
87	430	1.651E+01	1.698E+03	8.065E+02	7.718E+00	1.935E+01	1.460E+01	6.552E+01	1.971E+01
88	435	1.609E+01	1.698E+03	8.062E+02	-1.352E+00	1.954E+01	-7.457E+00	6.537E+01	1.860E+01
89	440	1.525E+01	1.698E+03	8.051E+02	-4.720E+00	1.955E+01	-2.924E+01	6.574E+01	1.870E+01
90	445	1.508E+01	1.670E+03	8.046E+02	-7.212E+00	1.938E+01	-4.594E+01	6.645E+01	1.895E+01
91	450	1.445E+01	1.687E+03	8.041E+02	-8.170E+00	1.905E+01	-5.767E+01	6.702E+01	1.922E+01
92	455	1.713E+01	1.722E+03	8.036E+02	-9.593E+00	1.856E+01	-6.481E+01	6.697E+01	1.934E+01
93	460	1.733E+01	1.695E+03	8.031E+02	-1.053E+01	1.805E+01	-7.701E+01	6.595E+01	1.927E+01
94	465	1.709E+01	1.704E+03	8.027E+02	-1.207E+01	1.714E+01	-8.371E+01	6.392E+01	1.893E+01
95	471	1.655E+01	1.731E+03	8.022E+02	-1.445E+01	1.613E+01	-1.284E+02	6.111E+01	1.839E+01
96	475	1.594E+01	1.719E+03	8.018E+02	-1.744E+01	1.513E+01	-1.581E+02	5.902E+01	1.779E+01
97	480	1.554E+01	1.742E+03	8.011E+02	-2.047E+01	1.413E+01	-2.039E+02	5.522E+01	1.730E+01
98	485	1.558E+01	1.711E+03	8.005E+02	-2.309E+01	1.317E+01	-2.494E+02	5.308E+01	1.705E+01
99	490	1.582E+01	1.710E+03	7.999E+02	-2.525E+01	1.244E+01	-2.915E+02	5.184E+01	1.704E+01
100	495	1.644E+01	1.710E+03	7.994E+02	-2.690E+01	1.197E+01	-3.242E+02	5.174E+01	1.713E+01
101	500	1.693E+01	1.715E+03	7.990E+02	-2.804E+01	1.181E+01	-3.440E+02	5.200E+01	1.747E+01
102	505	1.719E+01	1.738E+03	7.986E+02	-2.859E+01	1.198E+01	-3.503E+02	5.453E+01	1.795E+01
103	510	1.690E+01	1.765E+03	7.982E+02	-2.872E+01	1.241E+01	-3.370E+02	5.439E+01	1.805E+01
104	515	1.634E+01	1.784E+03	7.977E+02	-2.873E+01	1.304E+01	-3.209E+02	5.339E+01	1.792E+01
105	521	1.657E+01	1.795E+03	7.973E+02	-2.844E+01	1.376E+01	-3.198E+02	5.205E+01	1.761E+01
106	525	1.654E+01	1.795E+03	7.968E+02	-2.813E+01	1.443E+01	-3.243E+02	5.141E+01	1.731E+01
107	530	1.620E+01	1.778E+03	7.963E+02	-2.784E+01	1.503E+01	-3.272E+02	5.078E+01	1.719E+01
108	536	1.569E+01	1.757E+03	7.959E+02	-2.791E+01	1.553E+01	-3.242E+02	5.056E+01	1.728E+01
109	540	1.629E+01	1.748E+03	7.955E+02	-2.811E+01	1.593E+01	-3.198E+02	5.056E+01	1.754E+01
110	545	1.703E+01	1.752E+03	7.952E+02	-2.832E+01	1.622E+01	-3.137E+02	5.092E+01	1.802E+01
111	550	1.750E+01	1.779E+03	7.949E+02	-2.850E+01	1.642E+01	-3.063E+02	5.147E+01	1.847E+01
112	555	1.763E+01	1.791E+03	7.946E+02	-2.858E+01	1.654E+01	-2.985E+02	5.200E+01	1.867E+01
113	560	1.716E+01	1.770E+03	7.942E+02	-2.851E+01	1.661E+01	-2.917E+02	5.230E+01	1.867E+01
114	565	1.656E+01	1.765E+03	7.938E+02	-3.107E+01	1.665E+01	-2.879E+02	5.247E+01	1.868E+01
115	571	1.650E+01	1.762E+03	7.933E+02	-3.487E+01	1.667E+01	-2.866E+02	5.255E+01	1.868E+01
116	575	1.690E+01	1.791E+03	7.927E+02	-3.743E+01	1.668E+01	-2.867E+02	5.259E+01	1.869E+01
117	580	1.698E+01	1.788E+03	7.922E+02	-3.825E+01	1.669E+01	-2.873E+02	5.260E+01	1.869E+01
118	585	1.725E+01	1.743E+03	7.917E+02	-3.801E+01	1.669E+01	-2.880E+02	5.260E+01	1.869E+01
119	590	1.817E+01	1.738E+03	7.911E+02	-3.722E+01	1.669E+01	-2.885E+02	5.260E+01	1.869E+01
120	595	1.884E+01	1.734E+03	7.911E+02	-3.611E+01	1.669E+01	-2.888E+02	5.260E+01	1.869E+01
121	600	1.903E+01	1.737E+03	7.906E+02	-3.478E+01	1.669E+01	-2.890E+02	5.260E+01	1.869E+01
122	605	1.876E+01	1.743E+03	7.900E+02	-3.341E+01	1.669E+01	-2.891E+02	5.260E+01	1.869E+01
123	610	1.815E+01	1.740E+03	7.902E+02	-3.219E+01	1.669E+01	-2.892E+02	5.260E+01	1.869E+01
124	615	1.784E+01	1.749E+03	7.899E+02	-3.145E+01	1.669E+01	-2.892E+02	5.260E+01	1.869E+01
125	620	1.772E+01	1.768E+03	7.894E+02	-3.099E+01	1.669E+01	-2.893E+02	5.260E+01	1.869E+01
126	626	1.841E+01	1.759E+03	7.889E+02	-4.019E+01	-1.044E+01	-3.001E+02	5.578E+01	1.898E+01
127	630	2.031E+01	1.752E+03	7.886E+02	-3.914E+01	-1.000E+01	-3.882E+02	5.040E+01	1.868E+01
128	635	2.253E+01	1.752E+03	7.883E+02	-3.805E+01	-1.040E+01	-3.844E+02	5.267E+01	1.873E+01
129	640	2.483E+01	1.755E+03	7.882E+02	-3.190E+01	-1.005E+01	-3.888E+02	5.496E+01	1.889E+01
130	645	2.696E+01	1.780E+03	7.882E+02	-2.795E+01	-1.084E+01	-2.834E+02	5.081E+01	2.100E+01
131	650	2.876E+01	1.730E+03	7.882E+02	-2.599E+01	-1.039E+01	-2.351E+02	8.379E+01	2.192E+01
132	655	3.013E+01	1.705E+03	7.880E+02	-2.465E+01	-1.008E+01	-2.291E+02	8.883E+01	2.266E+01
133	660	3.282E+01	1.741E+03	7.878E+02	-2.419E+01	-1.044E+01	-2.671E+02	8.739E+01	2.533E+01
134	665	3.633E+01	1.732E+03	7.875E+02	-3.244E+01	-1.770E+01	-3.194E+02	8.843E+01	2.608E+01
135	670	4.164E+01	1.668E+03	7.871E+02	-3.614E+01	-1.670E+01	-4.460E+02	9.179E+01	2.705E+01
136	676	4.814E+01	1.700E+03	7.866E+02	-3.281E+01	-1.670E+01	-5.392E+02	9.241E+01	2.829E+01
137	680	5.573E+01	1.647E+03	7.867E+02	-2.720E+01	-1.644E+01	-5.392E+02	9.494E+01	2.989E+01
138	685	6.322E+01	9.726E+02	7.869E+02	-1.893E+01	-1.610E+01	-5.474E+02	9.789E+01	3.189E+01
139	690	6.996E+01	1.018E+03	7.873E+02	-1.032E+01	-1.516E+01	-5.412E+02	1.007E+02	3.422E+01
140	695	7.604E+01	1.089E+03	7.877E+02	-4.569E+00	-9.761E+00	-5.453E+01	1.019E+02	3.653E+01
141	700	7.994E+01	1.158E+03	7.880E+02	-4.194E+00	-7.982E+00	-4.377E+01	9.999E+01	3.846E+01
142	706	7.936E+01	1.194E+03	7.879E+02	-1.094E+01	-6.040E+00	-9.701E+01	9.411E+01	3.959E+01
143	710	8.389E+01	1.174E+03	7.876E+02	-2.302E+01	-4.047E+00	-2.131E+02	8.780E+01	4.022E+01
144	715	9.039E+01	1.149E+03	7.866E+02	-3.719E+01	-2.084E+00	-4.901E+02	8.139E+01	4.065E+01

10000RPM =0TR0,25=FIRING 24PER 90K= KZ COMPENSATED, R=0.450

Fig.71
Data set X = 0.45"

CONVERT TAPE NO 4
1000RPM WOT*0.25,FIRING 24DEG SPK, KZ COMPENSATED, X=0.450
ANALOG TAPE 6 TRANSMITTAL TAPE 1558

SERIAL	RUN	CHANNEL	TYPE	NO PERIODS	COEFF
7	17	123	1	1	15

NO POINTS	INITIAL	MAX PERIODS
414	1	7

FOURIER COEFFICIENTS AT CYCLE FREQUENCY

CYCLE HARMONIC	TEMPERATURE (DEG.F)	PHASE ANGLE CRANK ANG.DEG)
1	14.949	127.63
2	5.290	145.20
3	2.953	188.23
4	1.502	215.79
5	.852	237.65
6	.776	240.03
7	.484	255.30
8	.349	256.06
9	.378	252.44
10	.426	267.04
11	.330	285.75
12	.204	290.03
13	.215	280.88
14	.255	278.67
15	.273	301.31
	8.2E+02	7.8E+02

Fig.72 Fourier Coefficients of Wall Temperature cycle following

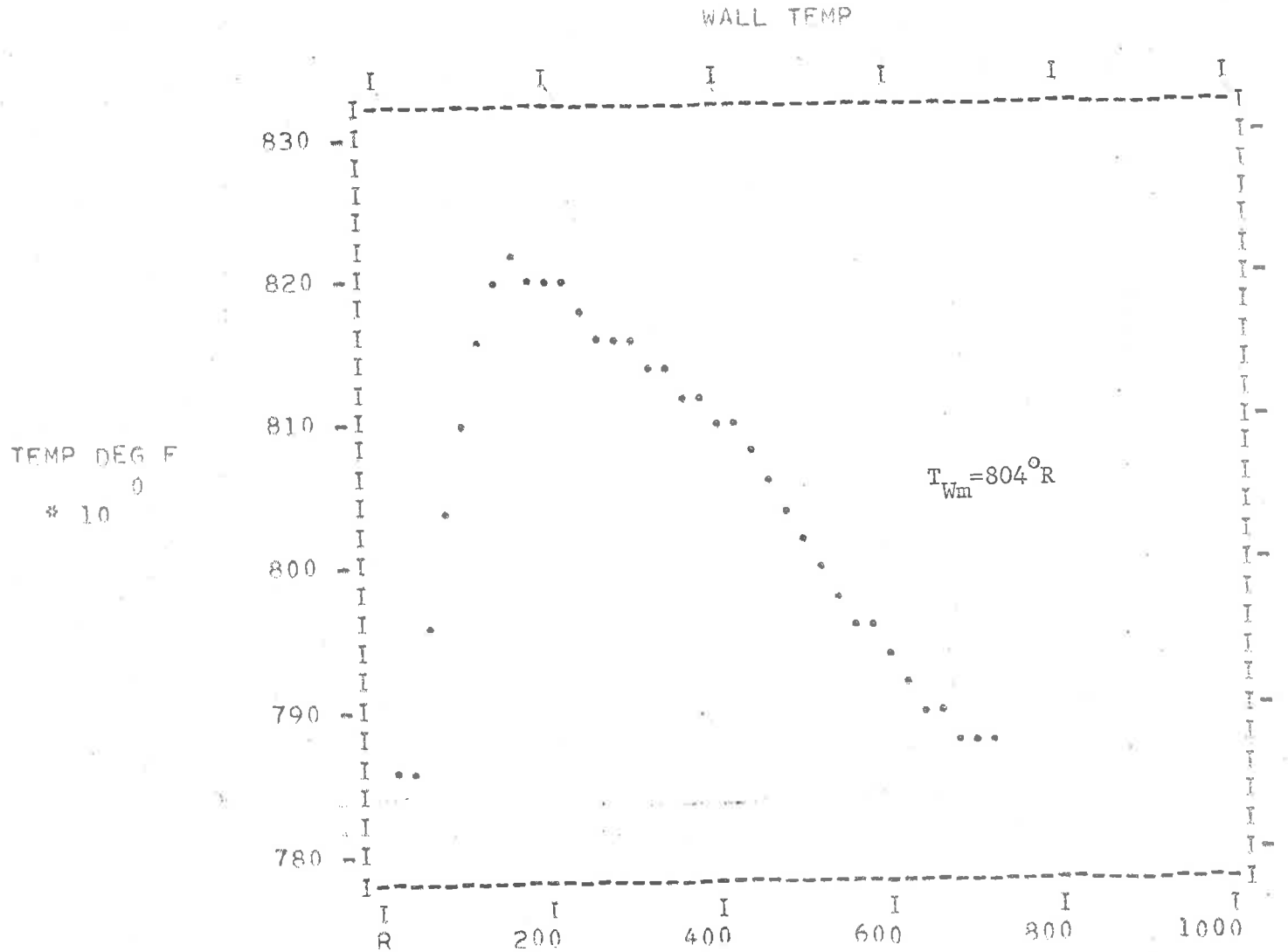

Fig.73 Wall Temperature cycle

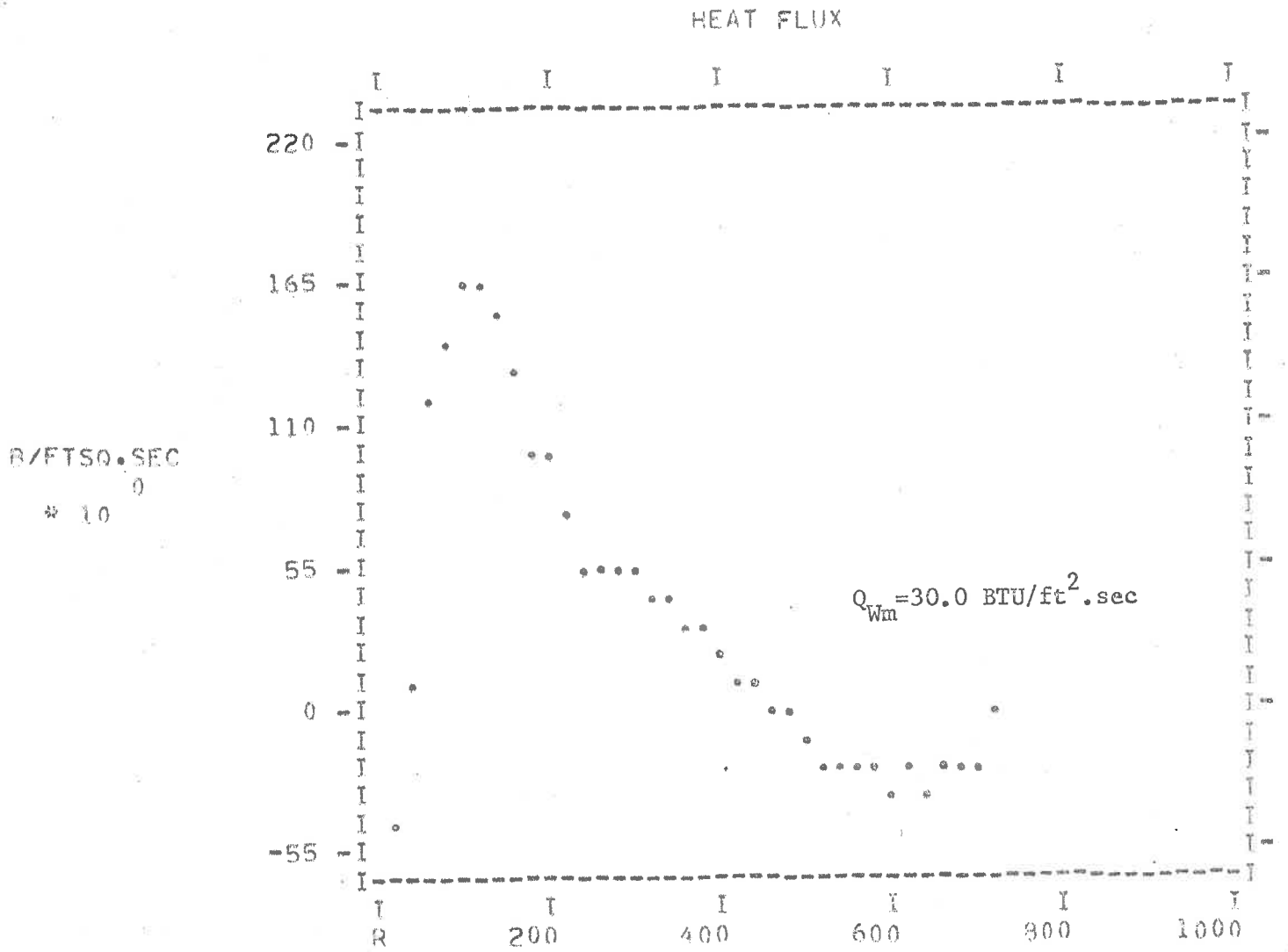

Fig.74 Heat Flux cycle derived from preceding T_w cycle

FOURIER COEFFICIENTS AT CYCLE FREQUENCY

CYCLE HARMONIC	TEMPERATURE (DEG.F)	PHASE ANGLE (CRANK ANG.DEG)
1	473.045	89.33
2	186.064	82.40
3	180.981	118.68
4	164.680	107.53
5	168.459	136.03
6	151.164	166.09
7	122.461	183.92
8	69.974	197.66
9	93.034	222.04
10	71.026	238.92
11	91.383	262.54
12	80.048	264.57
13	70.208	303.21
14	50.284	311.32
15	49.671	329.71
	3.2E+03	9.2E+02

Fig.75 Fourier Coefficients of Gas Temperature cycle following (X=0.450")

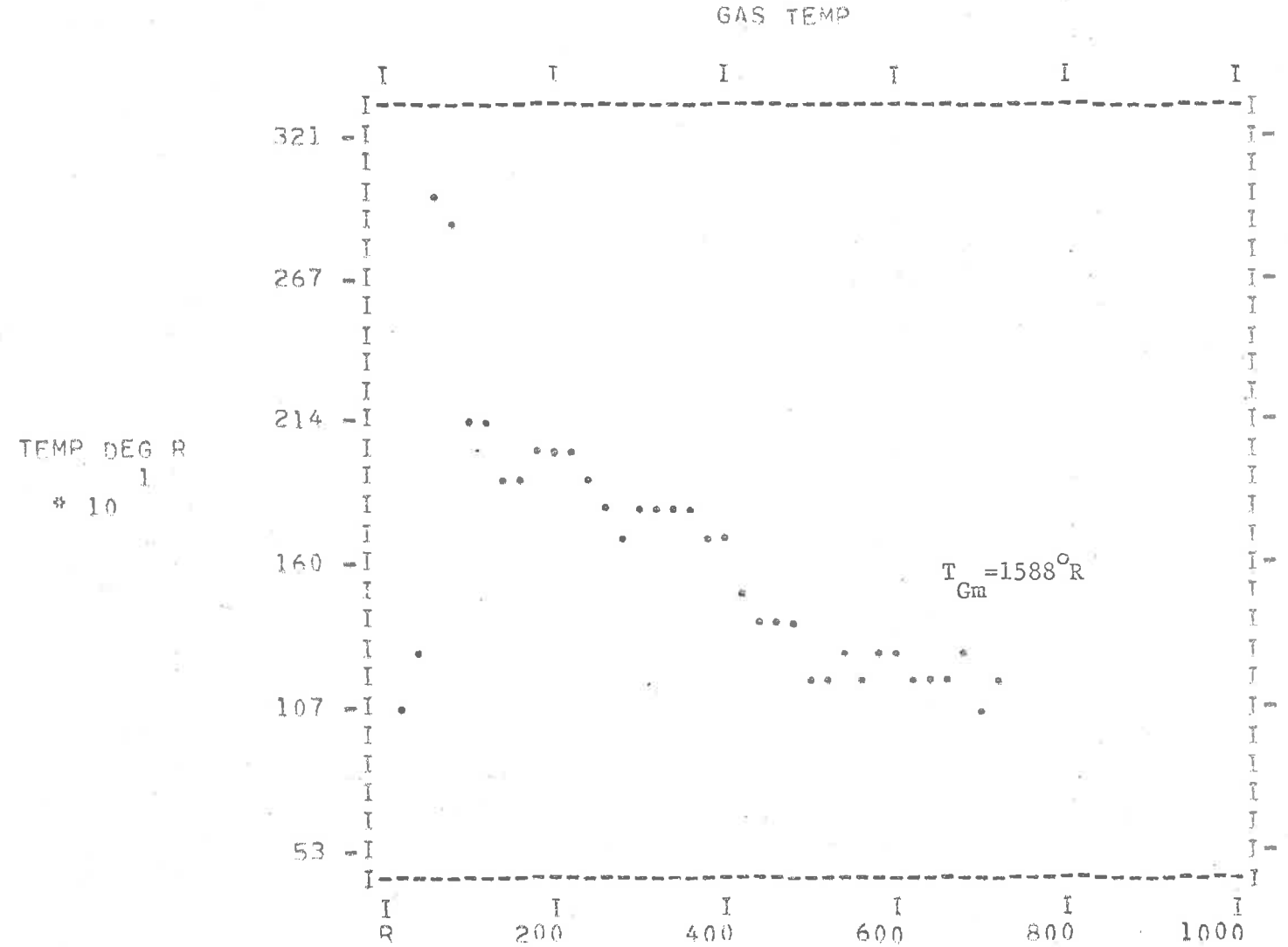

Fig.76 Gas Temperature cycle (X = 0.450")

FOURIER COEFFICIENTS AT CYCLE FREQUENCY

CYCLE HARMONIC	TEMPERATURE (DEG.F)	PHASE ANGLE CRANK ANG.DEG)
1	53.330	25.81
2	37.426	47.10
3	22.691	62.40
4	15.026	66.83
5	12.732	81.81
6	10.386	107.61
7	8.023	134.28
8	6.077	148.21
9	5.285	156.15
10	4.868	169.28
11	4.022	182.96
12	3.181	195.86
13	2.495	202.71
14	2.001	214.25
15	1.675	220.13
	2.3E+02 1.5E+01	

Fig.77 Fourier Coefficients of Gas Pressure cycle following

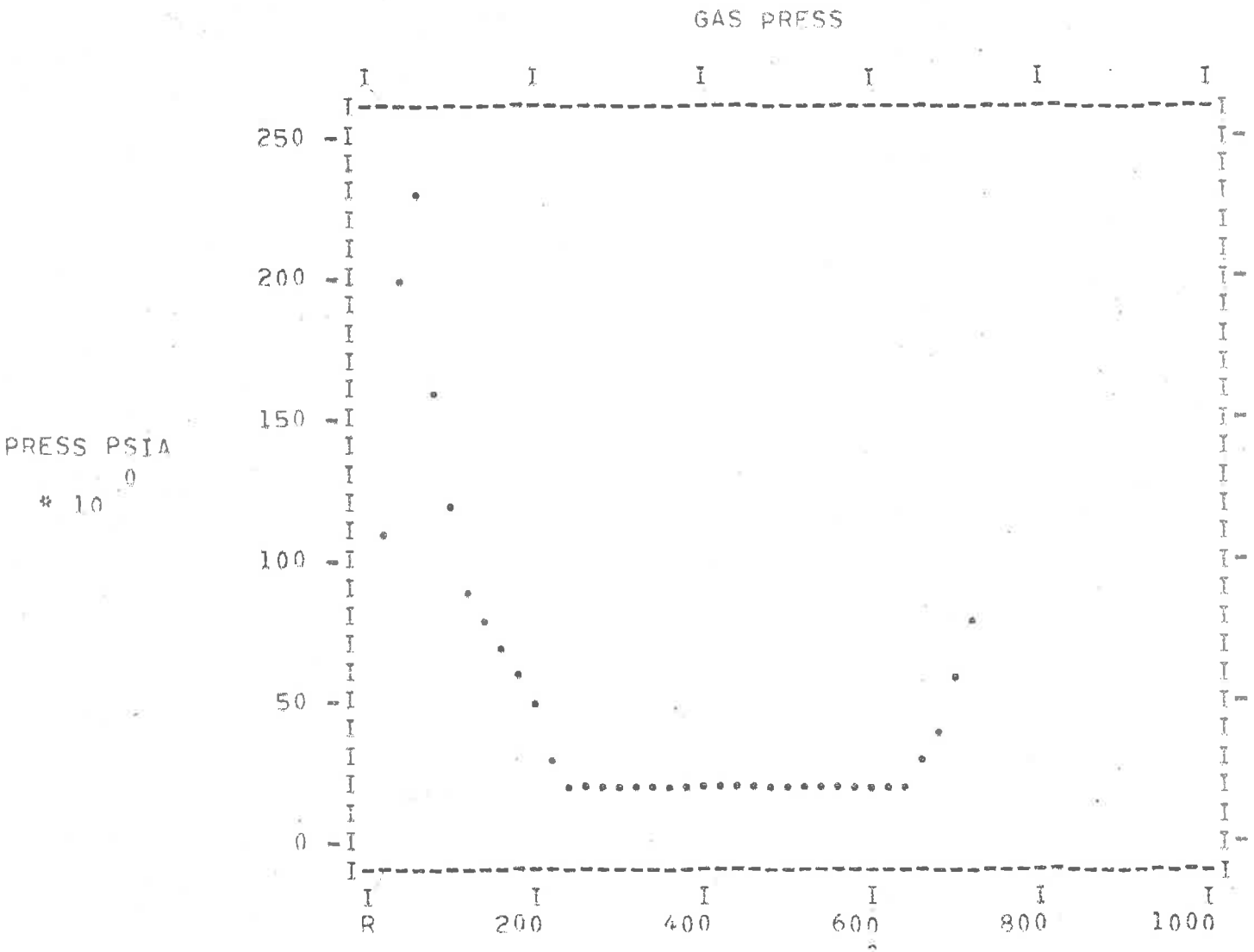

Fig.78 Gas Pressure cycle

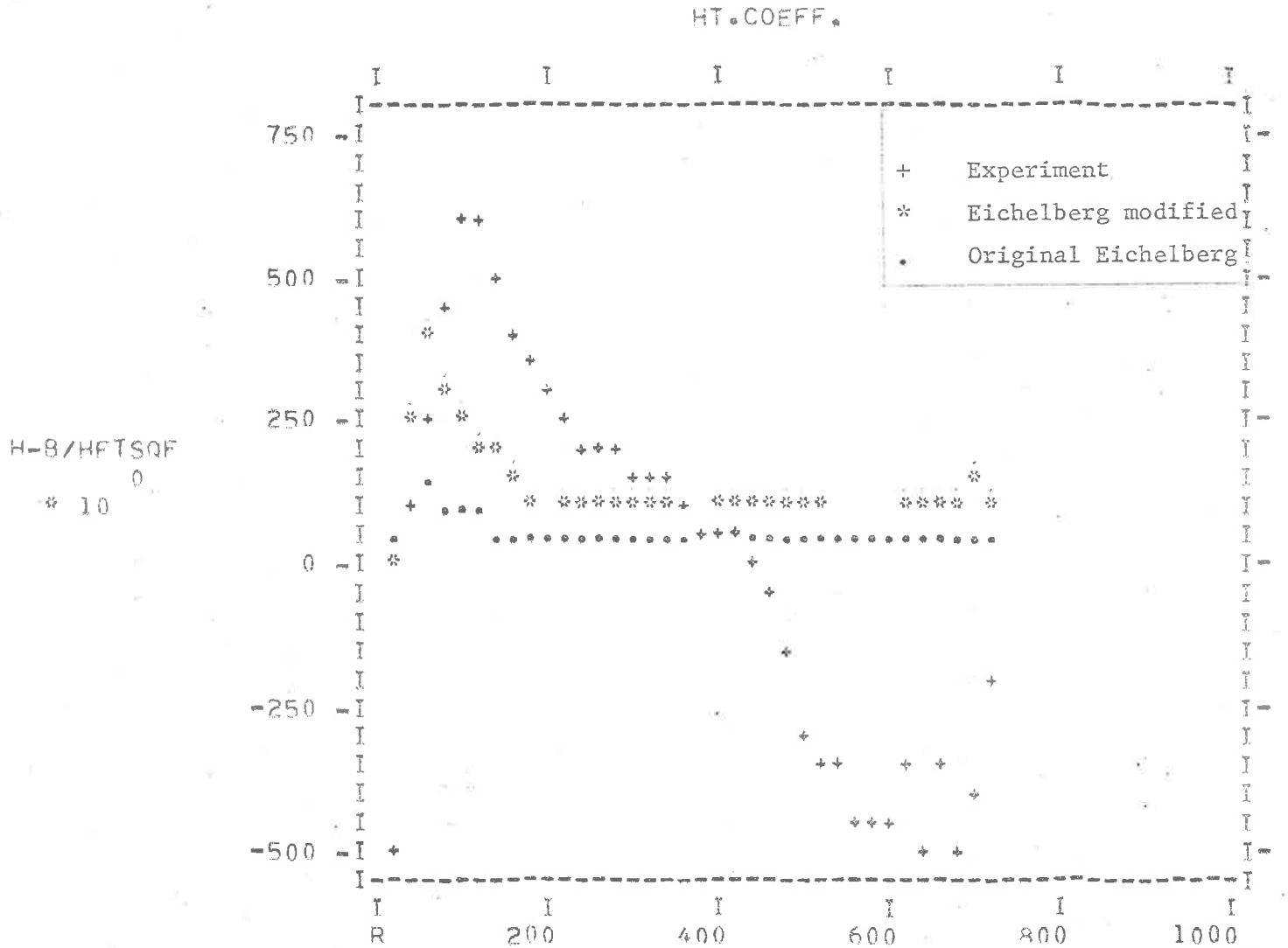

Fig.79 Cycle of Heat Transfer Coefficient
from preceding simultaneous data (X=0.450")

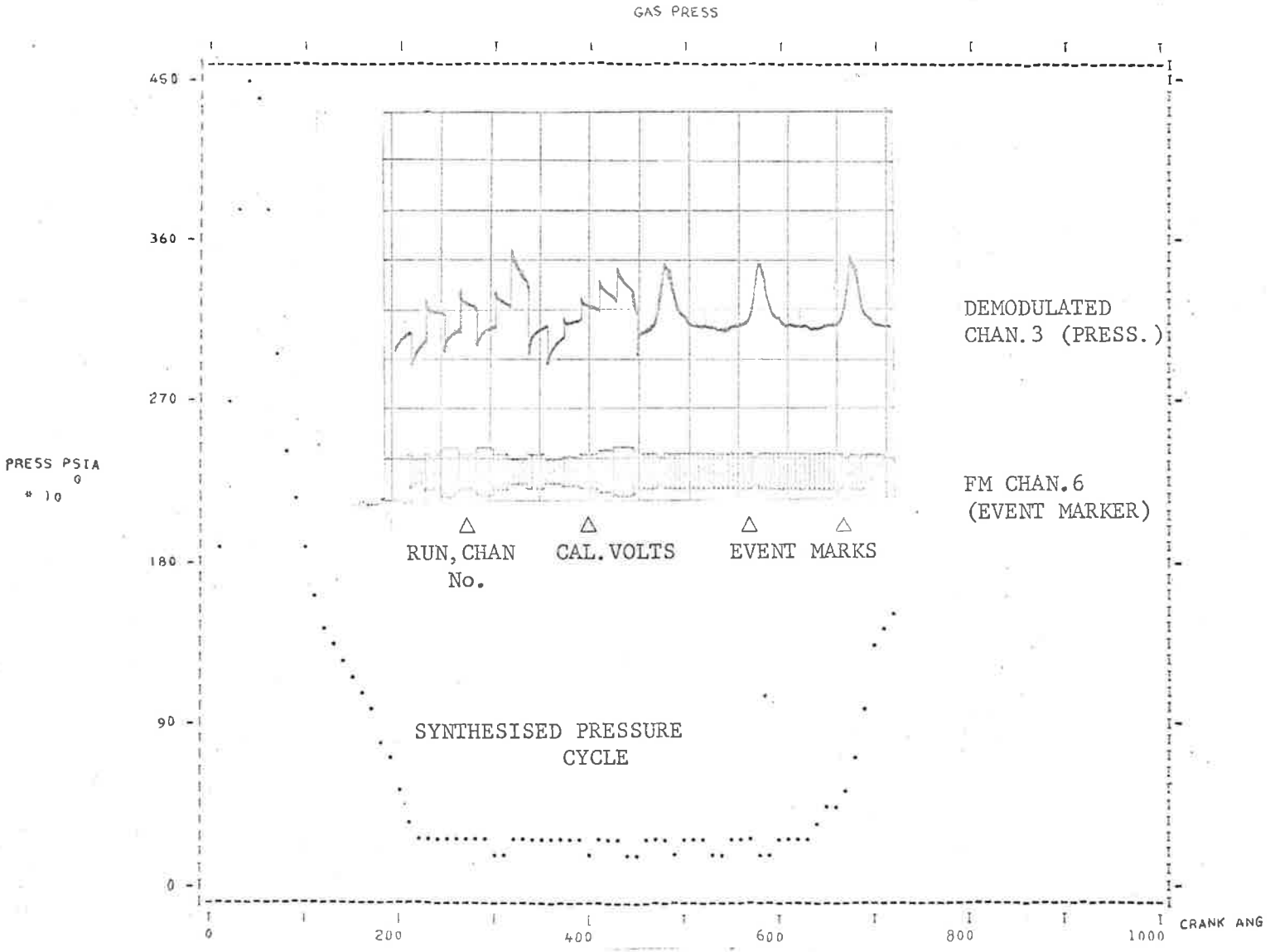

Fig.80 Example of a synthesised pressure cycle showing portion of a typical demodulated run simultaneously with the Event Marker track as recorded in FM form .(Tape Replay)

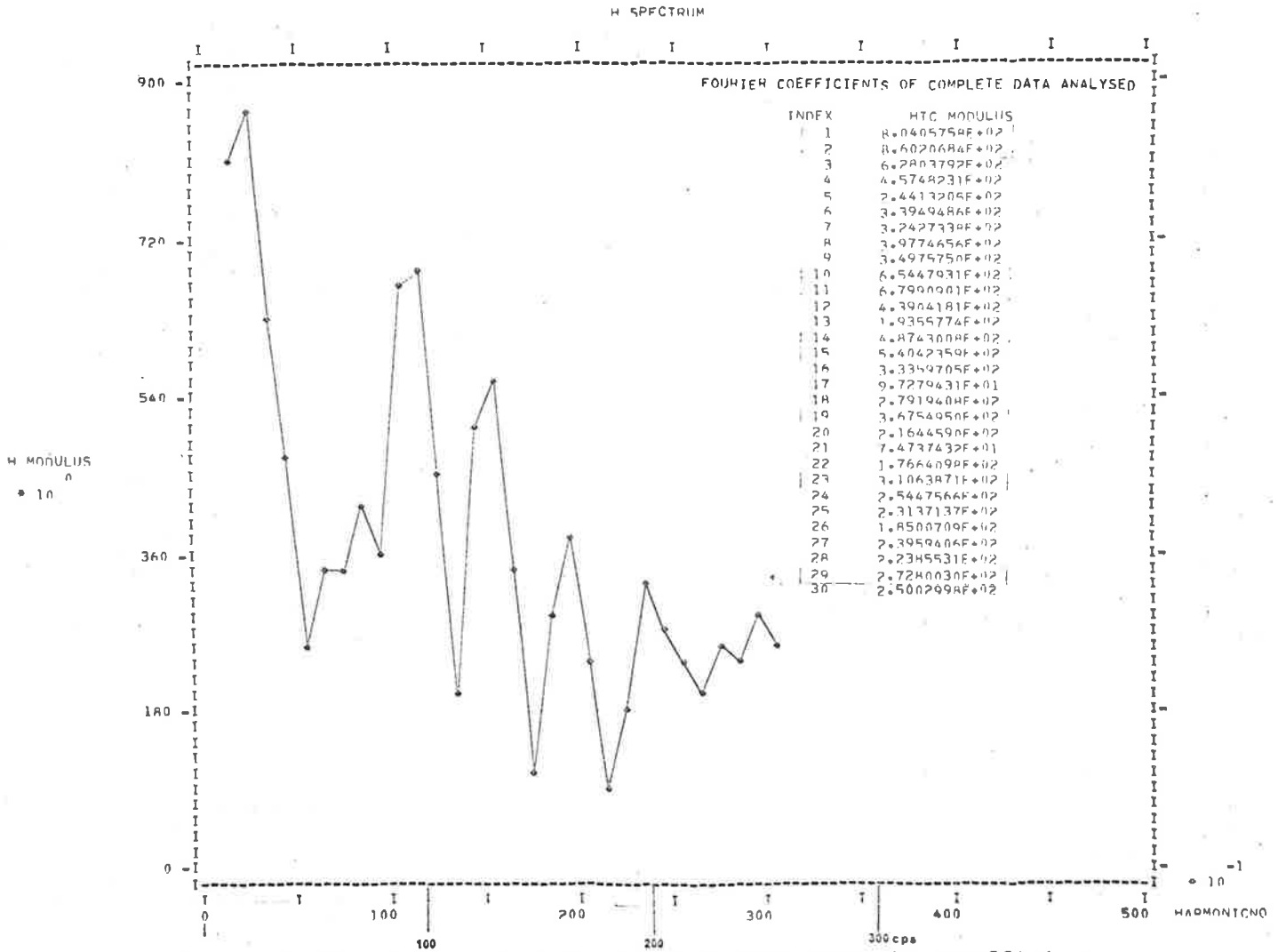

Fig.81 A typical Spectrum of Heat Transfer Coefficient

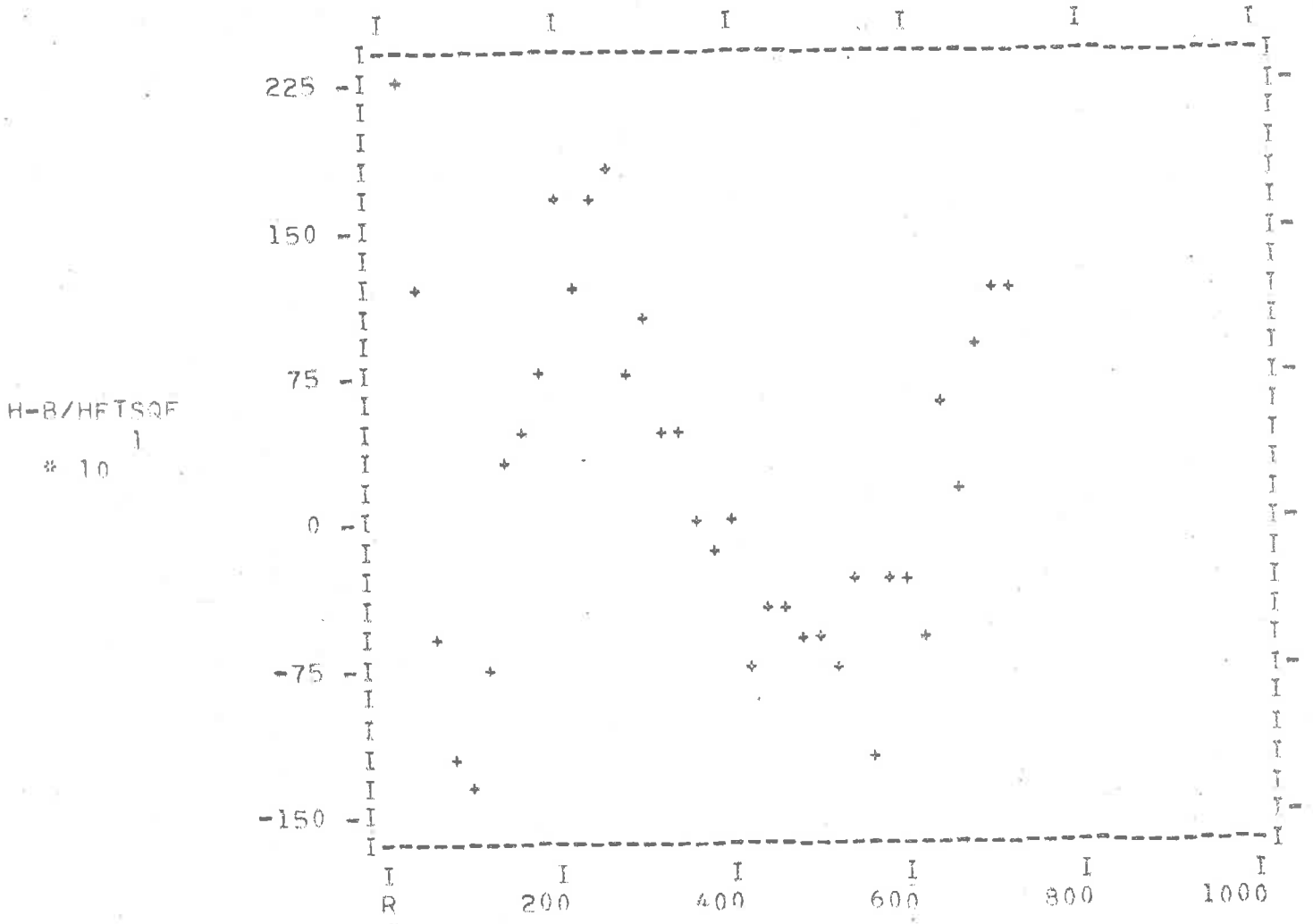

Fig.82 Synthesised Heat Transfer Coefficient cycle from Eqn,(78) for data of Fig.62 (X = 0.4")

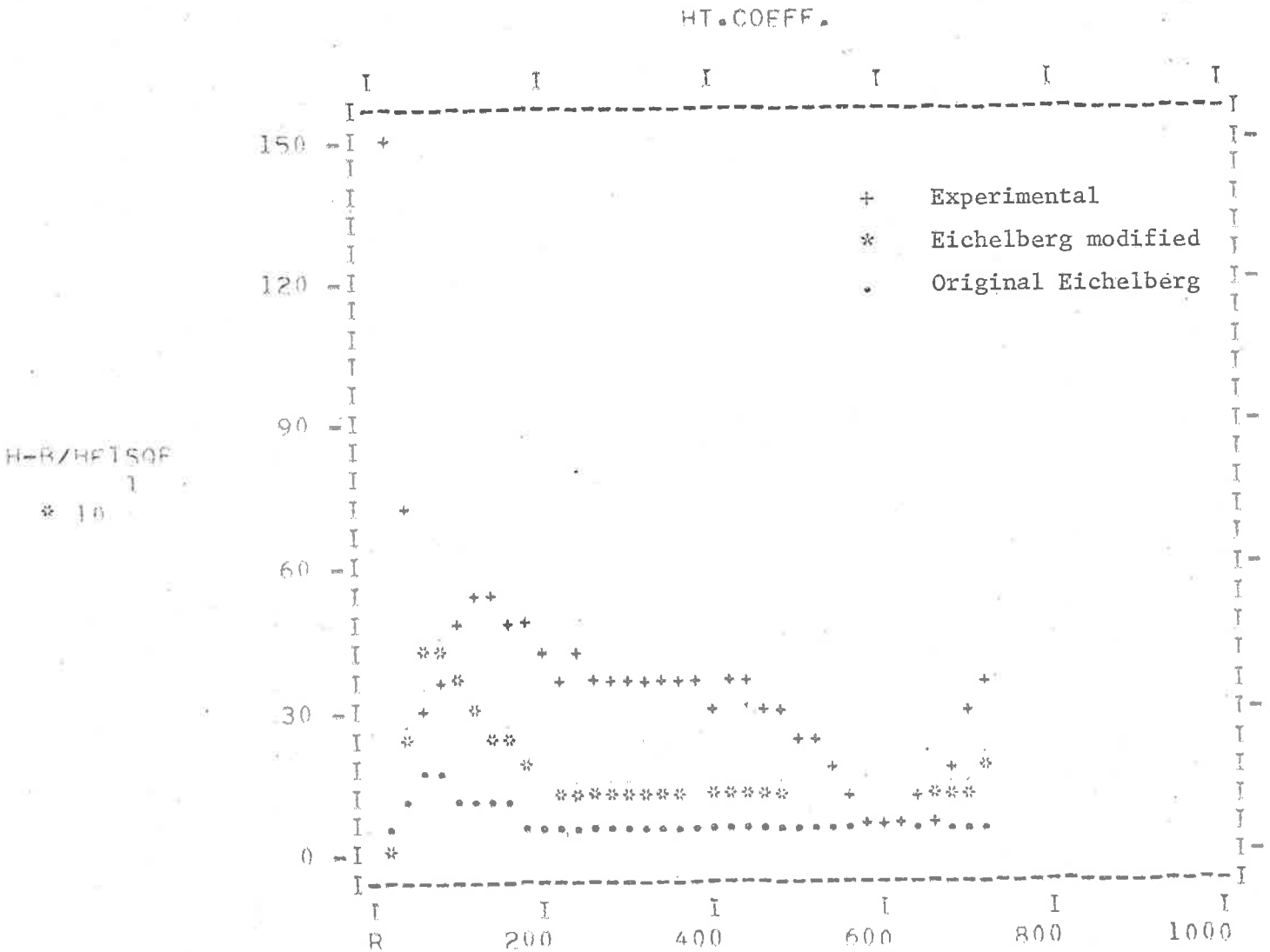

Fig.83 Heat Transfer Coefficient cycle resulting when heat flux is always positive over the cycle (Q_{Wm} put = 67.0 BTU/ft^{2}sec) (compare with that of Henien,Ref.30)

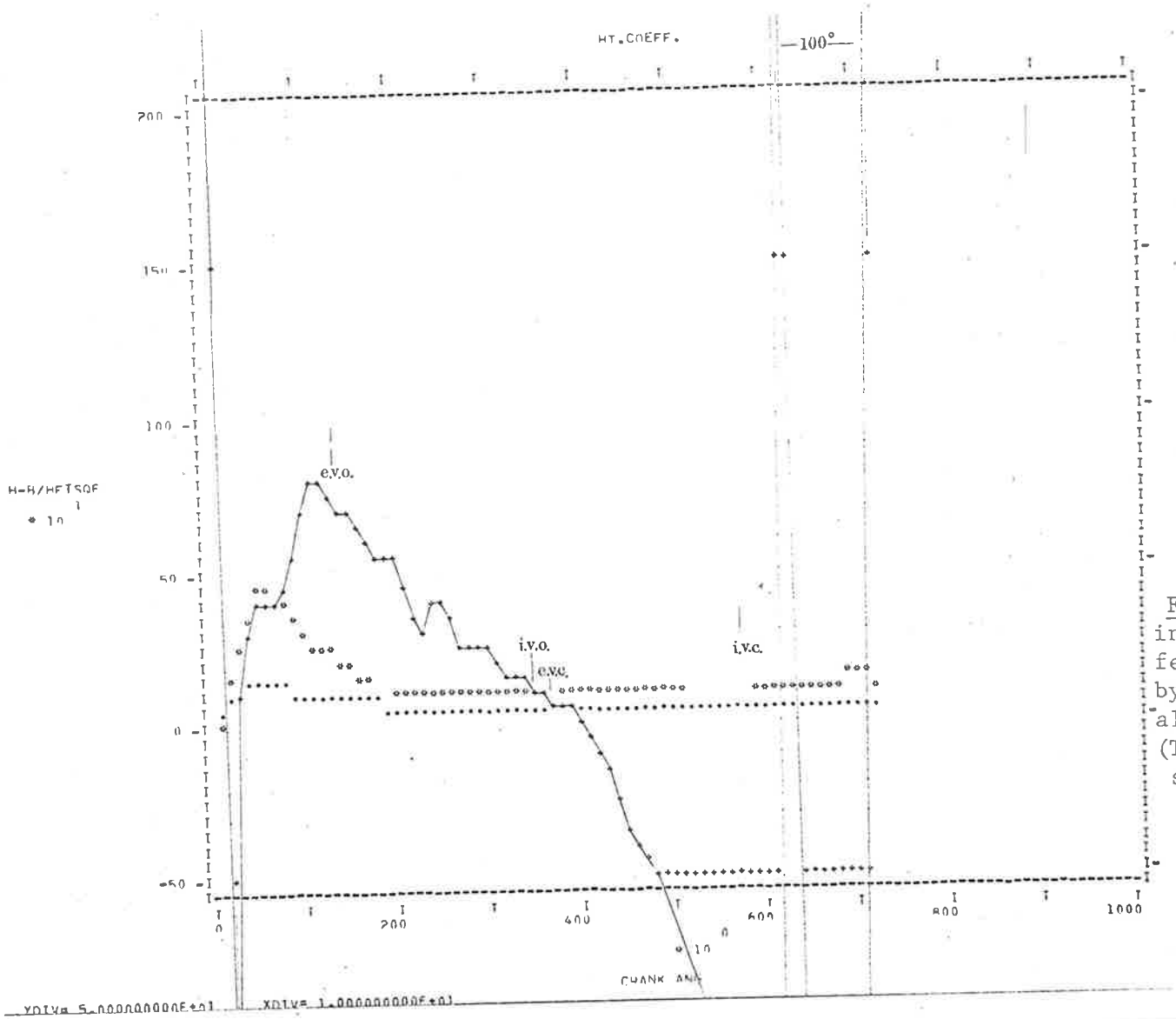

Fig.84 Fluctuation in cycle of Heat Tra fer coeff.accentuate by using an artifici ally high Wall temp. (T_{Wm} =896°R in data set of Fig.53)

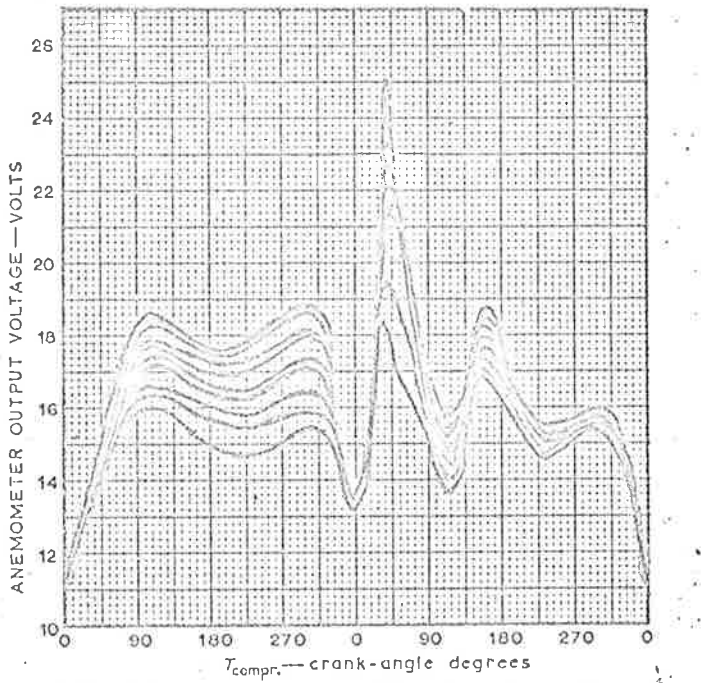

The different traces correspond to different angular positions of the wire probe, which was stepwise rotated through a total angle of 100°. From these data the instantaneous direction and magnitude of the velocity (mass flow) can be evaluated.

Fig.85 Reproduction of measurements by Horvatin(Ref.32) with a DISA type 55A 01 constant temperature anemometer in the combustion chamber of a motored diesel engine.

CONVERT TAPE NO 1
ANALOG TAPE # TRANSMITTAL TAPE 903
5000RPM KNOCK ZONE WOT FIRING 7/1CD 32DFB SPK TA0.250IN

SELECT 1	PERIODS INITIAL 2	MAX 3	NUMBER OF POINTS SELECT 985	INITIAL 1400	FINAL 2584	TOTAL 2934	PERIOD VARIATION 984	985

CYCLE COUNT	CRANK ANG	PRESSURE	GAS TEMP.	WALL TEMP.	HEAT FLUX	PISTON VELOC.	HEAT TRANSFER COEFF. EXPT.	ECH VP.	FICH. VPM
1	0	2.030E+02	2.428E+03	8.912E+02	1.945E+02	0.	4.290E+02	0.	1.127E+02
2	5	2.431E+02	2.443E+03	8.934E+02	1.899E+02	2.044E+00	4.350E+02	1.718E+02	1.037E+02
3	10	2.912E+02	2.490E+03	8.958E+02	1.819E+02	4.067E+00	4.391E+02	1.997E+02	9.983E+01
4	15	2.091E+02	2.552E+03	8.984E+02	1.751E+02	6.048E+00	4.330E+02	2.140E+02	9.004E+01
5	20	1.933E+02	2.629E+03	9.076E+02	1.719E+02	7.942E+00	4.32KE+02	2.247E+02	8.631E+01
6	25	1.830E+02	2.724E+03	9.089E+02	1.729E+02	9.751E+00	4.361E+02	2.339E+02	8.392E+01
7	30	1.734E+02	2.833E+03	9.082E+02	1.745E+02	1.145E+01	4.433E+02	2.407E+02	8.184E+01
8	35	1.620E+02	2.939E+03	9.017E+02	1.805E+02	1.301E+01	4.519E+02	2.431E+02	7.920E+01
9	40	1.479E+02	3.033E+03	9.031E+02	1.824E+02	1.443E+01	4.490E+02	2.401E+02	7.556E+01
10	45	1.321E+02	3.111E+03	9.043E+02	1.806E+02	1.570E+01	4.620E+02	2.322E+02	7.108E+01
11	50	1.147E+02	3.177E+03	9.053E+02	1.750E+02	1.679E+01	4.493E+02	2.216E+02	6.632E+01
12	55	1.044E+02	3.239E+03	9.060E+02	1.667E+02	1.770E+01	4.503E+02	2.111E+02	6.208E+01
13	60	9.523E+01	3.287E+03	9.066E+02	1.576E+02	1.844E+01	4.362E+02	2.033E+02	5.897E+01
14	65	9.029E+01	3.190E+03	9.067E+02	1.494E+02	1.899E+01	4.191E+02	1.991E+02	5.720E+01
15	70	8.791E+01	3.190E+03	9.069E+02	1.431E+02	1.935E+01	4.018E+02	1.977E+02	5.644E+01
16	75	8.631E+01	3.204E+03	9.071E+02	1.389E+02	1.954E+01	3.854E+02	1.972E+02	5.611E+01
17	80	8.519E+01	3.224E+03	9.073E+02	1.367E+02	1.959E+01	3.704E+02	1.954E+02	5.561E+01
18	85	8.410E+01	3.248E+03	9.075E+02	1.362E+02	1.948E+01	3.556E+02	1.913E+02	5.457E+01
19	90	7.519E+01	3.258E+03	9.076E+02	1.374E+02	1.909E+01	3.39KE+02	1.848E+02	5.301E+01
20	95	7.031E+01	3.259E+03	9.078E+02	1.398E+02	1.864E+01	3.217E+02	1.773E+02	5.127E+01
21	100	6.874E+01	3.249E+03	9.076E+02	1.429E+02	1.805E+01	3.027E+02	1.706E+02	4.985E+01
22	105	6.927E+01	3.234E+03	9.071E+02	1.467E+02	1.734E+01	2.846E+02	1.659E+02	4.912E+01
23	110	6.564E+01	3.218E+03	9.066E+02	9.772E+01	1.653E+01	2.683E+02	1.631E+02	4.909E+01
24	115	6.477E+01	3.206E+03	9.064E+02	9.298E+01	1.562E+01	2.576E+02	1.610E+02	4.936E+01
25	120	6.704E+01	3.196E+03	9.061E+02	9.039E+01	1.463E+01	2.523E+02	1.575E+02	4.936E+01
26	125	6.499E+01	3.189E+03	9.059E+02	8.955E+01	1.357E+01	2.512E+02	1.510E+02	4.852E+01
27	130	6.599E+01	3.181E+03	9.058E+02	8.914E+01	1.246E+01	2.516E+02	1.407E+02	4.650E+01
28	135	6.711E+01	3.149E+03	9.057E+02	8.790E+01	1.130E+01	2.480E+02	1.266E+02	4.324E+01
29	140	4.298E+01	3.149E+03	9.056E+02	8.494E+01	1.011E+01	2.460E+02	1.102E+02	3.986E+01
30	145	3.403E+01	3.124E+03	9.053E+02	8.026E+01	8.884E+00	2.370E+02	9.349E+01	3.459E+01
31	150	2.710E+01	3.098E+03	9.050E+02	7.449E+01	7.641E+00	2.248E+02	7.863E+01	3.067E+01
32	155	2.298E+01	3.072E+03	9.045E+02	6.885E+01	6.384E+00	2.122E+02	6.797E+01	2.808E+01
33	160	2.184E+01	3.052E+03	9.040E+02	6.457E+01	5.116E+00	2.027E+02	6.097E+01	2.711E+01
34	165	2.218E+01	3.038E+03	9.038E+02	6.242E+01	3.842E+00	1.981E+02	5.592E+01	2.735E+01
35	170	2.333E+01	3.031E+03	9.033E+02	6.249E+01	2.563E+00	1.988E+02	5.402E+01	2.800E+01
36	175	2.394E+01	3.027E+03	9.031E+02	6.411E+01	1.280E+00	1.954E+02	5.420E+01	2.834E+01
37	180	2.364E+01	3.024E+03	9.031E+02	6.621E+01	-6.819E-07	2.127E+02	5.928E+01	2.803E+01
38	185	2.204E+01	3.020E+03	9.031E+02	6.766E+01	-1.282E+00	2.181E+02	6.851E+01	2.714E+01
39	190	2.039E+01	3.015E+03	9.030E+02	6.772E+01	-2.563E+00	2.193E+02	7.457E+01	2.607E+01
40	195	1.936E+01	3.009E+03	9.029E+02	6.624E+01	-3.842E+00	2.155E+02	7.815E+01	2.530E+01
41	200	1.953E+01	3.005E+03	9.028E+02	6.362E+01	-5.116E+00	2.078E+02	7.725E+01	2.546E+01
42	205	2.100E+01	3.003E+03	9.026E+02	6.059E+01	-6.384E+00	1.982E+02	6.388E+01	2.639E+01
43	210	2.324E+01	3.004E+03	9.023E+02	5.789E+01	-7.641E+00	1.891E+02	7.137E+01	2.776E+01
44	215	2.540E+01	3.007E+03	9.020E+02	5.595E+01	-8.884E+00	1.823E+02	7.851E+01	2.905E+01
45	220	2.669E+01	3.009E+03	9.018E+02	5.478E+01	-1.011E+01	1.780E+02	8.404E+01	2.979E+01
46	225	2.667E+01	3.008E+03	9.015E+02	5.393E+01	-1.130E+01	1.755E+02	8.720E+01	2.978E+01
47	230	2.555E+01	3.002E+03	9.013E+02	5.292E+01	-1.246E+01	1.731E+02	8.801E+01	2.909E+01
48	235	2.388E+01	1.992E+03	9.011E+02	5.129E+01	-1.357E+01	1.692E+02	8.733E+01	2.808E+01
49	240	2.248E+01	1.981E+03	9.008E+02	4.889E+01	-1.463E+01	1.630E+02	8.682E+01	2.714E+01
50	245	2.194E+01	1.970E+03	9.005E+02	4.592E+01	-1.562E+01	1.554E+02	8.726E+01	2.676E+01
51	250	2.250E+01	1.962E+03	9.001E+02	4.282E+01	-1.653E+01	1.481E+02	8.984E+01	2.703E+01
52	255	2.375E+01	1.959E+03	8.997E+02	4.008E+01	-1.734E+01	1.362E+02	9.371E+01	2.775E+01
53	260	2.502E+01	1.960E+03	8.993E+02	3.800E+01	-1.805E+01	1.290E+02	9.748E+01	2.846E+01
54	265	2.559E+01	1.961E+03	8.990E+02	3.660E+01	-1.864E+01	1.240E+02	9.988E+01	2.882E+01
55	270	2.504E+01	1.961E+03	8.988E+02	3.567E+01	-1.909E+01	1.207E+02	9.939E+01	2.851E+01
56	275	2.348E+01	1.956E+03	8.983E+02	3.469E+01	-1.940E+01	1.180E+02	9.660E+01	2.756E+01
57	280	2.139E+01	1.947E+03	8.980E+02	3.343E+01	-1.955E+01	1.147E+02	9.226E+01	2.625E+01
58	285	1.960E+01	1.938E+03	8.976E+02	3.189E+01	-1.954E+01	1.101E+02	8.801E+01	2.505E+01
59	290	1.877E+01	1.929E+03	8.972E+02	2.995E+01	-1.935E+01	1.040E+02	8.554E+01	2.442E+01
60	295	1.915E+01	1.924E+03	8.968E+02	2.729E+01	-1.898E+01	9.709E+01	8.560E+01	2.460E+01
61	300	2.050E+01	1.902E+03	8.964E+02	2.520E+01	-1.844E+01	9.017E+01	8.755E+01	2.540E+01
62	305	2.215E+01	1.902E+03	8.960E+02	2.346E+01	-1.778E+01	8.398E+01	8.977E+01	2.648E+01
63	310	2.333E+01	1.905E+03	8.956E+02	2.206E+01	-1.679E+01	7.867E+01	9.080E+01	2.712E+01
64	315	2.349E+01	1.909E+03	8.952E+02	2.080E+01	-1.570E+01	7.385E+01	8.901E+01	2.725E+01
65	320	2.255C+01	1.911E+03	8.948E+02	1.945E+01	-1.443E+01	6.898E+01	8.495E+01	2.671E+01
66	325	2.092E+01	1.908E+03	8.944E+02	1.785E+01	-1.301E+01	6.339E+01	7.889E+01	2.570E+01
67	330	1.933E+01	1.899E+03	8.940E+02	1.605E+01	-1.145E+01	5.747E+01	7.250E+01	2.465E+01
68	335	1.853E+01	1.885E+03	8.935E+02	1.430E+01	-9.751E+00	5.190E+01	6.703E+01	2.404E+01
69	340	1.898E+01	1.868E+03	8.931E+02	1.295E+01	-7.942E+00	4.781E+01	6.295E+01	2.418E+01
70	345	2.035F+01	1.851E+03	8.927E+02	1.229E+01	-6.068E+00	4.620E+01	5.934E+01	2.497E+01
71	350	2.230E+01	1.834E+03	8.923E+02	1.237E+01	-4.067E+00	4.729E+01	5.421E+01	2.602E+01
72	355	2.394E+01	1.820E+03	8.920E+02	1.294E+01	-2.045E+00	5.020E+01	4.650E+01	2.685E+01
73	360	2.459E+01	1.807E+03	8.917E+02	1.349E+01	2.180E-06	5.308E+01	4.611E+01	2.711E+01
74	365	2.399E+01	1.791E+03	8.915E+02	1.346E+01	2.045E+00	5.374E+01	4.422E+01	2.686E+01
75	370	2.241E+01	1.780E+03	8.912E+02	1.276E+01	4.087E+00	5.048E+01	5.353E+01	2.569E+01
76	375	2.053E+01	1.765E+03	8.908E+02	1.039E+01	6.048E+00	4.279E+01	5.821E+01	2.469E+01
77	380	1.914E+01	1.750E+03	8.904E+02	7.564E+00	7.942E+00	3.167E+01	6.134E+01	2.356E+01
78	385	1.888E+01	1.737E+03	8.899E+02	4.548E+00	9.751E+00	1.934E+01	6.492E+01	2.328E+01
79	390	1.972E+01	1.726E+03	8.894E+02	1.994E+00	1.145E+01	8.459E+00	6.988E+01	2.373E+01
80	395	2.130E+01	1.718E+03	8.889E+02	2.304E-01	1.301E+01	1.001E+00	7.553E+01	2.461E+01
81	400	2.284E+01	1.712E+03	8.885E+02	-6.053E-01	1.443E+01	-2.646E+00	8.082E+01	2.544E+01
82	405	2.359E+01	1.708E+03	8.880E+02	-8.828E-01	1.570E+01	-3.877E+00	8.432E+01	2.581E+01
83	410	2.311E+01	1.702E+03	8.877E+02	-1.183E+00	1.679E+01	-5.227E+00	8.524E+01	2.552E+01
84	415	2.154E+01	1.695E+03	8.873E+02	-2.076E+00	1.770E+01	-9.247E+00	8.363E+01	2.460E+01
85	420	1.955E+01	1.687E+03	8.868E+02	-3.870E+00	1.844E+01	-1.741E+01	8.052E+01	2.336E+01
86	425	1.791E+01	1.678E+03	8.863E+02	-6.468E+00	1.898E+01	-2.940E+01	7.763E+01	2.230E+01
87	430	1.734E+01	1.672E+03	8.858E+02	-9.397E+00	1.935E+01	-4.305E+01	7.671E+01	2.190E+01
88	435	1.807E+01	1.668E+03	8.852E+02	-1.200E+01	1.954E+01	-5.516E+01	7.848E+01	2.233E+01
89	440	1.977E+01	1.669E+03	8.847E+02	-1.371E+01	1.955E+01	-6.289E+01	8.213E+01	2.337E+01
90	445	2.161E+01	1.673E+03	8.842E+02	-1.429E+01	1.940E+01	-6.519E+01	8.588E+01	2.450E+01
91	450	2.291E+01	1.678E+03	8.837E+02	-1.394E+01	1.909E+01	-6.328E+01	8.796E+01	2.523E+01
92	455	2.298E+01	1.682E+03	8.833E+02	-1.329E+01	1.864E+01	-5.994E+01	8.732E+01	2.524E+01
93	460	2.216E+01	1.680E+03	8.830E+02	-1.294E+01	1.805E+01	-5.850E+01	8.393E+01	2.452E+01
94	465	1.965E+01	1.674E+03	8.826E+02	-1.348E+01	1.734E+01	-6.130E+01	7.879E+01	2.333E+01
95	470	1.781E+01	1.664E+03	8.822E+02	-1.498E+01	1.653E+01	-6.899E+01	7.373E+01	2.218E+01
96	475	1.715E+01	1.654E+03	8.817E+02	-1.714E+01	1.562E+01	-7.992E+01	7.166E+01	2.167E+01
97	480	1.791E+01	1.645E+03	8.812E+02	-1.932E+01	1.463E+01	-9.102E+01	7.347E+01	2.208E+01
98	485	1.991E+01	1.641E+03	8.807E+02	-2.088E+01	1.357E+01	-9.873E+01	7.737E+01	2.325E+01
99	490	2.233E+01	1.641E+03	8.802E+02	-2.134E+01	1.246E+01	-1.010E+02	7.449E+01	2.462E+01
100	495	2.409E+01	1.644E+03	8.798E+02	-2.084E+01	1.130E+01	-9.810E+01	7.497E+01	2.568E+01
101	500	2.434F+01	1.647E+03	8.794E+02	-1.988E+01	1.011E+01	-9.312E+01	7.264E+01	2.576E+01
102	505	2.293F+01	1.648E+03	8.791E+02	-1.913E+01	8.884E+00	-8.962E+01	6.743E+01	2.495E+01
103	510	2.080E+01	1.643E+03	8.788E+02	-1.922E+01	7.641E+00	-9.079E+01	6.404E+01	2.336E+01
104	515	1.709E+01	1.635E+03	8.784E+02	-2.056E+01	6.384E+00	-9.785E+01	5.907E+01	2.151E+01
105	520	1.513E+01	1.629E+03	8.780E+02	-2.271E+01	5.116E+00	-1.094E+02	4.537E+01	2.017E+01
106	525	1.500E+01	1.617E+03	8.775E+02	-2.501E+01	3.842E+00	-1.217E+02	4.496E+01	2.004E+01
107	530	1.617E+01	1.614E+03	8.770E+02	-2.661E+01	2.563E+00	-1.300E+02	3.782E+01	2.117E+01
108	535	1.972E+01	1.614E+03	8.765E+02	-2.688E+01	1.282E+00	-1.308E+02	3.258E+01	2.297E+01
109	540	2.262E+01	1.623E+03	8.762E+02	-2.572E+01	-2.044E-06	-1.240E+02	4.104E+01	2.465E+01
110	545	2.424E+01	1.630E+03	8.759E+02	-2.363E+01	-1.282E+00	-1.129E+02	3.428E+01	2.558E+01
111	550	2.480E+01	1.633E+03	8.756E+02	-2.152E+01	-2.563E+00	-1.022E+02	4.450E+01	2.547E+01
112	555	2.210E+01	1.631E+03	8.754E+02	-2.027E+01	-3.842E+00	-9.710E+01	4.093E+01	2.442E+01
113	560	1.966E+01	1.623E+03	8.752E+02	-2.078E+01	-5.116E+00	-1.001E+02	5.167E+01	2.297E+01
114	565	1.812E+01	1.612F+03	8.749E+02	-2.268E+01	-6.384E+00	-1.108E+02	5.322E+01	2.198E+01
115	570	1.870E+01	1.603E+03	8.746E+02	-2.534E+01	-7.641E+00	-1.253E+02	5.725E+01	2.227E+01
116	575	2.179E+01	1.601E+03	8.742E+02	-2.768E+01	-8.884E+00	-1.371E+02	6.492E+01	2.402E+01
117	580	2.666E+01	1.607E+03	8.735E+02	-2.858E+01	-1.011E+01	-1.403E+02	7.412E+01	2.663E+01
118	585	3.180E+01	1.621E+03	8.732E+02	-2.754E+01	-1.130E+01	-1.327E+02	8.452E+01	2.920E+01
119	590	3.544E+01	1.637E+03	8.729E+02	-2.485E+01	-1.246E+01	-1.171E+02	9.375E+01	3.099E+01
120	595	3.644E+01	1.649E+03	8.728E+02	-2.152F+01	-1.357E+01	-9.983E+01	9.817E+01	3.154E+01
121	600	3.479E+01	1.651E+03	8.727E+02	-1.892E+01	-1.463E+01	-8.837E+01	9.403E+01	3.083E+01
122	605	3.178F+01	1.642F+03	8.726E+02	-1.817E+01	-1.562E+01	-8.501E+01	9.484E+01	2.939E+01
123	610	2.962E+01	1.623E+03	8.724E+02	-1.964E+01	-1.653E+01	-9.427E+01	9.374E+01	2.821E+01
124	615	3.049E+01	1.602E+03	8.721E+02	-2.280E+01	-1.734E+01	-1.124E+02	9.601E+01	2.863E+01
125	620	3.556E+01	1.586E+03	8.716E+02	-2.617E+01	-1.809E+01	-1.319E+02	1.046E+02	3.056E+01
126	625	4.435E+01	1.583E+03	8.712E+02	-2.809E+01	-1.864E+01	-1.420E+02	1.179E+02	3.409E+01
127	630	4.444E+01	1.594E+03	8.708E+02	-2.734E+01	-1.909E+01	-1.361E+02	1.124E+02	3.797E+01
128	635	4.336E+01	1.614E+03	8.706E+02	-2.378E+01	-1.946E+01	-1.149E+02	1.442E+02	4.115E+01
129	640	4.268E+01	1.636E+03	8.706E+02	-1.860E+01	-1.955E+01	-8.687E+01	1.504E+02	4.280E+01
130	645	4.460E+01	1.645E+03	8.707E+02	-1.730E+01	-1.954E+01	-8.183E+01	1.496E+02	4.258E+01
131	650	4.179E+01	1.638E+03	8.708E+02	-1.885E+01	-1.935E+01	-9.013E+01	1.432E+02	4.090E+01
132	655	3.767E+01	1.620E+03	8.708E+02	-1.181F+01	-1.898E+01	-9.792E+01	1.363E+02	3.915E+01
133	660	3.846E+01	1.598E+03	8.705E+02	-1.693F+01	-1.844E+01	-8.972E+01	1.363E+02	3.955E+01
134	665	3.603E+01	1.530E+03	8.701E+02	-2.209E+01	-1.770E+01	-1.230E+02	1.492E+02	4.388E+01
135	670	1.08AE+02	1.521E+03	8.696E+02	-2.882F+01	-1.679E+01	-1.448E+02	1.744E+02	5.227E+01
136	675	1.47AE+02	1.541E+03	8.692E+02	-2.616F+01	-1.570E+01	-1.257E+02	2.685E+02	6.381E+01
137	680	2.195E+02	1.656E+03	8.694E+02	-1.199E+01	-1.443E+01	-5.493E+01	2.642E+02	7.749E+01
138	685	2.865E+02	1.805E+03	8.702E+02	1.127E+01	-1.301E+01	4.324E+01	2.829E+02	9.217E+01
139	690	3.43RE+02	1.889E+03	8.719E+02	4.411E+01	-1.145E+01	1.421E+02	3.128E+02	1.064E+02
140	695	3.874E+02	2.183E+03	8.745E+02	8.277E+01	-9.751E+00	2.277E+02	3.298E+02	1.183E+02
141	700	4.089E+02	2.357E+03	8.778E+02	1.217E+02	-7.942E+00	2.963E+02	3.288E+02	1.263E+02
142	705	4.044E+02	2.484E+03	8.819E+02	1.554E+02	-6.068E+00	3.449E+02	3.073E+02	1.293E+02
143	710	3.836E+02	2.563E+03	8.851E+02	1.795E+02	-4.067E+00	3.474E+02	2.852E+02	1.273E+02
144	715	3.663E+02	2.592E+03	8.885E+02	1.922E+02	-2.044E+00	4.135E+02	2.808E+02	1.212E+02

Fig.86

CONVERT TAPE NO 1
500RPM KNOCK ZONE HOT FIRING 7/1CR 32DEG SPK X=0.250IN
ANALOG TAPE 8 TRANSMITTAL TAPE 503

SERIAL	RUN	CHANNEL	TYPE	NO PERIODS	COEFF
21	10	123	1	1	15

NO POINTS	INITIAL	MAX PERIODS
985	2	3

FOURIER COEFFICIENTS AT CYCLE FREQUENCY

CYCLE HARMONIC	TEMPERATURE (DEG.F)	PHASE ANGLE CRANK ANG.DEG)
1	16.162.	96.39
2	6.000	90.69
3	3.340	91.85
4	2.112	92.53
5	1.080	83.07
6	.825	63.65
7	.621	46.90
8	.482	39.55
9	.414	13.55
10	.410	7.57
11	.329	359.47
12	.269	353.07
13	.251	325.83
14	.285	325.10
15	.221	315.02
	9.1E+02	9.7E+02

Fig.87 Fourier Coefficients of Wall Temperature cycle following

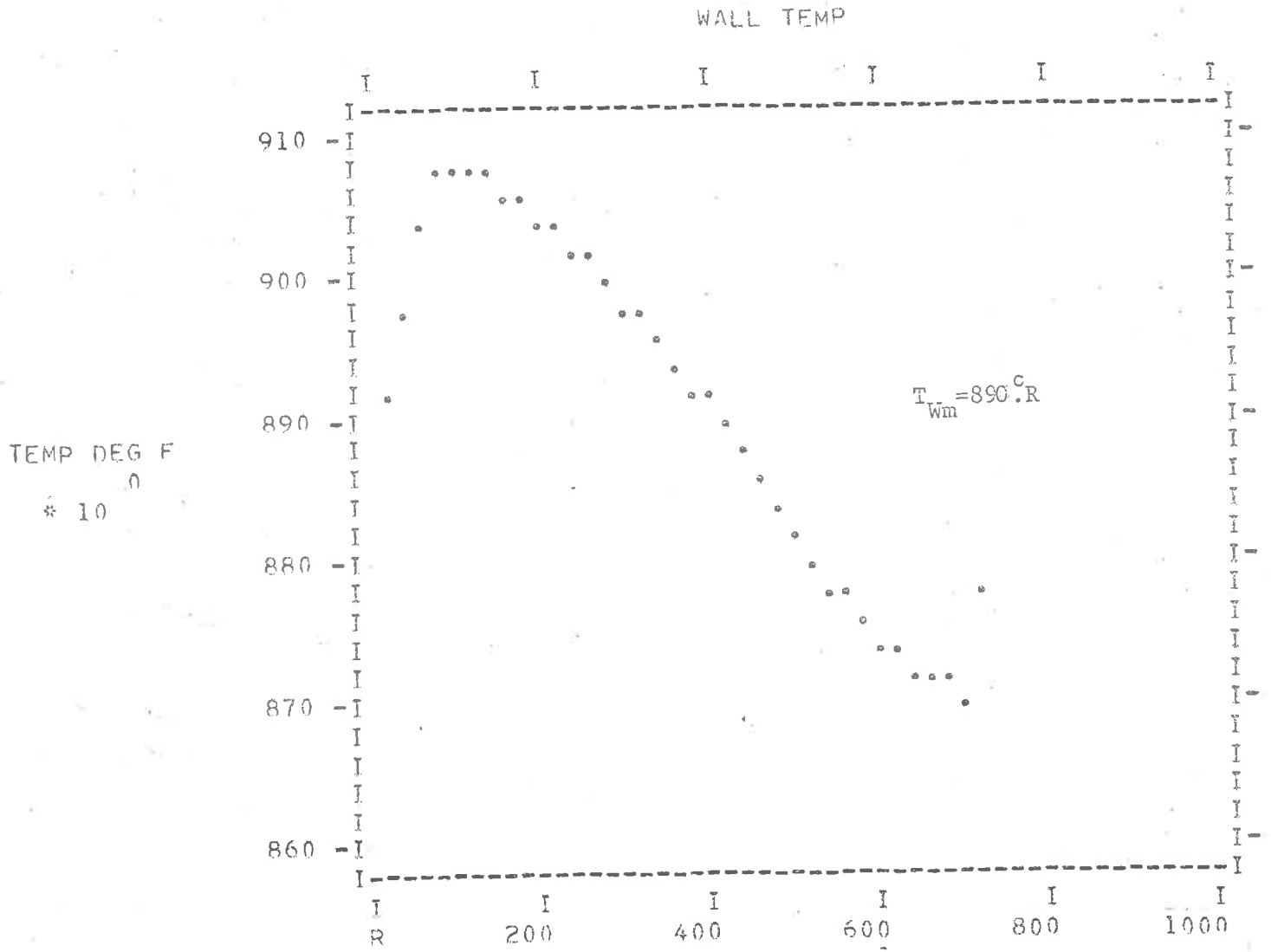

Fig.88 Wall Temperature cycle

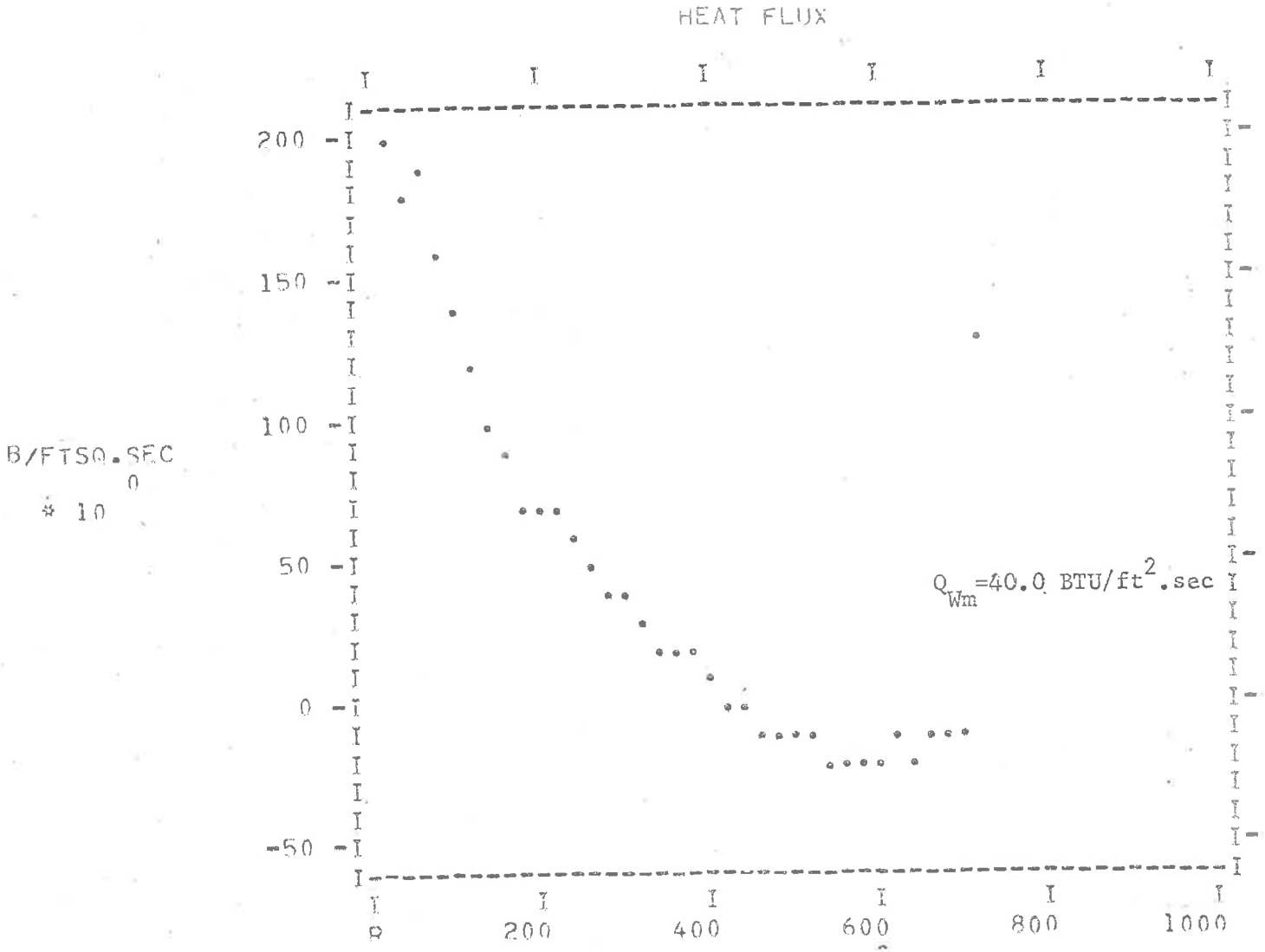

Fig.89 Heat Flux cycle derived from preceding T_w cycle

FOURIER COEFFICIENTS AT CYCLE FREQUENCY

CYCLE HARMONIC	TEMPERATURE (DEG.F)	PHASE ANGLE CRANK ANG.DEG)
1	308.591	60.48
2	131.577	43.38
3	99.639	47.89
4	62.431	17.13
5	63.414	9.08
6	66.657	354.42
7	49.165	358.51
8	36.126	338.91
9	29.594	322.08
10	27.824	302.35
11	25.692	297.51
12	27.122	272.14
13	25.982	271.17
14	22.845	255.37
15	17.683	245.26
	2.6E+03 1.5E+03	

Fig.90 Fourier Coefficients of Gas Temperature cycle following (X=0.250")

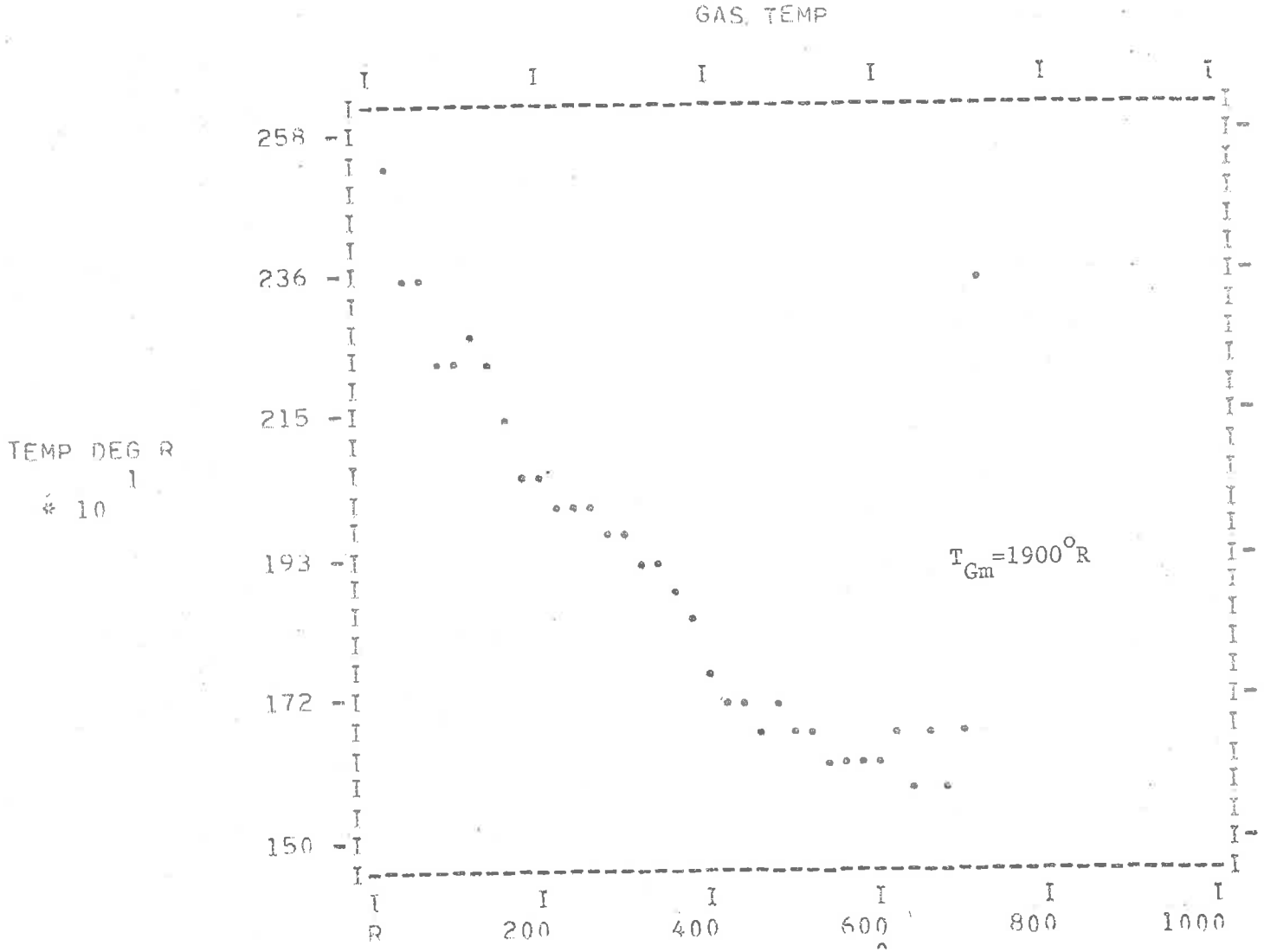

Fig.91 Gas Temperature cycle (X=0.250)

FOURIER COEFFICIENTS AT CYCLE FREQUENCY

CYCLE HARMONIC	TEMPERATURE (DEG.F)	PHASE ANGLE CRANK ANG.DEG)
1	77.585	2.07
2	59.471	359.14
3	41.855	351.07
4	31.643	337.33
5	28.116	325.50
6	24.423	321.33
7	18.102	310.66
8	14.029	291.10
9	13.066	273.24
10	12.387	262.38
11	10.502	251.74
12	8.220	235.82
13	7.333	216.28
14	6.800	201.60
15	5.843	187.14
	4.1E+02 1.5E+01	

Fig.92 Fourier Coefficients of Gas Pressure cycle following

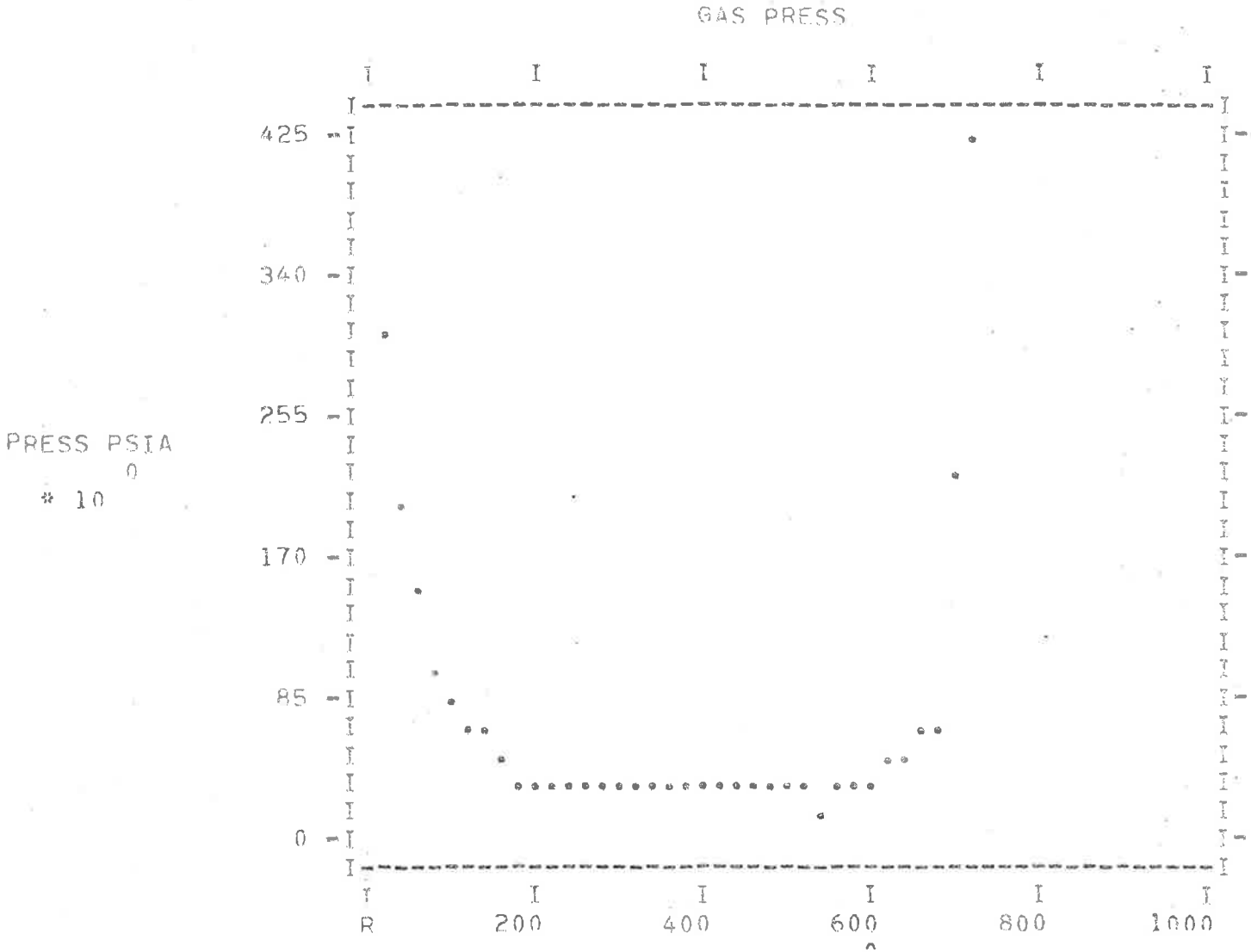

Fig.93 Gas Pressure cycle

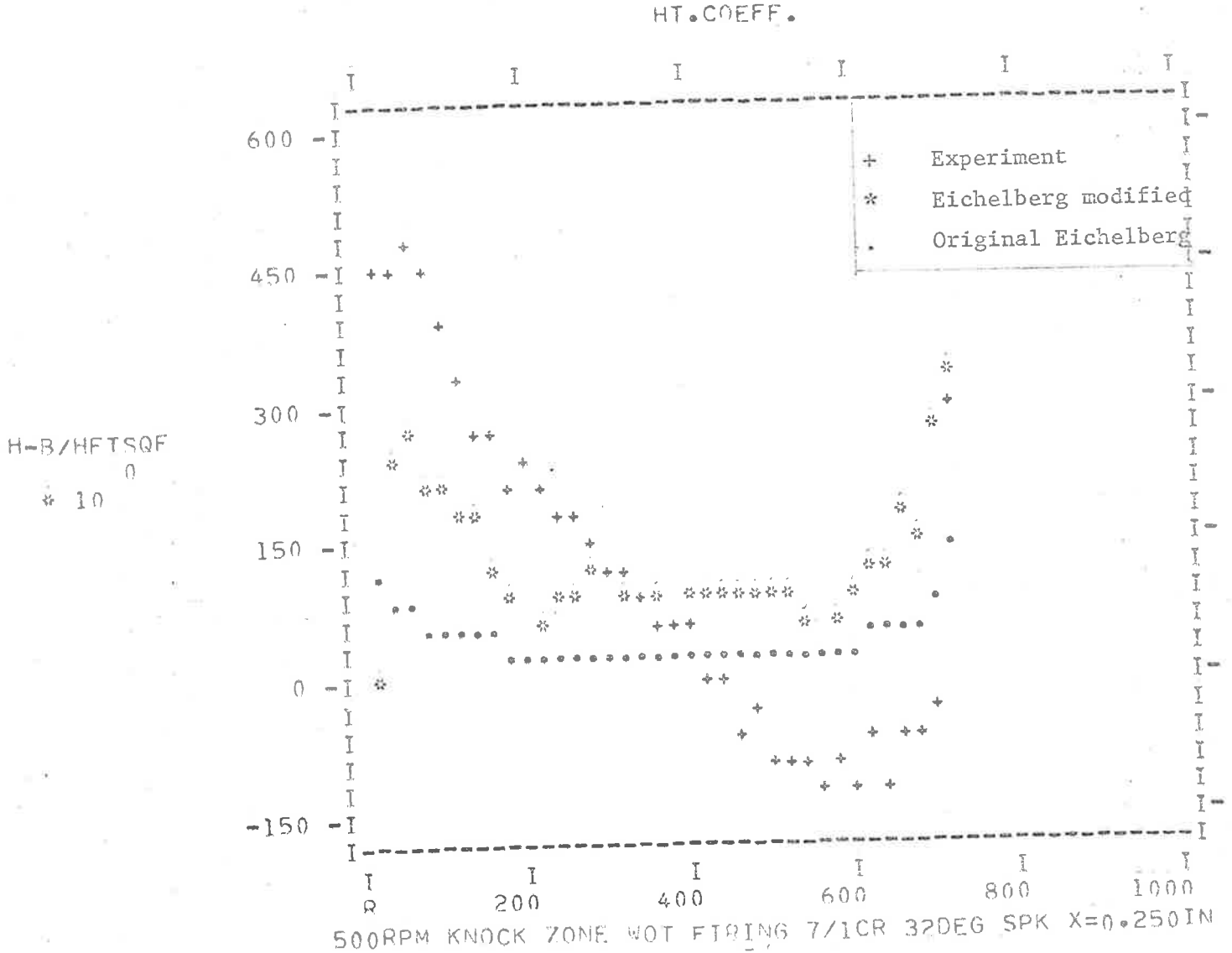

Fig.94 Cycle of Heat Transfer Coefficient from preceding simultaneous data (X=0.250)

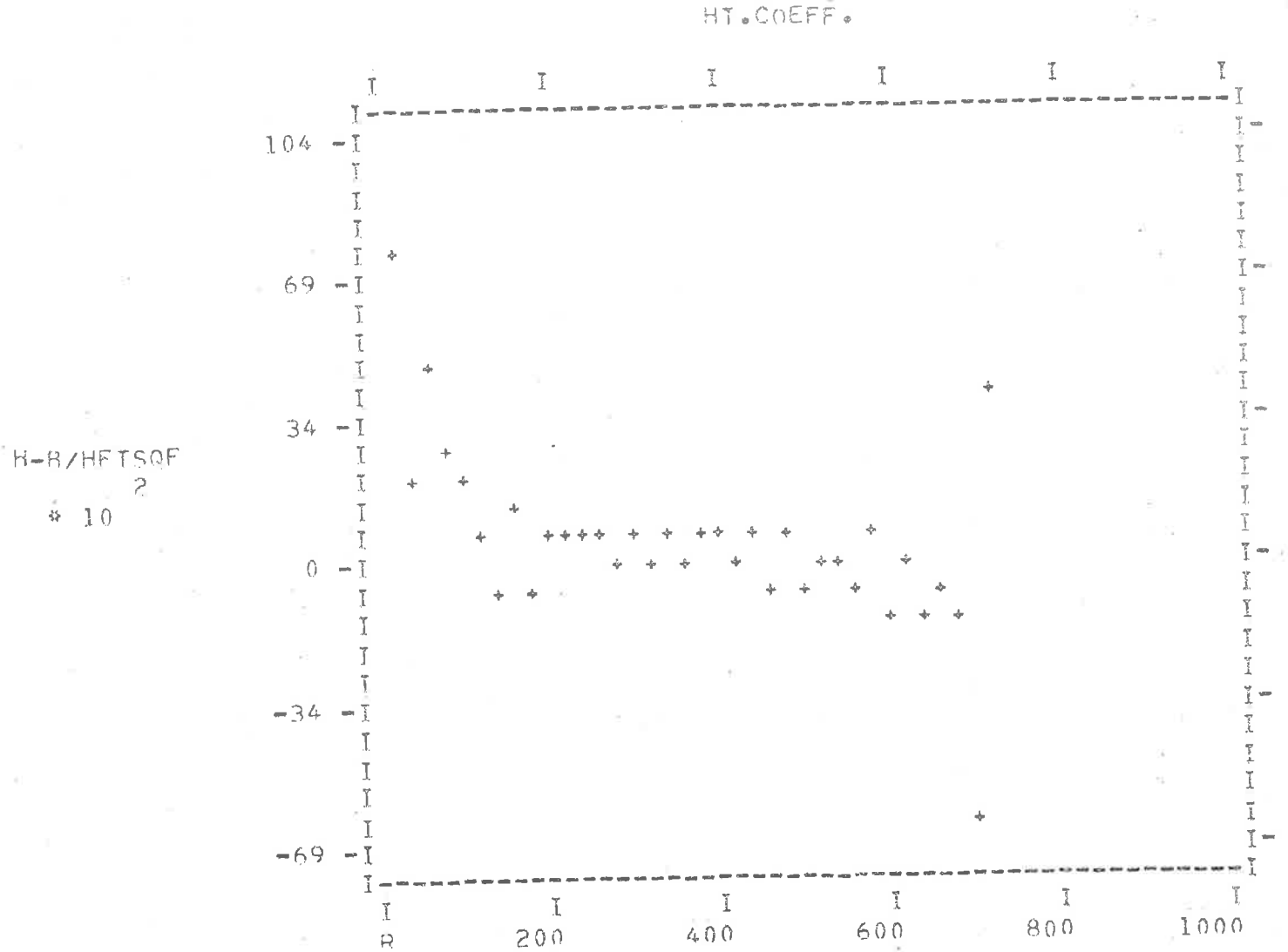

Fig.95 Synthesised Heat Transfer Coefficient cycle from Eqn.(78) for data set preceding (Fig.86)

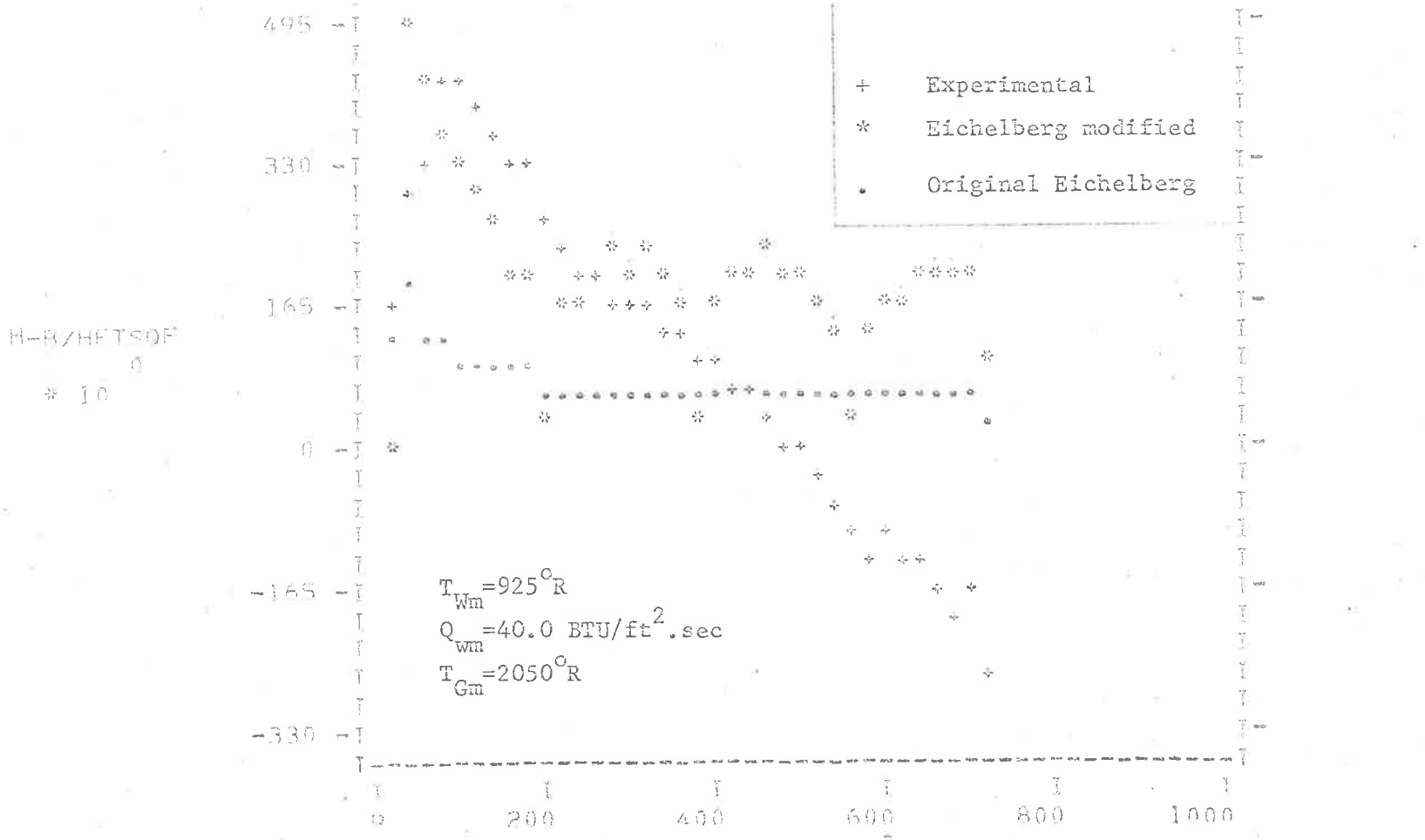

CONVERT TAPE NO 6
ANALOG TAPE 6 TRANSMITTAL TAPE 503
650RPM.KNOCK ZONE NOT.7/1CP.30 DEG SPK.(A/F)MAXP..X=0.400IN

PERIODS			NUMBER OF POINTS				PERIOD	
SELECT	INITIAL	MAX	SELECT	INITIAL	FINAL	TOTAL	VARIATION	
1	2	3	827	1284	2110	2892	824	826

Fig.96 Heat Transfer Coefficient cycle (MBT Spark)

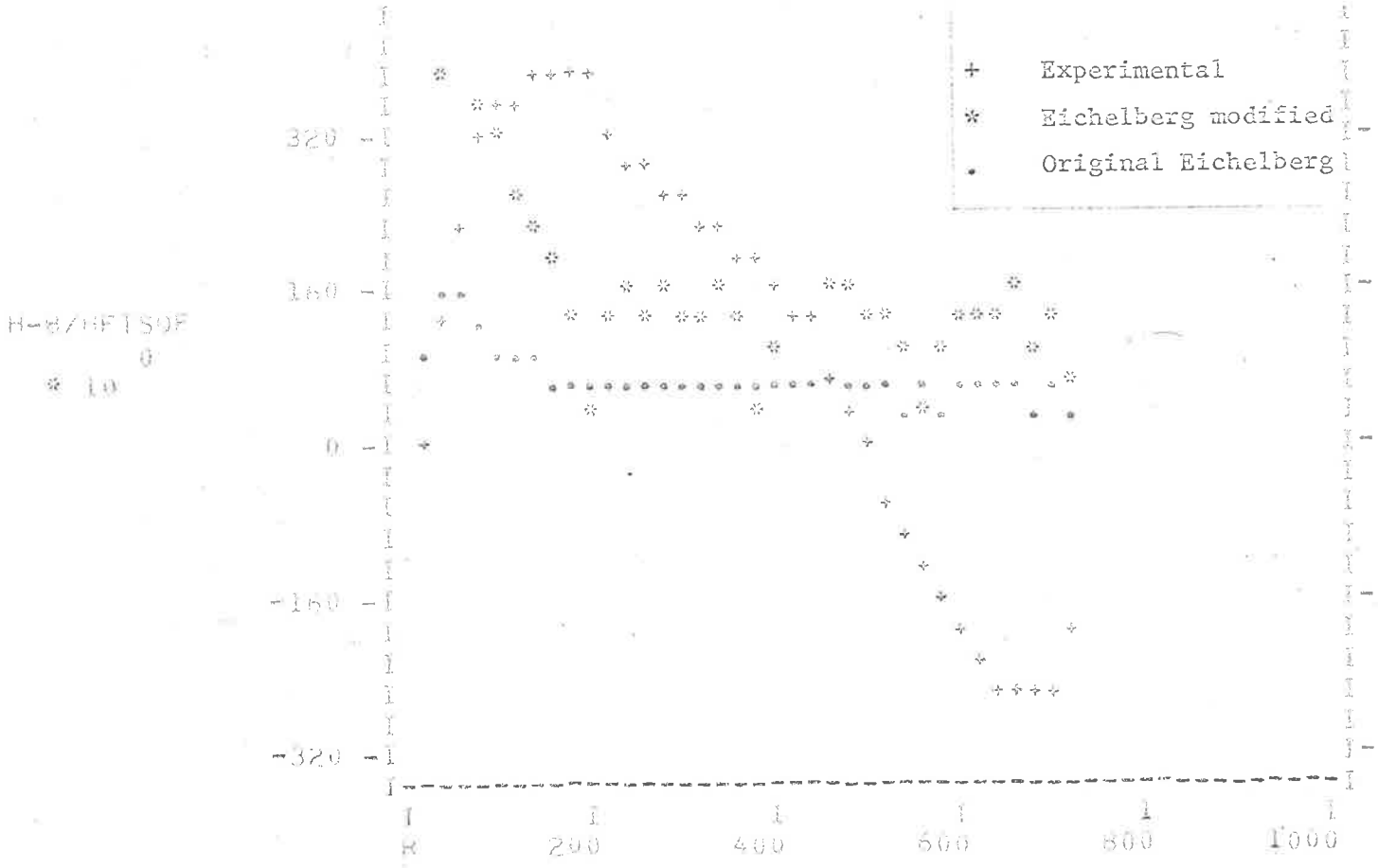

CONVERT TAPE NO 6
ANALOG TAPE 6 TRANSMITTAL TAPE 503
1000RPM,KNOCK ZONE WOT,7/1CR,2° DEG SPR,(A/F)MAXP,,X=0,400IN

PERIODS			NUMBER OF POINTS				PERIOD	
SELECT	INITIAL	MAX	SELECT	INITIAL	FINAL	TOTAL	VARIATION	
1	2	6	467	628	1094	2086	466	469

Fig.97 Heat Transfer Coefficient Cycle (Retarded Spark)

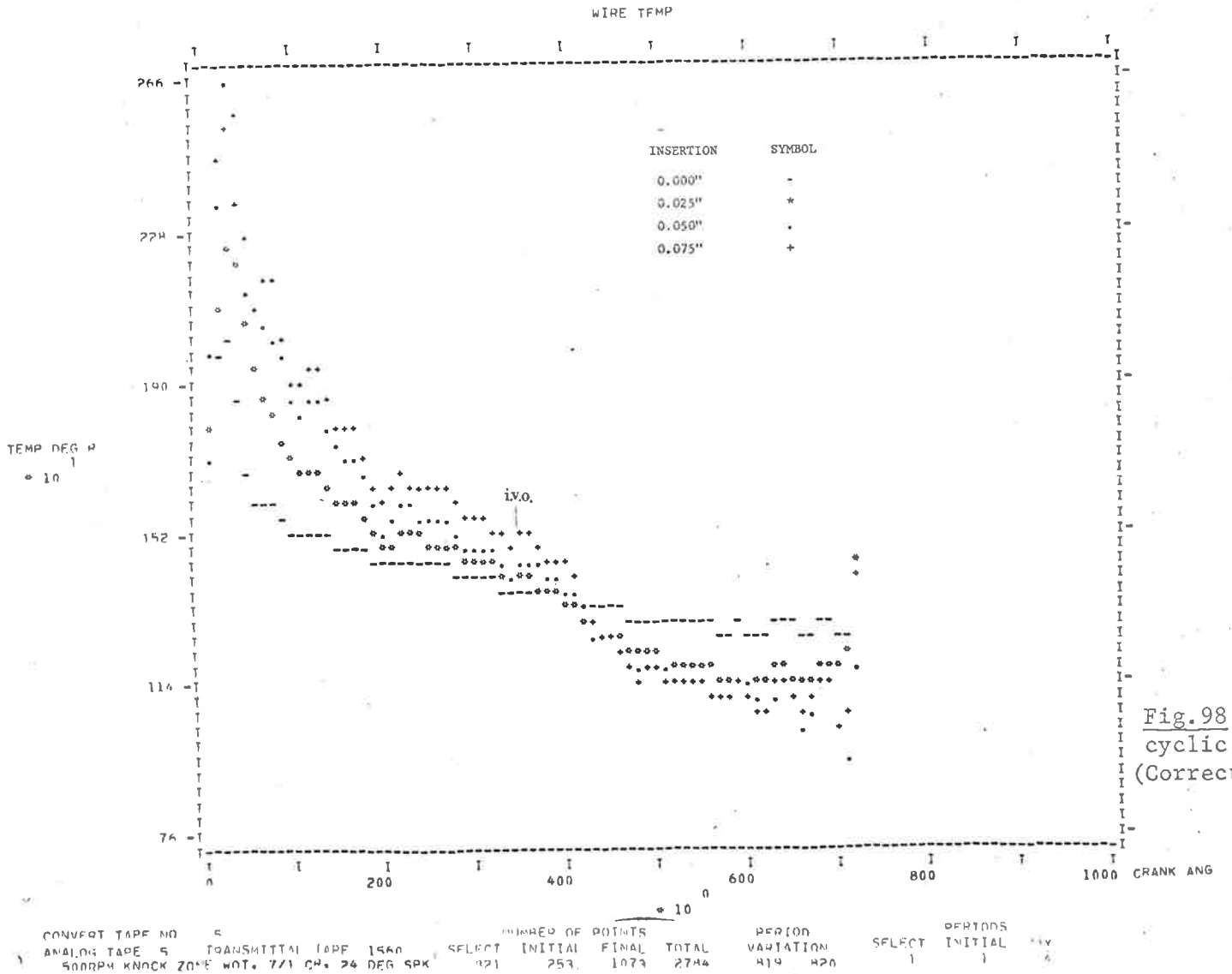

Fig.98 Knock-Zone cyclic traverse (Corrected)- Firing WO

CONVERT TAPE 50
500000 RANDOM ZONE WRITE 721 CP+ 24 DEC SPR
AFAIRE TAPE 4 INA SWITTAL TAPE 1001

TEMP DEG R

	0.0	0.021	0.050	0.075*
1	1.788268E+03	1.581319E+03	1.700148E+03	2.196476E+03
2	1.998086E+03	1.981135E+03	2.161704E+03	2.431806E+03
3	2.138086E+03	2.156571E+03	2.477005E+03	2.862766E+03
4	2.219092E+03	2.287774E+03	2.634610E+03	3.129446E+03
5	2.185211E+03	2.317231E+03	2.704468E+03	3.114686E+03
6	2.084278E+03	2.254856E+03	2.595629E+03	2.951110E+03
7	1.989561E+03	2.091745E+03	2.428784E+03	2.668770E+03
8	1.868001E+03	2.011345E+03	2.251101E+03	2.423275E+03
9	1.823761E+03	1.957 E+03	2.270629E+03	2.398110E+03
10	1.840845E+03	1.918032E+03	2.191328E+03	2.356785E+03
11	1.880827E+03	1.963728E+03	2.078635E+03	1.998488E+03
12	1.865335E+03	1.930112E+03	1.983728E+03	2.005708E+03
13	1.816031E+03	1.847131E+03	1.908619E+03	2.043134E+03
14	1.885332E+03	1.787 E+03	1.888778E+03	1.932966E+03
15	1.899624E+03	1.798358E+03	1.888158E+03	1.861309E+03
16	1.908870E+03	1.800 E+03	1.894548E+03	1.927811E+03
17	1.876602E+03	1.776437E+03	1.884508E+03	1.943715E+03
18	1.819926E+03	1.726464E+03	1.840102E+03	1.894925E+03
19	1.898084E+03	1.844341E+03	1.850418E+03	1.854876E+03
20	1.885906E+03	1.817 E+03	1.841208E+03	1.781925E+03
21	1.896731E+03	1.807415E+03	1.868098E+03	1.796155E+03
22	1.911130E+03	1.809206E+03	1.879035E+03	1.786425E+03
23	1.927731E+03	1.826 E+03	1.900018E+03	1.885108E+03
24	1.935862E+03	1.868 E+03	1.920408E+03	1.901368E+03
25	1.870001E+03	1.807 E+03	1.892954E+03	1.874791E+03
26	1.914878E+03	1.867561E+03	1.902 E+03	1.934184E+03
27	1.801631E+03	1.839988E+03	1.867 E+03	1.774209E+03
28	1.878488E+03	1.816 E+03	1.927 E+03	1.734388E+03
29	1.886032E+03	1.852 E+03	1.901132E+03	1.728158E+03
30	1.849137E+03	1.838 E+03	1.868398E+03	1.734058E+03
31	1.877131E+03	1.837 E+03	1.852 E+03	1.740 E+03
32	1.895018E+03	1.868 E+03	1.868 E+03	1.790 E+03
33	1.867 E+03	1.867 E+03	1.873 E+03	1.810 E+03
34	1.879 E+03	1.861 E+03	1.871 E+03	1.793 E+03
35	1.846 E+03	1.850 E+03	1.870 E+03	1.780 E+03
36	1.886 E+03	1.868 E+03	1.868 E+03	1.865 E+03
37	1.870 E+03	1.880 E+03	1.891 E+03	1.822 E+03
38	1.815 E+03	1.847 E+03	1.868 E+03	1.874 E+03
39	1.814 E+03	1.873 E+03	1.861 E+03	1.861 E+03
40	1.831 E+03	1.836 E+03	1.863 E+03	1.856 E+03
41	1.847 E+03	1.862 E+03	1.868 E+03	1.868 E+03
42	1.868 E+03	1.874 E+03	1.879 E+03	1.892 E+03
43	1.881 E+03	1.873 E+03	1.886 E+03	1.881 E+03
44	1.830 E+03	1.891 E+03	1.880 E+03	1.876 E+03
45	1.829 E+03	1.813 E+03	1.893 E+03	1.815 E+03
46	1.817 E+03	1.817 E+03	1.899 E+03	1.871 E+03
47	1.810 E+03	1.844 E+03	1.893 E+03	1.880 E+03
48	1.829 E+03	1.870 E+03	1.893 E+03	1.880 E+03
49	1.812 E+03	1.868 E+03	1.868 E+03	1.874 E+03
50	1.834 E+03	1.868 E+03	1.868 E+03	1.854 E+03
51	1.829 E+03	1.874 E+03	1.868 E+03	1.868 E+03
52	1.829 E+03	1.868 E+03	1.868 E+03	1.802 E+03
53	1.817 E+03	1.868 E+03	1.868 E+03	1.847 E+03
54	1.805 E+03	1.868 E+03	1.868 E+03	1.881 E+03
55	1.868 E+03	1.868 E+03	1.868 E+03	1.868 E+03
56	1.900 E+03	1.851 E+03	1.851 E+03	1.868 E+03
57	1.829 E+03	1.868 E+03	1.868 E+03	1.868 E+03
58	1.834 E+03	1.819 E+03	1.873 E+03	1.868 E+03
59	1.868 E+03	1.817 E+03	1.868 E+03	1.868 E+03
60	1.868 E+03	1.868 E+03	1.868 E+03	1.868 E+03
61	1.868 E+03	1.868 E+03	1.868 E+03	1.868 E+03
62	1.868 E+03	1.868 E+03	1.868 E+03	1.868 E+03
63	1.868 E+03	1.868 E+03	1.868 E+03	1.868 E+03
64	1.868 E+03	1.868 E+03	1.868 E+03	1.868 E+03
65	1.868 E+03	1.868 E+03	1.868 E+03	1.868 E+03
66	1.868 E+03	1.868 E+03	1.868 E+03	1.868 E+03
67	1.868 E+03	1.868 E+03	1.868 E+03	1.868 E+03
68	1.868 E+03	1.868 E+03	1.868 E+03	1.868 E+03
69	1.868 E+03	1.868 E+03	1.868 E+03	1.868 E+03
70	1.868 E+03	1.868 E+03	1.868 E+03	1.868 E+03
71	1.868 E+03	1.868 E+03	1.868 E+03	1.868 E+03
72	1.868 E+03	1.868 E+03	1.868 E+03	1.868 E+03
73	1.868 E+03	1.868 E+03	1.868 E+03	1.868 E+03
74	1.868 E+03	1.868 E+03	1.868 E+03	1.868 E+03
75	1.868 E+03	1.868 E+03	1.868 E+03	1.868 E+03
76	1.868 E+03	1.868 E+03	1.868 E+03	1.868 E+03
77	1.868 E+03	1.868 E+03	1.868 E+03	1.868 E+03
78	1.868 E+03	1.868 E+03	1.868 E+03	1.868 E+03
79	1.868 E+03	1.868 E+03	1.868 E+03	1.868 E+03
80	1.868 E+03	1.868 E+03	1.868 E+03	1.868 E+03
81	1.868 E+03	1.868 E+03	1.868 E+03	1.868 E+03
82	1.868 E+03	1.868 E+03	1.868 E+03	1.868 E+03
83	1.868 E+03	1.868 E+03	1.868 E+03	1.868 E+03
84	1.868 E+03	1.868 E+03	1.868 E+03	1.868 E+03
85	1.868 E+03	1.868 E+03	1.868 E+03	1.868 E+03
86	1.868 E+03	1.868 E+03	1.868 E+03	1.868 E+03

10

87	1.868 E+03	1.868 E+03	1.868 E+03	1.868 E+03
88	1.868 E+03	1.868 E+03	1.868 E+03	1.868 E+03
89	1.868 E+03	1.868 E+03	1.868 E+03	1.868 E+03
90	1.868 E+03	1.868 E+03	1.868 E+03	1.868 E+03
91	1.868 E+03	1.868 E+03	1.868 E+03	1.868 E+03
92	1.868 E+03	1.868 E+03	1.868 E+03	1.868 E+03
93	1.868 E+03	1.868 E+03	1.868 E+03	1.868 E+03
94	1.868 E+03	1.868 E+03	1.868 E+03	1.868 E+03
95	1.868 E+03	1.868 E+03	1.868 E+03	1.868 E+03
96	1.868 E+03	1.868 E+03	1.868 E+03	1.868 E+03
97	1.868 E+03	1.868 E+03	1.868 E+03	1.868 E+03
98	1.868 E+03	1.868 E+03	1.868 E+03	1.868 E+03
99	1.868 E+03	1.868 E+03	1.868 E+03	1.868 E+03
100	1.868 E+03	1.868 E+03	1.868 E+03	1.868 E+03
101	1.868 E+03	1.868 E+03	1.868 E+03	1.868 E+03
102	1.868 E+03	1.868 E+03	1.868 E+03	1.868 E+03
103	1.868 E+03	1.868 E+03	1.868 E+03	1.868 E+03
104	1.868 E+03	1.868 E+03	1.868 E+03	1.868 E+03
105	1.868 E+03	1.868 E+03	1.868 E+03	1.868 E+03
106	1.868 E+03	1.868 E+03	1.868 E+03	1.868 E+03
107	1.868 E+03	1.868 E+03	1.868 E+03	1.868 E+03
108	1.868 E+03	1.868 E+03	1.868 E+03	1.868 E+03
109	1.868 E+03	1.868 E+03	1.868 E+03	1.868 E+03
110	1.868 E+03	1.868 E+03	1.868 E+03	1.868 E+03
111	1.868 E+03	1.868 E+03	1.868 E+03	1.868 E+03
112	1.868 E+03	1.868 E+03	1.868 E+03	1.868 E+03
113	1.868 E+03	1.868 E+03	1.868 E+03	1.868 E+03
114	1.868 E+03	1.868 E+03	1.868 E+03	1.868 E+03
115	1.868 E+03	1.868 E+03	1.868 E+03	1.868 E+03
116	1.868 E+03	1.868 E+03	1.868 E+03	1.868 E+03
117	1.868 E+03	1.868 E+03	1.868 E+03	1.868 E+03
118	1.868 E+03	1.868 E+03	1.868 E+03	1.868 E+03
119	1.868 E+03	1.868 E+03	1.868 E+03	1.868 E+03
120	1.868 E+03	1.868 E+03	1.868 E+03	1.868 E+03
121	1.868 E+03	1.868 E+03	1.868 E+03	1.868 E+03
122	1.868 E+03	1.868 E+03	1.868 E+03	1.868 E+03
123	1.868 E+03	1.868 E+03	1.868 E+03	1.868 E+03
124	1.868 E+03	1.868 E+03	1.868 E+03	1.868 E+03
125	1.868 E+03	1.868 E+03	1.868 E+03	1.868 E+03
126	1.868 E+03	1.868 E+03	1.868 E+03	1.868 E+03
127	1.868 E+03	1.868 E+03	1.868 E+03	1.868 E+03
128	1.868 E+03	1.868 E+03	1.868 E+03	1.868 E+03

41

129	1.868 E+03	1.868 E+03	1.868 E+03	1.868 E+03
130	1.868 E+03	1.868 E+03	1.868 E+03	1.868 E+03
131	1.868 E+03	1.868 E+03	1.868 E+03	1.868 E+03
132	1.868 E+03	1.868 E+03	1.868 E+03	1.868 E+03
133	1.868 E+03	1.868 E+03	1.868 E+03	1.868 E+03
134	1.868 E+03	1.868 E+03	1.868 E+03	1.868 E+03
135	1.868 E+03	1.868 E+03	1.868 E+03	1.868 E+03
136	1.868 E+03	1.868 E+03	1.868 E+03	1.868 E+03
137	1.868 E+03	1.868 E+03	1.868 E+03	1.868 E+03
138	1.868 E+03	1.868 E+03	1.868 E+03	1.868 E+03
139	1.868 E+03	1.868 E+03	1.868 E+03	1.868 E+03
140	1.868 E+03	1.868 E+03	1.868 E+03	1.868 E+03
141	1.868 E+03	1.868 E+03	1.868 E+03	1.868 E+03
142	1.868 E+03	1.868 E+03	1.868 E+03	1.868 E+03
143	1.868 E+03	1.868 E+03	1.868 E+03	1.868 E+03
144	1.868 E+03	1.868 E+03	1.868 E+03	1.868 E+03

Data set for traverse...
of Fig.98

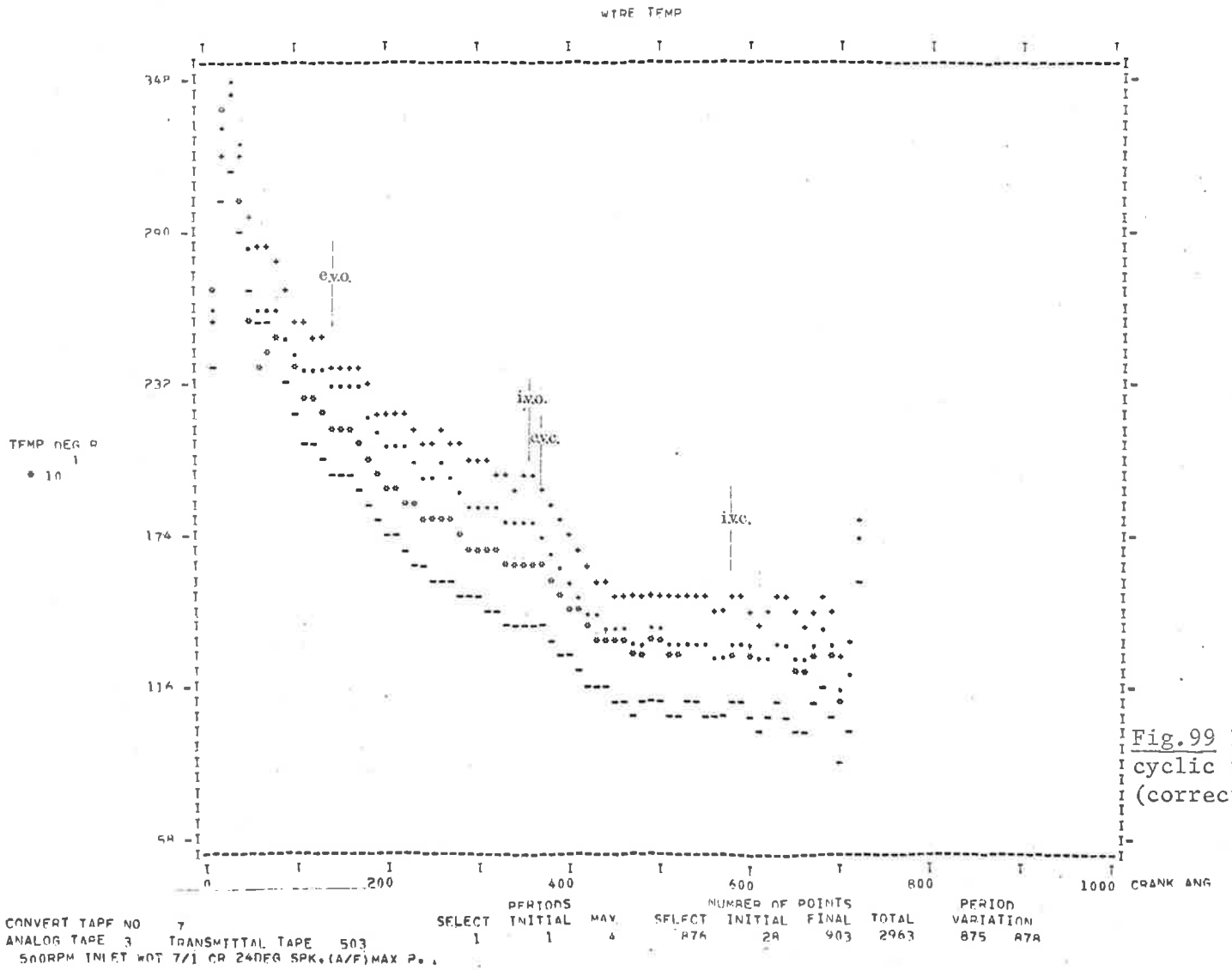

Fig.99 Inlet region cyclic traverse (corrected)-Firing WOT

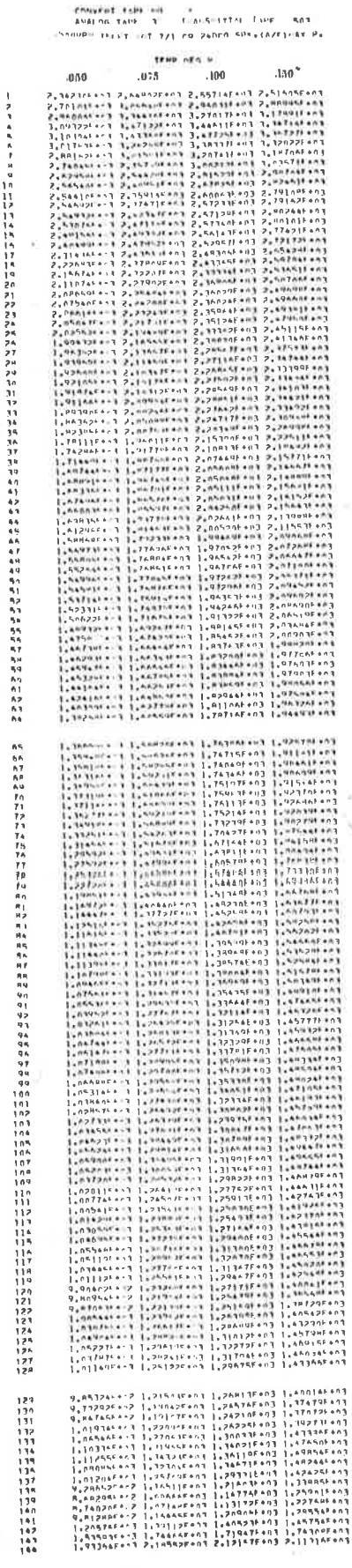

Data set for traverse of Fig.99

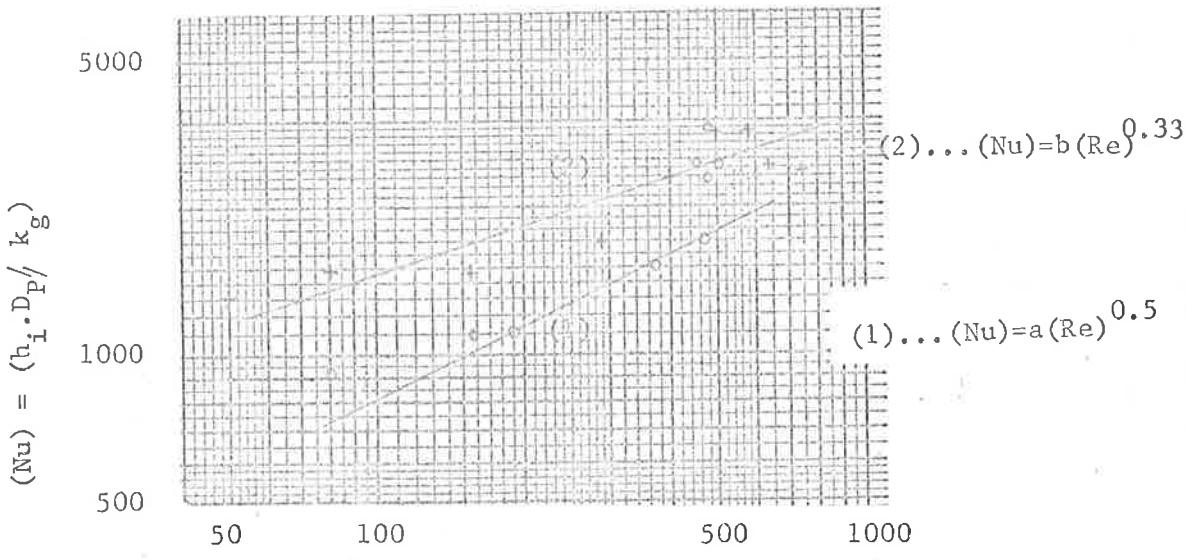

$$(Re) = (V_{Pm} . D_P \rho / \mu) \quad ....(1)$$

$$(Re) = (V_{Pi} . D_P \rho / \mu) \quad ....(2)$$

Fig.100 Annand type correlation for heat transfer coefficient over expansion-exhaust strokes (100°-200°ACTDC)for data of Fig.79.

7. CONCLUSIONS

From the theoretical and experimental work presented in this thesis the following conclusions may be drawn:

(1) In general, the steady-state overall and local heat transfer measurements agree with those of previous workers for variation in mixture strength, spark advance and fuel flow rate.

Local steady-state heat transfer rate was found to be proportional to $(r.p.m.)^{0.2}$. This agrees more closely with the formula of Eichelberg who used an exponent of 0.33 than with that of Annand who proposed an exponent of 0.8.

(2) The experimentally determined quasi-steady heat transfer coefficient breaks down during the induction-compression phase of the cycle by giving negative and infinite coefficients.

(3) These discontinuities were found to be the result of phase differences between heat flux and driving temperature difference The experimental evidence indicates that the phase relationships between the variables are more accurately predicted by the Heat Transfer Coefficient Concept than by the Temperature Profile Method despite the fact that the former theory assumes a constant heat transfer coefficient in its derivation. It was found that:

(a) A particular harmonic of the bulk gas temperature variation leads the corresponding wall surface temperature variation by 1/8th of its period or 90^{o} crank angle for the fundamental component.

(b) The wall surface heat flux variation is in phase with, and is also a replica of, the bulk gas temperature.

(4) The "thermal layer" thickness was found to vary considerably over the cycle, being thickest during induction and thinnest during compression. Increasing speed and C.R. was found to further reduce the layer thickness.

Good agreement was obtained between the experimental instantaneous gas temperature gradients and those predicted by using gas mixture thermal conductivity data.

(5) This "thermal layer thickness" appears not to be the true turbulent boundary layer thickness but most likely represents that of the "quench layer" extending to between 0.200 and 0.400" from the wall. The discontinuities in the heat transfer coefficient were less predominant when the bulk gas temperature was measured outside the quench layer.

A sub-layer was detected within the "thermal layer" under motoring conditions at the Inlet region.

The thickness of this sub-layer corresponds to the equivalent aerodynamic boundary layer thickness in turbulent pipe flow used by Knight.

(6) The cycle of heat transfer coefficient was found to resemble closely the cycle of mass velocity measured by Horvatin in a motored engine. In both cases large amplitude oscillations occur in the second half of the cycle having a period of 120^{o} crank angle.

(7) The expansion-exhaust strokes of the cycle showed a continuous variation of heat transfer coefficient with a maximum occuring near e.v.o.

(8) Using Annand's correlation ($(Nu)=a(Re)^{m}$) over this phase, a value for the exponent of 0.5 is obtained.

When instantaneous piston velocity is used rather than mean piston speed in the above expression, the resulting exponent is 0.33.

(9) The values for instantaneous heat transfer coefficient predicted by Eichelberg's formula are considerably lower than those measured experimentally. Better agreement with experimental values is obtained when Eichelberg's formula is arbitrarily multiplied by a factor of 3 and the mean piston speed is replaced by the instantaneous piston velocity.

RECOMMENDATIONS

(1) The most important direction for further research is that of instantaneous velocity measurement simultaneously with the other variables recorded in this investigation.

Since velocity is a vector quantity this will be extremely difficult but local gas velocity measurement appears to be a necessity for further understanding of the instantaneous heat transfer process. Semenov (31) and Horvatin (32), report on early attempts at velocity measurement by compensated hot wire anemometers.

(2) The method used herein for electrical compensation of the gas thermocouple could be simulated numerically by writing the appropriate inverse transfer function into the computer programme. This would allow a greater degree of accuracy since the thermocouple time constant could be included as a time-varying function of velocity over the cycle. Reliable local gas velocity data would thus also greatly improve the certainty of knowledge of local instantaneous gas temperatures.

(3) Regarding the apparent deficiencies of classical steady-state concepts, it is of interest to note recent advances in an allied field.

Biot (61), (62) found that spatial distribution of heat flux in both laminar and turbulent boundary layers with streamwise temperature variations was generally out of phase with the wall temperature.

He also observed that the concept of a surface heat transfer coefficient gave negative and infinite values in this situation.

Biot physically explained this behaviour as being a distortion of the temperature field by fluid motion.

Using variational principles, he successfully extended the Lagrangian thermodynamic equations of irreversible processes to describe the transient convective heat transfer.

This approach would also appear to point the way for further advances in the field of unsteady heat transfer in engines.

(4) Numerous applications of the 'MOVADAS' data acquisition system remain in areas of study which were barely mentioned in this thesis. Some of the more important possibilities seem to be:-

(a) Instrumentation of all three probe locations simultaneously to record on the present three data channels either gas temperatures or wall temperatures. This would provide valuable information on burning rates, flame velocities and regional differences. The completion of a multiplex system originated by this author would enable complete heat transfer information to be obtained from all locations simultaneously.

(b) A detailed study of instantaneous temperature gradients in the quench layer may yield knowledge on the mechanism of formation of the exhaust contaminants thought to contribute to air pollution or 'smog'. Daniel (63) reported that both original fuel hydrocarbons which fail to burn and non-fuel hydrocarbons produced by cracking are formed in the quench layer.

(c) Unsteady heat transfer under 'knocking' combustion would seem to be a fruitful area for further work and the sensitive pressure transducers developed by Barden (41) could be adapted to the system for this purpose.

BIBLIOGRAPHY

(1) OVERBYE, V.D., BENNETHUM, J.E., UYEHARA, O.A. and MYERS, P.S.; "Unsteady Heat Transfer in Engines"; SAE.TRANS, 1961, V69.

(2) ELSER, K.; "Der instationare Warmeubergangin Diesel-motoren" MITT. INST. THERMODYN - ZURICH, 1954 No. 15.

(3) NUSSELT, W.; "Die Warmeubergang in den Verbrennungs - Kraftmaschinen" S.V.D.I. 1923, V67.

(4) CLERK, D.; TRANS. FARADAY soc. 1926, V22.

(5) ANNAND, W.J.D. "Heat Transfer in the cylinders of Reciprocating Internal Combustion Engines"; PROC.I.MECH.E., LOND. 1963, V177, No. 36.

(6) STAMBULEANU, A "Contribution to the Study of the Distribution of Heat Transfer Coefficients during the phase of the working cycle of an I.C. Engine". PROC. 3RD INT. HEAT TRANSFER CONF., I.MECH.E, CHICAGO 1966, pp 339-358.

(7) TAYLOR, F.C. & TAYLOR, S.E.; "The Internal Combustion Engine" INTERNATIONAL TEXTBOOK CO, 1962 p168.

(8) SEMENOV, E.S. & SOKOLIK, A.S.; IZV. AN. SSR, 1958, 130, No. 8.

(9) JAKOB, M.; "Heat Transfer" V1, WILEY N.Y. 1956.

(10) STAMBULEANU, A.; Diss. Techn. Hochschule, Berlin, 1935.

(11) STEIGER, A. & AUE, G.K.; "The influence of the thermal loading criterion on the design of a turbo-charged two-stroke diesel engine". PROC. I.MECH.E., Lond. 1964-65, V179/3C, p68.

(12) WALKER, G.; "Computing the Performance of Gasoline Engines"; THE ENGINEER, Mar. 27, 1964 pp562-568.

(13) HENIEN, N.A., "Thermal Loading and wall temperatures as Functions of performance of turbo-charged Compression Ignition engines"; DISS. UNIV. MICHIGAN, 1957.

(14) BROWN, D.H.; "Diesel cylinder Heat Transfer design Criteria"; TRANS. SAE, 1958 V66, pp522-531.

(15) HUBER, P. & BROWN, J.R.; "Computation of instantaneous airflow and volumetric efficiency". PAPER 812B, SAE Auto.Eng.Congress 1964, pp698-717.

(16) WHITEHOUSE, N.D., STOTTER, A., GOUDIE, G.O. and PRENTICE, B.W.; "Method of predicting some aspects of performance of a diesel engine using a digital computer". PROC.I.MECH.E., LOND, 1962. V176, No. 9, p195.

(17) SMYTH, R. & WALLACE, F.J.; "Comparative performance assessment by digital computers of various compression-ignition engine configurations in combination with compressors and turbines". PROC.I.MECH.E., LOND, 1966-67, V181/1, No. 12, p259.

(18) BORMAN, G.L. etal "Development and evaluation of the Simulation of the compression-ignition engine". SAE paper 650451, Chicago, May, 1965.

(19) EICHELBERG, G.; "Temperaturverlauf und Warmespannung in Verbrennungsmotoren" FORSCH. ENG. WES, 1923, No. 263.

(20) HUG, K.; "Messung und Berechnung von Kdbentemperaturen in Dieselmotoren" MITT. INST. THERMODYN. ZURICH, 1937, No. 1.

(21) EICHELBERG, G.; "Some new investigations on old combustion engine problems" ENGINEERING, LOND, 1939, V148.

(22) PFLAUM, W.; "Warmeubergang bei Dieselmaschinen mit und ohne Aufladung" M.T.Z. 1961, V22, 70.

(23) VAN TIEJEN, H.W. & deMOOY, A.; "Cylinder wall temperature in Four- and Two-stroke diesel engines as dependent on mean indicated pressure, piston speed and bore" PROC. C.I.M.A.C., 1959, p405.

(24) WALKER, G.; "Heat Transfer in Gasoline Engines" THE ENGINEER, Nov. 24, 1967, pp690-695.

(25) MILLAR, G.E. etal; "Practical applications of engine flame temperature measurements" SAE NAT. FUELS & LUBRICANTS MTNG, CHICAGO, Nov. 1963, Paper 196.

(26) ELSER, K.; "Instanionare Warmeubertragung bei periodisch adiabater Verdichtung turbulenter gase" FORSCH. ING. WES.; 1955, V21, 65.

(27) OGURI, T.; "On the Coefficient of heat transfer between gases and cylinder walls of the spark ignition engine". BULL. JSME.; 1960, V3 No. 11. pp363-369.

(28) OGURI, T.; "Theory of heat transfer in the working gases of I.C. Engines". BULL. JSME, 1960, V3, No. 11, pp370-377.

(29) KNIGHT, B.E. "The problem of predicting heat transfer in diesel engines". PROC.I.MECH.E., LOND, 1964-65, V179/3C p99.

(30) HENIEN, N.A.; "Instantaneous heat transfer rates and coefficients between the gas and combustion chamber of a diesel engine". PAPER 969B, SAE Auto.Eng.Congress, Detroit, Jan. 1965.

(31) SEMENOV, E.S. "Device for measuring the turbulence in Piston engines". INSIRUMENTS & EXPERIMENTAL TECHNIQUES (RUSSIAN) No, 1 Jan-Feb 1958, pp102-111.

(32) HORVATIN, M.; "Messung des Luftdralls in einem fremd angetrieben Dieselmotor". DISS. TECH. HOCHSCHULE, MUNSCHEN, 1965.

(33) OVERBYE, V.D. "Variation of instantaneous wall temperature, heat transfer and heat transfer coefficients in a spark ignition engine". DISS. UNIV. WISCONSIN, 1960.

(34) BIRD, R.B., STEWART, W.E. & LIGHTFOOT, E.N.; "Notes on transport phenomena" WILEY, N.Y., 1958.

(35) HOBSON, E.W.; "Warmeleitung, Mathematischer Teil" ENCYKLOPADIE DER MATHEMATISCHEN WISSENSCHAFTEN, V5 Part 1, Article 4, B.G. Teubner Leipzig & Berlin, 1903-1921, p186.

(36) LORD KELVIN, "Linear motion of heat, Part 2". CAMBRIDGE MATHEMATICAL JOURNAL, V3 LONDON, 1943, pp206-211.

(37) PFRIEM, H.; "Periodic heat transfer at small pressure fluctuations" NACA TECH.MEMO 1048, 1940.

(38) KADRINOV, N.B.; "An approach to deriving a formula for determing the coefficient of heat transfer from a gas to a wall based on the Kinetic theory of matter" 12V. VYSSHIKH. UCHEBNYKH ZADEDENIY, Neft i Gaz, No. 11, 1960 pp95-100.

(39) BENNETHUM, J.E.; "Heat transfer and combustion chamber deposits in a spark ignition engine". DISS. UNIV. WISCONSIN, 1960.

(40) HARA, M. & OGURI, T.; "Measurement of piston temperature of a spark ignition engine". BULL. JSME. 1950 V2 No. 7 p388.

(41) BARDEN, R.G.; "An investigation of combustion phenomena associated with detonation in I.C. Engines". DISS. UNIV. ADELAIDE, 1956.

(42) BAKER, RYDER & BAKER; "Temperature measurements in Engineering" WILEY, N.Y., 1961.

(43) DAFT, C.H.J.; "Instruments used in the development of diesel engines". PAPER 4, PROC.I.MECH.E., 1965-66, V180/3G.

(44) SMYTH, R.; "Transient heat flow investigations using an on-line computer". PAPER 16, AUST. INST. NUCL.SCI & ENG. - 3RD FLUID MECH. CONF, 1967.

(45) MEYER, W.E. & DE CAROLIS, J.J.; "Compression Temperatures in diesel engines under starting conditions". SAE TRANS., 1962 V70, pp163-174.

(46) BENSON, R.S. & BRUNDRETT, G.W.; "Development of a resistance wire thermometer for measuring transient temperatures in exhaust systems of I.C. Engines". TEMP. MEAST. & CONTROL IN SCIENCE & INDUSTRY, V3, Part 2, 1962 pp631-653.

(47) SHANNON, C.E. & WEAVER, W.; "The mathematical Theory of communication" UNI. ILLINOIS PRESS, 1949.

(48) HAMMING, R.W.; "Numerical analysis for scientists & engineers". MCGRAW HILL, 1963.

(49) CLARKE, A.P.; "The computation of the coefficients of a Fourier series expansion of a function defined by sampled data points". AUST. DEPT. SUPPLY, ADSS, W.R.E. Tech.Memo TRD 71, June, 1964.

(50) CHISTYAKOV, U.S.; "Methods of measuring rapidly varying temperatures of gas streams". TEPLOFIZIKA VYSOKIKH TEMPERATUR (Rassian Transl.) V3, No. 6, Nov-Dec 1965.

(51) KERLEY, R.V. & THURSTON, K.W.; "Indicated performance of Otto cycle engines". TRANS. SAE, 1962, V70, 5.

(52) GORDOV, A.N. & KOVSHEV, B.I.; "Nature of dynamic errors in measuring pulsating temperatures of a gas flow with a pulsating speed" (Russian Transl.) IZMERITELNAYA TEKHNIKA No. 5, (MEASUREMENT TECHNIQUES) May, 1961, pp17-21.

(53) GOLDSTEIN, S., "Modern developments in fluid Dynamics" 1938 (OXFORD)

(54) JANEWAY, R.N.; "Quantitative analysis of heat transfer in engines" TRANS. SAE., Sept. 1938, V43 No. 3, pp 371-379.

(55) KU, P.M.; "Factors affecting heat transfer in I.C. Engines". N.A.C.A. Tech. Note TN787, 1940.

(56) TAYLOR, C.F. & TOONG, T.Y.; "Heat transfer in I.C. Engines". A.S.M.E. paper No. 57-HT-17, 1957.

(57) ALCOCK, J.F., "Heat transfer in diesel engines". PROC. INT. HEAT TRANSFER CONF., BOULDER, I.MECH.E. LOND. 1961, V174.

(58) TAYLOR, C.F.; "Heat transmission in internal combustion engines". PROC. GENERAL DISCUSSION ON HEAT TRANSFER, I.MECH.E. LOND. 1951, pp397-401.

(59) HOTTEL, H.C., WILLIAMS, G.C. & SATTERFIELD, C.N.; "Thermodynamic charts for combustion processes"; WILEY, N.Y. 1949.

(60) BREWSTER, B. & KERLEY, R.V.; "High temperatures trigger pre-ignition" SAE PAPER No. 725C, 1962.

(61) BIOT, M.A.; "Fundamentals of boundary layer heat transfer with streamwise temperature variations" JNL. AEROSPACE SCI. May, 1962, pp558-567. V 29, No.5.

(62) BIOT, M.A.; "Lagrangian thermodynamics of heat transfer in systems including fluid motion" JNL. AEROSPACE SCI. May, 1962, pp568-577.

(63) DANIEL, W.A. "Auto smog blamed on engines cold walls" MACHINE DESIGN, Feb. 1967, p8.

APPENDIX A1

THERMOCOUPLES FOR ENGINE GAS TEMPERATURE MEASUREMENT

by

G.A. MORGAN

UNIVERSITY OF ADELAIDE
DEPARTMENT OF MECHANICAL ENGINEERING
Report Mech.Eng. R67/1
November, 1967.

THERMOCOUPLES FOR ENGINE GAS TEMPERATURE MEASUREMENT

- Construction, Calibration & Correction

TABLE OF CONTENTS

THERMOCOUPLE PROBES FOR ENGINE GAS TEMPERATURE MEASUREMENT

1. INTRODUCTION

This report describes the construction, calibration and correction of fine wire thermocouples used in various probes designed to study the Phenomenon of Instantaneous Heat Transfer to the combustion chamber walls of a spark ignition engine.

A brief resume of the study area is followed by a critical survey of alternative methods of temperature measurement leading to justification of a suitable method for this application.

The errors involved in gas temperature measurement are explained and those pertinent to this study are detailed in a section dealing with the theory of element response to a step change in gas temperature. A method of thermocouple calibration using a shock tube is described.

This leads to a discussion of methods used for obtaining true gas temperature from recorded wire temperatures. The limitations of each method are briefly described and examples of corrected temperatures are compared to those from thermodynamic cycle calculations. Problems associated with the choice of thermoelements including the junction and its formation are described, together with the design of a special welder for producing impurity free miniature junctions.

2. GAS TEMPERATURE MEASUREMENT

Methods of measurement of gas temperature can be classified as follows:

(1) Indirect methods:

(a) by calculation

(b) indirect experimental methods

and (2) Direct methods:

(a) Resistance thermometers

(b) thermocouples

In this section the advantages and disadvantages of these methods will be discussed.

2.1 Indirect Methods

2.1.1. By calculation:

In the engine heat transfer literature, the perfect gas equation ($pv = mRT$) has often been used to calculate cyclic "mass average" gas temperatures from discrete time sampling of cylinder pressure records. This method has the following disadvantages:

(1) The effect of charge blow-by past the piston rings can introduce a significant error in estimations of charge mass at TDC from that at BDC.

(2) The use of perfect gas laws may hold approximately on the compression stroke and late in expansion but during combustion this is obviously unrealistic.

(3) Pressure and temperature are both variables requiring independent study in unsteady heat transfer work, and especially during conditions conducive to 'knocking' combustion.

(4) Pressure indicator diagrams are often obtained by "point-by-point" sampling, which method provides a psuedo-pressure cycle, thus masking cycle-to-cycle variations.

Different regions of the combustion chamber gas experience different temperature cycles as a result of local variations in flow velocities, density gradients, and wall temperatures.

The use of a "mass average" temperature calculated in this manner, is hardly ideal especially when use is made of this in correlations with measured local instantaneous wall temperature and heat-flux data

2.1.2 Indirect experimental methods

A comprehensive examination of methods of gas temperature measurement in engines was reported by the Co-ordinating Research Council (8), 1960, viz Sonic velocity measurement, Iodine Absorption method, Infrared Null and Sodium line reversal methods.

The latter three are all basically similar in principle, usually requiring extensive engine modifications e.g. quartz windows and special combustion chamber "pockets". Calculations of gas temperature are based on the absorption of light or a radiation source by the gas at various wavelengths corresponding to the absorption bands of iodine, water vapour and sodium (flame temperatures) respectively.

These all require a line of sight optical path through the gas, giving rise to an average gas temperature which, due to the unknown effects of thermal gradients in the gas near to the walls,

is found to depend on the device being used. The Infrared monochromator method tends to give an average temperature weighted toward the peak value.

The report mentioned above states that the free stream or peak fluid temperature can be estimated if some information about the thermal boundary layer thickness is available. A more accurate appraisal of the effects of gradients will probably require at least a crude attempt to measure the temperature profile - under very mild motoring conditions - with fast response thermocouples or resistance probes.

Another indirect method of obtaining gas temperature is by measurement of the sonic velocity between two probes in the gas, (8).

Although this method gives a more localised measurement, a serious drawback is brought about by the necessity to water-cool the probe tips. This imposes an 'artificial' temperature gradient across the acoustical path thus influencing the gas temperature.

A further disadvantage is that due to limitations in data acquisition techniques, all the above methods have used 'point-by-point' or null-point sampling whereby only one gas temperature is sampled per cycle at a particular crank-angle, and a 'psuedo-cycle is built up by sampling at different crank angles over a large number of cycles. Significant cycle-to-cycle variations show the desirability of recording all pertinent experimental data simultaneously.

2.2 Direct Methods

2.2.1 Resistance Thermometers

As described in a survey by Benson and Brundrett (10), 1962, a great deal of pioneering work with fine wires for engine gas temperature measurement was done toward the end of the last century (e.g. see Donkin (11), 1893, Coker & Scoble (12) 1913), the approach being to reduce wire size and thus thermal inertia. However, it was soon realised that even very fine wire thermocouples and resistance thermometers had a finite time-lag, Petersen (13), 1913.

Interest in fine-wire transient temperature measurement has renewed in recent years with application to compressors, jet engines, pulse-jets, re-entry heating and combustion studies.

This has lead to the availability of extremely fine wires - particularly by the Wollaston process, Hall (14), 1961 - down to 0.000015" Ø for use as resistance thermometers.

These have the advantage over thermocouples that a welded joint does not have to be made. Thus a resistance thermometer can have a shorter time lag than a thermocouple of the same diameter wire.

Still, resistance thermometers do have several drawbacks when applied to local instantaneous engine measurements:

(1) The resistance wire sensing element needs to be longer than the equivalent thermocouple in order to reduce end conduction temperature losses to its supports. This effectively measures the temperature over a longer finite volume of gas than does a thermocouple, which tends to give a point measurement.

(2) Also due to this inherently greater length, resistance thermometers cannot be made as mechanically strong as thermocouples.

(3) The wire materials commonly used for resistance thermometry are Platinum or Platinum-Rhodium, and Tongsten. Neither of these are entirely suitable for use in combustion chambers:

(a) Platinum alloys and other noble metals encounter surface catalytic effects in oxidising atmospheres above 1800^{o}F and thus suffer surface self-heating and changes in calibration.

(b) Tungsten, although robust, has the disadvantage of a very low oxidising temperature (830F); and a non-uniformity between samples due to its complex method of manufacture. This makes comparison between different sensors uncertain.

(4) A more general objection to resistance thermometry for the present work concerns the difficulty of monitoring and recording an instantaneous bridge balance current and applying the temperature-resistance calibration for the particular length of wire being used. To carry out this process automatically is far more difficult than the simple voltage recording required for thermocouples.

These considerations have eliminated the use of the above devices for the present application, and the remaining possibility, the fine wire thermocouple, will now be discussed.

To sum up; the forgoing sophisticated methods all suffer from the disadvantages that:

(1) They average temperatures over a finite (sometimes large) path length, thus obscuring:

(a) Gas boundary layer thermal gradients due to conductive heat transfer between the main gas 'core' and the containing walls.

(b) Local temperature differences due to gas velocity variations and regional 'hot-spots'.

(2) In the optical methods, dirty windows and non-equilibrium of the radiating atoms with the gas can introduce errors.

(3) Point-by-point recording methods can misrepresent comparisons of cyclic data.

2.2.2. Thermocouples

It is known that wires less than about 0.0015" Ø will respond to engine gas temperature variations:- Meyer & De Carolis, (15) 1962, and that wires less than about 0.0005" Ø will probably be destroyed by combustion.

Within these limits, therefore, the problem is to find a method of correcting the thermocouple signal for the errors inherent due to the finite size of the element, and the dynamic nature of the process being measured.

Some of the advantages of the fine-wire thermocouple can now be listed:

(1) It can provide a localised point temperature measurement suitable for an investigation of gas temperature gradients.

(2) A linear thermoelement (such as Chromel-Alumel) gives a self-generated output voltage directly proportional to temperature. This can be very easily displayed or continuously recorded thus obviating the need for energised bridge elements.

A high speed multichannel data-acquisition system (9) can be used to obtain a comparison between simultaneously recorded cycles from a number of thermocouples.

In this investigation, Chromel-Alumel was used exclusively for all thermocouples* because of its linear output and good high temperature stability.

(3) It will be shown that if the junction is made small enough, all measurement errors become small, the most predominant being due to thermal inertia of the element, for which corrections may be applied.

(4) It is not possible, for mechanical reasons, for layers of soot to form on fine wire thermocouple beads (Ref. (16)). This was borne out by the present work.

* Those used in this investigation are tradenamed:

"Thermocoax" made by Societe Anonyme d'Etudes et Realisations Nucleaires, France; and "Ceramo" made by Thermo-Electric Co., Inc., U.S.A.

3. ERRORS INVOLVED

A thermocouple junction may not attain the true temperature of the surrounding gas for the following reasons:

(1) Incomplete recovery of the Kinetic energy of the gas stream:

Total gas temperature = Static gas temp. + $RV^2/2gJC_p$

where R = recovery factor

V = gas velocity

g = gravitational constant

C_p = specific heat of gas

J = mechanical equivalent of heat

i.e. this error varies with the square of the velocity and inversely with temperature, since C_p increases with temperature. However, even for an expected gas velocity of 400ft/sec, assuming R = 1, and say T_g = 1200°F this error is only;

$(400)^2/64.4 \times 778 \times 0.28 = 11.4^{\circ}F$ i.e. about 1%.

(2) Conduction heat transfer to and from the probe support. Hunt (17), 1959 states that with fine wires supported by heavy leads this error can be reduced to less than 1% by making the distance from the support to the junction at least 5 times wire diameter.

End conduction error is not a problem with thermocouple junctions of the type being used. (See Fig. 25).

(3) Likewise, Radial temperature gradients in the wire have been shown by Benson & Brundrett to be negligible providing that the wire diameter is of the order of 0.001" Ø.

(4) Radiation to and from the surroundings

It has been shown in many previous studies (1), (2), (15) that the radiative mode of heat transfer from the combustion gases of a petrol engine is negligible compared to the convection mode and this is a working assumption of this thesis.

Both (10) and (15) report that radiation from combustion chamber walls gives an error of only 2-5^{o}F for a 0.0015" Ø wire for typical gas and wall temperatures of 932^{o}F and 572^{o}F respectively.

(5) Thermal capacity or thermal inertia of the junction - this together with rate of temperature change and heat transfer coefficient to the wire-determines the thermocouple response or lag time.

This is by far the most significant error and it will be shown that this can be approximately corrected for.

4. THEORY OF ELEMENT RESPONSE

Consider a straight fine wire element

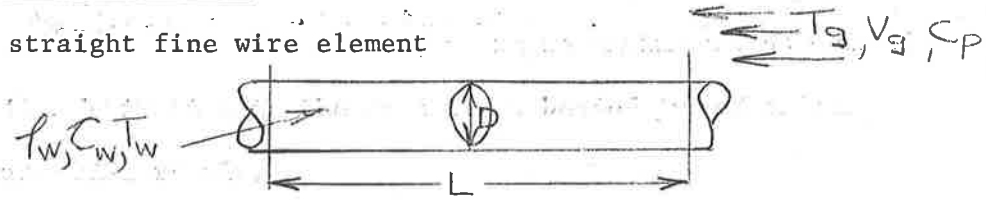

Consider an energy balance between the convective heat transfer to an element of length of wire and the rate of accumulation of heat in that element over the time interval $\delta\theta$. Neglect conduction temperature gradients within the wire and also neglect radiative heat transfer.

then: Heat input from gas = heat stored in wire

i.e. $hA(T'_g - Tw) = MC_w \frac{dTw}{d\theta} . \delta\theta$

where h = convective heat transfer coefficient, gas-wire

A = surface area of element

T_g' = total gas temperature

T_g = Static gas temperature

Tw = wire temperature

m = mass of element

C_w = specific heat of element

$dTw/d\theta$ = time rate of change of wire temperature.

Thus,

$$h\pi DL(T_g + V^2/2gJC_p).\delta\theta = \rho_w \frac{\pi}{4} D^2 LC_w . (dT_w/d\theta) . \delta\theta$$

or

$$(T_g + V^2/2gJC_p - T_w) = \frac{1}{h} \left(\frac{\rho CD}{4}\right)_w . (dT_w/d\theta)$$

and it was shown in Section 3 that the recovery of kinetic energy is also negligible.

i.e. $T_g = T_w + \frac{\rho CD}{4h} \cdot dT_w/d\theta$

or $T_g = T_w + \tau \cdot dT_w/d\theta$

where $\tau = \frac{\rho CD}{4h}$ is defined as the thermoelement time constant. The dependence of τ on the gas-wire heat transfer coefficient, infers a dependence on gas velocity which is not accurately known over the cycle. This is discussed later in Section 7.1.

The thermocouple time constant is thus defined as the ratio of the heat capacity per degree temperature rise to the rate of heat input per degree temperature difference between the gas and the wire. This can be determined experimentally by a number of methods, one of which, by shock tube tests, is detailed in Section 8.

The above reasoning may be applied for a beaded thermocouple junction, but the constant resulting in the expression for τ above will be different.

5. CORRECTION METHODS

To calculate the true gas temperature from the recorded wire temperature variation, the following methods are available:

1. The Single Wire Iterative Method.
2. Two-wire Methods.
3. The three-wire Method.
4. Network Compensation.

5.1 Single wire iterative method

This method is usually only successful in flow conditions where the heat transfer coefficient to the wire is known. It requires that the gas velocity is known throughout the cycle, or can be calculated from recorded gas pressure and temperature, (e.g. by the method of characteristics).

Alternatively, an estimate of heat transfer coefficient can be made from steady-state data for flow over small cylinders. (Spangenberg (18)).

However, Kudryavstev (19), 1961, warns that this approach is unreliable as the steady-state heat transfer coefficients are not the same as those obtained from steady-state experiments.

Velocity measurement in the combustion chamber is extremely difficult, the compensated hot wire method of Semonov (21), 1956, coming closest to direct local measurement, however this is not a working laboratory instrument at present.

Even prediction of instantaneous gas velocity is fraught with difficulty, the use of Piston Velocity as an approximation being unrealistic due to unknown gas swirl and valve motion effects.

This also precludes the use of the method of characteristics which would give planes of constant velocity at any distance from the piston i.e. "slug" flow. Hence this method was not attempted.

5.2 Two Wire Methods

5.2.1 Wires of different diameter

This method follows that of Aftalion (16) (thermocouples) and Benson & Brundrett (10) (Resistance thermometers). The derivation is the same for either configuration, the method making use of two elements of different diameter, but same thermal properties (thermal capacitance $\rho_w C_w$).

From equation (1)

$$T_g = T_{w_1} + \frac{1}{h_1}\left[\left(\frac{\rho C D}{4}\right)_1 \cdot \frac{dT_{w_1}}{d\theta}\right] \qquad (5)$$

$$T_g = T_{w_2} + \frac{1}{h_2}\left[\left(\frac{\rho C D}{4}\right)_2 \cdot \frac{dT_{w_2}}{d\theta}\right] \qquad (6)$$

These equations show the fallacy of merely attempting to extrapolate to zero wire diameter, as do Fishenden & Saunders (22), because this neglects the important rate of change of temperature term.

As we have only 2 equations with 3 unknowns (two unknown heat transfer coefficients and one unknown temperature); a further expression is required.

Aftalion (16) assumed that the gas-wire heat transfer coefficient could be expressed simply as a function of Reynolds No. i.e. for a cylinder exposed to continuum flow: $(Nu) = k\,(Re)^n \cdot (Pr)^m$ (7)

Aftalion further assumed that for engine exhaust gases (Re) fluctuates between 30 and 600 and that

$$(N_u) = 0.068 (R_e)^{0.466} \cdot (P_r)^{0.31} \qquad (8)$$

But Benson (20) pointed out that with the wire size commonly used for this method, the wire diameter is of the same order as the gas molecular free path and "slip flow" occurs.

Thus strictly the Reynold's No. (Re) should be replaced by the Knudson No. in equations (7) & (8).

However, Benson actually used the expression

$$(N_u) = A (R_e)^m \qquad (9)$$

where A & m are constants.

Thus the heat transfer coefficient to the wire

$$h = \frac{Ak}{D}\left(\frac{VD}{\nu}\right)^m \qquad (10)$$

and for two wires, the ratio of heat transfer coefficients is:

$$\frac{h_1}{h_2} = \left(\frac{D_2}{D_1}\right)^{1-m} \qquad (11)$$

substituting (11) in (6)/(5) gives:

$$T_g = T_{W1} + \Delta T$$

where

$$\Delta T = \left[\left(\frac{D_2}{D_1}\right)^{1-m} \cdot \left\{\left(\frac{fCD}{4}\right)_2 \cdot \frac{dT_{W2}}{d\theta} \Big/ \left(\frac{fCD}{4}\right)_1 \cdot \frac{dT_{W1}}{d\theta}\right\}\right]^{-1} - 1 \qquad (12)$$

Aftalion gives an example of a two wire calculation using (12) and wires of 0.002" and 0.004" diameter.

It will be shown later that this method has no advantage over Method 2.4 due to the assumption of the constant exponent 'm'.

Further, Benson & Brundrett point out that this method gives scattered results and propose smoothing out the measurement errors by means of the 3-wire technique.

The scatter inherent in the two wire method is a direct result of the methods used to evaluate the derivatives $dT_w/d\theta$:

1. Estimation of the tangent at a point by graphical means for which great accuracy is required.
2. Calculating the chordal slope between adjacent points on either side of the point required (Secant method).

   Chistyakov (23) criticises both these methods as being incapable of satisfactory results, and recommends differentiating the functions for the temperature cycle of each wire expressed in the form of a Fourier series (The function $T(\theta)$ always satisfies the Dirichlet conditions). This method is used in the present investigation and allows the derivatives to be determined with a high degree of accuracy.

5.2.2 Wires of different diffusivity

The method of Kobayashi (7) 1937, appears to be fundamentally more attractive than the method of Aftalion.

Kobayashi recognised the need for thermal lag (attenuation & phase) correction even for wires of 0.0005" and, probably following the suggestion of Pfriem (24) 1936, carried out experiments using two wires of the same diameter but with different thermal diffusivities ($\alpha = k/\rho c$).

This method has the distinct advantage that if the wires have the same surface smoothness and emissivity, then the heat transfer coefficient to each wire is the same. i.e. only two unknowns h & T_g remain and thus only two equations are needed for a solution.

Note that this method enables the gas-wire heat transfer coefficient to be determined whereas by method 5.2.1 any attempt to do this results in considerable error.

Kobayashi gave the derivation both for an infinitely long wire and for a resistance element of finite length, giving also corrections for radiant heat transfer.

In his experiments he used resistance elements of pure platinum (α= 0.0865 cgs units) and of 90% Platinum, 10% Rhodium (α = 0.036 cgs units) with apparently good results.

5.3 The Three-Wire method

Restating equation (1) Section 4.

$$\left[T_g + \frac{v^2}{2gJC_p} - T_w\right] = \frac{1}{h}\left(\frac{\rho CD}{4}\right)_w \cdot \frac{dT_w}{d\theta}$$

Benson & Brundrett continue as follows:

Since $(N_{v.}) = \frac{hD}{K_g}$ & $(N_u) = A(R_e)^m$

then $\frac{hD}{K_g} = A\left(\frac{V_g D \rho_g}{\mu_g}\right)^m$

or $$\frac{1}{h} = \frac{D}{k_g A}\left(\frac{\mu_g}{\rho_g V_g D}\right)^m$$

$$\text{in (1)} \rightarrow \left[T_g + \frac{V^2}{2gJC_p} - T_w\right] = \frac{D}{k_g A}\left(\frac{\mu_g}{\rho_g V_g D}\right)^m \left[\left(\frac{\rho CD}{4}\right)_w \cdot \frac{dT_w}{d\theta}\right] \qquad (13)$$

and under a given set of conditions they assume that

$$\mu, \rho_w, \rho_g, C_w, C_p, k_g \text{ \& } A$$

are constant and at any instant, neglecting the recovery term:

$$T_g = T_w + B \cdot D^{2-m} \cdot \frac{dT_w}{d\theta} \quad ; \quad B = \text{CONSTANT} \qquad (14)$$

Benson & Brundrett thus maintain that by plotting T_w as a function of $D^{2-m} \cdot \frac{dT_w}{d\theta}$ at each point in time for the 3 wires, a straight line should result with an intercept at Tg (See Fig. 1).

However, attractive as this method might seem, it contains a very serious difficulty: namely that the exponent 'm' is unknown, varying over the temperature cycle. Benson & Brundrett recognise this and state that the exponent 'm' strictly varies with (Re) & (Kn), but D^{2-m} is not sensitive to small changes in 'm' as $m \ll 2$.

In their example they used a constant value of m but did not give its magnitude.

It will be shown in the next section that this is a major discrepancy the effect of which is to render the 3-wire method redundant.

6. DIFFICULTIES IN THE 3-WIRE SOLUTION

6.1 The 3-wire Temperature Function

From (14):

$$T_g = T_w + K D^{2-m} \cdot \frac{dT_w}{d\theta} \qquad (K, T_g \text{ \& } m \text{ unknown})$$

where

$$K = \left(\frac{\lambda}{V}\right)_g^m \cdot \frac{\rho_w C_w}{4 k_g A}$$

A = a constant; and for a beaded thermocouple (not butt welded), the factor in the denominator is not necessarily = 4.0).

Now, following the simplifying notation of C.H.J. Daft (25), 1965 if the 3 wires are designated

	a	b	c
of diameter	$D_a = 1$	$\frac{D_b}{D_a} = d$	$\frac{D_c}{D_a} = D$
of temperatures	$T_a = A$	$T_b = B$	$T_c = C$
& of rates of change	$\frac{dT_a}{d\theta} = X$	$\frac{dT_b}{d\theta} = Y$	$\frac{dT_c}{d\theta} = Z$

then substituting in equation (14) gives:

$$T = A + KX \qquad (15)$$

$$T = B + K d^{2-m} \cdot Y \qquad (16)$$

$$T = C + K D^{2-m} \cdot Z \qquad (17)$$

$$(16) \rightarrow d^{2-m} = \frac{T-B}{KY} \rightarrow (2-m)\log d = \log\left[\frac{(T-B)}{KY}\right] \qquad (18)$$

$$(17) \rightarrow D^{2-m} = \frac{T-C}{KZ} \rightarrow (2-m)\log D = \log\left[\frac{(T-C)}{KZ}\right] \qquad (19)$$

$$\frac{(19)}{(18)} \rightarrow \frac{\log D}{\log d} = \frac{\log\left[\frac{T-C}{KZ}\right]}{\log\left[\frac{T-B}{KY}\right]} \qquad (20)$$

$$(15) \rightarrow K = \frac{T-A}{X} \text{ in (20) :-}$$

$$\frac{\log D}{\log d} = \frac{\log\left[\left(\frac{T-C}{T-A}\right)\cdot\frac{X}{Z}\right]}{\log\left[\left(\frac{T-B}{T-A}\right)\cdot\frac{X}{Y}\right]}$$

$$\therefore \frac{\log D}{\log d} \cdot \log\left[\frac{x}{y}\left(\frac{T-B}{T-A}\right)\right] = \log\left[\frac{x}{z}\cdot\left(\frac{T-C}{T-A}\right)\right] \qquad (21)$$

The following is the author's continuation:

Now if log D/log is written = n

then $\log\left[\frac{x}{y}\left(\frac{T-B}{T-A}\right)\right]^n = \log\left[\frac{x}{z}\cdot\left(\frac{T-C}{T-A}\right)\right]$

$$\therefore \frac{x}{z}\left(\frac{T-C}{T-A}\right) = \left[\frac{x}{y}\left(\frac{T-B}{T-A}\right)\right]^n \qquad (22)$$

& the RHS of (22) can be written as

$$\left(\frac{T-B}{T-A}\right)^n = \left[1+\left(\frac{A-B}{T-A}\right)\right]^n \qquad (23)$$

Now ignoring the trivial solution T = A, & cross multiplying (22)

$$(T-A)^{n-1} = \left[\frac{x}{y}\cdot(T-B)\right]^n \cdot \frac{z}{x}\cdot\left(\frac{1}{T-C}\right)$$

$$\therefore \left(\frac{T-A}{x}\right)^{n-1} = \left(\frac{T-B}{y}\right)^n \cdot \left(\frac{z}{T-C}\right)$$

thus, the 3-wire temperature function is defined according to

to the above terminology as

$$F(T) = \left(\frac{T-A}{x}\right)^{n-1} - \left(\frac{T-B}{y}\right)^n \cdot \left(\frac{z}{T-C}\right) = 0 \qquad (24)$$

The numerical solution of this function was attempted by various methods as follows:

6.2 Newton's Iteration

i.e. $T_{n+1} = T_n - \frac{F(T)}{F'(T)}$

& from (24) $F'(T) = \frac{n-1}{x^{n-1}}\cdot(T-A)^{n-2} - \frac{z}{y^n}\frac{(T-B)^{n-1}}{(T-C)}\cdot\left\{n-\left(\frac{T-B}{T-C}\right)\right\}$

for the first iteration say To = A, as the finest wire will be closest to the true gas temperature

i.e. $F(T_0) = -\frac{(A-B)^n}{Y^n} \cdot \left(\frac{Z}{A-C}\right)$

& $F'(T_0) = \frac{-Z(A-B)^{n-1}}{Y^n(A-C)} \cdot \left\{n - \left(\frac{A-B}{A-C}\right)\right\}$

& since $T_{n+1} = T_n - \frac{F(T_n)}{F'(T_n)}$

then $T_1 = \left(A^2(n-2) + AC(1-n) + 2AB - BC\right) / \left(n(A-C) - (A-B)\right)$

$\therefore F(T_1) = \ldots$ & $F'(T_1) = \ldots$ $\Big\} \therefore T_2 = T_1 - \frac{F(T_1)}{F'(T_1)}$ .... etc

This procedure was programmed and an iterative solution for T attempted on the CDC6400 computer of the University.

This was unsuccessful, however, due probably to the fundamental ill-conditioned nature of the 3-wire temperature function.

This ill-conditioning can be demonstrated by considering the following example:

From (22) $\frac{X}{Z}\left(\frac{T-C}{T-A}\right) = \left\{\frac{(T-B)}{(T-A)} \cdot \frac{X}{Y}\right\}^n$

in particular, if n = 2 (various actual values used for n were 1.58, 1.67, 2.25 & 3.30).

then: $\left(\frac{T-C}{Z}\right) = \frac{X(T-B)^2}{Y^2(T-A)}$

$\therefore (T-C)(T-A)Y^2 - XZ(T-B)^2 = 0$

$\therefore \underset{a}{(Y^2-XZ)}T^2 - \underset{b}{[(A+C)Y^2 - 2XZB]}T + \underset{c}{[ACY^2 - XZB^2]} = 0$

& $T = \left(-b \pm \sqrt{b^2-4ac}\right)/2a$

In general, terms (a), (b) and (c) will be very small leading to

6.3 The Bolzano Bisection Method

It was suspected that Newton's iteration method could be unreliable with the temperature function being used, so a method which would always converge to the roots of the equation was sought.

In order to choose suitable 'begin' and 'end' points for this iterative routine, an understanding of the relationship between true gas temperature over the cycle and the corresponding temperatures and rates of change of temperature of all three wires was required.

The setting of these limits is shown in a decision chart. (Fig. 2).

These decisions are understood if it is borne in mind that true gas temperature must always be greater in magnitude (±) than the temperature of the finest wire, and must lead this wire temperature in phase angle. Similarly, the other wire temperatures must show an attenuation and phase lag with respect to the finest wire.

The computer subroutine for this method is shown in Fig. (3a), Appendix A 4 . Unfortunately this method was also still unworkable over the whole cycle probably due to a data inconsistency discussed in Section 6.4.

Meanwhile, a further method was developed to solve the 3-wire problem 'direct' from the Fourier coefficients representing each wire temperature cycle.

This method, gave a useful insight into the shortcomings of the 3-wire method as applied to the particular set of data being examined.

6.4 Calculation Direct from Fourier Coefficients

Since a computer Fourier analysis was performed on all recorded data (Ref. (9)); it was possible to express the 3-wire equations in terms of the modulus and phase of each term of the Fourier series. The true gas temperature was then found by the least squares solution of two simultaneous equations.

From 6.1 $T = A + KX$ (15)

$T = B + Kd^{2-m}Y$ (16)

$T = C + KD^{2-m}Z$ (17)

Now by definition:

$$\left.\begin{aligned} T = A \text{ at wt} = \alpha \\ T = B \text{ at wt} = \beta \\ T = C \text{ at wt} = \gamma \end{aligned}\right\} \quad -(25)$$

where A, B & C are moduli α, β, γ are phase angles of a given component of the Fourier series for each wire in order of ascending diameter.

Let $T = P \cos wt + Q \sin wt$ (26)

where T = true gas temperature at any time in the cycle.

then

$$\left.\begin{aligned} A &= P\cos\alpha + Q\sin\alpha \\ B &= P\cos\beta + Q\sin\beta \\ C &= P\cos\gamma + Q\sin\gamma \end{aligned}\right\} \quad - (27)$$

Now let :

$$\left.\begin{aligned}(P\cos\alpha + Q\sin\alpha - A)^2 &= R_A^2\\ (P\cos\beta + Q\sin\beta - B)^2 &= R_B^2\\ (P\cos\gamma + Q\sin\gamma - C)^2 &= R_C^2\end{aligned}\right\} \qquad (28)$$

The conditions for a least squares solution are:

$$\left.\begin{aligned}&(a)\ \partial\Sigma R^2/\partial P = 0\\ \&\ &(b)\ \partial\Sigma R^2/\partial Q = 0\end{aligned}\right\} \qquad (29)$$

and this requires that both

$$\left.\begin{aligned}&P\cos^2\alpha + Q\sin\alpha.\cos\alpha - A\cos\alpha\\ &+P\cos^2\beta + Q\sin\beta\cos\beta - B\cos\beta\\ &+P\cos^2\gamma + Q\sin\gamma\cos\gamma - C\cos\gamma\end{aligned}\right) = 0 \qquad (30)$$

&

$$\left.\begin{aligned}&P\cos\alpha\sin\alpha + Q\sin^2\alpha - A\sin\alpha\\ &+P\cos\beta\sin\beta + Q\sin^2\beta - B\sin\beta\\ &+P\cos\gamma\sin\gamma + Q\sin^2\gamma - C\sin\gamma\end{aligned}\right) = 0 \qquad (31)$$

i.e. (30) and (31) have two unknowns, P & Q, for which they can be solved and then the true gas temperature is given by:

$$T = P\cos wt + Q\sin wt \qquad (32)$$

At any crank angle $\theta = wt$ in the cycle.

From this derivation it transpires that the only criterion for a solution is that A, B & C and α, β & γ should be in the logical order according to the respective wire diameters. For corresponding harmonic components of the temperature cycles, when progressing from the finest to the thickest wire, the

Moduli and phase angles should be decreasing and increasing respectively with respect to those of the finest wire.

This procedure was programmed in the sub-routine given in Fig. (3b) Appendix A4. Using this it was observed from the temperature records of the 3-wires under motoring conditions (Figs.4) that this criteria was not always satisfied for all harmonics. However, it will now be shown that the 3-wire method as solved by previous investigators (20), (10), (26), is not advantageous over the network compensation method.

7. THE NETWORK COMPENSATION METHOD

7.1 General

If in equation (14) a constant exponent is used, then we have

$$Tg = Tw + B^1 . \, dTw/d\theta \qquad (33)$$

where B^1 is a constant for each wire, and it can be shown that

$$B^1 = \tau = (\rho c D/4h)_w$$

and (33) becomes identical to (2) in Section 1.

i.e. $$Tg = Tw + \tau . dTw/d\theta$$

In this case, if τ is known, the necessary correction to recorded wire temperature can be conveniently provided by an electrical network.

In general, a thermocouple junction has a transfer function corresponding to that of a simple time-lag network. i.e. the voltage output of the thermocouple is attenuated from and lags behind the gas temperature input. This can also be seen from the frequency response curve (magnitude ratio MR) of a thermocouple (Fig. 5) which shows that above the cut off frequency of the thermocouple ($fc = 1/2\pi\tau$), higher frequency components are attenuated. A phase plot will similarly show increased phase lag of components above this frequency.

If, however, the voltage output of the thermocouple is modified by an electrical network having exactly the inverse transfer function of the thermocouple, then the resulting combined response is constant to a much higher frequency. (Fig.5).

This improved response is gained at the expense of an overall attenuation and the output signal level is reduced by the same factor (r) which extends the cut-off frequency.

This is the only limit to the extent of compensation requiring high gain-low noise preamplifiers in this application.

Thus the compensator can be thought of as a low frequency attenuator achieving an improvement in the response bandwidth by electrically solving equation (20). It provides a signal output proportional to the gas temperature by adding a correcting signal proportional to the rate of change of wire temperature to an input signal which is proportional to wire temperature (27).

Completeness of compensation of dynamic temperature measurements by this method depends on the assumption that thermocouple time constant is known and constant over the cycle.

It is doubtful whether this is so in this investigation due to variation in heat transfer coefficient from the gas to the wire, as the velocity varies over the cycle.

Thus the same problem arises which restricted the 3-wire method (Section 6).

However, in a recent reference, Simbirskiy (28) 1965, reports that 'τ' can be assumed constant over the cycle since it becomes independent of the heat transfer coefficient when the gas velocity is

high. According to his experiments, this condition is fulfilled over an engine cycle.

This latter observation is also verified by the cyclic velocity calculations of Knight (29) 1965, for the main chamber of a modern high-speed diesel engine.

Although an energy balance for a petrol engine would not include the injection velocity term, a similar gas velocity history to that shown by Knight could be expected. This has been reproduced in Fig. 6, from which it can be seen that gas velocities remain high (typically 400 ft/sec) for the majority of the cycle.

Following this observation, experimental values of 'τ' as a function of gas velocity (air) for a 0.001" ϕ thermocouple are given by Carbon et al (30) 1950. This shows that τ does in fact remain sensibly constant for velocities in excess of approximately 100 ft/sec for wires of this size.

Hence, based on Knight's calculations, the possibility of mismatch between the corrector and thermocouple is likely only for some 10^{o} crank angle quite early in the expansion stroke. Since final graphical results for all measured data were to be plotted at 20^{o} intervals, the error effects of mismatch were considered to be insignificant.

It is thus submitted here that the error involved in using electrical compensation with constant is no greater than that of the 3-wire method with constant m. Further, it is a simple technique to use and the processing and analysing of the gas temperature cycles is convenient as they are already in corrected form.

This gives the method a definite advantage over the complex numerical correction required for the 3-wire method.

The network approach was pursued in the following steps.

7.2 Analog Simulation

Using the Departmental Analog Computer (Heathkit ES200), a network was set up to simulate a thermocouple responding to a simulated "true gas temperature" input signal. (Fig.7).

The frequency of this ramp function input could be varied to cover the working range of the fundamental engine thermal cycle (4-20 cps).

Following the simulated thermocouple, a corrector network with a transfer function approximately inverse to that of the thermocouple was patched in.

The resulting corrected output signal was then compared on a dual beam oscilloscope with the simulated gas and simulated thermocouple signals over the frequency range. It was observed that with a thermocouple time constant of 10 msec, a correction to 1 msec was sufficient to get very close agreement with the input (Fig.7)

7.3 Active Corrector Network

At this stage a discrete electrical compensation network was built and tested on the analog computer. This was built as an "active" network i.e. making use of an operational amplifier as did the computer. However for economy and for 12 volt operation, an Operational/Differential chip amplifier was used (see Fig.8).

This circuit was also designed for an effective time constant of 1 msec assuming a 10 msec thermocouple, see time constant determination, Section 8.

This network compared very well (to 1/2 msec) with the analog computer correction using the same input. However, the output signal was considerably affected by 50 cps pickup from the computer power supply. This susceptibility to noise was further noticed during the shock-tube step-response tests (Fig. 13), and necessitated extensive modification to the basic corrector circuit (Fig. 8).

A special low-noise single ended thermocouple pre-amplifier was thus developed for the shock tube and engine tests and this is shown in Fig. .

As the same power supply was used for both the pre-amplifier and the corrector, further isolation was provided for the corrector by means of an FET input stage (see Fig. 9).

Motoring and firing runs were conducted on the engine using a 0.001" diameter thermocouple of approximately 10 msec time constant with a 10:1 correction factor.

The oscilloscope traces (Figs. 19-21) show considerable improvement in response for both motored and fired runs. However, this system was not entirely satisfactory for the following reasons:

1. The overall gain of the Pre-amplifier/Compensator network was not accurately known under engine conditions. The individual gains had been approximately determined for the Shock Tube case by separate tests. Since the gain of this type of active network is level-dependent due to feedback, an absolute calibration could not be made for the corrected engine temperature records.
2. The output signal from the corrector network was not compatible with the input requirement of the data acquisition system (9)

due to earth looping, and no satisfactory solution to this problem was found.

3. Despite extensive additions to the basic circuit to prevent interference, the corrector circuit remained highly susceptible to external electrical noise, especially that generated by the engine auxiliary DC motor drive and the temporary DC rectified power supply being used at that time.

4. The thermocouple pre-amplifier remained stable only for short periods of time under engine firing conditions, and frequent adjustment of the balancing potentiometers (Fig. 9) was required.

7.4 Passive Corrector Network

The active network was discarded for the foregoing reasons when it was realised that a simple passive network could be designed to perform the same corrective function.

Consider the circuit

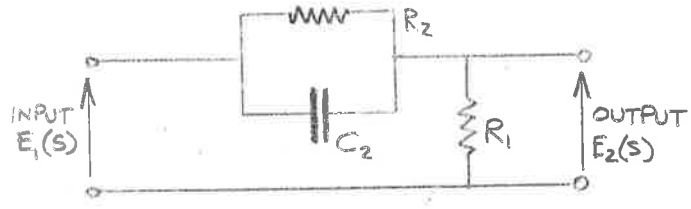

This circuit has a transfer function of the form $K\left(\frac{S+100}{S+1000}\right)$ with $K = 1$

i.e. $$\frac{E_2(S)}{E_1} = \frac{R_1}{R_1 + \frac{R_2}{1+R_2C_2S}}$$

$$= \frac{R_1(1+R_2C_2S)}{R_1(1+R_2C_2S)+R_2}$$

$$\therefore \frac{E_2(s)}{E_1} = \frac{R_1(1+R_2C_2s)}{(R_1+R_2)+R_1R_2C_2s}$$

$$= \frac{R_1\left(s+\frac{1}{R_2C_2}\right)}{s+\frac{R_1+R_2}{R_1}\left(\frac{1}{R_2C_2}\right)}$$

& if $R_2C_2 = 0.010$

$$\frac{E_2}{E_1} = \frac{s+100}{s+100F}$$

where $F = 1+(R_2/R_1)$

F is the factor by which the cut-off frequency of the thermocouple is effectively increased and the effective (corrected) time constant is equal to τ/F

if $R_2/R_1 = 9$, $F = 10$

then $\frac{E_2}{E} = \frac{S+100}{S+1000}$

e.g. A possible circuit is

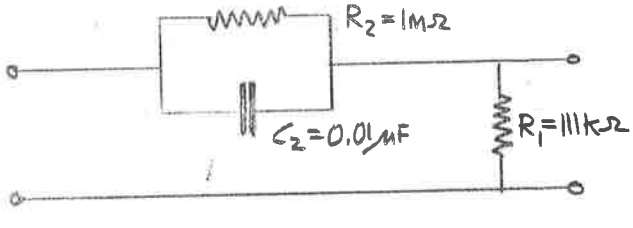

$\tau = R_2 C_2 = 0.010$ sec

& if $R_2/R_1 = 9$

$\therefore R_1 = \frac{R_2}{9} = \frac{1000}{9} = \underline{111\ K\Omega}$

This circuit can be magnitude scaled to give reasonable values for R & C.

The final form of the passive corrector used was

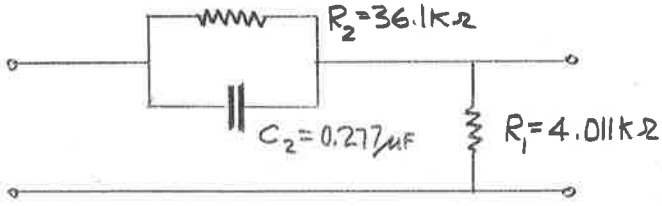

Note that R_1 should be adjusted to include the parallel input impedance of the device into which the corrector feeds its output signal e.g. C.R.O., Pre-amplifier, etc.

8. THERMOCOUPLE RESPONSE CALIBRATION

8.1 General

In order to correct the recorded wire temperature variations, a measurement of the thermocouple time constant under representative flow conditions must be made.

The Single-Shot Shock Tube facility available in this Department proved to be quite suitable for this purpose although other methods are given in (28), (30) & (31).

In the shock tube, (shown in Fig.10), still air at room temperature is suddenly heated by the passage of a shock wave caused by bursting a diaphragm under pressure.

A piezoelectric pressure transducer* was inserted in the wall of the test section adjacent to and upstream of the thermocouple under test. (Fig. 10). The rapid pressure rise due to the passage of the shock-front was used to trigger a dual-beam oscilloscope; the thermocouple response to the step temperature rise being recorded on the second beam. (See Figs.11-17).

The time difference between the initial points of the two traces gave a measure of the shock velocity between the two transducers.

It was found during early experimentation that the thermocouple had insufficient time to reach equilibrium due to temperature disturbances caused by reflected rarefaction waves from the open and closed ends of the tube.

* S.L.M. miniature ceramic-capacitive type.

These effects were successfully postponed until after the thermocouple had reached equilibrium by the addition of new tube sections to both ends. (See Fig10).

From the recorded response of the thermocouple, the time constant could be determined by the following methods:

1. From the temperature trace (Fig.11), the initial rate of rise of wire temperature could be measured.

   Then, by definition $\tau = \Delta T/(dT/dt)$

   where ΔT = step change in temperature due passage of shock,

   dT/dt = rate of rise of temp. (F^o/msec).

   ΔT was calculated from shock-tube data as shown in Section 8.1.

ie. τ can be estimated by the time taken for the wire to reach 63.2% of its final steady value.

2. τ can be found from the empirical formulae of Moffat (32), 1958.

$$\tau_o = \frac{3.5\times10^3 \rho_w C_w d^{1.25}}{T} \cdot G^{-15.8/\sqrt{T}} \qquad (34)$$

& for Chromel-Alumel using average values from Ref. (33)

$\rho_w = 540$ lb/ft^3, $C_w = 0.116$ BTU/lb°F

$$\tau_o = \frac{2.19\times10^5 d^{1.25}}{T} \cdot G^{-15.8/\sqrt{T}} \qquad (35)$$

where τ = sec.

G = mass veloc (lb/sec/ft^2)

T = total temperature (^{o}R)

d = wire diameter (ft.)

and correcting for bead-size effects

$$\left(\frac{\tau}{\tau_0}\right) = \left(\frac{D}{d}\right)^{0.375}$$

The time constant thus determined was then used to design the Corrector Network as described in Section 7.4.

8.1.1 Original Shock-Tube configuration

From Fig. (11) for the original shock tube, it can be seen that at only 4 msec after arrival of the shock front, a pressure drop occurs due to the reflected rarefaction wave from the open end of the tube.

This in turn causes a temperature drop long before the thermocouple reaches equilibrium. A further pressure drop occurs at 12 msec due to the reflected wave from the closed end.

At 10 msec a large scale disturbance to the temperature record is apparent. Although this effect was not studied in detail, it was quite repeatable and is thought to be a characteristic of the shock-tube rather than of the wire.* An explanation could be condensation of water vapour following the re-expansion and the subsequent impinging of droplets on the wire.

Fig. (12) shows the initial response of a 0.001" wire Ø thermocouple in the original shock tube with a 30 psig burst.

Fig. (13) shows the same thermocouple under the same conditions but corrected by the Active corrector network, (Fig. (8) using the special preamplifier in Fig. (9).

The overall system gain, experimentally determined by separate tests for both the preamplifier and the corrector was approximately 2250.

The susceptibility of the active system to noise can be seen in Fig. 13 and this influenced the decision to use the passive network.

* In Fig. (18), Schlieren photographs taken during a later test confirm that rapid flow density changes occur at this time.

8.1.2 Modified Shock Tube.

It was desirable to have a quantitative check on the effectiveness of correction, and hence the shock tube was lengthened to give the thermocouple a longer time at equilibrium conditions.

With new tube sections added to both ends (Fig. 10) about 12 msec was available post-shock during which conditions at the thermocouple were almost constant in time. There was a slow pressure drop during this period of about 0.1 psia/msec (Fig. 14) but this gave a calculated temperature drop of only $1F^{o}$/msec.

Approximately 9 msec after the shock wave passed the thermocouple, the gas temperature began to decrease. It was suspected that this due to the arrival of the "contact surface" moving at a much lower velocity. This was confirmed by the following calculations.

Sample calculations for 30 psig burst pressure

T_{amb} $62^{o}F$, P_{amb} = 30.2" H_g

Shock velocity C_1 = 1/0.7 = 1430 ft/sec (thermocouple 6" from pressure transducer)

Local sonic velocity $a_o = \sqrt{R_o T_o} = 49\sqrt{522}$ = 1110 ft/sec

Local Mach No. $M = C_1/a_o$ = 1430/1110 = 1.29

$(C_1/a_o)^2$ = 1.66

$(P/P_o) = 1/6(7(C_1/a_o)^2 - 1)$ = 1.77

This is < 2, so assume isentropic - Bannister & Mucklow, Ref. (33)

$(T/T_o) = (P/P_o)^{0.286} \doteq (1.77)^{0.286}$ = 1.18

$T = 1.18 \times 522 = 616^{o}R$ $\quad \Delta T = 616 - 522 = 94F^{o}$

Method 1

Initial rate of temperature rise from Fig. (14)

$dT/d\theta$ = 8.38 F^{o}/msec

$\therefore$ Time constant $\tau = \Delta T/(dT/d\theta) = 94/8.38 =$ 11.2 msec

Method 2 - Moffat, Ref. (32)

Mass flow rate $G = \rho_g C_2$ & $\rho_g = 1.325\ P/T$

& P = 1.77 x 14.7 psia

= 26 x 2.036 "Hg

= 53 "Hg

& T = $616^{o}R$

Now particle velocity

$$C_2 = 5a_o\ (P/P_o - 1) / \sqrt{7(P/P_o + 1)}$$

$$= 5 \times 1110 \times 0.77 \times \sqrt{7 \times 11.62}$$

= 474 ft/sec

$\therefore G = \rho_g C_2 = 0.114 \times 474 =$ 54 lb/sec/ft^2

$$\therefore \tau = \frac{219}{562} \cdot \frac{(54)}{616}^{-15.8/\sqrt{616}} = 7.95 \text{ msec}$$

Now allowing for bead size effect if d = 0.001" Ø and D=0.0027" Ø bead (measured) then

$$(\tau/\tau_o) = (D/d)^{0.375} = (2.7)^{0.375} \times 7.95 = 11.5 \text{ msec}$$

The uncorrected wire in Fig. (14) can be directly compared with Fig. (15) to the same scales for the same wire but corrected with a passive compensating circuit assuming 10 msec time constant.

$(dT/d\theta)$ corrected = 71.5 msec

$\therefore \tau_{corrected} = 94/71.5 =$ 1.32 msec

This corresponds to the time constant of a wire of approximately 0.0002" diameter. In both Figs. 14 & 15 the time of arrival of the "Contact Surface" can be found as follows:

Particle velocity C_2 = 474 ft/sec

and the thermocouple station is 6' from the diaphragm.

$\therefore$ Particles arrive 6/474 = 12.7 msec after burst.

Shock front arrives 6/1430 = 4.2 msec after burst.

Thus particles arrive at the thermocouple at approximately 8.5 msec after the shock front passes the thermocouple. This is confirmed by the temperature drop noticed at this time in both Figs. (14) & (15).

Sample calculations for 15 psig burst pressure

Shock velocity measurement C_1 = 1/0.8 = 1250 ft/sec

$\therefore$ $M = C_1/a_o = 1250/1110 = 1.126$

$\therefore$ $(C_1/a_o)^2 = 1.27$

$\therefore$ $(P/P_o) = 1/6\ (7(C_1/a_o)^2 - 1) = 1.32$ (2)

$\therefore$ $(T/T_o) = (P/P_o)^{0.286} = 1.08$

$\therefore$ $T = 1.08 \times 522 = 564^oR$

$\therefore$ $\Delta T = 564 - 522 = 42F^o$

Method 1:

From the uncorrected trace Fig. (16):

$(dT/d\theta') = 3.19F^o/msec$

$\therefore$ $\tau = \Delta T/(dT/d\theta') = 42/3.19 = 13.2$ msec

Method 2:

Particle velocity $C_2 = 5a_o (P/P_o - 1)/\sqrt{7(6(P/P_o) + 1)}$

$= \underline{224 \text{ ft/sec}}$

& density $\rho_g = 1.325P/T$

& $P = 1.32 \times 14.7 = 19.4$ psia

$= 19.4 \times 2.036$

$= \underline{39.4" \text{ Hg}}$

& $T = 564^{\circ}R$

$\therefore \rho_g = 1.325 \times 39.4/564 = \underline{0.0926 \text{ lb/ft}^3}$

$\therefore G = \rho_g C_2 = 0.0926 \times 224 = \underline{20.85 \text{ lb/sec/ft}^2}$

& From Moffat $\tau = \frac{219}{5.62} \frac{(G)}{T}^{-15.8/\sqrt{T}} = \underline{9.14 \text{ msec}}$

& Allowing for bead size effect:

$\tau = 9.14 (2.7)^{0.375} = \underline{13.25 \text{ msec}}$

Again using the 10 msec passive compensator, the corrected thermocouple Fig. (17) can be compared directly with the uncorrected trace Fig. (16).

$(dT/d\theta)$ corrected $= 22.4F^{\circ}/\text{msec}$

$\therefore \tau$ corrected $= \frac{42}{22.4} = \underline{1.88 \text{ msec}}$

Note that in this case, for a 15 psig burst, the indicated thermocouple temperature begins to drop soon after the pressure transducer indicates that a rarefaction wave has passed, i.e. at about 12 msec in Fig. (17), and not <u>before</u> this event as in the 30 psig case. This is due to the fact that with the much slower particle velocity, the contact surface arrives at the thermocouple

at: $\left(\frac{6}{224} - \frac{6}{1250}\right)$ = 22 msec after the shock front passes:

i.e. much later than the reflected wave.

Thus equilibrium of the thermocouple is again terminated by a limitation of the shock tube. Thermocouples much larger in diameter than those presently used would therefore not reach equilibrium.

The time constants of large thermocouples could still be determined using this facility, since from the above calculations it can be seen that it is only necessary to measure the initial rate of rise.

9. EFFECTIVENESS OF CORRECTION

9.1 Shock Tube

Comparative results for 30 psig and 15 psig burst pressures are tabulated in the table below from which a measure of the effect of gas velocity on response time can be ascertained.

Burst Pressure (psig)	30	15
Shock Pressure Ratio	1.77	1.32
ΔT (F^o)	94	42
$dT/d\theta$ (F^o/msec)	8.34	3.19
Shock velocity C_1 (ft/sec)	1430	1250
Particle velocity C_2 (ft/sec)	474	224
Thermocouple τ (msec)	11.2	13.2
Thermocouple + corrector τ (msec)	1.32	1.88
Equilibrium terminated by	Arrival of contact surface	Arrival of reflected rarefaction wave
.....At time after shock passes thermocouple (msec)	8.5	12.0

In view of Knight's calculations indicating gas velocities of the order 400ft/sec, Fig. (6): it was decided to design the passive corrector circuit for 0.001" diameter wire by assuming

a time constant of 10.0 msec and to use this in both the motored and fired engine experiments.

9.2 Motored Engine

The effectiveness of correction in the motored engine case is illustrated by the oscilloscope photograph Fig. (19) which shows (lower trace) an uncorrected thermocouple lagging the CTDC mark by 6 msec or 43^{o} crank angle. When using the preamplifier and active corrector (upper trace) the signal is in phase with the CTDC mark.

The high noise content characteristic of the active network is again evident from Fig. (19). Also, the gain factor is unknown.

The passive corrector gave a similar correction, but without the extraneous noise. A resynthesis of a motored engine cycle from Fourier coefficients of such a corrected thermocouple is shown in Fig. (23).

9.3 Fired Engine

Fig. (20) shows a typical oscilloscope recording of the uncorrected gas temperature from a fired engine compared with the adjacent wall temperature. It can be seen that the peak gas temperature lags even the wall temperature thus indicating the inadequate response of the gas thermocouple.

Fig. (21) shows the same comparison but with the gas thermocouple corrected by the active network. The marked improvement in response is evident. Again however, the gain factor for this system is unknown.

Fig. (22) shows a comparison between gas and wall temperatures, but this time using the passive network for gas thermocouple correction.

The similarity in form of this gas temperature cycle and that from the active network is apparent. In this case, however, the gain is known, and the trace can be calibrated.

i.e. ΔT peak-peak = 2.20 x 1000/22.4 $\frac{\mu V}{\mu V/^{o}F}$

= $\underline{1790F^{o}}$

Fig. (24) shows a resynthesised cycle plot from a Fourier analysis of passively corrected gas temperature data.

The direct influence of valve timing on the gas temperature cycle is also apparent from Fig. (24), and a comparison with values calculated at several state points from a thermodynamic (Hottel chart) analysis gives further confidence that the corrected thermocouple at least gives a fair approximation to instantaneous gas temperatures over the cycle.

10. JUNCTION WELDING

The most satisfactory type of thermocouple wire for use in the combustion chamber was found to be of the "thermocoax" type.

The two fine thermoelements (0.001" Ø wires of Chromel and of Alumel) are insulated by magnesium oxide from their stainless-steel sheathing which itself is only 0.010" Ø. (Fig 25) .

In earlier work with much larger gauge thermocoax (0.008" Ø wire), junctions were simply flame welded. However, with the use of the finer wires, this method was discontinued due to the likelihood of impurity inclusion and a desire for the smallest possible junction.

Thus an arc-welding technique using an inert gas atmosphere was devised following the principles of Stover (36) and of Gelb etal (37).

Figures (26 & 27) show the thermocouple welder. A hard carbon electrode is enclosed in a T-shaped glass working section and the stripped thermocoax is entered opposite this and moved slowly toward the electrode where a spark discharge forms the bead.

The thermocouple leads are maintained at a positive potential with respect to the electrode by means of a rectified AC power supply, the output voltage of which can be varied by means of a voltage dividing potentiometer.

The energy of the spark discharge is controlled by selecting any combination of capacitance from a bank of capacitors of varying size.

Optimum voltage and capacitor settings were found for various material and wire-gauge combinations and impurity-free junctions of minimum size could be consistently produced.

Prior to welding, the wires were cleaned in a solution of 16 parts Nitric acid, 16 parts water and 3 parts Hydrofluoric acid; this left the chromel wire bright and the alumel wire slightly dull. (Hunt (17)).

To prevent oxidation of the junction, an inert gas (Argon) was introduced into one arm of the glass working section of the welder.

11. CONCLUSIONS

This report has dealt with a number of alternative means of gas temperature measurement and correction techniques. The main conclusions can be summarised as follows:-

1. Instantaneous temperature at a point in a combustion chamber is apparently best measured directly by a very fine, fast response thermocouple.
2. The principal error involved is that due to the thermal inertia of the element itself.
3. The time constant of the element can be repeatedly and conveniently determined by Shock-Tube tests.
4. Most multiwire correction methods are unsatisfactory, requiring either complex numerical methods of solution or tedious graphical techniques.

   The 3-wire method in particular seems to have been solved only by making a basic assumption which renders the result no better than that from a simple passive compensating network.
5. This simple electrical method can effectively reduce the time constant of a given thermocouple by any required factor - within the limits of satisfactory amplification - giving a response time equivalent to that of a much finer wire.
6. The accuracy of this method depends on how closely the time constant of the thermocouple at any instant "matches" that for which the compensating network has been designed.

7. The effect of "mismatch" between the thermocouple and corrector is found to depend principally on gas-wire heat transfer which is some function of gas velocity. If velocity is high (above 200 ft/sec) then the gas-wire heat transfer coefficient approaches a constant value and the time constant tends to become independent of gas velocity.

8. From the technical literature, combustion chamber gas velocities in an engine are likely to be predominantly high over the cycle ($>$ 200 ft/sec). Thus, it may be expected that any mismatch effects will be slight.

9. By applying compensation to the output of a comparatively robust thermocouple, it is possible to simulate the behaviour of an extremely fine wire without the use of such a fragile element itself.

10. The correction technique is thought to be a useful approximation in experimentally measuring local instantaneous gas temperatures at a point in the combustion chamber of an I.C. Engine.

REFERENCES

(1) OVERBYE, V.D., BENNETHUM, J.E., UYEHARA, O.A. and MYERS, P.S.; "Unsteady heat transfer in engines"; SAE.TRANS. 1961, 69, p 461.

(2) ANNAND, W.J.D. "Heat Transfer in the cylinders of reciprocating Internal Combustion Engines"; PROC. I. MECH. E., LOND. 1963, 177, 36, p 973.

(3) HENEIN, N.A. & VINCENT, E.T.; "Thermal Loading and Wall Temperature as functions of performance of Turbocharged Compression Ignition engines" SAE.TRANS., 1959, 67, p 478.

(4) EICHELBERG, G.; "Temperaturverlauf und Warmespannung in Verbrennungs motoren"; FORSCH.ING.WES, 1923, No 263.

(5) ELSER, K.; "Der instationare Warmeuber gang in Dieselmotoren"; MITT.INST. THERMODYN-ZURUCH 1954 No 15.

(6) MILLAR, G.H., UYEHARA, O.A. & MYERS, P.S.; "Practical Application of Engine Flame temperature Measurements"; PAPER 196, SAE NATIONAL FUELS & LUBRICANTS MEETING, CHICAGO 1953.

(7) KOBAYASHI, A.; "Measurement of Fluctuating Temperature of Working Gas in Internal Combustion Engines" TRANS. J.S.M.E. V3, No 11, May, 1937 (in Japanese).

(8) COORDINATING RESEARCH COUNCIL INC.; "Development of Techniques for measuring Gas temperatures in Internal Combustion Engines - Final Summary Report" - CRC 347 - CRC Project No CM-1-58, March, 1960, N.Y.

(9) HALE, M.R. and MORGAN, G.A. "MOVADAS Data Acquisition System" UNIVERSITY OF ADELAIDE, MECH. ENG. DEPT. REPORT R66/2, November, 1966.

(10) BENSON, R.S. and BRUNDRETT, G.W.; "Development of a resistance wire Thermometer for measuring Transient Temperatures in Exhaust systems of I.C. Engines"; TEMPERATURE-MEAST. & CONTROL IN SCIENCE & INDUSTRY, V3, Part 2, 1962 p 631.

(11) DONKIN, B.; PROC. INST. CIVIL ENGRS. 115, Part 1, 1893 - 1894.

(12) COKER, E.G. & SCOBLE, W.A.; "Cyclic Changes of Temperature in a Gas Engine Cylinder"; PROC. INST. CIVIL ENGRS., 196, Part 2, 1913 - 1914.

(13) PETERSEN, A.; MITT. FORSCH. 143, 1913.

(14) HALL J.S.; "The Use of Fibro-Platinum in Thermocouple elements"; ENGLEHARD INDS. TECH. BULL. 2, 85, 1961.

(15) MEYER, W.E. & De CAROLIS, J.J.; "Compression Temperatures in Diesel Engines under starting conditions". SAE TRANS, 1962 V70, pp163-174

(16) AFTALION, S.; "The Determination of Rapidly Changing Exhaust-Gas temperatures in Internal Combustion engines"; SULZER TECH. REV. 2/1958 pp 67 - 74.

(17) HUNT, M.H.; "Design and Use of Fine Wire Thermocouples for Research"; U.S. NAVORD REPORT 5828, NAVAL ORDNANCE TEST STATION TP1919, 1959.

(18) SPANGENBERG, W.G.; "Heat Loss characteristics of Hot Wire Anemometers at various densities in Transonic and Supersonic Flow"; U.S. NACA TECH. NOTE 3381, 1955.

(19) KUDRYAVSTEV Y.V. etal; "Unsteady-State Heat Transfer" (RUSSIAN TRANSL.) ILLIFE, LOND., 1966.

(20) BENSON, R.S.; "Measurement of Transient Exhaust Temperatures in IC Engines". THE ENGINEER, Feb. 28, 1964, pp 377 - 383.

(21) SEMENOV, E.S.; "Device for Measuring the Turbulence in Piston Engines"; INSTS & EXPTL. TECHNIQUES. (RUSSIAN) No 1, Jan. - Feb. 1958, pp 102 - 11

(22) FISHENDEN, M. and SAUNDERS, O.A.; "The Errors in Gas Temperature Measurement and their Calculation"; JNL. INST. OF FUEL, March, 1939.

(23) CHISTYAKOV, V.S.; "Methods of Measuring Rapidly varying Temperatures of Gas Streams"; TEPLOFIZIKA VYSOKIKH TEMPERATUR (RUSSIAN TRANSL.) V3, No 6, Nov. - Dec. 1965.

(24) PFRIEM, H.; "Zue Messung Verandelisher Temperaturen von Ogasen und flussigkeiten" FORSCH. GEB. INGEN., 7, 2, 1936.

(25) DAFT, C.H.J.; "Instruments used in the Development of Diesel Engines" I.MECH.E. SYMPOSIUM-ACCURACY OF ELECTRONIC MEASUREMENTS IN I.C. ENGINE DEVELOPMENT - PROC. I. MECH. E. 1965 - 1966 v 180/3G.

(26) SMYTH, R.; "Transient Heat-flow investigations using an on-line Computer" PAPER 16 AUST. INST. NUCL. SCI. & ENG. 3RD FLUID MECH. CONF. 1967.

(27) SHEPARD, C.E., & WARSHAWSKY, I.; "Electrical Techniques for Compensation of Thermal Time Lag of Thermocouples and Resistance Thermometer Elements"; US. NACA. TECH. NOTE 2703, May, 1952.

(28) SIMBIRSKIY, D.F.; "Measurements of Rapidly Changing Temperatures of Gas Flows with the Application of Electronic Correction for the ThermalInertia of the Heat Detector"; IZVESTIA VYSSHIKH UCHEBNYKH ZAVEDENII; PRIBOROSTROENIE: INSTRUMENT BUILDING V8 No 4 1965, pp 141 - 145.

(29) KNIGHT, B.E.; "The problem of Predicting Heat Transfer in diesel engines"; I.MECH.E. SYMPOSIUM "THERMAL LOADING OF DIESEL ENGINES" PROC. I.MECH.E. 1964 - 1965 V179/3C pp 99 - 112.

(30) CARBON, M.W., KUTSCH, H.J. & HAWKINS, G.A.; "The response of Thermocouples to Rapid Gas Temperature Changes" TRANS. ASME, V72, pp 655 - 657, 1950.

(31) SCADRON, M.D. & WARSHAWSKY, I.; "Experimental Determination of Time Constants & (Nu) for bare-wire thermocouples in high velocity air streams ....." U.S. NACA TN 2599, 1952.

(32) MOFFAT, R.J. "Designing Thermocouples for Response Rate" TRANS. ASME Feb. 1958, pp 257 - 262.

(33) BANNISTER & MUCKLOW "Wave action following sudden release of compressed gas from a cyclinder" PROC. IMECH. E. 1948 v 159.

(34) DWYER, M.J. "A Study of Pressure Waves in a pipe with reference to I.C. Engine exhaust silencers." UNIV. OF SOUTHAMPTON ISAV No 114, August, 1964.

(35) STOVER, C.M.; "Method of Butt-Welding Small Thermocouples 0.001 to 0.010" Ø " REV. SCI. INSTS, V31, No 6, June, 1960.

(36) GELB, GH, MARCUS, B.D. & DROPKIN, D; "Manufacture of Fine Wire Thermocouple Probes" REV. SCI. INSTS. V35, No 1, January, 1964.

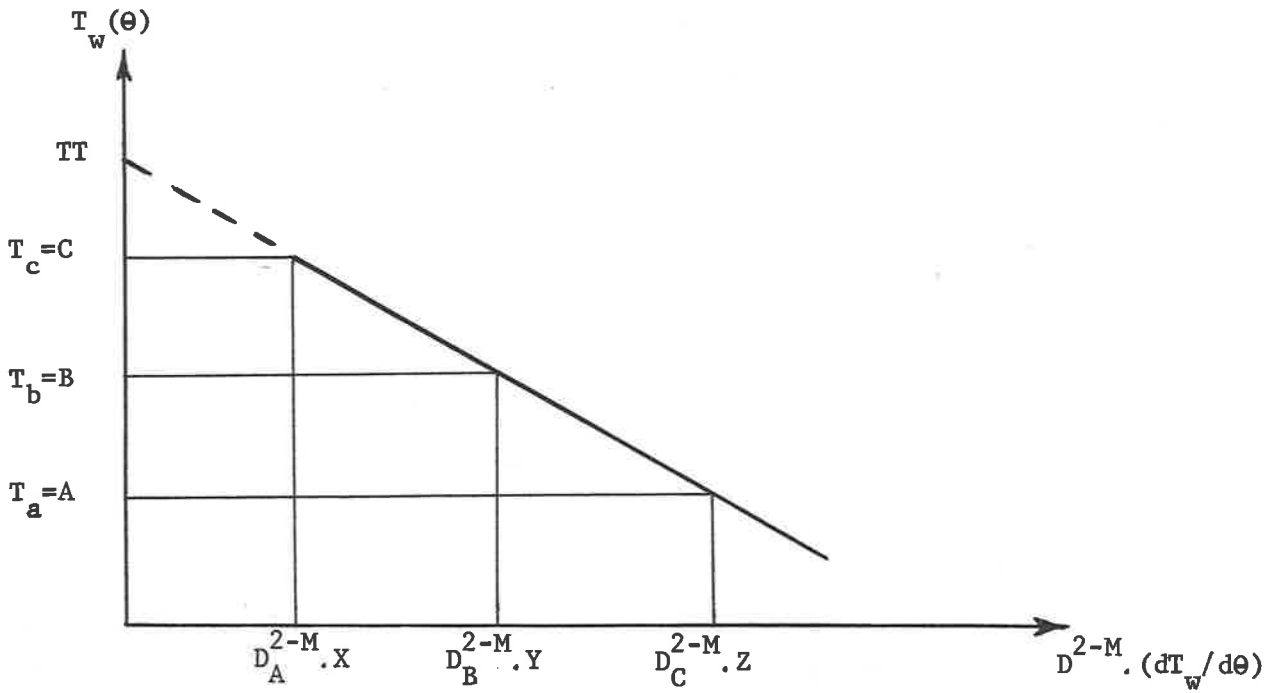

Fig. 1 Benson's 3-wire Extrapolation for True Gas Temperature at any time(θ).

A, B, C Wire temperatures
X, Y, Z Corresponding rates of change of wire temp.

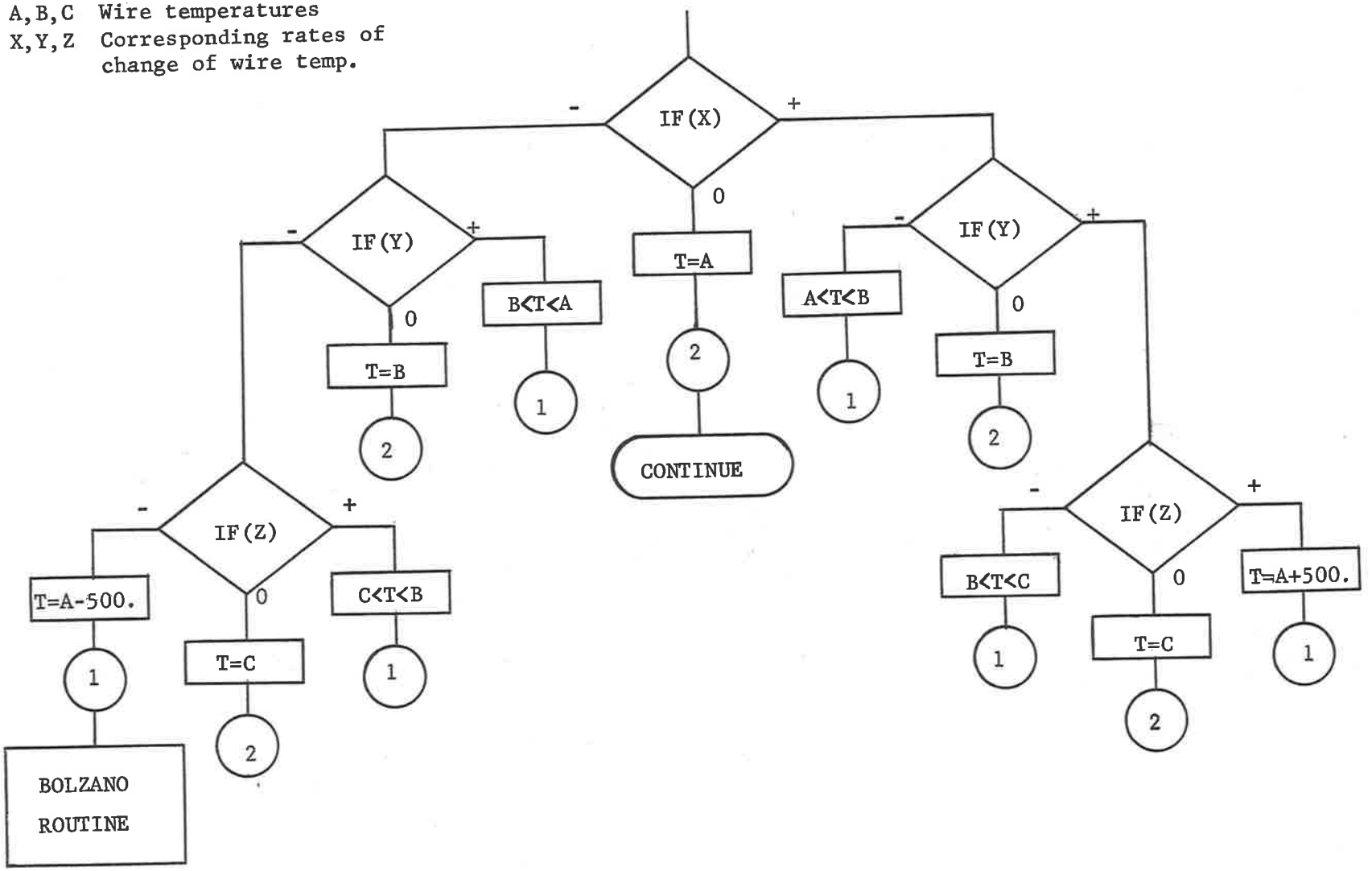

Fig. 2 Decision Chart prior to Bolzano Iteration Routine.

Fig.3(a) & 3(b) See Appendix A4

CONVERT TAPE NO 7
MOTORING 600RPM-P1 INLET 0.150IN A=1.9.B=2.2.C=3.1THOU DIAM
ANALOG TAPE 4 TRANSMITTAL TAPE 1558

SERIAL	RUN	CHANNEL	TYPE	NO PERIODS	COEFF	NO POINTS	INITIAL	MAX PERIODS
4	11	123	1	1	15	712	1	3

FOURIER COEFFICIENTS AT CYCLE FREQUENCY			FOURIER COEFFICIENTS AT CYCLE FREQUENCY			FOURIER COEFFICIENTS AT CYCLE FREQUENCY		
CYCLE HARMONIC	TEMPERATURE (DEG.F)	PHASE ANGLE (CRANK ANG.DEG)	HARMONIC	TEMPERATURE (DEG.F)	PHASE ANGLE (CRANK ANG.DEG)	HARMONIC	TEMPERATURE (DEG.F)	PHASE ANGLE (CRANK ANG.DEG)
1	36.53427	65.29	1	27.20991	73.76	1	26.44498	80.52
2	18.85701	58.56	2	12.44509	69.35	2	12.78323	75.22
3	9.26920	118.25	3	5.45609	121.70	3	6.22448	133.28
4	6.95166	78.46	4	3.80264	85.88	4	3.05124	78.69
5	2.72432	109.73	5	1.70373	129.12	5	1.72461	139.78
6	2.19746	126.90	6	1.22000	148.75	6	.32137	129.96
7	1.89554	127.15	7	.95721	142.17	7	.46316	136.85
8	.56864	94.28	8	.19076	114.05	8	.57754	27.97
9	1.25487	133.45	9	.95594	131.42	9	.49150	136.69
10	.23779	341.02	10	.21480	24.59	10	.86640	336.10
11	.94605	139.11	11	.32727	137.81	11	.51685	200.73
12	.55528	334.24	12	.17553	281.30	12	.91285	328.83
13	.80719	102.97	13	.91714	67.04	13	.76671	123.03
14	.76155	331.96	14	.46529	346.40	14	1.07673	11.35
15	.54539	100.88	15	.61296	98.05	15	.65264	118.92

Fig. 4 Fourier Coefficients for 3-wire data following.

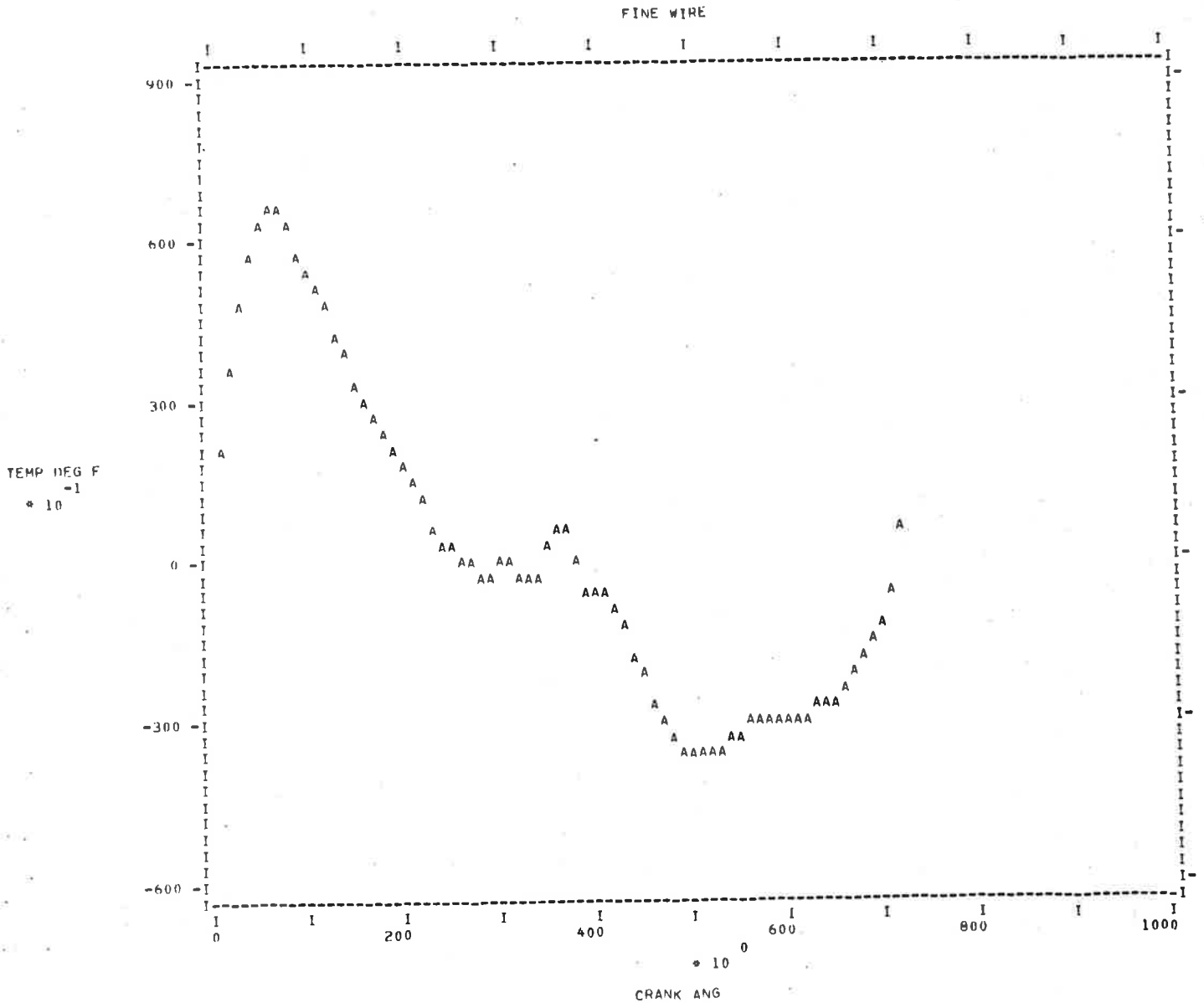
FINE WIRE
900
600
300
0
-300
-600
TEMP DEG F
-1
* 10
0
200
400
600
800
1000
0
* 10
CRANK ANG
YDIV= 3.000000000E+00
XDIV= 1.000000000E+01

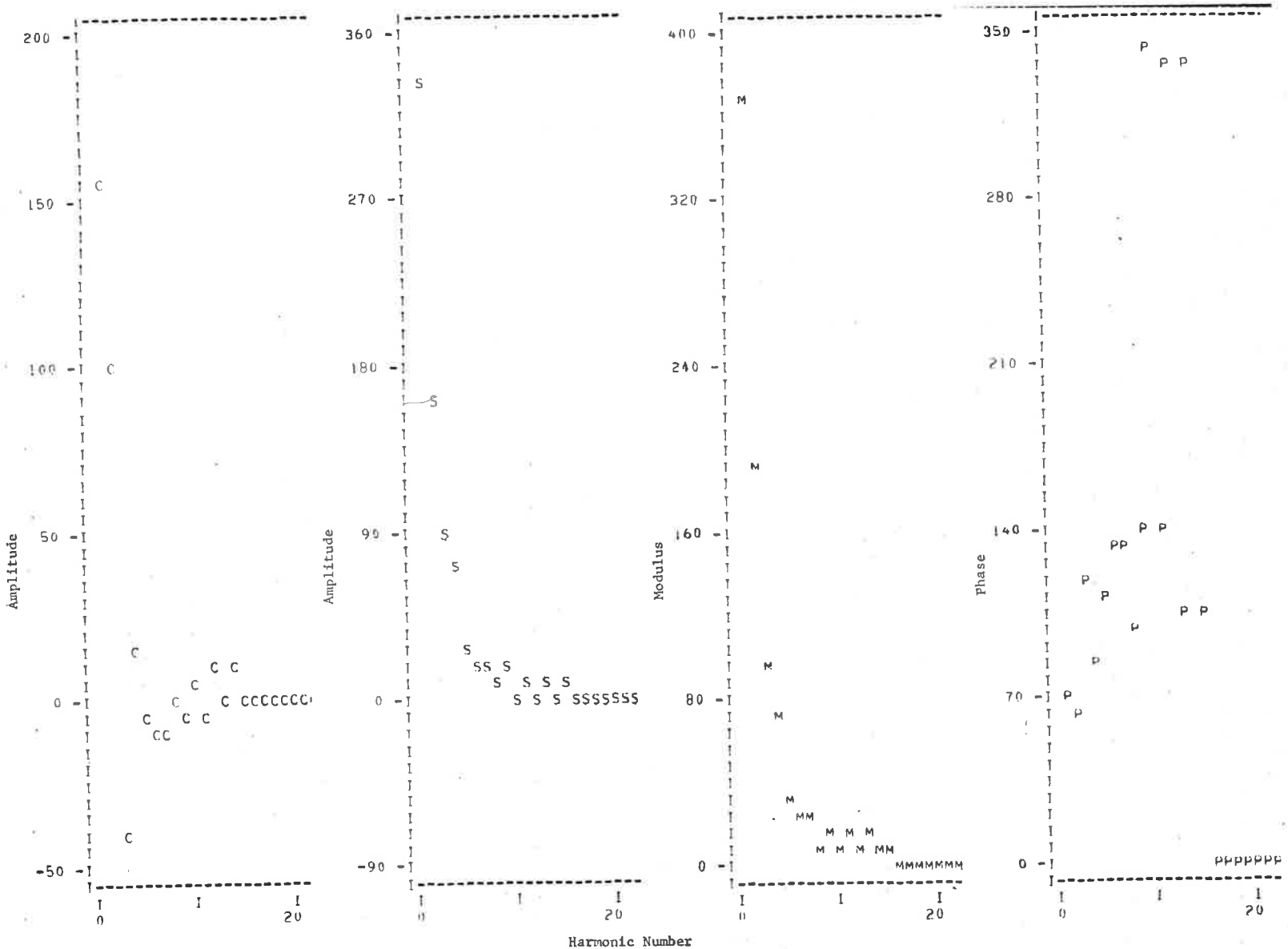

Fig. 4 (contd.) Fourier Spectra - Fine Wire.(A)

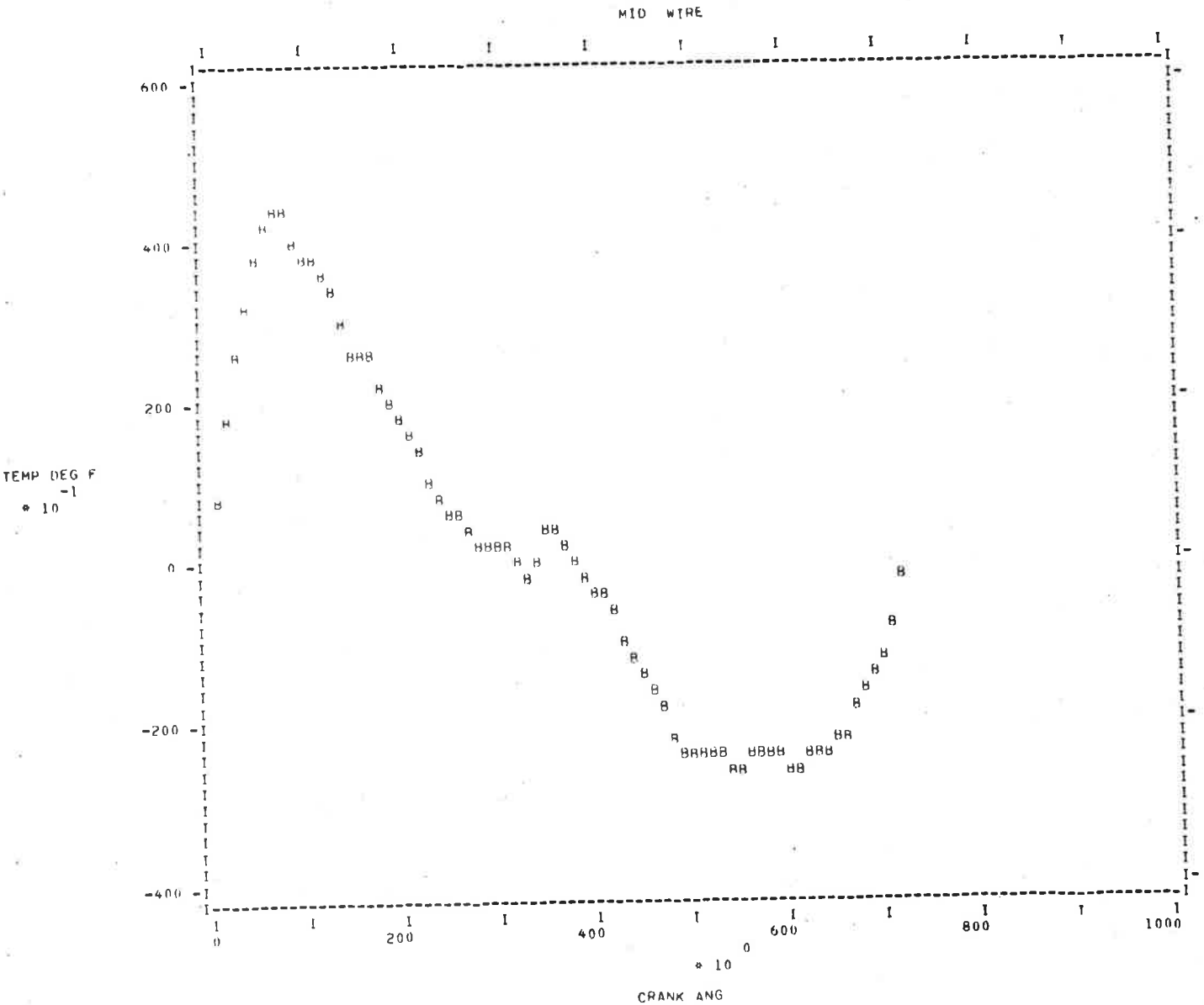
MID WIRE
600
400
200
0
-200
-400
TEMP DEG F
-1
* 10
0
200
400
600
800
1000
0
* 10
CRANK ANG
YDIV= 2.000000000E+00
XDIV= 1.000000000E+01

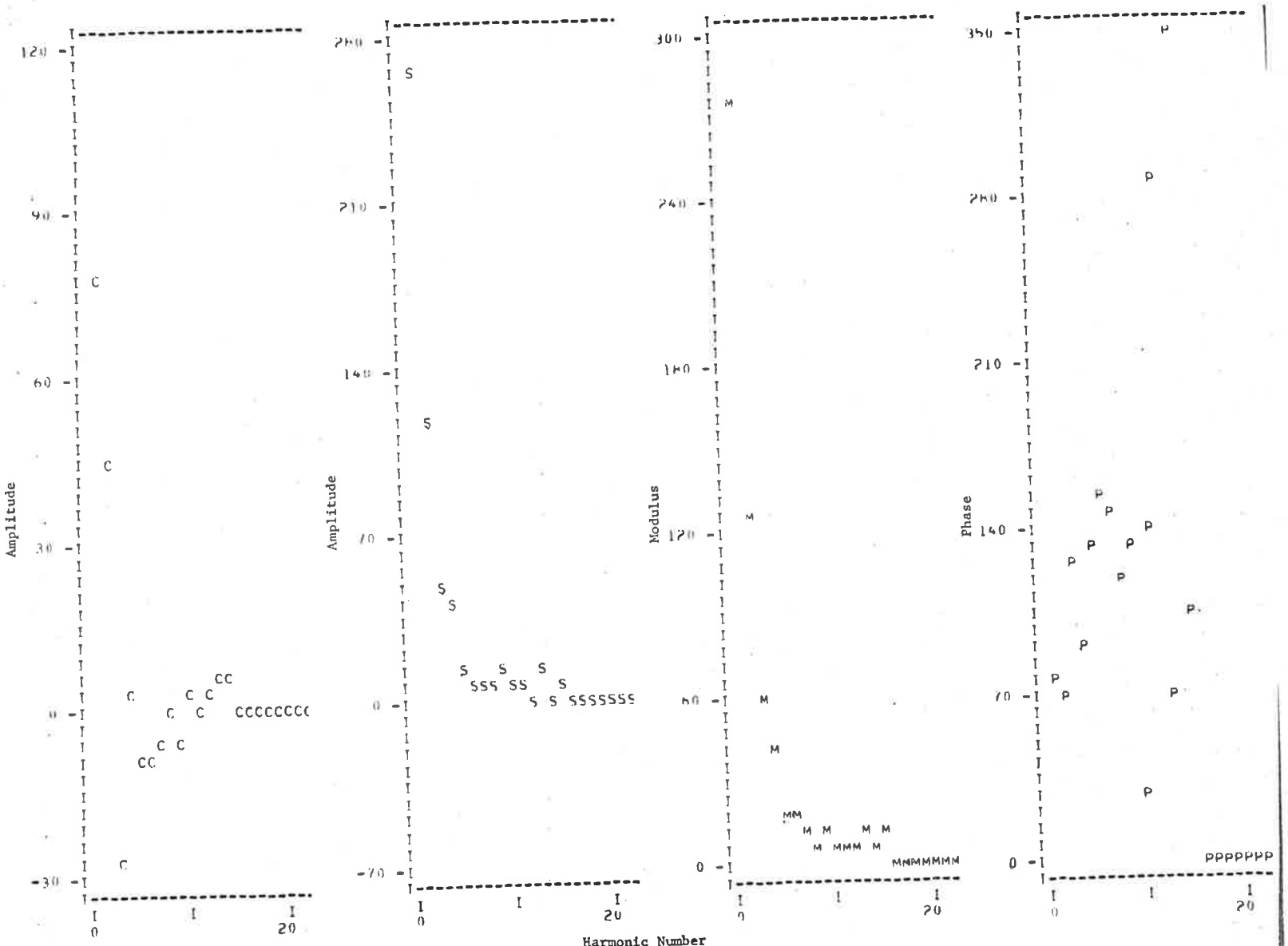

Fig. 4 (contd.) Fourier Spectra - Mid Wire (B).

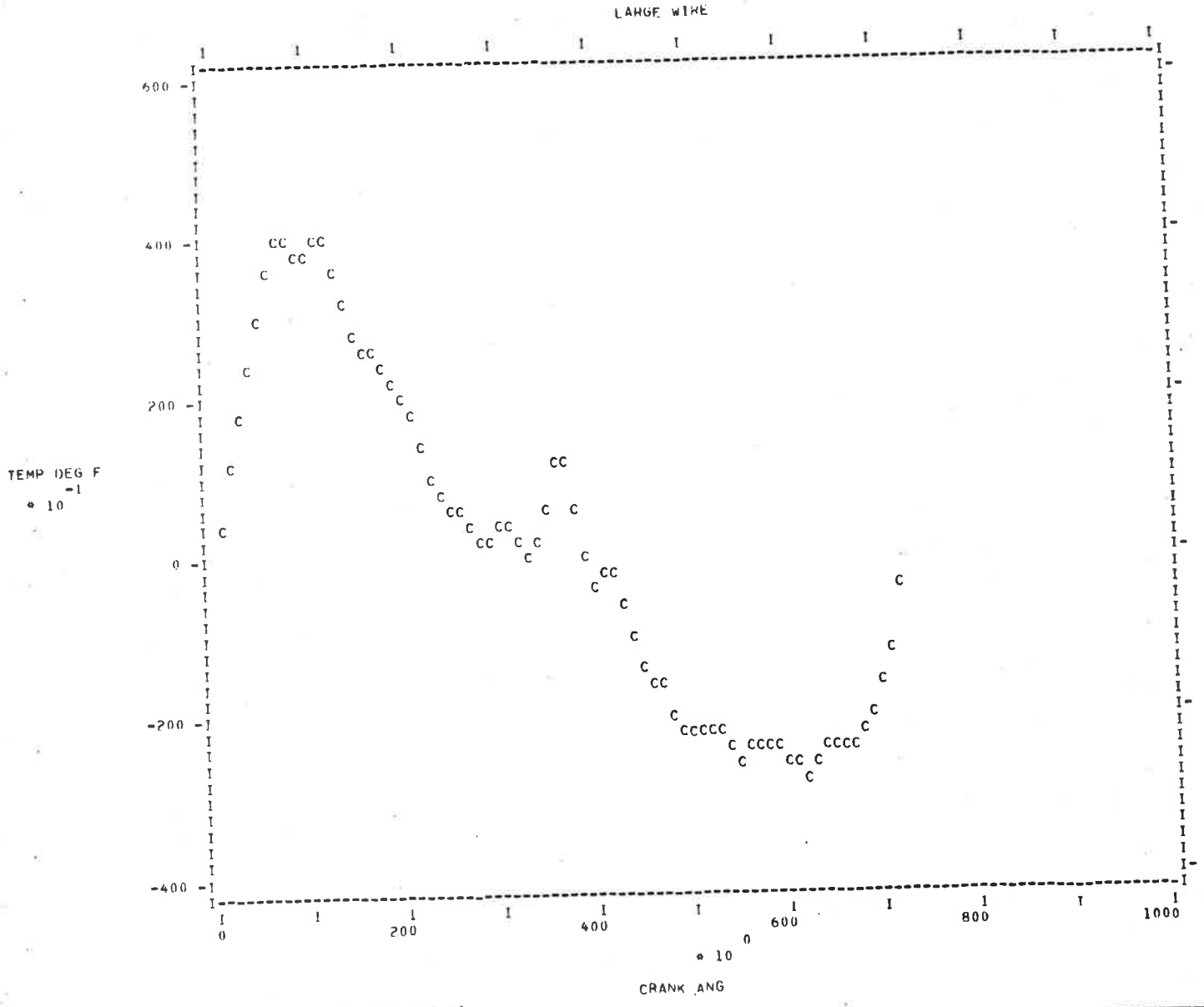
LARGE WIRE
600
400
200
0
-200
-400
TEMP DEG F
-1
* 10
0
200
400
600
800
1000
0
* 10
CRANK ANG
YDIV= 2.000000000E+00
XDIV= 1.000000000E+01

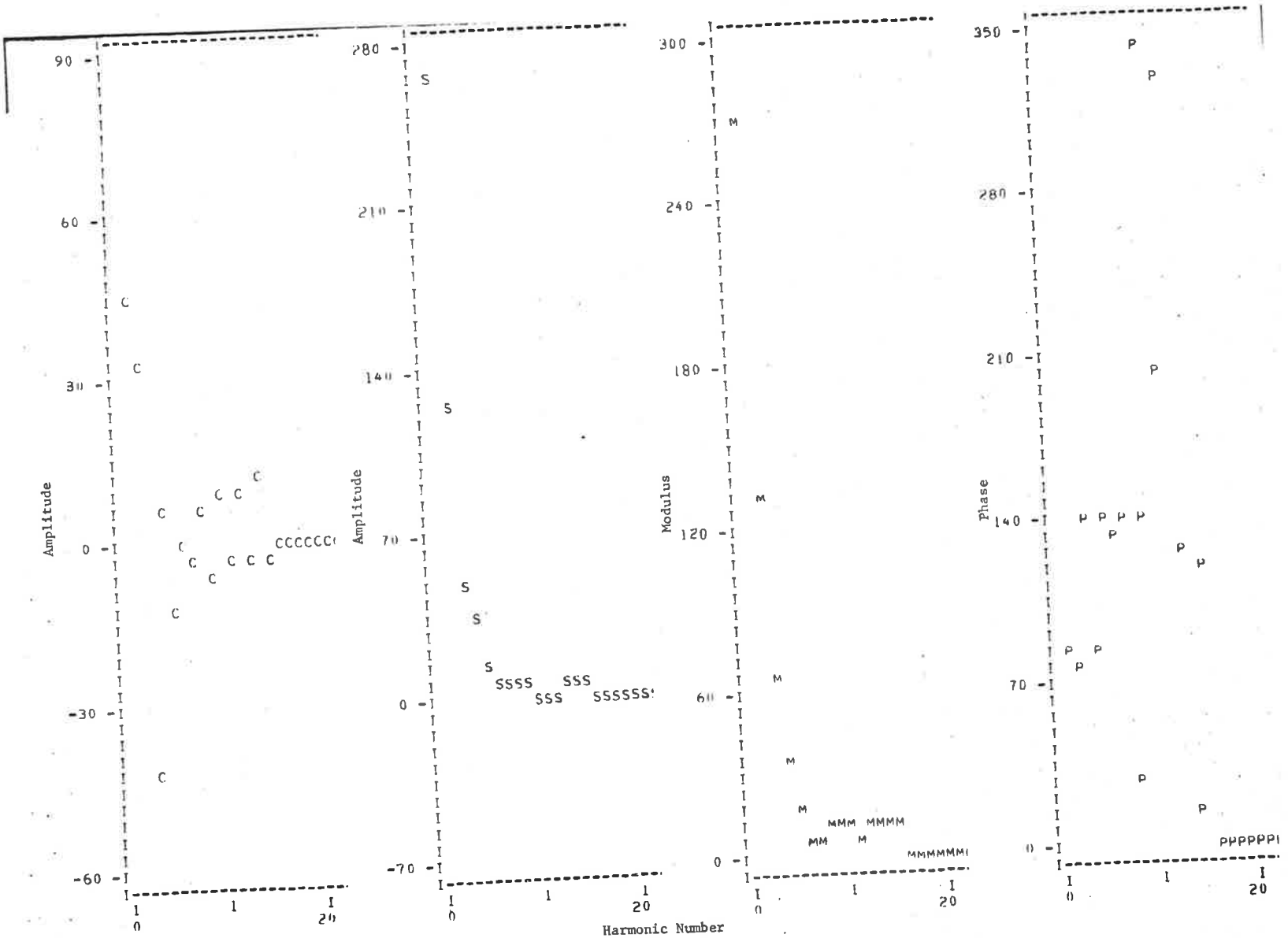

Fig. 4 (contd.) Fourier Spectra - Large Wire (C).

Component	Bode Plot	Transfer Function
(1) Thermocouple 	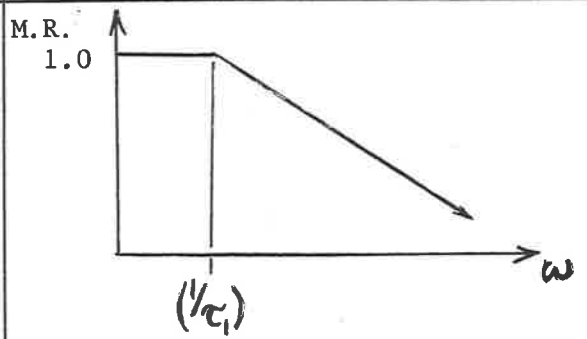	$\frac{1}{1+\tau_1 s}$
(2) Passive Corrector Network 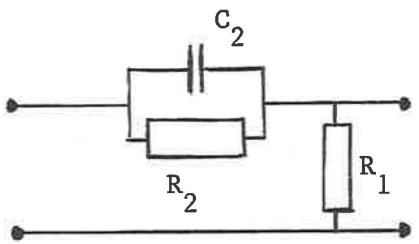	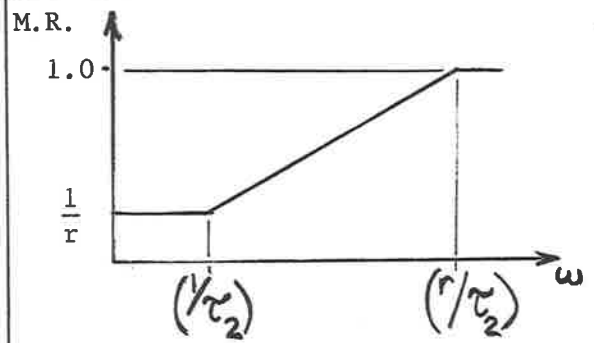	$\frac{1}{r} \cdot \frac{1+\tau_2 s}{1+\left(\frac{\tau_2}{r}\right)s}$ $r = \left(R_2/R_1\right) + 1$ $\tau_2 = R_2 C_2$
(1) & (2) 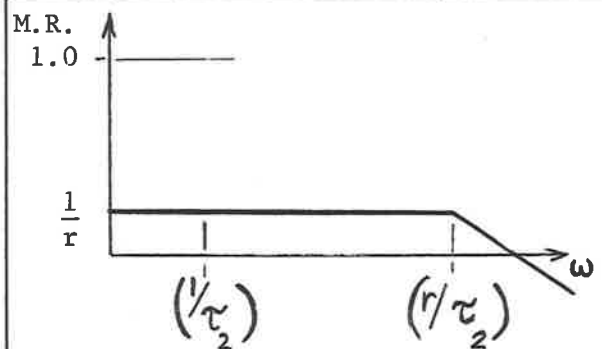		$\frac{1}{r} \cdot \frac{1}{1+\left(\frac{\tau_2}{r}\right)s}$ if $\tau_2 = \tau_1$

Fig. 5 Bode Plots for Thermocouple & Corrective Network

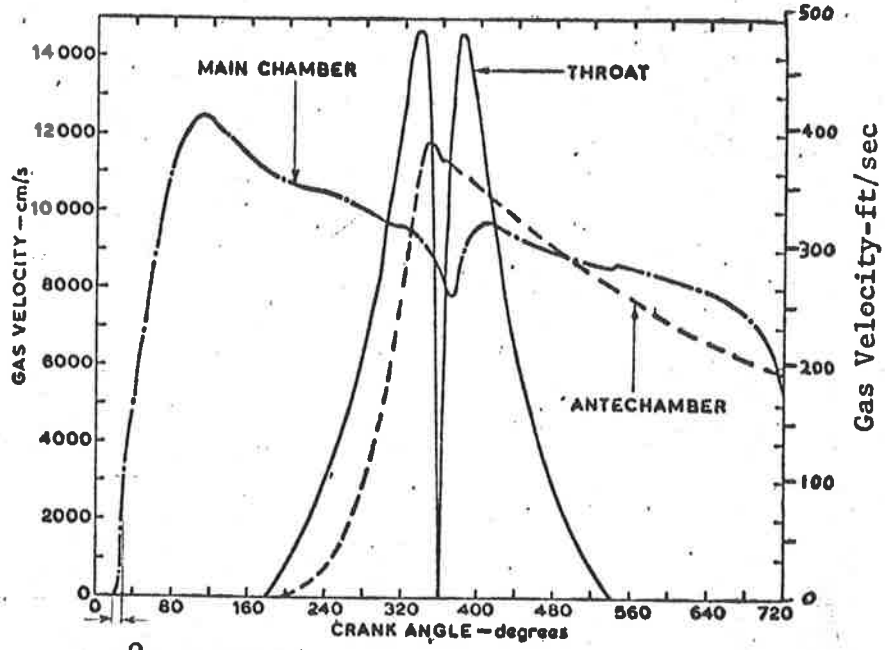

$10^{o} V_g < 100 ft/sec$

Fig.6 Gas Velocity cycle for a Diesel Engine 2000 rpm Fired (from Knight, Ref.29)

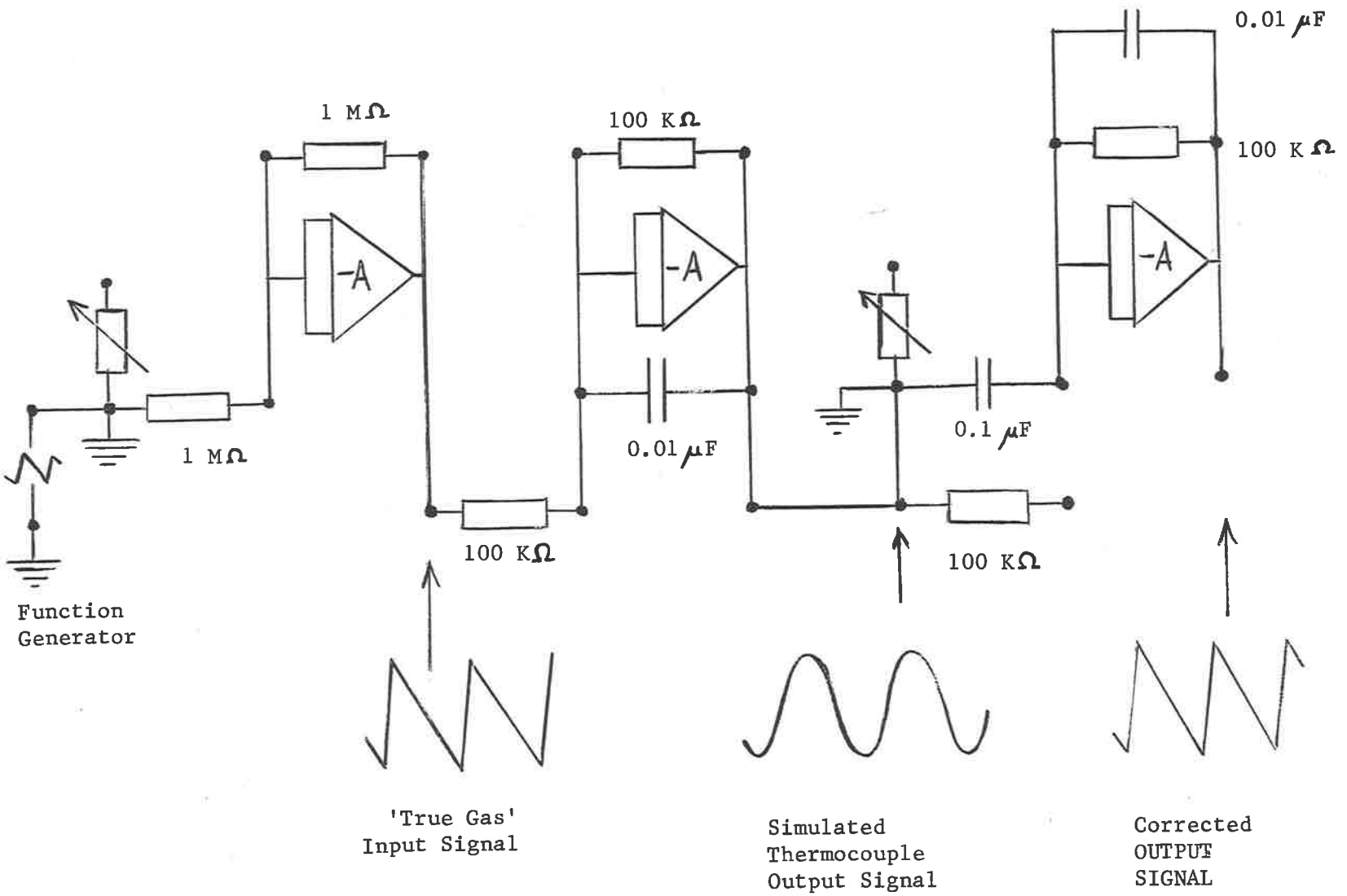

Fig. 7 Analog Computer Simulation of Thermocouple & Corrective Network.

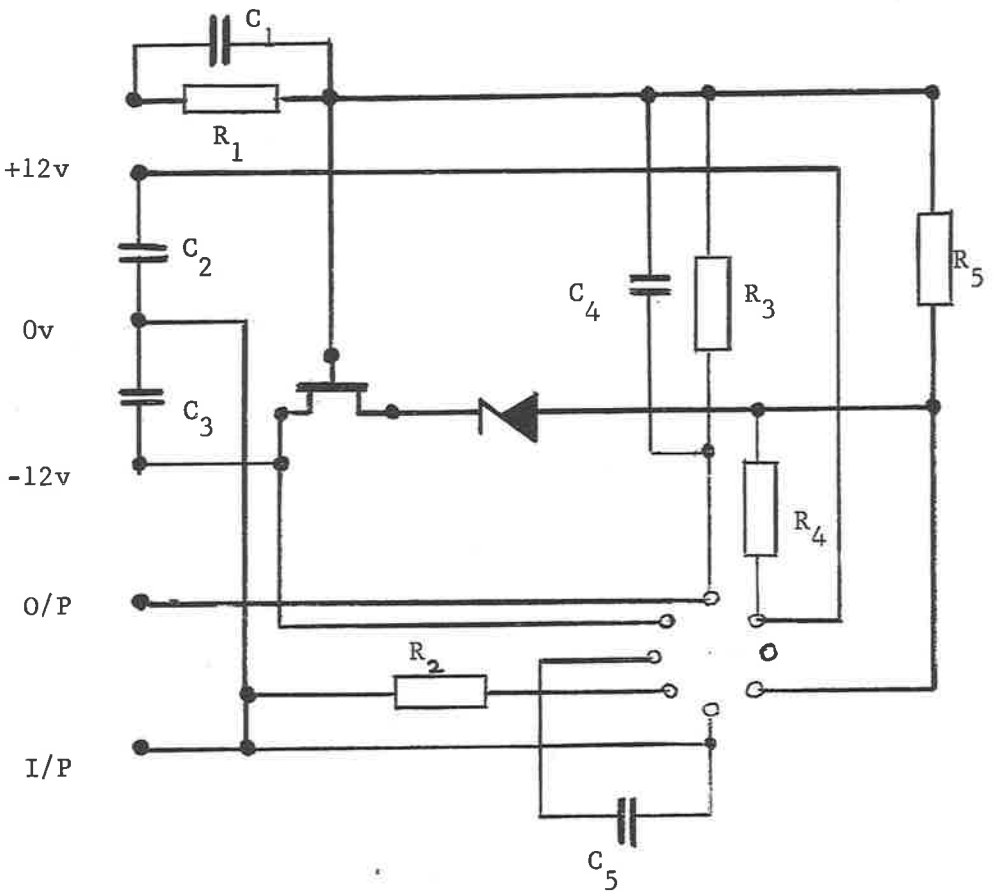

Chip Amp SN7241
FE Transistor 2N4360
Zener Diode Z4

Resistors

R_1	120 K Ω
R_2	1 M Ω
R_3	120 K Ω
R_4	390 K Ω
R_5	10 M Ω

Capacitors

C_1	0.10 μF
C_2	16 μF
C_3	16 μF
C_4	3300 pF
C_5	150 kpF

$\tau = R_1 C_1$

Fig. 8 Active Corrector Network.

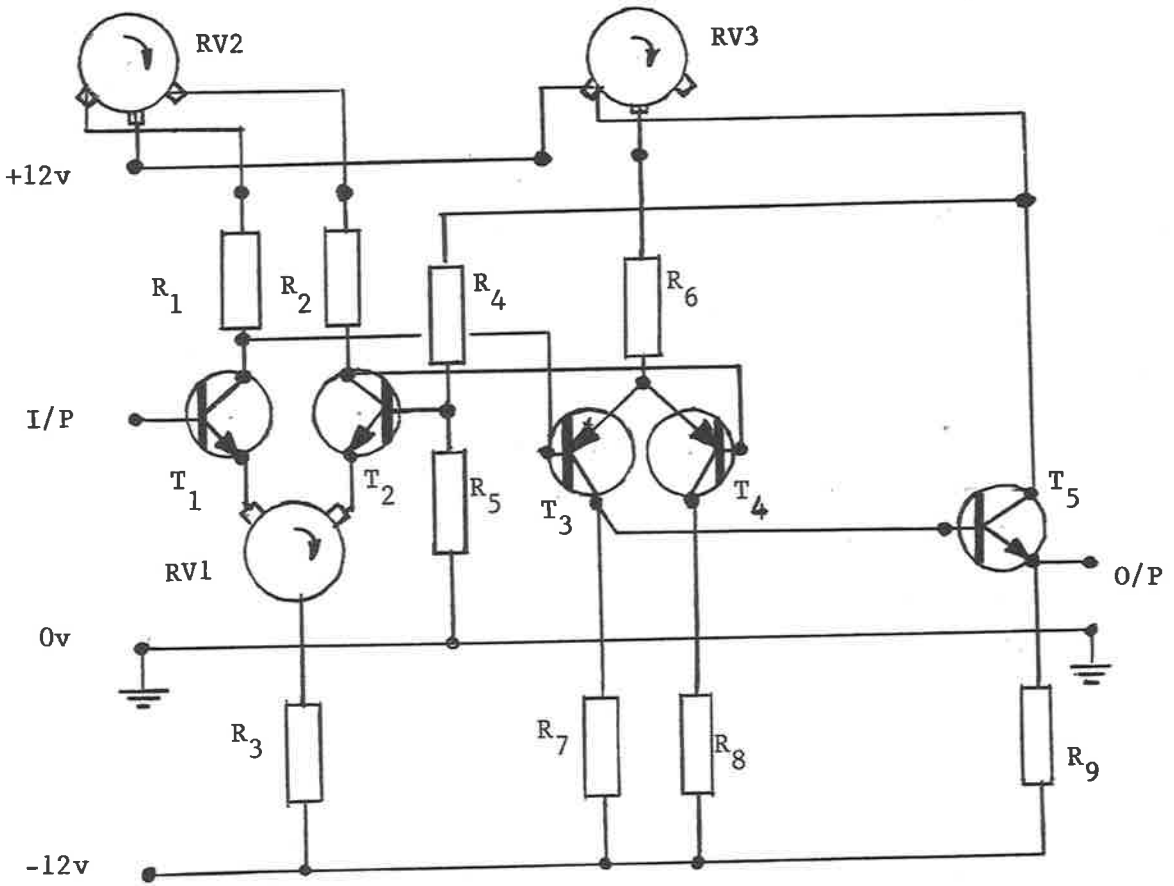

Transistors

T_1 SE4010
T_2 SE4010
T_3 2N3638
T_4 2N3638
T_5 2N3694

Resistors

R_1 30 KΩ
R_2 30 KΩ
R_3 7.5 KΩ
R_4 27 KΩ
R_5 270 Ω
R_6 4.7 KΩ
R_7 15 KΩ
R_8 15 KΩ
R_9 10 KΩ

Resistors Variable

RV1 100 Ω
RV2 5 KΩ
RV3 300 Ω

Fig. 9 Low Noise Single Ended Thermocouple Amplifier for Active Corrector Network.

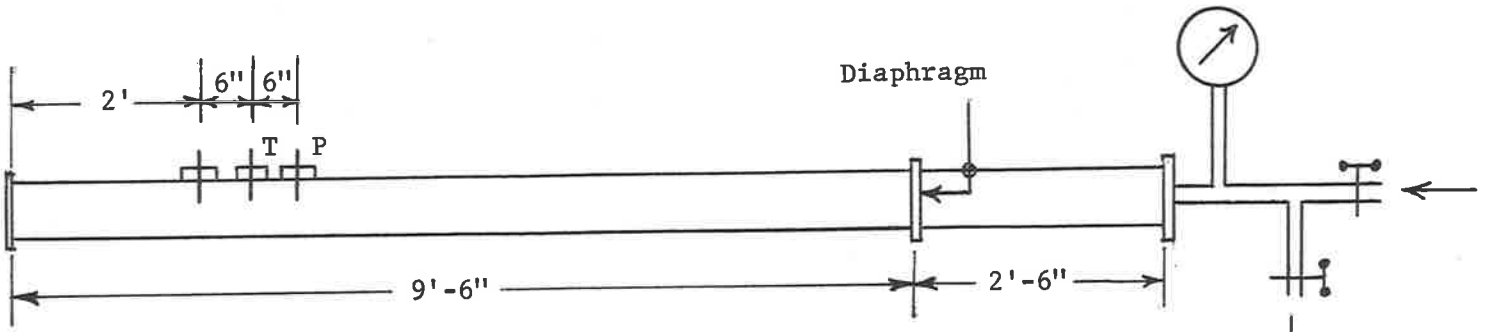

Original Shock Tube

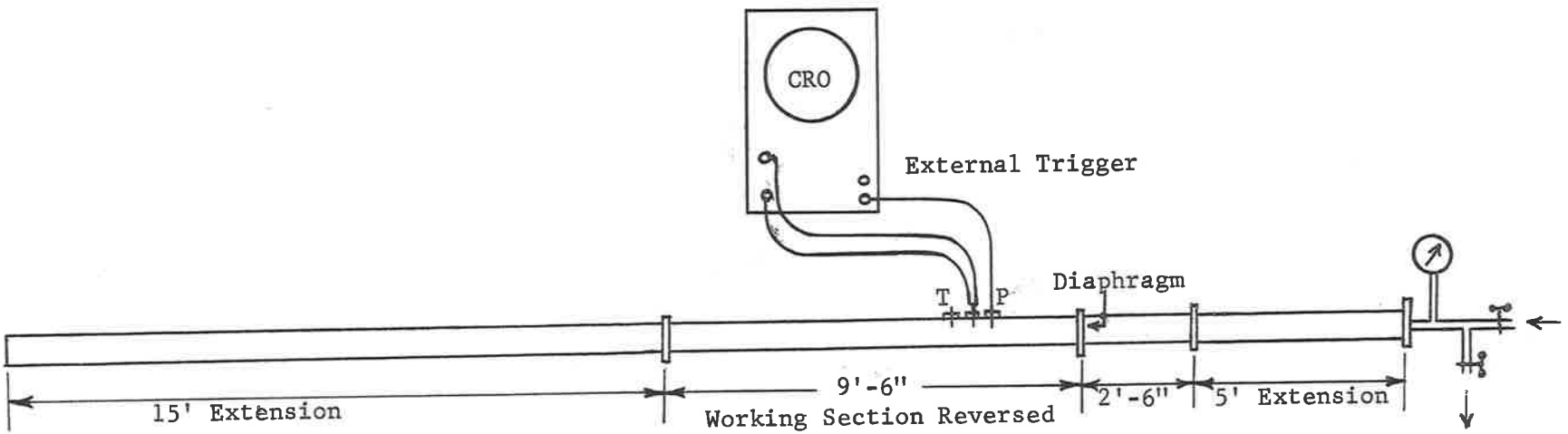

Modified Shock Tube

Fig. 10 Shock Tube Layout.

Response of Chromel-Alumel Thermocouple (0.001"Ø wires)

in, Original Shock-Tube with 30psig burst.pressure.

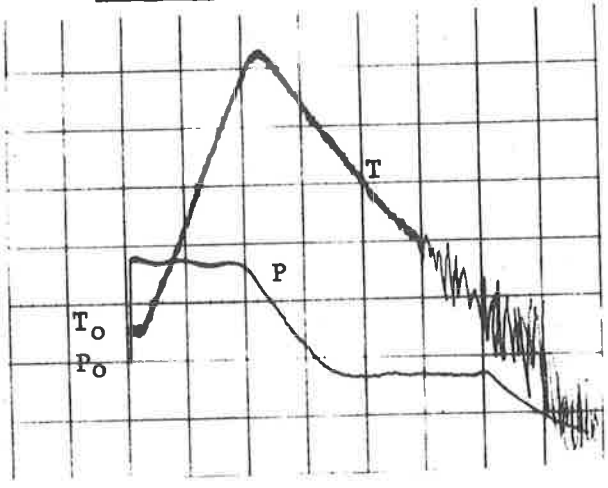

Fig.11

Uncorrected Thermocouple

Scales: Time=2.0msec/cm
Temp=100μv/cm
Press=100mv/cm

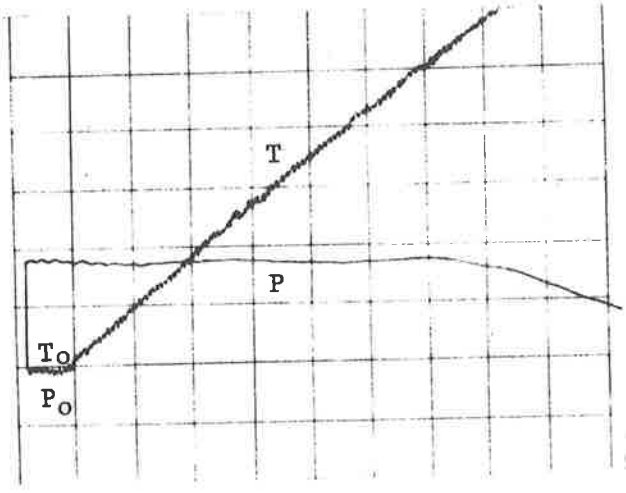

Fig.12

Uncorrected Thermocouple

Scales: Time=0.5msec/cm
Temp=100μv/cm
Press=100mv/cm

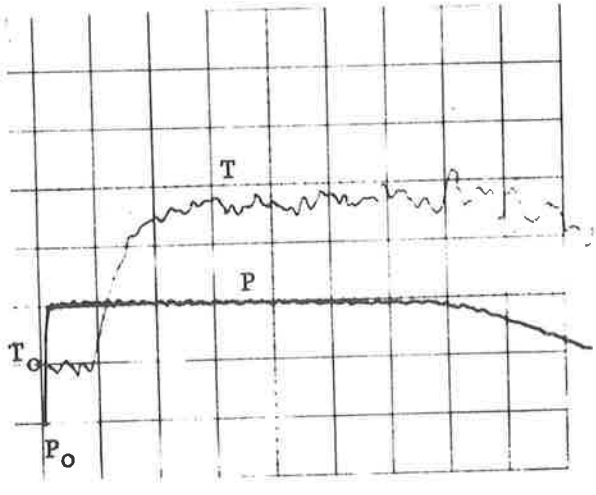

Fig.13

Thermocouple corrected by
ACTIVE Corrector:
Preamp gain=500
Corrector " = 4.5
Overall gain=2250

Scales: Time=0.5msec/cm
Temp=500mv/cm
Press=100mv/cm

Response of Chromel-Alumel Thermocouple (0.001"Ø wires)

in Modified Shock-Tube with 30psig burst pressure.

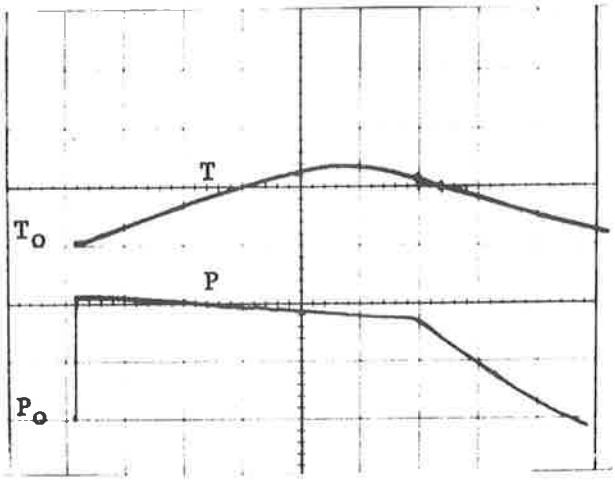

Fig.14

Uncorrected Thermocouple

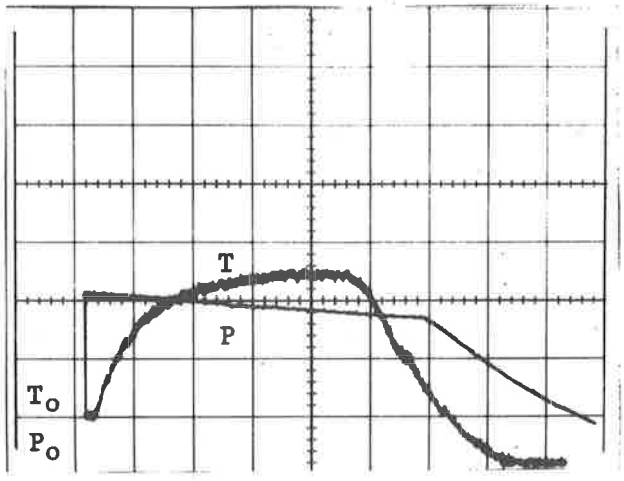

Fig.15

Thermocouple corrected with PASSIVE Network

Scales: Time=2.0 msec/cm
Temp=1.0 mv/cm
Press=100 mv/cm

Response of Chromel-Alumel Thermocouple (0.001"ϕ wires)

in Modified Shock-Tube with 15psig burst pressure.

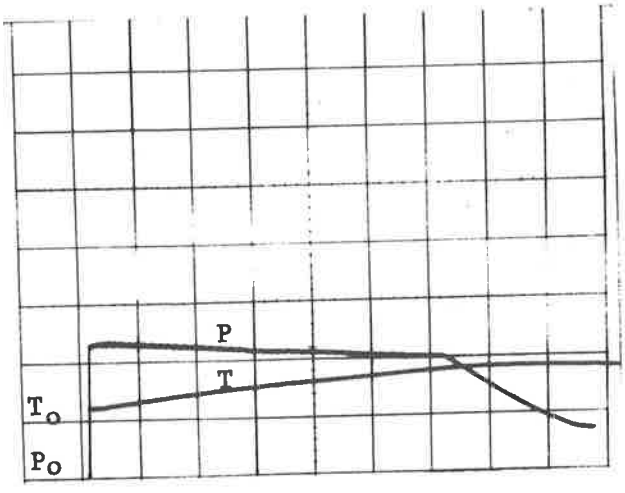

Fig.16

Uncorrected Thermocouple

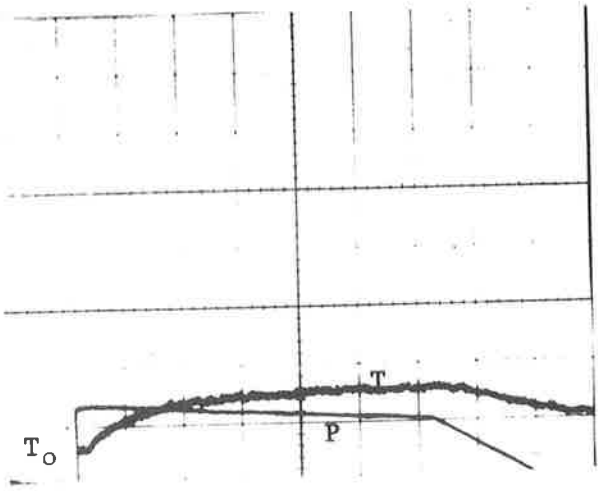

Fig.17

Thermocouple corrected with PASSIVE Network

Scales: Time=2.0msec/cm
Temp=1.0mv/cm
Press=100mv/cm

Thermocouple & Pressure Transducer at same location in Original Shock-Tube, 20psig burst, with Schlieren photographs taken simultaneously.

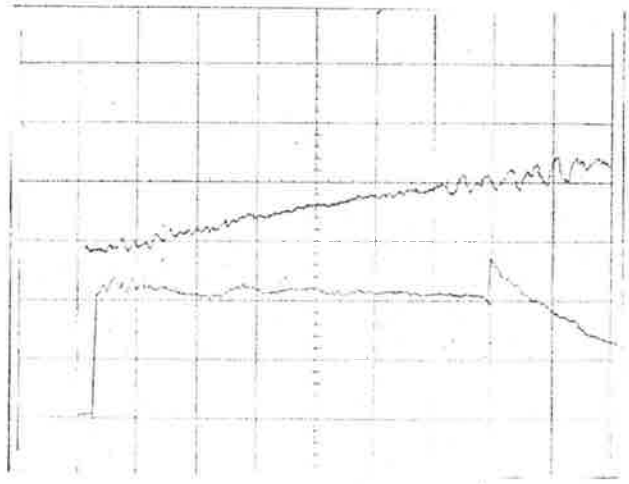

Fig.18.1 Uncorrected Thermocouple

Scales: Time= 1.0msec/cm
Temp= 200 v/cm
Press= 100mv/cm

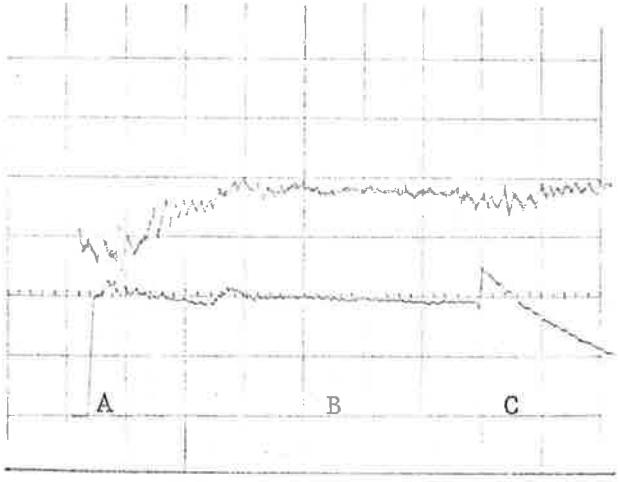

See Fig.18.3 .....

Fig.18.2 Corrected Thermocouple

Scales: Time= 1.0 msec/cm
Temp= 1.0 mv/cm
Press=100mv/cm

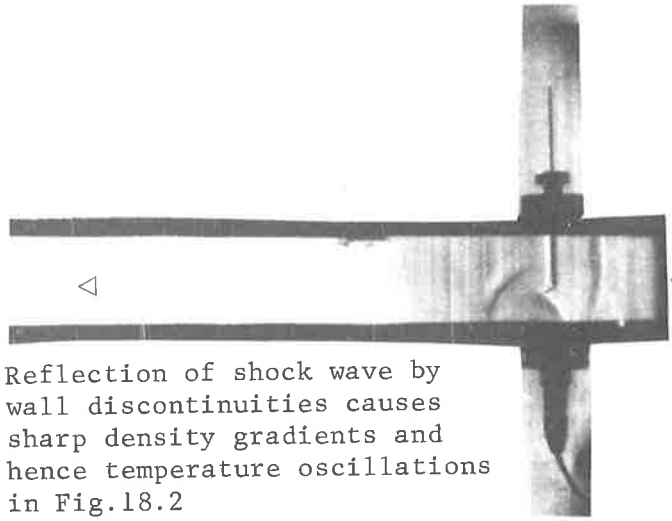

A - (0.4 msec)

Reflection of shock wave by wall discontinuities causes sharp density gradients and hence temperature oscillations in Fig.18.2

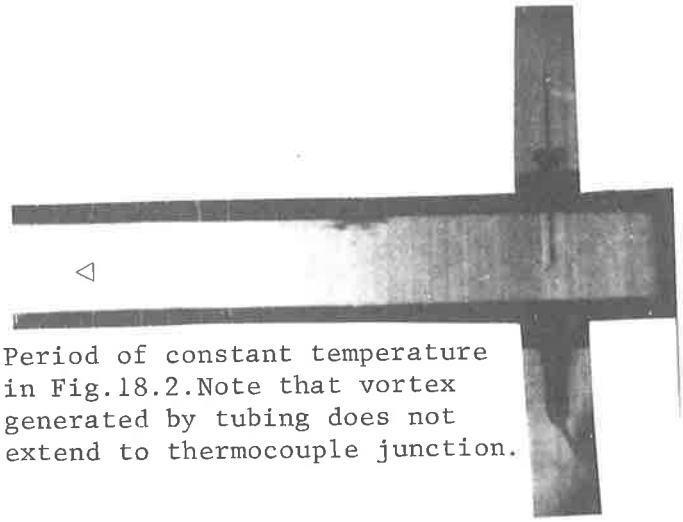

B - (4.0 msec)

Period of constant temperature in Fig.18.2.Note that vortex generated by tubing does not extend to thermocouple junction.

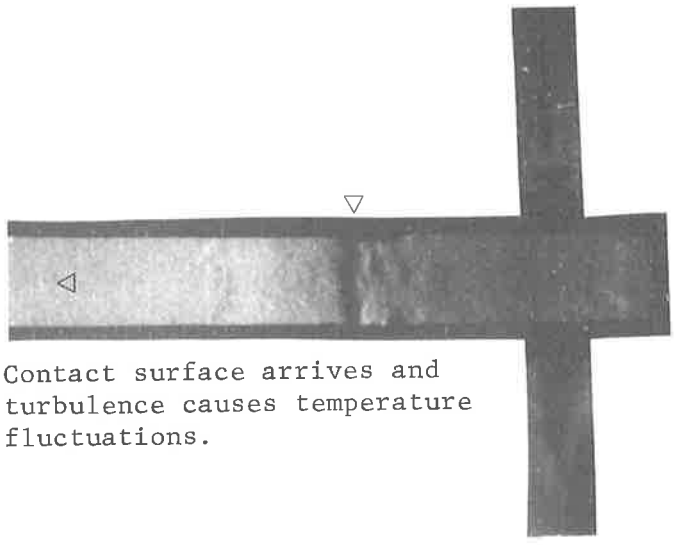

C - (7.0 msec)

Contact surface arrives and turbulence causes temperature fluctuations.

Fig.18.3 Schlieren Photographs showing flow conditions at thermocouple in Fig.18.2

Corrected & Uncorrected Traces for Motored & Fired Engine

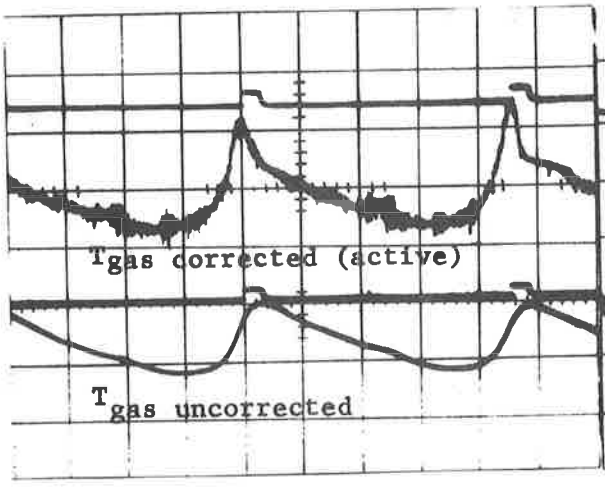

Fig.19

Motoring
CR 5:1 1300rpm WOT
Location: Knock Zone
Insertion: 0.100"
Scales: Time = 20 msec/cm
Temp = 2 v/cm(upper)
2 mv/cm(lower)

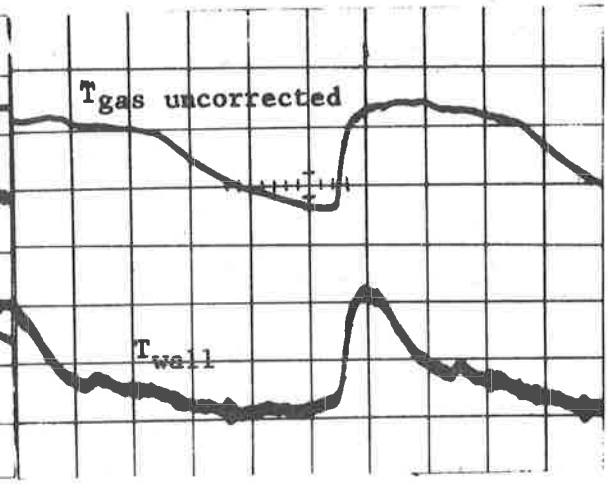

Fig.20

Firing
CR 5:1 1000rpm WOT 35°spk adv
Location: Knock Zone
Insertion: 0.100"
Scales: Time = 20 msec/cm
Temp = 2 mv/cm(upper)
200 μv/cm(lower)

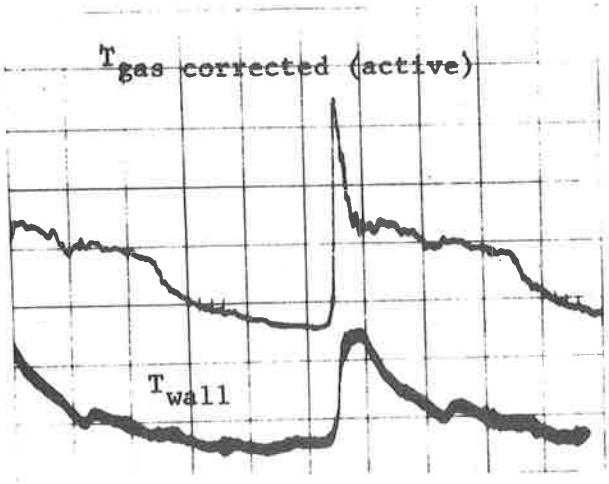

Fig.21

Firing
CR 5:1 1000rpm WOT 35°spk adv
Location: Knock Zone
Insertion: 0.100"
Scales: Time = 20 msec/cm
Temp = 2 v/cm(upper)
200 μv/cm(lower)

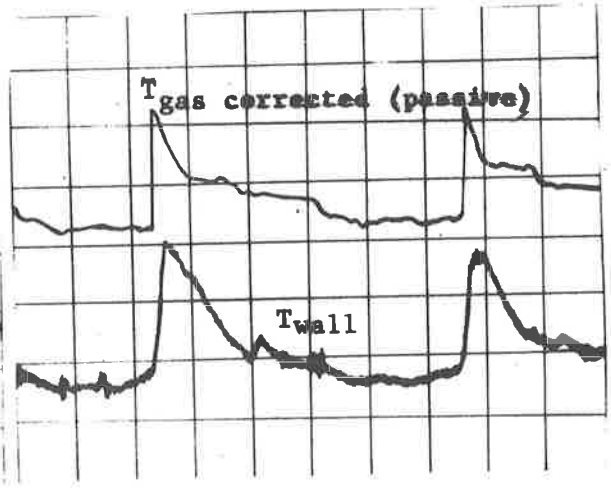

Fig.22

Firing
CR 5:1 1160rpm WOT 30°spk adv
Location: Knock Zone
Insertion: 0.300"
Scales: Time = 20 msec/cm
Temp = 2x10 mv/cm(upper)
200 μv/cm(lower)

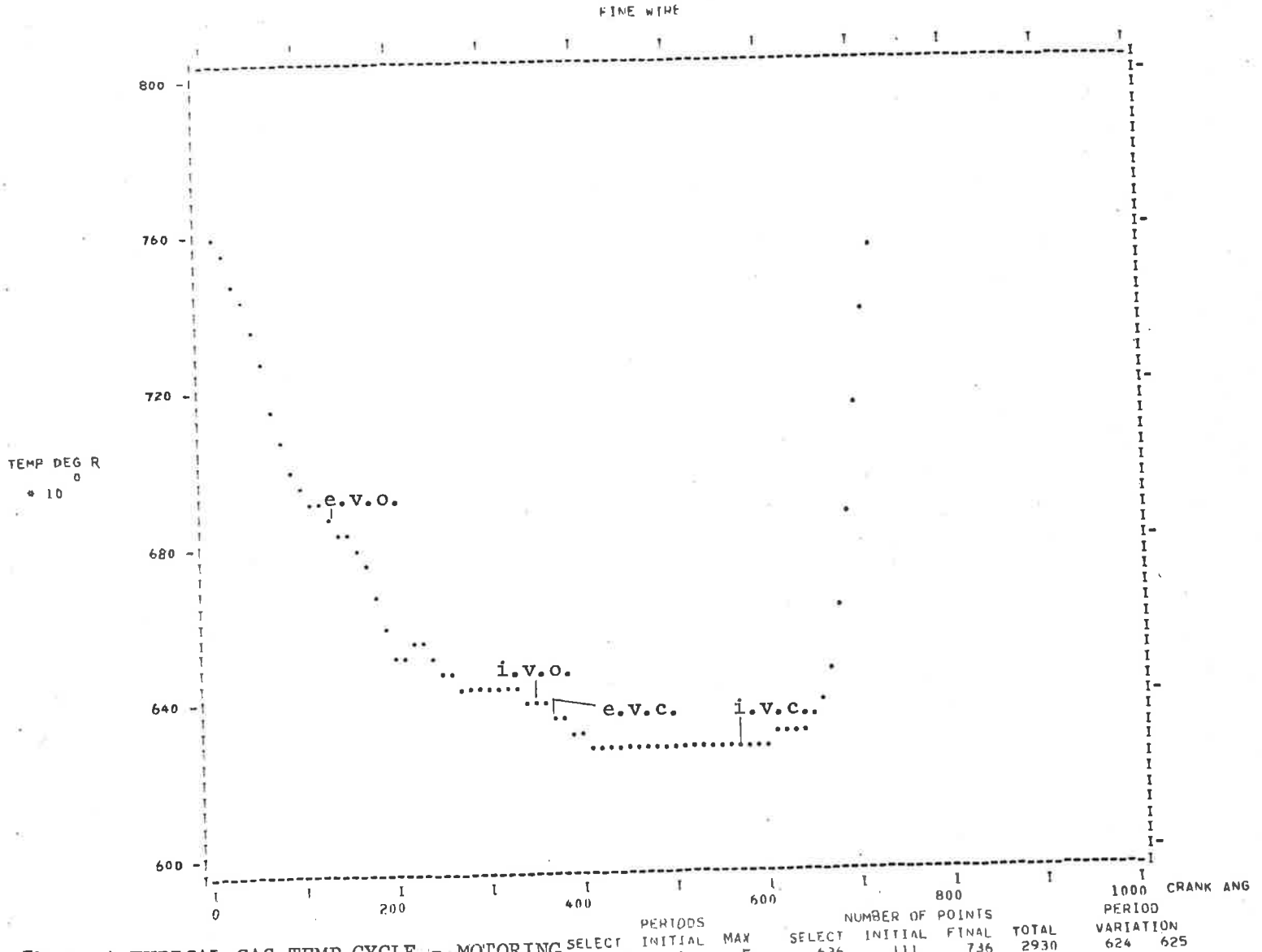

Fig.23 A TYPICAL GAS TEMP.CYCLE - MOTORING

700 RPM.CR 5/1. WOT MOTORING.INLET CORRECTED. X=0.200

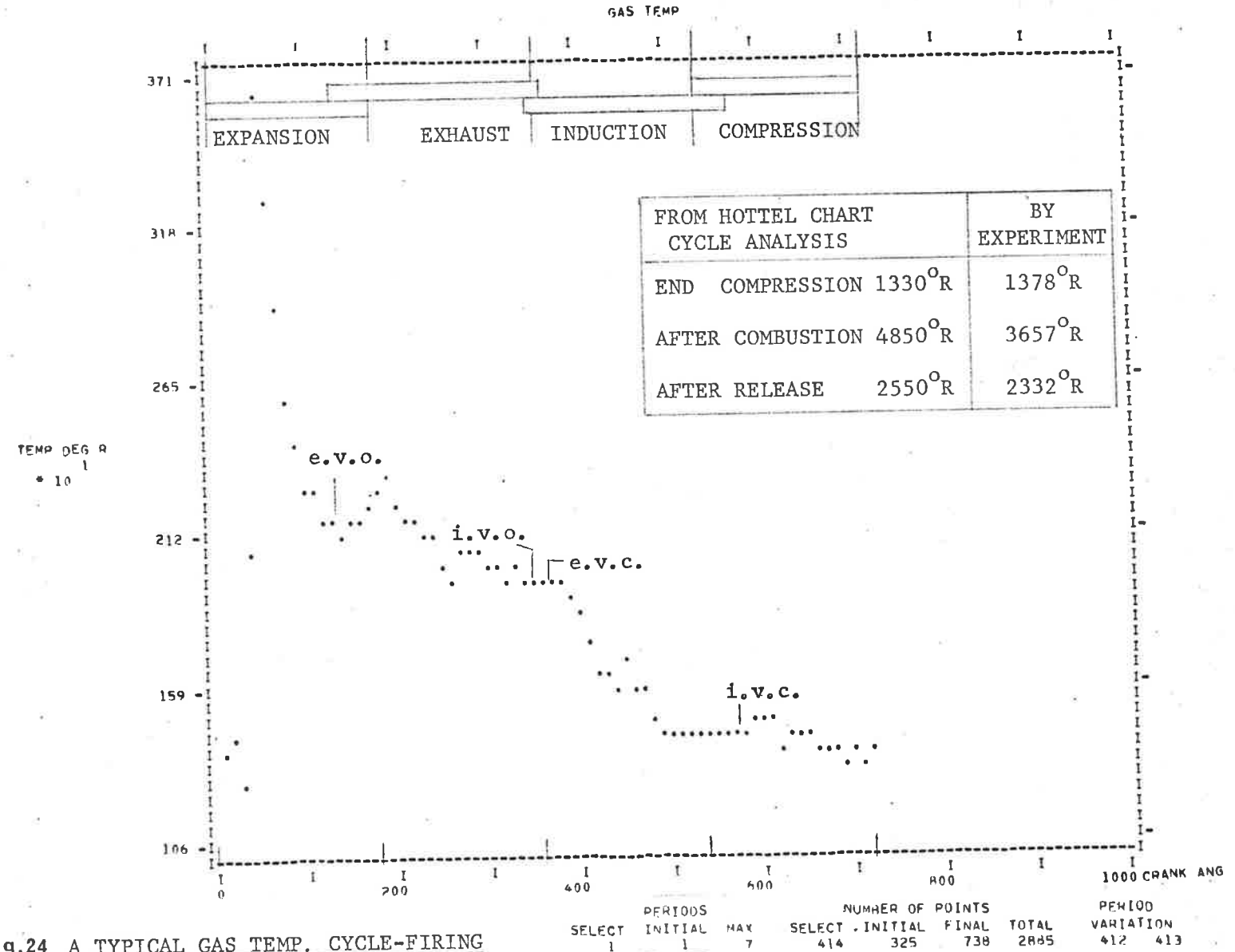

FROM HOTTEL CHART CYCLE ANALYSIS	BY EXPERIMENT
END COMPRESSION 1330°R	1378°R
AFTER COMBUSTION 4850°R	3657°R
AFTER RELEASE 2550°R	2332°R

Fig.24 A TYPICAL GAS TEMP. CYCLE-FIRING

CR 5/1,1000RPM WOT*0.25.FIRING 240EG SPK. KZ COMPENSATED. X=0.450

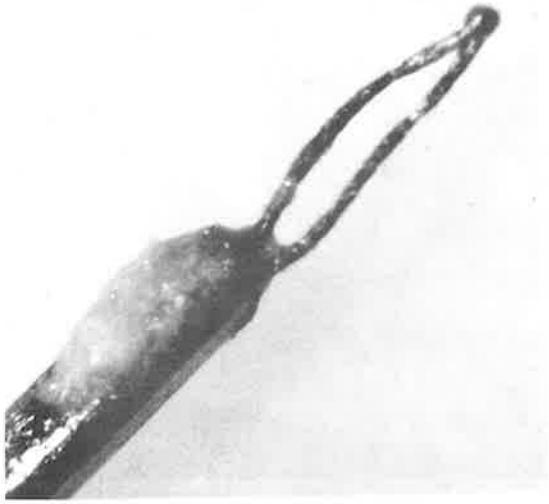

Single wire probe
Wire 0.001" Ø
(18X)

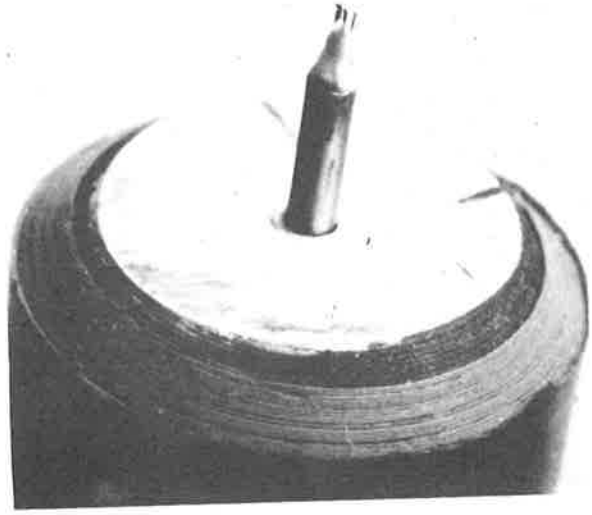

3-Wire probe
Wires 1.0, 1.5, 1.97X0.001"Ø
(8X)

Fig. 25

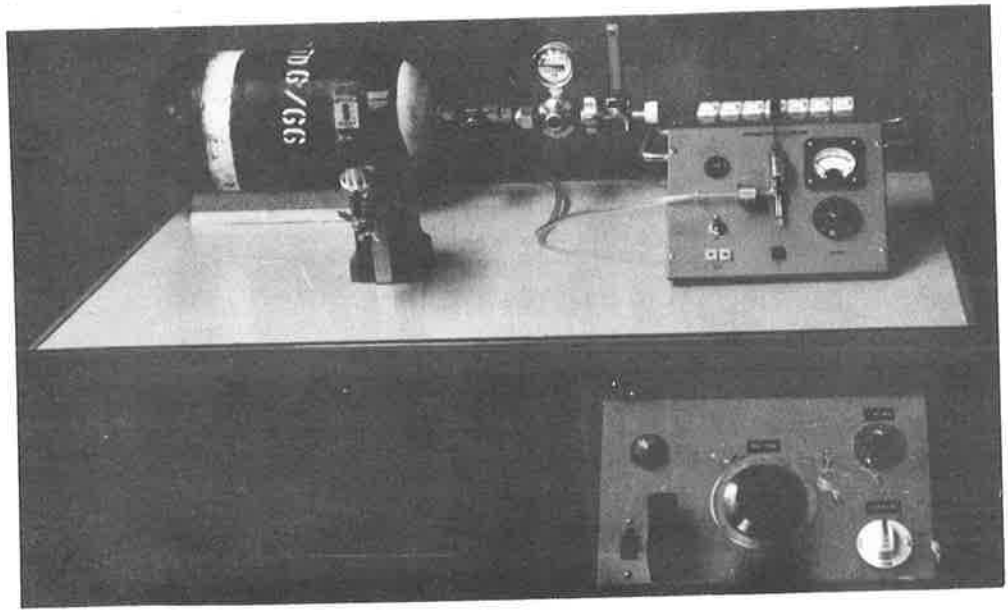

Fig. 26. Thermocouple Arc-Welder

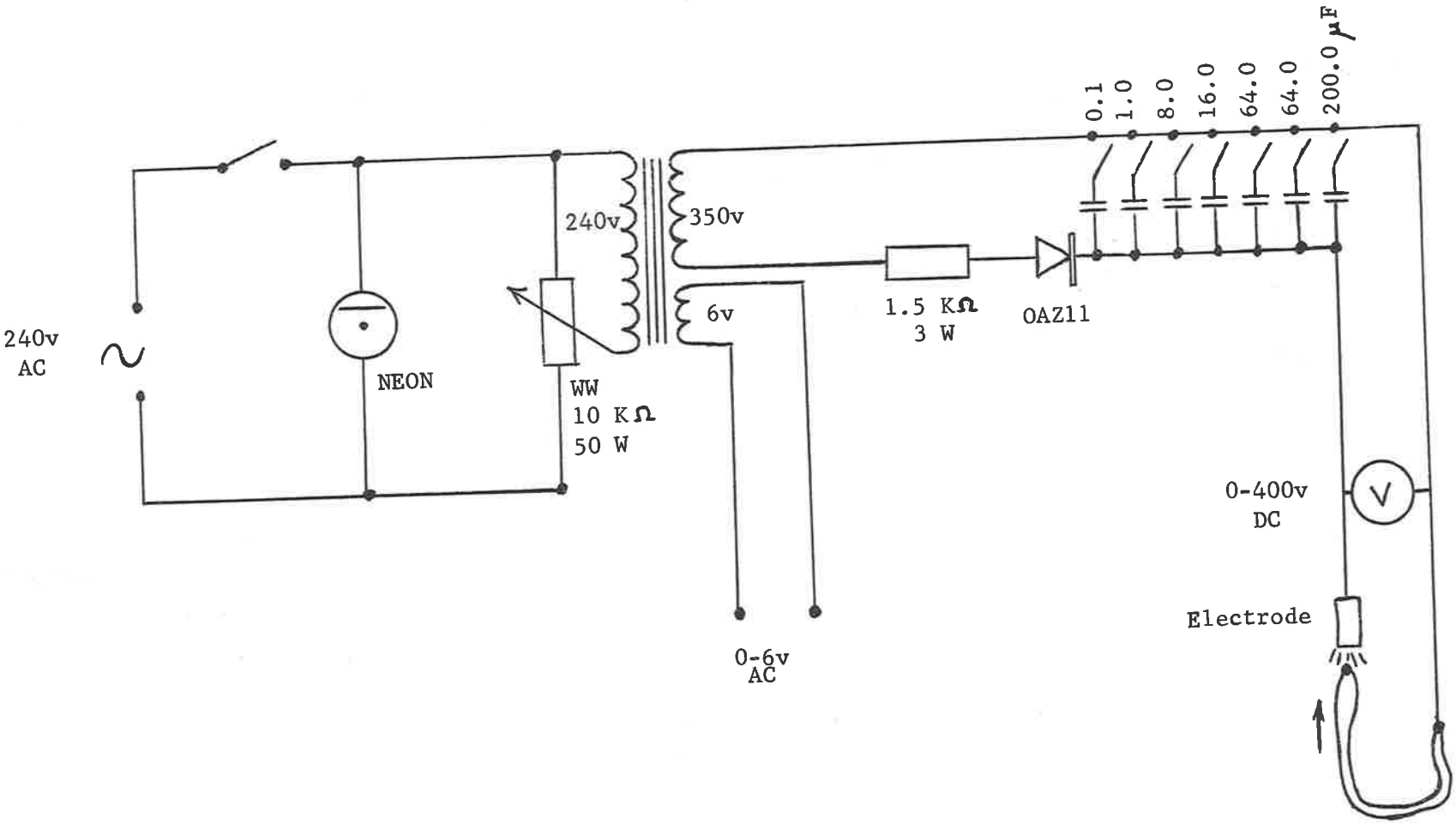

Fig. 27 THERMOCOUPLE ARC WELDER CIRCUIT

APPENDIX A2

THERMAL TRANSPORT PROPERTIES DURING AN OTTO CYCLE COMPRESSION

by

G.A. MORGAN

UNIVERSITY OF ADELAIDE
DEPARTMENT OF MECHANICAL ENGINEERING
Report Mech.Eng. R65/1
March, 1965.

TABLE OF CONTENTS

A DIGITAL COMPUTER PROGRAMME (FORTRAN) FOR CALCULATING THERMAL TRANSPORT PROPERTIES DURING AN OTTO CYCLE COMPRESSION

ABSTRACT

A programme is given for calculation of the thermal properties of an Otto cycle compression mixture as function of temperature.

Viscosity, conductivity, specific heat and Prandtl No. are calculated for a 7 component fuel/air/ residuals mixture up to the dissociation temperature limit.

Constituent viscosity calculations are based on the Chapman-Enskog molecular theory; conductivity being obtained by the Eucken approximation.

Mixture viscosity is calculated by the semi-empirical method of Wilke and mixture conductivity by an analogous method.

Using this programme, property predictions were made for the fuels Octane, Benzene, Ethanol, and Nitro-Methane over the temperature range 200-2000^{o}F. All except the oxy-nitrogen derivative had both viscosity and conductivity within 4% of the corresponding values for air over the temperature range.

However, the Prandtl number of all fuels was significantly (5-10%) greater than that of air over the temperature range and showed a marked deviation (10-20% from Annand's assumption of $(P_r) = 0.7$.

NOMENCLATURE

C_p	Specific heat at constant pressure	
d	Molecular diameter	
D	Typical dimension	
F	Force of interaction between a pair of molecules	
F'	Fuel/Air ratio (sometimes written F/A)	
Fcc	Stoichiometric Fuel/Air ratio	
h	Local gas-wall heat transfer coefficient	(Btu/hr.ft^{2}F^o)
k	Thermal conductivity	(Btu/ft.sec.^{o}F)
K	Boltzmann's constant = 3.29×10^{-4}	(cal/mol. ^{o}K)
m	Molecular mass	
M	Molecular weight	
n	Number of constituents in mixture	
Pc	Critical pressure of gas	(ATMOS)
Q	Potential energy between a pair of molecules	
(P_e)	Peclet No. = $\rho VDC_p/k$	
(P_r)	Prandtl No. = $C_p\mu/k$	
(R_e)	Reynold's No. = $VD\rho/\mu$	
R	The Universal Gas Constant = 1545	(ft.lbwt/lbmole^{o}R)
r	Molecular separation	
T	Gas Temperature	(^{o}F, ^{o}K)

T_W	Wall temperature	(^oF)
T_c	Critical temperature of Gas	(^oK)
T_b	Boiling temperature of liquid	(^oK)
V_c	Molecular volume of gas at critical point	(Cm^3/gm.mole)
V_b	Molecular volume of liquid at boiling point	(Cm^3/gm.mole)
V	Local gas velocity	(ft/sec)
x	Molar fraction of constituent in mixture	
α	Thermal diffusivity = $k/\rho C_p$	(ft^2/sec)
ε	Lennard-Jones force constant representing maximum energy of attraction between a pair of gas molecules.	
μ	Dynamic viscosity of gas	(lb/ft.sec)
ν	Kinematic viscosity of gas = μ/ρ	(ft^2/sec)
ρ	Gas Density	(lb/ft^3)
σ	Lennard-Jones parameter - characteristic molecular diameter or "collision diameter"	(Å)
ε/k	Lennard-Jones parameter = ratio	$\frac{\text{Lennard-Jones force constant}}{\text{Boltzmann's constant}}$ (^oK)
Ω_μ	Collision integral = $f(kT/\varepsilon)$	

1. INTRODUCTION

Current heat transfer investigations require an approximate knowledge of the thermal transport properties of the working fluid in the combustion chamber of a petrol engine at any stage in the cycle.

This preliminary programme is a procedure for calculating viscosity, thermal conductivity, specific heat and Prandtl Number, at any temperature over the induction and compression phases of the engine cycle.

Chemical dissociation of the constituent gases at approximately 2200^{o}F imposes an upper temperature limit on this programme.

The prime aims of this investigation are :-

(1) To determine the mixture transport properties as functions of temperature, type of fuel and mixture strength.

(2) To determine the Prandtl No. variation with temperature of a real fuel/air mixture and to compare this with the assumption of Annand (1)** that (Pr) = 0.7 is sufficient.

Although experimental values of constituent properties are obtainable from handbooks (4), (13), (15), (17), over a fairly wide temperature range; the use of these for computation of mixture properties requires the fitting of polynominal approximations to these data.

This method is unwieldly for manipulation and consumes valuable storage space in the computer.

Thus it seems more logical to resort to the fundamental equations derived directly from molecular theory for the prediction of these properties.

** Numbers in brackets refer to references given in Section 7.

2. THEORY

2.1 Transport Properties and Dimensionless Parameters

Diffusion, Viscosity and Thermal Conductivity are referred to as "Transport Phenomena" and are expressed by their respective "Transport Coefficients" i.e.

Diffusion is the transport of mass; and the Coefficient of Self Diffusion, D, in a gas in which the number of molecules per cm^3, n, varies with the coordinate Z is defined by the statement that the Number flux = -D'. dn/dz.

Viscosity is the transport of momentum; and the Coefficient of Viscosity, μ, in a gas in which the y component of the velocity, v_y, varies with z, is defined by the assertion that the Momentum flux in the y direction = $-\mu\, dv_y/dz$.

Conductivity is the transport of energy; and the Coefficient of thermal Conductivity, k, in a gas in which the temperature, T, varies with z is defined by the requirement that the Energy flux = - k dT/dz.

One of the applications of the kinetic theory of gases is the determination of D, μ and k in terms of the properties of the gas molecules.

Mass Diffusion does not concern us in this heat transfer investigation but Specific Heat, C_p. although not strictly a Transport Property, will be required.

A study of some of the dimensionless parameters often used in heat transfer investigations will demonstrate the significance of C_p, μ and k:-

Stanton No. (St).

$$(St) = \frac{h}{\rho C_p V} \equiv \frac{h\Delta T}{(\rho C_p \Delta T)V}$$

The denominator is a measure of convective heat transport and is proportional to the rate at which thermal energy is borne along by the flow i.e. if heat transfer is predominantly by convection, (St)→ constant.

Nusselt No. (Nu). $(Nu) = \frac{hD}{K} \equiv \frac{h\Delta T}{K\Delta T/D}$

In which the denominator is a measure of conductive heat transport and is proportional to the rate at which thermal energy is transferred through the flow by molecular motion. i.e. if heat transfer is exclusively by conduction, (Nu) tends to become constant.

Reynolds No. (Re). $(Re) = \frac{\rho VD}{\mu} \equiv \frac{(\rho V)V}{\mu V/D}$

In which the denominator represents the rate at which momentum is transported by molecular motion and the numerator represents the rate at which momentum is transported by fluid motion or, more simply, (Re)= Inertial forces/Viscous forces.

Peclet No. (Pe). $(Pe) = \frac{\rho C_p VD}{K} \equiv \frac{(\rho C_p \Delta T)V}{K\Delta T/D}$

In which the denominator represents the rate at which thermal energy is transported by molecular motion and the numerator represents the rate at which thermal energy is transported by fluid motion. i.e.Thermal similitude can be maintained in a flow, if, in addition to the numbers involved in dynamic similitude, the (Pe) is maintained the same. i.e. the (Pe) can be thought of as a thermal (Re).

Prandtl No. (Pr). $(Pr) = \frac{C_p \mu}{k} \equiv \frac{\rho C_p VD/k}{\rho VD/\mu}$

Thus (Pr) is a measure of the tendency of momentum to diffuse (μ) compared with thermal energy (k/C_p).

i.e. $(Pr) = \frac{\nu}{\alpha}$

$= \frac{\mu/\rho}{k/\rho C_p}$

or, (Pr) = $\frac{\text{Kinematic Viscosity (or Momentum Diffusivity)}}{\text{Thermal Diffusivity}}$

Of the above parameters (Pr) is attractive in that it is merely a fluid property, dependent on temperature.

2.2 Constituent Viscosity

The viscosity expression given by Annand (1) is:

$$\mu = \mu_0 T^m \qquad \text{lb/ft.sec} \qquad (1)$$

where:

T = Absolute Temperature (^oK)

m = 0.645

μ_0 tabulated for various gases for $T > 250^o$ K

This form is similar to that derived from the simplified molecular theory of gases at low density (2) and assumes a pure gas composed of rigid nonattracting spherical molecules.

The expression given in (2) is:-

$$\mu = 2/3 \cdot \pi^{-3/2} \cdot d^{-2} \cdot (mKT)^{1/2} \qquad (2)$$

where:

m = mass of molecules (rigid, nonattracting, spherical)

d = diameter of molecules

K = Boltzmann constant

T = Absolute Temperature

Bird, Stewart and Lightfoot (2) infer that this equation gives a qualitatively correct picture of momentum transfer in a low density gas and the absence of any pressure dependent term agrees with experimental data up to about 10 atmospheres.

However, the predicted temperature variation is less satisfactory; experimental data for various gases indicating that μ varies more rapidly than $T^{1/2}$ and is not accurately represented by any power function of T.

First trials of this programme did make use of Annand's viscosity expression but results gave poor agreement with experimental data from (4). See Fig. 3. Subsequently a correction to this expression in the form of a multiplying 5th order polynomial was applied but this was of limited success due to its cumbersome nature. This method was thus discontinued in favour of the more direct fundamental approach given here.

THE CHAPMAN-ENSKOG THEORY

To predict the temperature dependence of μ more accurately, resort must be made to a more rigorous molecular theory, replacing the rigid sphere model by a more realistic molecular force field.

Such a theory was developed by Chapman of England and independently by Enskog of Sweden, before the first World War.

This theory is very complicated mathematically, giving expressions for the transport properties in terms of the potential energy of interaction between a pair of molecules in the gas.

It is applicable for low density gases (where intermolecular collisions are considered unimportant) but not for densities so low that the dimensions of the vessel are large compared with the

mean free path of the molecules (i.e. Knudsen gases). For a discussion on the effect of pressure, See Appendix "C".

The final expression of the Chapman-Enskog Theory using the Lennard-Jones potential function for the Viscosity of a pure monatomic gas of molecular weight 'M' at absolute temperature 'T' is:

$$\mu = 2.6693\times10^{-5}\sqrt{MT}/\sigma^2\Omega_\mu \quad gm/cm.sec \qquad (3)$$

Ω_μ is a slowly varying function of KT/ε tabulated in (2) and shown in Fig. 2 where:

K = Boltzmann's Constant

ε = Maximum energy of attraction between a pair of molecules

and σ = A characteristic molecular diameter (NOTE: See Appendix 'A' and Fig. 1).

The function Ω_μ represents the deviation from rigid theory behavious i.e. if the gas were composed of rigid spheres of diameter σ instead of real molecules with attractive and repulsive forces, then Ω_μ would be unity.

Note that equation (3) predicts a viscosity increase roughly as the 0.6 to 1.0 power of absolute temperature and there is no pressure dependence in the low density region.

Strictly, the theory is applicable to monatomic gases only. Practically however, it is found that internal molecular motions are relatively unimportant in mass and momentum transfer. Hence the theory may be applied to calculation of mass diffusion and

viscosity coefficients of polyatomic molecules.

However, for thermal conductivity the same is not true, as internal modes of vibration make a substantial contribution to energy transport. This effect can be approximately compensated for by the Eucken approximation.

2.3 Constituent Conductivity

Bird, Stewart and Lightfoot (2) again illustrate the transport mechanisms by a simplified derivation from rigid sphere theory; and then compare the resulting expression with that of the more rigorous Chapman-Enskog theory.

Their final expressions for Conductivity are:

(1) Simple Theory:

$$k = \frac{1}{d^2}\sqrt{\frac{k^3 T}{\pi^3 m}} \qquad (4) \qquad \text{(monatomic)}$$

where:

k = Conductivity

d = Diameter of rigid nonattracting molecules

m = Mass of rigid monattracting molecules

K = Boltzmann's constant

T = Absolute temperature

This equation shows no pressure dependence; and this is in agreement with experimental data for monatomic gases up to about 10 atmospheres. However, as for viscosity, the temperature dependence predicted by this simple theory is inadequate.

(2) Chapman-Enskog Theory

$$k = 1.9891 \times 10^{-4}\sqrt{T/M}\,/\,\sigma^2 \Omega_k \qquad (5) \qquad \text{(monatomic)}$$

where:

k = Conductivity (cal/cm.sec.^{o}K)

T = Absolute temperature (^{o}K)

M = Molecular weight

σ = "Collision diameter" (Å)

$\Omega_k = \Omega_\mu = f(kT/\varepsilon)$

This equation affords an accurate prediction of monatomic gas thermal conductivity, and uses the same Lennard-Jones intermolecular force parameters, σ and ε_k, as used for the viscosity calculation.

However, an approximate generalisation of the above theory is required in order to compute the conductivity of polyatomic gases.

THE EUCKEN EQUATION

Polyatomic gas molecules have rotational and vibrational energy in addition to their kinetic energy of translation; and all these forms of energy may be exchanged during a collision.

A simple semi-empirical method of handling this energy exchange between polyatomic gas molecules was developed by Eucken (11) and results in the following equation:

$$k = \left(\hat{C}_p + \frac{5}{4} \cdot \frac{R}{M}\right) \qquad (6) \qquad \text{(polyatomic)}$$

where:

k = Conductivity

$\hat{C}_p$ = Specific Heat at constant pressure (per unit mass)

R = The Universal gas constant

M = Molecular weight

μ = gas viscosity

This equation gives conductivities within a few per cent of experimental values for all but the most complex gas molecules (See Fig. 4).

2.4 Constituent Specific Heat

The Constituent Specific heats were calculated by means of a fifth order polynomial expression using the coefficients of M.H. Edson (12) as listed in Table 1.

These polynomials had been fitted by Edson to experimental data of API Project 44 (13) and were also found in this investigation to agree completely with the data given in (4). (See Fig. 5).

This 5th order data was also considered to be an improvement over the simple second-order approximation used in (1).

MIXTURE PROPERTIES

3.1 Mixture Viscosity Calculation

The Chapman-Enskog theory has been extended to include multi-component gas mixtures at low density by Curtiss and Hirschfelder (8) but for engineering calculations, the semi-empirical formula of Wilke (14) is quite adequate:-

$$\mu_{MIX} = \sum_{i=1}^{n} \frac{x_i \mu_i}{\sum_{j=1}^{n} x_j \phi_{ij}} \qquad (7)$$

where

$$\phi_{ij} = \frac{1}{\sqrt{8}} \left(1+\frac{M_i}{M_j}\right)^{-1/2} \left[1+\left(\frac{\mu_i}{\mu_j}\right)^{1/2} \left(\frac{M_j}{M_i}\right)^{1/4}\right]^2 \qquad (8)$$

n = number of chemical species in mixture

M_i , M_j = Molecular weights of species i & j at mixture temperature & Pressure.

x_i , x_j = Molar fractions of species i & j at mixture temperature & Pressure.

μ_i, μ_j = Constituent viscosities species i & j at mixture temperature & Pressure.

ϕ_{ij} is dimensionless and when i = j, $\phi_{ij} = 1$

The seven constituents of the Otto cycle mixture under consideration are

O_2 , N_2 , CO , CO_2 , H_2O , H-C FUEL , and H_2

These constituents are listed in Table 2 together with their relevant molecular weights and molar fractions for a chemically correct mixture. Their Lennard-Jones intermolecular force

parameters σ and ε/k are also tabulated in Table 2.

3.2 Mixture Conductivity Calculation

The method of calculation of mixture conductivity, k_{mix}, is an approximation by Mason (16) to the more accurate method of Hirschfelder (7) and is exactly analogous to that previously given for mixture viscosity.

$$k_{mix} = \sum_{i=1}^{n} \frac{x_i k_i}{\sum_{j=1}^{n} x_j \phi_{ij}} \qquad (9)$$

where $$\phi_{ij} = \frac{1}{\sqrt{8}} \left(1 + \frac{M_i}{M_j}\right)^{-1/2} \left[1 + \left(\frac{\mu_i}{\mu_j}\right)^{1/2} \left(\frac{M_j}{M_i}\right)^{1/4}\right]^2$$

as for viscosity.

4. PROGRAMME

4.1 Calculation Procedure

From the preceding sections the following equations were used to calculate the properties of each constituent of the mixture (the j^{th} component):-

Specific Heat:

$$C_{pj} = a + bT + cT^2 + dT^3 + eT^4 + fT^5 \qquad (10)$$

Viscosity:

$$\mu_j = (\text{constant}) \times \sqrt{W_j T}/\Omega^2 \Omega_\mu \qquad (11)$$

Conductivity:

$$k_j = \mu_j \left(C_{p_j} + (\text{constant})/W_j\right) \qquad (12)$$

Prandtl No.:

$$(P_r)_j = C_{p_j} \mu_j / k_j \qquad (13)$$

These constituent properties were then combined to give the overall mixture properties by the following:

Mixture Molecular Weight

$$W_{MIX} = \sum_{j=1}^{n} (X_j W_j) \qquad (14)$$

Mixture Specific Heat:

$$C_{P_{MIX}} = \sum_{j=1}^{n} \left(X_j W_j C_{p_j}\right) / W_{MIX} \qquad (15)$$

Mixture Viscosity:

$$\mu_{MIX} = \sum_{j=1}^{n} \frac{X_j \mu_j}{\sum_{k=1}^{n} X_k \Phi_{jk}} \qquad (16)$$

where

$$\Phi_{jk} = \frac{1}{\sqrt{8}} \left(1 + \frac{W_j}{W_k}\right)^{-1/2} \left[1 + \left(\frac{\mu_j}{\mu_k}\right)^{1/2} \left(\frac{W_j}{W_k}\right)^{1/4}\right]^2 \qquad (17)$$

Mixture Conductivity:

$$k_{mix} = \sum_{j=1}^{n} \frac{X_j k_j}{\sum_{k=1}^{n} X_k \phi_{kj}} \quad , \phi_{kj} \text{ as above} \qquad (18)$$

Mixture Prandtl No.:

$$(P_r)_{mix} = C_{p_{mix}} \cdot \mu_{mix} / k_{mix} \qquad (19)$$

All constants in the above equations were adjusted to give properties in standard British units.

These basic equations were written in the FORTRAN 'AFIT' language for an IBM 1620 automatic digital computer, of 20K storage capacity.

The sequence of calculation is shown by means of the following Flow Chart (Section 4.3).

A listing of the actual Source Program used is shown in Table 8 while examples of the output results are given in Appendix 'D'.

4.2 Input Instructions

(1) Print Heading, Print Run No., read Run Comment and Print. Read number of temperatures for which properties are required, read number of constituents allowed for (7) *

Read constituent MW's in order: O_2, N_2, CO, CO_2, H_2O, (FUEL), H_2.

Read, (in above order) the molar fractions of each constituent in the mixture being considered.

Read the Lennard-Jones intermolecular force parameters in order.

Read the Lennard-Jones intermolecular force parameters ε/k in order.

Read Viscosity correction factors.

Read fifth order Specific-Heat polynomial coefficients for the constituents in order. Repeat for fourth down to zeroth order.

* If one or more constituents are absent, it is only necessary to put X(J)=0.0 for those constituents.

PROGRAMME FLOW CHART

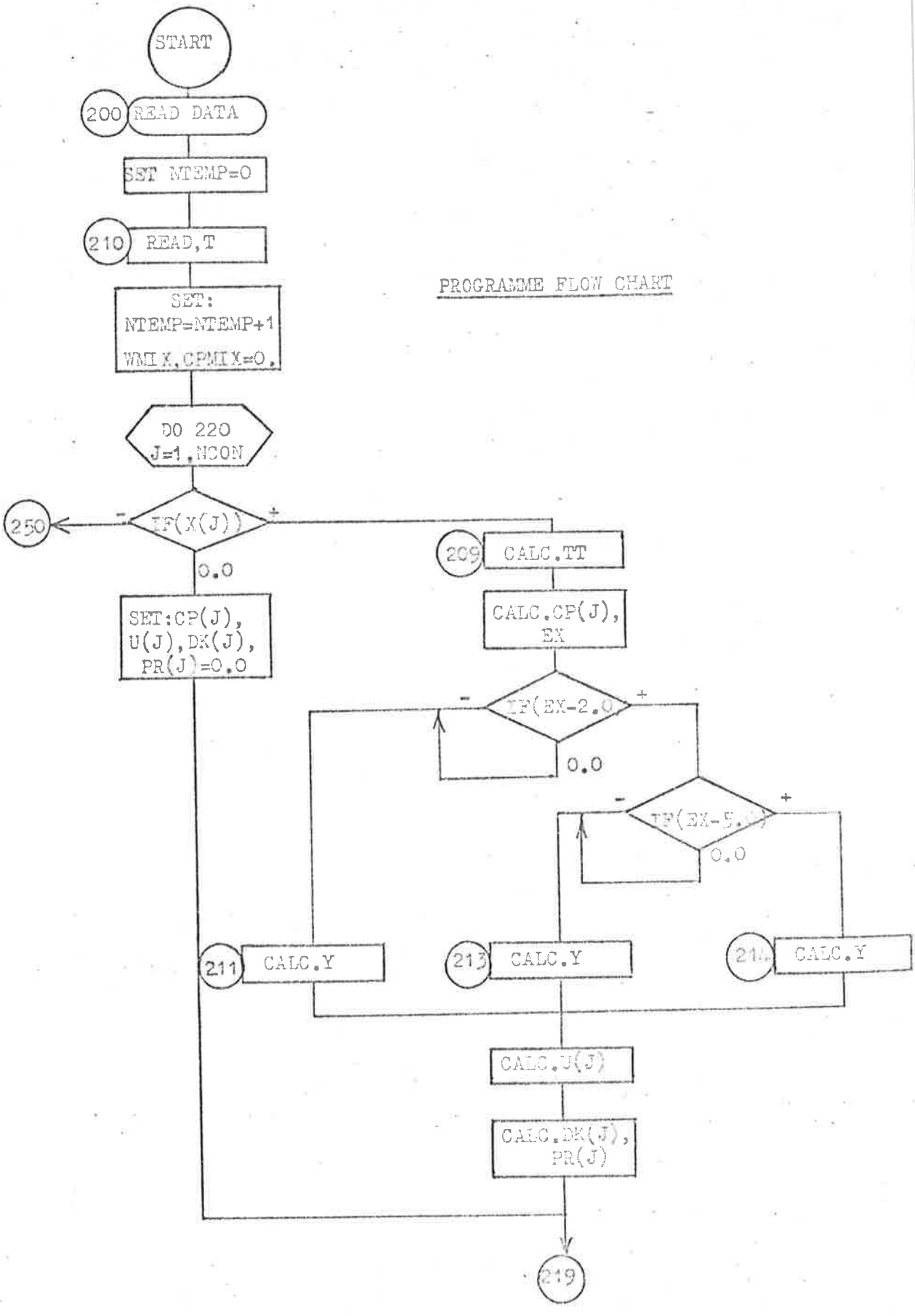

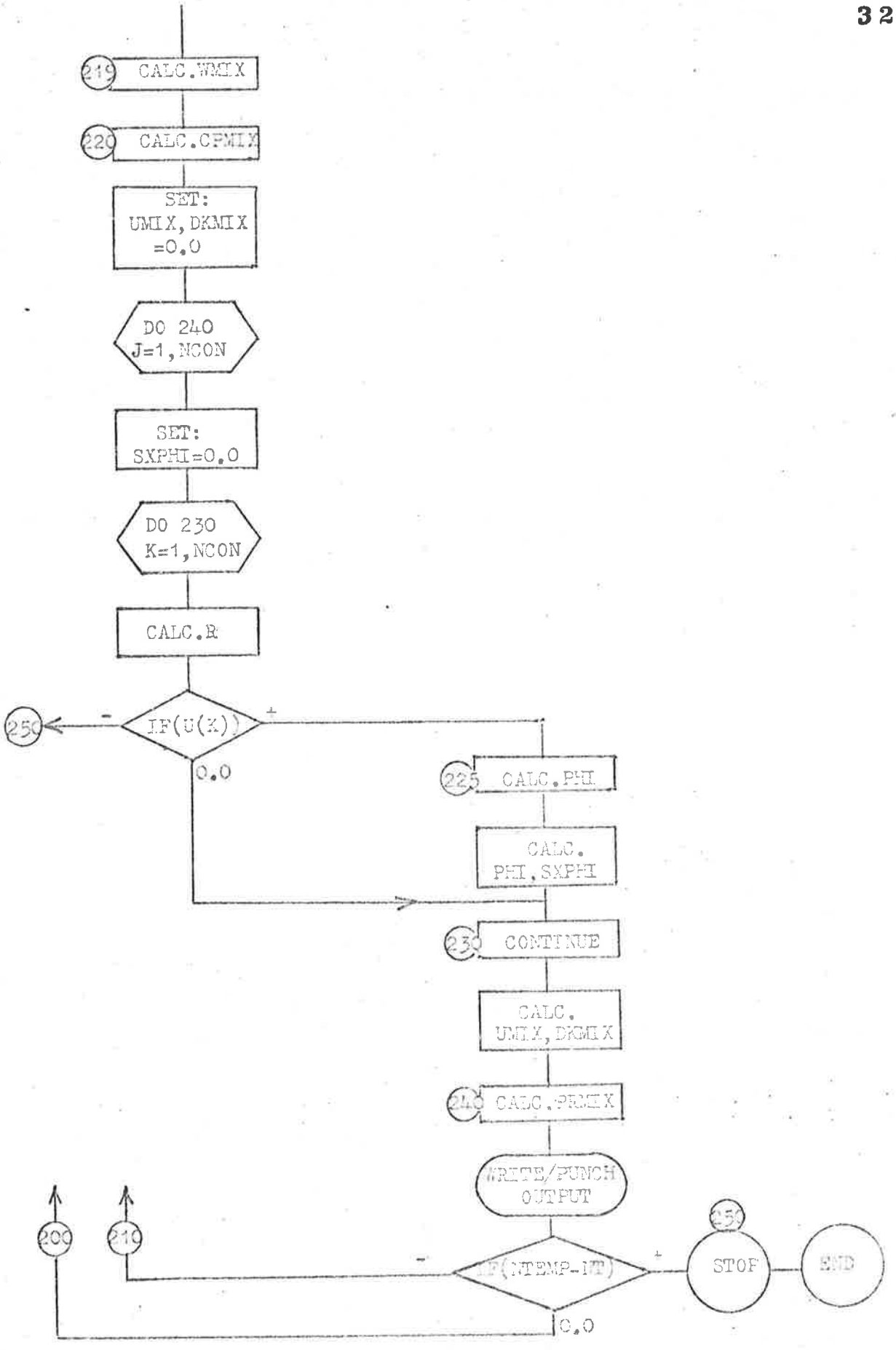
219
CALC.WMIX
220
CALC.CPMIX
SET:
UMIX, DKMIX
=0.0
DO 240
J=1, NCON
SET:
SXPHI=0.0
DO 230
K=1, NCON
CALC.R
250
IF(U(K))
-
+
0.0
225
CALC.PHI
CALC.
PHI, SXPHI
230
CONTINUE
CALC.
UMIX, DKMIX
240
CALC.PRMIX
WRITE/PUNCH
OUTPUT
200
210
IF(NTEMP-NT)
-
+
0.0
250
STOP
END

5. INVESTIGATIONS

5.1 Proving the Programme

5.1.1. Ternary Mixture

As a first check on the programmed computations, a thermal conductivity prediction was made for a ternary gas mixture (CO_2-O_2-N_2) from data given in ref. (2): see Appendix "D".

The programme output for this problem is given in Appendix "D", and a comparison with the manual solution of equations (7) and (9) using constituent conductivity data given in ref. (2) page 259 is also shown.

Whereas computed mixture viscosity agrees very well (0.1%); mixture conductivity is about 8% low possibly due to the approximate nature of the Eucken equation.

5.1.2. Comparison with Handbook Data

Another check on the accuracy of the computations was afforded by plotting constituent properties as a function of temperature at 200°F intervals and comparing these with data from ref. (4) See Figs. 3, 4, 5.

The Specific Heats calculated from the 5th order polynomial coefficients of Edson, ref. (12) were found to be in very close agreement with those from ref. (4); it is possible, however, that these were both from the same source (NBS C461, 1947) as Edson did not disclose the source of his table of coefficients.

The viscosity temperature relationships (Fig. 3) for the majority of constituents were also found to be in close agreement with data from ref. (4). The only constituent showing

appreciable deviation from the Handbook data was the polar type gas H_2O.

However, the computed viscosity-temperature curve for H_2O was adjusted by the use of:

(1) Intermolecular force parameters of the modified Stockmayer Potential as given by Joshi and Saxena, ref. (10); see Appendix 'B'. These parameters gave better agreement in slope of the curve than Lennard-Jones parameters.

(2) An arbitrary magnitude correction factor of 1/1.4 (AK(J(=1.4) was introduced to reduce the computed viscosities to approximately the same values over the range as ref. (4) data.

Viscosities calculated from Annand's equation $\mu = \mu_o T^m$ were also plotted in fig. 3 and are all somewhat lower than both the Handbook and the Computed values. Coefficients for Annand's equation were not available for O_2 or H_2.

Similarly, computed conductivities for each constituent were compared with the data of ref. (4) and with those calculated from the Eucken equation using Annand's viscosity expression (Fig. 4).

Because of the good agreement of constituent gas properties with data of ref. (4); it can be expected that mixture properties and Prandtl Nos. will be sufficiently accurate for the present purpose of comparison of various fuels and mixture strengths.

5.2.0. The effect of Mixture Strength on the Thermal Properties of an Octane-Air-Residuals Mixture over the Temperature Range 200-2000°F.

5.2.1. Chemical Reaction Equations

In order to determine the molar fractions of each constituent present at the various fuel-air ratios, the chemical reaction equations are first written for the combination of the fuel (Iso-octane; i-C_8H_{18}) with 75, 90, 100, 110, 125 and 150% of theoretical air.

The first three mixture strengths (RICH) require a different approach to the last three (LEAN) because of the excess O_2 present in the latter case.

Consider the rich mixtures first.

Rich Mixtures

If the air supplied is insufficient for complete combustion, the residual gas mixing with the incoming charge must contain CO and H_2 but no excess O_2.

To approximate the composition of the residual gas, the following procedure from ref. (18) is adopted:

Assume the residual gas to have the composition:

CO_2	$n_1 x$
CO	$n_1 (1-x)$
H_2O	$n_2 y$
h_2	$n_2 (1-y)$
N_2	n

The reaction equation provides the values of n_1, n_2 and n'' and one relation between x and y.

For example, consider the combination of C_8H_{18} with 'a' moles of O_2 where 'a' $<$ 12.5. The reaction equation is:

$$C_8H_{18} + aO_2 + 3.78aN_2 \rightarrow 8xCO_2 + 8(1-x)CO + 9yH_2O + 9(1-y)H_2 + 3.78aN_2$$

Comparing the number of atoms of O_2 on each side of the equation:

$$2a = 16x + 8(1-x) + 9y$$

or $$a = 4(1-x) + 4.5y$$

To obtain a second x/y equation, we make use of the fact that the gas is equilibrium during the expansion and is therefore at state-point 4 (Fig. 18) at the end of expansion. Here the relationship for water-gas equilibrium is valid:

$$K_{(w-g)} = y(1-x)/x(1-y) = c$$

A probable temperature at end of expansion T_4, is assumed and the constant c above is thus fixed.

Solution of the two equations gives x and y and hence the composition of the residual gas i.e. the RHS of the reaction equation.

For this programme, the involved iterative calculation of the equilibrium constant is not attempted; as the constituent molar fractions are considered as data-input to the programme.

However, Goodenough and Baker, ref. (18), give results of this calculation for the state points of an Otto cycle using Octane fuel; for various % theoretical air, and at various compression ratios. Their results are reproduced in Table 3 for a CR of 6.5:1.

Taking as an example 75% theoretical air:

$T_4 = 2995^{o}F$, $x_4 = 0.4875$, $y_4 = 0.7620$

$\therefore \quad K_{(w-g)} = c = y(1-x)/x(1-y)$

$= 0.7620(1-0.4875)/0.4875(1-0.7620)$

$= \underline{3.3660}$

and $a = 4(1+x) + 4.5y$

$= 4x1.4875 + 4.5x0.7620$

$= \underline{9.38}$

Thus the reaction equation for 75% theoretical air is:

$$C_8H_{18} + 9.38O_2 + 35.46N_2 \rightarrow 3.9CO_2 + 4.10CO + 6.86H_2O + 2.14H_2 + 35.46N_2$$

i.e. 45.84 moles charge form 52.46 moles products

and F/A ratio is $114/(9.38x32 + 35.46x28) = \underline{0.0882}$

This procedure is repeated for 90% and 100% theoretical air; the resulting reaction equations being listed in Table 3.

Lean Mixtures

With sufficient air, the products at the end of expansion contain relatively little CO and H_2 (assuming a homogeneous mixture with complete combustion). Thus, the residual gas that is mixed with the incoming charge may be considered as being composed of CO_2, H_2O, N_2 and excess O_2.

For 100% theoretical (no excess) air, the chemical reaction equation is:

$$C_8H_{18} + 12.5O_2 + 47.25N_2 \rightarrow 8CO_2 + 9H_2O + 47.25N_2$$

But if there is n% excess air, and air contains 21%O_2 and 79%N_2 by volume, then:

Excess O_2 present = nx12.5+100 = n/8

and N_2 present = ((100+n)/100 x 12.5) x 79/21

= (100+x)/8 x 79/21 by volume

For example, 125% Theor. Air or 25% excess air (n=25) :

Excess O_2 present = 25/8 = 3.125 moles

$\therefore$ O_2 present before combustion = 12.5 + 3.125 = 15.625 moles

and N_2 present = 125/8 x 79/21 = 58.78 Moles

Thus, the modified reaction equation is:

$$C_8H_{18} + 15.625O_2 + 58.78N_2 \rightarrow 8CO_2 + 9H_2O + 58.78N_2 + 3.125O_2$$

i.e. 75.41 moles charge form 78.91 moles products

and F/A ratio is 114/15.625x32 + 58.78x28 = 0.0531

Similarly for other rich mixtures, the resulting equations are listed in Table 3.

5.2.2. Calculation of Constituent Molar Fractions at Various Mixture Strengths

The procedure followed is that of Obert, ref. (19) section 7.1.

e.g. for 90% Theoretical air, the Reaction equation is:

$$C_8H_{18} + 11.25O_2 + 42.529N_2 \rightarrow 6.115CO_2 + 1.885CO + 8.385H_2O + 0.615H_2 + 42.529N_2$$

and multiplying through by molecular weights we have:

114 lb. mol. fuel + 1551. lb. mol. Air $\rightarrow$ 1665 lb. mol. Burned Prods.

Thus, F/A = 114+1551 = 0.0735

Considering 1 lb Air, this gives 1.0736 lb. Mixture; but the incoming charge is diluted in the cylinder by the weight fraction 'f' of residual gases trapped in the clearance space. If this residual fraction is 0.1, say, then the total weight of mixture in the cylinder will be:

0.9 lb Air + (0.9 x 0.0735 = 0.06615) lb Fuel + 0.10735 lb Burned Prods. which, from the reaction equation is equivalent to:

1 x (0.9/1551) = 0.000580 moles C_8H_{18}

11.25x(" ") = 0.006525 moles O_2 (New charge)

42.52x(" ") = 0.024667 moles N_2

and 0.10735 lb Burned Products is equivalent to:

6.115 x (0.10735/1665) = 0.000394 Moles CO_2

1.885 x (0.10735/1665) = 0.000122 Moles CO

8.385 x (0.10735/1665) = 0.000541 Moles H_2O (residual gases)

0.615 x (0.10735/1665) = 0.000040 Moles H_2

42.529 x (0.10735/1665) = 0.002742 Moles N_2

The moles of each constituent are then divided by the total No. of moles in the mixture to give the molar fraction of each constituent. These are listed in Table 4 for each mixture strength considered.

5.2.3. Computed Results

The molar fractions given in Table 4, together with constituent molecular weights, Lennard-Jones parameters and other input data, were submitted with the Programme to the IBM 1620 Computer

of the University. Thermal transport properties were computed from this data at 200F^{o} intervals over the range, 200 to 2000^{o}F as shown by the Output Listings in Appendix 'D'.

Prandtl Numbers from these results have been plotted in Fig. 6 over this temperature range, and show from 2 to 5% to variation with mixture strength.

Rich mixtures can be seen to have the highest (Pr) over the temperature range, whilst only extremely lean mixtures approach the characteristic of air *.

For comparison, Annand's assumption of (Pr) = 0.7 for the mixture is shown in Fig. 6, and can be seen to be inadequate both in its magnitude and in its temperature independance.

* NOTE: This curve for (Pr) AIR was computed in an earlier Stoichiometric Octane calculation, using the same basic Source Programme, but, however, using only 6 constituents in the mixture, i.e. the constituent molar fractions for O_2 and N_2 were combined and called "AIR" in the new charge calculations of 5.2.2.

This Programme became superseded by the present 7 component programme when it was decided to study the effect of mixture strength on the transport properties, i.e. O_2 had to be introduced in the lean mixture calculations.

5.3 Comparison with Other Mixture Data

5.3.1. Data of Taylor and Toong

Taylor and Toong (ref. 18) give graphs of gas temperature as a function of mixture strength with viscosity and conductivity plotted from standard tables for air at these temperatures.

By using their gas temperatures, and by calculating the molar fractions of the various constituents (octane fuel, see Table 4) at the mixture strengths corresponding to these temperatures; it was possible to use the Programme to calculate specific heat,viscosity,conductivity, and Prandtl No. of the true Fuel/Air mixture at each temperature.

A comparison of these results with Fig. 14, P.17 of Ref. 20, is given in Figs. 7 and 8, and shows that over the range of mixture strengths, mixture viscosity is only about 5% lower than that of air; while mixture conductivity is some 10% lower than that for air over the same range. This last figure could be slightly in error due to the Eucken approximation (see section 5.1.1.) and true mixture conductivity therefore, is probably only 5% lower than that of air.

The simplifying assumption of air for the working fluid in Ref. 20 thus seems to be quite valid for viscosity, and conductivity calculations. However, it is recommended that the procedure of this Programme should still be adopted as mixture specific heats are quite different to those for air (Fig. 14) and give rise to Prandtl Numbers bearing little resemblence to (Pr) AIR over the range of temperatures and mixture strengths being considered (Fig. 17).

5.3.2. Data of Pinkel and Zipkin and Sanders

A similar comparison to that in the preceding section was made to compare the thermal properties at two locations of different temperature in an engine.

This was possible through data presented by Taylor Fig. 2 Ref. 21 from Pinkel (Ref. 22) for "Cylinder head" gas temperature; and from Zipkin and Sanders (Ref. 23) for "exhaust-valve temperature" of an aircraft engine as a function of Fuel/Air ratio.

These two sets of temperatures were sampled at various mixture strengths as in 5.3.1.; and used as input temperatures to the Programme (see Figs. 9 to 13). The results show that for 100% difference in temperature over the mixture range, specific heats are different at the two "locations" by only about 10%; viscosities by about 40% conductivities by about 50% and Prandtl Nos. consequently by about 4%.

Thus specific heat and Prandtl No. do not vary greatly but viscosity and conductivity do show a significant spatial variation, due to large temperature differences within the combustion chamber.

5.4 Comparison of Thermal Properties of Stoichiometric Mixtures of Various Types of Fuel over the Temperature Range 200 to 2000°F.

The fuels selected for comparison together with their chemical symbols and petroleum families are:

(1) OCTANE - C_8H_{18} - a Paraffin

(2) BENZENE or BENZOL - C_6H_6 - An Aromatic

(3) ETHYL ALCOHOL or ETHANOL - $C_2H_5(OH)$ - an Alcohol

(4) NITROMETHANE - CH_3NO_2 - an Aliphatic Oxy-Nitrogen derivative.

Since the Specific-Heat polynomial coefficients for all these fuels were listed in Ref. 12 (see Table 1 this paper) the only other input data required was :-

(1) The molecular weights and Lennard-Jones Parameters

and (2) The molar fractions of the various constituents in a stoichiometric fuel-air-residuals mixture of each fuel.

The only difficulty in (1) above was in determining the Lennard-Jones parameters for Nitromethane. These could not be found in any reference data. However, they were eventually estimated by the method shown in Appendix 'A'.

The Lennard-Jones parameters for all the above fuels are listed in Table 2.

Constituent molar fractions as required in (2) above, were found by writing the chemical reaction equations (stoichiometric) as previously for Octane. These equations are listed in Table 6, and the resulting molar fractions are shown in Table 7.

Specific-Heat, Viscosity, Conductivity and Prandtl No. for Stoichiometric mixtures of the above 4 fuels are plotted in Figs. 14 to 17 respectively over the temperature range 200 to 2000^{o}F.

6. CONCLUSION

When compared with the viscosity of air, stoichiometric mixture viscosities predicted by this Programme for all fuels but Nitromethane, showed agreement within 4% over the temperature range 200 - 2000^{o}F.

The viscosity of Nitromethane was 15 - 25% lower than the viscosity of air over the same temperature range.

Similarly, comparing mixture thermal conductivities with those of air, all fuels but Nitromethane agree within 4% but the conductivity of Nitromethane was between 7 and 28% lower than that of air over the temperature range.

Mixture specific heats were between 3 and 25% higher than those for air over the temperature range, depending on the fuel.

This results in mixture Prandtl Nos. being between 5 - 10% greater than those for air. Variation of Fuel/Air ratio (for Octane) from rich to lean gave a further 2 - 5% difference in addition to this over the temperature range.

It was thus found that Annand's assumption of Prandtl Number constant at 0.70 was between 10% and 20% lower over the temperature range 200-2000^{o}F than the Prandtl Nos. predicted by this Programme for the stoichiometric Fuel/Air mixtures of four different fuels.

Although Annand's simple power-law viscosity equation may fit experimental viscosity-temperature curves with engineering accuracy, it is preferable to predict viscosities on a more fundamental basis. The computations involved may be more complex but the use of an automatic digital computer outweighs this objection, at the same time giving a quick accurate solution in a convenient format.

This approach is especially valuable when, for example, the effect of a new fuel on the thermal properties of the mixture is being studied. The calculation procedure is based on inter-molecular force parameters which have been extensively tabulated for most gases. However, if these parameters are not available, they are quite readily estimated from the relevant gas critical properties.

The procedure described is quite flexible in application, being neither limited by the number of constituents in the mixture, nor by the particular chemical species involved.

In fact, the only reason that this Programme was limited to undissociated constituents was that the time period allotted for this investigation precluded programming of the tedious equilibrium-constant calculation necessary for molar fraction determination of of the dissociated constituents.

It is anticipated that an addition to this initial programme to enable dissociated components to be handled will allow Transport Property calculation over the entire engine cycle; thus giving instantaneous properties from a recorded temperature cycle.

It is envisaged that this computational procedure will provide thermal property data for a quasi-steady heat-transfer model to aid in the understanding of instantaneous gas-to-wall heat-transfer.

7. REFERENCES

(1) ANNAND, W.J.D. "Heat Transfer in the cylinders of reciprocating Internal Combustion Engines"; PROC. I. MECH.E., LOND. 1963, 177, 36, P973.

(2) BIRD, R.B., STEWART, W.E., and LIGHTFOOT, E.N., "Notes on Transport Phenomena", WILEY, N.Y., 1958.

(3) KENNARD, E.H., "Kinetic Theory of Gases" McGRAW-HILL, N.Y., 1938.

(4) MAXWELL, J.B., "Data Handbook on Hydrocarbons", VAN NOSTRAND, N.Y., 1951.

(5) HIRSCHFELDER, J.O., CURTISS, C.F., and BIRD, R.B., "Molecular Theory of Gases and Liquids", WILEY, N.Y., 1954.

(6) HIRSCHFELDER, J.O. "Generalisation of the Eucken Approximation for Heat Conductivity of Polyatomic or Chemically reacting gas mixtures", JOINT CONF. I. MECH. E., LOND. ON THERMO. & TRANSPORT PROPERTIES OF FLUIDS, 1957.

(7) HIRSCHFELDER, J.O., - JNL. CHEM. PHYS. 26, 1957 pp 274 - 281.

(8) CURTISS, C.F., and HIRSCHFELDER, J.O., - JNL. CHEM. PHYS. 17, 1949 pp 550 - 555.

(9) BIRD, R.B., HIRSCHFELDER J.O., and CURTISS, C.F. "Theoretical Calculation of the Equations of State and Transport Properties of Gases and Liquids" ASME TRANS. V 76/2, 1954.

(10) JOSHI AND SAXENA, S.C., "Viscosity of Polar Gases" PHYSICA 27, 1961, pp 329 - 336.

(11) EUCKEN, A. - PHYSIK Z 14, 1913, pp 324 - 332.

(12) EDSON, M.H., "The influence of Compression ratio and dissociation on Ideal Otto cycle engine efficiency". SAE JNL, OCT. 1961.

(13) AMERICAN PETROLEUM INSTITUTE - "API Project 44", CARNEGIE INST. TECH. PITTSBURG, Pa.

(14) WILKE, C.R., "A Viscosity equation for Gas mixtures" JNL. CHEM. PHYS. 18, 1950, pp 517 - 519.

(15) REID, R.C., AND SHERWOOD, T.K., "The Properties of Gases and Liquids" McGRAW-HILL, N.Y., 1958, pp 228 - 231.

(16) MASON E.A. AND SAXENA, S.C., "The Physics of Fluids" 1, 1958, pp 361 - 369.

(17) EDULJEE - p 3.214, PERRY'S CHEMICAL ENGINEERING HANDBOOK, 4TH EDITION.

(18) GOODENOUGH, G.A. and BAKER, J.B. "A Thermodynamic Analysis of I.C. Engine Cycles" UNIV. ILLONOIS ENG. EXPT. STN. BULL, 160, 1927.

(19) OBERT, E.F. "Internal Combustion Engines; Analysis and Practice" INTERNATIONAL TEXT BOOK CO. SCRANTON, Pa. 1959.

(20) TAYLOR, C.F. and TOONG, T.Y. "Heat Transfer in I.C. Engines" ASME Paper No. 57-HT-17, 1957.

(21) TAYLOR, C.F. "Heat Transmission in I.C. Engines" IMECH.E/ASME GEN. DISCUSSION ON HEAT TRANSFER, ASME, 1951.

(22) PINKEL, B. "Heat Transfer Processes in Air Cooled Engine Cylinders" NACA TR-612, 1938.

(23) ZIPKIN, M.A. and SANDERS, J.C. "Correlation of Exhaust Valve Temperatures with engine operating conditions" NACA TR-813, 194!

(24) Private communications with Professor C.F. Taylor M.I.T. CAMBRIDGE, MASS.

APPENDIX 'A'

THE POTENTIAL FUNCTION

Only a brief outline as in (2) will be given here, but for the full theoretical development the reader should see (5), (7), (8), (9).

If the Potential Energy of interaction between any pair of molecules, distance 'r' apart, is 'Q'; and the force of interaction between them is 'F'; then the ensuing relation is;

$$F = dQ/dr$$

The exact form of the function Q(r) is not known; but a satisfactory function for elastic collisions between rigid, smooth, spherical, nonpolar molecules is the Lennard-Jones (6-12) Potential:

$$Q(r) = 4\varepsilon\left[\left(\frac{\sigma}{r}\right)^{12} - \left(\frac{\sigma}{r}\right)^{6}\right] \qquad (10) \quad \text{see fig. 1}$$

where

σ = a characteristic molecular diameter (the "collision" diam)

ε = a characteristic energy of interaction between a pair of molecules (the maximum energy of attraction)

r = the molecular separation

r_m = the molecular separation for maximum attraction

Values of σ and ε/k are known and tabulated, (2), (5) for many gases and when unknown can be estimated from the fluid properties at:

(1) The critical point for gases:

$$\varepsilon/k = 0.77\ T_c\ , \quad \sigma = 0.841\tilde{V}_c^{1/3} \quad \text{or} \quad \sigma = 2.44\left(\frac{T_c}{P_c}\right)^{1/3}$$

(2) The boiling point for liquids:

$$\varepsilon/k = 1.15\ T_b\ , \quad \sigma = 1.166\,\tilde{V}_b^{1/3}$$

where

K Is Boltzmann's Constant

ε/K and T are in ^{o}K

σ in Angstrom units ($1\text{Å} = 10^{-10}$ metre)

$\tilde{V}$ in $cm^3/gm.mole$

Pc in ATMOS

INTERMOLECULAR FORCE PARAMETERS AND COLLISION INTEGRAL

In the constituent viscosity calculation, the Lennard-Jones parameters, σ and ε/K were read in as data for each constituent. These were obtained from tabulations in refs. (2), (5) and (7).

When these parameters were not available from reference tables, they were estimated from critical properties.

$$\sigma = 2.44\ (T_c/P_c)^{1/3} \qquad (11)$$

and $$\frac{\varepsilon}{K} = 0.77\ T_c \qquad (12)$$

Some difficulty was experienced in finding critical temperature and pressure for Nitromethane and in this case critical properties were estimated by the method of Eduljee (15) p.3-214:

$$T_c = T_b\ /\ (\Sigma\Delta T/100)\ ) \qquad ^{o}K$$

and $$P_c = 10^4\ M\ /\ (\Sigma\Delta P)^2 \qquad \text{ATMOS}$$

where T_b = Normal boiling point (^{o}K)

M = Molecular weight

and ΔT, Δp represent contributions from the various types of atoms and bonds in the molecular structure being considered.

These estimated critical properties were then used in equations (11) and (12) to give approximate values of the Lennard-Jones force parameters.

The Collision Integral, Ω_μ , was tabulated in (2) as a function of KT/ε This was plotted in the form of a log-log graph and was approximated (Fig. 2) by 3 straight line equations of best fit for the purposes of the program. Curve fitting was carried out by using a standard Polynomial Regression program. (IBM Library Programme 7.0.002).

APPENDIX 'B'

POLAR MOLECULES

Equations (3), (10) are not strictly applicable to polar type or highly elongated molecules e.g. H_2O, NH_3, CH_3OH, NOCl; because of the highly angle-dependent force fields that exist between such molecules.

A Potential Function for simple polar molecules is the 'Stockmayer Potential":

$$Q(r,\theta_1,\theta_2,\phi_2-\phi_1) = 4\varepsilon\left[\left(\frac{\sigma}{r}\right)^{12}-\left(\frac{\sigma}{r}\right)^{6}\right]-\frac{\eta^2}{r^3}\cdot f(\theta_1,\theta_2,\phi_2-\phi_1)$$

in which the r^{-3} term represents the long range attraction between two point dipoles, the mutual orientation of which is described by the function:

$$f(\theta_1,\theta_2,\phi_2-\phi_1) = \left[2\cos\theta_1\cdot\cos\theta_2-\sin\theta_1\sin\theta_2\cdot\cos(\phi_2-\phi_1)\right.$$

η is the dipole moment of a single molecule.

Thus, the more complicated theory based on the Stockmayer Potential should be employed for Polar gases, Hirschfelder, Curtiss and Bird (5) summarise this theory and give values of $\Omega_{v,t}$ as a function of kT/ε and a dimensionless group t * involving the dipole moment.

However, this extension of the molecular theory appears not to have been developed and confirmed for convenient use in the estimation of gas viscosities.

In the absence of the necessary theory at this time, and in view of the fact that H_2O(the only strongly ** polar constituent in the mixture being considered) constitutes only about 1.5% of the mixture by weight; it seems reasonable to use the modified Stockmayer Force

Constants for H_2O as given by (7). These constants were found to give good agreement in form of the viscosity-temperature curve (Fig. 3) for H_2O; but a constant scaling factor was required to reduce the curve to the same order of magnitude as data from Ref. (4).

** The constituent CO is slightly polar for $kT/\varepsilon < 5.0$; i.e. for $T < 531^{\circ}F$. A modified Stockmayer Potential should give better results than the Lennard-Jones Potential. However, Fig. (3) shows good agreement between experimental data of (4) and viscosity and conductivity predicted by using the Lennard-Jones Potential.

APPENDIX 'C'

PRESSURE CORRECTION

It is necessary to determine whether or not the cylinder pressure variation (from approximately 1.0 to 50 atmos) has a significant effect on viscosity.

Two methods have been proposed for doing this:

(1) A method proposed by Reid and Sherwood based on that of Carr, Parent and Peck.

This makes use of reduced viscosity $\mu^{\#} = \mu/\mu_o$, versus reduced pressure, $P_r = P/P_c$ curves for various reduced temperatures, $T_r = T/T_c$; where the subscript c denotes the critical gas condition.

The above correction curves are given in (2) and are applied using Pseudo-critical temperatures and pressures obtained by Kay's Rule:

$$P_c' = \sum_{i=1}^{n} x_i P_{ci} \qquad \text{Then } P_r = P/P_c'$$

$$T_c' = \sum_{i=1}^{n} x_i T_{ci} \qquad T_r = T/T_c'$$

$$\mu_c' = \sum_{i=1}^{n} x_i \mu_{ci}$$

i.e. this rule weights the constituent critical properties according to their molar fraction in the mixture.

The constituent viscosities at the system temperature and pressure are then found by using the reduced viscosity/reduced pressure chart; and these values (which have been weighted by Kay's Rule) are used in the numerator of equation (7).

(2) The method recommended by Bird, Steward & Lightfoot (2) is to calculate the low pressure mixture viscosity by the semi-empirical formula of Wilke:

$$\mu^{\circ}_{Mix} = \sum_{i=1}^{n} \frac{x_i \mu_i}{\sum_{j=1}^{n} x_j \Phi_{ij}}$$

and then, using Kay's Rule for pseudo-critical properties, compute reduced pressures, temperatures and viscosities in terms of P_c', T_c' and μ_c' and use the chart in exactly the same way as for a pure fluid, i.e. $\mu^{\#} = \mu/\mu_o$ is obtained from the chart and this quantity multiplied by μ°_{mix} to give μ_{mix} at systems temperature and pressure. However, considering engine temperatures and pressures neither of these methods of pressure correction were warranted owing to the small pressure and temperature ranges considered.

It can be seen however, that if necessary a pressure correction can be quite easily inserted into the programme once the critical conditions are known and the reduced viscosity-pressure-temperature charts are approximated by equations of best fit.

TABLE 1 COEFFICIENTS FOR COMPUTING Cp AT $T^{\circ}K$

$$Cp(J) = A(J) + B(J)T + C(J)T^2 + D(J)T^3 + E(J)T^4 + F(J)T^5$$

J	A(J)	B(J)	C(J)	D(J)	E(J)	F(J)
DRY AIR	0.6126880E 01	0.2581011E-02	-0.1004231E-05	0.2167687E-09	-0.2444707E-13	0.1126386E-17
O_2	0.6014893E 01	0.3832211E-02	0.2106804E-05	0.6449786E-09	0.9553103E-13	0.5355434E-17
N_2	0.6170795E 01	0.2272505E-02	-0.7181618E-06	0.1037995E-09	-0.5571979E-14	0.
CO	0.6133285E 01	0.2539359E-02	0.8839086E-06	0.1399667E-09	-0.8205784E-14	0.
CO_2	0.6039775E 01	0.1208784E-01	-0.6892165E-05	0.1979687E-08	-0.2758421E-12	0.1483168E-16
H_2O	0.6987605E 01	0.2855764E-02	0.4082449E-06	-0.4530978E-09	0.9097223E-13	-0.5813041E-17
H_2	0.7034649E 01	-0.7481993E-03	0.1414508E-06	-0.5232309E-09	0.8176101E-13	-0.4673767E-17
i C_8H_{18}	0.2547736E 01	0.1536359E 00	-0.1333815E-04	-0.9377068E-07	0.7097913E-10	-0.1649594E-13
C_6H_6	-0.1062471E 02	0.1258172E 00	-0.8972832E-04	0.2003337E-07	0.8539103E-11	-0.3871192E-14
$C_2H_5(OH)$	0.2328293E 01	0.8250851E-01	-0.9886384E-04	0.9734339E-07	-0.5614683E-10	0.1291466E-13
CH_3NO_2	0.2914160E-01	0.3805755E-01	0.1122153E-05	-0.3146385E-07	0.2270921E-10	-0.5169621E-14

TABLE 2 LENNARD-JONES PARAMETERS

		M.W.	σ	ε/κ
	AIR	28.966	3.617	97.0
O_2	OXYGEN	32.0	3.433	113.0
N_2	NITROGEN	28.016	3.681	91.5
CO	CARBON MONOXIDE	28.011	3.641	101.2
CO_2	CARBON DIOXIDE	44.011	3.996	190.0
H_2O	WATER VAPOUR	18.016	3.059	231.7
H_2	HYDROGEN	2.016	2.915	38.0
C_8H_{18}	ISO OCTANE	114.14	7.451	320.0
C_6H_6	BENZENE	78.11	5.270	440.0
$C_2H_5(OH)$	ETHANOL	46.0	4.455	391.0
CH_3NO_2	NITROMETHANE	61.04	4.160	430.0

TABLE 3

Equilibrium Constants for various OCTANE mixture strengths at 6.5:1 CR
From Goodenough & Baker Ref. (18) Table No. 2 P38-39

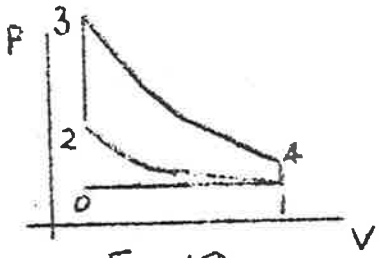

Fig 18

% AIR	T_1	P_1	T_2	P_2	T_3	P_3	x_3	y_3	T_4	P_4	x_4	y_4
75	594	14.7	1066	171.5	4810	882.3	0.4058	0.8333	2995	84.5	0.4875	0.7620
90	601		1098	174.6	5121	886.2	0.6925	0.9474	3355	89.0	0.7644	0.9317
100	605		1117	176.4	5108	863.4	0.8150	0.9724	3553	91.3	0.9858	0.9969
110	600		1119	178.2	4995	842.3	0.8868	0.9838	3327	85.6	0.9987	0.9997
125	595		1123	180.3	4774	803.5	0.9453	0.9927	3029	78.2	1.0000	1.000
150	595		1139	182.9	4406	734.4	0.9835	0.9988	2655	68.0	1.0000	1.000

TABLE 4

REACTION EQUATIONS FOR i-OCTANE OF VARIOUS MIXTURE STRENGTHS

%THEO.AIR	F/A	REACTION EQUATION
75	0.0882	$C_8H_{18} + 9.38O_2 + 35.46N_2 \rightarrow 3.9CO_2 + 4.1CO + 6.86H_2O + 2.14H_2 + 35.46N_2$
90	0.0735	$C_8H_{18} + 11.25O_2 + 42.529N_2 \rightarrow 6.115CO_2 + 1.885CO + 8.385H_2O + 0.615H_2 + 42.529N_2$
100	0.0665	$C_8H_{18} + 12.5O_2 + 47.25N_2 \rightarrow 8CO_2 + 9.0H_2O + 47.25N_2$
110	0.0604	$C_8H_{18} + 13.75O_2 + 51.726N_2 \rightarrow 8CO_2 + 1.25O_2 + 9.0H_2O + 51.726N_2$
125	0.0531	$C_8H_{18} + 15.625O_2 + 58.78N_2 \rightarrow 8.0CO_2 + 3.125O_2 + 9.0H_2O + 58.78N_2$
150	0.0443	$C_8H_{18} + 18.75O_2 + 70.54N_2 \rightarrow 8.0CO_2 + 6.25O_2 + 9.0H_2O + 70.54N_2$

TABLE 5

CONSTITUENT MOLAR FRACTIONS FOR i-OCTANE OF VARIOUS MIXTURE STRENGTHS

% THEO. AIR	O_2	N_2	CO	CO_2	H_2O	C_8H_{18}	H_2
75	0.18888	0.76939	0.00688	0.00656	0.01151	0.01511	0.00167
90	0.183229	0.769670	0.003426	0.011064	0.015192	0.016287	0.001123
100	0.185237	0.772010	0.0	0.013159	0.014796	0.014796	0.0
110	0.187068	0.774022	0.0	0.011972	0.013469	0.013469	0.0
125	0.189753	0.775910	0.0	0.010575	0.011879	0.011879	0.0
150	0.193127	0.778240	0.0	0.008797	0.009903	0.009316	0.0

TABLE 6

REACTION EQUATIONS FOR VARIOUS FUELS (STOICHIO. F/A)

FUEL	SYMBOL	MW	EQUATION
ISOOCTANE	C_8H_{18}	114.2	$C_8H_{18} + 12.5O_2 + 47N_2 \rightarrow 8CO_2 + 9H_2O + 47N_2$
BENZENE	C_6H_6	78.1	$C_6H_6 + 7.5O_2 + 28.2N_2 \rightarrow 6CO_2 + 3H_2O + 28.2N_2$
ETHANOL	$C_2H_5(OH)$	46.0	$C_2H_5(OH) + 3O_2 + 11.3N_2 \rightarrow 2CO_2 + 3H_2O + 11.3N_2$
NITROMETHANE	CH_3NO_2	61.04	$CH_3NO_2 + 0.75O_2 + 2.82N_2 \rightarrow CO_2 + 1.5H_2O + 3.32N_2$

TABLE 7

CONSTITUENT MOLAR FRACTIONS FOR VARIOUS FUELS (STOICHIO F/A)

FUEL	(F/A) STOICHIO	COMPONENT	MOLAR FRACTION
ISO OCTANE	= 0.067	C_8H_{18}	0.014796
		O_2	0.185237
		N_2	0.772010
		CO_2	0.013159
		H_2O	0.014796
BENZENE	= 0.076	C_6H_6	0.024496
		O_2	0.183660
		N_2	0.767376
		CO_2	0.016312
		H_2O	0.008156
ETHANOL	= 0.111	$C_2H_5(OH)$	0.058441
		O_2	0.175322
		N_2	0.733815
		CO_2	0.012969
		H_2O	0.019453
NITROMETHANE	= 0.594	CH_3NO_2	0.191669
		O_2	0.143741
		N_2	0.611288
		CO_2	0.021321
		H_2O	0.031981

TABLE 8.

```
C       G.A.MORGAN/FOWLER MECH ENG DEPT U OF A  TEL 461
C       OTTO CYCLE COMPRESSION MIXTURE TRANSPORT PROPERTIES
C       PROGRAMME NO  015/1620
      DIMENSIONW(7),X(7),S(7),EK(7),AK(7),F(7),E(7),D(7),C(7),B(7),A(7)
      DIMENSIONDK(7),PR(7),CP(7),U(7)
  010 FORMAT(1H1,9X,44HTHERMAL TRANSPORT PROPERTIES OF CONSTITUENTS)
  020 FORMAT(1H0,13X,41HAND MIXTURE DURING OTTO CYCLE COMPRESSION)
  030 FORMAT(1H0,8HRUN NO.=,I3)
  040 FORMAT(49H                                                  )
  110 FORMAT(1H0,5HTEMP=,F8.2)
  120 FORMAT(1H0,13X,2HCP,15X,1HU,15X,2HSK,15X,2HPR)
  130 FORMAT(1H0,2HO2,8X,E10.3,6X,E10.3,6X,E10.3,6X,E10.3)
  140 FORMAT(1H0,2HN2,8X,E10.3,6X,E10.3,6X,E10.3,6X,E10.3)
  150 FORMAT(1H0,2HCO,8X,E10.3,6X,E10.3,6X,E10.3,6X,E10.3)
  160 FORMAT(1H0,3HCO2,7X,E10.3,6X,E10.3,6X,E10.3,6X,E10.3)
  170 FORMAT(1H0,3HH2O,7X,E10.3,6X,E10.3,6X,E10.3,6X,E10.3)
  180 FORMAT(1H0,5HC8H18,5X,E10.3,6X,E10.3,6X,E10.3,6X,E10.3)
  185 FORMAT(1H0,2HH2,8X,E10.3,6X,E10.3,6X,E10.3,6X,E10.3)
  190 FORMAT(1H0,3HMIX,7X,E10.3,6X,E10.3,6X,E10.3,6X,E10.3)
  200 PUNCH010
      PUNCH020
      READ,NRUN
      PUNCH030,NRUN
      READ040
      PUNCH040
      READ,NT,NCON
      READ,W(1),W(2),W(3),W(4),W(5),W(6),W(7)
      READ,X(1),X(2),X(3),X(4),X(5),X(6),X(7)
      READ,S(1),S(2),S(3),S(4),S(5),S(6),S(7)
      READ,EK(1),EK(2),EK(3),EK(4),EK(5),EK(6),EK(7)
      READ,AK(1),AK(2),AK(3),AK(4),AK(5),AK(6),AK(7)
      READ,F(1),F(2),F(3),F(4)
      READ,F(5),F(6),F(7)
```

```
      READ,E(1),E(2),E(3),E(4)
      READ,E(5),E(6),E(7)
      READ,D(1),D(2),D(3),D(4)
      READ,D(5),D(6),D(7)
      READ,C(1),C(2),C(3),C(4)
      READ,C(5),C(6),C(7)
      READ,B(1),B(2),B(3),B(4)
      READ,B(5),B(6),B(7)
      READ,A(1),A(2),A(3),A(4)
      READ,A(5),A(6),A(7)
      NTEMP=0
  210 READ,T
      NTEMP=NTEMP+1
      WMIX=0.0
      CPMIX=0.0
      DO220J=1,NCON
      IF(X(J))250,208,209
  208 CP(J)=0.0
      U(J)=0.0
      DK(J)=0.0
      PR(J)=0.0
      GOTO219
  209 TT=(T-32.0)/1.8+273.0
      CP(J)=((((F(J)*TT+E(J))*TT+D(J))*TT+C(J))*TT+B(J))*TT+A(J)
      CP(J)=CP(J)/W(J)
      EX=TT/EK(J)
      IF(EX-2.0)211,211,212
  211 Y=4.772*(10.0*EX)**(-0.4741428)
      GOTO215
  212 IF(EX-5.0)213,213,214
  213 Y=2.471*(10.0*EX)**(-0.2529181)
      GOTO215
  214 Y=1.648*(10.0*EX)**(-0.1495001)
  215 U(J)=17.936895E-07*SQRTF(W(J)*TT)/((S(J)**2.0)*Y)
      U(J)=U(J)/AK(J)
      DK(J)=U(J)*(CP(J)+2.48072/W(J))
```

```
      PR(J)=CP(J)*U(J)/DK(J)
  219 WMIX=WMIX+X(J)*W(J)
  220 CPMIX=CPMIX+X(J)*W(J)*CP(J)
      CPMIX=CPMIX/WMIX
      UMIX=0.0
      DKMIX=0.0
      DO240J=1,NCON
      SXPHI=0.0
      DO230K=1,NCON
      R=W(J)/W(K)
      IF(U(K))250,230,225
  225 PHI=(1.0+SQRTF(U(J)/U(K))/R**0.25)**2
      PHI=0.353553*PHI/SQRTF(1.0+R)
      SXPHI=SXPHI+X(K)*PHI
  230 CONTINUE
      UMIX=UMIX+X(J)*U(J)/SXPHI
      DKMIX=DKMIX+X(J)*DK(J)/SXPHI
  240 PRMIX=CPMIX*UMIX/DKMIX
      PUNCH110,T
      PUNCH120
      PUNCH130,CP(1),U(1),DK(1),PR(1)
      PUNCH140,CP(2),U(2),DK(2),PR(2)
      PUNCH150,CP(3),U(3),DK(3),PR(3)
      PUNCH160,CP(4),U(4),DK(4),PR(4)
      PUNCH170,CP(5),U(5),DK(5),PR(5)
      PUNCH180,CP(6),U(6),DK(6),PR(6)
      PUNCH185,CP(7),U(7),DK(7),PR(7)
      PUNCH190,CPMIX,UMIX,DKMIX,PRMIX
      IF(NTEMP-NT)210,200,250
  250 STOP
      END
```

NO.	ITEM	DESCRIPTION	UNITS	FORMAT	REQD.	REMARKS
INPUT DATA						
1	NRUN	Output identification No.	-	XX	1	
2	NT	No. of temperatures for which properties desired	-	XXX	1	
3	NCON	No. of constituent gases in mixture	-	x	1	This No. must be 7 whether all constituents present or not
4	W(J)	Molecular weight of jth constituent	lb. mol.	XXX.XXX	NCON	See Table 2
5	X(J)	Molar Fraction of jth constituent	-	X.XXXXXX	"	See Table 5,7
6	S(J)	Lennard-Jones parameter σ of jth constituent	^{o}A	X.XXX	"	See Table 2
7	EK(J)	Lennard-Jones parameter ε/k of jth constituent	^{o}K	XXX.X	"	See Table 2
8	AK(J)	Magnitude correction factor for mixture α	-	X.X	"	To correct Polar gases (esp. H_2O)
9	F(J)	5th order Poly. coeff.	cal/mole.^{o}K	$\pm$(X.XXXXXXX)$10^{\pm xx}$	"	See Table 1
10	E(J)	4th order " "	"	"	"	"
11	D(J)	3rd order " "	"	"	"	"
12	C(J)	2nd order " "	"	"	"	"
13	B(J)	1st order " "	"	"	"	"
14	A(J)	Zeroth order "	"	"	"	"
15	T	Temperature at which transport properties reqd.	^{o}F	XXXX.XX	NT	Limited to range 0-2200^{o}F

NO.	ITEM	DESCRIPTION	UNITS	FORMAT	REQD.	REMARKS
OUTPUT	CP(J)	Specific heat (at constant pressure) of jth constituent	BTU/lb.^{o}F	(X.XXX)10$^{\pm xx}$	NCØN	See Eqn.10
16						
17	U(J)	Dynamic viscosity of jth constituent	lb/ft.sec.	"	"	See Eqn. 3, 11
18	DK(J)	Thermal conductivity of jth constituent	BTU/ft.sec.^{o}F	"	"	See Eqn. 6, 12
19	PR(J)	Prandtl Number of jth constituent	-	"	"	See Eqn. 13
20	CPMIX	Specific heat (at constant pressure) of mixture	BTU/lb.^{o}F	(X.XXX)10$^{\pm xx}$	1	See Eqn. 15
21	UMIX	Dynamic Viscosity of mixture	lb/ft.sec.	"	1	See Eqn. 7, 16
22	DKMIX	Thermal conductivity of mixture	BTU/ft.sec.^{o}F	"	1	See Eqn. 9, 18
23	PRMIX	Prandtl Number of mixture	-	"	1	See Eqn. 19
COMPUTATION						
24	NTEMP	Temperature cycle counter	-			1st set NTEMP = 0 LAST NTEMP = NT
25	TT	Absolute Temperature	^{o}K			
26	EX	Ratio: Absolute Temp./ Lennard-Jones ε/k	-		(	See Fig. 1
27	Y	Lennard-Jones Collison Integral $\Omega_{11} = f(kT/\varepsilon)$	-		(	
28	WMIX	Molecular weight of mixture	lb.mol			See Eqn. 14
29	R	Ratio W(J)/W(K)	-		(	
30	W(K)	Mol. weight of kth constituent	lb.mol		(	See Eqn. 17
31	X(K)	Molar fraction " " "	-		(	
32	U(K)	Dynamic viscosity" " "	lb/ft.sec.		(	
33	PHI	Equation 17	-			
34	SXPHI	Denominator of Equation 17	-			

* If any of the 7 constituents are not present in the mixture it is only necessary to put X(J) = 0 0

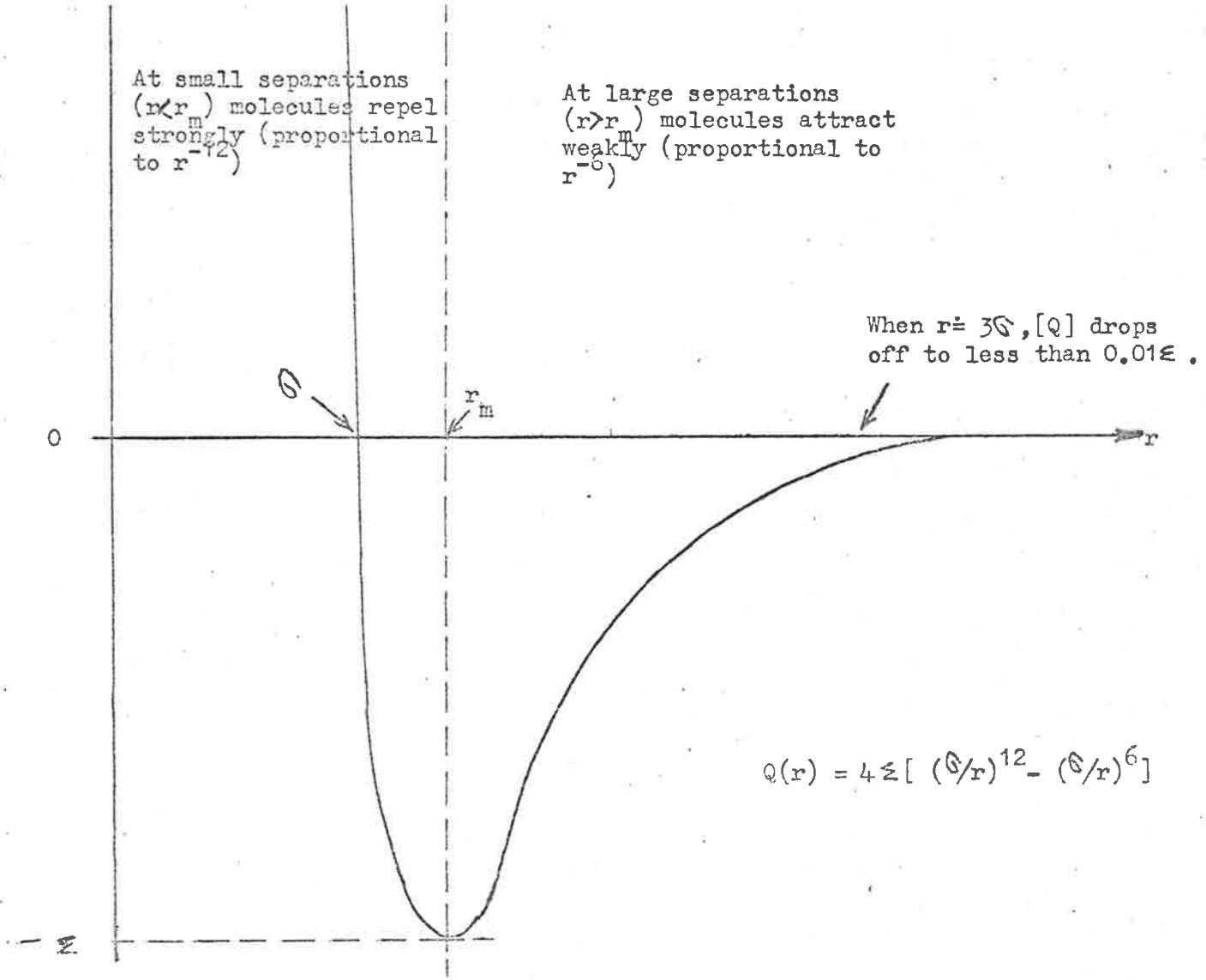

FIG.1 THE LENNARD-JONES POTENTIAL FUNCTION (FROM REF.2)

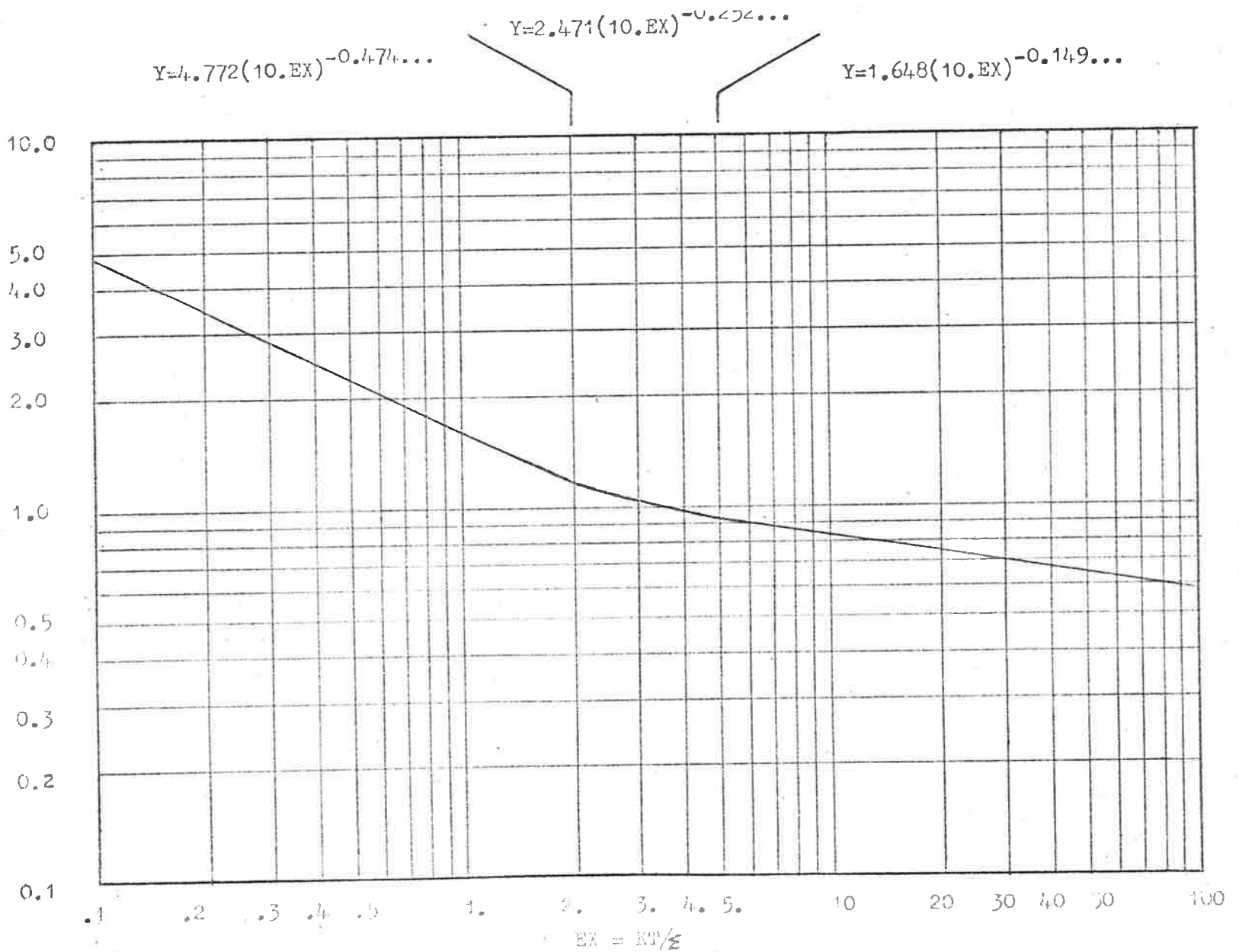

FIG.2 COLLISION INTEGRAL PLOTTED FROM REF.2, TABLE B2.

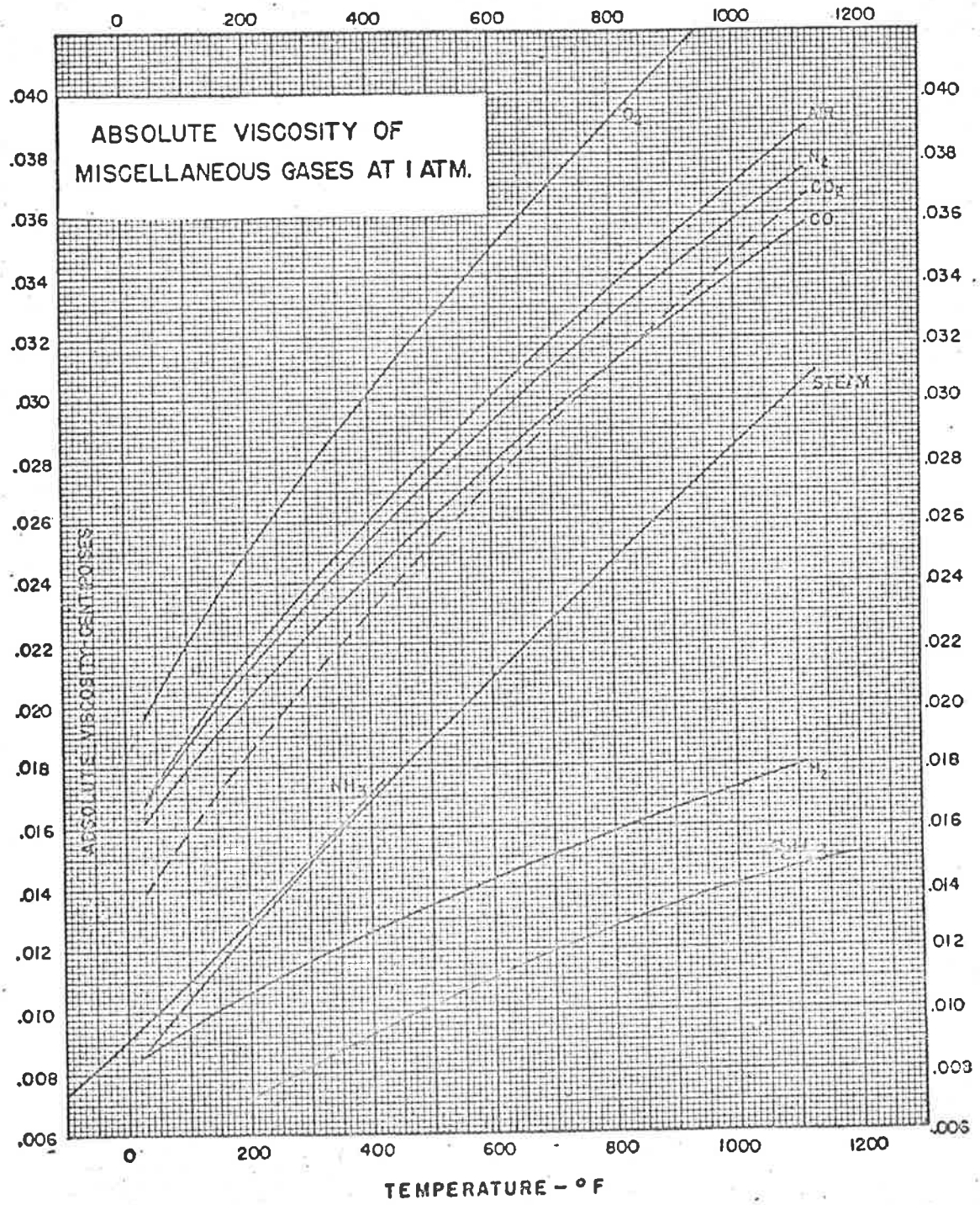

FIG. 3a CONSTITUENT VISCOSITIES REPRINTED FROM REF. 4

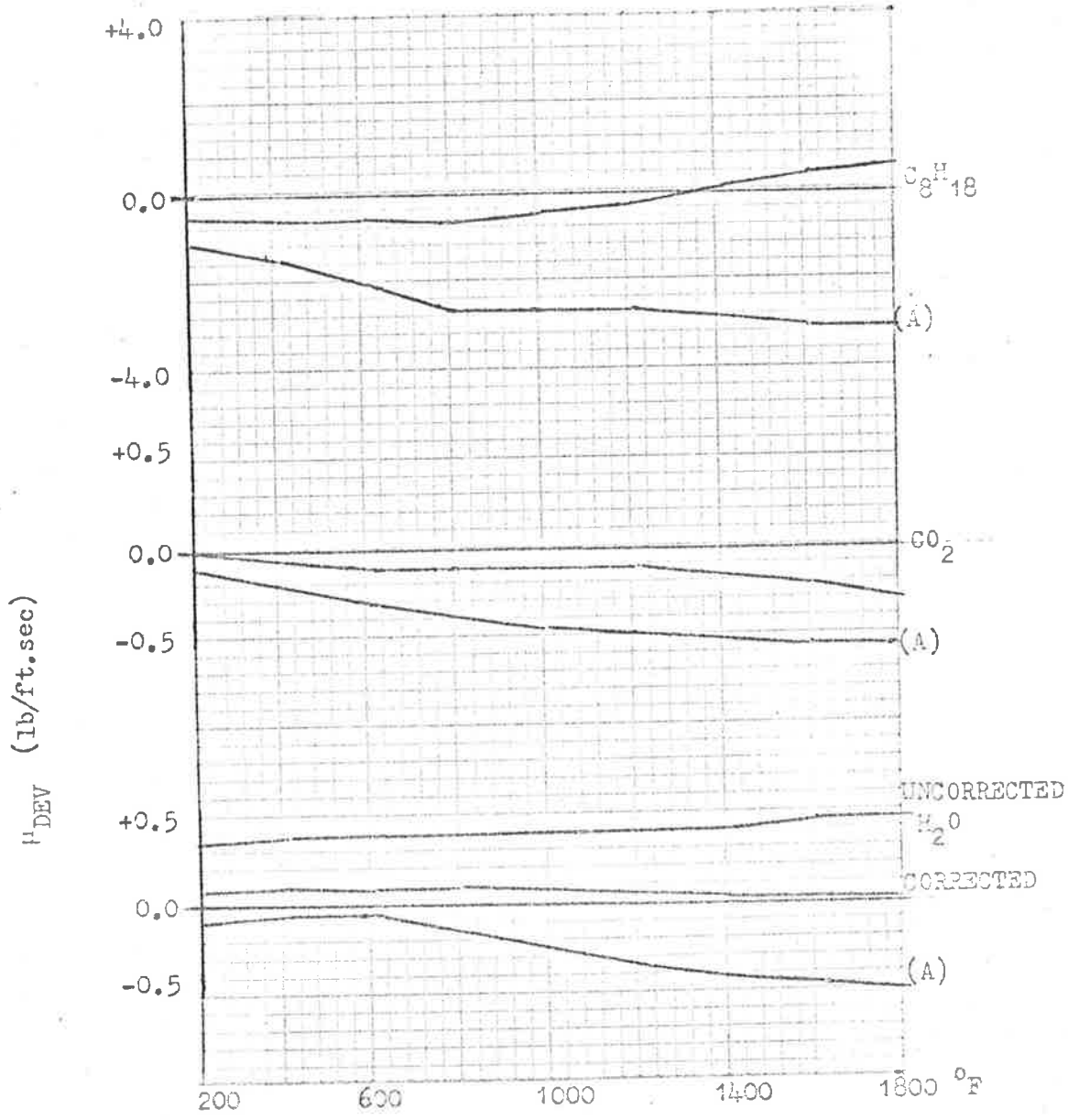

FIG. 3b DEVIATIONS OF COMPUTED CONSTITUENT VISCOSITIES FROM DATA OF REF.4

$$\mu_{DEV} = (\mu_{ref.4} - \mu_{calc.})$$

DEVIATIONS FOR H_2, O_2, AIR, & N_2 WERE 2% OVER THE RANGE WHILE CO DEVIATED 2% - 6%.

(A) SHOWS DEVIATION OF μ CALCULATED FROM $\mu = \mu_o T^m$.

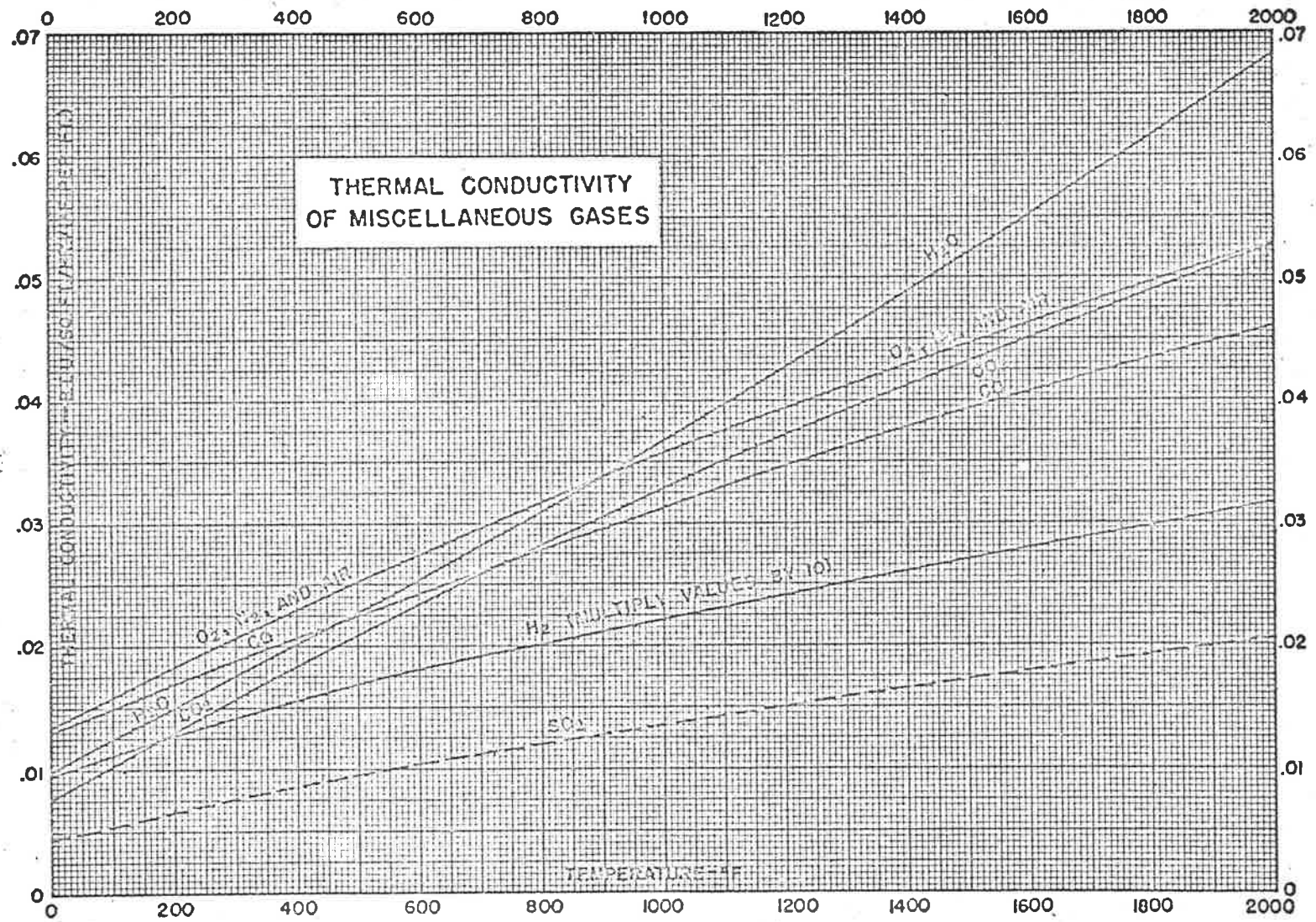

FIG.4a CONSTITUENT CONDUCTIVITIES REPRINTED FROM REF.4

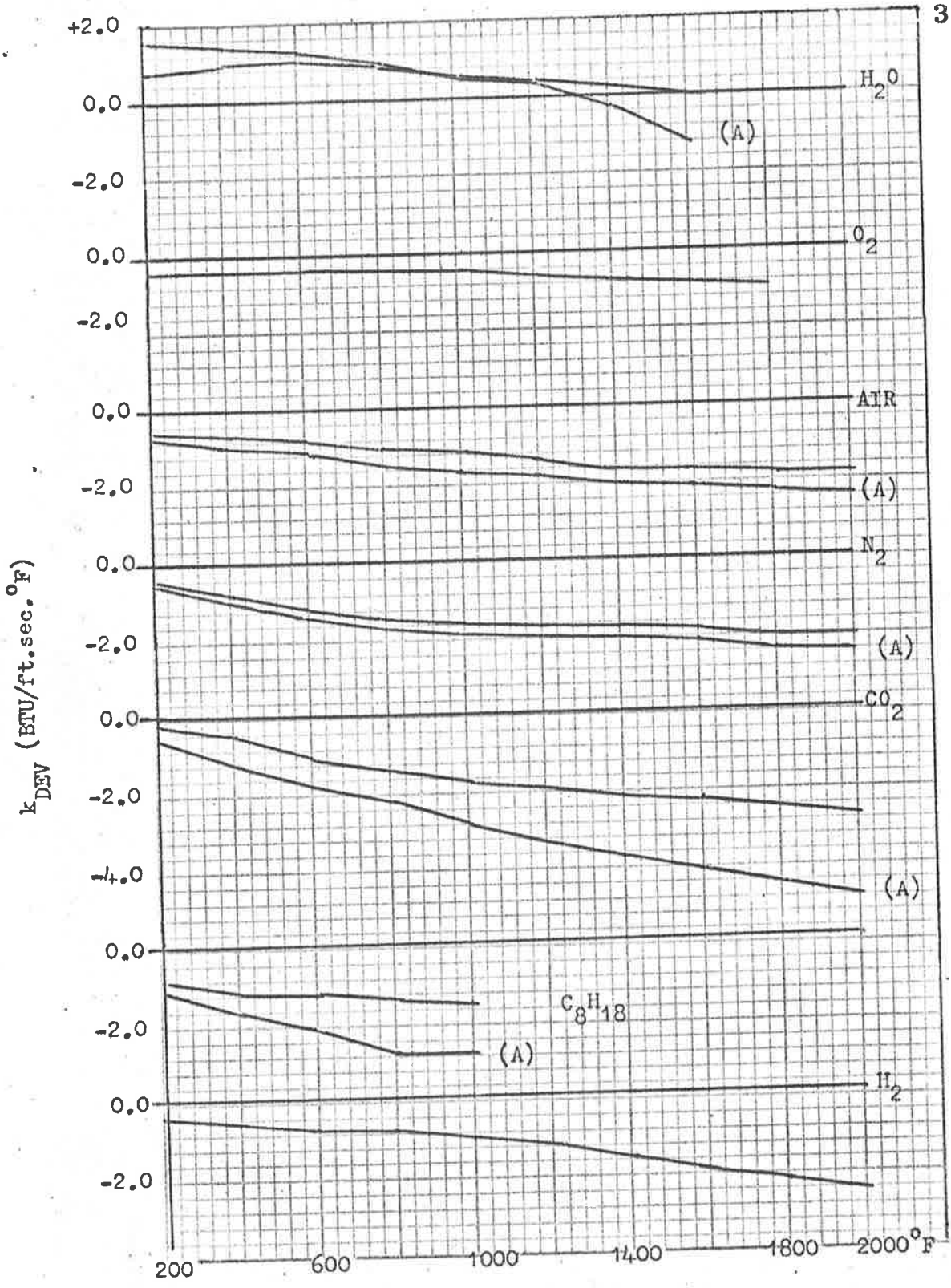

FIG. 4b DEVIATIONS OF COMPUTED CONSTITUENT THERMAL CONDUCTIVITIES FROM DATA OF REF.4

$$k_{DEV} = (k_{ref.4} - k_{calc.})$$

DEVIATION OF CO WAS ZERO.
(A) SHOWS DEVIATION OF k CALCULATED FROM THE EUCKEN EQN. BUT USING VISCOSITY FROM $\mu = \mu_o T^m$.

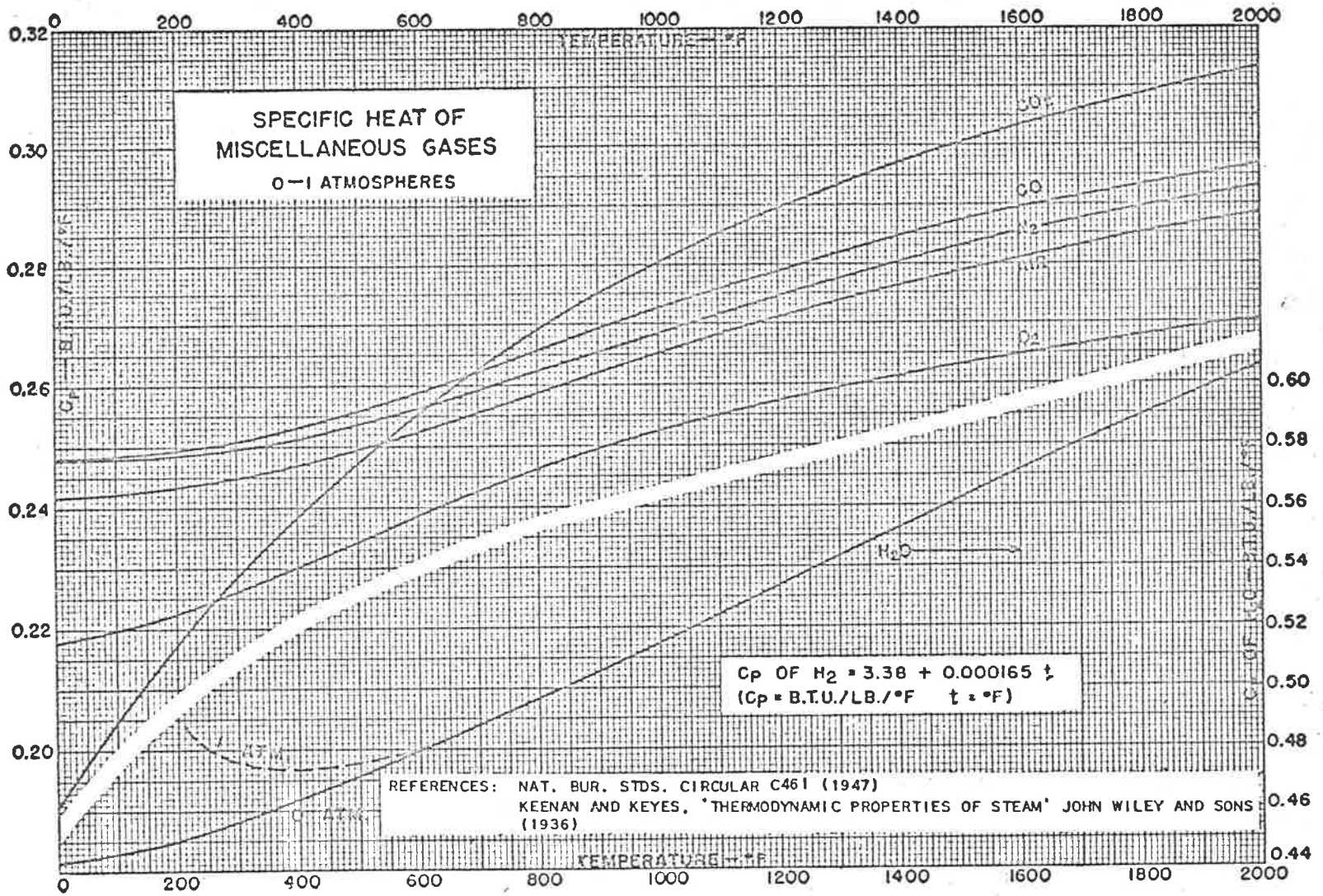

FIG.5 CONSTITUENT SPECIFIC HEATS REPRINTED FROM REF.4

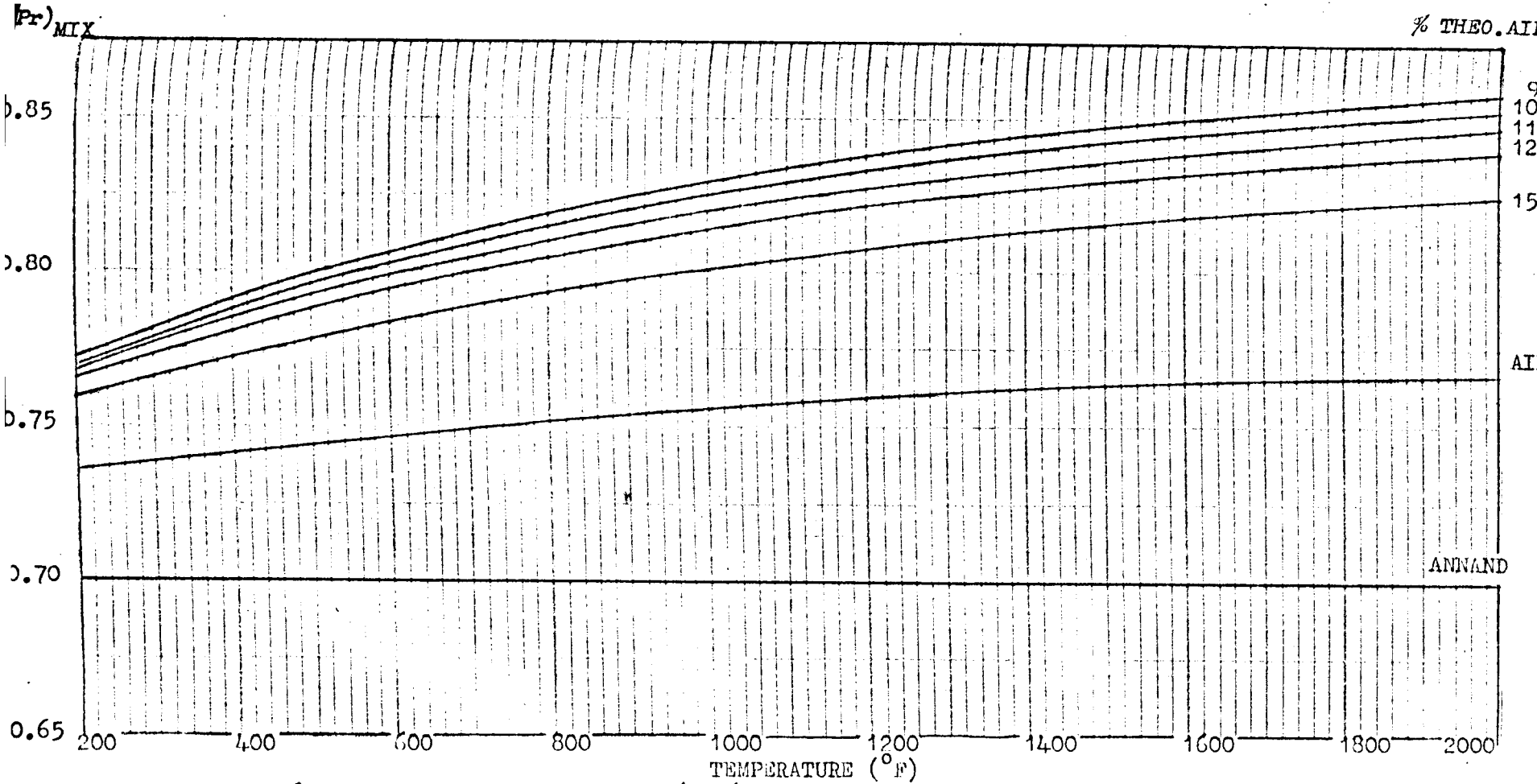

FIG.6 PRANDTL NO. OF OCTANE/AIR/RESIDUALS MIXTURE OF VARIOUS STRENGTHS.

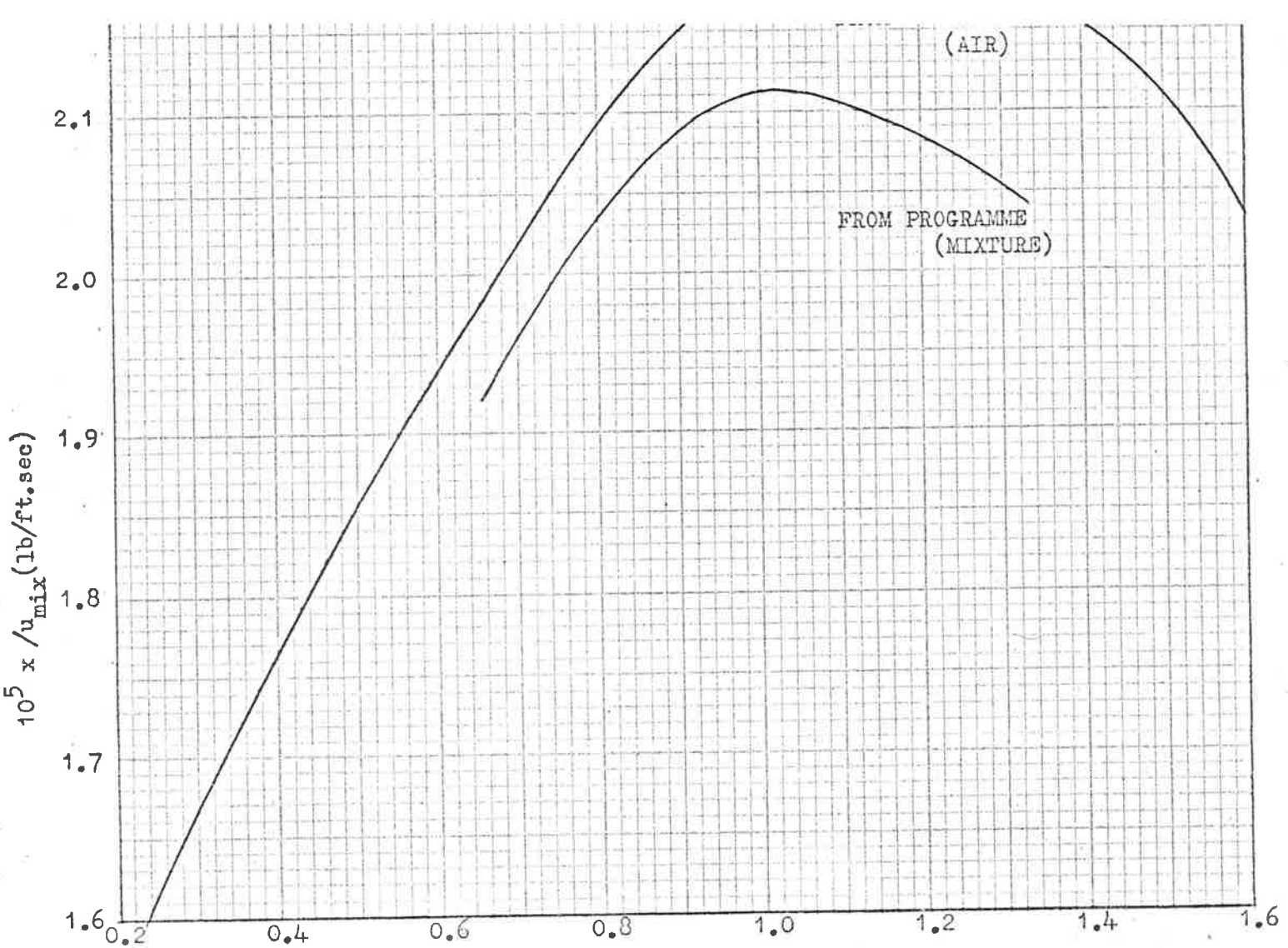

FIG.7 MIXTURE VISCOSITY(OCTANE) OF VARIOUS STRENGTHS COMPARED WITH DATA OF REF.18 FOR AIR AT SAME TEMPERATURE.

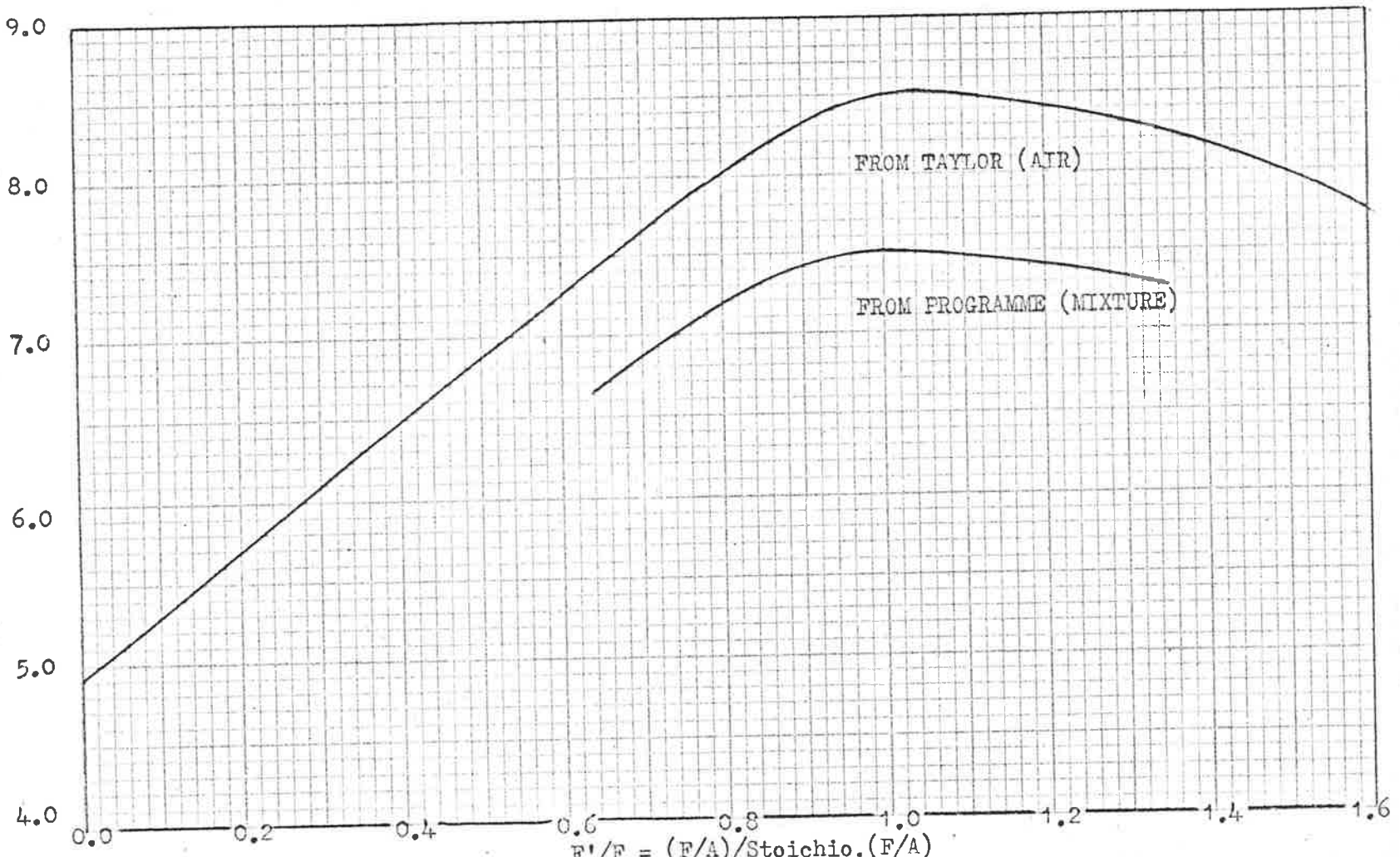

FIG.8 MIXTURE CONDUCTIVITY (OCTANE OF VARIOUS STRENGTHS) COMPARED WITH DATA OF REF.18 FOR AIR AT SAME TEMPERATURE.

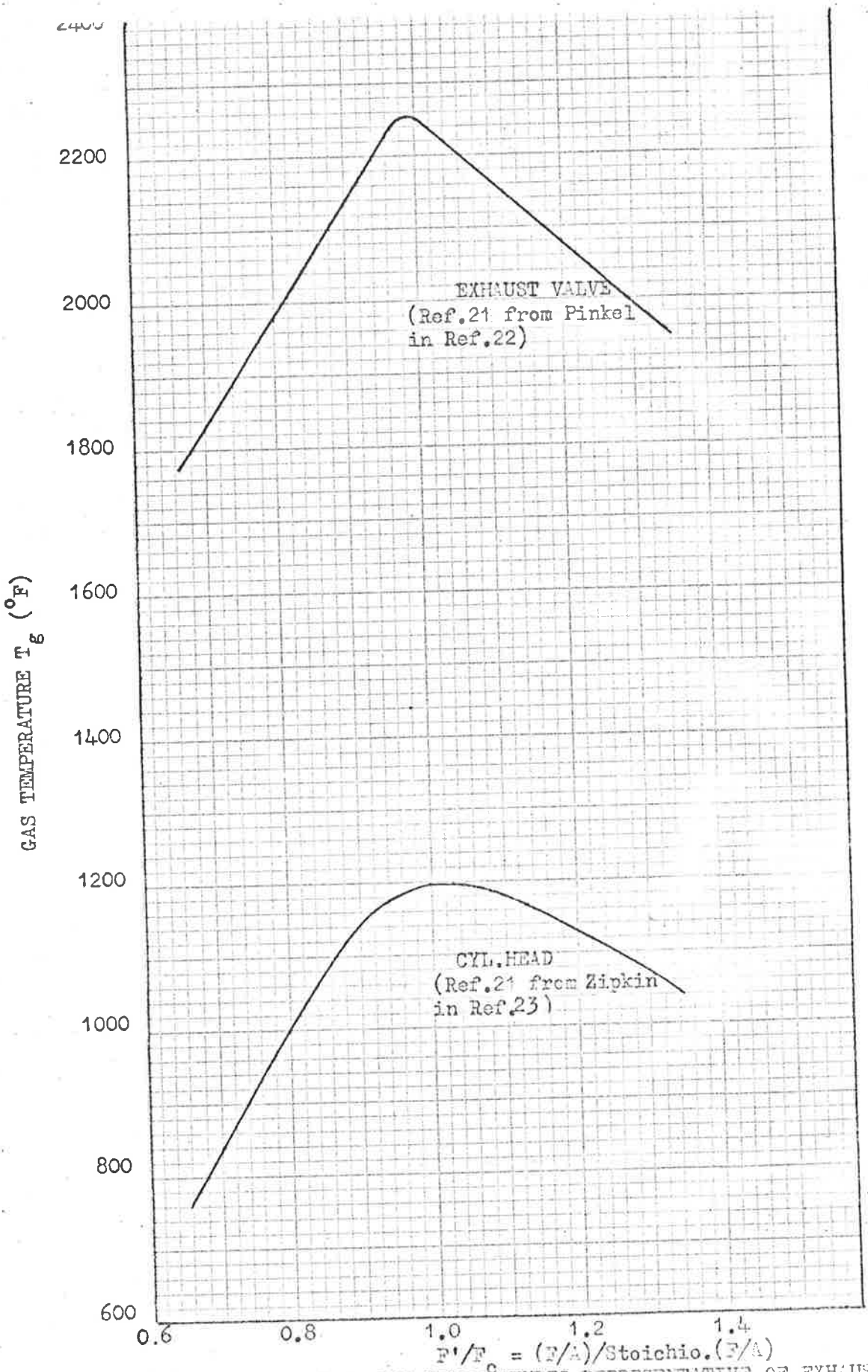

FIG.9 GAS TEMPERATURES REPRESENTATIVE OF EXHAUST-VALVE AND 'CYLINDER-HEAD' LOCATIONS FROM REF.21.

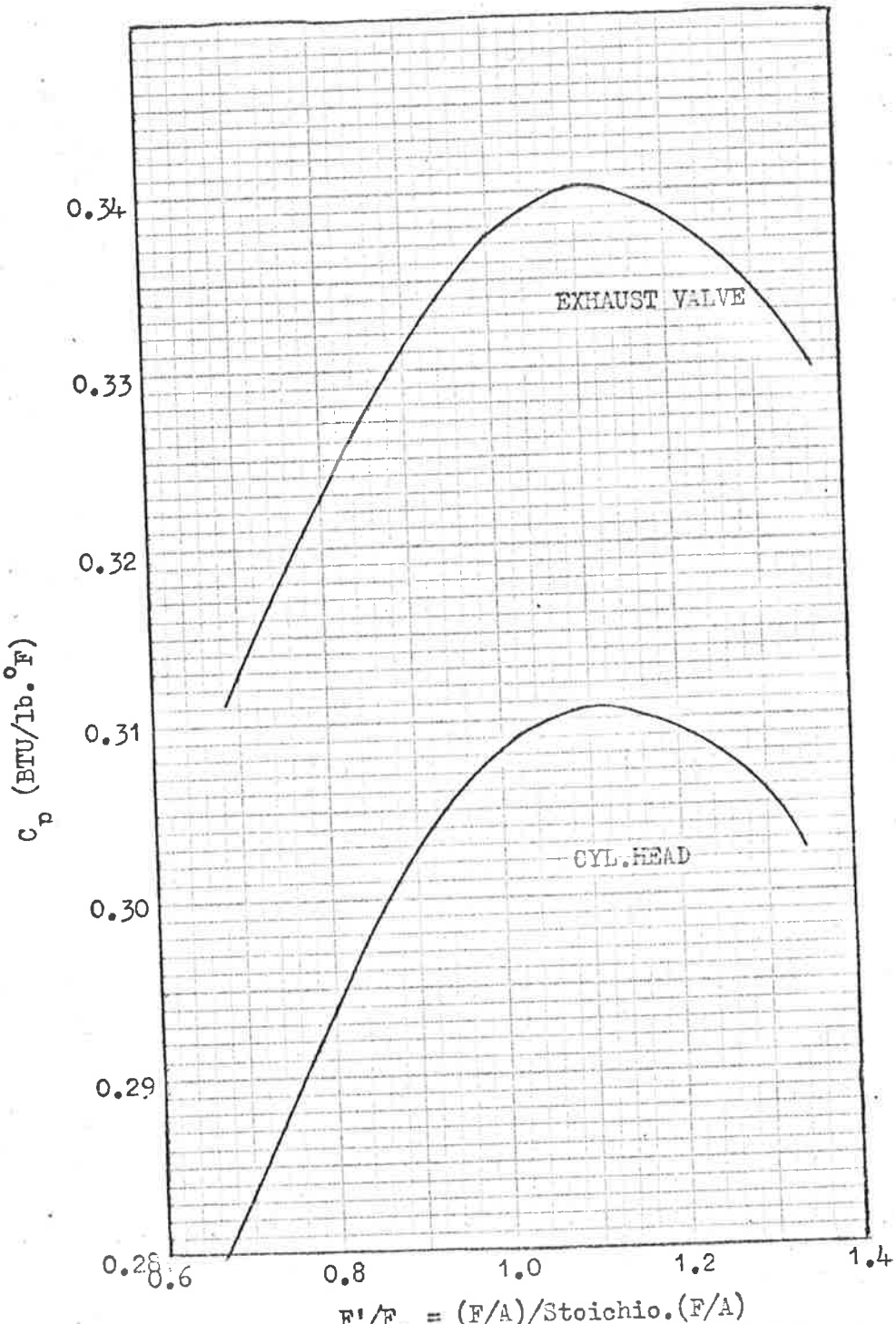

FIG.10 SPECIFIC HEATS FROM TEMPERATURES REPRESENTATIVE OF EXHAUST VALVE AND 'CYLINDER-HEAD' LOCATIONS(REFS.21,22,23) AS A FUNCTION OF OCTANE MIXTURE STRENGTH.

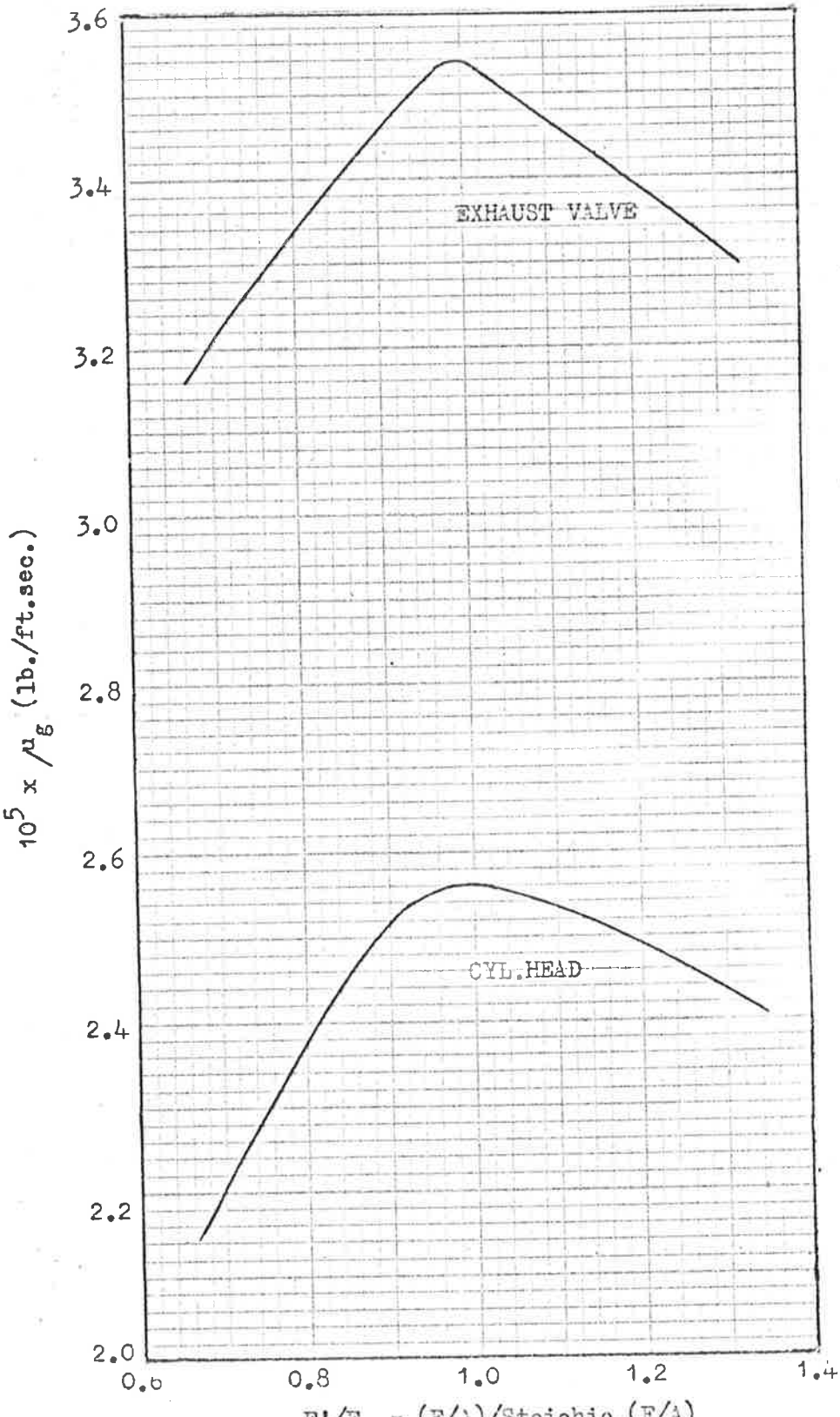

FIG.11 GAS VISCOSITIES FROM TEMPERATURES REPRESENTATIVE OF EXHAUST VALVE AND 'CYLINDER-HEAD' LOCATIONS (REFS.21,22,23) AS A FUNCTION OF OCTANE MIXTURE STRENGTH.

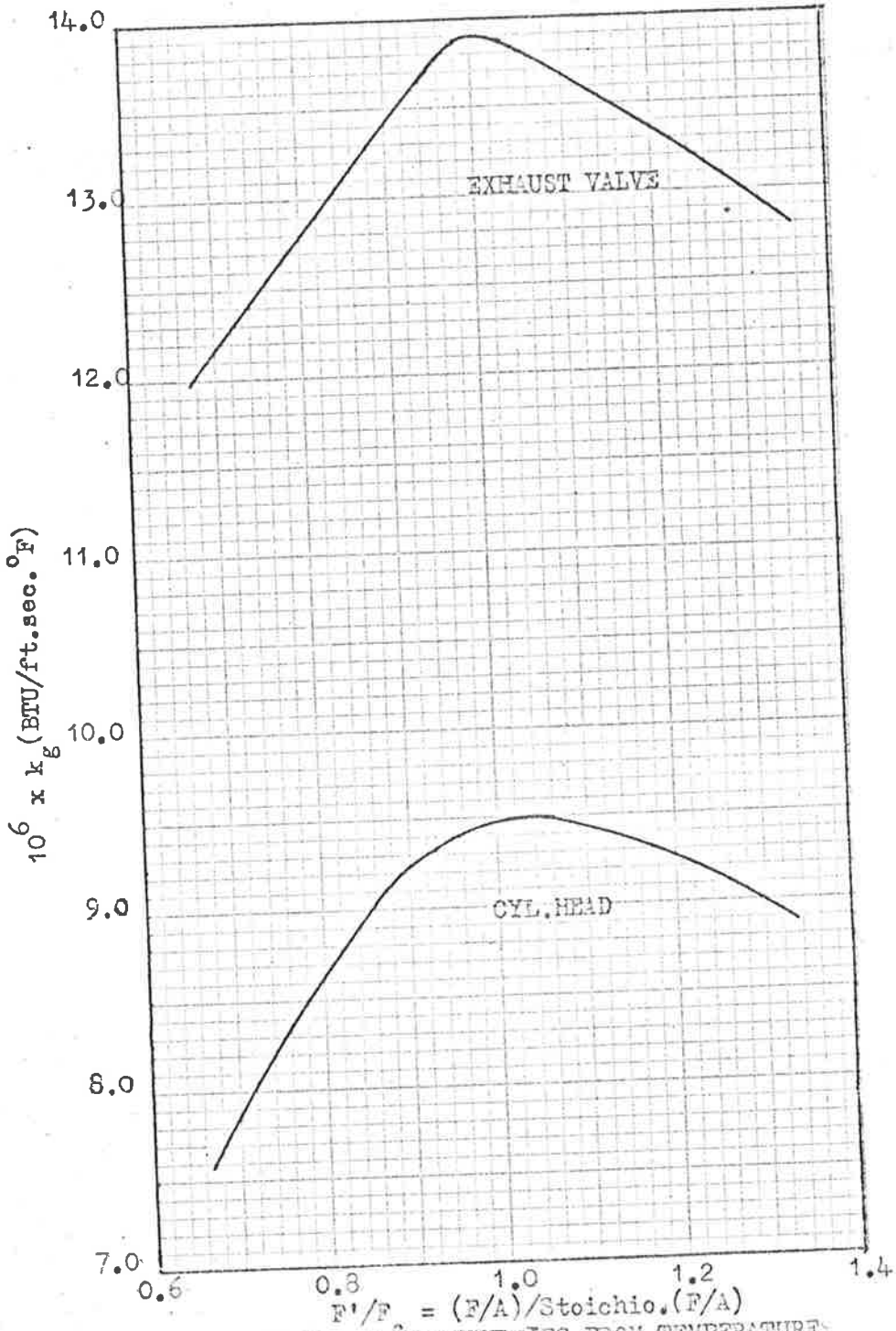

FIG.12 GAS CONDUCTIVITIES FROM TEMPERATURES REPRESENTATIVE OF EXHAUST VALVE AND 'CYLINDER-HEAD LOCATIONS (REFS.21,22,23) AS A FUNCTION OF OCTANE MIXTURE STRENGTH.

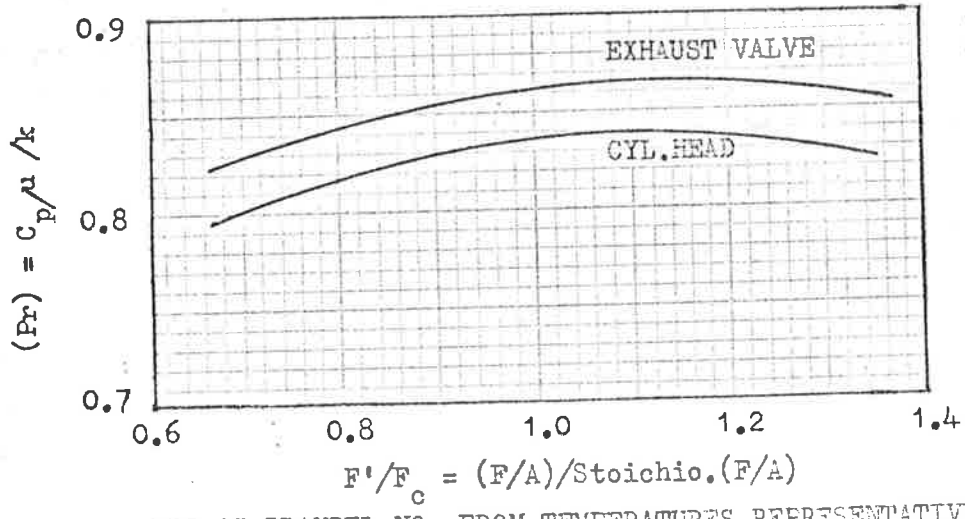

FIG.13 PRANDTL NO. FROM TEMPERATURES REPRESENTATIVE OF EXHAUST AND 'CYLINDER-HEAD'LOCATIONS(REFS.21,22,23)

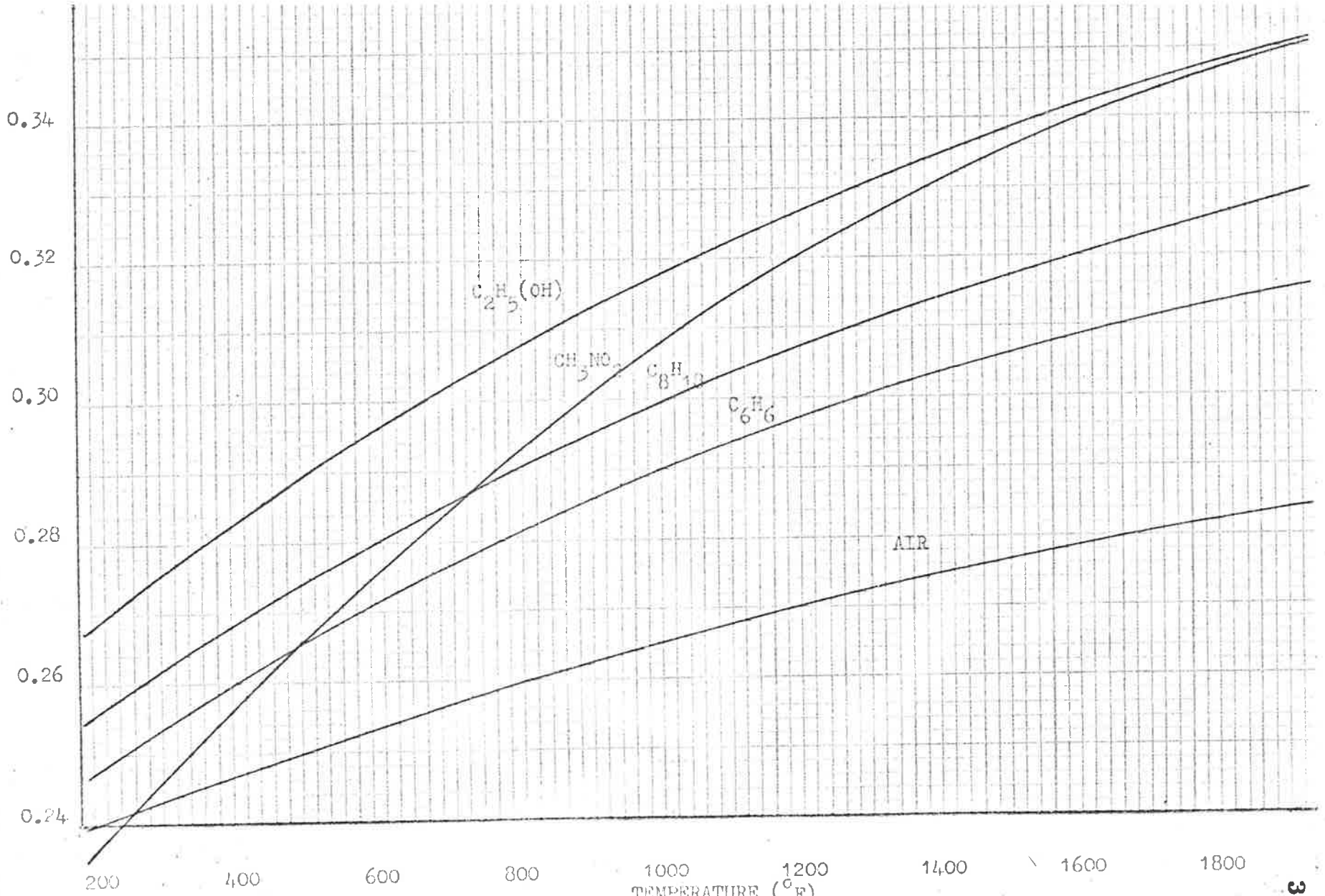

FIG.14 SPECIFIC HEATS FOR VARIOUS FUELS (STOICHIOMETRIC MIXTURES)

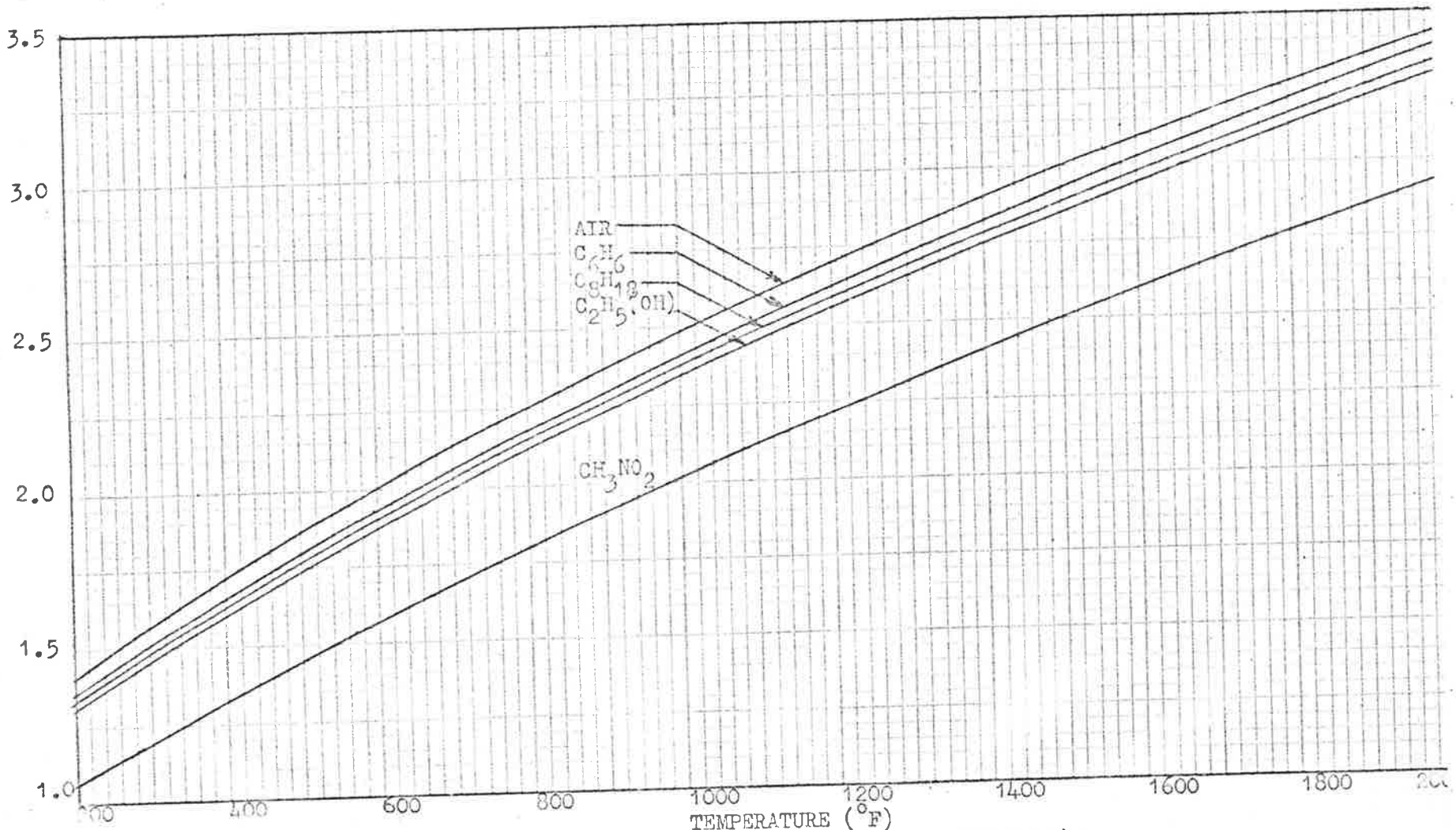

FIG.15 VISCOSITIES OF VARIOUS FUELS (STOICHIOMETRIC MIXTURES)

FIG.16 THERMAL CONDUCTIVITY OF VARIOUS FUELS (STOICHIOMETRIC MIXTURES)

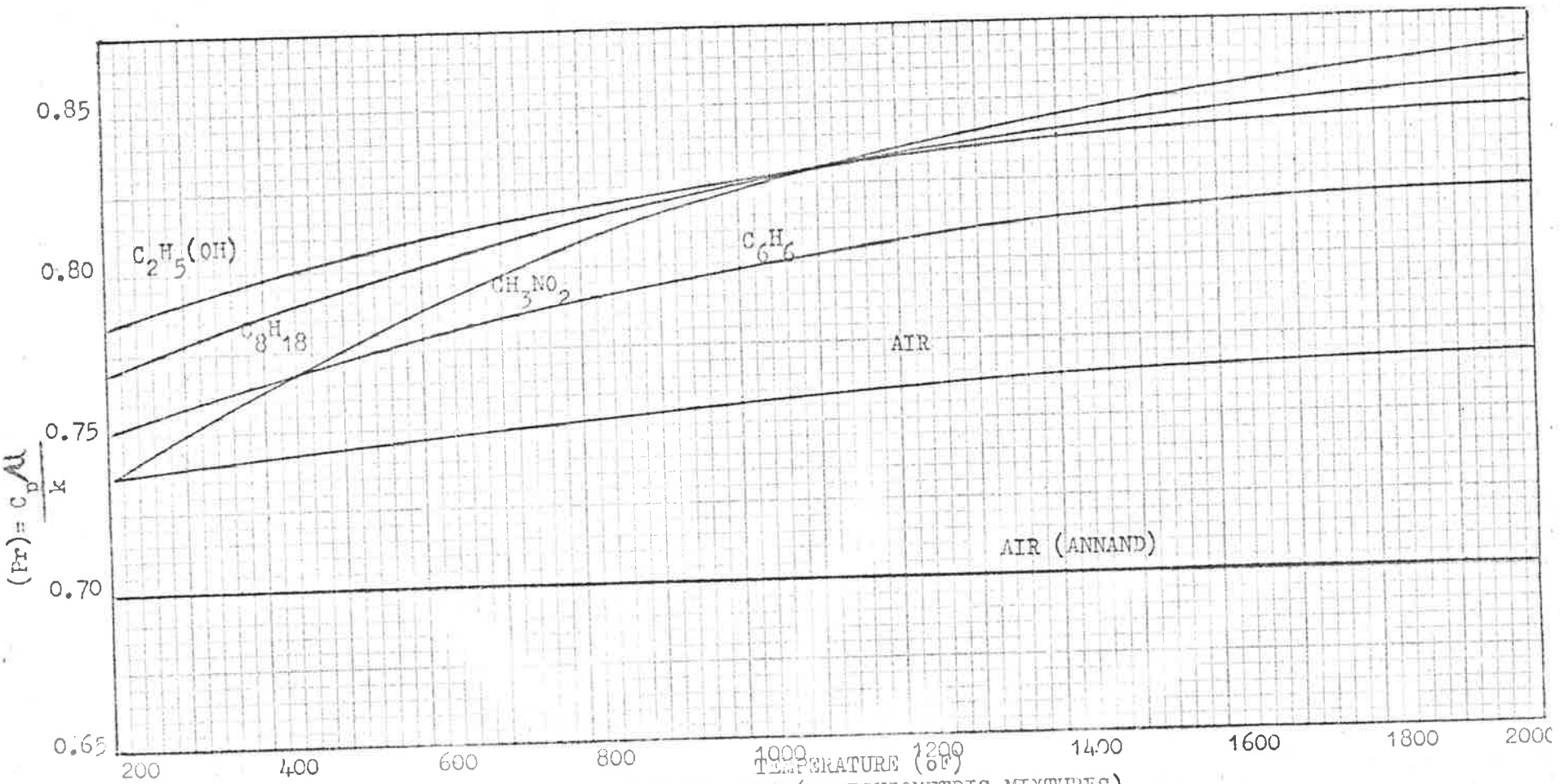

FIG.17 PRANDTL NO. OF VARIOUS FUELS (STOICHIOMETRIC MIXTURES)

APPENDIX 'D' SAMPLE OUTPUT LISTINGS

For detailed listings corresponding to results plotted in text see original Report R65/1

THERMAL TRANSPORT PROPERTIES OF CONSTITUENTS

VISCOSITY PROBLEM - B.S.L PG 25 (REF. 2)

RUN NO.= 17

TEMP= 68.00

	CP	U	SK	PR
O2	2.178E-01	1.358E-05	4.013E-06	7.375E-01
N2	2.419E-01	1.166E-05	3.854E-06	7.320E-01
CO	.000E-99	.000E-99	.000E-99	.000E-99
CO2	2.053E-01	9.780E-06	2.559E-06	7.846E-01
H2O	.000E-99	.000E-99	.000E-99	.000E-99
C8H18	.000E-99	.000E-99	.000E-99	.000E-99
H2	.000E-99	.000E-99	.000E-99	.000E-99
MIX	2.338E-01	1.141E-05	3.637E-06	7.338E-01

COMPARISON OF TEXTBOOK AND COMPUTER SOLUTIONS (REF. 2)

CONSTIT.	$U \times 10^5$ lb/ft.sec		$SK \times 10^6$ BTU/ft.sec.°F		%DEVIATION	
	TEXT	PROG	TEXT	PROG	U	SK
O_2	1.365	1.358	4.110	4.013	-0.51	-2.4
N_2	1.179	1.166	4.211	3.854	-0.10	-8.5
CO_2	0.983	0.987	2.572	2.559	0.51	-0.5
MIX	1,152	1.141	3.922	3.637	-0.10	-7.8

THERMAL TRANSPORT PROPERTIES OF CONSTITUENTS
AND MIXTURE DURING OTTO CYCLE COMPRESSION

RUN NO.=19

90% THEO.AIR, F/A=0.0735, F/FC=1.1053

TEMP= 200.00

	CP	U	SK	PR
O2	2.239E-01	1.607E-05	4.845E-06	7.428E-01
N2	2.467E-01	1.379E-05	4.626E-06	7.358E-01
CO	2.482E-01	1.374E-05	4.630E-06	7.369E-01
CO2	2.189E-01	1.215E-05	3.347E-06	7.952E-01
H2O	4.478E-01	8.629E-06	5.052E-06	7.648E-01
C8H18	4.695E-01	4.398E-06	2.160E-06	9.557E-01
H2	3.350E+00	6.891E-06	3.157E-05	7.314E-01
MIX	2.576E-01	1.347E-05	4.498E-06	7.719E-01

TEMP= 400.00

	CP	U	SK	PR
O2	2.321E-01	1.962E-05	6.077E-06	7.496E-01
N2	2.535E-01	1.677E-05	5.740E-06	7.411E-01
CO	2.556E-01	1.678E-05	5.776E-06	7.426E-01
CO2	2.372E-01	1.489E-05	4.372E-06	8.080E-01
H2O	4.662E-01	1.104E-05	6.670E-06	7.719E-01
C8H18	5.776E-01	5.692E-06	3.412E-06	9.637E-01
H2	3.302E+00	8.185E-06	3.710E-05	7.285E-01
MIX	2.712E-01	1.647E-05	5.649E-06	7.908E-01

TEMP= 600.00

	CP	U	SK	PR
O2	2.394E-01	2.288E-05	7.253E-06	7.553E-01
N2	2.598E-01	1.922E-05	6.697E-06	7.458E-01
CO	2.624E-01	1.934E-05	6.792E-06	7.476E-01
CO2	2.530E-01	1.743E-05	5.395E-06	8.178E-01
H2O	4.844E-01	1.293E-05	8.044E-06	7.786E-01
C8H18	6.709E-01	6.979E-06	4.835E-06	9.686E-01
H2	3.247E+00	9.376E-06	4.198E-05	7.251E-01
MIX	2.833E-01	1.900E-05	6.681E-06	8.062E-01

TEMP= 800.00

	CP	U	SK	PR
O2	2.457E-01	2.560E-05	8.277E-06	7.601E-01
N2	2.656E-01	2.150E-05	7.618E-06	7.500E-01
CO	2.686E-01	2.164E-05	7.734E-06	7.520E-01
CO2	2.667E-01	1.985E-05	6.415E-06	8.255E-01
H2O	5.023E-01	1.472E-05	9.427E-06	7.848E-01
C8H18	7.502E-01	8.062E-06	6.224E-06	9.718E-01
H2	3.184E+00	1.049E-05	4.632E-05	7.212E-01
MIX	2.940E-01	2.131E-05	7.654E-06	8.188E-01

TEMP= 1000.00

	CP	U	SK	PR
O2	2.512E-01	2.817E-05	9.265E-06	7.642E-01
N2	2.710E-01	2.366E-05	8.511E-06	7.537E-01
CO	2.743E-01	2.382E-05	8.646E-06	7.559E-01
CO2	2.783E-01	2.218E-05	7.427E-06	8.316E-01
H2O	5.199E-01	1.645E-05	1.082E-05	7.906E-01
C8H18	8.170E-01	9.008E-06	7.556E-06	9.740E-01
H2	3.113E+00	1.154E-05	5.014E-05	7.167E-01
MIX	3.034E-01	2.348E-05	8.593E-06	8.292E-01

TEMP= 1200.00

	CP	U	SK	PR
O2	2.561E-01	3.062E-05	1.022E-05	7.676E-01
N2	2.760E-01	2.572E-05	9.378E-06	7.571E-01
CO	2.795E-01	2.589E-05	9.532E-06	7.593E-01
CO2	2.882E-01	2.444E-05	8.424E-06	8.364E-01
H2O	5.369E-01	1.812E-05	1.223E-05	7.959E-01
C8H18	8.731E-01	9.923E-06	8.880E-06	9.757E-01
H2	3.031E+00	1.254E-05	5.348E-05	7.112E-01
MIX	3.117E-01	2.555E-05	9.508E-06	8.377E-01

TEMP= 1400.00

	CP	U	SK	PR
O2	2.604E-01	3.297E-05	1.114E-05	7.706E-01
N2	2.805E-01	2.770E-05	1.022E-05	7.601E-01
CO	2.842E-01	2.788E-05	1.039E-05	7.623E-01
CO2	2.966E-01	2.641E-05	9.325E-06	8.403E-01
H2O	5.534E-01	1.975E-05	1.364E-05	8.007E-01
C8H18	9.205E-01	1.081E-05	1.018E-05	9.769E-01
H2	2.938E+00	1.351E-05	5.633E-05	7.048E-01
MIX	3.190E-01	2.753E-05	1.039E-05	8.448E-01

TEMP= 1600.00

	CP	U	SK	PR
O2	2.641E-01	3.524E-05	1.204E-05	7.731E-01
N2	2.847E-01	2.960E-05	1.104E-05	7.627E-01
CO	2.884E-01	2.979E-05	1.123E-05	7.650E-01
CO2	3.037E-01	2.822E-05	1.016E-05	8.434E-01
H2O	5.692E-01	2.132E-05	1.507E-05	8.052E-01
C8H18	9.612E-01	1.167E-05	1.147E-05	9.778E-01
H2	2.832E+00	1.443E-05	5.867E-05	6.971E-01
MIX	3.255E-01	2.944E-05	1.126E-05	8.507E-01

TEMP= 1800.00

	CP	U	SK	PR
O2	2.675E-01	3.742E-05	1.291E-05	7.753E-01
N2	2.885E-01	3.143E-05	1.185E-05	7.651E-01
CO	2.923E-01	3.164E-05	1.205E-05	7.674E-01
CO2	3.097E-01	2.997E-05	1.097E-05	8.460E-01
H2O	5.843E-01	2.269E-05	1.638E-05	8.092E-01
C8H18	9.964E-01	1.251E-05	1.274E-05	9.786E-01
H2	2.714E+00	1.533E-05	6.045E-05	6.880E-01
MIX	3.313E-01	3.128E-05	1.211E-05	8.557E-01

TEMP= 2000.00

	CP	U	SK	PR
O2	2.704E-01	3.954E-05	1.376E-05	7.772E-01
N2	2.919E-01	3.321E-05	1.264E-05	7.673E-01
CO	2.957E-01	3.343E-05	1.285E-05	7.694E-01
CO2	3.146E-01	3.167E-05	1.175E-05	8.480E-01
H2O	5.986E-01	2.397E-05	1.765E-05	8.130E-01
C8H18	1.026E+00	1.334E-05	1.399E-05	9.792E-01
H2	2.581E+00	1.620E-05	6.177E-05	6.772E-01
MIX	3.364E-01	3.307E-05	1.293E-05	8.600E-01

APPENDIX A3

'MOVADAS'

DATA ACQUISITION SYSTEM

by

M.R. HALE and G.A. MORGAN

UNIVERSITY OF ADELAIDE
DEPARTMENT OF MECHANICAL ENGINEERING
Report Mech.Eng. R66/2
November, 1966.

TABLE OF CONTENTS

ABSTRACT

A modulated Voltage Analogue Data Acquisition System (MOVADAS) built to IRIG* Specifications is described.

Basic units are D.C. Voltage Preamplifiers, High-Pass Filters, Driver Amplifiers, Voltage-to-Frequency Converters, Programming Switch and High-speed Tape Transport.

Immediately prior to recording of transducer signals, binary coded identification pulses representing Run, Channel and Calibration signals are simultaneously impressed on all data channels. This provides a time datum for subsequent computer analysis enabling data to be correlated between channels.

A reference frequency is recorded on one channel to facilitate accurate analogue to digital conversion independent of tape speed fluctuations.

The computing procedure also included, describes how the digital data files are recognised, related to a cyclic "Event" signal and reduced to numerical values of the recorded phenomena.

This enables a Fourier analysis to be performed on all recorded data between any predetermined cycles of the event.

* Inter-Range Instrumentation Group

INTRODUCTION

The development of a high speed data acquisition system was commenced in mid-1964 when it became apparent that the available recording instruments within the Department of Mechanical Engineering severely limited current and proposed research projects.

The research projects concerned required measurement of dynamic and cyclically fluctuating data from various transducers and sensors, e.g.; strain guages, thermocouples and pressure transducers. In each investigation, instantaneous data from two or more transducers was required to be recorded simultaneously, thus enabling a Fourier analysis and other computations to be conducted on a digital computer.

The existing techniques available in the department for recording and analysing fluctuating data were as follows:-

(1) Displays on dual-beam oscilloscopes were recorded by either drum or 35 mm camera; and analysed by manual measurement of ordinates.

Disadvantages of this method were:

(i) Excessive handling and film processing time

(ii) Limited sampling due to restricted length of trace

(iii) Required an optical comparator for the accurate measurement of ordinates; or

(iv) Reliance on manual measurement and human error.

(2) Multichannel pen recording and analysis by automatic digital curve reader (Reference 2)

(i) Limitations due to the capability of the curve reader to analyse only in polar co-ordinates.

(ii) Limited frequency response of pen recorders.

(iii) Necessity for manual conversion of curve reader printed output to punched cards for subsequent computer analysis.

(iv) Slow reading process.

It was decided at a Departmental meeting in September, 1964, that a versatile high speed data acquisition system, compatible with the data processing facilities of the Department of Computing Science, should be purchased or built. It was also resolved that this system should incorporate a high speed, multichannel magnetic tape recorder using 1/2" wide tape.

W.R.E. Scientific personnel generously offered advice on the design of such a data acquisition system based on their W.R.E. Mk. II Recorder. Arrangements were also made to purchase from W.R.E. an "Epsylon 1/2" tape transport which was subsequently modified to IRIG tape speed and track specifications.

In December 1964 the first "breadboard" mockup of a voltage to frequency converter was built and tested successfully and plans were made for the construction of three such modulator channels together with power supplies, preamplifiers and driver amplifiers for an FM Analogue recording system to be known as " MOVADAS" -- MODULATED VOLTAGE ANALOGUE DATA ACQUISITION SYSTEM.

APPENDIX A 3

A 3.0 MOVADAS - DATA ACQUISITION SYSTEM

MOVADAS - (Modulated Voltage Analogue Data Acquisition System) is a Frequency Modulated Recording System based on the Standard Bandwidth IRIG Specifications as follows:

Tape speed	ips	60	30
Carrier frequency	Kc/S	54	27
Modulation range	% of carrier	±40	±40

MOVADAS consists of the following basic units:

(1) Signal Amplifiers and conditioning units.

(i) D.C. Voltage pre-amplifiers.

(ii) Driver Amplifier

(iii) Voltage-frequency (V-F) Converters.

(iv) Programming switch.

(v) Event Marker.

(vi) Reference frequency.

(2) High speed tape recorder.

A simplified layout of MOVADAS is given in Fig. 1.

A3.1 SIGNAL AMPLIFIERS AND CONDITIONING UNITS

(1) D.C. Voltage Pre-amplifiers

The circuit for the D.C. Pre-amplifier was based on a Texas SN724 integrated circuit 'chip' amplifier. The circuit diagram is shown in Fig. 2.0.

Gains settings of 10.0, 20.0, 40.0 and 60.0 were provided by switching feedback resistors. At each gain setting a roll-off compensating capacitor was automatically coupled to prevent self-oscillation or phase shift.

To provide the same sensitivity for each setting a push-pull, single-ended voltage dividing network with frequency compensation was coupled to the inverting input of the chip amplifier.

D.C. balance control was provided by an offset voltage from a voltage divider.

A brief specification of the Pre-amplifiers follows:-

Input Impedance	0.5MΩ
Input noise level	40μV broadband
Supply voltage	± 12V D.C.
Output Impedance	1KΩ

(2) Driver Amplifier

This provided either D.C. or A.C. coupled inputs through two Nuvistor Triodes in push-pull cathode follower configuration.

The triodes gave a high input impedance and a low output impedance to connect directly to two push-pull transistor amplifier stages (Reference 1) The gain control was obtained by feedback. The output voltage from an emitter follower to the V-F converter was limited by the forward conduction of silicon diodes.

The circuit diagram is shown in Figs. 2.1 and 2.2.

(3) Voltage-Frequency Converter

The IRIG specification as follows was adopted.

Carrier frequency	54 Kc/s at 60"/s
Modulation range	±40% of carrier frequency
Input voltage	±1.4 volts for f.s.d.

Each V-F converter consisted of:

(i) Input stage

(ii) Modulator

(iii) Schmitt Trigger

(iv) Binary divider/flip-flop plus output stage.

The circuit diagrams are given in Figs. 3.1 to 3.6.

(i) Input Stage

Provided approximately 10,000Ω input impedance through an OC 140 emitter follower. This was temperature compensated by another OC 140 in the emitter circuit.

(ii) Modulator

This was a free-running voltage controlled R-L multivibrator adjusted to 54 Kc/s at zero input. The allowable linear deviation from this centre frequency was ±40%. The input signal was fed in through two 10mH

inductances, each one coupled to an emitter follower. A further emitter follower supplied a low output impedance to the Schmitt trigger.

(iii) Schmitt Trigger

This unit converted the Modulator output voltage to a "square" wave form.

(iv) Binary divider/Flip-flop

At a recording speed of 30 ips both inputs A & B at this stage were connected to output B of the Schmitt Trigger to provide a binary division prior to the flip-flop.

At 60 ips both outputs A & B of the Schmitt were connected to inputs A & B respectively of the Flip-flop which acted as a signal clean-up stage.

A low impedance output stage followed to match that of the Record/Reproduce tape head.

(4) Programming Switch

This unit controlled the recording sequence and inserted pulses of known amplitudes to identify the recorded information, i.e. run and channel identification. An instantaneous calibration of the V-F converter was also provided, immediately prior to the recording of real data.

Format details of the recorded information can be found in a following Section A3.4.

A block diagram of the programming switch is given in Fig. 6.1 and the circuit of the basic monostable multivibrator used is given in Fig. 6.2 .

The programming switch inserted the identification marks simultaneously on all active channels, except that channel which recorded the reference frequency [see (6) following].

(5) Event Marker

An FM signal changing from a static level of 54 Kc/s to a transient value of 70 Kc/s upon occurrence of a cyclic "Event" was recorded on a separate data channel during each recording sequence.

The event was signified by the interruption of a light beam impinging on a photo-cell.

An OC 71 transistor, which had the paint removed from its cover, was used as the photocell.

The voltage signal was fed into an AC coupled, two-stage pulse amplifier which provided a heavy positive pulse to the monostable multivibrator.

A variable pulse length was provided by the switching of a capacitor C3. (Refer Figs. 5.1 and 5.2)

The stages following were identical to those of the V-F converter. An improved event marker using integrated circuits is shown in Fig. 5.3.

(6) Reference Frequency

This was required for the analogue-to-digital conversion and was a 50 Kc/s, F-M signal recorded on a separate track of the magnetic tape.

The unit was controlled by a Venner Crystal Oscillator Type TS 25.

The basic layout for this unit is given in Fig. 4.

A3.2 HIGH SPEED TAPE RECORDER

An Epsylon Multitrack high speed tape recorder was modified to take 0.500 of an inch tape width at speeds of 60 and 30 ips. The magnetic heads were replaced with DRICO Series 50, Record/Reproduce heads to IRIG 7 track specifications.

A3.3 ANALOGUE - DIGITAL CONVERSION

The recorded F.M. information was converted into binary information at the rate of 4000 samples per second at an analogue tape speed of 60 ips. The recording mode of the digital information was compatible with IBM 7090 digital computer

i.e.		
	Packing density	200 bits per inch
	MOVADAS Data word	10 reading bits plus 2 parity bits
	Computer word	36 bits or three MOVADAS data words
	Record length	324 words

Because the A-D Converter used for the conversion was programmed to accept multiplexed telemetery data, the resulting structure of each computer record was as follows:

Each recorded track was converted separately and the digital information was recorded end-for-end on the digital tape or "transmittal tape."

The list of numbers which represented a complete single recorded run was termed a file. After each file an end of file

mark was recorded on the digital tape.

In the first record of a file, between the first (1) and the twenty-fourth (24) MOVADAS word, a time word of three (3) MOVADAS words in length was automatically inserted. The time word had the following structure, in octal notation.

$$4000_8, \quad XXXX_8, \quad YYYY_8$$

where $XXXX_8$ was greater than 40_8

$YYYY_8$ was greater than 4000_8

After every twenty-fourth MOVADAS word the time word was repeated until the end of file.

This information was a real time count and was redundant in the subsequent analysis.

A3.4 FORMAT OF RECORDED INFORMATION, ANALOGUE AND DIGITAL

The form of the input voltage to the V-F converter in MOVADAS, on automatic record mode, is sketched in Fig. 9.

The corresponding F.M. signal and digital output is also given in Fig. 9.

It was found necessary to commence each recording by a period of constant voltage, i.e. constant frequency on the F.M. signal, because the A-D Converter had to be manually operated.

The identification pulses prior to the recorded data represented the run number and channel (or track) number in binary form.

The run number consisted of five bits of information giving run numbers from 0 to 31 and the channel identification consisted of three bits. After this information a series of calibration voltages followed, enabling an instantaneous calibration to be made of the V-F converter.

The identification pulses and calibration voltages were applied to all active channels simultaneously. This was necessary because the recorded data from several tracks had to be phase compared in subsequent analysis.

The information recorded on the digital tape is as sketched in Fig. 9. The list of digits which constitutes a single experimental reading was termed a file and was terminated with an end of file mark. It should be noted that due to the programming switch in MOVADAS, the actual digital pulses were not ideally 'square cornered.' The initial discontinuity and leading edge was as desired, but oscillations did exist on the pulse top and trailing edge. These irregularaties presented difficulties, when developing a technique for detecting the identification pulses during computer analysis of the data.

The bit structure of the recorded digital data is quoted in Section 3.3 and details of the analysis of the data are given in Appendix A.4.

REFERENCES

.1 GRIGSON, C.W.B.,

"Some Precision Direct-Coupled Transistor Amplifiers and Approximate Design"

Electronic Engineering July-August, 1964.

Vol. 36, Nos. 437, 438.

.2 NORRIE, D.H.; WALL, I. & WOOD, A.E.R.,

"An Automatic Digital Curve Reader"

Journal of Scientific Instruments, May, 1965.

Vol. 42, pp 356 - 357.

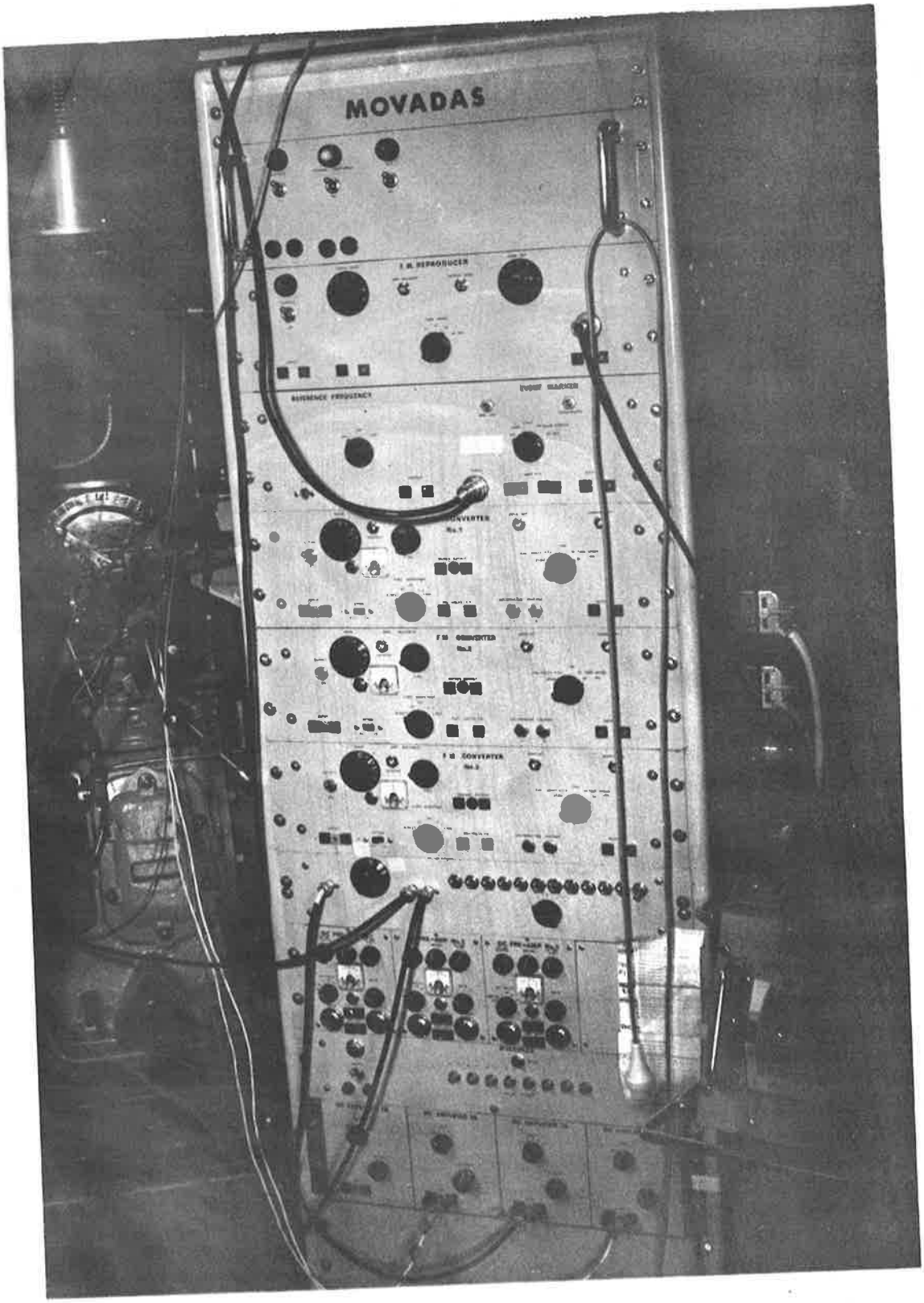

MOVADAS

Fig. 1

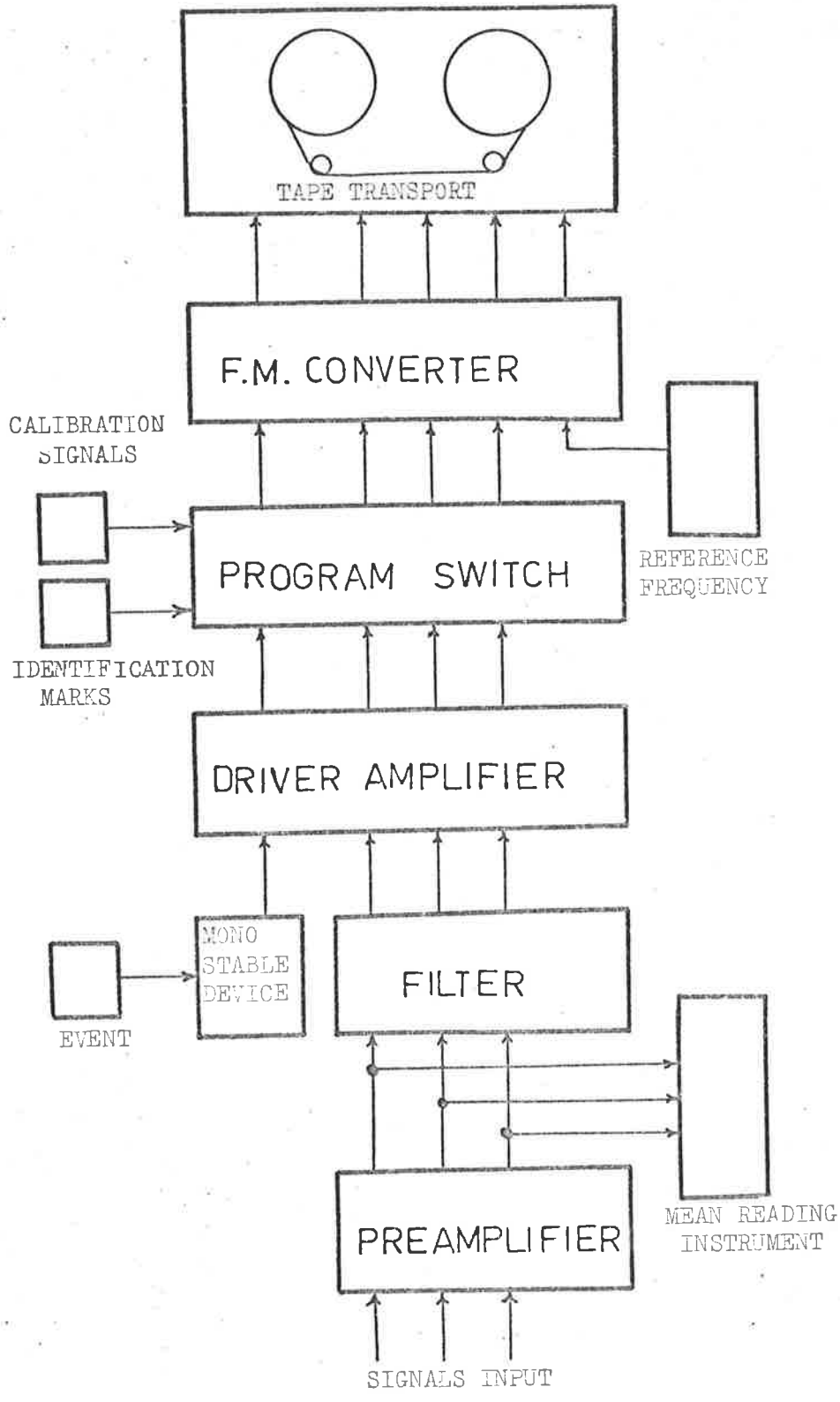

Fig. 1 - Layout of Movadas

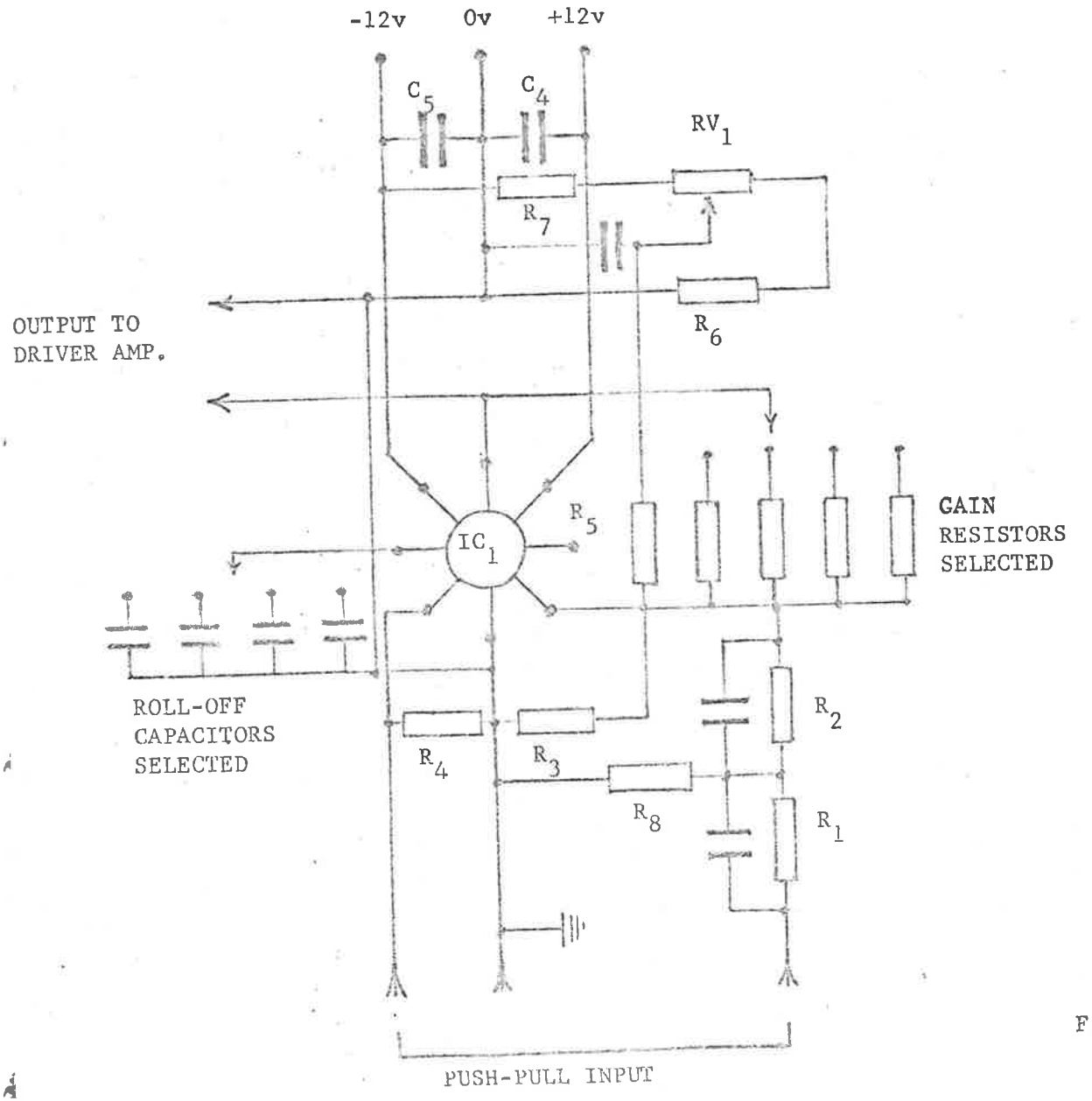

RESISTORS		CAPACITORS	
R_1	10K	C_1	0.47μF
R_2	22K	C_2	180pF
R_3	10K	C_3	0.047μF
R_4	560K	C_4	10μF
R_5	12K	C_5	10μF
R_6	3K] High Stability		
R_7	3K]		
R_8	6.8K		

VARIABLE RESISTORS		INTEGRATED CIRCUITS	
RV_1	100Ω 2W	IC_1	SN724

Fig. 2.0 D.C. Pre-Amplifier

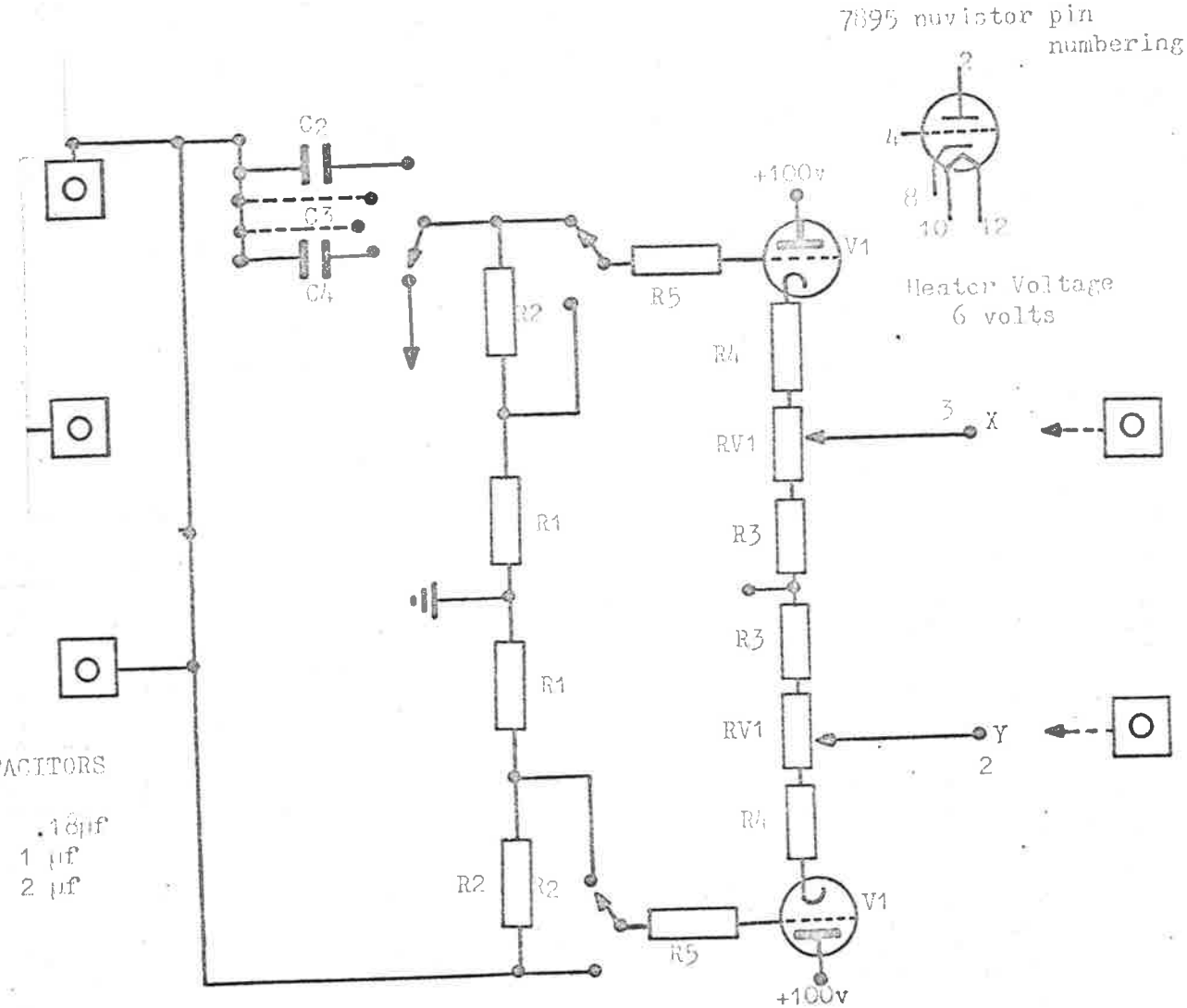

V_1 Nuvistor 7395

RESISTORS		CAPACITORS	
R1	350K		
R2	150K	C2	.1 µf
R3	50K	C3	1 µf
R4	500	C4	2 µf
R5	100		

RESISTOR VARIABLE
RV1 1K

Fig. 2.1 - Driver Amplifier
Filter and High Input Impedance Stage

Fig. 2.2

TRANSISTORS

T1 2S 303
T2 2S 703
T3 2S 303

DIODES

D1 10D4
D2 10D4

RESISTORS

R1 390
R2 390
R3 Variable so RV2
R4 works at 0.V
R5 between T1 & T2
R6 33K
R7 5.6K
R8 1K
R9 1.2K
R10 1K
R11 220
R12, R13, R14, R15, R16 } Gain setting resistor selected

RESISTORS VARIABLE

RV1 10K fine } balance
RV2 500 coarse }

CAPACITORS

C1, C2, C3, C4, C5 } Selected for each gain Setting

Fig. 2.2 - Driver Amplifier Amplification Stage.

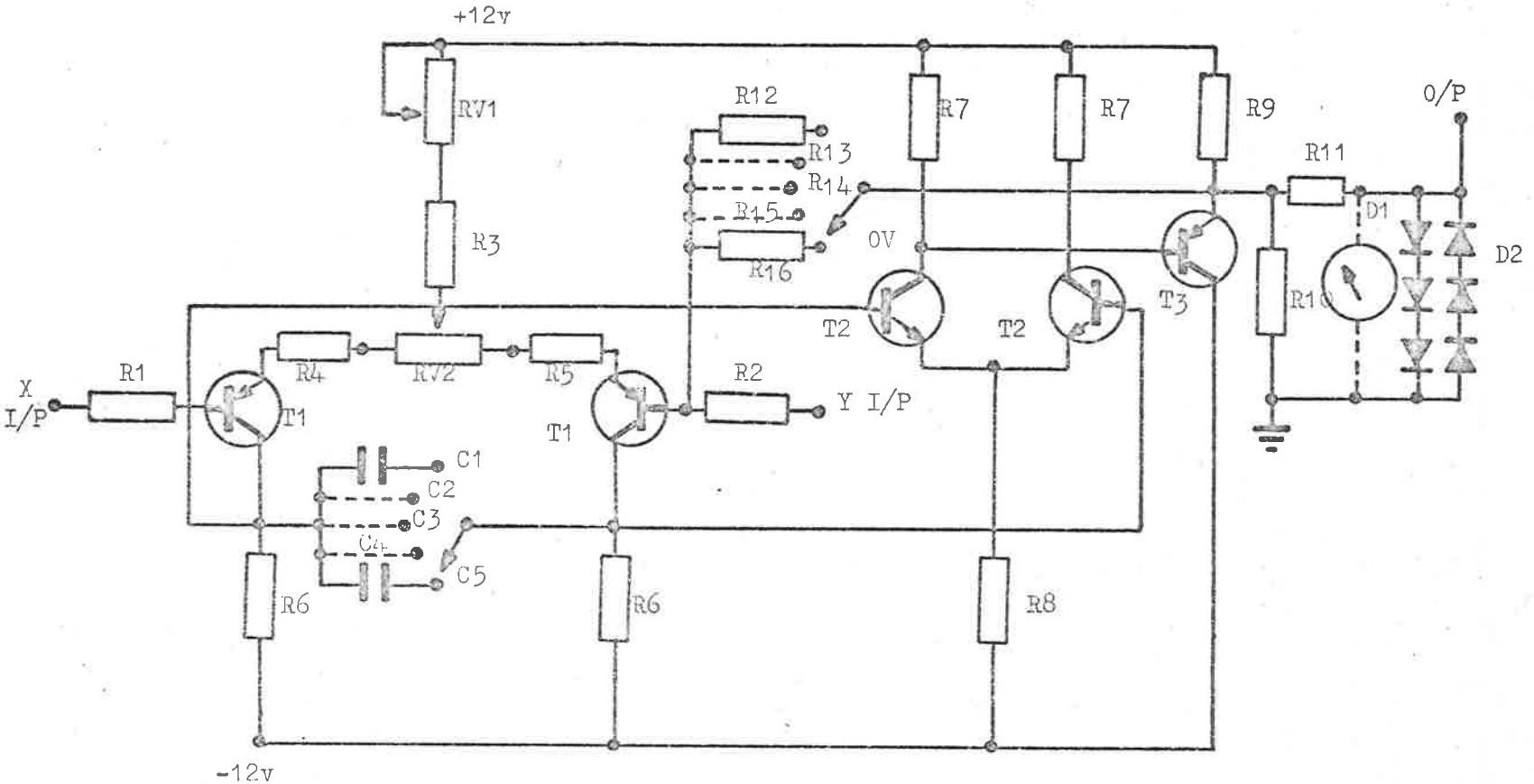

Fig. 2.2 - Driver Amplifier Amplification Stage.

Fig. 2.2

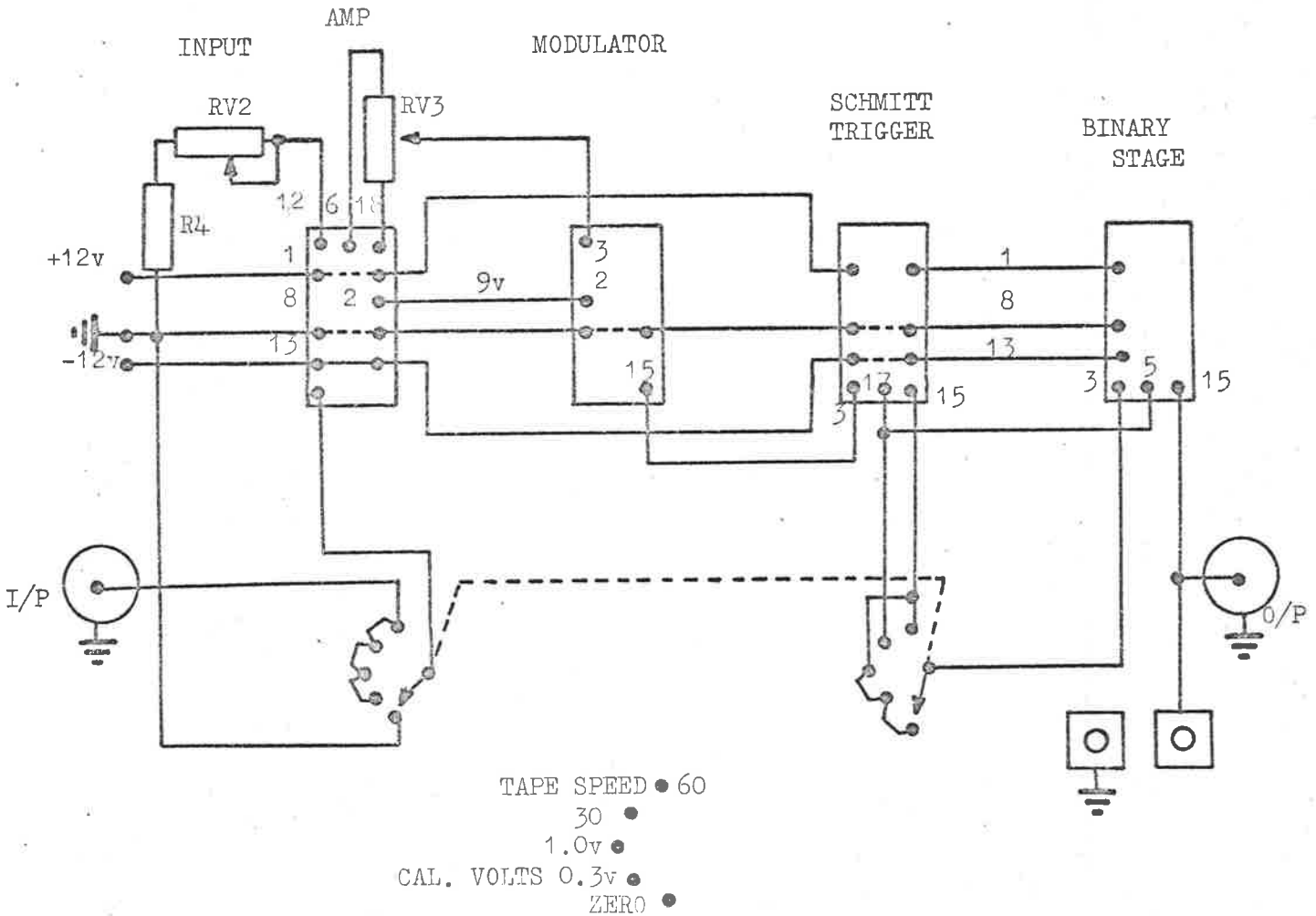

RESISTORS

R4 2.7K to 3.3K

RESISTOR VARIABLE

RV2 5K sensitivity
RV3 100 zero set

Fig. 3.1 - V-F Converter
Block Diagram of Wiring between Basic Cards.

Fig. 3.1

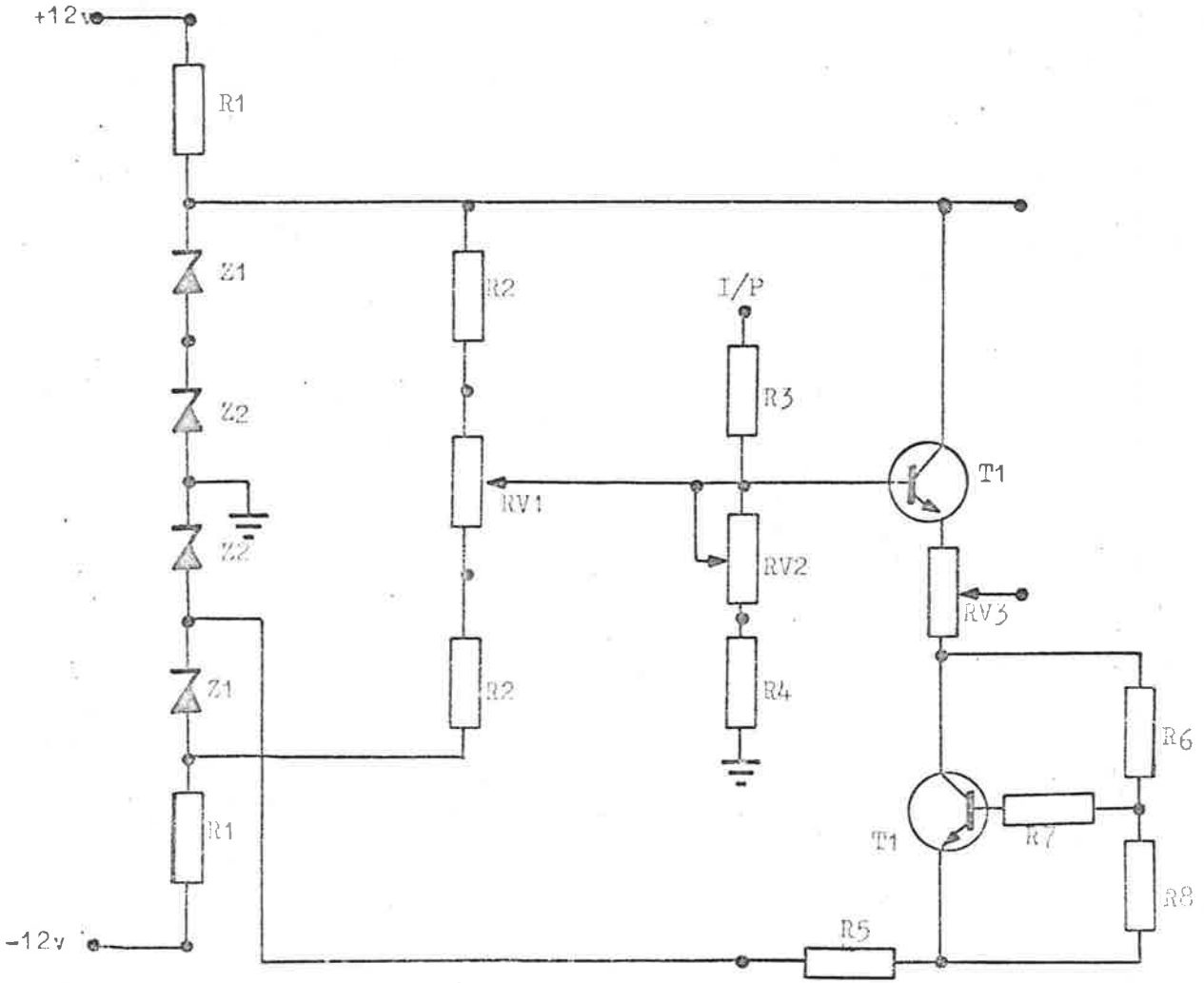

Fig. 3.2 - V - F Converter
Input Amplifier

TRANSISTORS
T1 OC140

ZENER DIODE
Z1 1Z4.7T5
Z2 1Z5.6T5

RESISTORS
R1 33
R2 100K Electrosil
R3 10K
R4 2.7K to 3.3K
R5 0-330
R6 47K
R7 33K
R8 100K

RESISTORS VARIABLE
RV1 25K
RV2 5K
RV3 100

Fig. 3.2

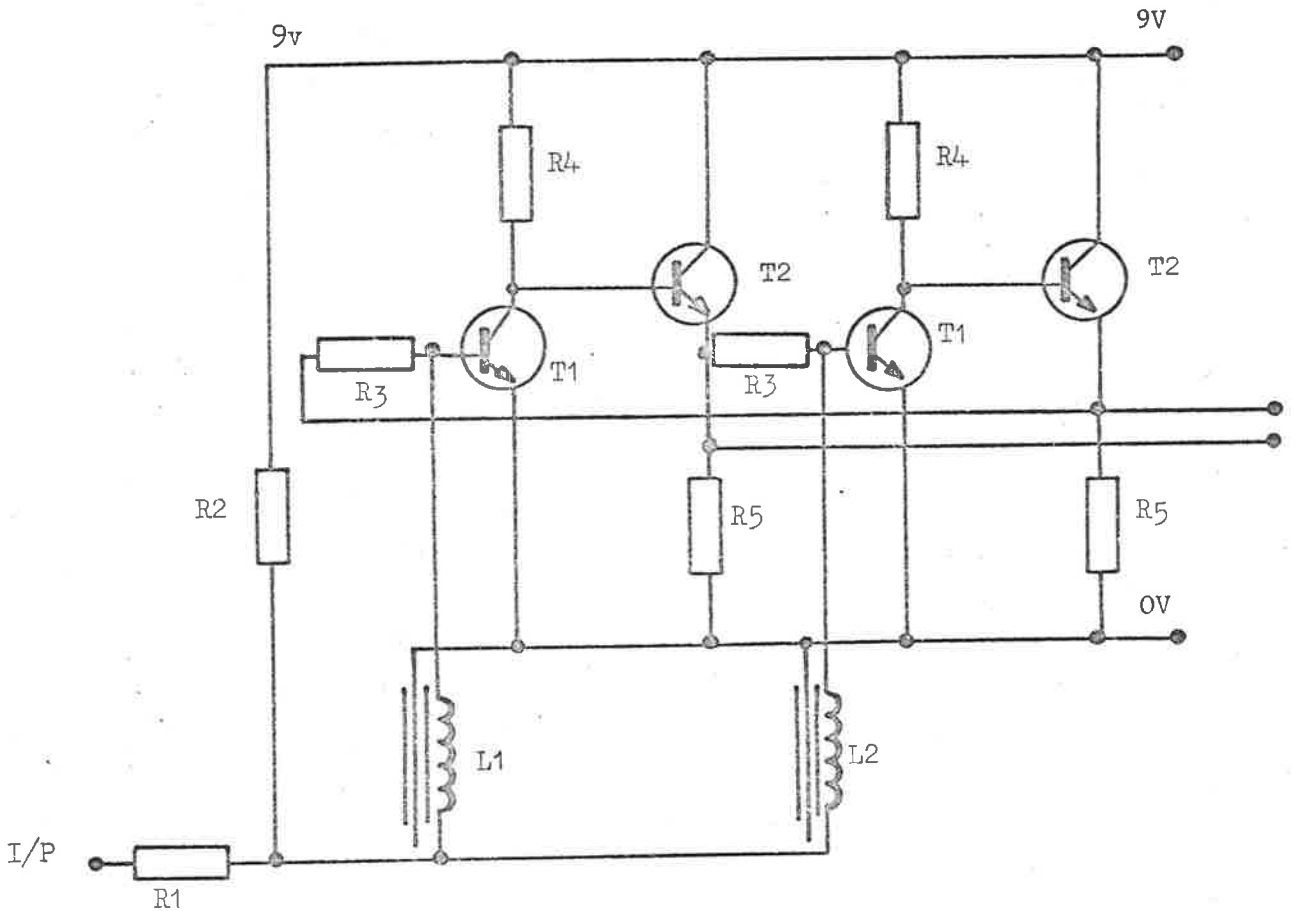

TRANSISTORS
T1 2S703
T2 OC140

INDUCTANCE
L1 10m H
L2 10m H

RESISTORS
R1 100 high stabili
R2 100 " "
R3 12K " "
R4 4.7K " "
R5 3.3K

Fig. 3.3 - V-F Converter
Astable Multivibrator - Voltage Controlled Modulator.

Fig. 3.3

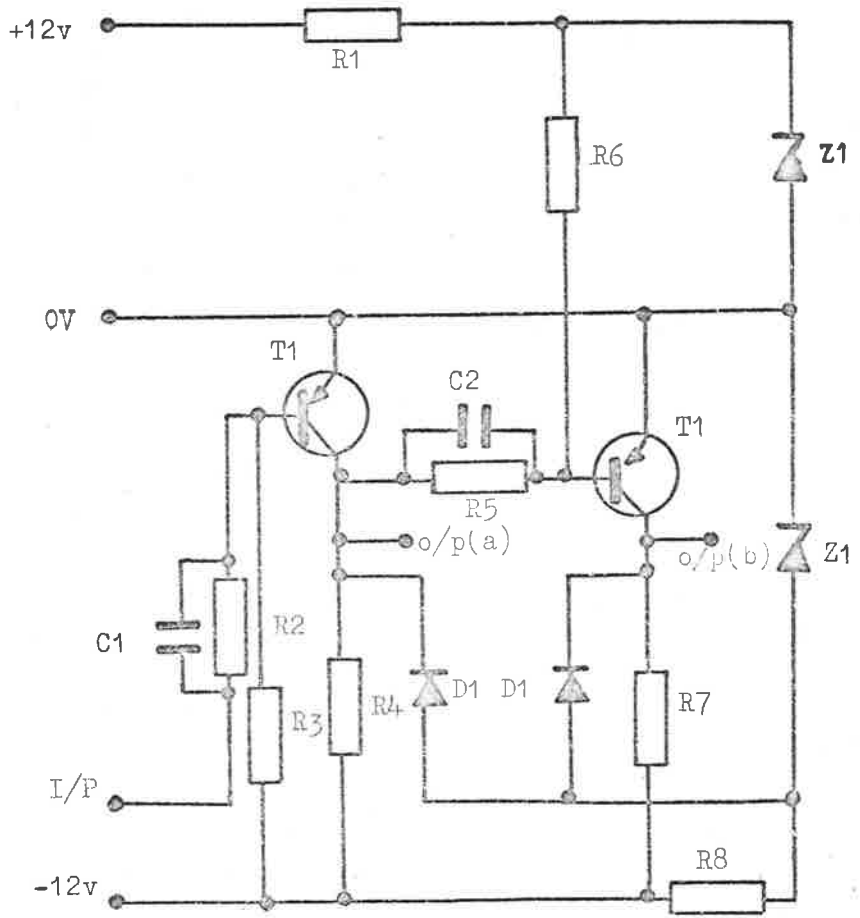

Fig. 3.4 - V-F Converter
Schmitt Trigger.

TRANSISTORS
T1 2N1309

ZENER DIODE
Z1 Z2A5.6

DIODE
D1 1N914

RESISTORS
R1 560
R2 22K
R3 82K
R4 3.9K
R5 15K
R6 68K
R7 3.9K
R8 150

CAPACITORS
C1 180pf
C2 180pf

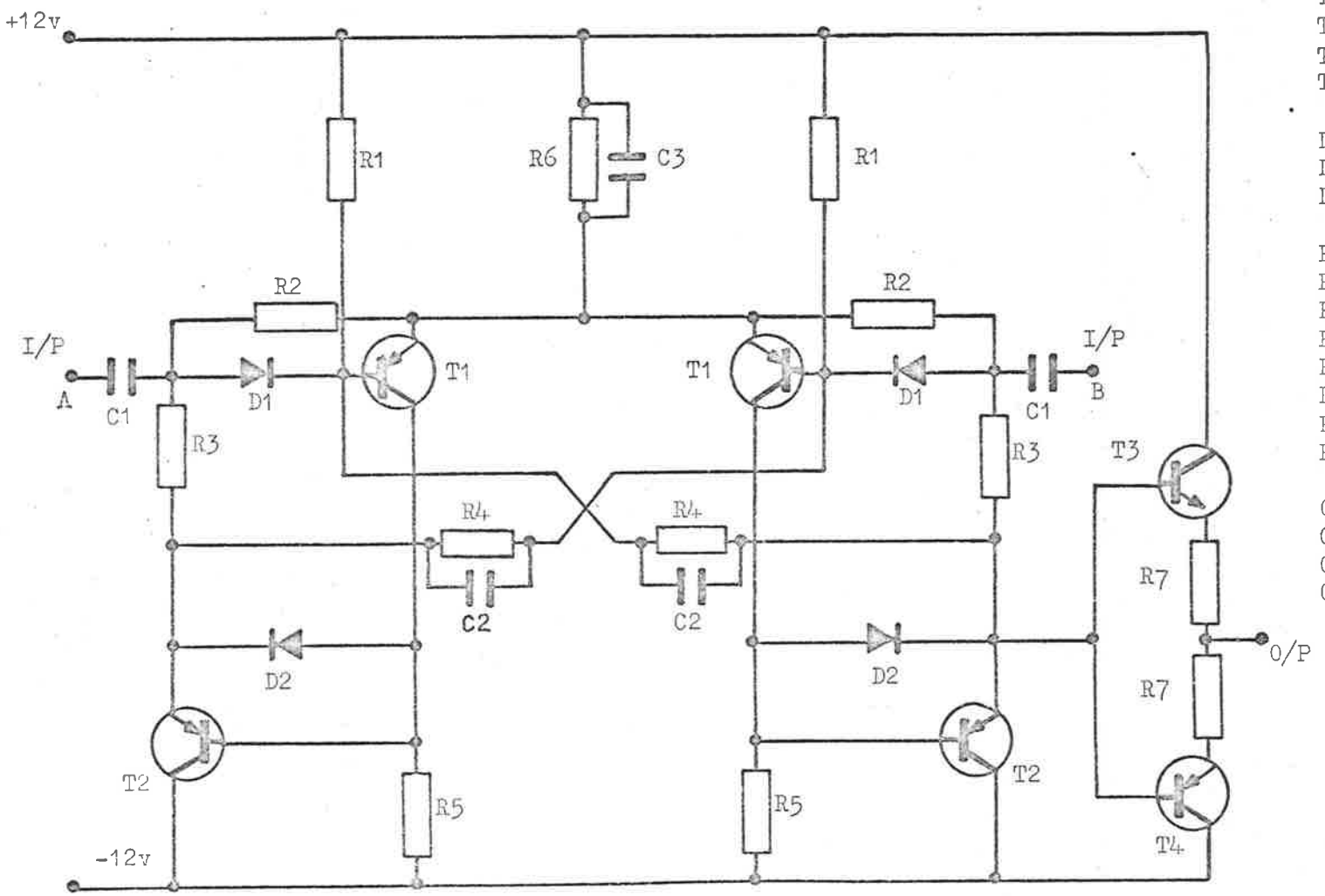

TRANSISTORS
T1 ASZ20N
T2 ASZ20N
T3 2N1308
T4 2N1309

DIODES
D1 1N914
D2 1N914

RESISTORS
R1 10K
R2 2.7K
R3 39K
R4 56K
R5 4.7K
R6 68
R7 1K

CAPACITORS
C1 180pf
C2 100pf
C3 8μf

Fig. 3.5 - V-F Converter
Binary Divide/Astable Multivibrator

Fig. 3.5

SELECTOR SWITCH ON V-F CONVERTER

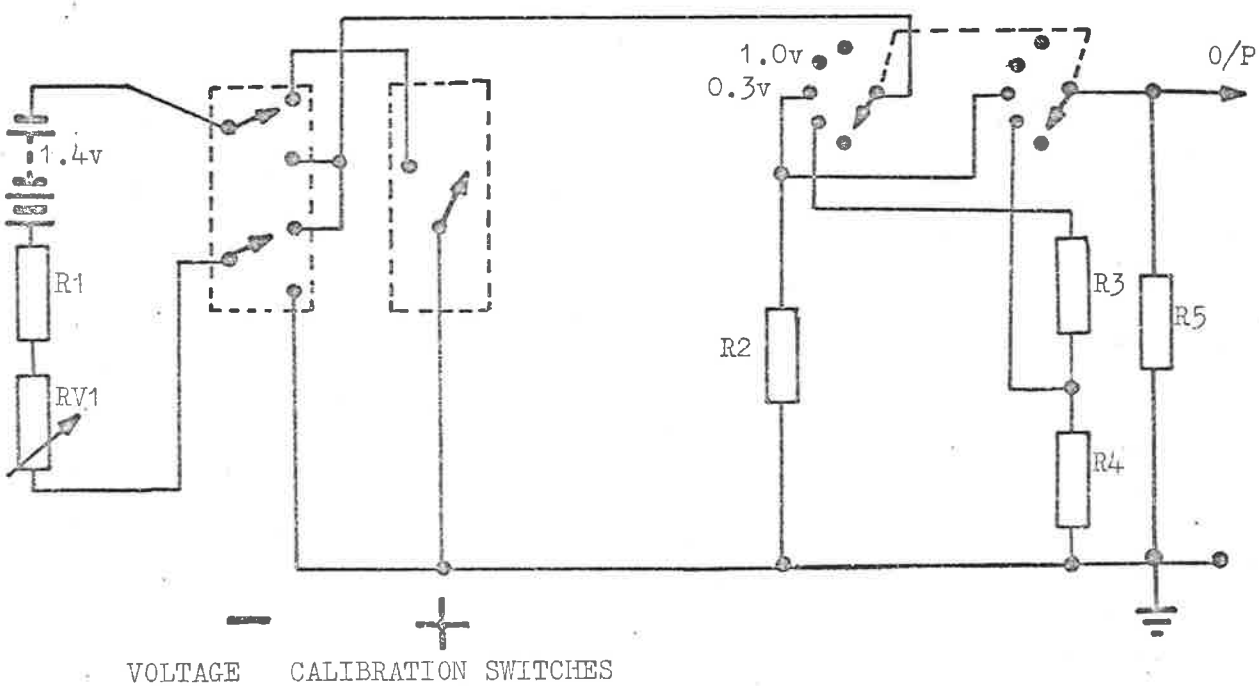

RESISTORS

R1 270
R2 1K
R3 636.36
R4 280. 37
R5 10K

RESISTOR VARIABLE

RV1 200

Fig. 3.6 - V-F Converter
Calibration Voltage Supply.

Fig. 3.6

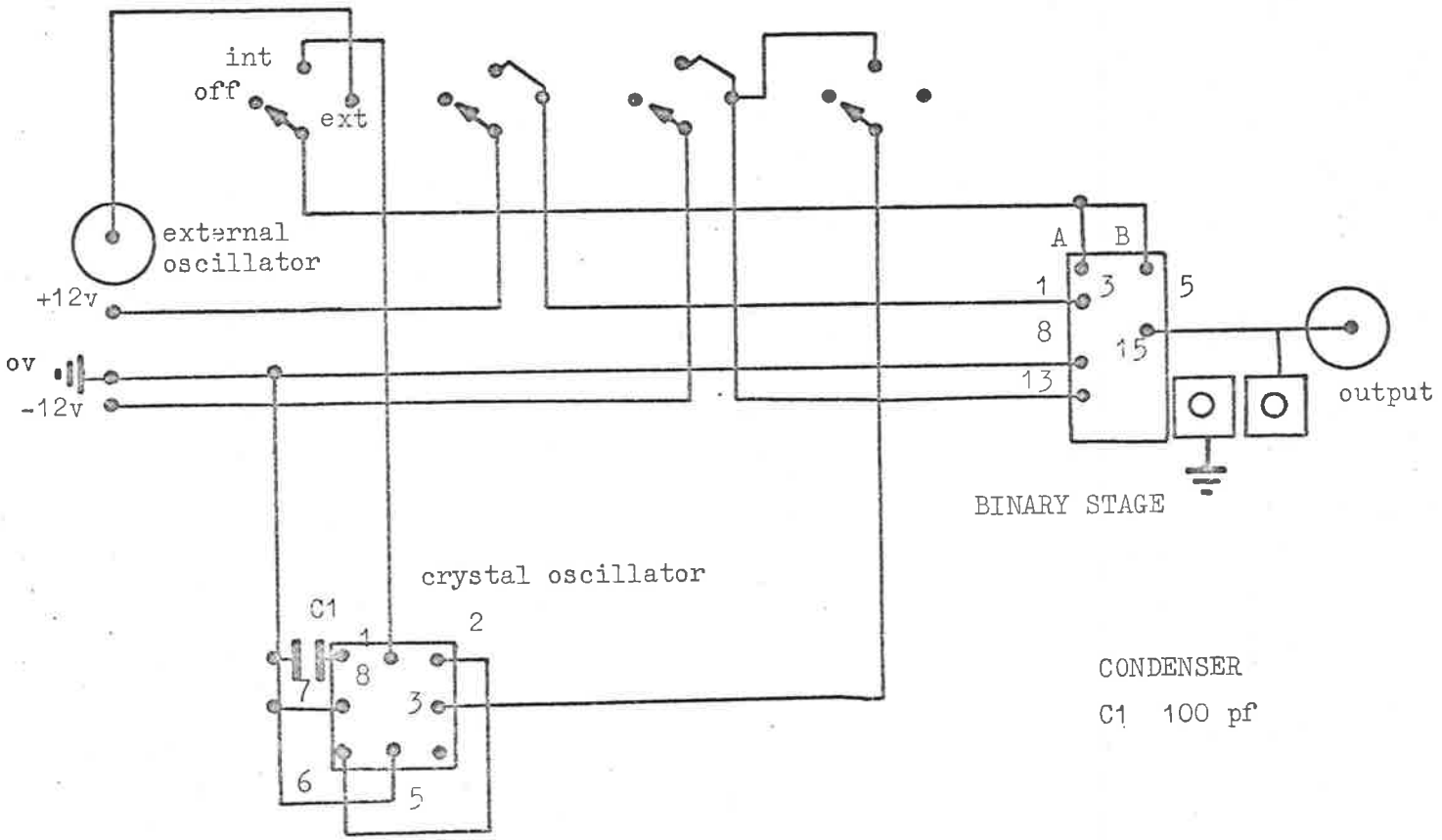

Fig. 4 - Reference Frequency
Block Diagram of Wiring between Basic Cards.

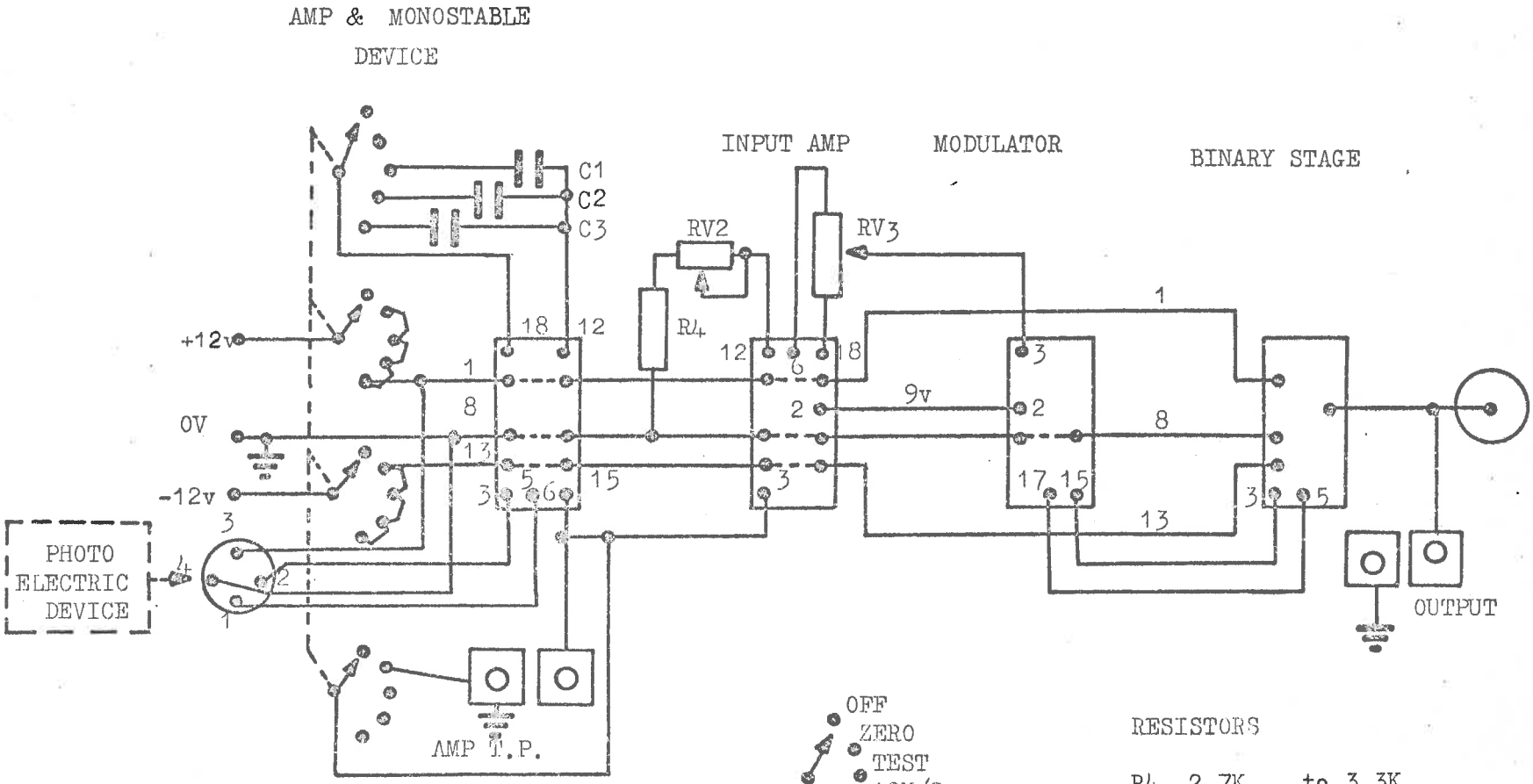

CAPACITORS

C1 64μf
C2 0.47μf
C3 1μf

RESISTORS

R4 2.7K to 3.3K

RESISTORS VARIABLE

RV2 5K sensitivity
RV3 100 zero set

Fig. 5.1 - Event Marker

Block Diagram of Wiring between Basic Cards.

Fig. 5.2

RESISTORS

R1 10K
R2 56K
R3 10K
R4 82K
R5 1K
R6 5.6K
R7 1K
R8 10K
R9 1meg
R10 33K
R11 5.6K
R12 2.2K
R13 33K
R14 2.2K
R15 560
R16 5.6K

CAPACITORS

C1 0.047μf
C2 100μf
C3 2.5μf
C4 0.01μf
C5 4700pf
C6 Variable time delay
C7 0.01μf
C8 1.0μf
C9 25μf

TRANSISTORS

T1 0C71
T2 0C74N
T3 AF114N
T4 2S303
T5 0C71
Paint removed to make transistor light sensitive

DIODE

D1 1N914

Fig. 5.2 - Event Marker
Amplifier and Monostable Multivibrator.

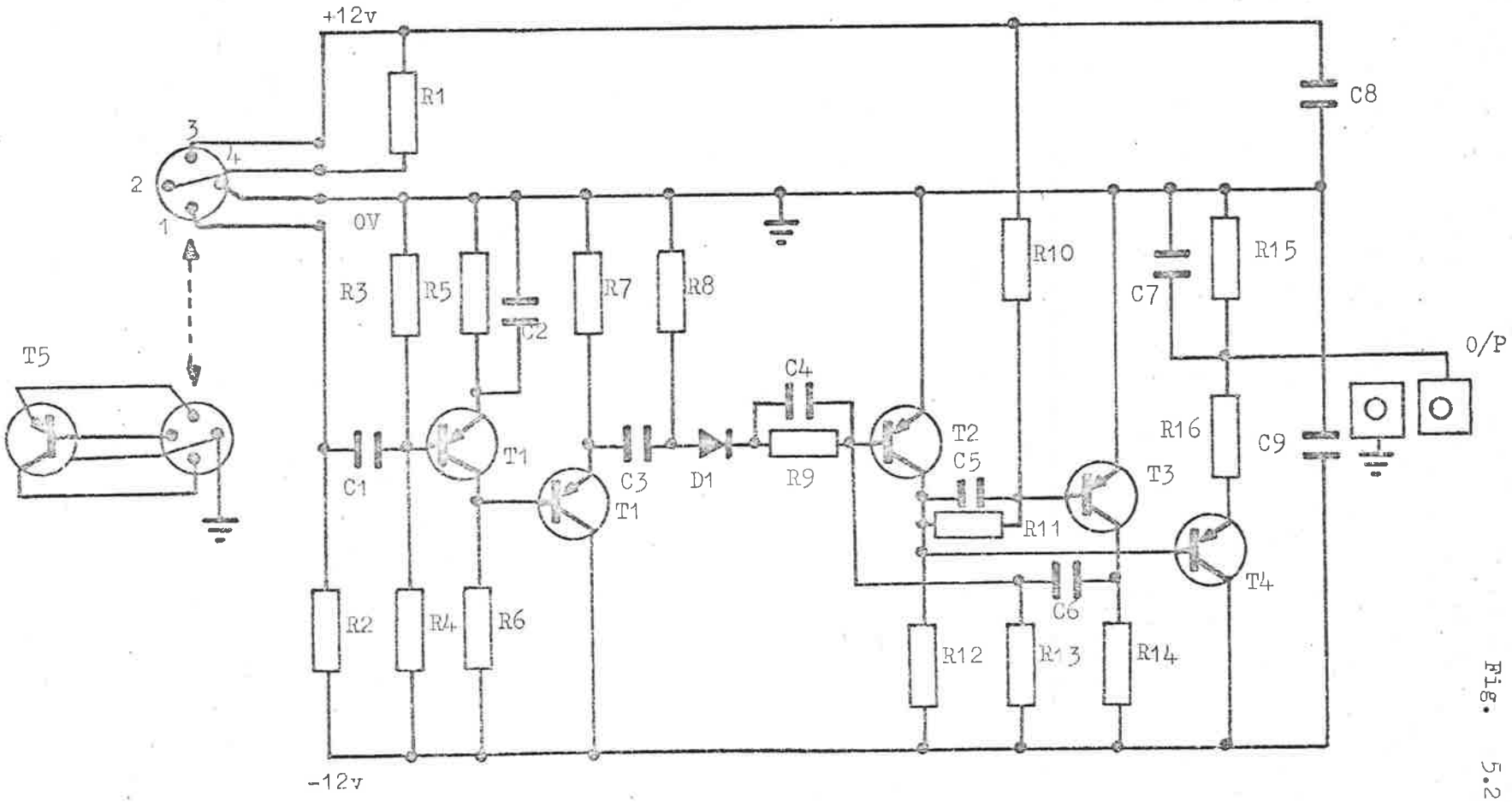

Fig. 5.2 - Event Marker - MK I
Amplifier and Monostable Multivibrator.

RESISTORS

R1 10K
R2 56K
R3 1.5K
R4 220K
R5 27K
R6 270Ω
R7 3.9K
R8 470Ω
R9 1.5K

CAPACITORS

C1 4μF

TRANSISTORS

T1 OC71 Photocell
T2 2N3694

DIODES

D1 AN1101

ZENER DIODES

Z1 1Z4.7T5

INTEGRATED CIRCUITS

IC1 μL914
IC2 μL914

Fig.5.3 Event Marker MK II
Integrated Circuit Monostable.

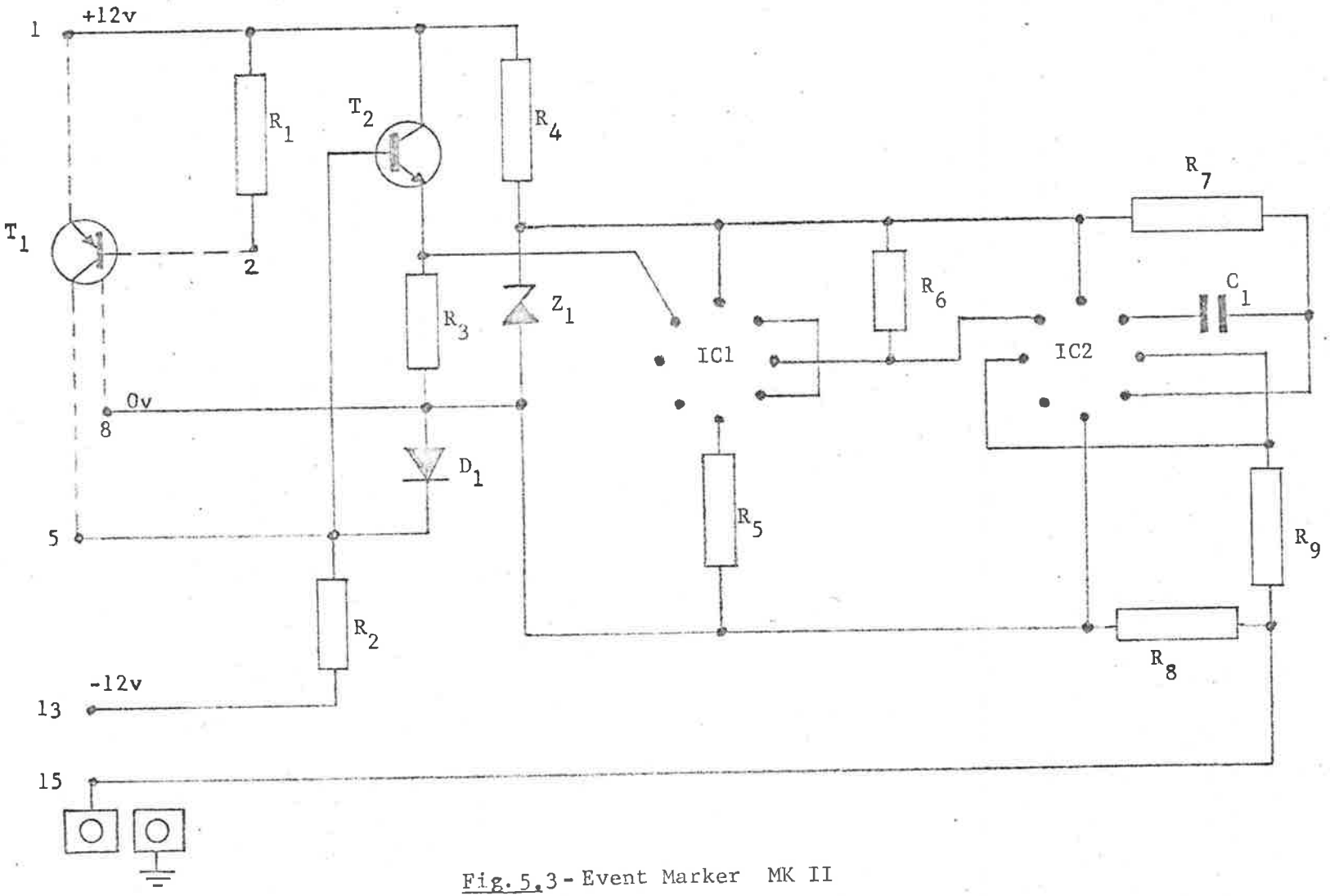

Fig. 5.3 - Event Marker MK II

Fig. 6.1

TRANSISTORS

T1	OC71
T2	AD140
T3	OC71
T4	AC128
T5	2N3638

ZENER DIODE

Z1 1Z30 T5

RESISTORS

R1	68 Ω
R2	1 K
R3	10 K
R4	15 K
R5	10 K

CAPACITORS

C1	1 µf
C2	1 µf
C3	1000 µf
C4	.68 µf

MONOSTABLE DEVICE

F/F1
F/F2
F/F3
F/F4

RELAYS SIEMENS

RL 1	6500/416
RL 2	"
RL 3	"
RL 4	"
RL 5	"
RL 6	6500/418

RL 1, Rl 2 } Connect Record/Reproduce Heads to V-F Converters

RL 3, RL 4 } Controls Tape Recorder Operation

RL 5 Connects Driver Amplifier and V-F Converters

RL 6 Controls Drive Coil of Uni-selector

Fig. 6.1 - Programme Switch
Block Diagram of Basic Cards.

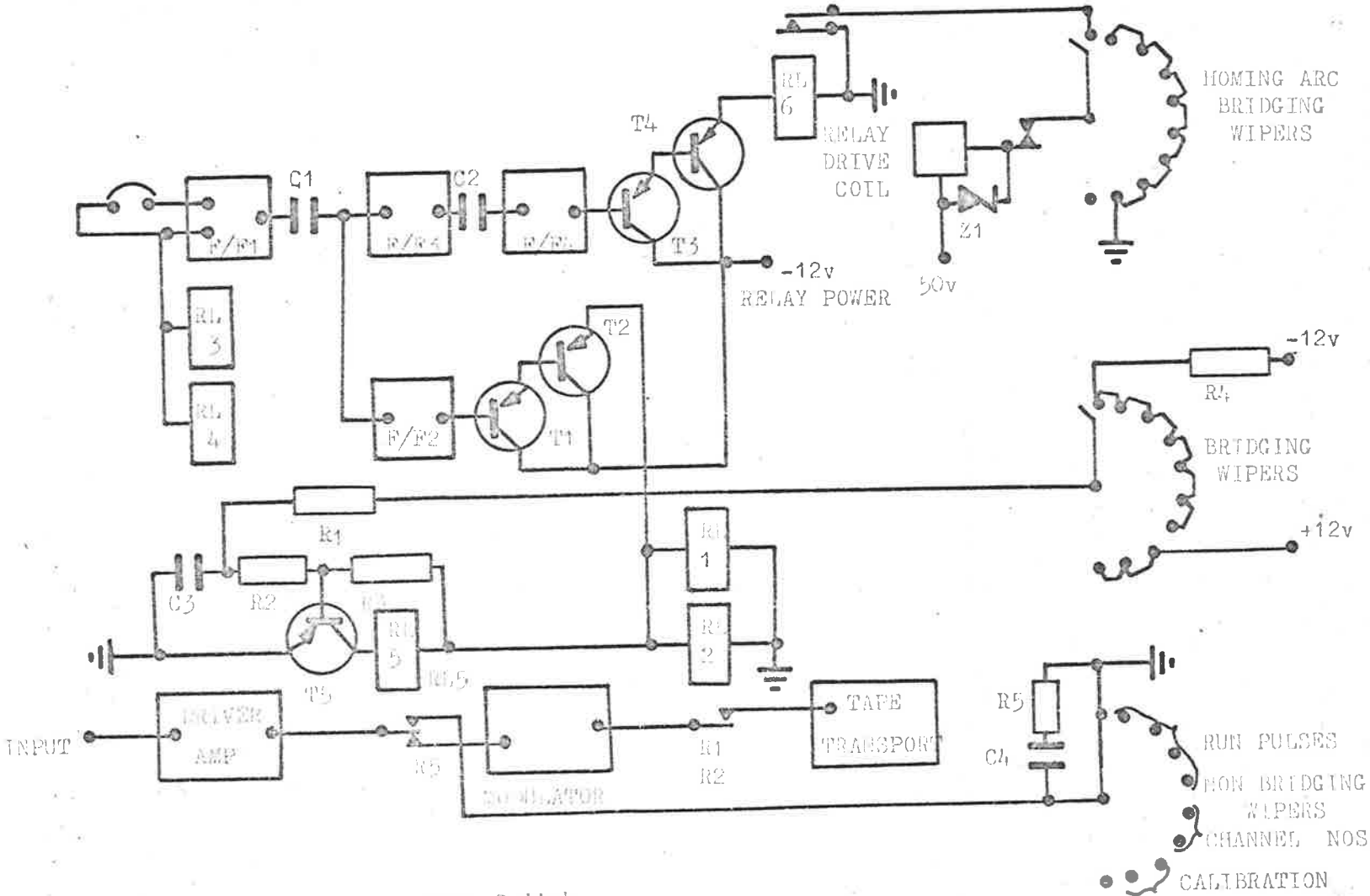

Fig. 6.1 - Programme Switch
Block Diagram of Basic Cards

Fig. 6.1

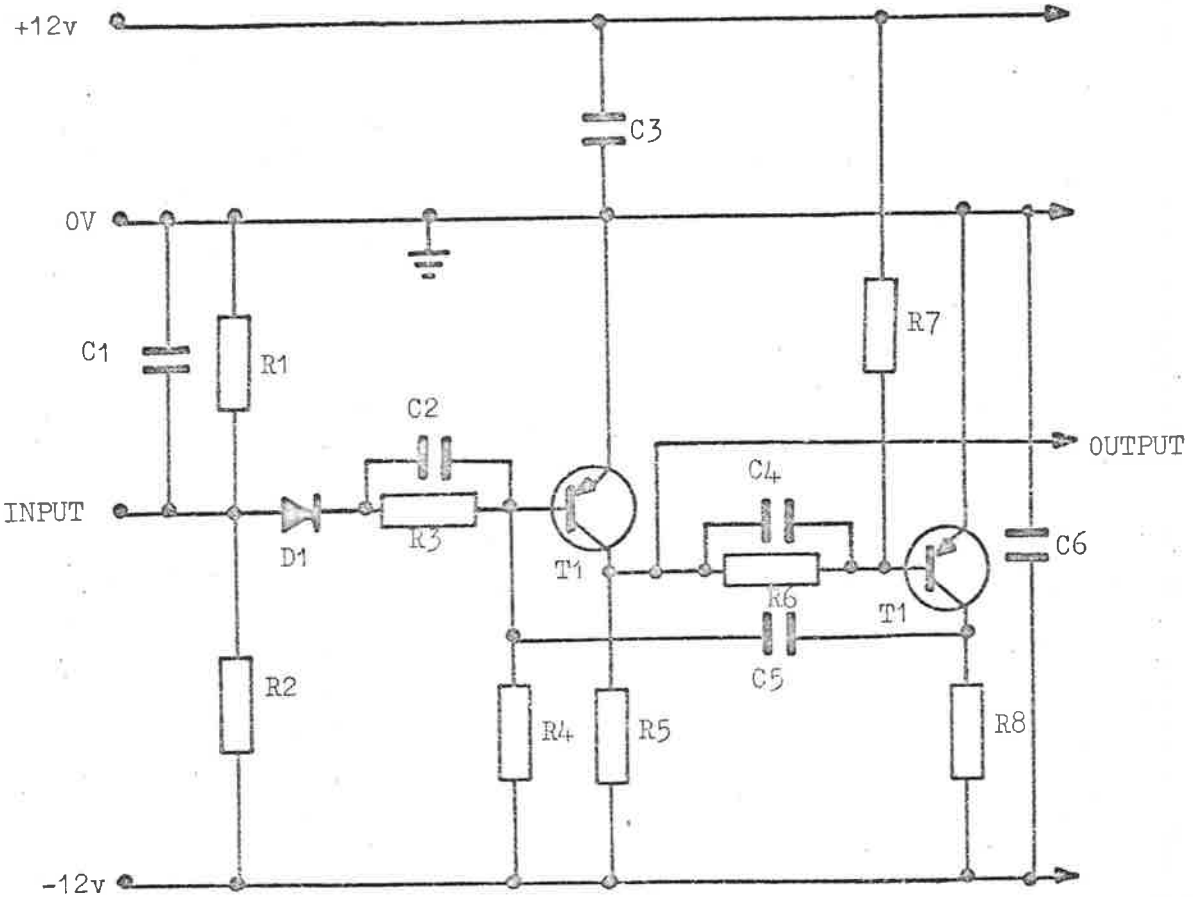

TRANSISTOR

T1 0C74N

DIODE

D1 1N914

RESISTOR

R1	10K
R2	39K
R3	1m
R4	33K
R5	2.2K
R6	1m
R7	33K
R8	2.2K

CAPACITOR

C1	560pf
C2	0.01µf
C3	25µf
C4	0.01µf
C5	time delay
C6	250µf

Fig. 6.2 - Programme Switch
Monostable Multivibrator.

Fig. 6.2

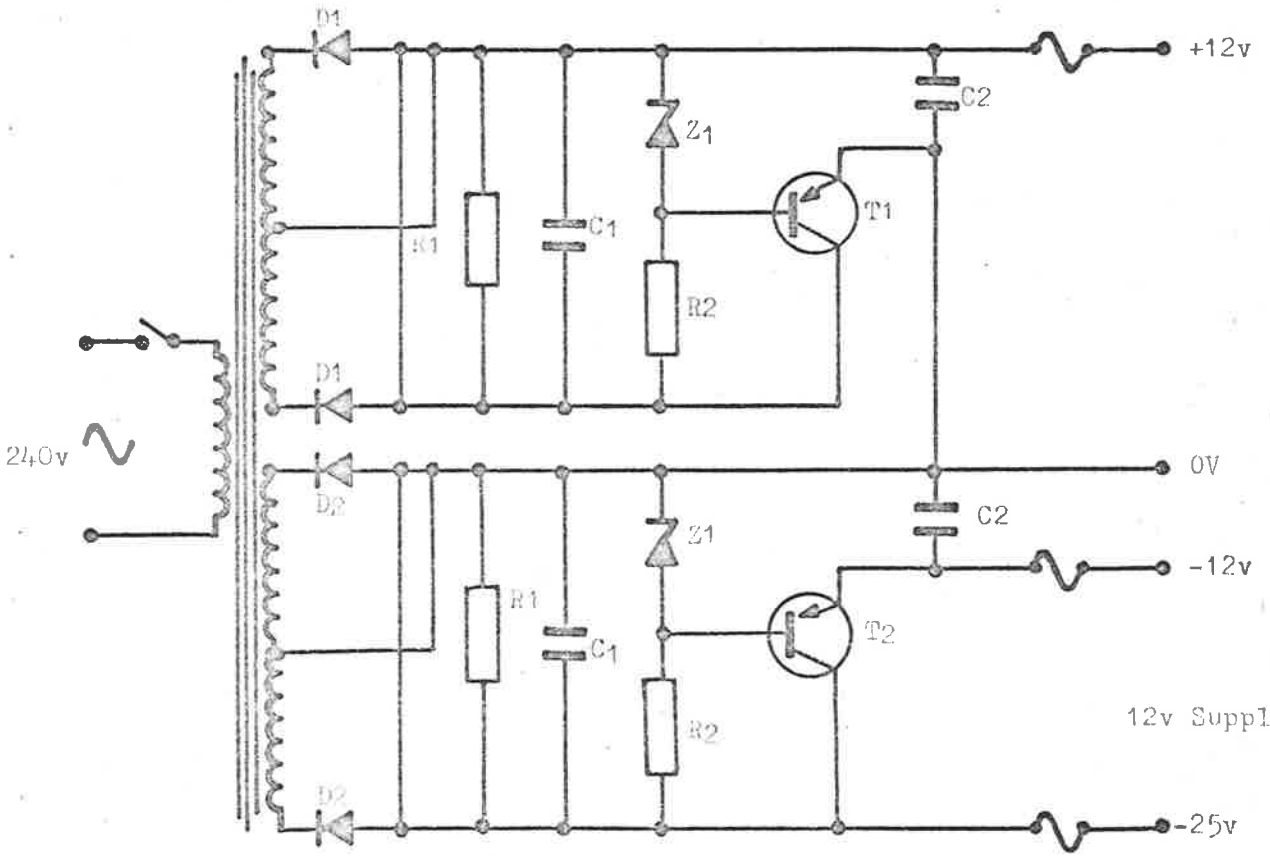

TRANSISTORS
T1) OC22 or
T2) AD140

ZENER DIODES
Z1 1Z12T5

DIODES
D1 1S023
D2 1S023

RESISTORS
R1 1K 1 watt
R2 390 1 watt

CAPACITORS
C1 500 µf
C2 640 µf

+12v
12v Supply 750 ma Fuse
-12v

+12v
Battery charge 1 amp fuse
-25v

Fig. 8.1 - D.C. Power Supply ± 12 volts.

Fig. 8.1

Fig. 8.2

VALVES

V1 6x4
V2 6x4
V3 6u8 two in one valve
V4 6u8 " " "
V5 5651

RESISTORS

R1 100KΩ
R2 47KΩ
R3 100KΩ
R4 47KΩ
R5 220KΩ
R6 220KΩ
R7 1KΩ
R8 3.3KΩ
R9 3.3KΩ
R10 1KΩ
R11 1mΩ
R12 1mΩ
R13 39KΩ
R14 33KΩ
R15 6.8KΩ

RESISTORS VARIABLE

RV1 10KΩ
RV2 10KΩ

CAPACITORS

C1 70µf
C2 .02µf
C3 2.0µf
C4 0.1µf
C5 40µf

Fig. 8.2 - D.C. Power Supply
High Tension ± 100v

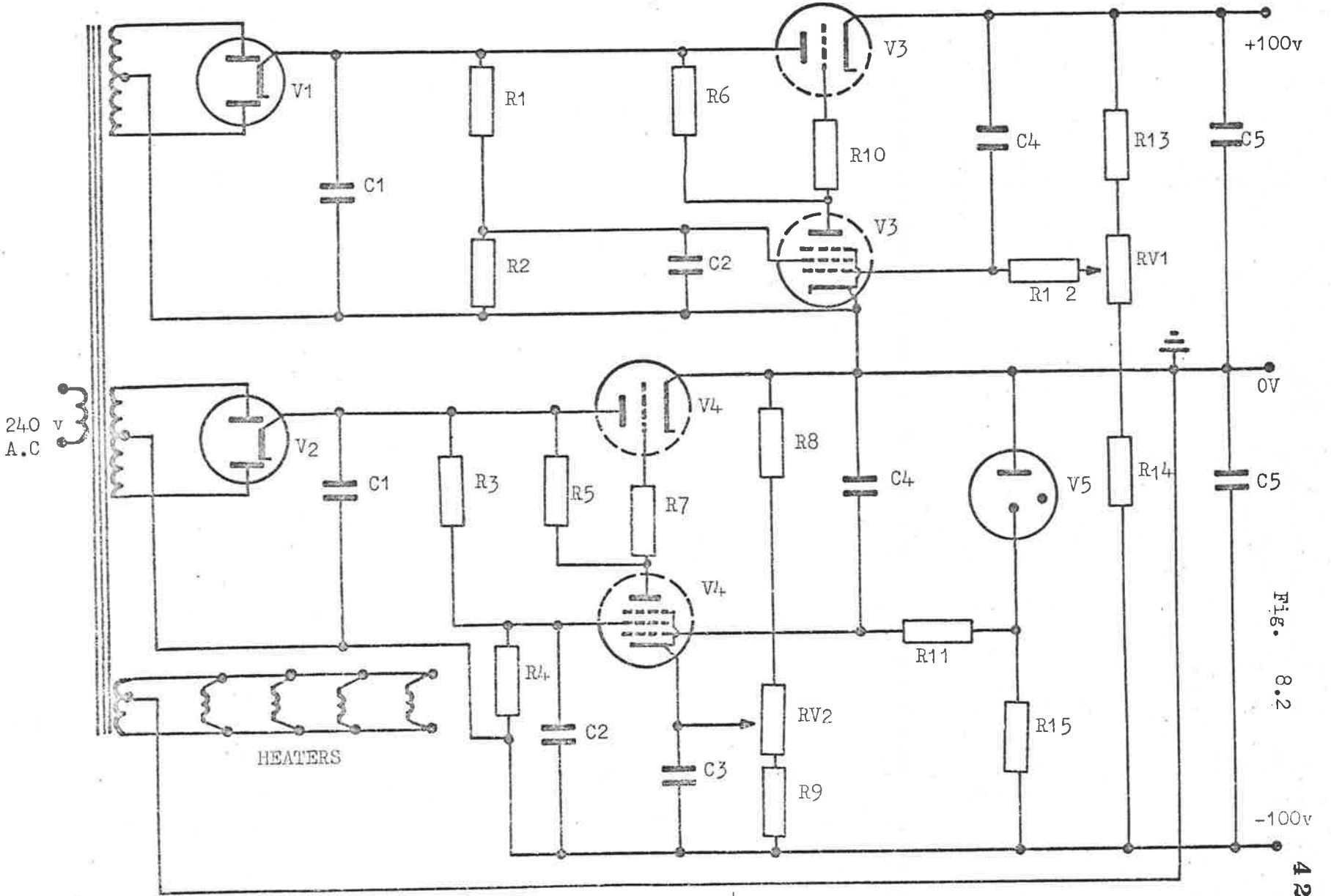

Fig. 8.2 - D.C. Power Supply. High Tension ± 100v

Fig. 8.2

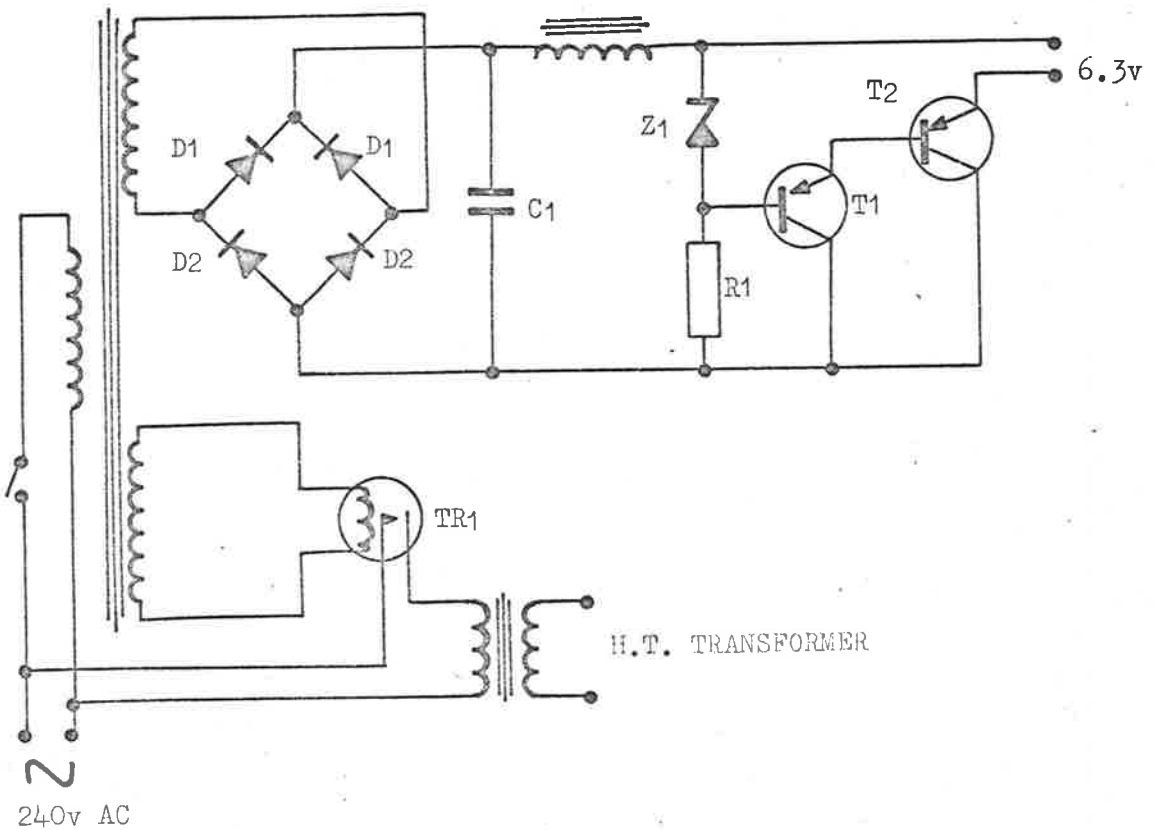

TRANSISTORS
T1 OC74N
T2 AD140

ZENER DIODE
Z1 1Z6.3T5

DIODES
D1 0A210
D2 0A210

RESISTORS
R1 180 1 watt

CAPACITORS
C1 4000μf

THERMAL RELAY
TR1 VLS631

Fig. 8.3 - DC Power Supply
Heaters of Driver Amplifier.

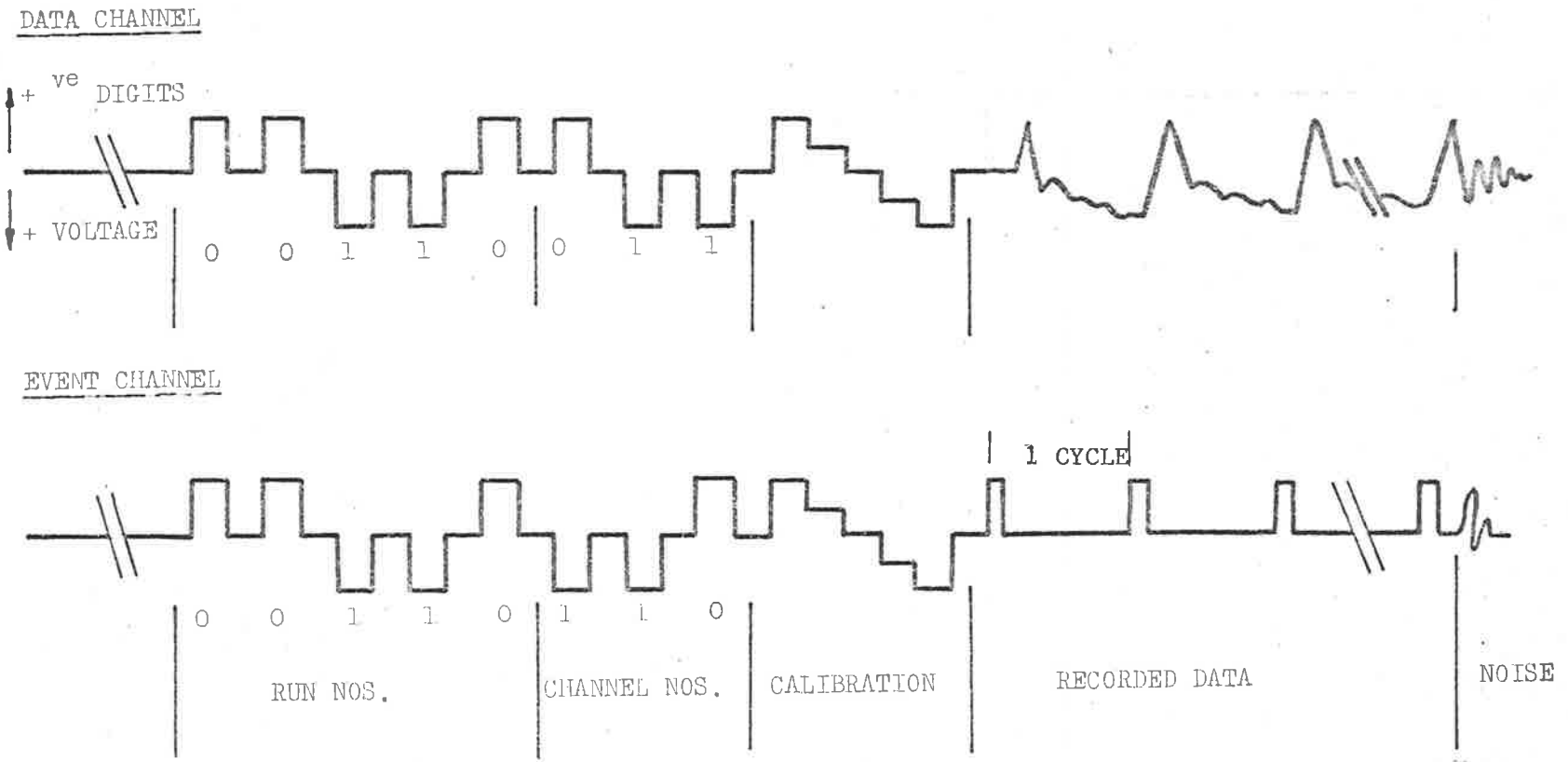

Fig. 9, Characteristics of a Single File from MOVADAS

APPENDIX A4

COMPUTING PROCEDURES

PROGRAMMES AND SUB-ROUTINES

TABLE OF CONTENTS

* Refer to Appendix A1

APPENDIX A 4

COMPUTING PROCEDURE - PROGRAMMES & SUBROUTINES

A4.0 GENERAL

In the course of the work many computer programmes were written for the digital computers of the University. Those listed in this Appendix are:-

TABLE	TITLE	REF.TEXT	COMPUTER
1	Programme CONVERT	5.1	CDC 3200
2	Programme CONTROL	6.4.3	CDC 6400
3(a)	Subroutine for 3-Wire Iteration by Bolzano Bisection Method	A1/6.3	These routines replace S/R Wire3 in Table 2 when signals recorded on 3 channels are from different size thermocouples.
3(b)	Subroutine for direct calculation of True Gas Temp. from 3-Wire Fourier coefficients.	A1/6.4	
4	Engine Performance Data Reduction	6.2	IBM 1620
5	Engine Heat Transfer Data Reduction	6.4.1	IBM 1620

Tables 1 and 2 only will be detailed under 'Computing Procedure' since these programmes are concerned with the processing, analysis and resynthesis of the instantaneous heat transfer data.

A4.1 COMPUTING PROCEDURE

The information recorded on magnetic tape by MOVADAS (Appendix A3) was in Frequency Modulated (FM) form. Before this could be processed by a digital computer, this information had to be converted to an array of digits in Binary Coded Decimal (BCD) format which represented the recorded signal sampled at equal intervals of time. The FM Analogue to Digital (A-D) Conversion was carried out at the Mathematical Services Division of the Weapons Research Establishment South Australia. Subsequent analysis of the data was conducted on the digital

computers at the University

The analysis of the data was divided into the following stages.

(1) PROGRAMME CONVERT (Table 1)

The digital information in the form discussed in A3.3 and A3.4 of Appendix A3 was firstly decoded into a format compatible with theinternal word structure of the University computers, and then data files were recognised from the identification pulses. This conversion was necessary because the digital (binary) output from the A-D Converter was to IBM 7090 format which was incompatible with the requirement of the CDC computers at the University.

As mentioned in Section A3.4 of Appendix A3, the analogue information was simultaneously applied to all active channels of MOVADAS and recorded on separate tracks of the magnetic tape. Included in this analogue information were the identification pulses, i.e., run and channel numbers, and instantaneous V-F Converter calibrations. The analogue information was converted separately for each track to digital information at the same sampling frequency of 4000 samples per second. After A-D conversion, digital files were then written consecutively 'end-to-end' on the digital(or 'Transmittal')tape. The occurrence of the last calibration voltage pulse was taken as the time zero origin, and was thus accurate to 1/4000 of a second. Hence a digital sample from one channel counted from the time origin had a corresponding sample at the same instant of time on all other channels.

The digital samples after time zero origin were selected and recorded, together with various identification numbers, on to another magnetic tape(the 'Convert'tape) for subsequent analysis by programme CONTROL.

(2) PROGRAMME CONTROL (Table 2)

This acts principally as the controlling and output programme for all the following subroutines. Using the recorded data from CONVERT and with input instructions from punched data cards, the analysis was as follows:-

Subroutines SYNC1 & SYNC2

These routines selected from the digital files of each experimental data channel in turn an array of numbers which corresponded to a given number of recorded cycles.

As previously mentioned, the digital information from CONVERT contained all samples from time zero origin. From the digital event file, the particular locations of the event pulses from the time origin were determined. The corresponding points on the data files were also located. Thus, it was possible to select from the complete digital file an array of numbers between any two event pulses.

Subroutines CONV & REDFA

The data were converted into real values of the measured variables (temperature and pressure) since the sensitivities of each unit in the recording system were known. The V-F converter sensitivity was obtained from the known instantaneous calibration levels which preceded the recorded data. (Section A3.4 Appendix A3).

Subroutines FASQW & CALC

A Fourier analysis of the data over the selected cycle was performed by the square-wave infinite series method of Clarke(Ref.49). Output was in the form of the Modulus, Cosine and Sine components of the variable for each harmonic of engine cyclic frequency; and their phase angles with respect to the CTDC (Event) point.

Subroutine HFLUX

This synthesises the wall temperature fluctuations from the Fourier coefficients, adds the mean wall temperature and plots the values over the selected cycle. The Fourier coefficients of the corresponding heat flux cycle are determined by differentiating the series representing the wall temperature. The cyclic component of heat flux is then synthesised, the measured mean value added and the total instantaneous heat flux cycle plotted.

Subroutine WIRE3

From the Fourier coefficients for corrected instantaneous gas temperature the cyclic component is synthesised, the recorded mean value added and the cycle plotted. The same procedure is repeated for gas pressure.

Eichelberg's heat transfer coefficient is calculated at each crank angle sample and so is the modified value using instantaneous piston speed.

These values are returned to Programme CONTROL where they are plotted together with the experimental quasi-steady coefficient. Also in CONTROL, the moduli of heat flux, gas temperature and wall temperature for each harmonic is used to plot the spectrum of heat transfer coefficient; and a synthesised coefficient is also plotted over the cycle.

Subroutine MEKPLT

This is an automatic plotting routine developed to enable a line printer to plot the values stored in a double subscripted array. This routine provides automatic scaling and choice of origin for up to 10 separate functions plotted on the one sheet. The coordinate axes are anotated and the titles may be specified for each axis. The input instructions are given at the beginning of subroutine MEKPLT in Table 2.

A 4.2 PROGRAMME INPUT INSTRUCTIONS

The programmes are listed in the tables following. The definitions of the input variables are as follows:-

(1) PROGRAMME CONVERT

ITAPTRN	Transmittal or digital tape number
ITAPCON	The number of the CONVERT output tape
NNSER	Series run number
LIST	Output format control: -ve lists the data points only 0 lists the data points and writes also on to magnetic tape. +ve writes on magnetic tape only
LLEST(N,M)	File numbers to be listed,skipped,listed,.....etc
LSKFLD	The number of times required to(list,skip)

(2) PROGRAMME CONTROL

ITAPA	F.M.Analogue tape number
ITAPT	Transmittal or Digital tape number
ITAPCON	Convert (BCD) tape number
ITAPSYN	Extra file identification if required
NPI	Number of the cycle of the Event at which analysis is to begin
NP	The number of cycles over which the analysis is performed
LIST	-ve or 0 lists the data points over one cycle and the Fourier coefficients of the NP cycles +ve does not list the above
ICHN	No. of the data channel to be investigated
NTYPE	Identification for the type of data
KKD	Number of Fourier coefficients required per engine cycle

VOLTC(I),I=1,5 Values of the 5 calibration voltage levels which were supplied automatically to the FM Converters when recording a run

ALPHA(I),I=1,8 A heading card characterising the experimental run

NSER Serial number of experimental group

IRUN Run number for the particular experimental recording and also the file number on the digital tape

NOCHN(I),I=1,7 The channel number corresponding to the recorded data to be investigated.The Event Marker channel number precedes all others

REV Rotational speed of the engine (r.p.m.)

IRAM Number of samples synthesised per cycle (usually 144=5^{o}crankangle)

ALFA Thermal diffusivity of probe wall

CON Thermal conductivity of probe wall

IFMC FM Converter (or Channel No.) for required data

IG2,IG3,IG4 Gain switch positions of Preamplifiers,Attenuation switch and Driver amplifiers.The gain figures are given in the programme as GG2(I,J),GG3(I,J),GG4(I,J) for each channel (I) and each setting (J)

G1 Thermocouple and Pressure transducer sensitivities

G2,G3,G4 Gain values consequent on switch settings above

TWM Mean or steady-state value of recorded wall surface temperature

QM Mean or steady-state heat flux from the calorimeter probe

TM Mean or steady-state value of gas temperature

PM Atmospheric pressure

TABLE 1

```
      PROGRAM CONVERT
C     CONVERTS MAG. TAPE FROM A-D CONVERTER INFORMATION RECORDED
C      INITIALLY ON MOVADAS IN FM ANALOG FORM
C     CONVERTS THE LIST OF NUMBERS IN EACH FILE NAMED FROM IBM 7090
C      FORMAT TO CDC 3200 OR 6400 FORMAT
C     THE TIME WORDS ARE REMOVED, FILES THAT ARE NOT DATA FILES ARE
C      REJECTED, IDENTIFICATION AND CALIBRATION PULSES ARE LOCATED
C      AND DECODED, THE TRUE DATA IS PLACED ON MAG. TAPE WITH THE
C      NECESSARY IDENTIFICATION
C     DATA OUTPUT IN BLOCKS OF 864 NUMBERS WITH DUMMY EOF AFTER EACH
C      BLOCK (-1,100,-10)
C     AFTER THE LAST BLOCK A DUMMY EOF IS (-2,-200,-20)
C     THIS IS FOLLOWED BY A TRUE END OF FILE
      INTEGER SHIFT
      INTEGER VAL,AND
      DIMENSIONINPT(486),VAL(1836),IFILE(8),ICAL(5)
      DIMENSIONLLEST(60,2)
      DIMENSIONIV(3),IW(3)
    5 FORMAT(55X,10HEOF SENSED)
    6 FORMAT(10X,22HEOF WRITTEN ON OUTTAPE)
   10 FORMAT(10X,33HPARITY ERROR DETECTED AND IGNORED)
   15 FORMAT(20X,19HCONVERTED RECORD NO,I5)
   20 FORMAT(1X,20HTOTAL NUMBER RECORDS,I6)
   25 FORMAT(1H-,11HFILE NUMBER,I6)
   30 FORMAT(1X,20I5)
   35 FORMAT(24I3)
   40 FORMAT(50X,22HDATA FILE NOT DETECTED)
   45 FORMAT(5X,9HRECORD NO,I5)
   50 FORMAT(5I5)
   55 FORMAT(20H TRANSMITTAL TAPE NO,I6,3X,15HCONVERT TAPE NO,I6)
   60 FORMAT(1X,9I5)
   65 FORMAT(50X,25HEOF DETECTED BEFORE IDENT)
   70 FORMAT(7X,14HGOOD DATA FILE)
   75 FORMAT(15X,18HLOOKING FOR IDENTS)
   80 FORMAT(10X,10HFILE IDENT,I5,3H  =,I2,4X,11HNO OF STEPS,I3)
   85 FORMAT(3X,12HSKIP FILE NO,I5)
```

```
   90 FORMAT(50X,29HCALIBRATION SIGNALS INCORRECT)
   95 FORMAT(9I5)
   96 FORMAT(20I5)
   97 FORMAT(3I5)
      IV(1)=-1
      IV(2)=-100
      IV(3)=-10
      IW(1)=-2
      IW(2)=-200
      IW(3)=-20
C     READS TRANSMITTAL AND CONVERT TAPE NOS, SERIAL NO. OF DATA
C     LIST +VE IF MAG. TAPE ONLY IS REQUIRED
C     LIST ZERO FOR MAG. TAPE AND LIST OF POINTS
C     LIST -VE FOR LIST OF POINTS ONLY
      READ(60,50)ITAPTRN,ITAPCON,NNSER,LIST,LSKFLD
      WRITE(61,55)ITAPTRN,ITAPCON
      IF(LIST)103,102,102
  102 REWIND11
  103 CALL DENS(10,1,REJ)
C     READS NO. OF FILES TO BE LISTED, SKIPPED, LISTED, SKIPPED, ...ETC.
      READ(60,35)((LLEST(N,M),M=1,2),N=1,LSKFLD)
      NOFILE=0
      DO106N=1,LSKFLD
      IF(LLEST(N,1).EQ.0.AND.LLEST(N,2).EQ.0)1000,104
  104 IF(LLEST(N,1))1000,105,109
  105 IF(LLEST(N,2))1000,1000,107
  106 CONTINUE
  107 LL=LLEST(N,2)
      DO108LT=1,LL
      NOFILE=NOFILE+1
      WRITE(61,85)NOFILE
  108 CALL SKIP(10)
      GOTO106
  109 NL=LLEST(N,1)
      DO990LT=1,NL
      NOREC=0
```

```
      NODIS=0
      IDENT=0
      IP=0
      JS=0
      KFILE=1
      JTEST=1
      JDTEST=6
      IYD=35
      IIYD=30
      NOFILE=NOFILE+1
      WRITE(61,25)NOFILE
      BUFFERIN(10,1)(INPT(1),INPT(486))
  100 CALL UNITST(10,K)
      GOTO(100,136,110,120),K
  110 IF(IP)1000,985,95
  120 WRITE(61,10)
  136 NOREC=NOREC+1
      WRITE(61,45)NOREC
C     BY MASKING BREAKS THE WORD INTO TWO WORDS
      DO140I=1,486
      J=2*I-1+JS
      VAL(J)=SHIFT(INPT(I),-12)
  140 VAL(J+1)=AND(INPT(I),7777B)
      BUFFERIN(10,1)(INPT(1),INPT(486))
      NUM=972+JS
C     CHECKING FOR TIME WORDS AND REMOVING THEM
      IF(AND(VAL(JS+971),4000B).EQ.4000B.AND.AND(VAL(JS+972),40B).EQ.40B
     1.AND.AND(VAL(JS+1),4000B).EQ.4000B)150,170
  150 II=1+JS
      III=969+JS
      DO160I=II,III
  160 VAL(I)=VAL(I+1)
      NUM=NUM-3
      GOTO200
  170 IF(AND(VAL(JS+972),4000B).EQ.4000B.AND.AND(VAL(JS+1),40B).EQ.40B.A
     1ND.AND(VAL(JS+2),4000B).EQ.4000B)180,200
```

```
  180 II=1+JS
      III=969+JS
      DO190I=II,III
  190 VAL(I)=VAL(I+2)
      NUM=NUM-3
  200 I=1+JS
  210 IF(AND(VAL(I),4000B).EQ.4000B.AND.AND(VAL(I+1),40B).EQ.40B.AND.AND
     1(VAL(I+2),4000B).EQ.4000B)220,235
  220 NUM=NUM-3
      DO230J=I,NUM
  230 VAL(J)=VAL(J+3)
  235 I=I+1
      IF(I-NUM+2)210,210,237
  237 WRITE(61,15)NOREC
      IF(JS)1000,236,25
  236 JS=864
      GOTO100
  250 GOTO(400,455,700),KFILE
C     CHECKING FOR A DATA FILE, IE, INITIAL POINTS ARE APPROX. CONSTANT
  400 IF(NOREC-3)405,405,450
  405 DO420I=36,864,18
      IF(IABS(VAL(I)-VAL(I-18))-IYD)420,420,410
  410 JTEST=JTEST+1
  420 CONTINUE
      GOTO(1000,900,430),NOREC
  430 IF(JTEST-JDTEST)445,440,440
  440 WRITE(61,40)
      CALL SKIP(10)
      GOTO990
  445 WRITE(61,70)
  450 KFILE=2
      L=39
  455 WRITE(61,75)
  500 L=L+1
      IF(L-903)520,520,510
  510 L=39
```

```
C       IDENTIFYING THE IDENTIFICATION PULSES
        GOTO900
  520   IF(IABS(VAL(L)-VAL(L-1))-IIYD)500,500,525
  525   IF(IABS(VAL(L)-VAL(L-10))-IIYD)500,500,530
  530   IF(IABS(VAL(L)-VAL(L-20))-IIYD)500,500,535
  535   IF(IABS(VAL(L-1)-VAL(L+1))-IYD)540,540,545
  540   IF(IABS(VAL(L-1)-VAL(L+2))-IYD)500,500,545
  545   LTEST=1
C       CHECKING THAT IT IS A PULSE
        DO555M=20,40
        MN=L+M
        IF(IABS(VAL(MN)-VAL(MN-1))-IYD)555,555,550
  550   LTEST=2
  555   CONTINUE
        GOTO(575,560,1000),LTEST
C       ANOTHER CHECK FOR THE PULSE
  560   DO570M=40,60
        MN=L+M
        IF(IABS(VAL(MN)-VAL(MN-1))-IYD)570,570,565
  565   LTEST=3
  570   CONTINUE
        GOTO(1000,575,500),LTEST
C       KEEPS RUNNING COUNT OF THE NO. OF DISCONTINUITIES AND SQUARE PULSES
  575   IF(NODIS-16)590,640,640
  590   NODIS=NODIS+1
        IF(NODIS/2-(NODIS+1)/2)600,630,1000
  600   IDENT=IDENT+1
        IF(VAL(L)-VAL(L-1))620,1000,610
  610   IFILE(IDENT)=0
        GOTO630
  620   IFILE(IDENT)=1
  630   L=L+100
        WRITE(61,80)IDENT,IFILE(IDENT),NODIS
        GOTO500
  640   IDENT=IDENT+1
        ISUM=0
```

```
C       DETERMINING THE CALIBRATION LEVELS
        DO670I=20,80
        IAL=I+L
  670   ISUM=ISUM+VAL(IAL)
        SUM=ISUM
        ICAL(IDENT-8)=SUM/61.0
        IF(IDENT-13)675,680,1000
  675   L=L+100
        GOTO500
C       DECODES RUN AND CHANNEL NOS.
  680   IIRUN=IFILE(1)*16+IFILE(2)*8+IFILE(3)*4+IFILE(4)*2+IFILE(5)
        IICHN=IFILE(6)*4+IFILE(7)*2+IFILE(8)
        WRITE(61,60)NNSER,IIRUN,IICHN,(ICAL(I),I=1,5),ITAPCON
        WRITE(61,97)(IV(I),I=1,3)
C       CHECK ON VALUES FOR CALIBRATION
        IF(ICAL(1).GT.ICAL(3).AND.ICAL(5).LT.ICAL(3))684,984
C       VARIOUS OUTPUT FORMATS DEPENDING ON THE VALUE OF LIST
  684   IF(LIST)690,685,685
  685   WRITE(11,95)NNSER,IIRUN,IICHN,(ICAL(I),I=1,5),ITAPCON
        WRITE(11,97)(IV(I),I=1,3)
  690   KFILE=3
        LLL=L+250
        IP=0
        DO695J=LLL,1728
        IP=IP+1
  695   VAL(IP)=VAL(J)
        IF(864-IP)720,100,100
  700   DO710J=865,1728
        IP=IP+1
  710   VAL(IP)=VAL(J)
  720   IF(LIST)730,735,740
  730   WRITE(61,30)(VAL(I),I=1,864)
        WRITE(61,97)(IV(I),I=1,3)
        GOTO750
  735   WRITE(61,30)(VAL(I),I=1,864)
        WRITE(61,97)(IV(I),I=1,3)
```

```
740 WRITE(11,96)(VAL(I),I=1,864)
    WRITE(11,97)(IV(I),I=1,3)
750 IP=IP-864
    DO760J=1,IP
760 VAL(J)=VAL(J+864)
    GOTO100
900 DO910I=1,864
910 VAL(I)=VAL(I+864)
    GOTO100
950 IF(IDENT-13)985,955,1000
955 IF(LIST)960,965,970
960 WRITE(61,30)(VAL(I),I=1,IP)
    WRITE(61,97)(IW(I),I=1,3)
    GOTO980
965 WRITE(61,30)(VAL(I),I=1,IP)
    WRITE(61,97)(IW(I),I=1,3)
970 LLL=IP+1
    DO975I=LLL,864
975 VAL(I)=0
    WRITE(11,96)(VAL(I),I=1,864)
    WRITE(11,97)(IW(I),I=1,3)
980 WRITE(61,20)NOREC
    WRITE(61,5)
    GOTO990
984 WRITE(61,90)
    CALL SKIP(10)
    GOTO990
985 WRITE(61,65)
    WRITE(61,20)NOREC
990 CONTINUE
    GOTO105
1000 CALL DENS(10,2,REJ)
    IF(LIST)1002,1001,1001
1001 END FILE 11
    WRITE(61,6)
1002 STOP
    END
```

TABLE 2

```
      PROGRAM CONTROL(TAPE62,INPUT,TAPE60=INPUT,OUTPUT,TAPE61=OUTPUT,TAP
     1E10)
C     COMPLETE FOURIER ANALYSIS OF DATA FROM MOVADAS CONVERSION
C      TO CDC 6400 WORD STRUCTURE (SEE PROGRAM 'CONVERT')
      COMMONIY(4321),Y(4321),ITAPCON,NSER,IRUN,NOCHN(8),ICAL(5)
      COMMONVOLTC(5),NPI,NP,NPD,NPTS,LIST,ISTOP
      COMMON NTEST,CAL(5),NPERD,MI,MF,KKD
      COMMON TMOD(250),TPHI(250),REV
      COMMON YS(250,2),YC(250,2)
      COMMON G1,G2,G3,G4
      COMMON NCO
      COMMON AW(144),BW(144),CW(144),DW(144),EW(144),FW(144),GW(144)
      DIMENSION GG2(3,6),GG3(3,2),GG4(3,10)
      DIMENSION ALPHA(8),MPLT(3)
      DIMENSION TW(144),QW(144),TG(144),H(144,3)
      DIMENSION YWC(144),YWS(144),YFC(144),YFS(144),YGC(144),YGS(144),Q(
     1144),DTC(144),DTS(144),DT(144),BH(144),BBH(150),SDT(144)
      DO9999 I=1,10185
 9999 IY(I)=0
   10 FORMAT(9I3)
   50 FORMAT(1H0,10HERROR TYPE,3(2X,I5))
   60 FORMAT(1H0,7HCHAN NO,I6)
   11 FORMAT(1H0,12I5)
   95 FORMAT(4I5)
   96 FORMAT(1H1,15HCONVERT TAPE NO,I5)
   97 FORMAT(1H ,11HANALOG TAPE,I3,4X,16HTRANSMITTAL TAPE,I6)
   98 FORMAT(3I3/3I4/5F10.3)
  100 FORMAT(8A10)
  101 FORMAT(1H ,8A10)
  110 FORMAT(3E10.3)
  120 FORMAT(F6.0)
  130 FORMAT(I4,F6.2,F6.1)
  180 FORMAT(1H0,7H SERIAL,5X,3HRUN,5X,7HCHANNEL,5X,4HTYPE,3X,10HNO PERI
     1ODS,3X,10HCOEFF      ,3X,9HNO POINTS,3X,21HINITIAL - MAX PERIODS)
  190 FORMAT(1H0,I6,4(5X,I5),2(8X,I5),I9,I8)
  195 FORMAT(4I3)
```

```
  111 FORMAT(I3)
  112 FORMAT(I4,2X,F5.0,8(2X,E10.3))
  113 FORMAT(1H1,*CYCLE  CRANK  PRESSURE   GAS TEMP.   WALL TEMP.    HEA
     1T       PISTON*,12X,*HEAT TRANSFER COEFF.*,/,1X,*COUNT  ANG*,41X,
     1*FLUX       VELOC.       EXPT.     EICH VP.    EICH. VPM*)
 1200 FORMAT(1H1,46HFOURIER COEFFICIENTS OF COMPLETE DATA ANALYSED)
 1300 FORMAT(1H0,9X,5HINDEX,8X,11HHTC MODULUS)
  140 FORMAT(11X,I4,4X,E14.7)
  150 FORMAT(1H0,9X,11HCYCLE COUNT,8X,9HSYNTH HTC)
 2001 FORMAT(X,I4,5X,2E12.5)
C     CALIBRATION VALUES FOR FM CONVERTER NO. 1
C     PREAMPLIFIER GAINS
      GG2(1,1)=10.0
      GG2(1,2)=20.0
      GG2(1,3)=40.0
      GG2(1,4)=60.0
C     ATTENUATION SWITCH POSITION
      GG3(1,1)=1.00
      GG3(1,2)=0.10
C     DRIVER AMPLIFIER GAINS
      GG4(1,1)=10.10
      GG4(1,2)=14.5
      GG4(1,3)=20.5
      GG4(1,4)=31.2
      GG4(1,5)=41.5
      GG4(1,6)=60.8
      GG4(1,7)=90.7
      GG4(1,8)=116.0
C     CALIBRATION VALUES FOR FM CONVERTER NO. 2
C     PREAMPLIFIER GAINS
      GG2(2,1)=10.0
      GG2(2,2)=20.0
      GG2(2,3)=40.0
      GG2(2,4)=60.0
C     ATTENUATION SWITCH POSITION
      GG3(2,1)=1.00
```

```
      GG3(2,2)=0.10
C     DRIVER AMPLIFIER GAINS
      GG4(2,1)=10.10
      GG4(2,2)=14.50
      GG4(2,3)=20.9
      GG4(2,4)=32.3
      GG4(2,5)=43.3
      GG4(2,6)=65.0
      GG4(2,7)=94.0
      GG4(2,8)=129.0
C     CALIBRATION VALUES FOR FM CONVERTER NO. 3
      GG2(3,1)=10.0
      GG2(3,2)=20.0
      GG2(3,3)=40.0
      GG2(3,4)=60.0
C     ATTENUATION SWITCH POSITION
      GG3(3,1)=1.00
      GG3(3,2)=0.10
C     DRIVER AMPLIFIER GAINS
      GG4(3,1)=11.70
      GG4(3,2)=16.60
      GG4(3,3)=23.60
      GG4(3,4)=38.75
      GG4(3,5)=49.50
      GG4(3,6)=84.00
      GG4(3,7)=108.0
      GG4(3,8)=150.0
      READ(60,095)ITAPA,ITAPT,ITAPCON,ITAPSYN
      READ(60,098)NPI,NP,LIST,ICHN,NTYPE,KKD,(VOLTC(I),I=1,5)
  205 READ(60,100)(ALPHA(I),I=1,8)
      IF(ENDFILE 60)1000,200
  200 READ(60,010)NSER,IRUN,(NOCHN(I),I=1,7)
      READ(60,120)REV
      READ(60,130)IRAM,ALFA,CON
      WRITE(61,096)ITAPCON
      WRITE(61,097)ITAPA,ITAPT
```

```
      WRITE(61,011)NSER,IRUN,(NOCHN(I),I=1,7),NPI,NP,LIST
      NTEST=1
      NCHN=1
      CALL SYNC1
  211 NCHN=NCHN+1
      IF(NOCHN(NCHN))213,205,215
  213 IERR=006
      WRITE(61,050)IERR,NCHN,NCHN
      GOTO1000
  215 READ(60,195)IFMC,IG2,IG3,IG4
      IF(IFMC.EQ.3)216,217
  216 G1=1.12E-03
      GOTO218
  217 G1=22.4E-06
  218 G2=GG2(IFMC,IG2)
      G2=GG2(IFMC,IG2)
      G3=GG3(IFMC,IG3)
      G4=GG4(IFMC,IG4)
      CALL SYNC2(NCHN)
  220 GOTO(221,222),NTEST
  221 CALL CONV
  222 GOTO(230,205),NTEST
  230 CALL REDFA
      WRITE(61,096)ITAPCON
      WRITE(61,100)(ALPHA(I),I=1,8)
      WRITE(61,097)ITAPA,ITAPT
      WRITE(61,180)
      WRITE(61,190)NSER,IRUN,ICHN,NTYPE,NPD,KKD,NPTS,NPI,NPERD
      CALL FASQW
      CALL CALC
      J=NPD
      KK=KKD*NPD
      IF(NCHN-3)231,232,233
  231 DO234K=J,KK,J
C     FOURIER COEFFS OF WALL TEMP  RETURNED FROM S/R CALC
      YWC(K)=YC(K,1)
      YWS(K)=YC(K,2)
C     FOURIER COEFFS OF HEAT FLUX
      YFC(K)=YC(K,2)+YC(K,1)
```

```
  234 YFS(K)=YC(K,2)-YC(K,1)
      GOTO233
  232 DO235K=J,KK,J
C     FOURIER COEFFS OF GAS TEMP  RETURNED FROM S/R CALC
      YGC(K)=YC(K,1)
  235 YGS(K)=YC(K,2)
  233 GOTO(240,238,241)IFMC
  240 READ(60,120)TWM
      READ(60,120)QM
      CALL HFLUX(IRAM,ALFA,CON,KK,QM,TWM)
      DO242I=1,IRAM
      TW(I)=AW(I)
  242 QW(I)=BW(I)
      GOTO243
  238 READ(60,120)TM
      TGM=TM
      CALL WIRE3(IRAM,NCHN,KK,TM)
      DO239I=1,IRAM
  239 TG(I)=CW(I)
      GOTO243
  241 READ(60,120)PM
      TM=PM
      CALL WIRE3(IRAM,NCHN,KK,TM)
      K=0
      K=K+1
      DO244I=1,IRAM
C     MODIFIED EICHELBERG H.T.COEFF.  RETURNED FROM S/R WIRE3
  244 H(I,K)=EW(I)
      K=K+1
      DO245I=1,IRAM
C     EICHELBERG H.T.COEFF.  RETURNED FROM S/R WIRE3
  245 H(I,K)=FW(I)
  243 GOTO(1000,211,211,236)NCHN
  236 K=K+1
C     LOCAL QUASI-STEADY H.T.COEFF. FROM DIRECT EXPERIMENTAL DATA
      DO300I=1,IRAM
```

```
  300 H(I,K)=(3600.0*QW(I))/(TG(I)-TW(I))
      PI=3.1415927
      PIA=2.0*PI/IRAM
      WRITE(61,113)
      DO424N=1,IRAM
      AN=N-1
      AN=AN*PIA
      AN=AN*360.0/PI
  424 WRITE(61,112)N,AN,DW(N),CW(N),AW(N),BW(N),GW(N),H(N,3),H(N,1),H(N,
     12)
C     LIMITING EXPERIMENTAL H.T.COEFF. TO FINITE VALUES FOR PLOTTING
      DO420N=1,IRAM
      IF(H(N,3).GT.1500.0)410,405
  405 IF(H(N,3).LT.(-500.0))412,420
  410 H(N,3)=1500.0
      GOTO420
  412 H(N,3)=-500.0
  420 CONTINUE
      CALL MERPLT(H,IRAM,1,3,1,10HHT.COEFF. ,10HCRANK ANG ,10HH-B/HFTSQF
     1,5.0,1H*,1H.,1H+)
      WRITE(61,1200)
      WRITE(61,1300)
      J=NPD
      REV=REV*60.0*PI
      DO500K=J,KK,J
C     MODULUS OF HEAT FLUX CONVERTED TO PHYSICAL UNITS
      Q(K)=SQRTF(YFC(K)**2+YFS(K)**2)
      Q(K)=Q(K)*SQRT(FLOAT(K/J))
      Q(K)=Q(K)*CON*(REV/(2.0*ALFA))**0.5
      DTC(K)=YGC(K)-YWC(K)
      DTS(K)=YGS(K)-YWS(K)
C     MODULUS OF GAS-WALL TEMP DIFF
      DT(K)=SQRTF(DTC(K)**2+DTS(K)**2)
C     MODULUS OF EXPERIMENTAL H.T.COEFF.
      BH(K)=Q(K)/DT(K)
  500 WRITE(61,140)K,BH(K)
```

```
      CALL MEKPLT(BH,KK,1,1,1,10HH SPECTRUM,10HHARMONICNO,10H H MODULUS,
     11,0,1H*)
      PI=3.1415927
      PIA=2.0*PI/IRAM
      BHM=QM*3600.0/(TGM-TWM)
      WRITE(61,150)
      DO700N=1,IRAM
      AN=N-1
      AN=AN*PIA
      BBH(N)=BHM
      SDT(K)=QM
C     SYNTHESISED CYCLE OF WEIGHTED H.T.COEFF.
      DO600K=J,KK,J
      FI=ATANF(YFS(K)/YFC(K))
  600 BBH(N)=BBH(N)+BH(K)*COSF(AN*K/J-FI)
  700 WRITE(61,140)N,BBH(N)
      CALL MEKPLT(BBH,IRAM,1,1,1,10H HT.COEFF.,10HCRANK ANG ,10HH-B/HFTS
     1QF,5.0,1H+)
      GOTO205
 1000 STOP
      END
```

```
      SUBROUTINE SYNC1
C     SELECTS INITIAL/FINAL POINT NOS FROM EVENT TRACK FOR REQD CYCLES
      DIMENSIONNPT(50)
      DIMENSION IX(3)
      COMMONIY(4321),Y(4321),ITAPCON,NSER,IRUN,NOCHN(8),ICAL(5)
      COMMONVOLTC(5),NPI,NP,NPD,NPTS,LIST,ISTOP
      COMMON NTEST,CAL(5),NPERD,MI,MF,KKD
      COMMON TMOD(250),TPHI(250),REV
      COMMON YS(250,2),YC(250,2)
      COMMON G1,G2,G3,G4
      COMMON NCO
      COMMON AW(144),BW(144),CW(144),DW(144),EW(144),FW(144),GW(144)
    4 FORMAT(7H STOP 4)
    6 FORMAT(10X,44HIDENTIFICATION BETWEEN DATA BLOCKS INCORRECT)
   10 FORMAT(1H ,35HCONVERT TAPE IS NOT THE TAPE CALLED/10H TAPE READ,I5
     1/12H TAPE CALLED,I5)
   35 FORMAT(1H0,8X,7HPERIODS,15X,16HNUMBER OF POINTS,12X,6HPERIOD)
   36 FORMAT(67H SELECT  INITIAL  MAX    SELECT  INITIAL  FINAL  TOTAL
     1  VARIATION)
   40 FORMAT(1H ,I5,I8,I7,I10,2I8,I7,I8,I6)
   50 FORMAT(1H0,10HERROR TYPE,3(2X,I5))
   95 FORMAT(9I5)
   96 FORMAT(20I5)
   97 FORMAT(3I5)
      NOCHN(8)=0
      NT=5
      IYD=5
      IIYD=50
      NPTDD=5
  100 REWIND02
      DO115N=1,4321
  115 IY(N)=0
C     READS MAG. TAPE AND SELECTS FILE REQUIRED FOR EVENT MARKER
  118 READ(02,95)NNSER,IIRUN,IICHN,(ICAL(I),I=1,5),ITAPCO
      IF(ENDFILE 02)1000,117
  117 IF(ITAPCON-ITAPCO)600,119,600
```

```
  119 IF(IRUN-IIRUN)150,120,150
  120 IF(NOCHN(1)-IICHN)150,160,150
  150 CALL SKIP(02)
      GOTO118
  160 NPF=NP+NPI
      NPERD=0
      NTOTE=0
      KTEST=1
      DO105I=1,50
  105 NPT(I)=0
      M=-863
      MM=0
C     READS DATA POINTS FROM EVENT MARKER FILE
  170 M=M+864
      MM=MM+864
      READ(02,97)(IX(I),I=1,3)
      IF(IX(1).EQ.-1.AND.IX(2).EQ.-100.AND.IX(3).EQ.-10)162,161
  161 IF(IX(1).EQ.-2.AND.IX(2).EQ.-200.AND.IX(3).EQ.-20)174,900
  162 READ(02,96)(IY(I),I=M,MM)
      IF(ENDFILE 02)174,171
  171 IF(MM-3456)170,170,172
  172 CALL SKIP(02)
  174 N=9
  175 N=N+1
      IF(N-MM+30)178,245,245
C     DETERMINING THE EVENT PULSES
  178 IF(IY(N)-1000)240,240,180
  180 IF(IABS(IY(N)-IY(N-1))-IYD)175,175,181
  181 IF(IABS(IY(N)-IY(N-4))-IYD)175,175,182
  182 IF(IABS(IY(N)-IY(N-9))-IYD)175,175,183
  183 IF(IABS(IY(N-1)-IY(N+1))-IYD)173,173,189
  173 IF(IABS(IY(N-1)-IY(N+2))-IYD)175,175,189
  189 LTEST=1
C     CHECK TO MAKE SURE THAT IT IS AN EVENT PULSE
      DO185M=4,14
      MN=N+M
```

```
      IF(IABS(IY(MN)-IY(MN-1))-IYD)185,185,184
  184 LTEST=2
  185 CONTINUE
      GOTO(200,186,1000),LTEST
  186 DO188M=15,25
      MN=N+M
      IF(IABS(IY(MN)-IY(MN-1))-IYD)188,188,187
  187 LTEST=3
  188 CONTINUE
      GOTO(1000,200,240),LTEST
  200 IF(IY(N)-IY(N-1)-IYD)220,220,205
  205 IF(IY(N)-IY(N-1)-IIYD)175,175,210
C     NOTES PERIOD NO. AND POINT NO. WHERE EVENT OCCURED
  210 NPERD=NPERD+1
      NPT(NPERD)=N
  220 N=N+15
      GOTO175
  240 NTOTE=N-1
  245 REWIND02
C     CHECK THAT PERIODS DID OCCUR IN EVENT SIGNAL
      IF(NPERD)250,250,255
  250 IERR=0003
      NTEST=2
      WRITE(61,050)IERR,NPERD,NTOTE
      GOTO1001
C     CHECK THAT VARIATION IN NO. OF POINTS PER PERIOD IS ACCEPTABLE
  255 NMIN=NPT(2)-NPT(1)
      NMAX=NMIN
      NN=NPERD-1
      DO290N=2,NN
      NPTD=NPT(N+1)-NPT(N)
      IF(NMAX-NPTD)260,270,270
  260 NMAX=NPTD
      GOTO290
  270 IF(NMIN-NPTD)290,290,280
  280 NMIN=NPTD
```

```
  290 CONTINUE
      IF(NMAX-NMIN-NPTDD)305,305,300
  300 IERR=004
      WRITE(61,050)IERR,NMIN,NMAX
      NTEST=2
      GOTO1001
C     CHECK THAT DESIRED NO. OF PERIODS IS OBTAINABLE
  305 IF(NPERD-NPF)310,320,320
  310 IERR=005
      WRITE(61,050)IERR,NPERD,NPF
      NPP=NPERD
      GOTO330
  320 NPP=NPF
  330 NPD=NPP-NPI
      IF(NPD)331,331,332
  331 NTEST=2
      GOTO1001
C     HENCE DETERMINE INITIAL AND FINAL POINT NOS.
C      (TOTAL NO. OF POINTS)
  332 MI=NPT(NPI)
      MF=NPT(NPP)
      NPTS=MF-MI+1
      WRITE(61,035)
      WRITE(61,036)
      WRITE(61,040)NPD,NPI,NPERD,NPTS,MI,MF,NTOTE,NMIN,NMAX
      GOTO1001
  600 WRITE(61,10)ITAPCO,ITAPCON
      GOTO1000
  900 WRITE(61,6)
      GOTO 1001
 1000 PRINT 4
      STOP
 1001 REWIND02
      RETURN
      END
```

```
      SUBROUTINE SYNC2(NCHN)
C     SELECTS DATA POINTS CORRESPONDING TO REQD CYCLES OF EVENT
C     FROM PARTICULAR DATA FILE DESIRED
      COMMONIY(4321),Y(4321),ITAPCON,NSER,IRUN,NOCHN(8),ICAL(5)
      COMMONVOLTC(5),NPI,NP,NPD,NPTS,LIST,ISTOP
      COMMON NTEST,CAL(5),NPERD,MI,MF,KKD
      COMMON TMOD(250),TPHI(250),REV
      COMMON YS(250,2),YC(250,2)
      COMMON G1,G2,G3,G4
      COMMON NCO
      COMMON AW(144),BW(144),CW(144),DW(144),EW(144),FW(144),GW(144)
      DIMENSION IX(3)
   95 FORMAT(9I5)
   96 FORMAT(20I5)
   97 FORMAT(3I5)
    5 FORMAT(7H STOP 5)
    6 FORMAT(10X,44HIDENTIFICATION BETWEEN DATA BLOCKS INCORRECT)
   20 FORMAT(1H ,27HDATA POINT APPEARS IN ERROR,I8,3X,5HPOINT/15H ORIGIN
     1AL POINT,I6,3X,12HCORRECTED TO,I6/23H SURROUNDING POINTS ARE,5I8)
   70 FORMAT(1H0,10I5)
   80 FORMAT(1X,20I5)
      INTPOL=600
      REWIND02
      DO360N=1,4321
  360 IY(N)=0
  390 READ(02,95)NNSER,IIRUN,IICHN,(ICAL(I),I=1,5),ITAPCO
      IF(ENDFILE 02)1000,391
  391 IF(IRUN-IIRUN)430,400,430
  400 IF(NOCHN(NCHN)-IICHN)430,435,430
  430 CALL SKIP(02)
      GOTO390
  435 KTEST=1
      M=-863
      MM=0
C     READ DATA FROM MAG. TAPE
  440 M=M+864
```

```
      MM=MM+864
      READ(02,97)(IX(I),I=1,3)
      IF(IX(1).EQ.-1.AND.IX(2).EQ.-100.AND.IX(3).EQ.-10)442,441
  441 IF(IX(1).EQ.-2.AND.IX(2).EQ.-200.AND.IX(3).EQ.-20)500,900
  442 READ(02,96)(IY(I),I=M,MM)
      IF(ENDFILE 02)500,450
  450 IF(MM-3456)440,440,460
  460 CALL SKIP(02)
  500 GOTO(510,1001),NTEST
  510 WRITE(61,070)NSER,IIRUN,IICHN,(ICAL(I),I=1,5),NPTS,NPD
C     CHECKS FOR ERRORS IN DATA AND INTERPOLATES FOR THE POINT
      DO512I=MI,MF
      IF(IABS(2*IY(I-1)-IY(I-2)-IY(I))-INTPOL)512,511,511
  511 IYY=IY(I)
      IY(I)=(IY(I-1)+IY(I+1))/2
      WRITE(61,020)I,IYY,IY(I),IY(I-2),IY(I-1),IY(I),IY(I+1),IY(I+2)
  512 CONTINUE
      IF(LIST)515,515,1001
  515 IF(MF-MI-79)520,530,530
  520 WRITE(61,080)(IY(M),M=MI,MF)
      GOTO1001
  530 MM=MI+79
      WRITE(61,080)(IY(M),M=MI,MM)
      MM=MF-79
      WRITE(61,080)(IY(M),M=MM,MF)
      GOTO1001
  900 WRITE(61,6)
 1000 PRINT 5
      STOP
 1001 REWIND02
      RETURN
      END
```

```
      SUBROUTINE CONV
C     CONVERTS SAMPLED DATA POINTS INTO FLOATING POINT NUMBERS
      COMMONIY(4321),Y(4321),ITAPCON,NSER,IRUN,NOCHN(8),ICAL(5)
      COMMONVOLTC(5),NPI,NP,NPD,NPTS,LIST,ISTOP
      COMMON NTEST,CAL(5),NPERD,MI,MF,KKD
      COMMON TMOD(250),TPHI(250),REV
      COMMON YS(250,2),YC(250,2)
      COMMON G1,G2,G3,G4
      COMMON NCO
      COMMON AW(144),BW(144),CW(144),DW(144),EW(144),FW(144),GW(144)
      II=0
      DO100I=MI,MF
      II=II+1
  100 Y(II)=IY(I)
      DO300I=1,5
  300 CAL(I)=ICAL(I)
      RETURN
      END
```

```
      SUBROUTINE REDFA
C     FROM CALIBRATION VALUES DETERMINES BEST FIT STRAIGHT LINES AND
C      CONVERTS SAMPLES TO PHYSICAL UNITS OF THE MEASURED VARIABLE
      COMMONIY(4321),Y(4321),ITAPCON,NSER,IRUN,NOCHN(8),ICAL(5)
      COMMONVOLTC(5),NPI,NP,NPD,NPTS,LIST,ISTOP
      COMMON NTEST,CAL(5),NPERD,MI,MF,KKD
      COMMON TMOD(250),TPHI(250),REV
      COMMON YS(250,2),YC(250,2)
      COMMON G1,G2,G3,G4
      COMMON NCO
      COMMON AW(144),BW(144),CW(144),DW(144),EW(144),FW(144),GW(144)
      PI=3.1415927
      XP=CAL(1)+CAL(2)+CAL(3)
      XN=CAL(3)+CAL(4)+CAL(5)
      YP=VOLTC(1)+VOLTC(2)+VOLTC(3)
      YN=VOLTC(3)+VOLTC(4)+VOLTC(5)
      ZP=CAL(1)**2+CAL(2)**2+CAL(3)**2
      ZN=CAL(3)**2+CAL(4)**2+CAL(5)**2
      WP=CAL(1)*VOLTC(1)+CAL(2)*VOLTC(2)+CAL(3)*VOLTC(3)
      WN=CAL(3)*VOLTC(3)+CAL(4)*VOLTC(4)+CAL(5)*VOLTC(5)
      AP=(ZP*YP-WP*XP)/(3.0*ZP-XP*XP)
      AN=(ZN*YN-WN*XN)/(3.0*ZN-XN*XN)
      BP=(3.0*WP-XP*YP)/(3.0*ZP-XP*XP)
      BN=(3.0*WN-XN*YN)/(3.0*ZN-XN*XN)
      SEN=1.0/(G1*G2*G3*G4)
      CALINT=(AP-AN)/(BN-BP)
      DO290I=1,NPTS
      IF(Y(I)-CALINT)270,280,280
  270 YY=(Y(I)*BN+AN)*SEN
      Y(I)=YY
      GOTO290
  280 YY=(Y(I)*BP+AP)*SEN
      Y(I)=YY
  290 CONTINUE
      RETURN
      END
```

```
      SUBROUTINE FASQW
C     DETERMINES THE FOURIER COEFFICIENTS OF THE VARIABLE
      COMMONIY(4321),Y(4321),ITAPCON,NSER,IRUN,NOCHN(8),ICAL(5)
      COMMONVOLTC(5),NPI,NP,NPD,NPTS,LIST,ISTOP
      COMMON NTEST,CAL(5),NPERD,MI,MF,KKD
      COMMON TMOD(250),TPHI(250),REV
      COMMON YS(250,2),YC(250,2)
      COMMON G1,G2,G3,G4
      COMMON NCO
      COMMON AW(144),BW(144),CW(144),DW(144),EW(144),FW(144),GW(144)
  150 FORMAT(1H8,27H COUNTING ERROR EXIT CALLED)
      N=NPTS
      KK=NPD*KKD
      PI=3.1415927
      THETA=2.0*PI/FLOAT(N-1)
      Y(1)=0.5*Y(1)
      DO50K=1,KK
      ALPHA=PI/(FLOAT(K)*THETA)
      BETA=1.0
      YS(K,1)=0.0
      YS(K,2)=0.0
      DO50J=1,2
      L=1
      BETA=BETA+ALPHA/2.
      GAMMA=BETA
      DO50I=1,N
      IF(FLOAT(I)-GAMMA)20,20,11
   11 DELTA2=FLOAT(I)-GAMMA
      GAMMA=GAMMA+ALPHA
      IF(L-1)96,12,13
   12 L=2
      YS(K,J)=YS(K,J)+.5*Y(I-1)-DELTA2*(Y(I)+Y(I-1))-0.5*Y(I)
      IF(I-N)50,14,96
   13 L=1
      YS(K,J)=YS(K,J)-.5*Y(I-1)+DELTA2*(Y(I)+Y(I-1))+0.5*Y(I)
      IF(I-N)50,14,96
```

```
14 A=YS(K,J)-0.5*Y(I)
   YS(K,J)=1.57079632*A/FLOAT(N-1)
   GOTO50
20 M=L
   IF(M-1)30,30,45
30 YS(K,J)=YS(K,J)+Y(I)
   IF(I-N)50,39,50
39 A=YS(K,J)-0.5*Y(I)
   YS(K,J)=1.57079632*A/FLOAT(N-1)
   GOTO50
45 YS(K,J)=YS(K,J)-Y(I)
   IF(I-N)50,49,50
49 A=YS(K,J)+0.5*Y(I)
   YS(K,J)=1.57079632*A/FLOAT(N-1)
50 CONTINUE
   JJ=(2*KK)/3-1
   YC(KK,1)=YS(KK,1)
   YC(KK,2)=YS(KK,2)
   J=KK-1
   JX=J
   DO95L=1,JX
   YC(J,1)=YS(J,1)
   YC(J,2)=YS(J,2)
   IF(L-JJ)95,70,70
70 DO91LL=1,L
   M=J+LL
   KA=M/J
   MM=M
71 IF(MM-J)91,80,72
72 MM=MM-J
   GOTO71
80 KKA=KA
73 IF(KKA-2)90,91,74
74 KKA=KKA-2
   GOTO73
90 YC(J,1)=YC(J,1)-YC(M,1)/(FLOAT(KA*(-1)**((KA/2)+2)))
```

```
      YC(J,2)=YC(J,2)-YC(M,2)/(FLOAT(KA))
   91 CONTINUE
   95 J=J-1
      DO97K=1,KK
      C=SQRTF(YC(K,1)**2+YC(K,2)**2)
      PHI=ATANF(YC(K,2)/YC(K,1))*180.0/PI
      PHI=ABSF(PHI)
      IF(YC(K,2))470,510,540
  470 IF(YC(K,1))480,490,500
  480 PHI=180.0+PHI
      GOTO98
  490 PHI=270.0
      GOTO98
  500 PHI=360.0-PHI
      GOTO98
  510 IF(YC(K,1))520,530,530
  520 PHI=180.0
      GOTO98
  530 PHI=0.0
      GOTO98
  540 IF(YC(K,1))550,560,98
  550 PHI=180.0-PHI
      GOTO98
  560 PHI=90.0
   98 TMOD(K)=C
      TPHI(K)=PHI
   97 CONTINUE
      GOTO99
   96 WRITE(61,150)
      NTEST=2
   99 RETURN
      END
```

```
      SUBROUTINE CALC
C     LISTS COMPUTED FOURIER COEFFICIENTS (SINE, COSINE, MODULUS AND
C      PHASE) FOR EACH DATA CHANNEL (WALL TEMP, GAS TEMP, PRESS.)
      COMMONIY(4321),Y(4321),ITAPCON,NSER,IRUN,NOCHN(8),ICAL(5)
      COMMONVOLTC(5),NPI,NP,NPD,NPTS,LIST,ISTOP
      COMMON NTEST,CAL(5),NPERD,MI,MF,KKD
      COMMON TMOD(250),TPHI(250),REV
      COMMON YS(250,2),YC(250,2)
      COMMON G1,G2,G3,G4
      COMMON NCO
      COMMON AW(144),BW(144),CW(144),DW(144),EW(144),FW(144),GW(144)
  120 FORMAT(1H1,46HFOURIER COEFFICIENTS OF COMPLETE DATA ANALYSED)
  125 FORMAT(1H0,10X,39HFOURIER COEFFICIENTS AT CYCLE FREQUENCY)
  130 FORMAT(1H0,9X,5HINDEX,8X,6HCOSINE,13X,4HSINE,12X,7HMODULUS,9X,5HPH
     1ASE//)
  135 FORMAT(1H0,45H CYCLE HARMONIC    TEMPERATURE    PHASE ANGLE)
  136 FORMAT(1H ,21X,7H(DEG.F),6X,15H CRANK ANG.DEG)//)
  140 FORMAT(11X,I4,3(4X,E14.7),4X,F6.1)
  145 FORMAT(1H0,6X,I4,10X,F8.3,9X,F7.2)
      WRITE(61,125)
      WRITE(61,135)
      WRITE(61,136)
      KK=KKD*NPD
      M=0
      J=NPD
      DO570K=J,KK,J
      M=M+1
  570 WRITE(61,145)M,TMOD(K),TPHI(K)
      NCO=KK/NPD
      IF(LIST)580,580,99
  580 WRITE(61,120)
      WRITE(61,130)
      DO590K=1,KK
  590 WRITE(61,140)K,YC(K,1),YC(K,2),TMOD(K),TPHI(K)
   99 RETURN
      END
```

```
      SUBROUTINE HFLUX(IRAM,ALFA,CON,KK,QM,TWM)
C     BY DIFFERENTIATION OF FOURIER SERIES OF WALL SURFACE TEMPERATURE,
C      DETERMINES FOURIER COEFFICIENTS FOR HEAT FLUX AND PLOTS
C      SYNTHESISED CYCLE
      DIMENSION T(144),Q(144)
      COMMONIY(4321),Y(4321),ITAPCON,NSER,IRUN,NOCHN(8),ICAL(5)
      COMMONVOLTC(5),NPI,NP,NPD,NPTS,LIST,ISTOP
      COMMON NTEST,CAL(5),NPERD,MI,MF,KKD
      COMMON TMOD(250),TPHI(250),REV
      COMMON YS(250,2),YC(250,2)
      COMMON G1,G2,G3,G4
      COMMON NCO
      COMMON AW(144),BW(144),CW(144),DW(144),EW(144),FW(144),GW(144)
  120 FORMAT(1H1,16X,46HFOURIER COEFFICIENTS OF COMPLETE DATA ANALYSED)
  130 FORMAT(1HO,9X,5HINDEX,8X,6HCOSINE,13X,4HSINE,12X,7HMODULUS,9X,5HPH
     1ASE//)
  140 FORMAT(11X,I4,3(4X,E14.7),4X,F6.1)
      J=NPD
      PI=3.1415927
      REV=REV*60.0*PI
      PIA=2.0*PI/IRAM
C     SETS CRANK ANGLE PLOTTING INTERNAL
      DO370N=1,IRAM
      AN=N-1
      AN=AN*PIA
      T(N)=0.0
      DO500K=J,KK,J
C     FOURIER SERIES FOR WALL TEMP. CYCLE
  500 T(N)=T(N)+YC(K,1)*COSF(AN*K/J)+YC(K,2)*SINF(AN*K/J)
  370 CONTINUE
      DO380I=1,IRAM
C     ADDING MEAN(RECORDED) WALL TEMP.
  380 AW(I)=T(I)+TWM
C     SYNTHESISED WALL TEMP. PLOT
      CALL MEKPLT(AW,IRAM,1,1,1,10H WALL TEMP,10HCRANK ANG ,10HTEMP DEG
     1F,5.0,1H.)
```

```
      WRITE(61,120)
      WRITE(61,130)
      DO650K=J,KK,J
      YFC=YC(K,2)+YC(K,1)
      YFS=YC(K,2)-YC(K,1)
      C=SQRTF(YFC**2+YFS**2)
      PHI=ATANF(YFS/YFC)*180.0/PI
      PHI=ABSF(PHI)
      IF(YFS)470,510,54
  470 IF(YFC)480,490,505
  480 PHI=180.0+PHI
      GOTO98
  490 PHI=270.0
      GOTO98
  505 PHI=360.0-PHI
      GOTO98
  510 IF(YFC)520,530,53
  520 PHI=180.0
      GOTO98
  530 PHI=0.0
      GOTO98
  540 IF(YFC)550,560,98
  550 PHI=180.0-PHI
      GOTO98
  560 PHI=90.0
   98 TMOD(K)=C
      TPHI(K)=PHI
C     LIST OF FOURIER COEFFS OF HEAT FLUX CYCLE
  650 WRITE(61,140)K,YFC,YFS,TMOD(K),TPHI(K)
      DO700N=1,IRAM
      AN=N-1
      AN=AN*PIA
      Q(N)=0.0
      DO600K=J,KK,J
C     FOURIER SERIES FOR HEAT FLUX CYCLE
      QQ=(YC(K,2)-YC(K,1))*SINF(AN*K/J)+(YC(K,2)+YC(K,1))*COSF(AN*K/J)
```

```
  600 Q(N)=Q(N)+QQ*SQRT(FLOAT(K/J))
      Q(N)=Q(N)*CON*(REV/(2.0*ALFA))**0.5
C     ADDING MEAN(MEASURED) HEAT FLUX
      Q(N)=(Q(N)/3600.0)+QM
  700 CONTINUE
C     SYNTHESISED HEAT FLUX CYCLE PLOT
      CALL MEKPLT(Q,IRAM,1,1,1,10HHEAT FLUX ,10HCRANK ANG ,10HB/FTSQ.SEC
     1,5.0,1H.)
      DO780I=1,IRAM
  780 BW(I)=Q(I)
      REV=REV/(60.0*PI)
      RETURN
      END
```

```
      SUBROUTINE WIRE3(IRAM,NCHN,KK,TM)
C     FROM FOURIER COEFFICIENTS, SYNTHESISES CYCLES OF GAS TEMPERATURE
C      AND PRESSURE AND CALCULATES EMPIRICAL H.T.COEFF.(EICHELBERG)
      COMMONIY(4321),Y(4321),ITAPCON,NSER,IRUN,NOCHN(8),ICAL(5)
      COMMONVOLTC(5),NPI,NP,NPD,NPTS,LIST,ISTOP
      COMMON NTEST,CAL(5),NPERD,MI,MF,KKD
      COMMON TMOD(250),TPHI(250),REV
      COMMON YS(250,2),YC(250,2)
      COMMON G1,G2,G3,G4
      COMMON NCO
      COMMON AW(144),BW(144),CW(144),DW(144),EW(144),FW(144),GW(144)
      DIMENSION T(144),DT(144),ABW(144),VP(144)
    7 FORMAT(7H STOP 7)
    8 FORMAT(7H STOP 8)
    9 FORMAT(7H STOP 9)
   10 FORMAT(1H0,I5,2E10.2)
   20 FORMAT(1H0,I5,3E10.2)
   30 FORMAT(1H0,I5,E10.2)
   50 FORMAT(1H0,3E10.2)
   80 FORMAT(2X,I5,2X,10E10.2)
  101 FORMAT(1H0,21HINTERPOLATE THIS TEMP)
      J=NPD
      PI=3.1415927
      R=2.1875
      EL=9.5
      Q=R/EL
      R=R/12.0
      PIA=2.0*PI/IRAM
      WM=REV*PI/30.0
C     SETS CRANK ANGLE PLOTTING INTERVAL
  180 DO370 N=1,IRAM
      AN=N-1
      AN=AN*PIA
      T(N)=0.0
      DT(N)=0.0
C     INSTANTANEOUS PISTON VELOCITY
```

```
      VP(N)=WM*R*(SINF(2.0*AN)+Q*SINF(4.0*AN)/2.0)
      GW(N)=VP(N)
      DO190K=J,KK,J
      T(N)=T(N)+YC(K,1)*COSF(AN*K/J)+YC(K,2)*SINF(AN*K/J)
      DT(N)=DT(N)-YC(K,1)*(K/J)*SINF(AN*K/J)
  190 DT(N)=DT(N)+YC(K,2)*(K/J)*COSF(AN*K/J)
  370 CONTINUE
      GOTO(1001,1001,200,300)NCHN
  200 DO201N=1,IRAM
C     ADDING MEAN(RECORDED) GAS TEMP.
  201 CW(N)=T(N)+TM
C     SYNTHESISED GAS TEMP. CYCLE PLOT
      CALL MEKPLT(CW,IRAM,1,1,1,10H GAS TEMP ,10HCRANK ANG ,10HTEMP DEG
     1R,5.0,1H.)
      GOTO1000
C     ADDING CYCLIC PRESSURE ABOVE ATMOS.
  300 PMIN=T(1)
      DO302N=1,IRAM
      IF(T(N).LT.PMIN)301,302
  301 PMIN=T(N)
  302 CONTINUE
      DO303N=1,IRAM
  303 DW(N)=T(N)-PMIN+TM
C     SYNTHESISED GAS PRESS. CYCLE PLOT
      CALL MEKPLT(DW,IRAM,1,1,1,10H GAS PRESS,10HCRANK ANG ,10HPRESS PSI
     1A,5.0,1H.)
      R=4.375
C     MEAN PISTON SPEED
      VPM=REV*R/360.0
      DO900K=1,IRAM
      ABW(K)=CW(K)*DW(K)
      VP(K)=ABS(VP(K))
C     MODIFIED EICHELBERG H.T.COEFF.
      HTC=0.168*((VP(K))**0.333)*(ABW(K))**0.5
      HTC1=HTC
      EW(K)=HTC1
```

```
C       ORIGINAL EICHELBERG H.T.COLFF.
        HTC=0.056*((VPM)**0.333)*(ADW(K))**0.5
        HTC2=HTC
  900 FW(K)=HTC2
        GOTO1000
 1001 PRINT7
        STOP
 1002 PRINT8
        STOP
 1000 RETURN
        END
```

```
      SUBROUTINE SKIP(LU)
C     ROUTINE TO SKIP A FILE
      DIMENSION IX(3)
    2 FORMAT(8H STOP 02)
   97 FORMAT(3I5)
  100 READ(02,97)(IX(I),I=1,3)
      IF(ENDFILE02)1000,200
  200 IF(IX(1).EQ.-1.AND.IX(2).EQ.-100.AND.IX(3).EQ.-10)400,300
  300 IF(IX(1).EQ.-2.AND.IX(2).EQ.-200.AND.IX(3).EQ.-20)900,1000
  400 DO500I=1,44
  500 READ(02,97)(IX(I),I=1,3)
      GOTO100
 1000 PRINT 2
      STOP
  900 RETURN
      END
```

```
      SUBROUTINE MEKPLT(YPT,IMAX,IMIN,JMAX,JMIN,GTITLE,XTITLE,YTITLE,
     1FACTOR,GP0,GP1,GP2,GP3,GP4,GP5,GP6,GP7,GP8,GP9)
C     GENERAL PURPOSE PLOTTING ROUTINE, AUTOMATIC SCALING, PLOTS UP TO
C      10 ARRAYS
C     YPT= NAME OF ARRAY TO PLOT WITH DIMENSIONS (IMAX; JMAX)
C     PLOTS POINTS FROM THE IMIN VALUE OF THE ARRAY TO THE IMAX VALUE
C     PLOTS ONLY THE JMIN TO JMAX ARRAY OF POINTS IN YPT.
C     GTITLE = NAME OF GRAPH
C     XTITLE = NAME OF X AXIS
C     YTITLE = NAME OF Y AXIS
C     FACTOR = SCALE FACTOR TO CHANGE VALUES OF SUBSCRIPT I OF
C      YPT(I,J) TO PHYSICAL UNITS
C     GP0 ... GP9  CHARACTER TO DESIGNATE PARTICULAR PLOT J OF YPT(I,J)
      DIMENSION YPT(IMAX,10),APT(100,10),ALPHA(100),BETA(10),IBETA(6)
   10 FORMAT(1H1,65X,A10)
   20 FORMAT(1H ,20X,2H I,10A10)
   30 FORMAT(1H ,20X,2HI-,10A10,1HI)
   40 FORMAT(1H ,I18,4H -I ,100A1,3HI- )
   50 FORMAT(1H ,20X,2HI ,100A1,1HI)
   60 FORMAT(1H ,A10,10X,2HI ,100A1,1HI)
   61 FORMAT(1H ,4X,I4,12X,2HI ,100A1,1HI)
   62 FORMAT(1H ,2X,4H* 10,14X,2HI ,100A1,1HI)
   70 FORMAT(1H ,18X,I4,16X,I4,16X,I4,16X,I4,16X,I4,16X,I4)
   71 FORMAT(1H ,73X,I4)
   72 FORMAT(1H ,71X,4H* 10)
   80 FORMAT(1H ,65X,A10)
   90 FORMAT(1H )
  100 FORMAT(1H ,5HYDIV=,E16.9,5X,5HXDIV=,E16.9)
  101 FORMAT(1H ,10X,E9.1,4X,E9.1)
C     CALCULATE RANGE OF VALUES OF VARIABLE Y
      AMAX=YPT(IMIN,1)
      AMIN=YPT(IMIN,1)
      DO94K=JMIN,JMAX
      DO94I=IMIN,IMAX
      IF(YPT(I,K).GT.AMAX)91,92
   91 AMAX=YPT(I,K)
```

```
      GOTO94
   92 IF(YPT(I,K).LT.AMIN)93,94
   93 AMIN=YPT(I,K)
   94 CONTINUE
      PRINT101,AMAX,AMIN
      RY=AMAX-AMIN
C     CALCULATE FACTOR TO EXPAND RANGE TO .GT. 50
      IF(RY.GT.50)95,96
   95 RF=1.0
      IRF=1
      GOTO97
   96 RF=50/RY
      IRF=ALOG10(RF)+1.
      RF=10**IRF
      AMIN=AMIN*RF
   97 AMAX=AMAX*RF
      DO98I=IMIN,IMAX
      DO98K=JMIN,JMAX
   98 YPT(I,K)=YPT(I,K)*RF
      PRINT10,GTITLE
      PRINT90
C     CALCULATE RANGE OF VALUES OF VARIABLE X
      IRX=IMAX-IMIN+1
      IF(IRX.LT.100)110,180
C     FOR .LT. 100 POINTS, CALCULATE 'BEST FIT' X-RANGE, AND NO. SPACES/POINT
  110 IRX5=(IRX+4)/5
  120 IF(IRX5.EQ.(10*(IRX5/10)))140,130
  130 IRX5=IRX5+1
      GOTO120
  140 IRX=5*IRX5
      IC=100/IRX
      RC=IRX/100.0
      IXMIN=IRX5*(IMIN/IRX5)
      DO170K=JMIN,JMAX
      DO170I=1,100,IC
      IXGRAD=IXMIN+(I-1)/IC
```

```
      IF(IXGRAD.LT.IMIN)170,150
  150 IF(IXGRAD.GT.IMAX)170,160
C     DISTRIBUTE POINTS OVER THE FIELD OF 100 SPACES
  160 APT(I,K)=YPT(IXGRAD,K)
  170 CONTINUE
      GOTO250
C     FOR .GT. 100 POINTS, CALCULATE 'BEST FIT' X-RANGE AND NO. POINTS/SPACE
  180 IRX5=(IRX+4)/5
  190 IF(IRX5.EQ.(20*(IRX5/20)))210,200
  200 IRX5=IRX5+1
      GOTO190
  210 IRX=5*IRX5
      IC=IRX5/20
      RC=IC
      IXMIN=IRX5*(IMIN/IRX5)
      DO240K=JMIN,JMAX
      DO240I=1,100
      IXGRAD=IMIN+(I-1)*IC
      IF(IXGRAD.LT.IMIN)240,220
  220 IF(IXGRAD.GT.IMAX)240,230
C     DISTRIBUTE POINTS OVER THE FIELD OF 100 SPACES
  230 APT(I,K)=YPT(IXGRAD,K)
  240 CONTINUE
  250 RB=AMAX-AMIN
C     CALCULATE 'BEST FIT' Y-RANGE
      IRY=RB
  260 IF(IRY.EQ.(50*(IRY/50)))280,270
  270 IRY=IRY+1
      GOTO260
  280 C=IRY/50
C     CHOOSE MIN Y VALUE
      IYMIN=AMIN
      IRY5=IRY/5
  284 IF(IYMIN.EQ.(IRY5*(IYMIN/IRY5)))285,286
  286 IYMIN=IYMIN-1
      GOTO284
```

```
  285 YMIN=IYMIN
      YMAX=YMIN+50.0*C
      IF(YMAX.LT.AMAX)270,287
C     PRINT GRADUATION MARKS ACROSS TOP
  287 DO290K=1,10
  290 BETA(K)=10H          I
      PRINT20,(BETA(K),K=1,10)
C     PRINT LINE ACROSS TOP
      DO300K=1,10
  300 BETA(K)=10H------
      PRINT30,(BETA(K),K=1,10)
      DO410J=1,51
      DO310K=1,100
C     SET WHOLE FIELD BLANK
  310 ALPHA(K)=1H
      YGRAD=YMAX-(J-1)*C
      YGRAD2=YGRAD-C
      IF(IRX.LT.100)320,330
  320 IXDIV=100/IRX
      GOTO340
  330 IXDIV=1
C     IF Y-VALUE LIES BETWEEN VALUES OF 2 LINES, SET A POINT ON LOWEST LINE
  340 DO365K=JMIN,JMAX
      DO365I=1,100,IXDIV
      IX=I*RC+IXMIN
      IF(IX.LT.IMIN)365,341
  341 IF(IX.GT.IMAX)365,342
  342 IF(APT(I,K).LE.YGRAD)345,365
  345 IF(APT(I,K).GT.YGRAD2)350,365
  350 GOTO(500,501,502,503,504,505,506,507,508,509)K
  500 ALPHA(I)=GP0
      GOTO365
  501 ALPHA(I)=GP1
      GOTO365
  502 ALPHA(I)=GP2
      GOTO365
```

```
503 ALPHA(I)=GP3
    GOTO365
504 ALPHA(I)=GP4
    GOTO365
505 ALPHA(I)=GP5
    GOTO365
506 ALPHA(I)=GP6
    GOTO365
507 ALPHA(I)=GP7
    GOTO365
508 ALPHA(I)=GP8
    GOTO365
509 ALPHA(I)=GP9
    GOTO365
365 CONTINUE
    IF(RY.GT.50)367,366
367 IF(YMAX.LT.0)375,376
375 IPY10=ALOG10(-YMAX)
    GOTO377
376 IPY10=ALOG10(YMAX)
377 YGRAD=YGRAD/(10**IPY10)
    IPY10=IPY10-2
    IF(YGRAD.LT.0.0)371,372
371 IYGRAD=100*YGRAD-1.0E-01
    GOTO368
372 IYGRAD=100*YGRAD+1.0E-01
    GOTO368
366 IPY10=-IRF
    IF(YGRAD.LT.0.0)373,374
373 IYGRAD=YGRAD-1.0E-01
    GOTO368
374 IYGRAD=YGRAD+1.0E-01
368 IF(J.EQ.25)370,38
370 PRINT60,YTITLE,(ALPHA(I),I=1,100)
    GOTO410
380 IF(J.EQ.26)381,382
```

```
  381 PRINT61,IPY10,(ALPHA(I),I=1,100)
      GOTO410
  382 IF(J.EQ.27)383,385
  383 PRINT62,(ALPHA(I),I=1,100)
      GOTO410
  385 IF((J-10*(J/10)-1).EQ.0)390,400
  390 PRINT40,IYGRAD,(ALPHA(I),I=1,100)
      GOTO410
  400 PRINT50,(ALPHA(I),I=1,100)
  410 CONTINUE
C     PRINT LINE ACROSS BOTTOM
      PRINT30,(BETA(K),K=1,10)
C     PRINT GRADUATION MARKS ACROSS BOTTOM
      DO430K=1,10
  430 BETA(K)=10H          I
      PRINT20,(BETA(K),K=1,10)
C     PRINT X-GRADUATIONS
      XMAX=IMAX
      IPX10=ALOG10(XMAX)
      IX10=IPX10
      PFAC=ALOG10(FACTOR)
      IF(PFAC.LT.0.0)600,650
  600 IPFAC=1.0-PFAC+1.0E-01
      FAKTOR=FACTOR*(10**IPFAC)
      IPFAC=-IPFAC
      GOTO700
  650 IPFAC=PFAC+1.0E-01
      FAKTOR=FACTOR/(10**IPFAC)
  700 DO440I=1,6
      BETA(I)=(IXMIN+(I-1)*IRX5)*FAKTOR
      BETA(I)=BETA(I)/(10**IX10)
  440 IBETA(I)=100*BETA(I)+1.0E-01
      IPX10=IPX10-2+IPFAC
      PRINT70,(IBETA(I),I=1,6)
      PRINT71,IPX10
      PRINT72
```

```
      PRINT90
      PRINT80,XTITLE
C     PRINT VALUES OF LINE AND SPACE
      XDIV=IRX5/20*FACTOR
      YDIV=C/RF
      PRINT100,YDIV,XDIV
      DO800I=IMIN,IMAX
      DO800K=JMIN,JMAX
  800 YPT(I,K)=YPT(I,K)/RF
      RETURN
      END
```

Fig. 3(a) Subroutine for the 3-Wire Iteration by the Bolzano bisection method.

```
      SUBROUTINE WIRE3(IRAM,NCHN,KK)
      COMMONIY(4321),Y(4321),ITAPCON,NSER,IRUN,NOCHN(8),ICAL(5)
      COMMONVOLTC(5),NPI,NP,NPD,NPTS,LIST,ISTOP
      COMMON NTEST,CAL(5),NPERD,MI,MF,KKD
      COMMON TMOD(250),TPHI(250),REV
      COMMON YS(250,2),YC(250,2)
      COMMON G1,G2,G3,G4
      COMMON NCO
      COMMON AW(150),BW(150),CW(150),XW(150),YW(150),ZW(150)
      DIMENSION T(150),DT(150)
    7 FORMAT(7H STOP 7)
    8 FORMAT(7H STOP 8)
    9 FORMAT(7H STOP 9)
   10 FORMAT(1H0,I5,2E10.2)
   20 FORMAT(1H0,I5,3E10.2)
   30 FORMAT(1H0,I5,E10.2)
   50 FORMAT(1H0,3E10.2)
   70 FORMAT(1H0,12HSAMPLE COUNT  ,19HTRUE GAS TEMP-DEG F)
   75 FORMAT(5X,I4,5X,E12.5)
   80 FORMAT(2X,I5,2X,10E10.2)
  101 FORMAT(1H0,21HINTERPOLATE THIS TEMP)
      J=NPD
      PI=3.1415927
      REV=REV*60.0*PI
      PIA=2.0*PI/IRAM
  180 DO370 N=1,IRAM
      AN=N-1
      AN=AN*PIA
      T(N)=0.0
      DT(N)=0.0
      DO190K=J,KK,J
      T(N)=T(N)+YC(K,1)*COSF(AN*K/J)+YC(K,2)*SINF(AN*K/J)
      DT(N)=DT(N)-YC(K,1)*(K/J)*SINF(AN*K/J)
  190 DT(N)=DT(N)+YC(K,2)*(K/J)*COSF(AN*K/J)
  370 CONTINUE
      GOTO(1001,200,300,400),NCHN
```

```
200 DO201N=1,IRAM
    AW(N)=T(N)
201 XW(N)=DT(N)
    CALL MEKPLT(AW,IRAM,1,1,1,10HFINE WIRE ,10HCRANK ANG ,10HTEMP DEG
   1F,5.0,1HA)
    GOTO1000
300 DO301N=1,IRAM
    BW(N)=T(N)
301 YW(N)=DT(N)
    CALL MEKPLT(BW,IRAM,1,1,1,10HMID  WIRE ,10HCRANK ANG ,10HTEMP DEG
   1F,5.0,1HB)
    GOTO1000
400 DO401N=1,IRAM
    CW(N)=T(N)
401 ZW(N)=DT(N)
    CALL MEKPLT(CW,IRAM,1,1,1,10HLARGE WIRE,10HCRANK ANG ,10HTEMP DEG
   1F,5.0,1HC)
    DA=1.9
    DB=2.2
    DC=3.1
    DAB=DB/DA
    DCB=DC/DB
    DO800K=1,IRAM
    IF(XW(K))420,410,420
410 T=AW(K)
    GOTO740
420 IF(YW(K))440,430,440
430 T=BW(K)
    GOTO740
440 IF(ZW(K))460,450,460
450 T=CW(K)
    GOTO740
460 IF(XW(K)*YW(K))470,480,490
480 GOTO1003
470 IF(AW(K)-BW(K))500,510,520
500 T1=AW(K)+0.01
```

```
      T2=BW(K)-0.01
      GOTO620
  520 T1=BW(K)+0.01
      T2=AW(K)-0.01
      GOTO620
  510 WRITE(61,101)
      WRITE(61,010)K,AW(K),BW(K)
      ABE=XW(K)/YW(K)
      IF(ABE.LE.0)GOTO515
      PM1=ALOG(ABE)/ALOG(DAB)
      GOTO516
  515 PM1=0.0
  516 WRITE(61,030)K,ABE
      WRITE(61,030)K,PM1
      T=0.0
      GOTO740
  490 IF(YW(K)*ZW(K))530,540,550
  540 GOTO1003
  530 IF(BW(K)-CW(K))560,570,580
  560 T1=BW(K)+0.01
      T2=CW(K)-0.01
      GOTO620
  580 T1=CW(K)+0.01
      T2=BW(K)-0.01
      GOTO620
  570 WRITE(61,101)
      WRITE(61,010)K,BW(K),CW(K)
      BCE=YW(K)/ZW(K)
      IF(BCE.LE.0)GOTO575
      PM2=ALOG(BCE)/ALOG(DCB)
      GOTO576
  575 PM2=0.0
  576 WRITE(61,030)K,BCE
      WRITE(61,030)K,PM2
      T=0.0
      GOTO740
```

```
550 IF(AW(K)-CW(K))590,600,610
590 T1=AW(K)-200.0
    T2=AW(K)-0.01
    GOTO620
610 IF(XW(K).AND.YW(K).AND.ZW(K).LT.0)GOTO612
    T1=AW(K)+0.01
    T2=AW(K)+200.0
    GOTO620
612 T1=CW(K)-0.01
    T2=CW(K)-100.0
    GOTO620
600 WRITE(61,101)
    WRITE(61,010)K,AW(K),CW(K)
    T=0.0
    GOTO740
620 J=10
    GOTO640
615 T1=T1+10.0
640 FT2=FTN(K,T2)
    FT1=FTN(K,T1)
    IF(FT2*FT1)650,670,680
680 GOTO615
670 T=T2
    GOTO740
650 FT3=FT1
    T3=T1
    FT1=FT2
    T1=T2
    T2=(T1+T3)*0.5
    DO720I=1,J
    FT2=FTN(K,T2)
    IF(FT2*FT1)700,690,710
690 T=T2
    GOTO740
700 FT3=FT1
    T3=T1
```

```
  710 FT1=FT2
      T1=T2
  720 T2=(T1+T3)*0.5
      T=T2
  740 T(K)=T
  800 CONTINUE
      DO900N=1,IRAM
      TT=0.0
      AN=N-1
      AN=AN*PIA
      I=0
      DO790K=J,KK,J
      I=I+1
  790 TT=TT+(PP(I)*COSF(AN*K/J))+(QQ(I)*SINF(AN*K/J))
  900 T(N)=TT
      WRITE(61,070)
      WRITE(61,075)((K,T(K)),K=1,IRAM)
      CALL MEKPLT(T,IRAM,1.1,1,10HTRUE GAS T,10HCRANK ANG ,10HTEMP DEG F
     1,5.0,1H*)
      GOTO1000
 1001 PRINT 7
      STOP
 1002 PRINT 8
      STOP
 1003 PRINT9
      STOP
 1000 RETURN
      END
```

```
      FUNCTIONBOLZANO(BEGIN,FIN,STEP,K)
      A=BEGIN
      FA=FTN(K,A)
      ASSIGN10TOL
      IF(FIN.LT.BEGIN)ASSIGN20TOL
      GOTOL
   10 IF(A.GT.FIN)GOTO50
      B=A+STEP
      GOTO30
   20 IF(A.LT.FIN)GOTO50
      B=A-STEP
   30 FB=FTN(K,B)
      IF(FA*FB)80,70,40
   40 A=B
      FA=FB
      GOTOL
   50 BOLZANO=0.0
      PRINT60,BEGIN,FIN,STEP,K
   60 FORMAT(5X,12H****BOLZANO(,3(E10.2,2H**),I4,20H)ERROR**ZERO  RETURN
     1)
      RETURN
   70 BOLZANO=B
      RETURN
   80 N=ALOG(STEP*100.0)/0.6931+1.0
      DO110I=1,N
      C=(A+B)/2.0
      FC=FTN(K,C)
      IF(FB*FC)90,120,100
   90 A=B
      FA=FB
  100 B=C
  110 FB=FC
  120 BOLZANO=C
      RETURN
      END
```

```
      FUNCTION FTN(K,T)
      COMMONIY(4321),Y(4321),ITAPCON,NSER,IRUN,NOCHN(8),ICAL(5)
      COMMONVOLTC(5),NPI,NP,NPD,NPTS,LIST,ISTOP
      COMMON NTEST,CAL(5),NPERD,MI,MF,KKD
      COMMON TMOD(250),TPHI(250),REV
      COMMON YS(250,2),YC(250,2)
      COMMON G1,G2,G3,G4
      COMMON NCO
      COMMON AW(150),BW(150),CW(150),XW(150),YW(150),ZW(150)
   40 FORMAT(1H0,I5,8E10.2)
      REAL NN
      NN=2.5445
      FTN=(((T-AW(K))/XW(K))**(NN-1))*((T-CW(K))/ZW(K))-((T-BW(K))/YW(K)
     1)**NN
      WRITE(61,040)K,AW(K),BW(K),CW(K),XW(K),YW(K),ZW(K),T,FTN
      RETURN
      END
```

Fig. 3(b) Subroutine for direct calculation of True Gas Temperature from 3-Wire Fourier Coefficients.

```
      SUBROUTINE WIRE3(IRAM,NCHN,KK)
C     FROM DIRECT FOURIER COEFFICIENTS OF 3-WIRE DATA
      COMMONIY(4321),Y(4321),ITAPCON,NSER,IRUN,NOCHN(8),ICAL(5)
      COMMONVOLTC(5),NPI,NP,NPD,NPTS,LIST,ISTOP
      COMMON NTEST,CAL(5),NPERD,MI,MF,KKD
      COMMON TMOD(250),TPHI(250),REV
      COMMON YS(250,2),YC(250,2)
      COMMON G1,G2,G3,G4
      COMMON NCO
      COMMON AW(150),BW(150),CW(150),XW(150),YW(150),ZW(150)
      DIMENSIONT(150),DT(150),AA(250),BB(250),CC(250)
      DIMENSIONALPA(250),BETA(250),GAMA(250),QQ(250),PP(250)
    7 FORMAT(7H STOP 7)
    8 FORMAT(7H STOP 8)
    9 FORMAT(7H STOP 9)
   10 FORMAT(1H0,I5,2E10.2)
   20 FORMAT(1H0,I5,3E10.2)
   30 FORMAT(1H0,I5,E10.2)
   50 FORMAT(1H0,3E10.2)
   70 FORMAT(1H0,12HSAMPLE COUNT  ,19HTRUE GAS TEMP-DEG F)
   75 FORMAT(5X,I4,5X,E12.5)
   80 FORMAT(2X,I5,2X,10E10.2)
  101 FORMAT(1H0,21HINTERPOLATE THIS TEMP)
      J=NPD
      PI=3.1415927
      REV=REV*60.0*PI
      PIA=2.0*PI/IRAM
  180 DO370 N=1,IRAM
      AN=N-1
      AN=AN*PIA
      T(N)=0.0
      DT(N)=0.0
      DO190K=J,KK,J
      T(N)=T(N)+YC(K,1)*COSF(AN*K/J)+YC(K,2)*SINF(AN*K/J)
      DT(N)=DT(N)-YC(K,1)*(K/J)*SINF(AN*K/J)
  190 DT(N)=DT(N)+YC(K,2)*(K/J)*COSF(AN*K/J)
```

```
370 CONTINUE
    GOTO(1001,200,300,400),NCHN
200 DO201N=1,IRAM
    AW(N)=T(N)
201 XW(N)=DT(N)
    CALL MEKPLT(AW,IRAM,1,1,1,10HFINE WIRE ,10HCRANK ANG ,10HTEMP DEG
   1F,5.0,1HA)
    DO202I=1,KK
    AA(I)=TMOD(I)
202 ALPA(I)=TPHI(I)
    GOTO1000
300 DO301N=1,IRAM
    BW(N)=T(N)
301 YW(N)=DT(N)
    CALL MEKPLT(BW,IRAM,1,1,1,10HMID  WIRE ,10HCRANK ANG ,10HTEMP DEG
   1F,5.0,1HB)
    DO303I=1,KK
    BB(I)=TMOD(I)
303 BETA(I)=TPHI(I)
    GOTO1000
400 DO401N=1,IRAM
    CW(N)=T(N)
401 ZW(N)=DT(N)
    CALL MEKPLT(CW,IRAM,1,1,1,10HLARGE WIRE,10HCRANK ANG ,10HTEMP DEG
   1F,5.0,1HC)
    DO404I=1,KK
    CC(I)=TMOD(I)
404 GAMA(I)=TPHI(I)
    DO800I=1,KK
    F11=0.5*(COSF(2.0*ALPA(I))+COSF(2.0*BETA(I))+COSF(2.0*GAMA(I)))
    F1=1.5+F11
    F2=(SINF(ALPA(I)))*(COSF(ALPA(I)))+(SINF(BETA(I)))*(COSF(BETA(I)))
   1+(SINF(GAMA(I)))*(COSF(GAMA(I)))
    F3=AA(I)*COSF(ALPA(I))+BB(I)*COSF(BETA(I))+CC(I)*COSF(GAMA(I))
    F4=F2
    F5=1.5-F11
```

```
      F6=AA(I)*SINF(ALPA(I))+BB(I)*SINF(BETA(I))+CC(I)*SINF(GAMA(I))
      FM=-(F1/F4)
      QQ(I)=(F3+(FM*F6))/((FM*F5)+F2)
      PP(I)=(F3-(F2*QQ(I)))/F1
  800 CONTINUE
      DO900N=1,IRAM
      TT=0.0
      AN=N-1
      AN=AN*PIA
      I=0
      DO790K=J,KK,J
      I=I+1
  790 TT=TT+(PP(I)*COSF(AN*K/J))+(QQ(I)*SINF(AN*K/J))
  900 T(N)=TT
      WRITE(61,070)
      WRITE(61,075)((K,T(K)),K=1,IRAM)
      CALL MEKPLT(T,IRAM,1,1,1,10HTRUE GAS T,10HCRANK ANG ,10HTEMP DEG F
     1,5.0,1H*)
      GOTO1000
 1001 PRINT 7
      STOP
 1002 PRINT 8
      STOP
 1003 PRINT9
      STOP
 1000 RETURN
      END
```

TABLE 4

```
C       G.A.MORGAN/FOWLER  MECH ENG DEPT U OF A  TEL 461
C       ENGINE PERFORMANCE DATA REDUCTION
C       PROGRAMME NO 013/1620
        DIMENSIONMX(9),MS(9),FC(9),AC(9),W(9),H(9),T1(9),T2(9),FA(9),F(9)
        DIMENSIONAF(9),FD(9),HP(9),BC(9),BP(9),EV(9),EC(9),HT(9),A(9)
   10 FORMAT(1H ,49H                                                )
   20 FORMAT(1H ,6HNTEST=,I3,3X,5HNRUN=,I3)
   30 FORMAT(1H ,3HCR=,F4.1,6H NOCT=,I3,7H THROT=,F6.3)
   40 FORMAT(1H0,6HNRPM =,I9)
   50 FORMAT(1H ,6HMIX  =,3X,I2,8I7)
   60 FORMAT(1H ,6HMBT  =,1X,I3,8I7,4X,7HDEGBTDC)
   70 FORMAT(1H ,6H  F  =,9F7.2,1X,5HLB/HR)
   80 FORMAT(1H ,6H  A  =,9F7.2,1X,5HLB/HR)
   90 FORMAT(1H ,6H AF  =,1X,9F7.3)
  100 FORMAT(1H ,6H FA  =,2X,F6.3,8F7.3)
  110 FORMAT(1H ,6HFA/FC=,9F7.2)
  120 FORMAT(1H ,6HBHP  =,9F7.2)
  130 FORMAT(1H ,6HBSFC =,1X,9F7.3,9HLB/BHP.HR)
  140 FORMAT(1H ,6HBMEP =,F6.1,8F7.1,2X,3HPSI)
  150 FORMAT(1H ,6HEVOL =,9F7.2)
  160 FORMAT(1H ,6HECFLO=,F6.1,8F7.1,2X,6HGAL/HR)
  170 FORMAT(1H ,6HHTRE =,9F7.2,1X,7HKBTU/HR)
  220 FORMAT(2I6)
  230 FORMAT(F6.1,I6,F6.3)
  240 FORMAT(2F6.1,2F6.2,F6.4)
  250 FORMAT(I6)
  260 FORMAT(9I6)
  280 FORMAT(9F6.2)
  200 READ010
      PUNCH010
      READ220,NTEST,NRUN
```

```
      PUNCH020,NTEST,NRUN
      READ230,CR,NOCT,THROT
      PUNCH030,CR,NOCT,THROT
      READ240,DB,WB,HG,S,PWV
      READ250,NRPM
      PUNCH040,NRPM
      READ260,MX(1),MX(2),MX(3),MX(4),MX(5),MX(6),MX(7),MX(8),MX(9)
      READ260,MS(1),MS(2),MS(3),MS(4),MS(5),MS(6),MS(7),MS(8),MS(9)
      READ280,FC(1),FC(2),FC(3),FC(4),FC(5),FC(6),FC(7),FC(8),FC(9)
      READ280,AC(1),AC(2),AC(3),AC(4),AC(5),AC(6),AC(7),AC(8),AC(9)
      READ280,W(1),W(2),W(3),W(4),W(5),W(6),W(7),W(8),W(9)
      READ280,T1(1),T1(2),T1(3),T1(4),T1(5),T1(6),T1(7),T1(8),T1(9)
      READ280,T2(1),T2(2),T2(3),T2(4),T2(5),T2(6),T2(7),T2(8),T2(9)
      READ280,H(1),H(2),H(3),H(4),H(5),H(6),H(7),H(8),H(9)
      DO360I=1,9
      RPM=NRPM
      F(I)=0.798*FC(I)+0.288
      C=1.0-0.0015*(DB-68.0)
      B=46.08*C*AC(I)
      A(I)=B/S
      AF(I)=A(I)/F(I)
      FA(I)=1.0/AF(I)
      FD(I)=FA(I)/0.0665
      TT=DB+460.0
      HP(I)=W(I)*RPM/3500.0
      BC(I)=F(I)/HP(I)
      P=HG
      HP(I)=HP(I)*(29.92/(P-PWV))*SQRTF(TT/520.0)
      BP(I)=7.31*W(I)
      BP(I)=BP(I)*(29.92/(P-PWV))*SQRTF(TT/520.0)
      EV(I)=111.75*B/RPM
      DET=T2(I)-T1(I)
      EC(I)=6.0*(8.006+28.09*H(I)-2.851*(H(I)**2.0))
360   HT(I)=(18.0*EC(I)*DET)/1000.0
      PUNCH050,MX(1),MX(2),MX(3),MX(4),MX(5),MX(6),MX(7),MX(8),MX(9)
      PUNCH060,MS(1),MS(2),MS(3),MS(4),MS(5),MS(6),MS(7),MS(8),MS(9)
```

```
PUNCH070,F(1),F(2),F(3),F(4),F(5),F(6),F(7),F(8),F(9)
PUNCH080,A(1),A(2),A(3),A(4),A(5),A(6),A(7),A(8),A(9)
PUNCH090,AF(1),AF(2),AF(3),AF(4),AF(5),AF(6),AF(7),AF(8),AF(9)
PUNCH100,FA(1),FA(2),FA(3),FA(4),FA(5),FA(6),FA(7),FA(8),FA(9)
PUNCH110,FD(1),FD(2),FD(3),FD(4),FD(5),FD(6),FD(7),FD(8),FD(9)
PUNCH120,HP(1),HP(2),HP(3),HP(4),HP(5),HP(6),HP(7),HP(8),HP(9)
PUNCH130,BC(1),BC(2),BC(3),BC(4),BC(5),BC(6),BC(7),BC(8),BC(9)
PUNCH140,BP(1),BP(2),BP(3),BP(4),BP(5),BP(6),BP(7),BP(8),BP(9)
PUNCH150,EV(1),EV(2),EV(3),EV(4),EV(5),EV(6),EV(7),EV(8),EV(9)
PUNCH160,EC(1),EC(2),EC(3),EC(4),EC(5),EC(6),EC(7),EC(8),EC(9)
PUNCH170,HT(1),HT(2),HT(3),HT(4),HT(5),HT(6),HT(7),HT(8),HT(9)
GOTO200
END
```

TABLE 5

```
C       G.A.MORGAN  MECH ENG DEPT U OF A TEL 461
C       ENGINE HEAT TRANSFER DATA REDUCTION
C       PROGRAMME NO 007/1620
        DIMENSIONNRPM(5),W(5),FCM(5),ACM(5),H(5),TE1(5),TE2(5),TIME(5)
        DIMENSIONTIN(5),TOUT(5),TG(5),TW(5),BHP(5),F(5),A(5),FA(5),AF(5)
        DIMENSIONEC(5),HTRE(5),CFLO(5),HTR(5),HFLUX(5),HTC(5)
   10 FORMAT(1H ,49H                                                )
   20 FORMAT(1H ,3HCR=,F4.1,7H THROT=,F6.3,6H NOCT=,I3)
   30 FORMAT(1H ,5HNSPK=,I3,9H DEG.BTDC)
   40 FORMAT(1H0,5HNRPM=,4X,I9,4I10)
   50 FORMAT(1H ,4HBHP=,8X,F5.2,4F10.2)
   60 FORMAT(1H ,2HF=,11X,F5.3,4F10.3,8H  LB/MIN)
   70 FORMAT(1H ,2HA=,11X,F5.3,4F10.3,8H  LB/MIN)
   80 FORMAT(1H ,4HF/A=,4X,5F10.3)
   90 FORMAT(1H ,4HA/F=,4X,5F10.3)
  100 FORMAT(1H ,6HECFLO=,5F10.1,10H    LB/MIN)
  110 FORMAT(1H ,5HHTRE=,F12.1,4F10.1,1 H    BTU/HR)
  120 FORMAT(1H ,5HCFLO=,2X,5F10.2,7H LB/MIN)
  130 FORMAT(1H ,4HHTR=,2X,5F10.1,8H  BTU/HR)
  140 FORMAT(1H ,6HHFLUX=,5F10.1,11H  BTU/HFTSQ)
  150 FORMAT(1H ,4HHTC=,2X,5F10.1,12H  BTU/HFTSQF)
  200 READ010
      PUNCH010
      READ,CR,THROT,NOCT,K
      PUNCH020,CR,THROT,NOCT
  220 READ,NSPK
      READ,NRPM(1),NRPM(2),NRPM(3),NRPM(4),NRPM(5)
      READ,W(1),W(2),W(3),W(4),W(5)
      READ,FCM(1),FCM(2),FCM(3),FCM(4),FCM(5)
      READ,ACM(1),ACM(2),ACM(3),ACM(4),ACM(5)
      READ,DB,S
      READ,H(1),H(2),H(3),H(4),H(5)
      READ,TE1(1),TE1(2),TE1(3),TE1(4),TE1(5),TE2(1),TE2(2),TE2(3)
```

```
      READ,TE2(4),TE2(5)
  230 READ,TIME(1),TIME(2),TIME(3),TIME(4),TIME(5)
      READ,TIN(1),TIN(2),TIN(3),TIN(4),TIN(5),TOUT(1),TOUT(2),TOUT(3)
      READ,TOUT(4),TOUT(5)
      READ,TG(1),TG(2),TG(3),TG(4),TG(5),TW(1),TW(2),TW(3),TW(4),TW(5)
      DO260I=1,5
      RPM=NRPM(I)
      BHP(I)=W(I)*RPM/3500.0
      F(I)=FCM(I)/76.9
      C=1.0-0.0015*(DB-68.0)
      A(I)=0.768*C*ACM(I)/S
      FA(I)=F(I)/A(I)
      AF(I)=1.0/FA(I)
      EC(I)=6.45*H(I)+23.03
      DET=TE2(I)-TE1(I)
      HTRE(I)=108.0*EC(I)*DET
      CFLO(I)=33.0/TIME(I)
      DT=TOUT(I)-TIN(I)
      HTR(I)=CFLO(I)*DT*60.0
      D=0.483
      DD=D*D
      AR=0.78539816*DD/144.0
      HFLUX(I)=0.0
      HFLUX(I)=HTR(I)/AR
      IF(K)240,240,250
  240 HFLUX(I)=HFLUX(I)-5.0E4
      GOTO255
  250 HFLUX(I)=HFLUX(I)-7.5E4
  255 DTEMP=TG(I)-TW(I)
  260 HTC(I)=HFLUX(I)/DTEMP
      PUNCH030,NSPK
      PUNCH040,NRPM(1),NRPM(2),NRPM(3),NRPM(4),NRPM(5)
      PUNCH050,BHP(1),BHP(2),BHP(3),BHP(4),BHP(5)
      PUNCH060,F(1),F(2),F(3),F(4),F(5)
      PUNCH070,A(1),A(2),A(3),A(4),A(5)
      PUNCH080,FA(1),FA(2),FA(3),FA(4),FA(5)
```

```
PUNCH090,AF(1),AF(2),AF(3),AF(4),AF(5)
PUNCH100,EC(1),EC(2),EC(3),EC(4),EC(5)
PUNCH110,HTRE(1),HTRE(2),HTRE(3),HTRE(4),HTRE(5)
READ010
PUNCH010
READ010
PUNCH010
PUNCH120,CFLO(1),CFLO(2),CFLO(3),CFLO(4),CFLO(5)
PUNCH130,HTR(1),HTR(2),HTR(3),HTR(4),HTR(5)
PUNCH140,HFLUX(1),HFLUX(2),HFLUX(3),HFLUX(4),HFLUX(5)
PUNCH150,HTC(1),HTC(2),HTC(3),HTC(4),HTC(5)
GOTO200
END
```